

Fatigue of E-glass fiber reinforced composite materials and substructures
by Daniel David Samborsky

A thesis submitted in partial fulfillment of the requirements for the degree of Master of Science in Civil Engineering
Montana State University
© Copyright by Daniel David Samborsky (1999)

Abstract:
Fiberglass composites have been used in thousands of applications since their inception in the late 1930's despite an incomplete understanding and characterization of their mechanical fatigue properties. Wind turbine blades, which are the main focus of this research, experience between10^8 to10^9 significant fatigue (loading-unloading) cycles in their 20 to 30 year lifetime, and fatigue is a major factor in their design. This thesis presents a detailed analysis of the DOE/MSU Composite Material Fatigue Database, which has been developed over the last nine years. The database currently includes over 6000 static and fatigue test results covering 148 different fiberglass materials and numerous loading conditions. Trends in fatigue resistance with various materials and loading parameters are explored, including: reinforcement fabric architecture, fiber content, content of fibers orientated in the load direction, matrix material and loading conditions (tension, compression and reversed loading).

The results show unexpected transitions in fatigue resistance with fiber content and fabric architecture. Transitions to increased fatigue sensitivity have been related to fiber packing characteristics through detailed microscopy study. Material characteristics which produce maximum fatigue resistance have been established. Very high cycle tensile fatigue behavior (10^9 cycles) has been explored with a novel high frequency apparatus using impregnated strands. The strand data suggest a reduction in fatigue sensitivity in the 10^8 to 10^9 cycle range, but a material endurance limit has not been seen. Larger impregnated glass strands tested in excess of 10^8 cycles using conventional testing equipment provide similar results to the smaller strands.

The study has also explored the application of the database to the prediction of the fatigue response of small composite substructures representative of wind turbine blades. Thirty six I-beams were tested under four-point bending. The beams were constructed of materials which showed a range of fatigue resistance in the materials coupon tests. The coupon database accurately predicted the performance of the beams when the failure modes were predominately tensile or compressive. Delamination of the tensile flange in the beams with improved fatigue resistance materials, due to the increase in bending loads and flange operating strains, provided less conclusive results. The effect of flaws (through-thickness holes) was also explored. A second geometry, hollow tubes, was also explored in conjunction with field tests on a small wind turbine. Twenty seven hollow tube test sections were tested under four-point and cantilever bending. Due to the hollow tube geometry, the compressive buckling behavior was the limiting static design parameter, and the obtained compressive strains in the tubes were slightly lower than the database compressive strength values (which used very short specimens).

FATIGUE OF E - GLASS FIBER REINFORCED COMPOSITE MATERIALS AND SUBSTRUCTURES

by

Daniel David Samborsky

A thesis submitted in partial fulfillment
of the requirements for the degree

of

Master of Science

in

Civil Engineering

MONTANA STATE UNIVERSITY
Bozeman, Montana

December 1999

© COPYRIGHT

by

Daniel David Samborsky

1999

All Rights Reserved

N378
Sa44

APPROVAL

of a thesis submitted by

Daniel David Samborsky

This thesis has been read by each member of the thesis committee and has been found to be satisfactory regarding content, English usage, format, citations, bibliographic style, and consistency, and is ready for submission to the College of Graduate Studies.

Dr. John F. Mandell — Chairperson, Graduate Committee — Date 12/2/99

Approved for the Department of Civil Engineering

Dr. Don Rabern — Head, Civil Engineering Department — Date 12/1/99

Approved for the College of Graduate Studies

Dr. Bruce McLeod — Graduate Dean — Date 12-6-99

STATEMENT OF PERMISSION TO USE

In presenting this thesis in partial fulfillment of the requirements for a master's degree at Montana State University, I agree that the Library shall make it available to borrowers under rules of the Library.

I have indicated my intention to copyright this thesis by including a copyright notice page, copying is allowable only for scholarly purposes, consistent with "fair use" as prescribed in the U.S. Copyright Law. Requests for permission for extended quotation from or reproduction of this thesis in whole or in parts may be granted only by the copyright holder.

Signature 

Date 12/2/1999

ACKNOWLEDGMENTS

I have been both a student and a research engineer at MSU for over 10 years and this thesis is a collection of some of the research I have performed. I estimate 63,000 machine hours and over 16,000 personal hours are present in this document, and as no good deed goes unpunished, and I have made many personal sacrifices in performing this research, but it has been my choice, as it was the only way to get it done and to accomplish something that needed to be done.

This is by no means an average masters thesis, and both the amount, and detail of research can only be attributed to the truly outstanding mentors, and friends, I work with, notably: Dr. John Mandell (composites), Dr. Jerry Stephens (engineering) and Dr. Doug Cairns (composites).

No one can achieve work like this without exceptional parents and family, like my father James Samborsky, P. Eng. (B.S., M.S. civil, B.S. mechanical engineering (all MSU)), mother Judith; brothers Richard (B.Ed.) and Scott, and a special sister Tanya. I wish that my mother and Scott were alive to celebrate this achievement with me. I want to also mention a special friend, who, unfortunately, at the time, did not understand my engineering passion, Teresa Keef, and my other friends and co-workers, who, at the time, did not understand the humor or t-shirts, which were (actually) funny.

This work was supported by the following: Sandia National Laboratories, subcontracts 40-8875, 18-3958, AN-0412 and BC7159; the National Renewable Energy Laboratory, subcontracts XF-1-11009-5 and XAF-5-14076-04; and the Department of Energy through the DOE EPSCoR Program, contract DE-FC02-91ER75681.

TABLE OF CONTENTS

LIST OF TABLES viii

LIST OF FIGURES x

ABSTRACT xxiv

1. INTRODUCTION 1

2. FABRICATION OF MATERIALS 7
- Fabric Reinforcement 7
- Resins 9
- Flat Rectangular Plate Construction 12
- E - Glass Prepreg 14
- Industrial Supplied Materials 15
- Machining 15
- Test Specimen Geometries 16
- I - Beam Construction 20
- Cylindrical Tubes 24
- Fiber Volume Fraction (V_F) Determination 25

3. MECHANICAL TESTING EQUIPMENT 29
- Load Cells 29
- Extensometers 31
- Actuator Position (LVDT) 32
- Strain Gages 33
- Testing Machine Load Train Alignment 35
- Fiber Testing Apparatus 37

4. TESTING AND TEST DEVELOPMENT 40
- Coupon Tests 40
- Tensile Tests 41
- Tensile Test Development 45
- Test Coupon Gripping 48
- Compressive Test Development 54
- I - Beam 4 Point Bending Development 59
- Cylindrical Tube Bending Tests 62

5. COUPON TESTS 63
- Unidirectional Materials 63
  - Fiber Packing 63
  - Strand Deformations in Fabrics 64

Unidirectional fatigue behavior 76
Background 76
Results and Discussion 78
Variability in Properties of Strands Taken From Fabric 79
Unidirectional Laminates 87
±45° Fabrics 101
Materials With Varying Amounts of ±45° and 0° Plies 107
Fatigue Trends 108
Effect of R Value 120
Comparison of Materials 120
Failure Modes 130
Fabric Architecture Effects 138
Conclusions 144

6. BALANCED ANGLE PLY LAMINATES 146
Background Information 146
Testing Methods 150
Results and Discussion 152
Laminate Analysis Predicted Properties 158
Fatigue Testing 165
Failure modes 174
Conclusions for Balanced Ply Laminates 183

7. I-BEAMS 184
Experimental Investigation Of Beam Static and Fatigue Behavior 185
Material and Beam Description 187
Studies of Beams with Triax Material Flanges 191
Behavior of Beams 193
Studies of Beams with Improved Flange and Web Materials 199
Material Development and Coupon Results 200
Beam Test Results 200
Conclusions for Beams With Improved Flange and Web Materials . . . 207
Stiffness Changes 208
Studies Of Structural Details 213
Effects of Through-Thickness Holes 213
Coupon Results With Holes 214
Beam Results With Holes 219
Beams Utilizing a Balsa Wood Core 220
Conclusions for I-beam Study 222

8. CYLINDRICAL TUBES 224
Static 4-Point Bending Tests 225
Static and Fatigued Cantilever Beam Tests 239

Comparison with Coupon Tests 250
Conclusions for Cylindrical Tubes 253

9. CONCLUSIONS AND RECOMMENDATIONS 254
High Cycle Fatigue Behavior of Glass Strands 254
Reinforcement Fabric Architecture Effects 255
Fiber Content 257
Content of Fibers in the Loading Direction 257
Matrix Materials 258
Optimum Laminates for Blade Primary Structure 259
I-Beams 259
Cylindrical Tubes 260
Recommendations 260

REFERENCES 262

APPENDICES 270
Appendix A - DOE/MSU Composite Material Fatigue Database 271
Appendix B - Summary of I-Beam Tests 448

LIST OF TABLES

2.1. Summary of E - Glass fabrics 11

2.2. Summary of resin matrix materials 11

2.3. Summary of test coupon geometries 17

2.4. Summary of Tab Materials 20

2.5 Summary of web I-shapes used in Beams 6 through 59. 23

2.6. Summary of additional beam components 24

3.1. Summary of mechanical testing equipment 30

3.2. Summary of Load cells 31

3.3. Summary of extensometers 32

3.4. Summary of strain gages 34

3.5 Summary of applicable bending standards for uniaxial testing machines 36

5.1. Summary of previous fatigue results on individual E-glass fibers and tows 80

5.2. Impregnated strands tested in fatigue 82

5.3. Summary of fatigue properties for the unidirectional materials tested 89

5.4. Summary of static properties for the unidirectional materials tested 95

5.5. Summary of the ±45° materials tested 102

5.6. Summary of materials with 16 to 63 percent 0's. 109

5.7. Summary of materials with 69 to 85 percent 0° plies. 110

5.8. Lay-up summaries with 55 to 63 percent 0° plies. 119

5.9. Summary of fatigue results: tensile (R = 0.1), compressive (R = 10) and reversed loading (R = -1). 125

6.1. Measured angles of 0/±45 and ±45 materials listed in the database. 147

6.2. Properties of MSU manufactured (RTM) fiberglass materials with balanced angle plies. 149

6.3. Tension and compression test coupon gage lengths. 151

6.4. Ply properties used in the laminate theory analysis (static) and values used for million cycle fatigue predictions adjusted to a fiber volume fraction of 0.39. . 159

6.5. Failure criterion failure mode predictions for the balanced angle ply laminates with a fiber volume fraction of 0.39. 165

7.1. Static and fatigue data for beams with AA flanges and material CH10 webs. 188

7.2. Static and fatigue data for beams with DD5P flanges and CH10 webs. 189

7.3. Fatigue data for beams with DD5P flanges and CH3 webs. 189

7.4. Static and fatigue data for beams with DD5P flanges and CH12 webs. 190

7.5. Fatigue data for beams with DD5P flanges and DD5P webs. 190

7.6. Fatigue data for beams with DD22 flanges (with balsa wood), and CH12 webs. . 190

8.1. Summary of static four - point bending tests performed on tube sections 227

8.2. Test summary for tubes T120 through T137. 242

LIST OF FIGURES

1.1. Modified Bergey 10 kW wind turbine at Rice Ridge Renewable Energy Park. 3

1.2. Maximum recorded turbine blade strains, Bergey 10 kW, 7.5 m/s wind speed. 4

1.3. AOC 15/50 wind turbine. 4

1.4. Typical wind turbine blade cross sections. 6

2.1. D155 fabric. 8

2.2. A130 fabric. 8

2.3 DB120 fabric. 8

2.4. Lamina (plies) and laminate description. 10

2.5. Flat plate RTM mold. 13

2.6. Test coupon geometries. 19

2.7. Instron 8511 and 8872 test coupon geometry. 20

2.8. C-Channel RTM mold. 21

2.9. Web I-section RTM mold. 22

2.10. Assembled I-beam. 23

2.11. Cylindrical tube RTM mold. 26

2.12. Aluminum 2024-T3 tube end fittings. 26

2.13. Tube testing assembly. 27

2.14. Fiber volume content versus RTM composite thickness. 28

3.1. Strain gage photograph showing tensile strain cracks. 34

3.2. Clip strain gage. 36

3.3. High frequency strand testing apparatus and test coupon geometry. 39

4.1. Constant stress amplitude sine waveforms for different R values. 41

4.2. Stress-strain curves for material DD5P at different testing rates. 42

4.3. Tensile strength versus testing displacement rate (25 mm wide coupons with a 100 mm gage length). 43

4.4. Tensile strength versus coupon width (100 mm gage length, 13 mm/s testing rate). 43

4.5. ASTM D3039 tensile test coupon geometry. 46

4.6. Width tapered coupon (DD5P material) with shoulder splitting. 48

4.7. Grip damage in test coupons, with and without tabs. 49

4.8. Tensile fatigue damage present under tab material. 50

4.9. Instron hydraulic wedge grip cross section. 50

4.10. Applied axial load to the test coupon versus the grip body hydraulic pressure. . . . 51

4.11. Applied axial tensile load versus the hydraulic grip clamping force on the test coupon. 52

4.12. Steel wedge grip face contact area with the test coupon. Shown by pressure film. 53

4.13. Hydraulic grip head translation versus side loading force. 57

4.14. Anti-translation and anti-rotation devices. 57

4.15. Typical compressive stress-strain curves with back-to-back strain gages. 58

4.16. Material compressive strength versus testing displacement rate (25 mm wide test coupons with a 13 mm gage length). 58

4.17. Apparent compressive strength versus coupon width (13 mm gage length with a 13 mm/s testing rate). 59

4.18. I-beam four-point bending test set-up. 60

4.19. Cylindrical tube cantilever beam testing set-up. 62

5.1. Fiber volume fraction versus the average fiber spacing in a composite with theoretical square and hexagonal packing geometries. 65

5.2. Fiber volume fraction versus the normalized maximum principal stress for a transversely loaded composite. 66

5.3. Micrographs of prepreg and D155 fabric composites. 68

5.4. Composite fiber volume content versus D155 confined fiber tow area in Materials DD6, DD2 and DD7. 69

5.5. Composite fiber volume fraction versus average number of fibers in contact with each other for materials DD6, DD5, DD2, DD9 and DD10. 70

5.6. Stacking geometries of unidirectional fiber bundles. 72

5.7 Fabric stitching interaction with adjacent plies. 73

5.8. Fabric stitching interaction with adjacent ply stitching and the effects of removing the stitching. 74

5.9. A130 fabric with woven architecture with cracking around thermoplastic bead in coupon DD11-107 after fatigue testing. 75

5.10. Normalized S-N fatigue data for unimpregnated single glass fibers. 81

5.11. Normalized S-N fatigue data for unimpregnated glass fiber strands, R = 0.1. 81

5.12. Normalized S-N fatigue data for impregnated glass fiber strands, R = 0.1. 82

5.13. S-N fatigue data for impregnated fiber strand, R = 0.1. 83

5.14. Normalized S-N fatigue data for impregnated fiber strand, R = 0.1. 83

5.15. Applied tensile load versus time for a 45 fiber test coupon. 84

5.16. S-N fatigue data for D155 impregnated fiber strand, R = 0.1. 84

5.17. Normalized S-N fatigue data for impregnated D155 fiber strand, R = 0.1. 85

5.18. Strength distributions for strands from individual D155 rolls with Weibull fit parameters. 85

5.19. Weibull distribution of pooled D155 strand ultimate tensile strengths from rolls 1 through 6. 86

5.20. S-N fatigue data for D155 strands from D155 rolls 4 and 5. 87

5.21. Schematic representation of the development of damage during the fatigue life of a multidirectional composite laminate. 88

5.22. Normalized fatigue data for fabrics D072 and D092, R = 0.1. 90

5.23. Maximum initial fatigue strain data for fabrics D072 and D092, R = 0.1. 90

5.24. Normalized fatigue data for D155 fabrics (with and without stitching), R=0.1. . . 91

5.25. Maximum initial fatigue strain for D155 fabrics (with and without stitching), R = 0.1. 91

5.26. Normalized fatigue data for woven fabrics, R = 0.1. 92

5.27. Maximum initial fatigue strain data for woven fabrics, R = 0.1. 92

5.28. Normalized fatigue data for industrial materials A, B and L (with and without thickness tapering), R = 0.1. 94

5.29. Maximum initial fatigue strain data for industrial materials A, B and L (with and without thickness tapering), R = 0.1. 94

5.30. Fiber tensile strength versus fiber content for unidirectional materials. 95

5.31. Ultimate compressive stress versus fiber volume for unidirectional materials. . . . 96

5.32. Compressive failure strain versus fiber volume for unidirectional materials. 97

5.33. Million cycle tensile strain versus fiber volume for unidirectional materials, R=0.1. 99

5.34. Tensile fatigue coefficient, b, versus fiber volume for unidirectional materials. . . 99

5.35. Normalized compressive fatigue data for various unidirectional materials, R = 10. 100

5.36. Comparison of maximum initial fatigue strain data for various unidirectional materials and impregnated strand tests, R = 0.1. 100

5.37. Normalized Fatigue SN data for materials with DB120 ±45 fabric (R=0.1 and 10). 103

5.38. Initial fatigue strain data for materials with DB120 ±45 fabric (R=0.1 and 10). . 103

5.39. Initial fatigue strain data for materials with DB240 ±45 fabric (R=0.1 and 10). . 104

5.40. Initial fatigue strain data for materials with DB400 ±45 fabric (R=0.1 and 10). . 104

5.41. Normalized fatigue SN data for ±45 composites constructed with D155 fabric and different matrix materials (R=0.1 and 10). 105

5.42. Initial fatigue strain data for ±45 composites constructed with D155 fabric and different matrix materials (R=0.1 and 10). 105

5.43. Million cycle strain versus fiber volume fraction for ±45 materials. 106

5.44. Tensile fatigue coefficient, b, versus fiber volume fraction for ±45 materials. . . 106

5.45. Normalized S-N fatigue data for materials with 16 percent 0° plies, $[\pm 45/0/\pm 45]_S$ layup with D092 and DB240 fabrics, R=0.1 and 10. 111

5.46. Maximum initial fatigue strain data for materials with 16 percent 0° plies, $[\pm 45/0/\pm 45]_S$ layup with D092 and DB240 fabrics, R=0.1 and 10. 111

5.47. Normalized S-N fatigue data for materials with 24 percent 0° plies, $[\pm 45/0/\pm 45]_S$ layup with D155 and DB240 fabrics, R=0.1 and 10. 112

5.48. Maximum initial fatigue strain data for materials with 24 percent 0° plies, $[\pm 45/0/\pm 45]_S$ layup with D155 and DB240 fabrics, R=0.1 and 10. 112

5.49. Normalized S-N fatigue data for materials with 28 percent 0° plies, $[\pm 45/0/\pm 45]_S$ layup with D092 and DB120 fabrics, R=0.1 and 10. 113

5.50. Maximum initial fatigue strain data for materials with 28 percent 0° plies, $[\pm 45/0/\pm 45]_S$ layup with D092 and DB120 fabrics, R=0.1 and 10. 113

5.51. Normalized S-N fatigue data for materials with 39 percent 0° plies, $[\pm 45/0/\pm 45]_S$ layup with D155 and DB120 fabrics, R=0.1 and 10. 114

5.52. Maximum initial fatigue strain data for materials with 39 percent 0° plies, $[\pm 45/0/\pm 45]_S$ layup with D155 and DB120 fabrics, R=0.1 and 10. 114

5.53. Normalized S-N fatigue data for materials with 50 percent 0° plies, $[\pm 45/0/]_N$ layup with stitched triax fabrics, R=0.1 and 10. 115

5.54. Maximum initial fatigue strain data for materials with 50 percent 0° plies, $[\pm 45/0]_N$ layup with triax fabrics, R=0.1 and 10. 115

5.55. Normalized S-N fatigue data for materials with 55 to 63 percent 0° plies, R=0.1. 116

5.56. Maximum initial fatigue strain data for materials with 55 to 63 percent 0° plies, R=0.1. 116

5.57. Million cycle tensile strain data versus fiber volume fraction for materials with 19 to 63 percent 0° plies, R=0.1. 117

5.58. Tensile fatigue coefficient, b, versus fiber volume fraction for materials with 19 to 63 percent 0° plies, R=0.1. 118

5.59. Normalized S-N fatigue data for materials with 72 to 85 percent 0° plies. 119

5.60. Maximum fatigue strain versus cycles for material DD5P, R = 0.1, 10 and -1. . . 121

5.61. Maximum fatigue stress versus cycles for material DD5P, R = 0.1, 10 and -1. . . 121

5.62. Tensile fatigue data for various MSU and industrial materials, R = 0.1. 123

5.63. Extremes of normalized S-N tensile fatigue data (R = 0.1) for fiberglass laminates with at least 25 percent of the fiber in the 0° direction. 123

5.64. Normalized compressive fatigue data for standard coupons with 25 percent or greater percent 0° fibers, R = 10. 124

5.65. Reversed loading fatigue data normalized by the compressive strength for materials with 25 percent or greater percent 0° fibers, R = -1. 124

5.66. reversed loading fatigue data normalized by the tensile strength for materials with 25 percent or greater 0° fibers, R = -1. 125

5.67. Strain fatigue data for $[\pm 45]_S$ and $[0/\pm 45/0]_S$ materials, R=0.1. 128

5.68. Effect of fiber content on the normalized S-N data, R=0.1, for DD materials $[0/\pm 45/0]_S$. 129

5.69. Fiber content versus fatigue sensitivity coefficient, b, for DD materials. 129

5.70. Initial strain for 10^6 cycles (R = 0.1) versus percent 0° plies, D155, CH and DD materials. 130

5.71. Comparison of tensile fatigue test coupons, unidirectional Material A. 132

5.72. Unidirectional materials based on A130 fabric. 132

5.73. Unidirectional low fiber content materials based on D155 fabric. 133

5.74. Unidirectional high fiber content materials based on D155 fabric. 133

5.75. Material GG showing heavy brooming upon failure, tensile fatigue. 134

5.76. Material CH9 coupon failures. 134

5.77. Low fiber content, low percent 0's coupon failures. 135

5.78. High fiber content, low percent 0's coupon failures. 135

5.79.Moderate fiber content and percent 0's coupon failures. 136

5.80. Standard structural material at low fiber content, 72% 0's coupon failures. 136

5.81. Standard structural material with 72% 0's coupon failures. 137

5.82. Standard structural material at moderate fiber content coupon failures. 137

5.83. Standard structural materials at higher fiber content coupon failures. 138

5.84. Photographs of unidirectional stitched and adhesively bonded fabrics. 141

5.85. Photographs of woven unidirectional and stitched ±45° fabrics. 142

5.86. Photographs of stitched Triax fabrics. 143

6.1. Tensile stress - strain curves for balanced ±10°, ±20°, ±30°, and ±33° angle ply laminates (D155 fabric, $V_F = 0.39$). 153

6.2. Tensile stress - strain curves for balanced ±40°, ±45°, and ±50° angle ply laminates (D155 fabric, $V_F = 0.39$). 153

6.3. Tensile stress - strain curves for balanced ±60°, ±70°, ±80° and 90° angle ply laminates (D155 fabric, $V_F = 0.39$). 154

6.4. Ultimate tensile failure strain versus balanced ply angle. 155

6.5. Compressive stress - strain curves for balanced ±10°, ±20°, ±30° and ±40° angle ply laminates. 156

6.6. Compressive stress - strain curves for balanced ±50°, ±60°, ±70° and 90° angle ply laminates. 157

6.7. Calculated average ultimate compressive failure strain versus ply angle. 157

6.8. Longitudinal elastic modulus versus laminate theory predicted values. 159

6.9. Major Poisson's ratio versus laminate theory predicted values. 160

6.10. Calculated shear modulus versus balanced ply angle. 160

6.11. In - plane laminate stresses versus balanced ply angle. 161

6.12. Ultimate tensile strength versus balanced ply angle with laminate theory predicted values from the maximum stress, maximum strain and quadratic failure theories. 164

6.13. Ultimate compressive strength versus balanced ply angle with laminate theory predicted values from the maximum stress, maximum strain and quadratic failure theories. 164

6.14. First cycle hysteresis loops for balanced angle ply laminates from ±10° to 90°with a maximum stress equal to 50% of the laminates UTS. 166

6.15. Hysteresis energy generated on the first cycle for angle ply laminates from 0° to 90°with a maximum stress equal to 50% of the laminates UTS. 167

6.16. Tensile fatigue stress versus cycles to failure data for balanced ±10° to ±50°laminates ($\pm[\theta]_3$ laminates with D155 fabric, $V_F = 0.39$). 169

6.17. Tensile fatigue strain versus cycles to failure data for balanced ±10° to ±50°laminates ($\pm[\theta]_3$ laminate with D155 fabric, $V_F = 0.39$). 169

6.18. Tensile fatigue stress versus cycles to failure data for balanced ±60° to 90°laminates ($\pm[\theta]_3$ laminate with D155 fabric, $V_F = 0.39$). 170

6.19. Tensile fatigue strain versus cycles to failure data for balanced ±60° to 90°laminates (±[θ]$_3$ laminate with D155 fabric, $V_F = 0.39$). 170

6.20. One million cycle tensile fatigue failure strain versus balanced ply angle with laminate analysis predicted first ply static cracking strain and predicted million cycle strain. (±[θ]$_3$ laminate with D155 fabric, $V_F = 0.39$, R = 0.1). . . 171

6.21. Tensile fatigue coefficient, b, versus balanced ply angle. 171

6.22. Compressive fatigue stress versus cycles to failure data for balanced ±30° to 90°laminates (±[θ]$_3$ laminate with D155 fabric, $V_F = 0.39$). 172

6.23. Calculated compressive fatigue strain versus cycles to failure data for balanced ±30° to 90°laminates. 172

6.24. One million cycle compressive fatigue strain versus balanced ply angle with laminate analysis predicted first ply static cracking strain and predicted million cycle fatigue strain. 173

6.25. Compressive fatigue coefficient, b, versus balanced ply angle. 173

6.26. Failed tensile fatigue coupons from ±10° to ±30° laminates showing delamination and cracking of plies with edge effects. 176

6.27. Failed tensile fatigue coupon 20D155112 177

6.28. Failed tensile fatigue coupons from ±40° to ±45° laminates showing delamination and cracking of plies. 178

6.29. Failed tensile fatigue coupons from ±60° to 90° laminates showing cracking of plies. 178

6.30. Failed compressive fatigue coupons from ±30° to ±40° laminates showing cracking and shearing of plies. 180

6.31. Failed compressive fatigue coupons from ±50° to 90° laminates showing cracking and shearing of plies. 180

6.32. Static tensile failure of ±10°, ±20° and ±30° coupons showing lamina cracks parallel to the fiber direction. 181

6.33. Static tensile failure of ±40°, ±45° and ±50° coupons showing lamina cracks parallel to the fiber direction and delaminations causing matrix yielding and fiber movement. 182

6.34. Static tensile failure of ±60°, ±70°, ±80°and 90° coupons showing lamina cracks parallel to the fiber direction. 182

7.1 Sketch and photograph of composite I-beam. 186

7.2. Fatigue data for materials AA and DD5P, R = 0.1. 192

7.3. Fatigue data for materials AA and DD5P, R = 10. 192

7.4. Fatigue data for materials CH3, CH10, CH12 and DD5P, R = 0.1. 193

7.5. Fatigue data for material AA, R = 0.1 and 10. 195

7.6. Beams 6 - 14, 22 and 23 with material AA flanges and material CH10 web compared with material AA coupon fatigue data. 195

7.7. Beams 6 - 14, 22 and 23 with material AA flanges and material CH10 web. Compensated for flange thickness compared with CH10 coupon fatigue data. 196

7.8. Tensile and compressive flanges of failed beams with material AA flanges and material CH10 webs. 197

7.9. Beam 13 static compression flange failure. 198

7.10. Beam 8 tension flange failure. 198

7.11. Beam 14 tension flange fatigue failure. 199

7.12. Beams 18 - 21 and 24 - 29 with material DD5P flanges and material CH10 web compared with material DD5P coupon fatigue data. 202

7.13. Beams 18 - 21 and 24 - 29 with material DD5P flanges and material CH10 web compensated for flange thickness compared with material CH10 coupon fatigue data. 202

7.14. Photograph of web from Beam 10 showing extensive cracking of the web near tension flange. 203

7.15. Tension flanges of failed beams with material DD5P flanges and material CH3 webs. 203

7.16. Beams 30 - 33 with material DD5P flanges and material CH3 web compared with DD5P coupon fatigue data. 204

7.17. Beams 30 - 33 with material DD5P flanges and material CH3 web compensated for flange thickness compared with CH3 coupon fatigue data. . . 205

7.18. Beams 34 and 35 with material DD5P flanges and material CH12 web compared with material DD5P coupon fatigue data. 205

7.19. Beams 34 and 35 with material DD5P flanges and material CH12 web compensated for flange thickness compared with CH12 coupon fatigue data. . 206

7.20. Beams 51 - 54 with DD5P flanges and web compared with DD5P coupon fatigue data. 206

7.21. Tension and compression flanges of failed beams with material DD5P flanges and webs. 207

7.22. Shear stress XY at the adhesive interface of flanges (17.8 kN load). 209

7.23. Shear stress XZ at the adhesive interface of flanges (17.8 kN load). 210

7.24. Shear stress YZ at the adhesive interface of flanges (17.8 kN load). 211

7.25. Normalized Von Mises stress on the centerline of the beam. 212

7.26. Matrix cracking at tensile flange in Beam 28 (x = 178 mm) at delamination initiation location. 212

7.27. Beam stiffness versus lifetime. 214

7.28. Tensile fatigue data for material AA coupons with and without a 13 mm diameter hole, R = 0.1. 215

7.29. Tensile fatigue data for material AA coupons with and without a 13 mm diameter hole, R = 0.1. 216

7.30. Normalized tensile fatigue data for material AA coupons with and without a 13 mm diameter hole, R = 0.1. 216

7.31. Compressive fatigue data for material AA coupons with and without a 13 mm diameter hole, R = 10. 217

7.32. Fatigue data for material AA coupons with and without a 13 mm diameter hole, R = -1. 217

7.33. Damage around the 13 mm diameter hole versus fatigue lifetime. 218

7.34. Photograph of damage around the 13 mm diameter hole at different stress levels, R = 0.1. 218

7.35. Delamination on a compression fatigue coupon (coupon 127AA). 219

7.36. Comparison of AA material flange beams without holes to AA beams with 13 mm diameter holes in the flanges. 220

7.37. Comparison of AA material flange beams with holes to AA material coupons with 13 mm diameter holes. 221

7.38. Beam 15 with holes, static compression flange failure. 221

8.1. Hollow cylindrical tapered tube geometry. 225

8.2. Bending moment versus bending strain for T110. 228

8.3. T110 failed tube surface. 228

8.4. Bending moment versus bending strain for T111. 229

8.5. T111 failed tube surface. 229

8.6. Bending moment versus bending strain for T112. 230

8.7. T112 failed tube surface. 230

8.8. Bending moment versus bending strain for Tube T113. 231

8.9. T113 failed tube surface. 232

8.10. Bending moment versus bending strain for T114. 232

8.11. T114 failed tube surface. 233

8.12. Bending moment versus bending strains for T115. 233

8.13. T115 failed tube surface. 235

8.14. Bending moment versus bending strains for T116. 235

8.15. T116 failed tube surface. 236

8.16. Bending moment versus bending strains for T117. 236

8.17. Bending moment versus bending strains for T118. 237

8.18. T118 failed tube surface. 237

8.19. Bending moment versus bending strains for T119. 238

8.20. T119 failed tube surface. 238

8.21. Cantilever tube end fixture failures. 239

8.22. Normalized maximum bending stress vs. position on the tube. 241

8.23. T121 failed tube surface. 243

8.24. T122 failed tube surface. 243

8.25. T123 failed tube surface. 244

8.26. T124 failed tube surface. 244

8.27. T126 failed tube surface. 245

8.28. T129 failed tube surface. 245

8.29. Bending strain versus bending stress for T122. 246

8.30. Polished end of T130 showing adhesive cracking. 247

8.31. T137 fixed end support showing extensive cracking. 248

8.32. T130 fixed end support showing cracking. 248

8.33. Axial stress in the gage length versus axial strain for tube T130 tested in uniaxial tension after 1,800,000 bending fatigue cycles. 249

8.34. Axial stress in the gage section versus axial strain for tube T133, tested in uniaxial tension without prior fatigue testing. 249

8.35. Fixed end of tube T134 showing a metal fatigue crack after 3,200,000 cycles. . . 250

8.36. Tubes T120 - T137 compared with material DD5P Tensile (R=0.1) and Compressive (R=10) coupons. 251

8.37. Compressive fatigue data for Tubes T120 - T137 compared with material DD5P compressive (R=10) coupons. 252

8.38. Normalized compressive fatigue data for Tubes T120 - T137 compared with material DD5P compressive (R=10) coupons. 252

ABSTRACT

Fiberglass composites have been used in thousands of applications since their inception in the late 1930's despite an incomplete understanding and characterization of their mechanical fatigue properties. Wind turbine blades, which are the main focus of this research, experience between 10^8 to 10^9 significant fatigue (loading-unloading) cycles in their 20 to 30 year lifetime, and fatigue is a major factor in their design. This thesis presents a detailed analysis of the DOE/MSU Composite Material Fatigue Database, which has been developed over the last nine years. The database currently includes over 6000 static and fatigue test results covering 148 different fiberglass materials and numerous loading conditions. Trends in fatigue resistance with various materials and loading parameters are explored, including: reinforcement fabric architecture, fiber content, content of fibers orientated in the load direction, matrix material and loading conditions (tension, compression and reversed loading).

The results show unexpected transitions in fatigue resistance with fiber content and fabric architecture. Transitions to increased fatigue sensitivity have been related to fiber packing characteristics through detailed microscopy study. Material characteristics which produce maximum fatigue resistance have been established. Very high cycle tensile fatigue behavior (10^9 cycles) has been explored with a novel high frequency apparatus using impregnated strands. The strand data suggest a reduction in fatigue sensitivity in the 10^8 to 10^9 cycle range, but a material endurance limit has not been seen. Larger impregnated glass strands tested in excess of 10^8 cycles using conventional testing equipment provide similar results to the smaller strands.

The study has also explored the application of the database to the prediction of the fatigue response of small composite substructures representative of wind turbine blades. Thirty six I-beams were tested under four-point bending. The beams were constructed of materials which showed a range of fatigue resistance in the materials coupon tests. The coupon database accurately predicted the performance of the beams when the failure modes were predominately tensile or compressive. Delamination of the tensile flange in the beams with improved fatigue resistance materials, due to the increase in bending loads and flange operating strains, provided less conclusive results. The effect of flaws (through-thickness holes) was also explored. A second geometry, hollow tubes, was also explored in conjunction with field tests on a small wind turbine. Twenty seven hollow tube test sections were tested under four-point and cantilever bending. Due to the hollow tube geometry, the compressive buckling behavior was the limiting static design parameter, and the obtained compressive strains in the tubes were slightly lower than the database compressive strength values (which used very short specimens).

CHAPTER 1

INTRODUCTION

The selection of a material and prediction of the service lifetime for a fatigue dominated structural design, whether using metal, plastic, or composite, is one of the most difficult tasks faced by an engineer. Glass fiber reinforced plastics (GFRP) have been available for over 60 years and are presently incorporated into thousands of different applications ranging from consumer products to aerospace applications. However, fatigue research is time consuming and costly, and generally has been limited to the high technology areas, such as aerospace and defense, which can support these costs. The availability of fatigue data for the wide variety of GFRP materials has generally been very limited compared with carbon fiber composites used in aerospace. Furthermore, much of the available fatigue data for GFRP is flawed hysteretic heat generated failures at high frequencies using thick materials, and very few results are at lifetimes greater than 10^6 cycles for any composite system. This lack of fatigue information has led to apparent fatigue failures and overly conservative designs.

Wind turbine blades, such as those shown on the Bergey Excel 10 KW machine in Figure 1.1, operate at up to 300 rpm and typically experience more than 10^9 rotations over their 20 to 30 year design lifetime. Typical complex fatigue loading which occurs in

these blades is shown in Figure 1.2, recorded on the experimental Bergey Excell 10 kW machine at the Rice Ridge Renewable Energy Park operated by Montana Tech of the University of Montana and Montana State University-Bozeman. Figure 1.3 shows an Atlantic Orient Corporation (AOC) 15/50 wind turbine whose blades have been a focus of portions of the present study; this turbine has been installed at the Madison Valley Distributed Generation Demonstration site. Most wind turbine designs use relatively heavy, stiff blades which are designed to operate at maximum strains in the range of a few tenths of a percent, at most. While this approach may be necessary for the poorest of the GFRP material systems, it results in costly, inefficient blades compared with the best material systems found in the present study.

Variables which are generally manipulated in GFRP material systems include: fabric reinforcement type, fiber orientation angle, matrix material, fiber volume fraction and laminate lay-up (the sequence of plies of varying orientation). There is also a range of loading parameters to be studied, including various combinations of tension and compression cycling (R value), high and low cycle ranges, and spectrum loading with varying loads on each cycle.

The main focus of this research has been the development of a GFRP fatigue database including the materials and loading parameters of interest to the wind turbine blade application. Also, specialized strand tests are used to achieve higher cycle data than has been previously reported. (It must be noted that wind turbine blades are one extreme application of this fatigue research. Materials constructed and discussed in the database could be applied to any other structural component.) Most of this research has been

summarized in References 1 through 17.

The database related study has also been extended to small substructural elements, typical of wind turbine blades, which are shown in Figure 1.4. These blades can range in length from 3.3 m for the 10 KW Bergey Excell to 49 m for the 3.2 MW Boeing Aerospace turbine [18]. Reference [18] is a good overview of present wind turbine technologies and their fundamental operating principles. These turbine blades have an aerodynamic structural skin with internal stiffeners and spars which increase the rigidity of the blade structure.

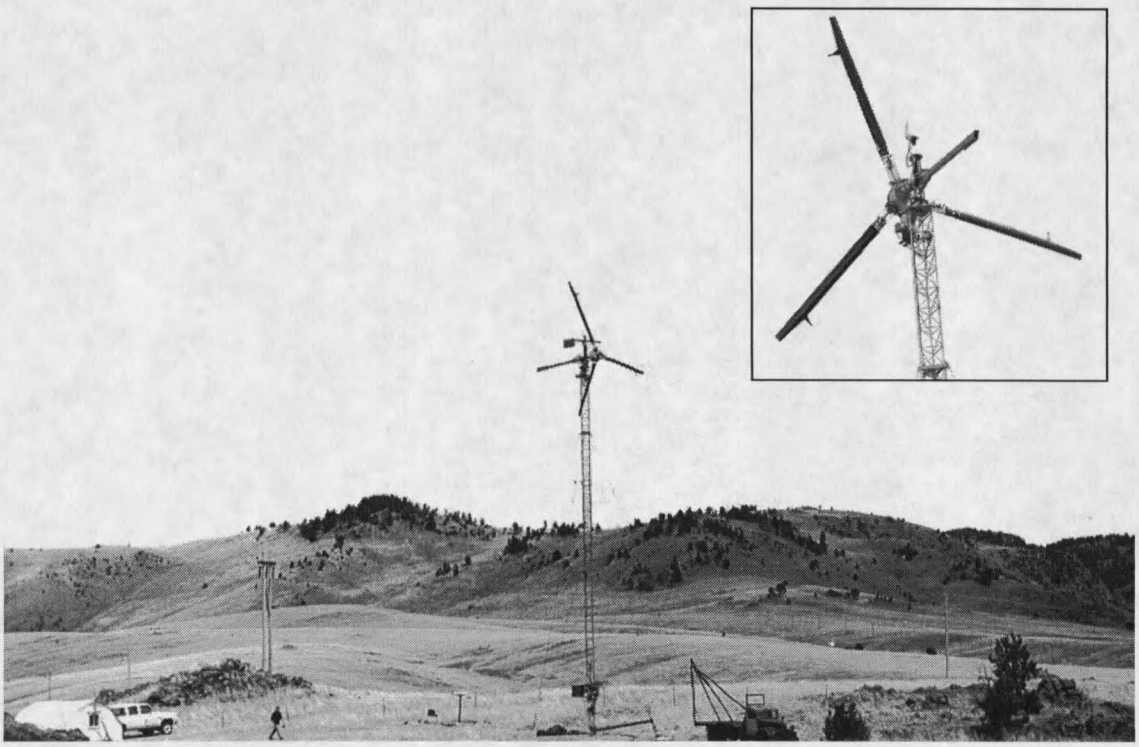


Figure 1.1. Modified Bergey 10 kW wind turbine at Rice Ridge Renewable Energy Park. Insert shows special test section with tube specimens at the blade root.

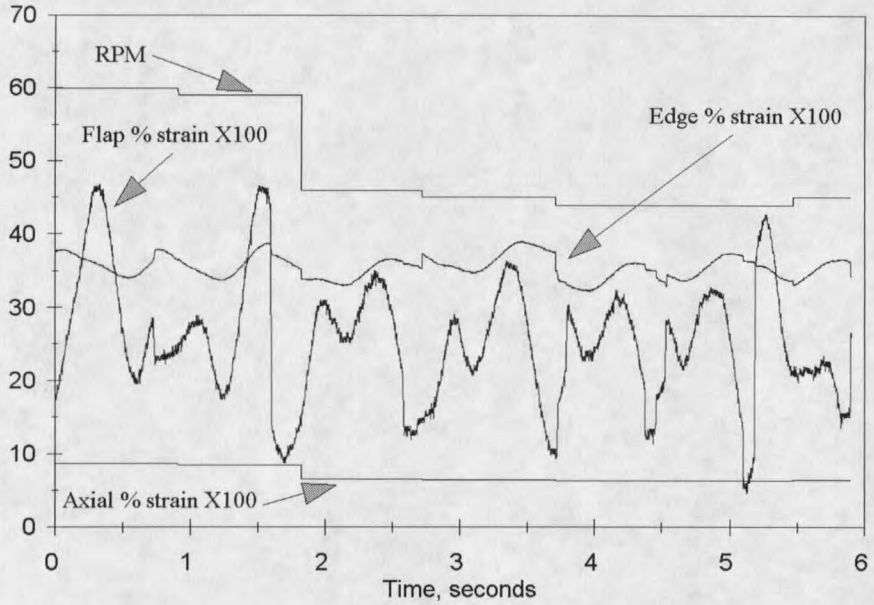


Figure 1.2. Maximum recorded turbine blade strains, Bergey 10 kW, 7.5 m/s wind speed.

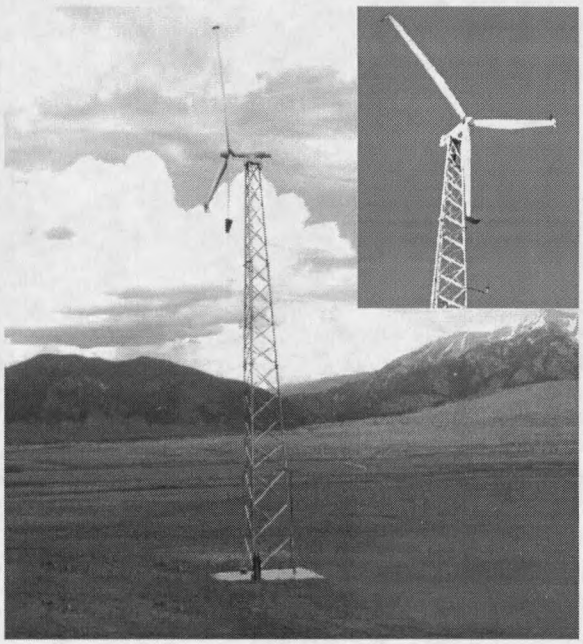


Figure 1.3. AOC 15/50 wind turbine.

The geometry and manufacturing of composite structures of this type can strongly affect the performance of composite materials relative to simple test coupons used in the database. Thus, this study has also included tests on a number of structural details and substructures typical of blades, to explore the structural performance relative to predictions from the database. Substructures included in this study are structural details, such as ply drops for thickness tapering, incorporated into test coupons, as well as structural geometries including hollow cylindrical tubes and I-beams. Future work will include full scale 8 m long AOC 15/50 blades which incorporate these substructures and details.

Due to the large amount of data presented in the DOE/MSU Wind Turbine Blade Composite Material Fatigue Database (hereafter referred to as "the database"), it is suggested that the reader become familiar with the introductory comments of the database presented in Appendix A. Generation of data for the database involved performing over 6,000 fatigue tests over a time period of approximately nine years, with many additional substructure tests. The author hopes to focus the reader on the most significant aspects of the database, fatigue testing and the mechanical fatigue behavior of fiberglass structures.

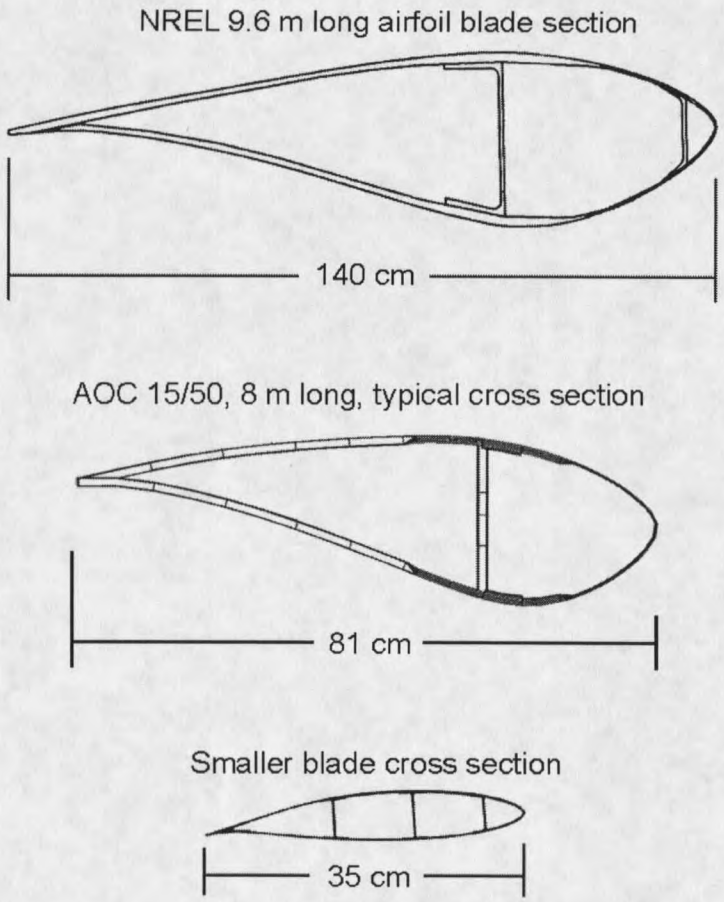


Figure 1.4. Typical wind turbine blade cross sections.

CHAPTER 2

FABRICATION OF MATERIALS

All of the materials manufactured at MSU for this study involved resin transfer molding (RTM). This process produces a composite with uniform thickness, excellent fiber wet out, low porosity and negligible fiber wash. It can also be used to produce materials typical of related processes, including hand lay-up used for many commercial blades. The process allows easy manipulation of ply lay-up and fiber volume content and produces more consistent material characteristics as compared to hand lay-up. A rigid and consistent approach to manufacturing was adopted from the start of the program and was applied to the RTM process to ensure consistent results.

Fabric Reinforcement

Stranded fabrics are available in a variety of stitched and woven architectures with varying strand (tow) size and fabric tightness. Examples of these fabric architectures are shown in Figures 2.1, 2.2 and 2.3 from Owens Corning Fabrics (formerly Knytex). Figure 2.1 shows a D155 unidirectional fabric which has a transverse (weft direction), polymer thread chain stitched to keep the fabric together. Figure 2.2 shows an A130 woven unidirectional fabric. These strands are woven over a transverse polymer thread coated

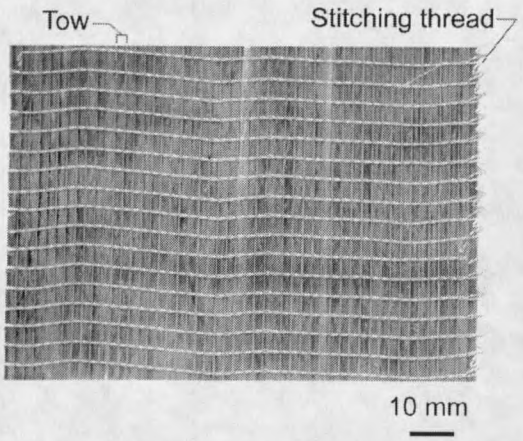


Figure 2.1. D155 fabric.

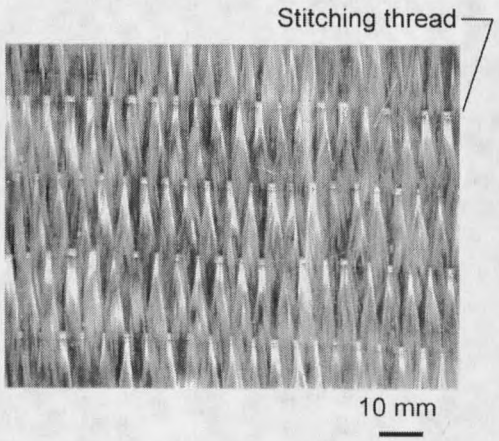


Figure 2.2. A130 fabric.

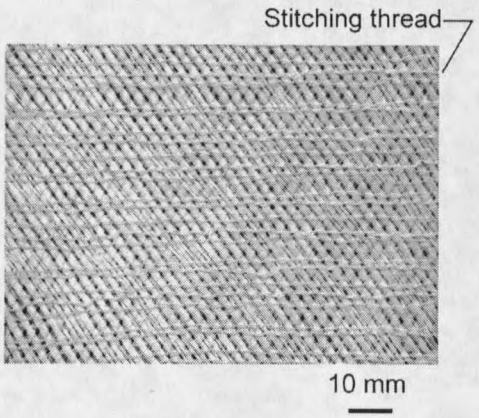


Figure 2.3 DB120 fabric.

with a thermoplastic adhesive which is melted and holds the architecture together. Figure 2.3 shows a DB120 fabric which is a stitched ±45° fabric. The +45° and - 45° fabrics are individually stitched with a polymer thread and then the two are stitched together to form the ±45° fabric. Thicker and multiple angled fabrics are also constructed using this process. The additional transverse stitching allows handling and placement of the fabrics with very little fabric movement or tow rotation. Laminates are constructed with individual layers (plies) or stitched multilayer fabrics as detailed in Figure 2.4.

E-glass fabric reinforcement was provided by (or purchased from) Owens Corning Fabrics, Collins Craft Incorporated, and Brunswick Technologies Incorporated and was delivered on 127 cm wide rolls. The fabrics were unrolled onto a table where rectangular patterns were cut using a standard rotary fabric cutter, with the 0^{O} fibers in the long dimension to aid in resin flow and fiber wet out. Fabrics in most of this study were limited to 0^{O}, $\pm 45^{O}$ and $0^{O}/\pm 45^{O}$ stitched fabrics, which are summarized in Table 2.1. These rectangular cut fabric patterns were then placed in the RTM mold and stacked as per the specific ply arrangement desired.

Resins

Five different resins were used in this study: CoRezyn 63-AX-051, an unsaturated orthophthalic polyester resin obtained from Interplastic Corporation, Derakane 411-C-50 and Derakane 8084 (rubber modified) vinyl esters produced by Dow Chemical Company, Epon epoxy resin 9410 with 9450 Epon curing agent, a modified bisphenol "A" epoxy resin system and liquid MDA based aromatic amine curing system obtained from Shell

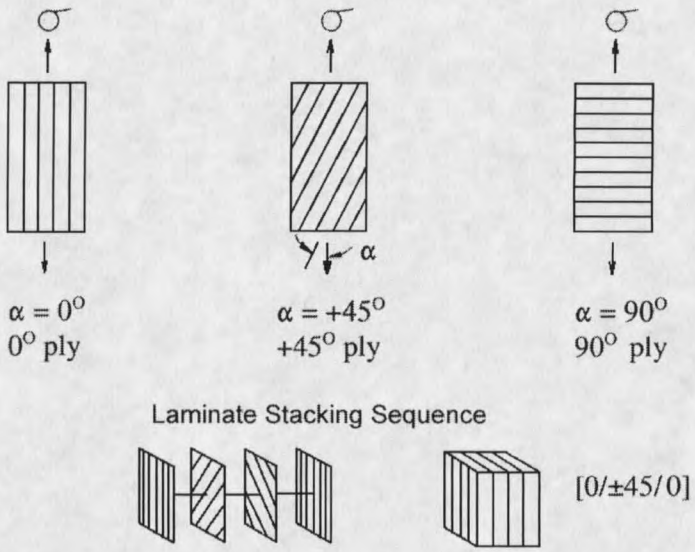


Figure 2.4. Lamina (plies) and laminate description.

Chemical Company, and a toughened epoxy (two-phase acrylate modified) system, SC-14, obtained from Applied Poleramic Incorporated. The mixing and cure schedules are summarized in Table 2.2, as recommended by each respective manufacturer. Methyl Ethyl Ketone Peroxide (MEKP) was the catalyst used by both the CoRezyn and the Derakane 411C. The 411C and 8084 Derakane were the only resins which had to be promoted with cobalt naphthenate (CoNap) and dimethylaniline (DMA) prior to mixing with the MEKP catalyst. Trigonox 239A (2%) was substituted for MEKP in the Derakane 8084 which reduced the amount of foaming.

Most of the RTM composites in this study involved the CoRezyn polyester resin, which is a common wind turbine blade manufacturing resin. The other resin systems were chosen for specific properties like toughness and heat resistance, and due to their wide commercial acceptance and general use in industry. The resin systems were initially stored at approximately -15 ^{o}C until needed. The resin was allowed to warm up to room

Table 2.1. Summary of E - Glass fabrics.

E - glass fabric	Description	Total weight g/m^2	Dry thickness mm	Manufacturer
A060	woven 0^o	206	0.35	Owens Corning Fabrics
A130		444	0.53	
A260		868	0.91	
CDB200	$0^o/\pm45^o$	759	0.86	
CM1701	0^o plus mat	587	0.78	
D072A	stitched 0^o	230	0.40	
D092		310	0.48	
D155		527	0.53	
DB120	45^o	393	0.53	
DB240		837	0.86	
DB400		1,349	1.24	
UC1018V	0^o	620	0.52	Collins Craft
TVM3408	$0^o/\pm45^o$	1,150	1.42	Brunswick

Table 2.2. Summary of resin matrix materials.

Resin	Catalyst	Promoter	Cure cycle
CoRezyn 63-AX-051	2% by vol. MEKP	----------	min. 4 hours in the mold +2 hours at 60^oC
Derakane 411-C-50	1.5% by vol. MEKP	0.3% CoNap 0.05% DMA	
Derakane 8084	2% by vol. Trigonox 239A	6% CoNap	min. 4 hours in the mold +2 hours at 60^oC
SC14	100:35 A:B mix ratio by weight		3 hours at 60^oC +5 hours at 100^oC
Epon 9410	Epon 9450 - 35% by weight		10 hours at 80^oC

temperature, 18 to 22 °C, for 24 hours before mixing with MEKP or mixing the two component Epon system. For the CoRezyn, if the room temperature was greater than 25 °C, the percentage of MEKP was reduced to 1.5% to ensure a minimum 30 minutes before it gelled. The catalyzed resin was then pumped into the two center injection holes in the aluminum baseplate using a peristaltic pump (Cole-Parmer Instruments Company Model 7553) and silicone tubing. The resin was transferred to the mold over a 5 to 15 minute period, with pressures less than 150 kPa, depending upon fiber reinforcement lay up, angle and fiber volume. Approximately 50 ml of resin was allowed to flow out of the exit ports at each end of the mold to ensure that all the layers had been wet out. The pump was then stopped and the center injection ports were plugged. The resin exit ports at the ends of the mold were left open to equalize the resin pressure throughout the mold. This action prevented pressure induced deflection of the mold faces, which would vary the thickness of the composite plate. The CoRezyn and Derakane plates were removed from the mold after a minimum of four hours from the time of the MEKP addition and placed in a post cure oven at 60 °C for two hours. The Epon epoxy plates were injected and directly placed in an 80 °C oven for ten hours and then allowed to cool down slowly to room temperature overnight. References 19 and 20 provide a detailed discussion of the resin transfer molding process used here.

Flat Rectangular Plate Construction

The most common flat rectangular plate resin transfer mold used in this study consisted of a lower 13 mm aluminum baseplate with a gasket channel milled around its

perimeter, as shown in Figure 2.5. This channel allowed the placement of a 13 mm by 13 mm extruded Buna N (nitrile rubber) gasket. The relative height of the top of this gasket to the top of the baseplate could be changed by adding sheet metal spacers under the gasket, allowing the thickness of the composite plate to be changed. A 13 mm thick tempered glass plate acted as the top of the mold, allowing visual examination of the mold filling process as the resin was injected into the mold. A positive seal was produced between the glass, gasket and the aluminum plate with ten C-clamps. Steel blocks were placed between the C-clamp heads and the glass plate to provide a bearing surface and to prevent fracturing of the glass. The clamps were torqued to 35 cm-kg. This torque setting was established at the beginning of the project and provided reproducible composite plate thicknesses throughout the study. A second, fixed thickness mold was later constructed to manufacture larger composite plates with dimensions 51 cm x 81 cm and a thickness of 3.15 ±0.05 mm.

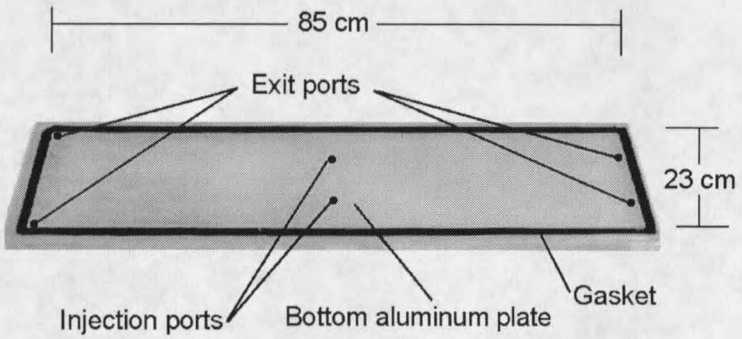


Figure 2.5. Flat plate RTM mold.

Both inside surfaces of the mold were coated with external mold release agent F-57NC, from Axel Plastics Research Laboratories Incorporated or Frekote 700 - NC mold release agent by the Dexter Corporation. The aluminum plate was initially surface

polished with 600 grit emery paper which produced an excellent carrier surface for the mold release. The mold release was applied over both the aluminum and the glass surfaces using a small cloth and approximately 10 to 15 ml of mold release. The release agent was then air dried for 15 minutes producing a viable film which lasted for 30 to 40 plates. When this film was exhausted, the mold surfaces were cleaned with acetone and a new film layer was applied.

For composite plates with fiber volume contents greater than 0.5 or fabrics with poor resin transfer channels, a special method of resin injection was developed. A special process was necessary to prevent fiber wet out problems, fiber wash in the mold or injection pressures greater than 200 kPa, which was the capacity of the pumping system. A layer of double sided mounting tape (Scotch 110) was placed between the glass and the rubber gasket and initially, very lightly clamped (surface contact). The mold was then completely injected with resin before the C-clamps were torqued up to 35 cm-kg. This caused the foam tape to compress from 1.6 mm to approximately 0.4 mm, causing excess resin to flow out the vent ports of the mold. The maximum fiber volume fraction produced by this process was 0.67 with excellent fiber wet out with negligible porosity.

E - Glass Prepreg

Scotchply reinforced epoxy unidirectional prepreg, SP-250E, was also prepared as coupon tabbing material, as well as a comparison material to some of the RTM materials. The storage and processing conformed to 3M Aerospace specifications. The prepreg tape was stored at -15 ^{o}C and was allowed to warm up to room temperature before handling.

The tape was cut into 29 cm long strips and placed on a 30 cm by 30 cm aluminum plate where additional layers of prepreg were added to obtain the required lay-up and thickness. This prepreg preform was then transferred to two electrically heated platens in an Instron 8562 servo-electric testing machine. Teflon release film, bleeder cloth and a peel ply sheet were placed between the two heated platens and the prepreg preform. The platens were preheated to 120 ^{o}C. The preform was heated under contact pressure with the heated platens for five minutes. The pressure on the preform was slowly increased over an additional five minutes and finally held at 340 kPa. The temperature and pressure were held for a period of two hours. At the end of this period the prepreg plate was taken out of the heated platens and placed in a post-cure oven for an additional 14 hours at 120 ^{o}C. The plate was then taken out and allowed to cool down to room temperature.

Industrial Supplied Materials

Materials were supplied by various wind turbine blade manufacturers for fatigue testing and evaluation. Most of these materials were supplied as hand laid-up flat sheets, and one manufacturer supplied a pultruded turbine blade from which test coupons (material EE) were cut. In most cases, details of the resin systems or the reinforcing fabrics used in these industrial composites were not available.

Machining

The edges of the RTM, prepreg and industrial plates were trimmed off to eliminate any edge composition variability, ensuring representative, uniform material

properties. The trimmed plates were then cut to produce flat rectangular coupons for testing. The plates were cut into 25 mm or 38 mm wide strips depending upon the required coupon width. From these strips, at least two tensile and two compressive coupons were cut. This stratified random sampling scheme, with replication, was necessary to produce the required number of testing specimens and to achieve the required statistical confidence in the experimental design. The plates were cut with a 20 cm diameter diamond coated blade rotating at 3,450 rpm (36 m/s), which was water cooled and lubricated. The feed rate of the composite plates during cutting was less than approximately 5 mm/second to ensure clean, perpendicular cut edges. Coupons which had to be thickness or width tapered were dry machined with a three flute carbide router bit rotating at 23,000 RPM. The final test coupons did not undergo any form of edge surface modification or polishing, they were tested "as cut". For materials which had a 12.7 mm diameter hole, the holes were drilled using a four step process. An originating locator hole was first drilled using a 3 mm diameter twist drill. This allowed for precise placement of the hole center and minimized the amount of drilling induced delamination damage. A second 7.9 mm diameter and a final 12.3 mm diameter twist drill followed. Final preparations involved polishing the circumference of the hole with 240, 400 and 600 grit polishing cloths.

Test Specimen Geometries

Determining accurate and representative material fatigue properties involved a number of tradeoffs. The material tests ideally would involve a representative material

volume, require low forces to test (which prevents load transfer problems and grip failures), a short gage length to achieve higher fatigue frequencies for a given hydraulic capacity and a gage area of uniform axial strain where the material modulus can be determined. Table 2.3 and Figure 2.6 summarize the nominal geometry of the test coupons with relation to the mechanical test to be performed. These developed geometries worked well in the static and fatigue tests performed on the MTS 880 and Instron 8501, 8511, 8872 and 1350 testing machines. The coupons tested in the Instron 8511 and 8872, due to the machine capacity, had to have smaller coupon cross sectional areas which are detailed in Figure 2.7. Additional tab material was added in the coupon gripping areas to reduce the stress concentration generated by clamping the coupon and to provide a wear surface between

Table 2.3. Summary of test coupon geometries.

Test	% zero's in composite	Coupon geometry	Materials	Gage Length
Static tensile and fatigue at R = 0.1	< 50%	rectangular, as cut	A-Y, AA, CH, $\pm 20^{O}$ - 90^{O}	100 mm
			$\pm 10^{O}$	160 mm
	50% to 84%	width tapered	BB, CC, DD, FF, GG	135 mm
	100%	thickness tapered	Axxx, Dxxx, CM1701	100 mm
Static compressive and fatigue at R = 10 and R = -1	All cases	rectangular, as cut	All cases	13 mm

the test specimen and the steel wedge grips. Additional tab material was bonded to the coupons, when necessary, as the last step in the manufacturing process. The tab material utilized in this study included electronic protoboard, fiberglass prepreg ($0^{o}/90^{o}$ and $\pm 45^{o}$ lay-ups) and, with limited success, aluminum with chopped glass fiber mat. These are summarized in Table 2.4. Different tab materials and adhesives were tried in order to produce good failure modes in the gage length of the coupons while avoiding grip induced damage or failures.

For tab material attachment, the areas of the coupon and the tab material surface were lightly roughened with 180 grit emery cloth, cleaned with a sponge and water, and air dried to produce clean bonding surfaces. Each surface was then smeared with a thin layer (0.1 to 0.4 mm) of Hysol EA 9309.2NA adhesive and assembled. Paper binder clips, 50 mm wide, were used to apply pressure to the assembly and keep the tabs aligned. The assembly was then cured in a convection oven at 60 ^{o}C for two hours, as recommended by the adhesive manufacturers. This adhesive cure cycle also served as the coupon material post cure treatment. After curing, the clamps were removed and the tab faces were lightly sanded to remove any excess adhesive and to provide flat and parallel clamping surfaces. The coupons were labeled for identification with a unique material letter label and a sample number. The finished test coupon was then measured for its average and minimum cross sectional area in the gage length using a Mitutoyo Digimatic digital caliper, or equivalent, with a minimum resolution and accuracy of 0.01 mm.

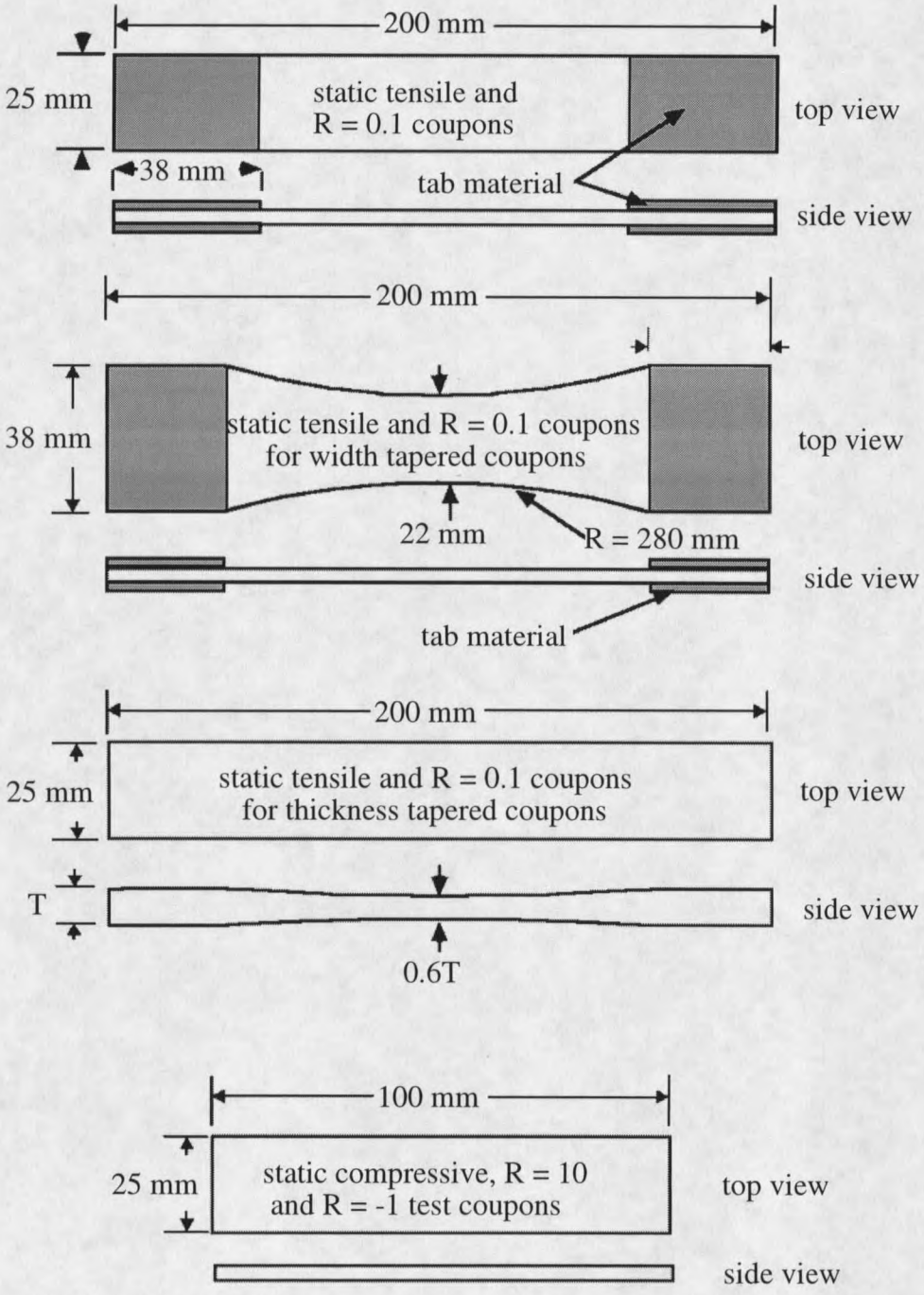


Figure 2.6. Test coupon geometries.

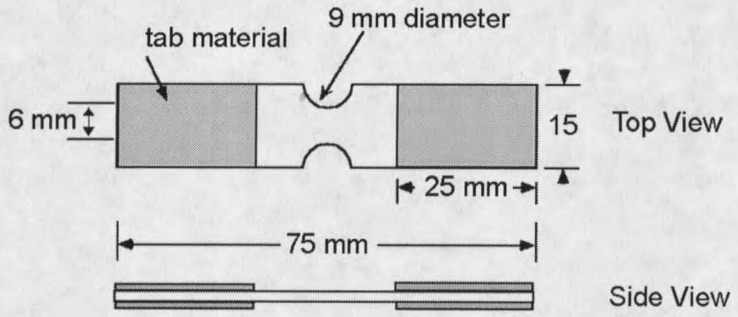


Figure 2.7. Instron 8511 and 8872 test coupon geometry.

Table 2.4. Summary of Tab Materials.

Material	Description
Protoboard	Radio Shack catalog number 276-1396, 1.6 mm epoxy sheet with 1 mm diameter holes spaced 2.5 mm in a rectangular grid.
Fiberglass[1]	Plastifab G10, 1.6 mm, $[0/90]_7$, $V_F = 35\%$. With and without 10^O tapered ends.
Fiberglass	3M SP250 prepreg, $[\pm 45]_{10}$, $V_F = 55\%$.
Aluminum	6061-T6, 2.5 mm with 10^O tapered ends with resin impregnated chopped mat (170 g/m^2) between the aluminum and the composite.
[1] most common and most successful tab material used in this research	

I - Beam Construction

Most of the developmental work on the composite I-beams and their initial construction was detailed by Combs [21] and involved Beams 1 through 5. The basic construction of the beams involved the resin transfer molding of two fiberglass C-channels, which were then secondary bonded together to form a I-shape. Flange material to be tested was then attached to this I-shape. For the C-channel mold, the glass fabric reinforcement was cut into 12 cm by 91 cm rectangular patterns and placed on the lower

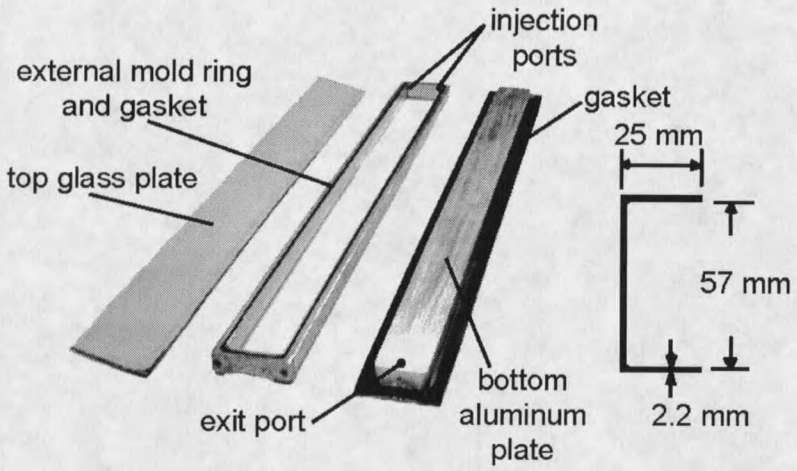


Figure 2.8. C-Channel RTM mold.

mold, which is shown in Figure 2.8. The external mold ring was then placed on top of the fabric and carefully pushed over the lower mold to create a C shape. The glass top plate was then placed on top and clamped down using twelve C-clamps torqued to 17 cm-kg. This mold was then injected identically to the large flat plates previously described. The two C-channel exterior web faces were lightly sanded with 180 grit emery cloth and wiped clean with a sponge and water. After air drying, the two C-channels were bonded together to form an I-section. The adhesive used exclusively during this I-beam study was Hysol EA 9309.2NA; it was cured using the manufacturers recommended procedures.

Beams numbering 30 and higher involved an I-channel mold which is shown in Figure 2.9. This mold operated exactly as the C-channel mold, but eliminated sanding and the other intermediate steps involved with secondary bonding of the two C-channels; it produced an I-section with less dimensional variability. Previous dimensional variability was caused by surface sanding and a poorly controlled adhesive layer thickness. Table 2.5 summarizes the beams and the different I-shapes used. To this I-Section was added

additional shear and torsional stiffeners in the load reaction areas to prevent shear failures between loading points. These additional elements are summarized in Table 2.6. Flange material on this I-Section was manufactured using the large flat RTM mold, cut up into 54 mm by 760 mm flange test sections, lightly sanded on one side and bonded to the I-Section external flanges. Load pads were then attached to the flanges. These pads were necessary to provide a wear surface for fatigue and to distribute the loading. Surfaces which were bonded together were mechanically clamped using C-clamps and load transfer bars, while the adhesive cured over a 24 hour period at room temperature. The completed beam was then post cured at 60 ^{o}C for two hours. The load pads on the beam, shown in Figure 2.10, were then machined in a vertical milling machine so that they were perpendicular to the web and parallel to the flange plane.

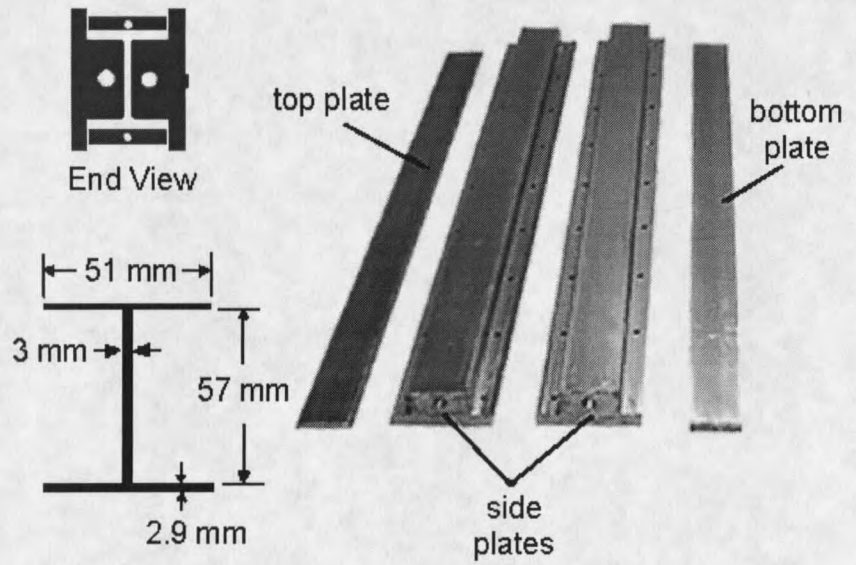


Figure 2.9. Web I-section RTM mold.

Table 2.5 Summary of web I-shapes used in Beams 6 through 59.

Beams	Web lay-up	Web database material	Average thickness, mm		V_F, %	
			Web	Flange[2]	Web	Flange
6 - 29	$(\pm 45)_3$	CH10	5.3 (0.11)[1]	2.3 (0.14)	34	33
30 - 33	$(\pm 45/0/\pm 45)_S$	CH3	5.5 (0.16)	2.1 (0.21)	30	31
34, 35	$(\pm 45/0/\pm 45)_S$	CH12	3.0 (0.10)	1.6 (0.19)	34	28
51 - 59	$(0/\pm 45/0)_S$	DD5	3.0 (0.13)	1.6 (0.13)	33	28

[1]Numbers shown in parenthesis are the sample standard deviation.
[2] Flange portion of the web I-shape, not the total flange.

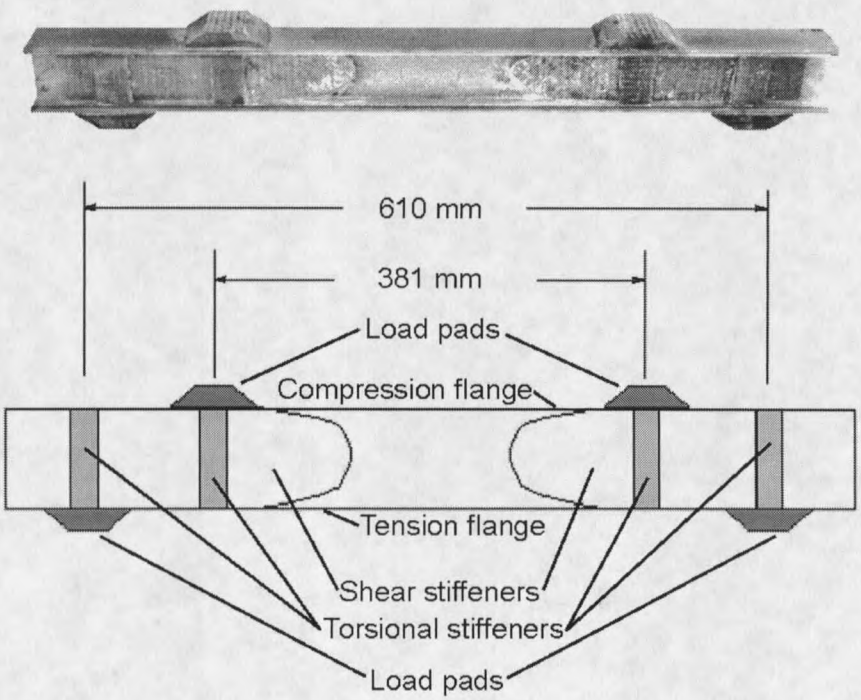
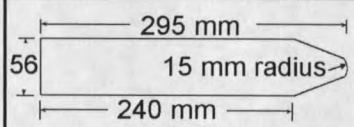
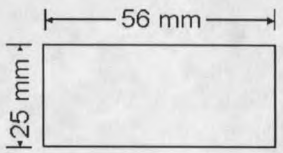
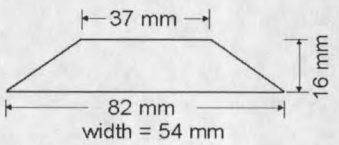


Figure 2.10. Assembled I-beam.

Cylindrical Tubes

The tapered cylindrical tubes were manufactured by placing the fabric around a two piece tapered steel mandrel, one ply at a time, with no circumferential overlap. The fabrics were held in place by tacking small areas of the fabric surface with 3M spray adhesive number 77. The 45° plies were placed on the mold individually, which required removing the stitching thread (de-coupling) from the ±45° fabrics. With the completed lay-up on the steel mandrel, this section was then placed in a two piece clam-shell (external) mold. The ends of the mold were then sealed and filled with resin. After two hours, the mold clamping bolts and the internal mandrels were removed. After an additional four hours, the external mold was separated and the tube removed. This mold

Table 2.6. Summary of additional beam components.

Beam Component	Lay-up	Fabric	V_F	Thickness	Drawing
Shear stiffener	$(\pm 45)_6$	DB400	0.40	8.5 mm	
Torsional Stiffener	$(\pm 45)_6$	DB400	0.40	8.5 mm	
Load Pad	$(\pm 45)_{14}$	DB400	0.42	16 mm	

is shown in Figure 2.11. These tubes were then attached to structural load transfer ends, which allowed the tube to be tested. The details of these aluminum 2024-T3 ends are shown in Figure 2.12. The ends consisted of an internal plug which was inserted and attached to the tube end using Hysol EA 9309.2NA adhesive. The aluminum ends were prepared for bonding following the ASTM standard D2651 involving P-2 etchant, Turco 4215NC-LT alkaline cleaner and acetone. Prior to the bonding of the external ring, approximately ten meters of glass roving was impregnated with polyester and wrapped around the ends of the tubes to aid in filling the space between the tube outside diameter and the inside diameter of the external ring. After curing the polyester, the external ring was attached and the void space filled with the Hysol adhesive. The entire assembly was then post cured at 60 °C for two hours. The finished assembly is shown in Figure 2.13.

Fiber Volume Fraction (V_F) Determination

In all the composites, the percentage of glass reinforcement was determined by the matrix burn off method described in ASTM D2584. This process involved taking a known volume of composite material and placing it in an electric muffle furnace at a temperature of 550 ^{o}C for one hour or until all of the carbon on the glass fibers had been removed. This glass reinforcement was then weighed on a Ohaus 1500 D digital balance with a resolution of 0.01 grams or a Sartorius BP210S digital balance with a resolution of 0.0001 g. The glass volume was calculated by dividing the glass fiber mass by a confirmed glass density of 2.56 g/cm^3. This glass volume divided by the original volume equaled the fiber volume fraction. The only deviation from the ASTM standard was the

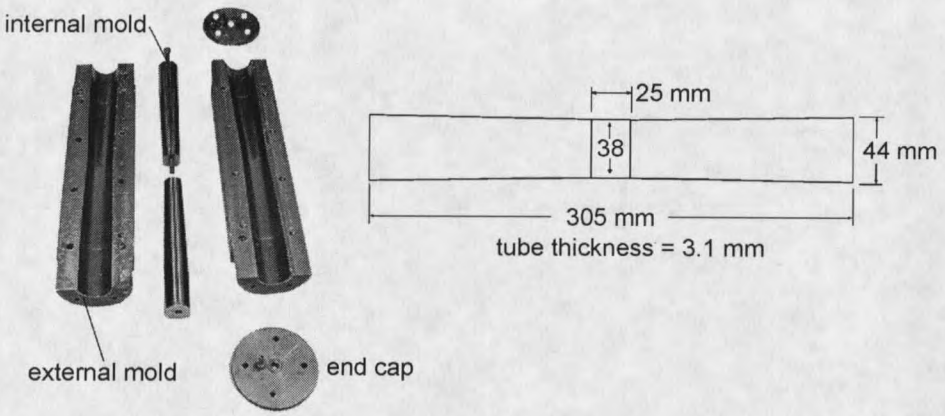


Figure 2.11. Cylindrical tube RTM mold.

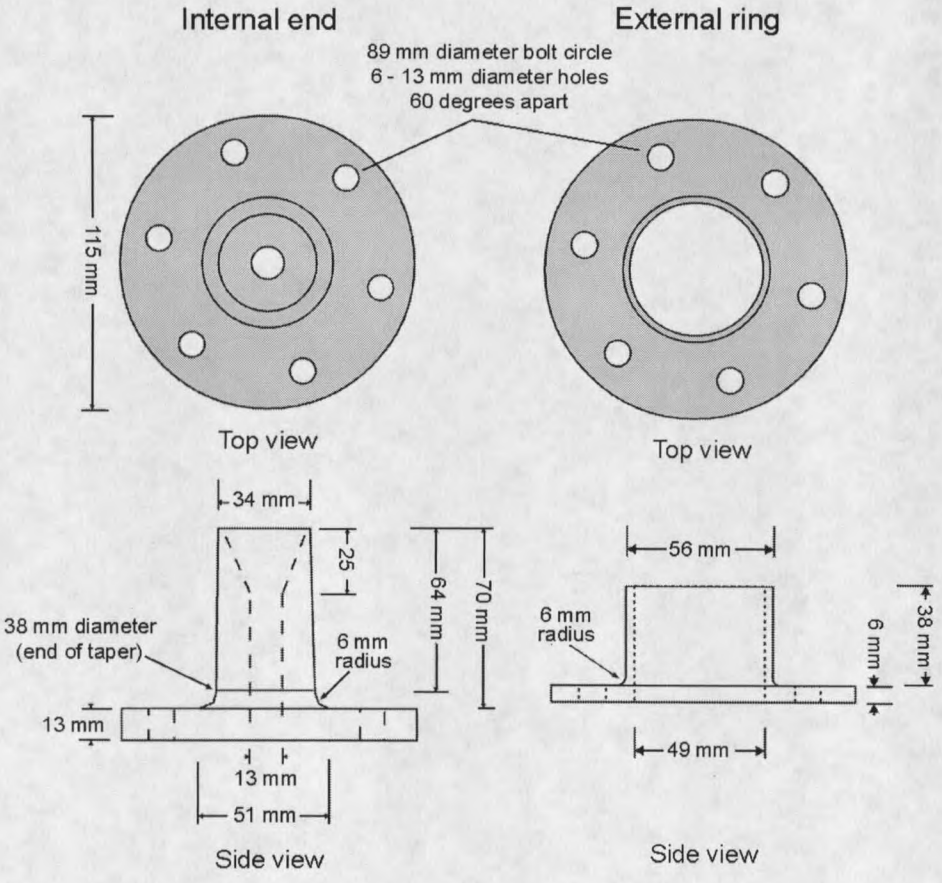


Figure 2.12. Aluminum 2024-T3 tube end fittings.

amount of material to be used in the burn off test. The standard requires five grams of material which works well with uniform, thin plied prepreg materials, but it was felt that the ASTM standard would not generate a representative average fiber volume fraction due to the coarse architecture, size and spacing of the fiber bundles in the stitched fabrics. Thus, a greater amount of material, 15 to 25 grams, was used. This fiber volume fraction was associated with the average thickness of the burn off specimen. If there was a difference between this thickness and the average thickness of the tested coupons, a linear

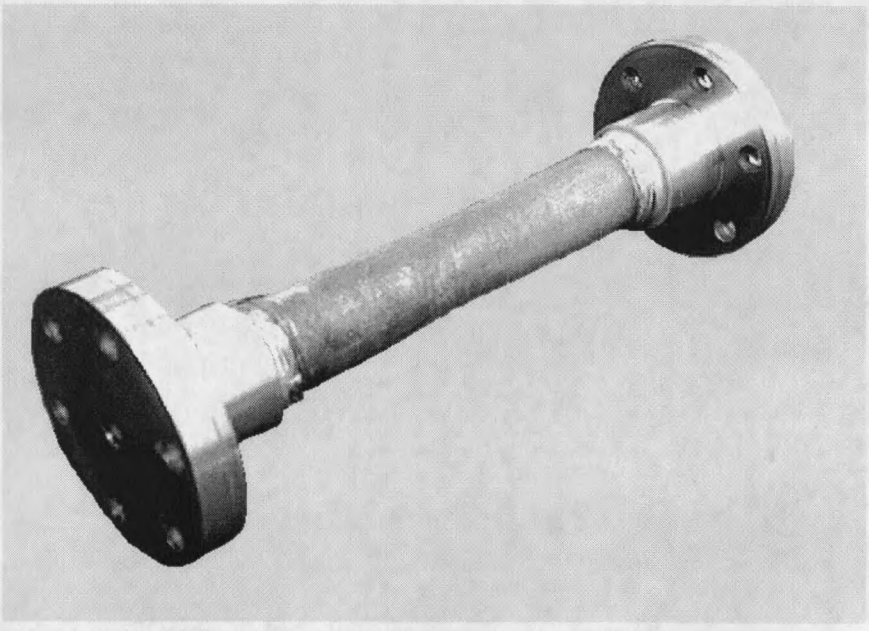


Figure 2.13. Tube testing assembly.

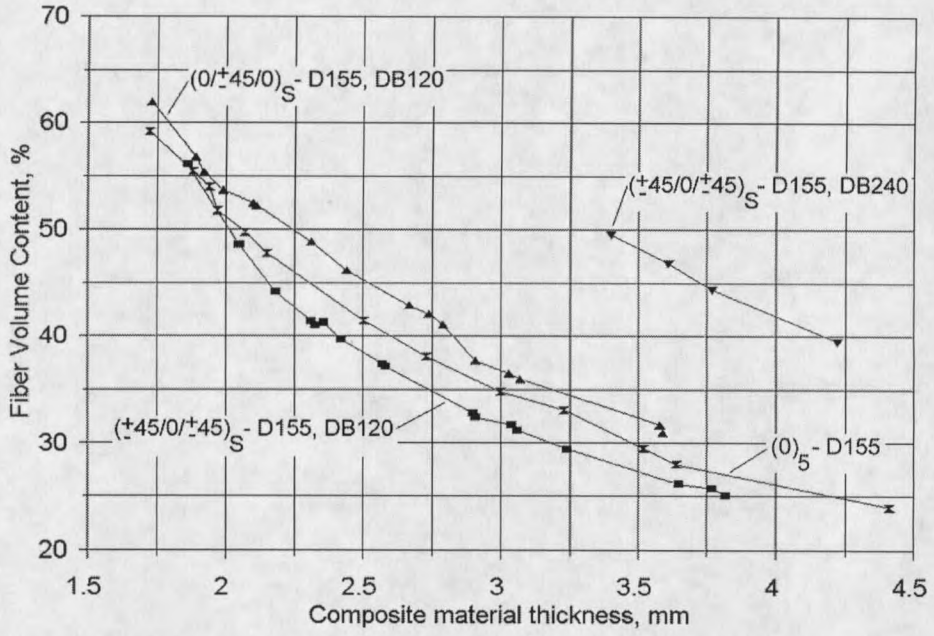


Figure 2.14. Fiber volume content versus RTM composite thickness.

adjustment to the fiber volume fraction was made and recorded. Figure 2.14 shows the fiber volume content versus thickness for different lay-ups studied. Generally, the V_F varied only by 1 - 2% between the average thickness of the burn off specimen and the tested coupons. Quantitative microscopy using Jandel Scientific Incorporated, Sigma ScanPro software was also used to determine the fiber volume content and porosity of smaller cross sections.

CHAPTER 3

MECHANICAL TESTING EQUIPMENT

The static, fatigue and four point bending tests were performed on nine different testing machines listed in Table 3.1. The Fiber Testing Apparatus used a unique audio speaker as an actuator and an Instron 8500 electronic console to provide control and feedback. Approximately 80 percent of the tests were performed on the Instron 8501, five percent on the MTS 880 with the remainder of the tests on the other machines. The MTS 440 structural testing system has interchangeable actuators which were used in cantilever fatigue tests of the cylindrical tube sections. All the hydraulic machines utilized 21 kPa hydraulic pressures. The testing machines had their respective transducers: load cell, extensometer and actuator LVDT, calibrated to their respective ASTM standards.

Load Cells

The load cells in each of the mechanical testing machines, along with their associated readout electronics, were calibrated as a complete system following the standards in ASTM E4 and E74. These procedures were also used for additional piggy back load cells used with lower force tests. These ASTM standards allow a maximum of ±1 percent error. The Instron 8501, 8562, 8511 MTS 440 and 880 had maximum errors less than ±0.4 percent during the entire duration of this study. The load cells were

Table 3.1. Summary of mechanical testing equipment.

Machine	Actuator control	Capacity	Stroke	Servo valve capacity
Instron 1350	Servo hydraulic	98 kN	±51 mm	0.32 L/s
Instron 8562	Servo electric	100 kN	±51 mm	--------
Instron 8501	Servo hydraulic	100 kN	±51 mm	0.64 L/s
Instron 8511	Servo hydraulic	10 kN	±25 mm	0.32 L/s
Instron 8872	Servo hydraulic	20 kN	±51 mm	0.64 L/s
MTS 440	Servo hydraulic	50, 100 kN	±75, ±127 mm	0.64, 0.96 L/s
MTS 440A[1]	Servo hydraulic	50 kN	±267	1.92 L/s
MTS 880[2]	Servo hydraulic	250 kN	±140 mm	0.64 L/s
Fiber Testing Apparatus	electric	10 N	±3 mm	--------
		22 N	±4 mm	

[1] - The original 406 test controller was replaced with a new digital 407 controller
[2] - The original 880 controller was retrofitted with Instron 8500 Plus electronics

calibrated or verified every four to six months using standard calibration cells calibrated through Morehouse Instrument Company and by additional ASTM E617 Class 1 precision dead weights, calibrated directly against secondary national standards. The dead weights were necessary to calibrate the load cells in the zero to two kN range where the extensometers were used to measure the initial elastic modulus of the test coupons; they consisted of ten separate 44.48 N weights. The standard test weights were not corrected for gravimetric differences between the standards calibration laboratory and the testing machine locations, as this effect was considered negligible. Smaller, NIST (National Institute of Standards and Technology) traceable weights under 10 N, were also employed to calibrate equipment which operated in these lower ranges. The load cells used in the testing machines are listed in Table 3.2.

Table 3.2. Summary of Load cells.

Machine	Load Cell Capacity	Manufacturer Serial Number
Instron 1350	100 kN	Lebow 3116-136, sn 2133
Instron 8501	100 kN	Instron, sn UK515
Instron 8511	22 kN	Sensotec, sn 336154
Instron 8562	100 kN	Instron, sn UK 517
Instron 8872	25 kN	2527-101, sn 10787
MTS 440	45 kN	MTS 661.21, sn 442
	100 kN	MTS 661.21, sn 585
	250 kN	MTS 661.22, sn 461
MTS 880	250 kN	MTS 380041-04, sn 69
General Use (Piggy back)	2.2 kN	Lebow 3132, sn 8796
	1.1 kN	Interface 1010AJ-250-B, sn 103726A
Fiber Testing Apparatus	4.45 N	Omega Engineering Inc. LCL-454G, 981077894
	9.8 N	Omega Engineering Inc. LCFA-1KG, 970805
	22.2 N	Omega Engineering Inc. LCL-005, 05993101-016

Extensometers

Contact extensometers and their associated electronics were directly calibrated and verified to ASTM E 83 and classified as class B2 extensometers with a maximum error of ± 0.5 percent. The seven extensometers used during this study are summarized below in Table 3.3. The extensometers were calibrated using a Boeckeler Instruments mechanical micrometer model 4-MBR which had a resolution of 0.0005 mm (0.5 μm) and a certified maximum error of 0.00033 mm (0.33 μm). A Mitutoyo IDC - 112E digital gage with a resolution of 0.001 mm was also used. The gage length was measured with an optical microscope calibrated with a Nikon MBM11100 objective micrometer.

Table 3.3. Summary of extensometers.

Extensometer	S/N	Range	Gage Length	Machine
2620-524	6236	± 5 mm	12.70 mm	Instron 1350
2620-525	6237	± 5 mm	12.70 mm	Instron 8501
2620-528	8405	± 5 mm	12.70 mm	Instron 8501
2620-824	185	± 5 mm	12.70 mm	Instron 8501
2620-826	251	± 2.5 mm	12.70 mm	Instron 8501
2620-528	8405	± 1.3 mm	12.70 mm	Instron 8511
632.12B-20	430	+13/-2.5 mm	25.40 mm	MTS 880

The gage lengths of the extensometers were checked with this digital gage and an optical microscope as described in ASTM E 83 using the indirect method. During tensile strain measurements, the extensometer was attached to the edge of the test coupon, or when possible, on the face of the coupon using rubber bands. When placed on the face of the coupon, it was necessary to attach two pieces of self adhering 240 grit polishing paper (extensometer mounts) to prevent the knife blades from slipping and to prevent the blades from damaging the composite surface. The knife blades were sharpened or replaced when they were damaged or failed to track the composite surface strain. Generally, the extensometer was removed prior to catastrophic failure of the test specimen to prevent damage to the device. The extensometer was not used during compression tests due to the short gage length of the compression coupon and the possibility of extensometer damage, so strain gages were generally used instead.

Actuator Position (LVDT)

The actuator position was calibrated using a CDI J4-C100-5000 mechanical

displacement gage with a resolution of 0.0254 mm (0.001 inches). Gage blocks were used to check displacements and set compression gage lengths (12.70 mm). The gage blocks were of grade A+ or better. Although no ASTM standard was referenced for this procedure, the maximum amount of error was less than ±1 percent over the entire actuator travel range.

Strain Gages

A Measurements Group Incorporated 2100 system strain gage conditioner and amplifier system with eight strain channels was used to measure strains. The strain gages were calibrated using the internal shunt calibration of the 2100 system. This active gage method of calibration and operation used a three lead wire circuit as recommended by Measurements Group TT-612 technical bulletin and conformed to ASTM E251. A minimum wire gage of 26 was used for connecting the gages to the instrumentation and the total length of connection wire was minimized to reduce lead wire resistance effects. In all cases, the excitation voltage was 2.000 Vdc with 120 and 350 ohm strain gages. Electronic gains of approximately 500 were used for strains up to 13.6 percent and gains of 5000 allowed measurement of strains up to 1.36 percent. Generally, one quarter Wheatstone bridges were used for strain measurements. The strain gages used in this study are summarized in Table 3.4. In all cases, the life of the strain gage was limited to a few hundred cycles, as matrix cracks on the surface of the composite opened and damaged the strain gage, as shown in Figure 3.1 from Beam 29.

Table 3.4. Summary of strain gages.

Company	Catalog Number
BLH	FAE-25-35-S13EL[1] FAET-2SA-3S-S13 PA - 7
Micro-Measurements	CEA-00-250UW-350[1] EA-00-015EH-350 EA-06-250-BF-350 ED-DY-125AD-350 WA-00-015-EH-350 WK-06-250AF-350 WK-00-250-BG-350
[1] - These gages had the longest lifetimes	

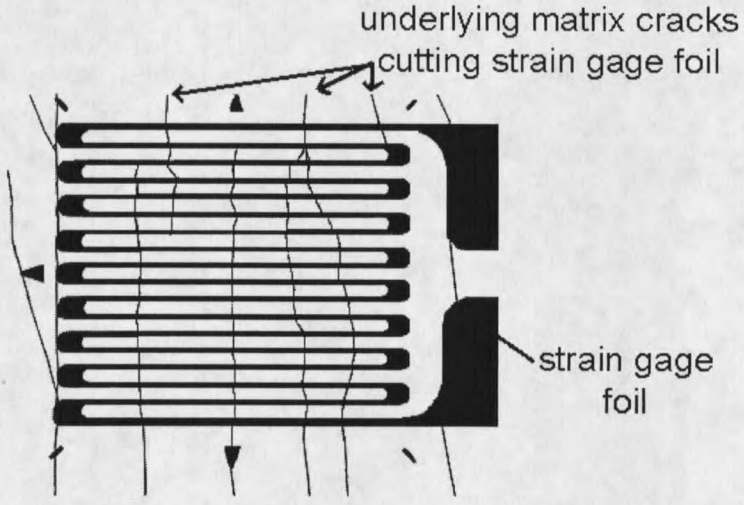


Figure 3.1. Strain gage photograph showing tensile strain cracks.

Using extensometers on the fatigue coupon for extended periods caused damage and subsequent failure of the coupon, as the knife edges of the extensometer dug into the coupon. Thus measurement problems were addressed with the development of strain clips which are shown in Figure 3.2. These devices reduced the running strain that the strain gage experienced, which prevented fatigue failure of the gage and eliminated strain gage failure by matrix cracking. Of the many methods tried to measure the fatigue running strain of the composites, this method yielded the best results. The clip gage was manufactured from 0.15 mm brass (C26000) shim stock, using a one half Wheatstone strain gage bridge with temperature compensation which minimized any material thermal mismatch and produced a durable gage. An additional aspect associated with this gage was that it initially had to be calibrated on each specimen with an extensometer or another strain gage on the composite surface. Adhesives used to bond the strain gages to the composite surface included Loctite 496 cyanoacrylate ester and Micro-Measurements Incorporated M - Bond AE 15 epoxy resin. The AE 15 was used when the expected strains were greater than two percent.

Testing Machine Load Train Alignment

Alignment of the load train of the mechanical testing machines was critical to ensure a uniform stress distribution across the test coupon, especially during compression tests. The grip and actuator travel centerline was adjusted to conform to ASTM E3039 even though the main standard concerning alignment is detailed in ASTM E1012. ASTM E1012 does not address the acceptable amount of bending in a testing setup, whereas

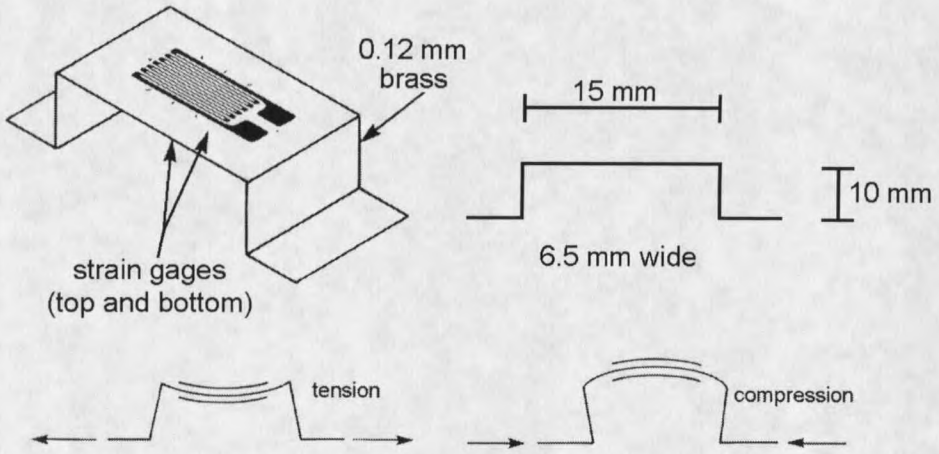


Figure 3.2. Clip strain gage.

ASTM D 3039 addresses it as an additional aspect to composite testing. Table 3.5 summarizes the available standards and their recommended allowable bending strains. The amount of bending during an axial test must be minimized, but it cannot be totally eliminated, so every effort was made to limit the amount of bending strain to less than five percent of the axial strain. The load train alignment had to be checked every time the hydraulic grips were removed from the machine or just prior to compression testing.

Table 3.5. Summary of applicable bending standards for uniaxial testing machines.

Standard	Maximum allowed bending strain (% of axial strain)
ASTM E 1012	Not stated
ASTM D 3039	5%
General Electric S-400	10% for ductile materials 5% for brittle
Military Standard 1312B	6%

To measure the amount of bending, four strain gages were placed on a thin (3 mm) rectangular, 4130 steel, coupon, as per ASTM D3039. The 3 mm thick by 50 mm wide steel calibration coupon was chosen as it was similar in dimensions to the fiberglass coupons. Although aluminum could yield higher sensitivity, gripping indentation by the steel grip faces could influence the results. The coupon was loaded up to a calibration load of 53 kN and the maximum amount of bending was calculated using the equation in Section 10 of ASTM D 3039. This maximum load, 53 kN, was used to prevent yielding of the calibration coupon. If the amount of bending strain was greater than five percent of the axial strain, the load train of the testing machine was adjusted. This alignment procedure was performed with the actuator at the position it was to be used during the material test to ensure test alignment. The hydraulic wedge grip faces were cleaned and freshly coated with MolyKote molybdenum disulfide lubricant between the grip body and the grip faces. Required cleaning of the grip faces was necessary as the fatigue tests wore down the lubricant and produced a hard black film between the grip face and the grip body. This film, if not cleaned and replaced regularly, caused angularity of the grip faces and nonuniform grip pressures and, therefore, grip misalignment.

Fiber Testing Apparatus

Standard testing machines are limited in their frequency and displacement response by low force noise and hydraulic oil pumping requirements. Testing to high cycles requires high frequencies to be practical, and high frequencies can only be used for very thin specimens to avoid hysteretic heating. In order to test a very small tow of 45

glass fibers to one billion cycles (or more), it was necessary to build a separate testing apparatus. The required maximum load was less than 15 N, and the desired frequency was 200 to 300 Hz (or higher). The Instron 8511 was used to test the D155 tows to 10^8 to 10^9 cycles, but the maximum acceptable frequency was judged to be only 80 Hz, and one test required 97 days. A new apparatus was constructed using a standard 25 cm diameter audio speaker (Radio Shack 40-1028) as the actuator. A second apparatus using a 30 cm diameter speaker (Radio Shack 40-1029) was later constructed.

A grip for load transfer to the coupon was constructed out of carbon fiber to minimize the grip mass (18 g with bolts). The test coupon was gripped in a sandwich friction grip system where two bolts clamped the grip assembly around the coupon. Self adhesive 1000 grit polishing paper lined the internal surface of the grip plates to ensure coupon gripping with the low clamping pressures generated by the 2 mm diameter clamping bolts. This low clamping pressure also minimized any clamping damage to the coupon. This grip assembly was then bonded to both the speaker dome and the cone with Plexus AO425 adhesive. The upper grip assembly was bolted to a bending beam load cell, which completed the load transfer path. This testing apparatus is shown in Figure 3.3 along with the coupon geometry. The crosshead was moveable by two 6 mm bolts, which were used to apply the mean cyclic load to the test coupon. An Instron 8500 electronic display tower was used to condition the load cell. The display also provided a sine wave frequency and cycle counting for the test. The Instron electronics were only capable of providing a low power frequency output up to 200 Hz, which was used as an audio input to an 80 watt amplifier to power the speaker. For frequencies greater than 200 Hz, a separate frequency generator was used.

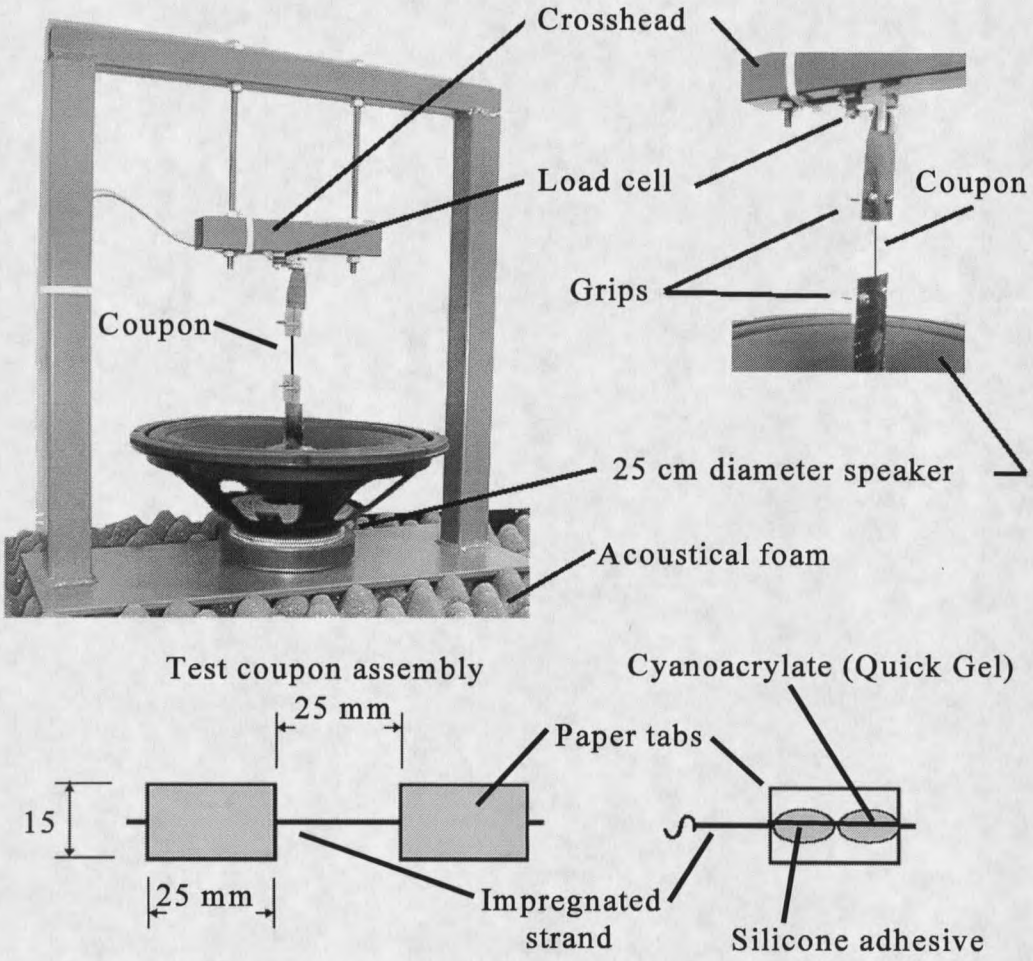


Figure 3.3. High frequency strand testing apparatus and test coupon geometry.

CHAPTER 4

TESTING AND TEST DEVELOPMENT

Coupon Tests

Unless noted, all fatigue tests were run at constant load amplitude with a sine waveform. Individual test coupons were selected from all available test coupons using a simple random sampling without replacement scheme, for static and fatigue tests at the different R values. The fatigue test R value is calculated by:

$$R\ Value = \frac{Minimum\ cyclic\ stress}{Maximum\ cyclic\ stress} \tag{4.1}$$

The three most common R values used in this study were: R = 0.1, 10 and -1. The relationships of stress, or strain, versus time for a sine waveform for these R values are shown in Figure 4.1. When additional test coupons were needed from two or more material plates, every effort was made to randomly select coupons from all the different material plates prior to initial testing to ensure a random selection from all the possible test material. For all the tensile tests, static and fatigue, an initial material elastic modulus, E, was calculated by taking the least squares fit of at least five evenly spaced axial stress-strain data points at total strains less than approximately 0.12 percent. This procedure allowed for modulus calculations with little, if any matrix cracking and to

ensure no extensometer slippage. The extensometer was used to obtain the initial fatigue running strain of the coupon and then removed to prevent damage to the test coupon. Compression tests utilized strain gages for the static tests and the fatigue tests used the average material modulus to calculate the fatigue running strains.

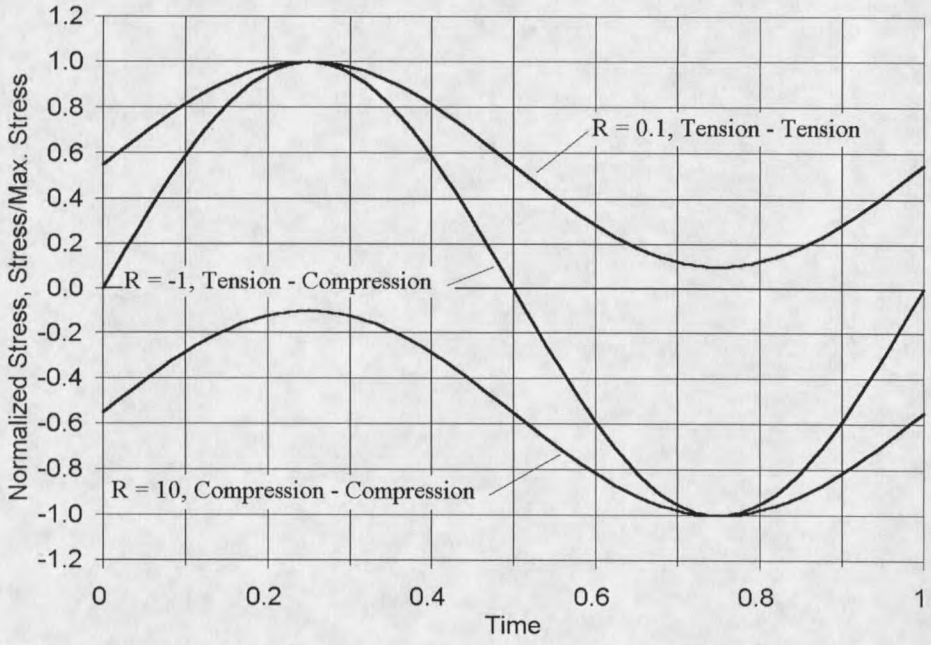


Figure 4.1. Constant stress amplitude sine waveforms for different R values.

Tensile Tests

A minimum of three static tensile tests were performed for each material, with the testing machine under displacement control, using a linear displacement - time ramp rate of 13 mm per second. This ramp rate provided similar strain rates to the fatigue tests. Figure 4.2 shows typical stress-strain diagrams for material DD5P for different testing rates. Figure 4.3 shows the trend of ultimate tensile strength versus the testing

displacement rate. The testing rate does significantly influence the static tensile ultimate strength, but does not significantly alter the elastic modulus over the strain rate range of $2.5x10^{-5}$ to 1.27×10^{-1}. The effect of coupon width was also studied and is shown in Figure 4.4. As long as the coupon width has a representative number of fiber bundles to minimize the effects of edge bundles, thicknesses greater than approximately 20 mm showed little sensitivity in ultimate tensile strength.

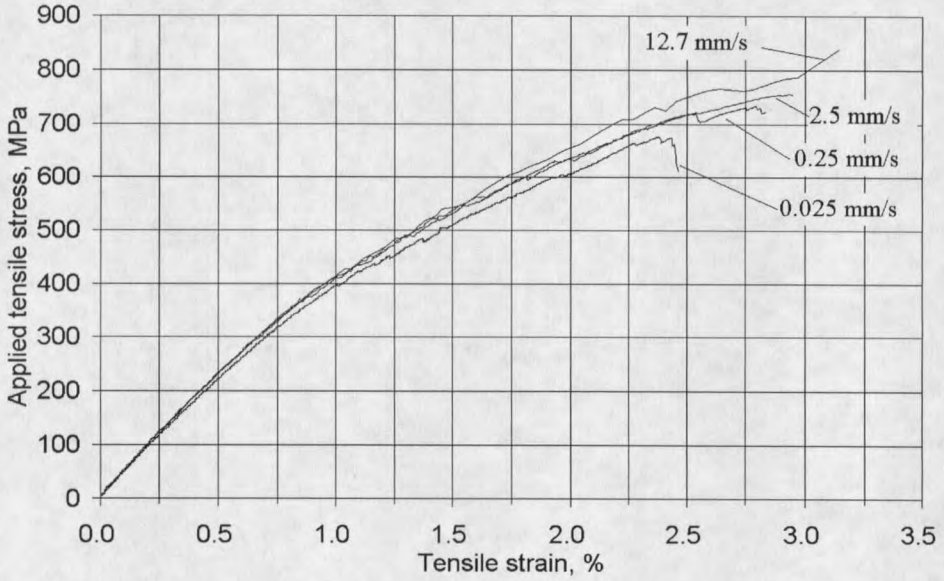


Figure 4.2. Stress-strain curves for material DD5P at different testing rates.

Most of the tensile tests were performed without computer data acquisition and relied upon the testing machine instrumentation to accurately record the maximum load applied to the test coupon. This method was periodically checked with an HP 5452A 500 MHz digital oscilloscope with no noticeable problems. With the ultimate tensile strength calculated, the first fatigue test was then run at approximately 60 percent of the static

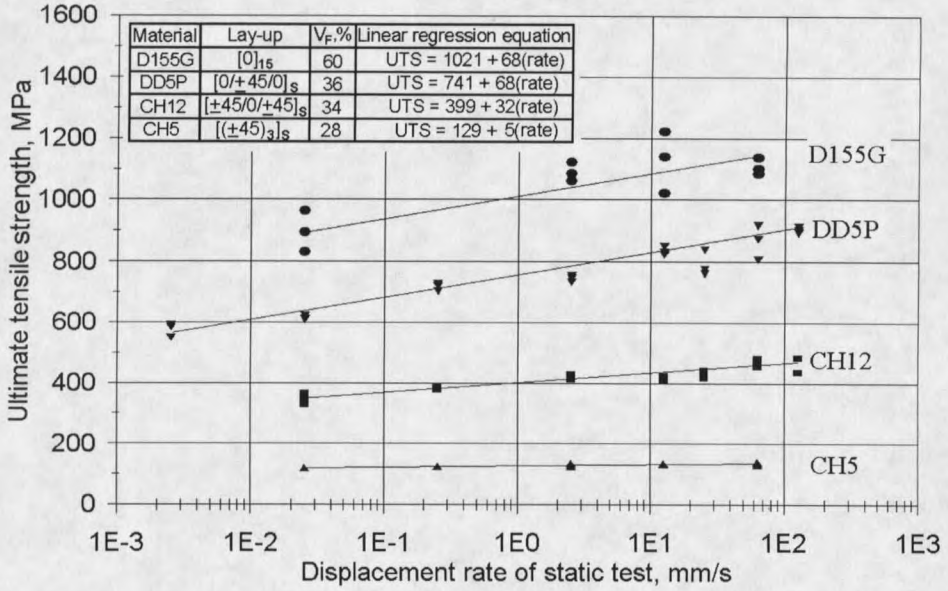


Figure 4.3. Tensile strength versus testing displacement rate (25 mm wide coupons with a 100 mm gage length).

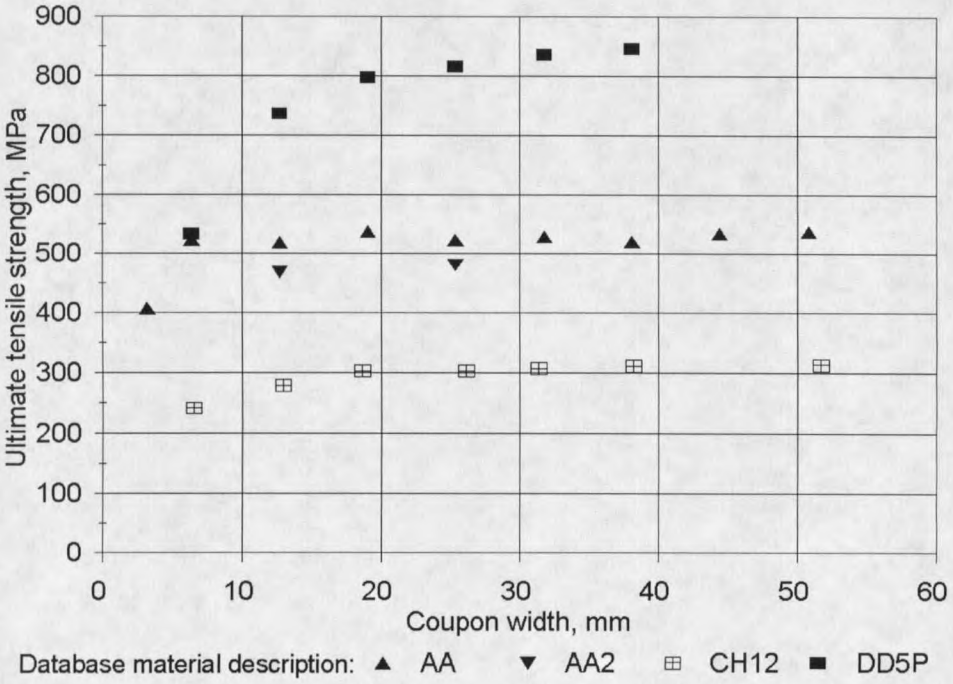


Figure 4.4. Tensile strength versus coupon width (100 mm gage length, 13 mm/s testing rate).

strength, usually at an R value of 0.1. This fatigue data point was then used to approximate the fatigue sensitivity coefficient b from the linear semi-log relationship [2]

$$\frac{S}{S_O} = 1 - b\ Log\ N \tag{4.2}$$

where S is the maximum stress, S_O is the single cycle strength and N is the total cycles to failure. This equation was used to determine all stress levels of an S-N data set. Stresses were picked to obtain fatigue failures in each log decade (2, 3, 4, 5, 6 and 7) of the fatigue semi-log plot to accurately determine the fatigue trend. Test coupons were then randomly assigned to these stress levels, with a minimum of three coupons per stress level. These coupons were then tested in their assigned order. Most materials were tested to beyond 10^5 cycles, with some more fatigue resistant materials tested to the 10^6 to 10^8 cycle range.

Fatigue tests used a sine-wave cyclic waveform with the testing machine under load control, with active amplitude control, which increased the internal gain of the machine as the coupon compliance changed during the testing. The frequency of the waveform was varied approximately inversely with the maximum stress level, which maintains an approximate constant load rate. This limits the hysteretic heating within the coupon at higher loads and prevents thermal failures. The frequency was varied between 1 and 20 Hz in most cases. All the test coupons were ambient air cooled with an air flow velocity of approximately two meters per second measured one cm away from the coupon surface. This limited the maximum coupon surface temperatures to less than 5 ^{o}C above ambient room temperature. Surface temperatures of the composite were monitored

throughout the test using a Omega Engineering Incorporated HH23 digital thermometer with a Cole-Parmer E-08533-96 fast response thermocouple, with a time constant of 0.1 seconds. All the tests were performed at ambient room temperatures, 15 to 27 ^{o}C, and at low relative humidities, 10 - 50%, unless otherwise indicated.

Generally, the test coupons were not removed from the hydraulic grips once the fatigue test was started. Occasionally, tests were stopped and the test coupon removed for examination. The coupons were then placed back in the grips and testing continued. Fatigue tests were generally performed until coupon failure, which was defined as the inability of the coupon to sustain the applied fatigue loading. Some of the tests were stopped before coupon failure (and after a large number of cycles) due to testing and time constraints. These coupons were labeled as "run outs". With the completed fatigue diagram, the fatigue sensitivity coefficient b was then calculated using a least squares fit of the data points an a linear stress versus log cycles to failure plot, assuming equation (4.1). The goodness of fit coefficient of the least squares fit was generally greater than 0.96. This testing procedure was then repeated for different R values (R = 10, -1).

Tensile Test Development

Most of the test development involving the tensile coupons was done in redefining a suitable geometry which minimized mechanical grip induced failures and produced fatigue failures in the gage length. Geometries different than the flat rectangular coupons with tapered tabs in the gripping areas, as described in ASTM D3039 and shown in Figure 4.5, were studied. It should be noted that ASTM D3039 was changed in 1993 to

allow the optional use of coupon tabs, which was done so that the test standard would be technically equivalent to the European ISO 527 standard. This process was necessary, as the initial number of grip induced failures (using the earlier coupon geometry), was quite high, which is a common testing problem [22 to 25]. It is unlikely that a universal test coupon geometry could be developed which would work for all the composite lay-ups; therefore, it was necessary to design specific test geometries for different lay-ups.

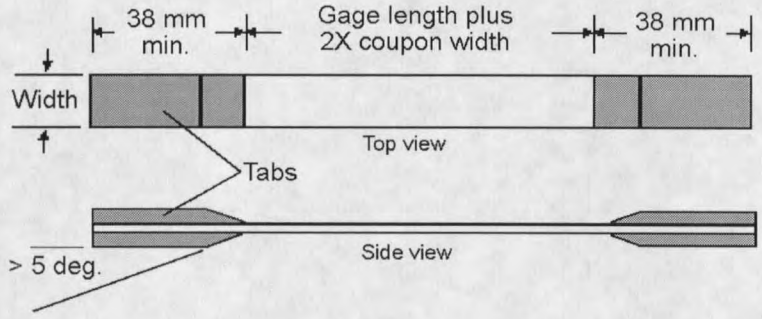


Figure 4.5. ASTM D3039 tensile test coupon geometry.

The highest percentage of grip failures involved the unidirectional, 100% 0^{O} fabric, materials. The best testing geometry found for these materials involved tapering the thickness of the coupon by at least 40 percent. When tested, the thickness tapered coupon did start to delaminate at the shoulder, tending to create a rectangular cross section, but the delaminations stopped at the point where the coupon was clamped in the hydraulic grips. This method of thickness tapering was similar to placing additional tab material on the rectangular ASTM D3039 coupon, but during initial fatigue experiments with tabs, tab failures occurred, as the adhesives used to bond the tabs onto the coupon

failed. This type of failure did not occur with the thickness tapered coupons. It was assumed that slight thickness-direction (Z direction) waviness in the glass fabrics created some additional through-the-thickness reinforcement, and thus more shear resistance as compared with bonded tabs. Adams and Finley [26] labeled these cracks "thickness taper release cracks" in compressive coupons and believed that these cracks reduce the stress concentrations associated with the taper radius and gripping effects. It is assumed that this same beneficial effect occurs in the tensile coupon geometries tested in this study.

Thickness tapering only worked for unidirectional materials. For materials with additional ply orientations, a width taper, resulting in a cross sectional area reduction of approximately 40 percent, or more, proved acceptable and minimized the number of grip failures. Careful width selection ensured that a representative volume of material was present in the gage section. This geometry still had grip failures, especially with high percentages of zero fibers in the load direction and fiber volume fractions greater than 0.35. Most of the coupons with grip failures did have other damage nucleation sites all over the gage length before final failure. Width tapered coupons did split at the shoulders, which tended to create a rectangular coupon. The shoulder cracks stopped in the compressive zone created by the gripping force, similar to the thickness tapered coupons. The coupons developed cracks and delamination during the first few hundred cycles which initiated in the taper radius region of the coupon and propagated along the coupon length and arrested in the compressive zone produced by the clamping action of the wedge grips shown in Figure 4.6. Coupons of the width tapered geometry were tried with and without additional tabs with no noticeable difference in the number of grip failures or

the number of fatigue cycles to failure. In fact, the presence of a tab produced no beneficial effect on the grip induced damage in the composites with fatigue lifetimes less than approximately a million cycles. It has also been reported that some material coupons without tabs provide consistently better testing results than those with tabs [22]. This gripping damage is also illustrated in Figures 4.7 and 4.8. The tab material, however, did provide abrasive protection to the test coupon on higher cycle (> 1 million) fatigue tests. Composite coupons with 50 or less percent 0° material did not generally need any special machining or tabs. These coupons had very few grip failures and the flat rectangular geometry proved acceptable.

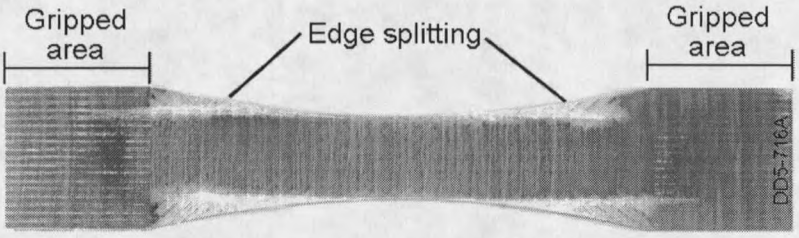


Figure 4.6. Width tapered coupon (DD5P material) with shoulder splitting.

Test Coupon Gripping

Hydraulically operated wedge grips were used to clamp the test coupons into the axial load train of the testing machines using externally generated and controlled hydraulic pressure. A tensile or compressive stress was applied to the coupon through a

mechanical shear interface over the clamped coupon ends. The clamping force on the coupon is directly proportional to the applied hydraulic pressure, as shown in Figure 4.9. The hydraulic pressure caused the grip body to move down, causing the wedge grips to close and clamp onto the test coupon. The hydraulic pressure in the grips was also dependant upon the applied tensile load being transferred through the test coupon. Due to the hydraulic grip design, the hydraulic fluid pressure caused any axial load transmitted through the test coupon to be transmitted through the hydraulically prestressed grip body. When the load transferred through the test coupon was greater than the load induced by the hydraulic grip prestress, the hydraulic pressure in the grip body increased as the fluid started to transfer more load, as shown in Figure 4.10. This Figure shows three different initial grip hydraulic pressures which, as the axial tensile load on the test coupon was

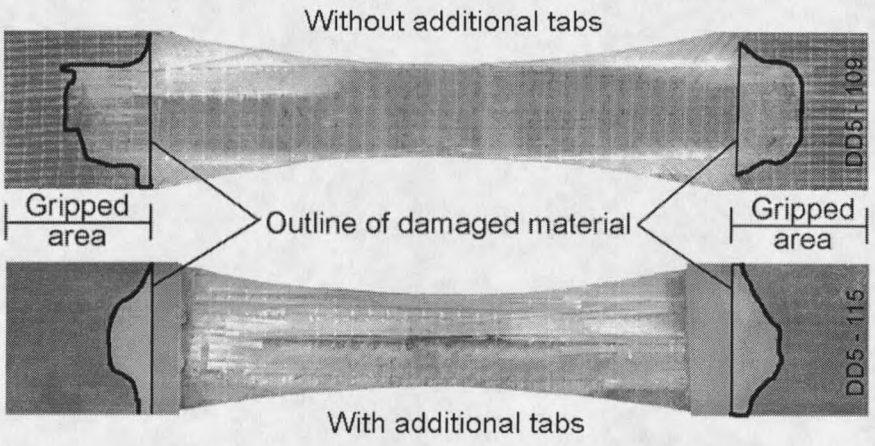


Figure 4.7. Grip damage in test coupons, with and without tabs.

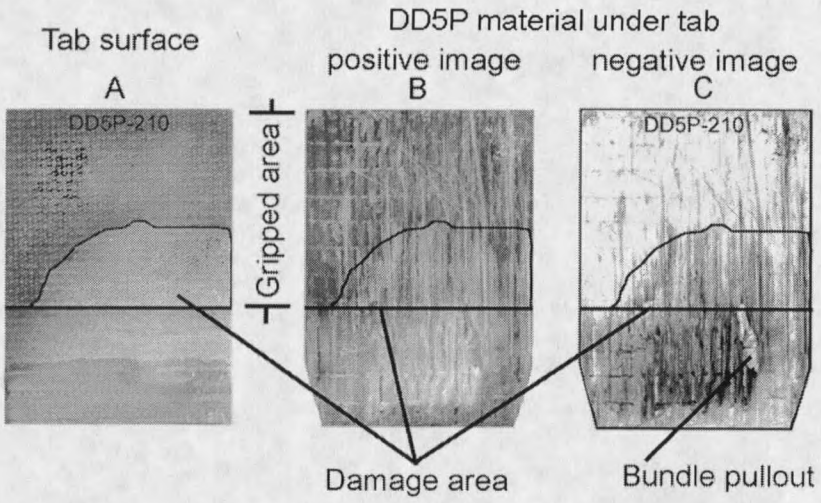


Figure 4.8. Tensile fatigue damage present under tab material.

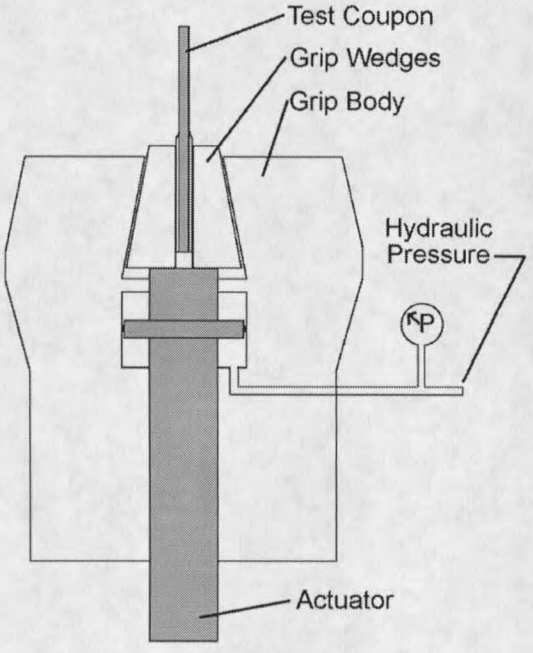


Figure 4.9. Instron hydraulic wedge grip cross section.

increased, remained constant until the prestress was not enough to handle the transmitted axial load causing the internal hydraulic pressure to increase. This increase in hydraulic pressure causes an increase in the test coupon clamping force, which is shown in Figure 4.11. This force divided by the composite gripped area determined the average compressive stress in the through-thickness direction (Z axis) of the test coupon in the grip area. Figure 4.11 was used to determine the correct hydraulic gripping pressure for the fatigue tests. This data was obtained with an Omega Engineering Incorporated PX602 pressure transducer and DP41S digital meter.

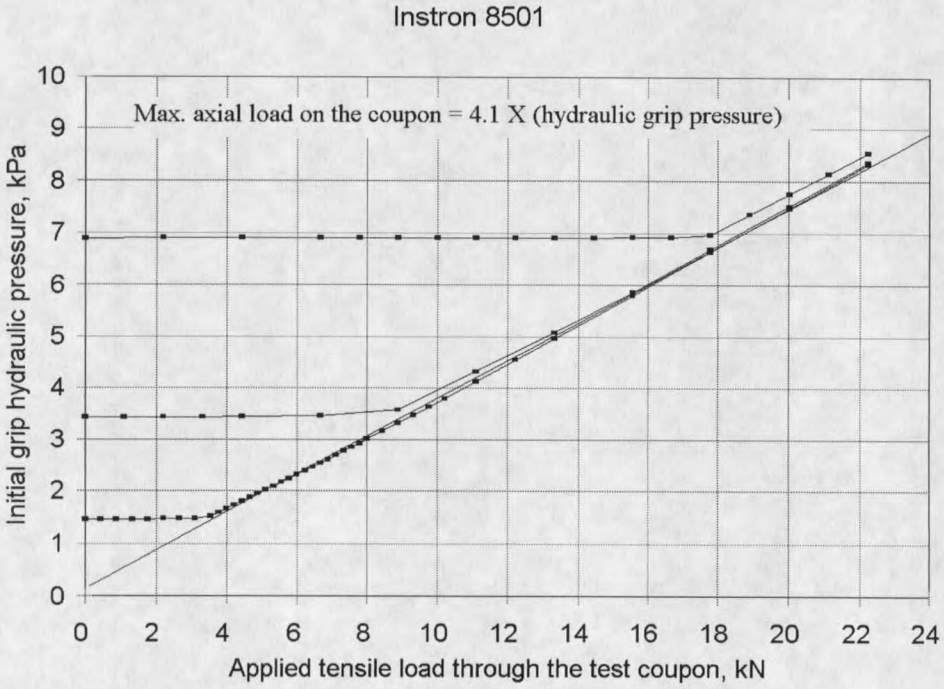


Figure 4.10. Applied axial load to the test coupon versus the grip body hydraulic pressure.

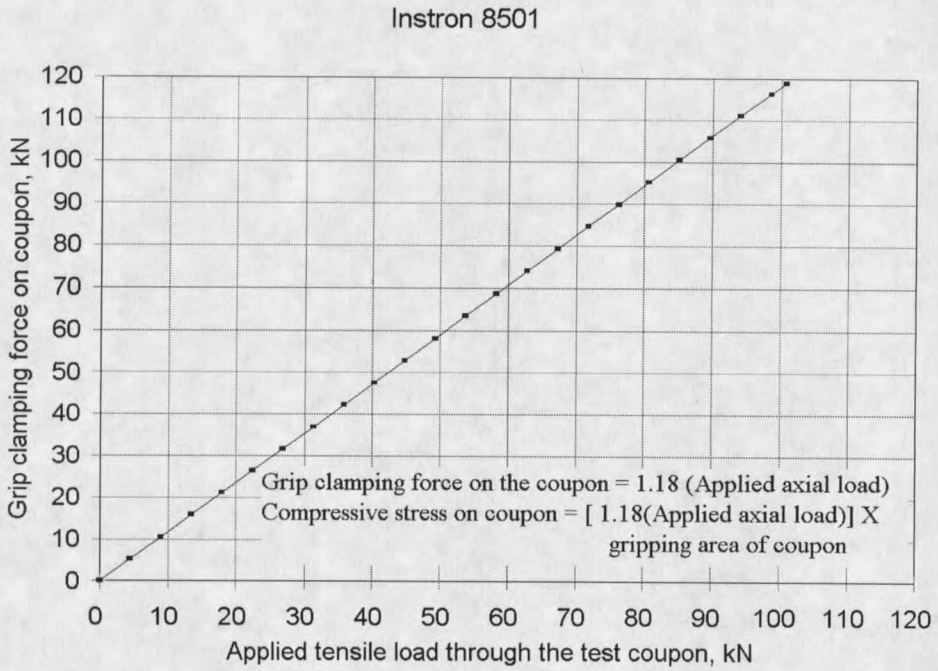


Figure 4.11. Applied axial tensile load versus the hydraulic grip clamping force on the test coupon.

The gripping force was measured with a 6.350 mm thick Mitutoyo steel gage block with a full strain gage bridge attached to its surface and the Measurements Group Incorporated 2100 system strain gage conditioner.

Under cyclic fatigue loading, if the initial grip hydraulic pressure was insufficient to apply the correct amount of prestress to the grip body, the increasing and decreasing hydraulic grip pressure caused the corresponding coupon clamping force to increase and decrease. This varying clamping force caused the steel wedge grips to bed-down and abrade the tab surface which caused premature failure of the coupon. When the grip hydraulic pressure was too high, the excessive clamping force also caused a premature coupon failure due to the increased stress concentration at the grip edge. This clamping-

force-hydraulic pressure interaction did not occur during pure compression tests. Due to the design of the hydraulic grips, compressive loads were transferred directly into the steel load train structure and actuator. The hydraulic pressure just secured and clamped the test coupon in place.

With the correct grip clamping pressure, the tensile coupon failures shown in Figures 4.6, 4.7 and 4.8 still occurred. It was suspected that the steel grip faces were not applying a uniform gripping pressure to the test coupon. The pressure distribution of the grip faces was checked using Pressurex tactile pressure measuring film manufactured by Fuji Photo Film Company Limited. The film is shown at four different clamping pressures on a 4.7 mm thick by 50 mm wide steel specimen (machinist's precision flat and parallel) in Figure 4.12. The color contact film revealed a grip face clamping area at the top of the steel wedge faces which had no contact pressure on the coupon. The rest of the grip face had a uniform pressure distribution over the test coupon clamped areas. This steel grip face wear zone at the top of the faces was the result of long term fiberglass test

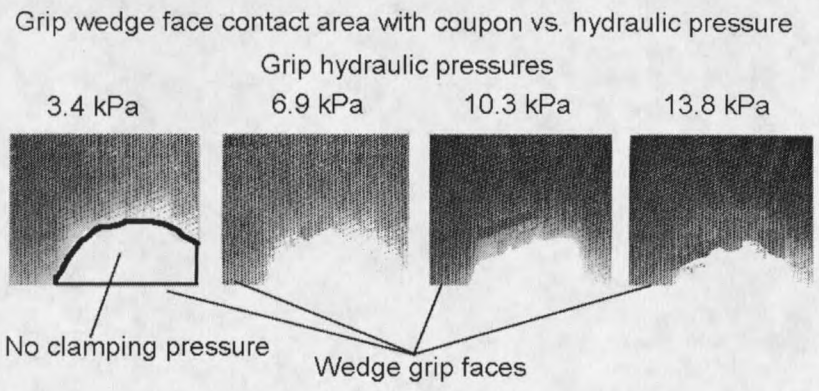


Figure 4.12. Steel wedge grip face contact area with the test coupon. Shown by pressure film.

coupon movement, and corresponding wear in this area. Fatigue tests were then performed with the test coupons clamped in the grip areas with no noticeable wear under a uniform pressure distribution, with the same fiberglass gripping damage as before. This damage area in the fiberglass test coupon must have been caused by active movement of the fiberglass over the steel grip face. This active movement is probably the result of a Poisson's ratio thickness shrinkage effect under axial loading, shear load transfer effects and material stiffness mismatch, but the reason this wear zone on the steel grip face is not symmetric is still unclear.

Compressive Test Development

Compressive testing of materials is always a difficult and controversial process as premature failure, or buckling of the coupon can undermine the test. Presently, ASTM specifies only three different methods of axial compression testing under ASTM D3410, while approximately 17 other methods are also used [27], and each method has been shown to produce different results. All these methods represent an attempt to obtain representative compression properties of the material being tested while limiting the amount of buckling. Buckling can be prevented by continuously supporting the faces of the test coupon and having the gage length as short as possible. Continuous support is not very practical in fatigue tests, as the supports cause abrasive damage to the coupon. Exploratory tests at the beginning of this study led to the choice of an unsupported gage length of 12.7 mm, which has given results consistent with compression failures in composite beam flanges (discussed later). This gage length is also required by the IITRI

(Illinois Institute Technology Research Institute, ASTM D3410), Celanese (ASTM D3410) and Wyoming modified Celanese compression test procedures. The tendency of a compression coupon to exhibit buckling is indicated by its slenderness ratio. With a 12.7 mm gage length, and a rectangular cross section, the column slenderness ratio is calculated by [28]

$$Slenderness\ ratio = \frac{\sqrt{12}\ L_E}{t} \qquad 4.3$$

where L_E is the effective length of the test coupon, which, for fixed-fixed end conditions is equal to 12.7 mm x 0.5 = 6.35 mm, and t is the composite thickness in the gage length. A study by Adams and Lewis [29] indicated that a slenderness ratio less than 30 was not prone to cause buckling failure in glass epoxy unidirectional composites. A 12.7 mm gage length and a slenderness ratio of 30 limited acceptable compressive testing, according to the above criteria, to test coupons which had a thickness greater than 1.5 mm.

The initial compression tests performed on the Instron 8501 provided very low ultimate compressive stress values as the actuator moved sideways under the side loads produced by the coupon during testing, causing premature buckling failure due to eccentric compressive loading. This side movement of the actuator was due to the Instron 8501 actuator top hydrostatic bearing, whereas previous compression tests were performed on the MTS 880 which had both upper and lower labyrinth bearings which prevented this sideways translation. Figure 4.13 shows the applied lateral force vs. the lateral deflection of the hydraulic grip head. The translation of the Instron 8501 grip was

corrected by placing two needle bearings connected to the machine frame, on either side of the grip head, as shown in Figure 4.14. This assembly acted as a linear bearing guide for the grip and prevented the sideways translation of the grip head during compression. Figure 4.14 also shows the grip anti-rotation device which prevented the lower grip and actuator from rotating and causing premature coupon failure due to additional torsion loads.

Where necessary, strain gages were attached to both the front and back center surfaces of the compressive coupon for stress-strain measurements. The extensometer could not be used due the small gage length of the test coupon and the possibility of extensometer damage during the test. Using back-to-back strain gages on the compression coupon provided valuable information on any bending or buckling during the test, which is shown in Figure 4.15. This figure indicates that a perfect compression test would show no bifurcation, or separation of the stress-strain curves provided by the two strain gages. If bifurcation of the curve is present, it indicates the presence of bending, buckling or a combination of both, which would effect the validity of the results.

The effect of compressive strain rate was also studied and is summarized in Figure 4.16. The rate effects are similar to those of the tensile coupons in Figure 4.3. Figure 4.17 shows the effects of coupon width on the compressive strength and shows similar behavior to that observed in the tensile tests. Again, as long as there was a representative number of complete fiber bundles in the gage length, as compared with the number of partial bundles on the edges, the compressive strength was insensitive to widths greater than approximately 20 mm.

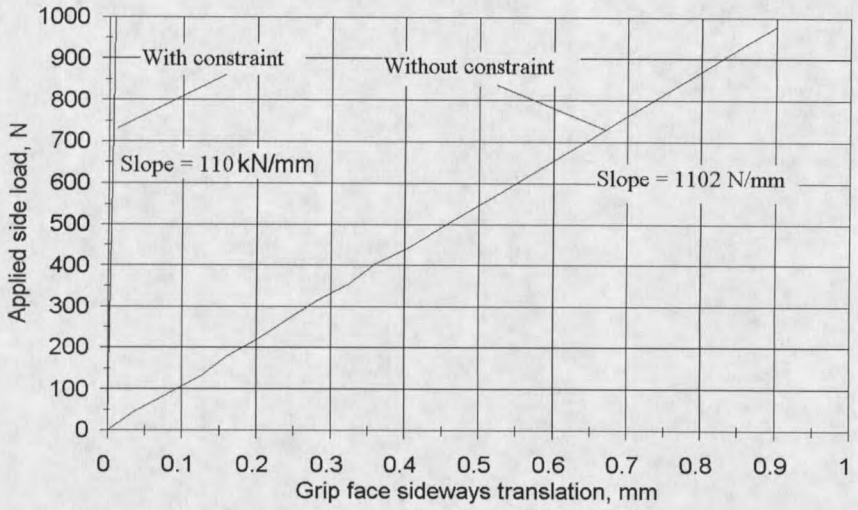


Figure 4.13. Hydraulic grip head translation versus side loading force.

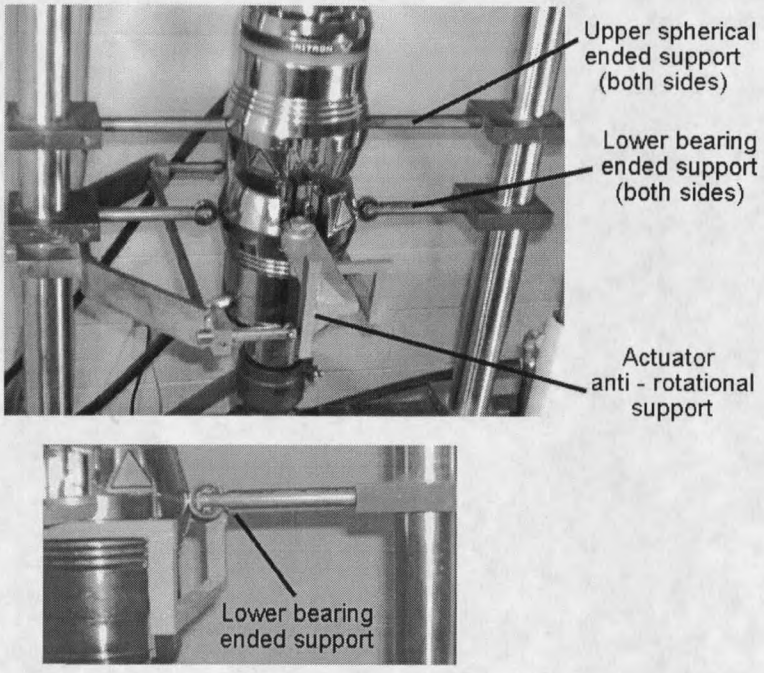


Figure 4.14. Anti-translation and anti-rotation devices.

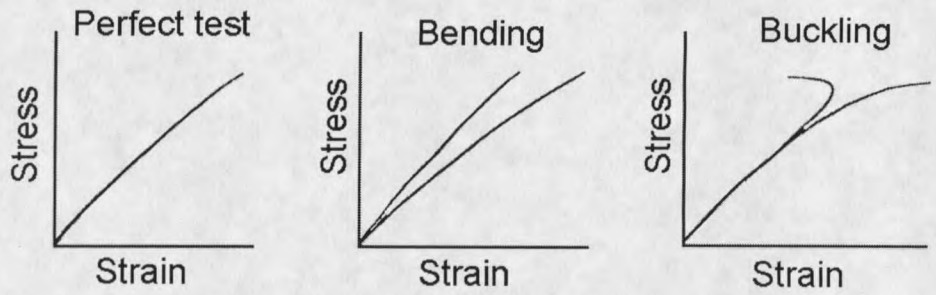


Figure 4.15. Typical compressive stress-strain curves with back-to-back strain gages.

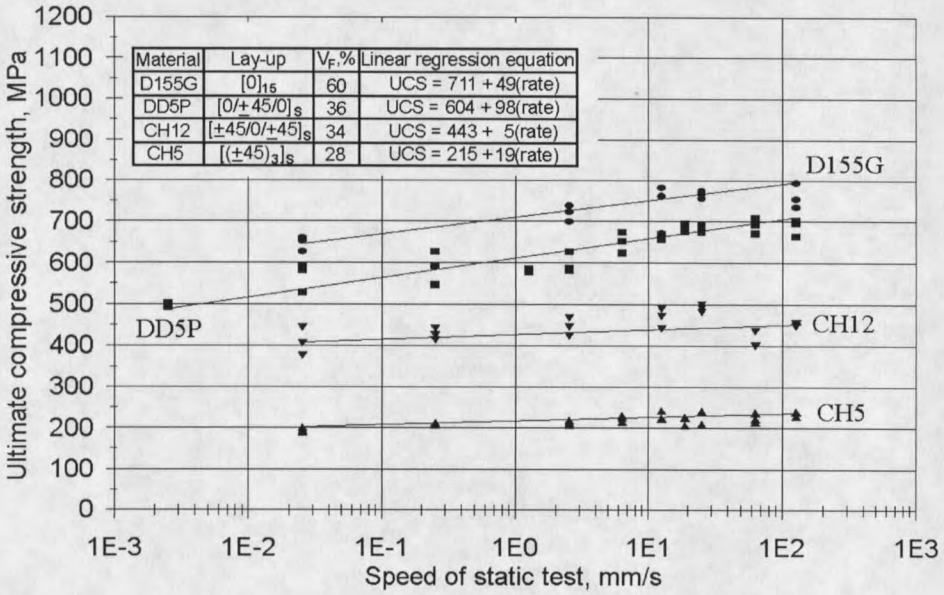


Figure 4.16. Material compressive strength versus testing displacement rate (25 mm wide test coupons with a 13 mm gage length).

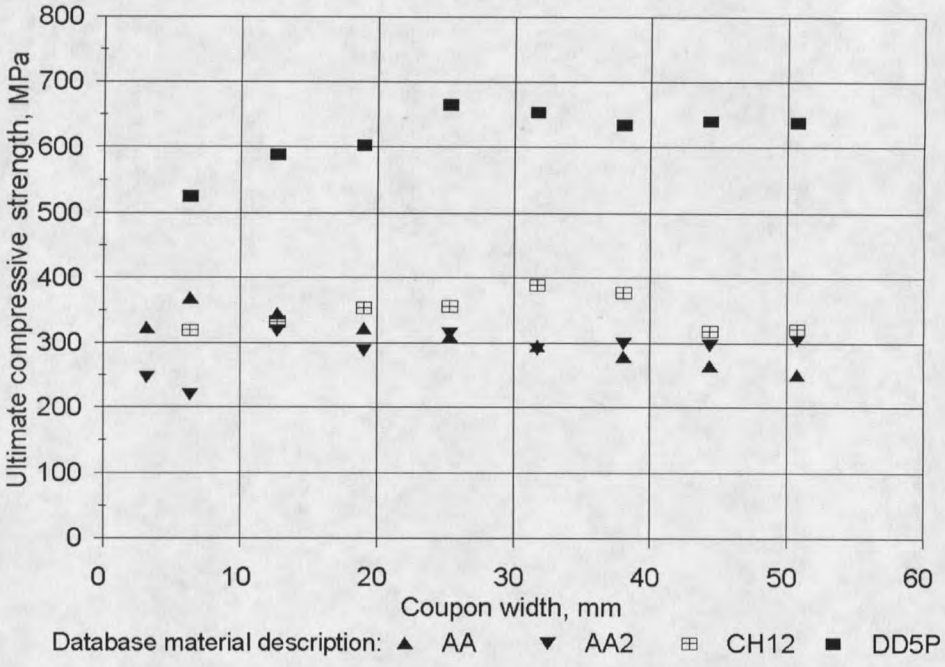


Figure 4.17. Apparent compressive strength versus coupon width (13 mm gage length with a 13 mm/s testing rate).

I - Beam 4 Point Bending Development

In order to perform the four point bending tests on the I-beams, the hydraulic grips of the Instron 8501 were removed and replaced with upper and lower two point loading platform which are shown in Figure 4.18. This assembly provided a more stable loading arrangement. The upper loading platform consisted of a W150 x 18 (AISC W6 x 12) steel I-beam with two 50 mm loading rollers spaced 610 mm apart, center-to-center. These rollers used needle bearings to allow easy rotation of the loading rollers during the testing. Combs [21] initially discovered that these rollers greatly reduced the amount of axial loading being introduced into the composite beam which was generated from contact friction. The lower loading platform consisted of two load rollers spaced 381 mm

apart, center-to-center, on a 127 x 127 x 6.35 hollow steel box beam (AISC ST5 X 5 X 0.25). Both steel platforms conformed to ASTM A500, Grade B steel specifications. Additional stiffeners were required on the W150 X 18 platform under the roller bearings to increase the lateral stability of the section. The loading platforms were centered on the load cell and actuator and bolted down. Four shear strain gages were initially placed on the steel I-beam to check for system alignment with the lower box beam and to ensure that half of the applied load was being transferred through each roller.

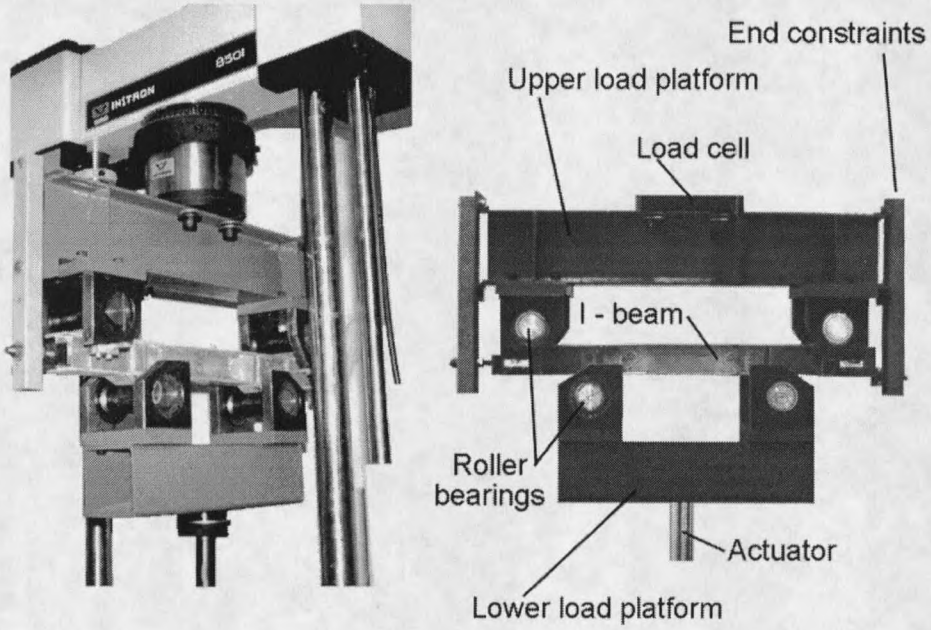


Figure 4.18. I-beam four-point bending test set-up.

The composite beam to be tested was placed in the four point loading apparatus under a pre-load of 100 N. This pre-load was used to ensure positive contact of all four load pads on the four rollers, for initial readings. With the beam centered on the loading

rollers, two longitudinal end constraints were adjusted to keep the composite beam from rolling off of the rollers. These supports allowed the beam to move only five mm longitudinally, and thus prevented the beam from slipping off of the load rollers. For lateral alignment, four aluminum supports, 4 mm x 10 mm, kept the composite beam centered, side-to-side, on the load rollers. These bars made contact with the shear stiffeners, outside of the loading areas. A Mitutoyo IDU25E digital indicator was placed in the center on the top tension flange of the I-beam to measure vertical displacement. Strain gages mounted in the longitudinal direction on the tension and compression flanges were connected to a Measurements Group Incorporated strain gage conditioner and zeroed at the 100 N preload.

The beams were loaded up to 18 kN in 8 steps, and readings from the two strain gages, the digital gage and the Instron 8500 electronics were taken. The digital displacement gage was then removed and the fatigue or static test was continued. These initial measurements were done for all the beams to obtain an indication of initial beam stiffness properties. The static tests were performed with the Instron 8501 in displacement control at a constant rate of 0.05 mm per second, while fatigue tests were run under load control with active amplitude control. During higher cycle tests, the beams were periodically taken out of the test setup and inspected for damage. Flexural tests were performed until beam failure, which was defined as either the inability of the beam to withstand the absolute maximum applied load or else total flange delamination. Upon failure, displacement safety limits terminated the test.

Cylindrical Tube Bending Tests

The first series of cylindrical tube tests were performed under 4-point bending in the same apparatus as used for the beams. The second series of tests loaded the tube as a cantilever beam which was more representative of an actual wind turbine blade in service. The setup is shown in Figure 4.19. The composite tube was mounted with aluminum end assemblies to transfer the loads through the tube. This assembly was fitted with a one meter long steel cantilever beam (free loading end), while the other end (fixed end) was bolted to a 127 x 127 x 6.35 HSS (AISC ST5 X 5 X 0.25) steel support, which in turn was bolted to a 30 cm thick structural floor with two 38 mm diameter bolts in the MSU Structures Testing Laboratory. The free end of the assembly was then loaded with a 45 kN MTS hydraulic actuator equipped with MTS 406 controllers.

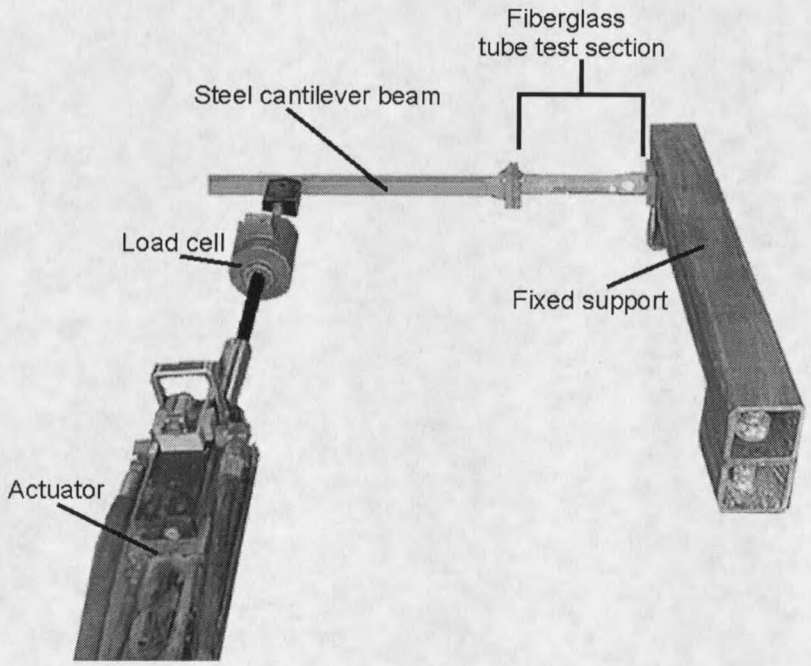


Figure 4.19. Cylindrical tube cantilever beam testing set-up.

CHAPTER 5

COUPON TESTS

The database includes a systematic variation in basic laminate parameters to establish basic trends in static and fatigue behavior. Ultimately, these tests are intended to identify materials with improved static and fatigue resistance. Over 6,000 static and fatigue tests were performed, covering 148 different materials. The database grew to these proportions in response to significant and unexpected variations in fatigue resistance which required detailed systematic study.

This chapter explores trends in static and fatigue resistance included in the database and attempts to identify the underlying mechanisms responsible for failure. Three levels of complexity are considered: simple unidirectional composites, unidirectional composites with stitched or woven reinforcing fabrics, and multidirectional laminates. Special attention is given to the high cycle behavior and basic mechanisms of breakdown in unidirectional materials.

Unidirectional Materials

Fiber Packing

An ideal composite lamina would have all the glass fibers aligned straight and

parallel to each other and to the load path, with just enough spacing between the fibers to prevent fiber-to-fiber contact. For this to occur, the arrangement of fibers would be in a uniform geometry, such as a square or hexagonal array. If all fibers have the same diameter, these arrangements would have a theoretical maximum fiber volume fractions of 0.79 (square) and 0.91 (hexagonal), shown in Figure 5.1. Random packing arrangements have a maximum fiber volume fraction which is between these limits and has a value of approximately 0.82 [30]. Practically, the fibers will involve a range of diameters, 10 to 20 μm, which could increase these fractions slightly. Increasing the fiber volume fraction is advantageous, as it increases the primary properties: longitudinal elastic modulus and tensile strength of the lamina. Above a fiber volume fraction of approximately 0.70, the transverse properties of the composite will degrade, as fibers contact each other and stress concentrations increase, which is detailed in Figure 5.2 [31, 32]. The stress concentrations around the fibers are higher when the fiber transverse modulus is higher relative to the matrix modulus. In a well bonded composite, a matrix material which would yield at a lower stress would decrease the local stress concentrations.

Strand Deformations in Fabrics

Glass fabrics are constructed using glass fiber strands or tows, which contain hundreds to thousands of continuous glass fibers, 10 to 20 μm in diameter, without any definite twisting of the fibers. These tows are stitched or woven together to form a fabric, which allows the fabric to be handled during composite manufacturing. Fiber handling

during fabric manufacturing significantly reduces the fiber strength, as shown later. The properties of the fibers can be further reduced by the stitching thread tightness, and the spacing of the stitching or weaving. The stitching pinches the tow and causes a slight curvature of the fibers on the outside of the glass strand as the diameter locally decreases. This curvature of the fibers introduces a bending stress in the fibers at the stitch, but it is postulated that the major effect is that the stitch decreases the average distance between fibers and causes the number of fibers in virtual contact, in that area, to increase. Virtual contact it is meant that the fibers appear in contact in micrographs; whether a thin matrix layer is present between the fibers is not known.

The reinforcing fabrics have bundles of glass fibers separated by an area without fibers which forms resin rich areas between the tows in stitched fabrics, and both above

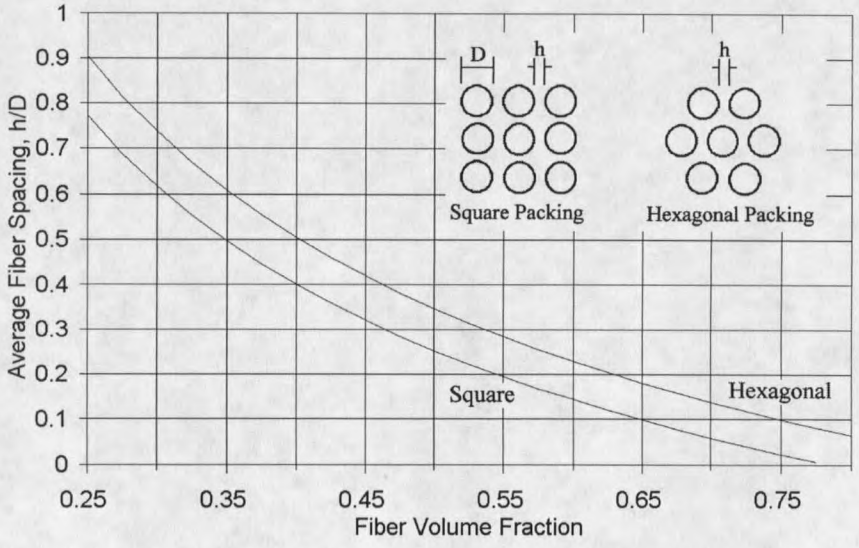


Figure 5.1. Fiber volume fraction versus the average fiber spacing in a composite with theoretical square and hexagonal packing geometries.

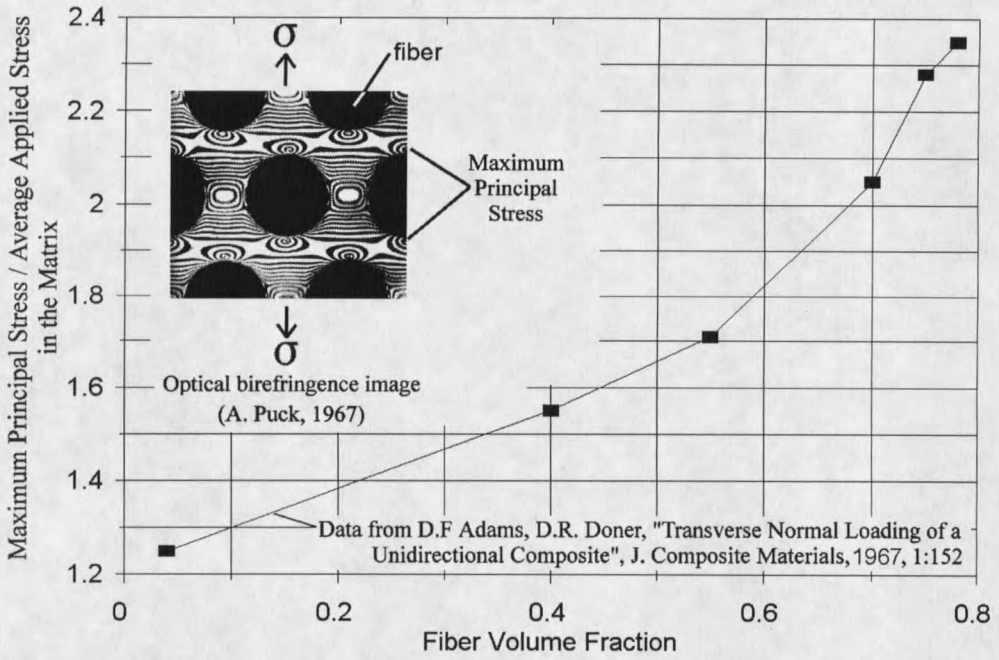
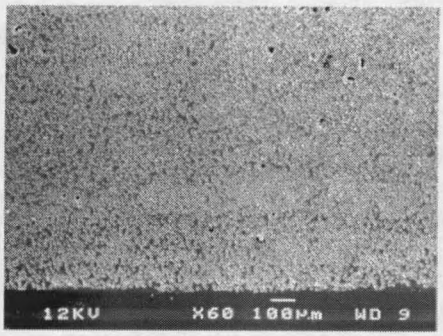


Figure 5.2. Fiber volume fraction versus the normalized maximum principal stress for a transversely loaded composite.

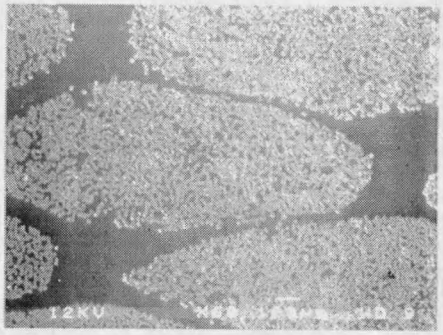
and below weave crossover points in woven fabrics. It is the presence of this resin rich channel between the tows which reduces the overall fiber content, and hence the lamina properties. In order to increase the fiber content, the elliptical fiber bundle cross section must be compressed and forced to spread out across the width of the lamina to fill this channel. The stitching or weave crossover points inhibit this spreading out from occurring. Figure 5.3 shows three different magnifications of Material PP, which used 3M-SP250 prepreg (no stitching or weaving), compared with a unidirectional composite with D155 stitched fabric. The prepreg material shows a uniform distribution of fibers with no large resin rich regions; the D155 composite, because of the stitching, has large resin rich regions between the tows. Figure 5.4 shows the D155 confined tow area versus

the overall ply fiber content for materials DD6, DD2 and DD7. As the composite fiber content increases, the cross-sectional area of the individual tows decrease (as expected), squeezing out the excess resin. The D155 fabric tows in Figure 5.4 start to interact and fill the matrix rich regions in the adjacent plies, and thus the elliptical tow cross-section geometry deforms. If this deformation of the tow is not uniform along the length, where the tow enters and exits the resin channel in the adjacent ply, a rotation of the strand occurs. The figure shows that the fiber content inside the fiber bundle does not change as significantly as the average composite fiber content, and that the fiber content in the fiber bundle changes along its length (x-axis) due to the periodic presence of stitching.

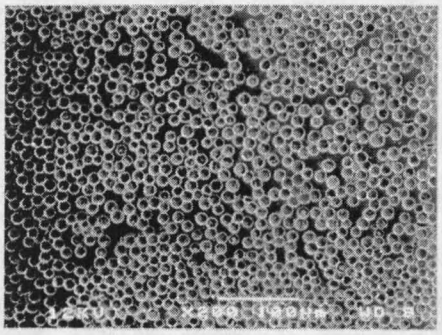
Figure 5.4 shows that the stitching causes up to a 10 percent local increase (from $V_F = 0.58$ to 0.68) in the fiber volume fraction of the strand contained within the stitching in the DD6 material; the DD7 material exhibited only a 2 percent increase (from $V_F =$ 0.70 to 0.72). The determination of strand fiber contents at higher individual ply fiber contents was not performed due to the difficulty in determination of the boundaries between adjacent strands. Figure 5.5 shows the number of fibers in direct contact with adjacent fibers versus the ply fiber volume fraction, both within and between stitching threads. A large increase in the number of fibers in contact occurs in the 0.31 to 0.36 fiber volume fraction region, which also coincides with the region where most of the composites in the database start to decrease in fatigue resistance. It should be noted that the D155 tow has stitching every 4 to 6 mm, which means that the tow fiber content varies between a maximum and a minimum value every 4 to 6 mm.



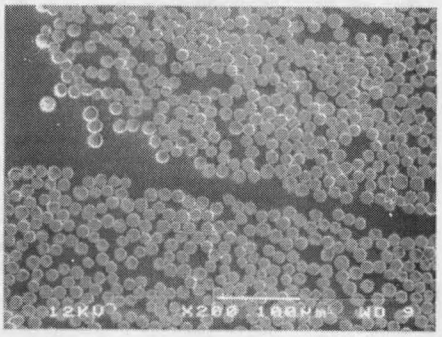
Prepreg (60X magnification)



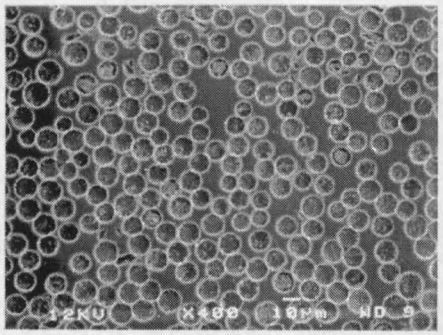
D155 (60X magnification)



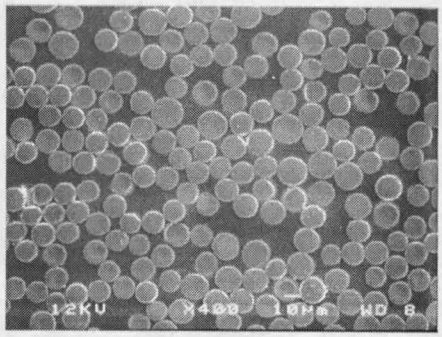
Prepreg (200X magnification)



D155 (200X magnification)

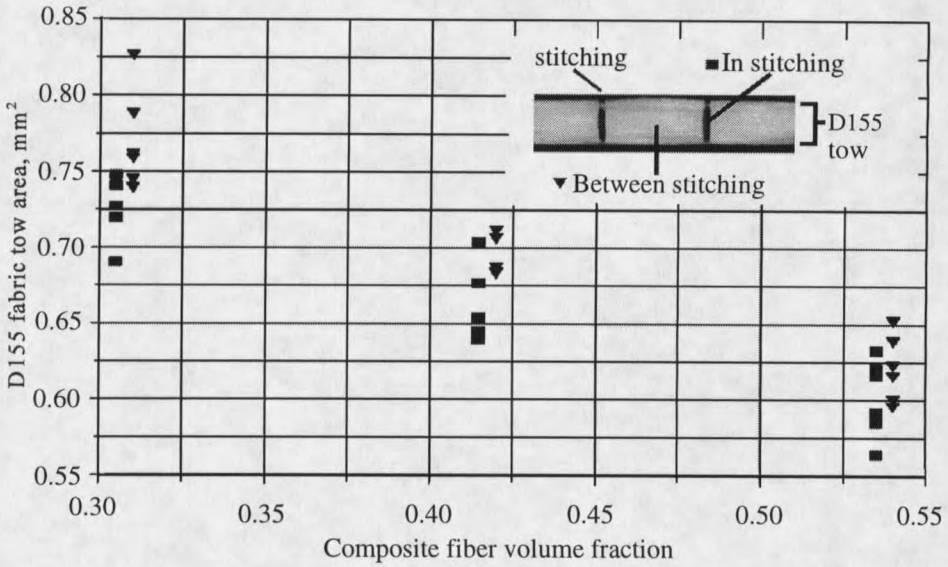


Prepreg (400X magnification)



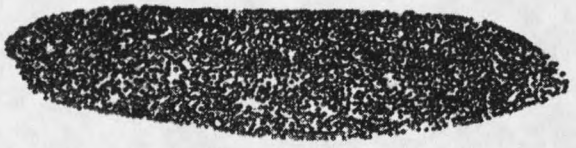
D155 (400X magnification)

Figure 5.3. Micrographs of prepreg and D155 fabric composites

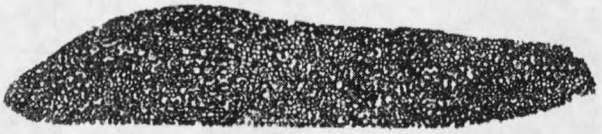




Material DD6 - composite $V_F = 0.31$, D155 tow $V_F = 0.58 - 0.68$



Material DD2 - composite $V_F = 0.42$, D155 tow $V_F = 0.65 - 0.69$



Material DD7 - composite $V_F = 0.54$, D155 tow $V_F = 0.70 - 0.72$

Figure 5.4. Composite fiber volume content versus D155 confined fiber tow area in Materials DD6, DD2 and DD7.

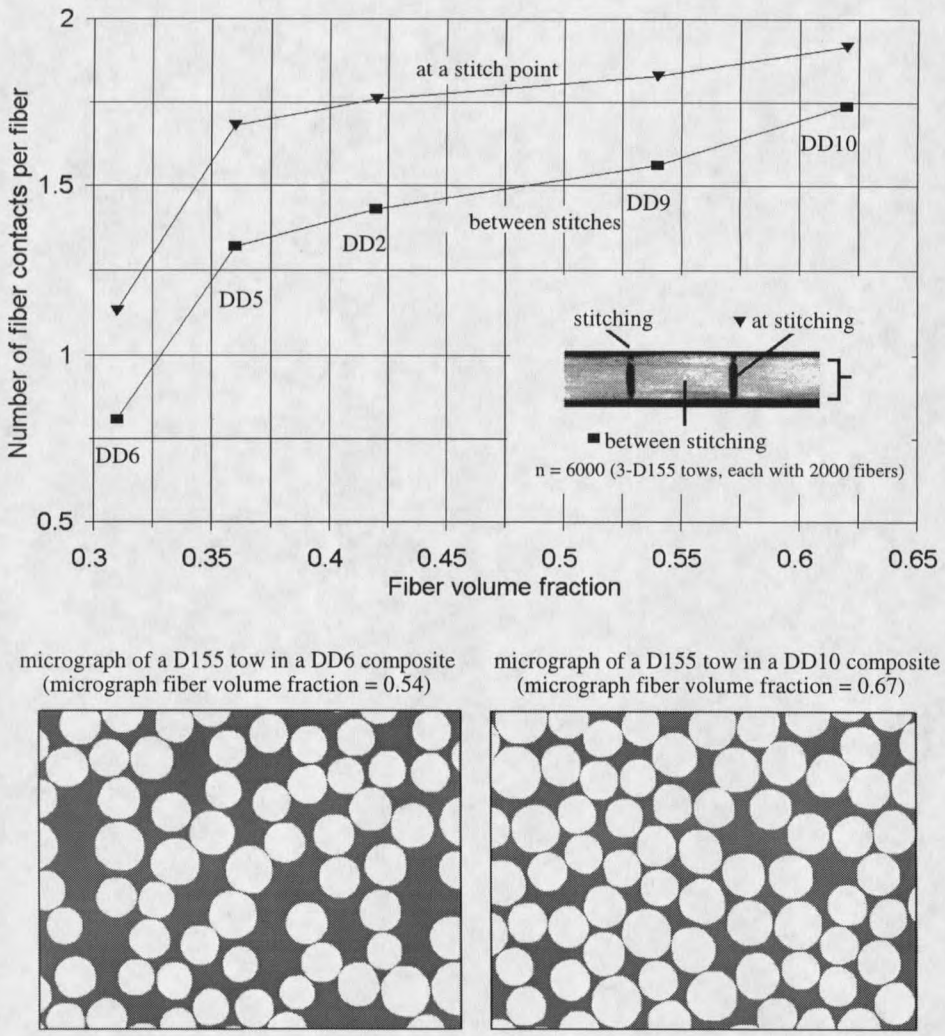


Figure 5.5. Composite fiber volume fraction versus average number of fibers in contact with each other for materials DD6, DD5, DD2, DD9 and DD10.

Since the fabrics are stitched or woven with a regular spacing, the tows can be stacked in or out of phase with the adjoining plies. Figure 5.6 shows three possible stacking possibilities. Each has some degree of tow compression and elliptical shape deformation with increasing average fiber content as the tow interacts with adjacent tows. The D092 fabric is a lighter fabric with a larger distance between the fiber tows and thus larger matrix rich regions. With the tows stacked directly in phase with each other (strands on top of each other) the resin rich areas can extend continuously through the composite thickness. When the tows are out of phase with the adjacent tows, the resin rich areas between the tows are partly filled in by deformed tows from adjacent layers, allowing for higher fiber contents. Figure 5.6 shows the D092 fabric at fiber volume fractions of 0.30, 0.41 and 0.50. At a fiber content less than approximately 0.30, the tows in all the fabrics are separated from the adjacent plies by a continuous matrix layer, and therefore do not have any direct fiber contact with the tows in the adjacent ply. As the fiber content is increased, the tows start to contact the tows in adjacent plies, causing elliptical tows to flatten out and fill the resin rich areas between the adjacent plies. Increasing the fiber content further causes the tows to deform in the width direction, filling in resin channels between the tows, within the ply. If this deformation is restricted by the weave or stitching, a pinched region along the strand will exist.

Since the stitching is physically on the surface above and below the tow, the stitch introduces additional "hard points" of contact, which cause localized pinching of the fiber tow as well as adjacent tows in contact with this stitching. This situation causes additional points of pinching. In the DD series of materials listed in the database, the stitching in the

D155 fabric starts to interact with the adjacent plies at a fiber volume fraction of approximately 0.36. This interaction effect is illustrated in Figure 5.7. Since the stitching thread is also on a regular spacing, the stitching in one ply can contact the stitching in an adjacent ply, creating another hard contact point or location of increased bundle fiber content. Figure 5.8 shows the interaction of the plies when the stitches are stacked on top of each other. The stacking of the stitching causes the plies to be separated more at the stitch points than between the stitches, causing the fibers to collapse into the resin rich region, creating a small fiber angle which might reduce the localized compressive strength. The figure shows the effects of removing the stitching thread from the D155 fabric. Without the restrictions of the stitching thread, the glass fibers disperse and form a more uniform geometry similar to the prepreg materials, minimizing the size of the matrix rich regions in the ply.

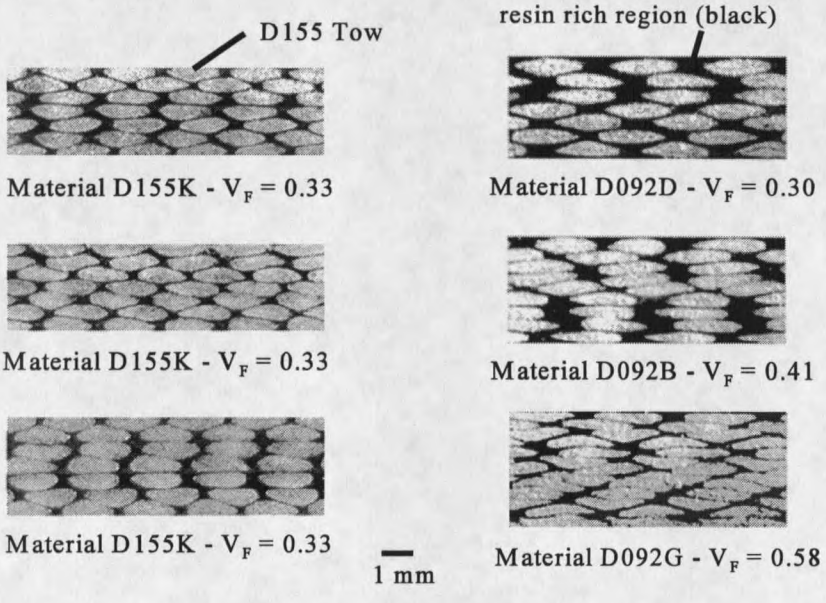


Figure 5.6. Stacking geometries of unidirectional fiber bundles.

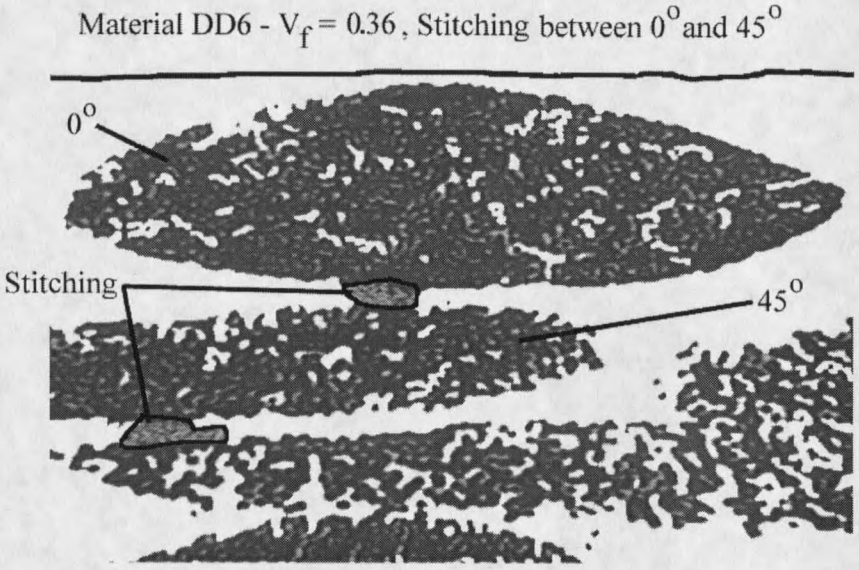
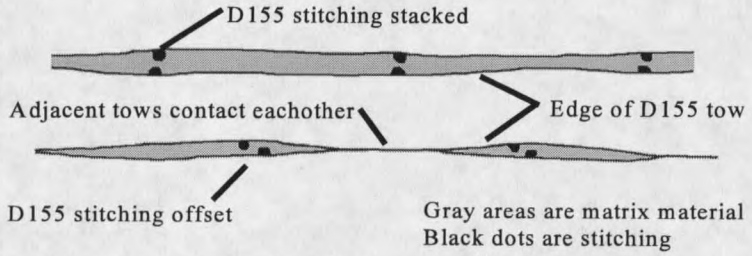
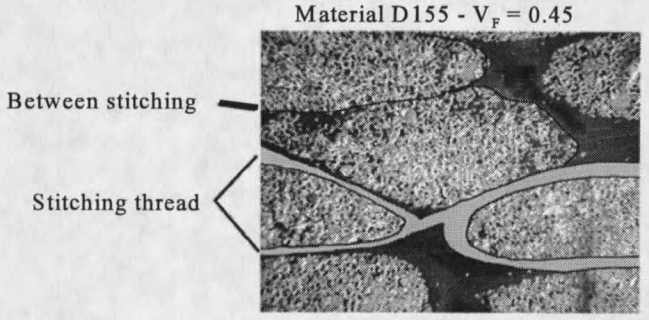


Figure 5.7 Fabric stitching interaction with adjacent plies.

The A130 fabric, which has a woven architecture shown in Figure 5.9, uses the same glass roving that is used in the D155 fabric. This fabric is woven around a weft glass strand which is coated with a thermoplastic hot melt adhesive. During fabric weaving, this strand thermoplastic bead is woven into the fabric. Heat is applied to melt the thermoplastic to encapsulate the glass strands in direct contact with it, locking the fabric architecture together. The bonding of the matrix materials to this thermoplastic bead is poor. Cracks readily form at the interface of this bead and the matrix for all the resin systems in the database.



Edge view of D155 plies (stitching spaced about every 4 mm)



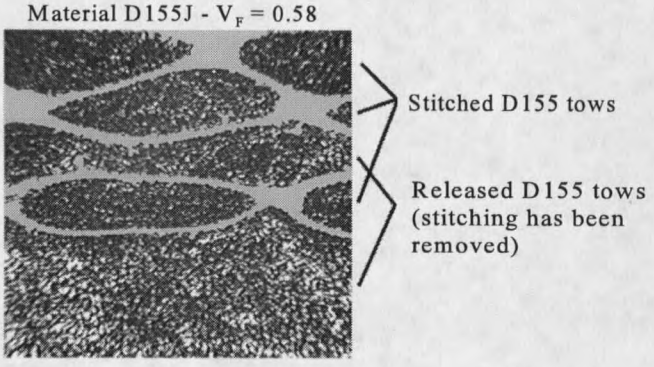


Figure 5.8. Fabric stitching interaction with adjacent ply stitching and the effects of removing the stitching.

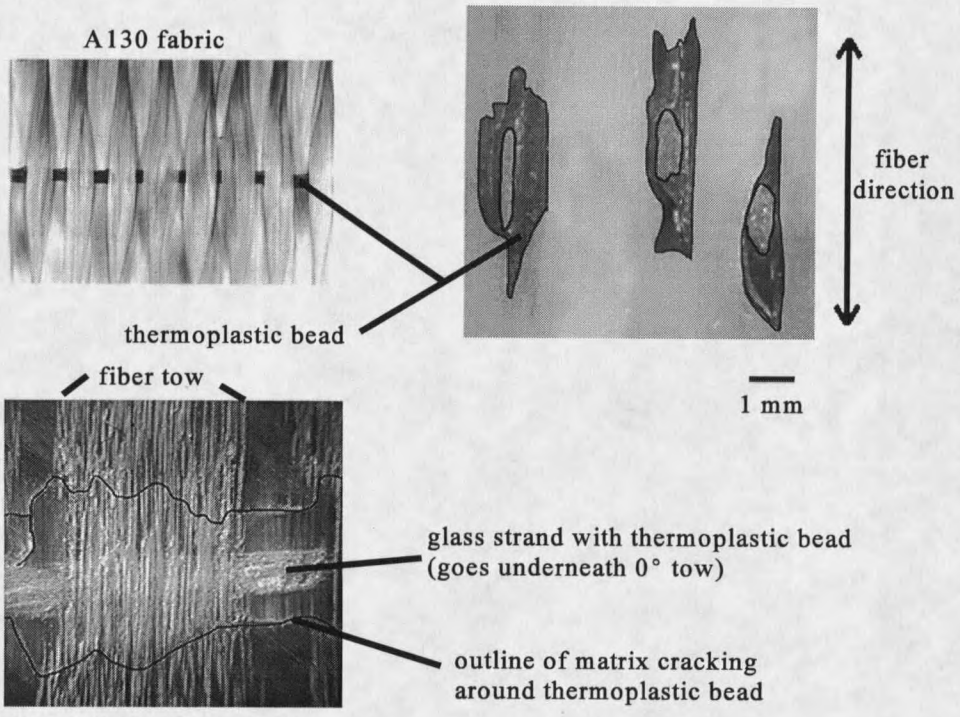


Figure 5.9. A130 fabric with woven architecture with cracking around thermoplastic bead in coupon DD11-107 after fatigue testing.

In summary, the following effects have been observed in strand-fabric interactions:

- Stitching or weaving is necessary in order to physically handle the fabric during composite manufacturing in low cost composites.
- The stitch or weave causes a local pinching and misorientation of the strands.
- The stitching causes the strand fiber content to locally increase periodically along the length of the strand.
- The stitching thread interacts with the strands as a hard contact point.
- The thermoplastic bead in the woven fabrics does not bond with the matrix materials used in this study and was a nucleation point for starter cracks.
- The strands deform in cross-section as the composite fiber content increases.

Unidirectional fatigue behavior

Background. Bulk glass and single glass fibers are not affected by the cycling of stress. However, inorganic glasses are affected by a stress-corrosion mechanism termed "static fatigue" where the tensile stress causing failure is reduced by 3 to 5 percent for each decade of time under load [33, 34]. This mechanism of stress-corrosion is caused by water molecules attacking the silica bonds of the glass, creating surface flaws, which propagate to produce failure [35]. The rate of this process is increased strongly by impurities such as sodium. This mechanism appears to be independent from the cyclic fatigue behavior of the composites [36, 37, 38]. Higher sodium content glasses are more sensitive to this corrosion and their strength can be reduced by as much as 10 percent for each additional decade of time under load.

The inherent fatigue behavior of individual glass fibers and strands has been reported in the literature [39-46] and is summarized in Table 5.1 and Figures 5.10 through 5.12. The individual fiber tests listed show the static fatigue (stress corrosion) mechanism inherent in bulk glass. The 500 μm diameter fiber had a complex composition which degraded at 9 percent per log decade. References 39 and 43 researched these 500 μm diameter fibers which could be manufactured with a surface compressive residual stress which eliminated the static, as well as the cyclic fatigue behavior of the glass. The major limitations of this fiber were their low initial strength compared to smaller, conventional reinforcing fibers and their high manufacturing cost. The surface compressed fiber data was not included in Table 5.1 or Figure 5.10.

Figure 5.11 shows unimpregnated fiber strands containing 5, 30 and 210 fibers.

The fatigue sensitivity coefficient, b, (equation 4.2) of these strands increased to 7 to 10 percent per log decade of cycles from the 4 percent per decade of the individual fiber shown in Figure 5.10. References 1 to 19, 47 and 48 all demonstrate that non-woven glass reinforced plastics degrade with a fatigue sensitivity coefficient, b, of approximately 0.10 or 10 percent per decade. Figure 5.12 details the impregnated strand data with strands varying from 30 to 2040 fibers. These data also show a b-value of approximately 0.10. This fatigue behavior must be inherent to the glass fiber as both the unimpregnated and the impregnated strands have approximately the same b-value and this also suggests that the fatigue behavior of the composites derives directly from the glass reinforcement [41- 44].

The basic mechanism of fatigue degradation in these composites appears to be some sort of glass fiber surface abrasion or friction and wear process. Looking at one glass fiber, the smallest incremental distance that a crack can grow in the glass is the diameter of the silicate ring, which is 0.4 to 0.5 nm (10^{-9} m) [35]. Using fracture mechanics to estimate flaw sizes at fiber failure, glass has a fracture toughness (K_{IC}) of approximately 0.7 $MN/m^{3/2}$ and at a tensile stress (σ) of 800 MPa (typical of fatigue tests to 10^6 cycles), using $K_I = 1.12\ \sigma\ (\pi\ a)^{1/2}$ [50], the crack length (a) equals 1.9×10^{-7}m or 190 nm. This is a crack length of a few hundred silica rings in a fiber that has a diameter of 12,000 nm (12μm). Attempts to find fatigue damage of this size on the glass strands have been unsuccessful. Fatigue damage generated on the surface of the glass fiber could not be differentiated from the longitudinal irregularities found on pristine fibers due to the fiber manufacturing process.

Results and Discussion. Only very limited fatigue data is available with results past a few million cycles. A b-value of 0.10 extrapolates (assuming a linear S-N curve on a semi-log plot) to zero strength after ten decades or 10 billion cycles. The slope of the fatigue trend must change slope at some level. In order to determine the high cycle behavior of impregnated glass strands, a specially constructed strand consisting of 45 fibers and a D155 strand of 2000 fibers were impregnated with polyester (CoRezyn 63-AX-051) and fatigue tested out to 10^9 cycles at R=0.1. These tests are detailed in Table 5.2. These are the first known fiberglass fatigue results at 10^9 cycles.

The 45 fiber strand was tested on the speaker cone based fiber testing apparatus discussed in Chapter 3, and the results are presented in Figures 5.13 and 5.14, as well as listed in the database (Appendix A). Figure 5.14 shows two plotted trend lines: one semi-log prediction line at 8.3 % / decade, with a corresponding statistical goodness of fit value (R^2) of 0.95, and a log-log prediction line. The log-log prediction line had a higher corresponding statistical goodness of fit value (0.93) when the static data was included in the line fit (forced through 1). The three fatigue coupons which went in excess of 1 x 10^9 cycles, unbroken, are considered "run-outs" and were included in the prediction line calculations. All calculated stresses and strains are based upon the actual glass fiber cross sectional area and an elastic modulus of 70 GPa. The static tests were performed by attaching a twelve volt battery across the speaker terminals, which drove the speaker at a displacement rate of 140 to 150 mm per second, similar to the fatigue rate. Figure 5.15 shows a typical static test applied load versus time diagram.

Most of the coupons failed in the gage section, with significant fiber failures and

transverse matrix cracks. The fiber volume fraction of the coupons ranged between 0.52 and 0.57. The polyester resin used to impregnate these fibers had an ultimate strain to failure of approximately 2 percent, and the test coupons showed numerous transverse matrix cracks along the strands length.

The D155 strand of 2000 fibers was tested in the Instron 8511 servo-hydraulic testing machine and the data presented in Figures 5.16 and 5.17. Figure 5.17 shows three predicted trend lines: two log-log and one semi-log. The semi-log predicted trend of 8.8 percent per decade had the highest corresponding statistical goodness of fit value into the 10^5 to 10^6 cycle range ($R^2 = 0.99$). Past this range, the power law prediction (linear on a log-log plot) incorporating only the fatigue data at stresses less than a normalized stress of 0.55 had a better fit ($R^2 = 0.97$ versus 0.69 for the entire data set).

Variability in Properties of Strands Taken From Fabrics. The D155 strands were carefully taken from different rolls of D155 fabric. A variation of the static strength of the D155 strands with different batches was noticed early on in the research and was monitored. Six rolls of D155 fabric were used to fabricate the materials in the database over a seven year period. Strands were carefully removed from these rolls, impregnated with polyester and statically tested. Thirty coupons were tested from each batch, and the scatter is detailed in the Weibull graph in Figure 5.18. The Weibull values of Eta (level at which 62 percent of the coupons have failed) and the Beta or Weibull modulus (m) are also listed in Figure 5.18. Roll 1 had the lowest strength of all the rolls tested. Figure 5.19 combines all the 300 static strength tests into one curve. Since most of the statistical tests

performed in this study required a normal or near normal statistical distribution, it was necessary to test the strength distribution to determine normality. Figure 5.19 shows the three best statistical models, and their coefficients for the data, as determined by the computer simulation program Unifit II, by Averill M. Law and Associates. The data are normally distributed. The strengths range from 912 N (3.1% strain to failure) to 1,487 N (5.1% strain to failure), again with roll 1 filling in the lower end of the curve. A Weibull modulus of 12.2 was obtained from the pooled data sets (all data), which is within the range for ceramic materials [49], but is much lower than the individual data sets from separate batches.

Table 5.1. Summary of previous fatigue results on individual E-glass fibers and tows.

Number of fibers	Fiber diameter μm	Matrix material and fiber volume fraction	UTS/V_F MPa	R = 0.1 b	R = 0.1 10^6 strain % [A]	Reference
1	25	none, 1	2130	0.040	2.31	39
1	500	none, 1	738	0.090	0.49	39, 43
5	25	none, 1	1490	0.068	1.26	40
30	25	none, 1	1390	0.099	0.81	39
210	9	none, 1	1530	0.091	0.99	41-44
30	25	epoxy, 0.40	2324	0.088	1.57	39
210	9	epoxy, 0.49	2255	0.096	1.37	41-44
210	9	epoxy, 0.45	2158	0.091	1.40	
210	9	polyester, 0.23	1980	0.100	1.13	
2040	13	epoxy, 0.16, (R=0)	1672	0.115[B]	0.74	45, 46
2040	13	epoxy, 0.33, (R=0)	1659	0.107[B]	0.85	
2040	13	epoxy, 0.50, (R=0)	1556	0.093[B]	0.98	

[A] 10^6 strain calculated using E = 70 GPa

[B] R = 0 data

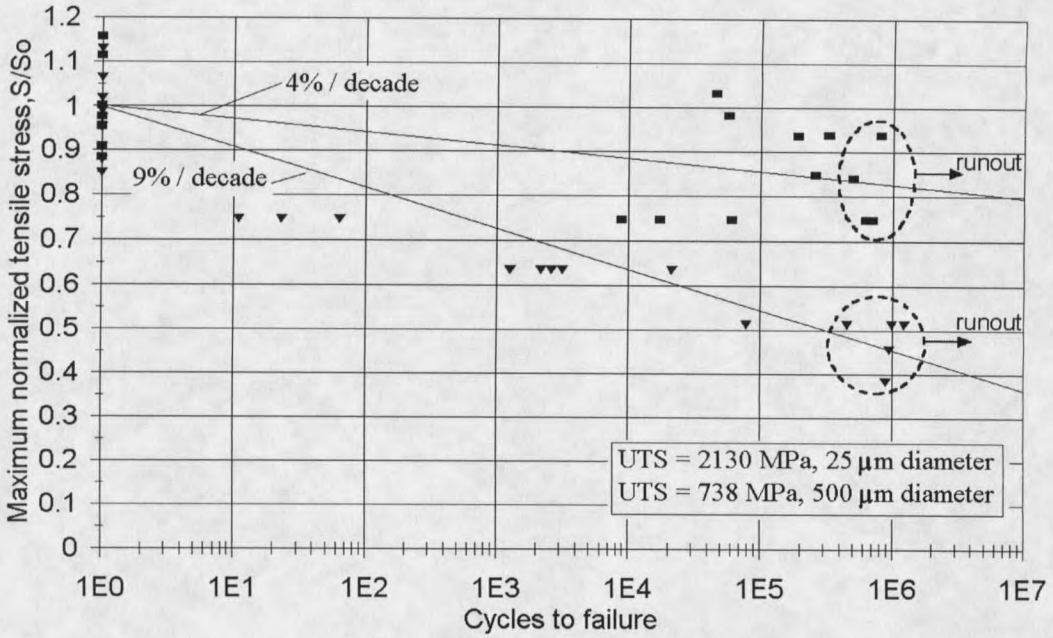


Figure 5.10. Normalized S-N fatigue data for unimpregnated single glass fibers (References 39, 43).

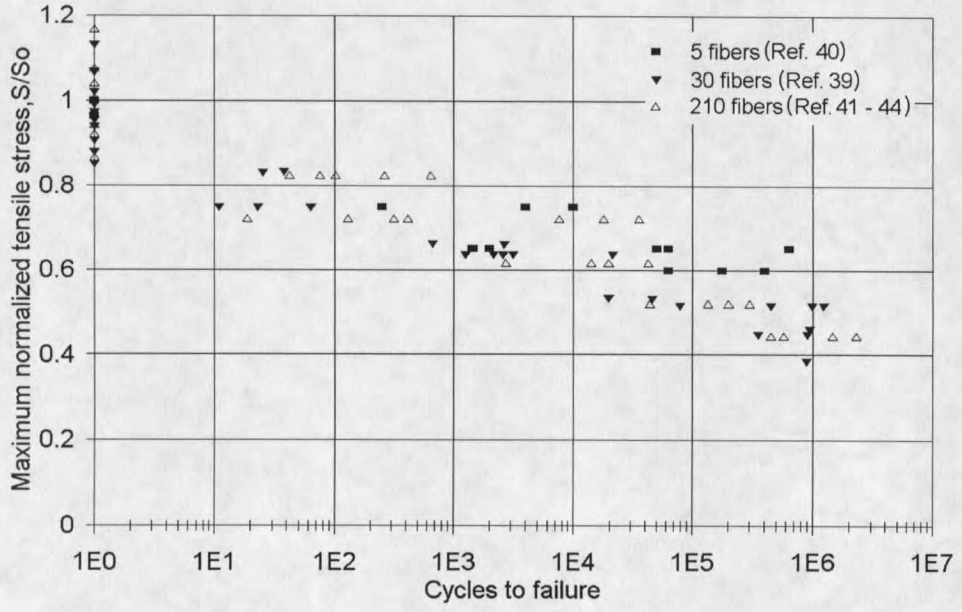


Figure 5.11. Normalized S-N fatigue data for unimpregnated glass fiber strands, R = 0.1 (References 39 - 44).

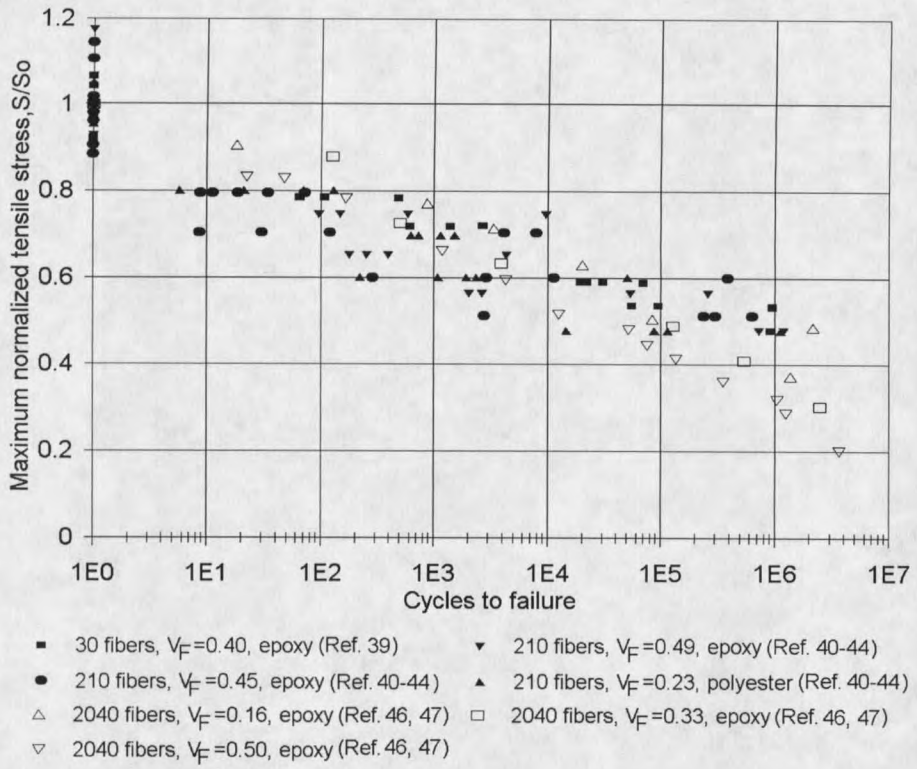


Figure 5.12. Normalized S-N fatigue data for impregnated glass fiber strands, R = 0.1 (References 39 - 47).

Table 5.2. Impregnated strands tested in fatigue.

Owens Corning Roving Number	OC-107B-AC-450 (roving used in D155 and A130 fabrics)	OC-990-BC-2385-4093
Number of fibers in roving	2000	208[A]
Average fiber diameter, µm	15.98	10.66
Standard deviation, µm	1.53	0.94
Maximum diameter, µm	19.00	8.33
Minimum diameter, µm	13.50	13.96
Sample size	12,000	2,800
Average UTS, MPa	2,750	3,126
UTS standard deviation, MPa	296	398
Average failure strain, % [B]	3.93	4.47

[A] To lower the required loads, this strand was split down to 45 fibers.
[B] Calculated using an elastic modulus of 70 GPa.

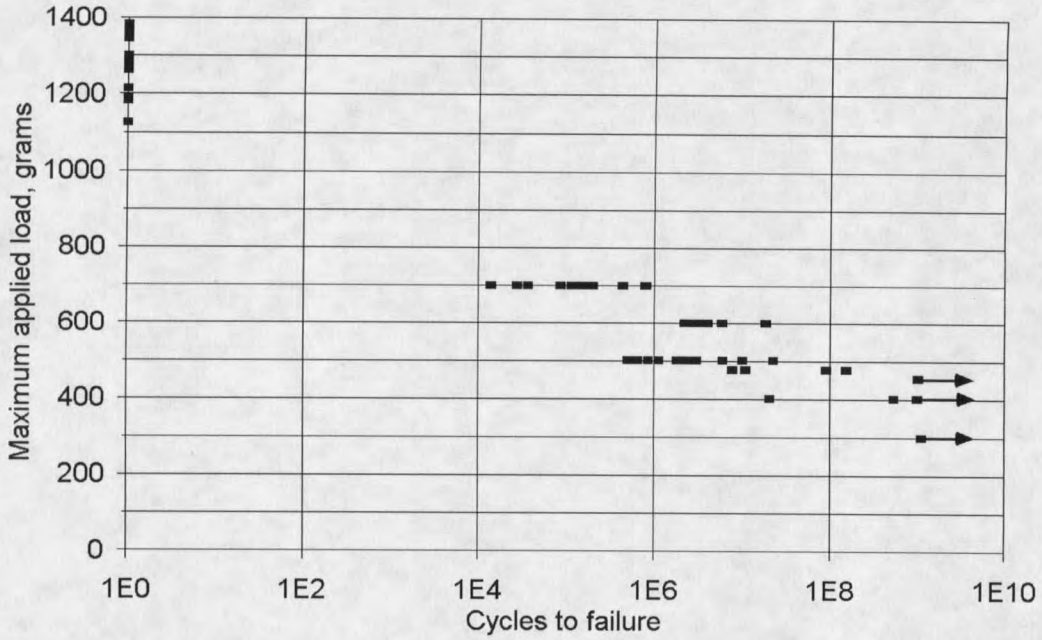


Figure 5.13. S-N fatigue data for impregnated fiber strand (45 fibers, average diameter = 10.76 μm, SD = 0.40 μm), R = 0.1 (obtained using the speaker cone apparatus).

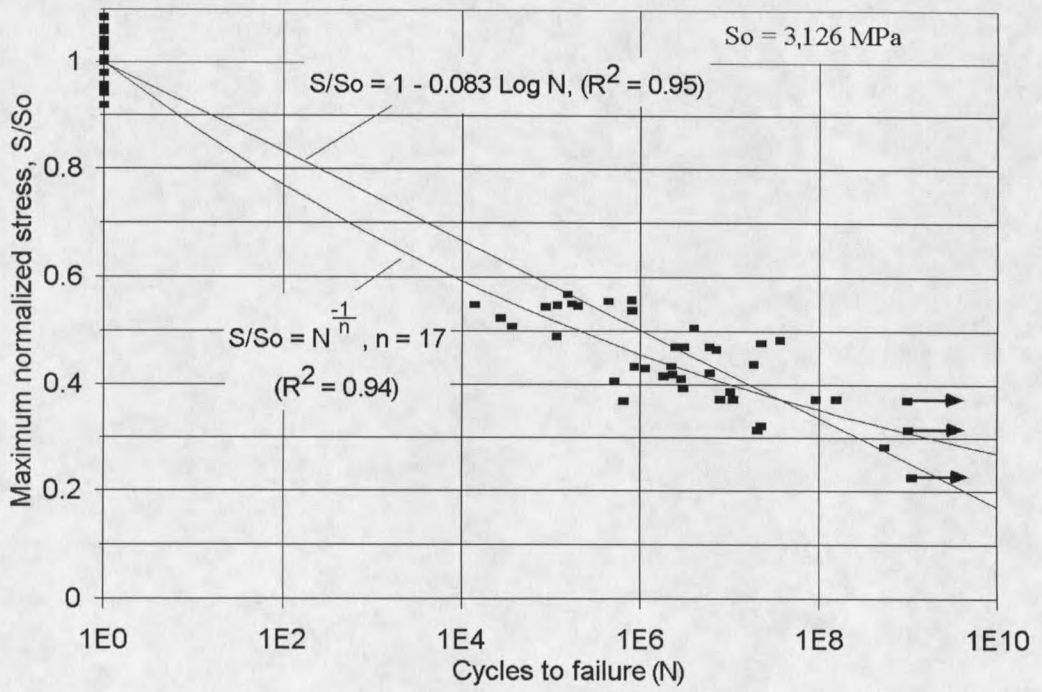


Figure 5.14. Normalized S-N fatigue data for impregnated fiber strand (45 fibers, average diameter = 10.76 μm, SD = 0.40 μm), R = 0.1.

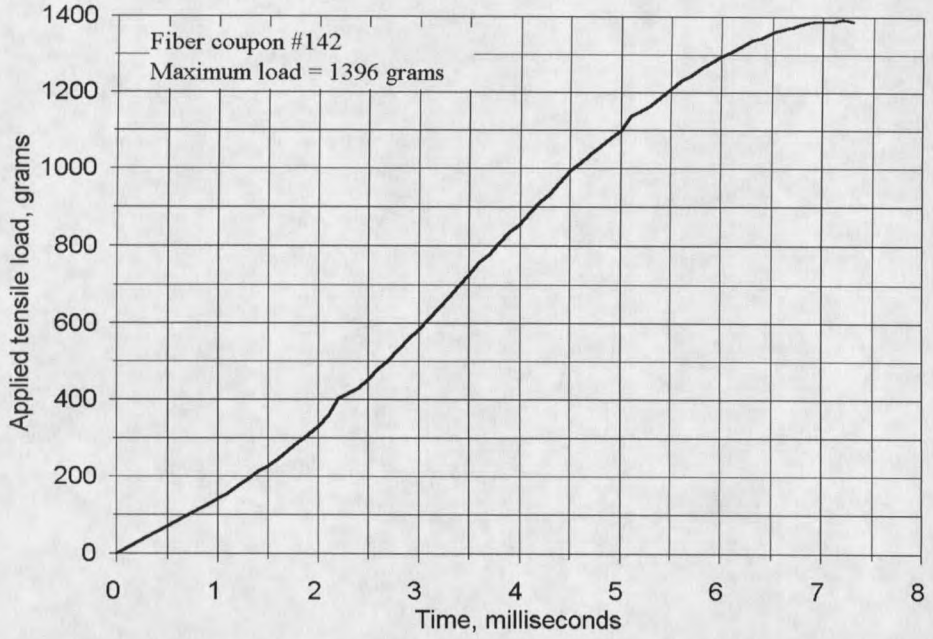


Figure 5.15. Applied tensile load versus time for a 45 fiber test coupon.

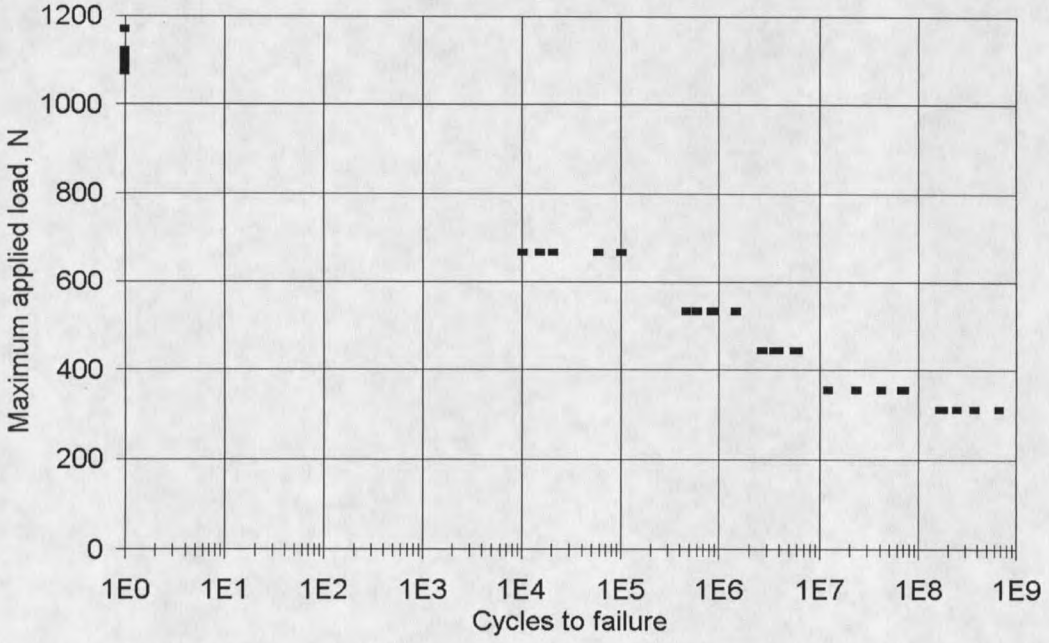


Figure 5.16. S-N fatigue data for D155 impregnated fiber strand (2000 fibers, average diameter = 15.98 μm, SD = 1.53 μm), R = 0.1 (tested in a servohydraulic machine).

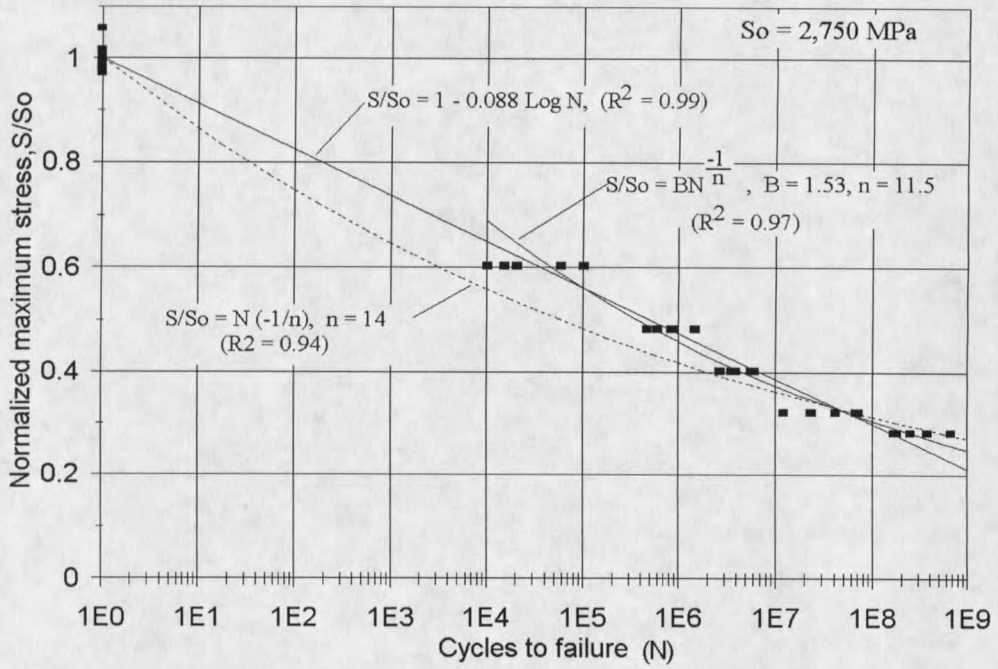


Figure 5.17. Normalized S-N fatigue data for impregnated D155 fiber strand (2000 fibers, average diameter = 15.98 μm, SD = 1.53 μm), R = 0.1.

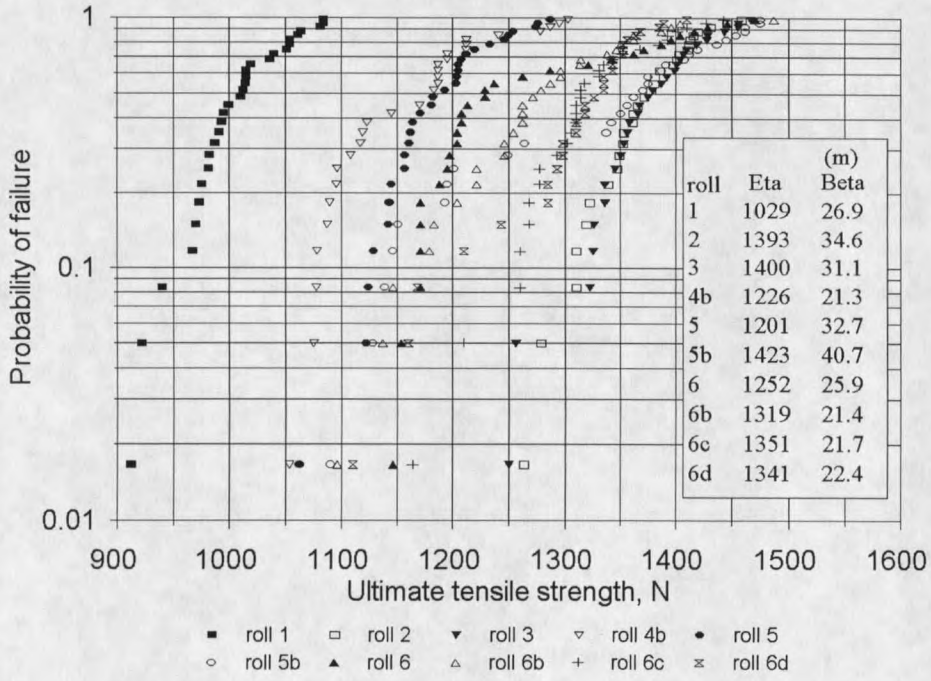


Figure 5.18. Strength distributions for strands from individual D155 rolls with Weibull fit parameters.

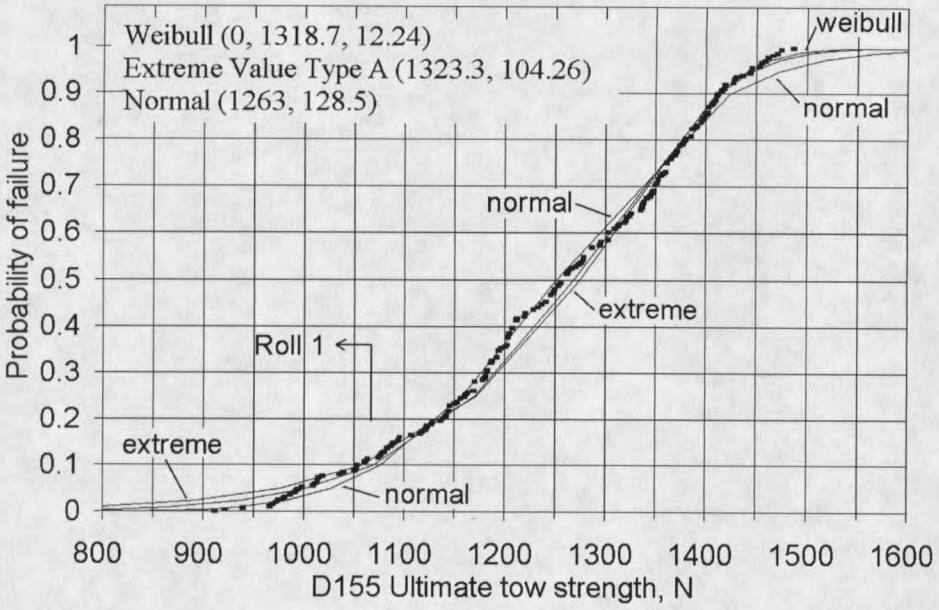


Figure 5.19. Weibull distribution of pooled D155 strand ultimate tensile strengths from rolls 1 through 6.

Fatigue tests were run with coupons from roll 4 and roll 5, which had significantly different static strengths (statistical p-value <0.0001), with the data shown in Figure 5.20. Although there was a statistical difference in the static strengths, past a fatigue lifetime of approximately a million cycles, little difference can be seen between the strands. This same check was performed on materials DD2 and DD2A in the database with the same conclusions (no difference).

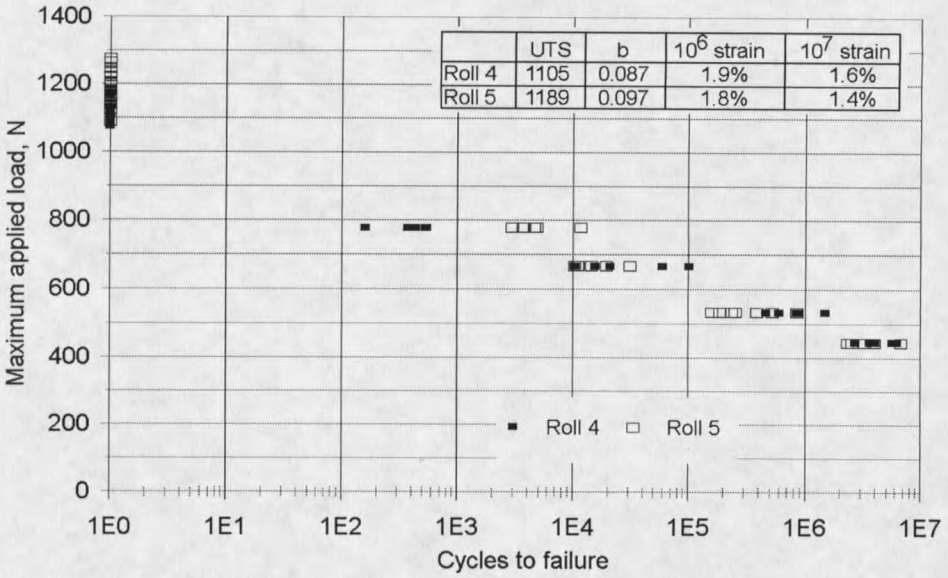


Figure 5.20. S-N fatigue data for D155 strands from D155 rolls 4 and 5.

Unidirectional Laminates

The strand data support the conclusion that the basic fatigue response is inherent in the glass fiber interactions. This section describes results for larger unidirectional specimens using laminates fabricated from fabrics, which include the complications of stitching, weaving and matrix rich areas. The unidirectional materials studied are listed in Table 5.3, with additional information about the fabrics and composites listed in the database.

Various authors have reported that the degradation in composite materials under fatigue loading results from the accumulation of stable cracking in the matrix and fiber-matrix interface [51]. This stable cracking increases in severity with cyclic loading, resulting in the gradual decrease in mechanical properties until final failure by overloading. Figure 5.21, from Reference 51, shows the generally accepted progression of

damage in a composite during fatigue. Further information on fatigue damage accumulation can be found in Reference 51. It is believed that this increased amount of damage in the matrix and at the matrix/fiber interface is what decreases the larger coupon fatigue behavior from the individual strand behavior.

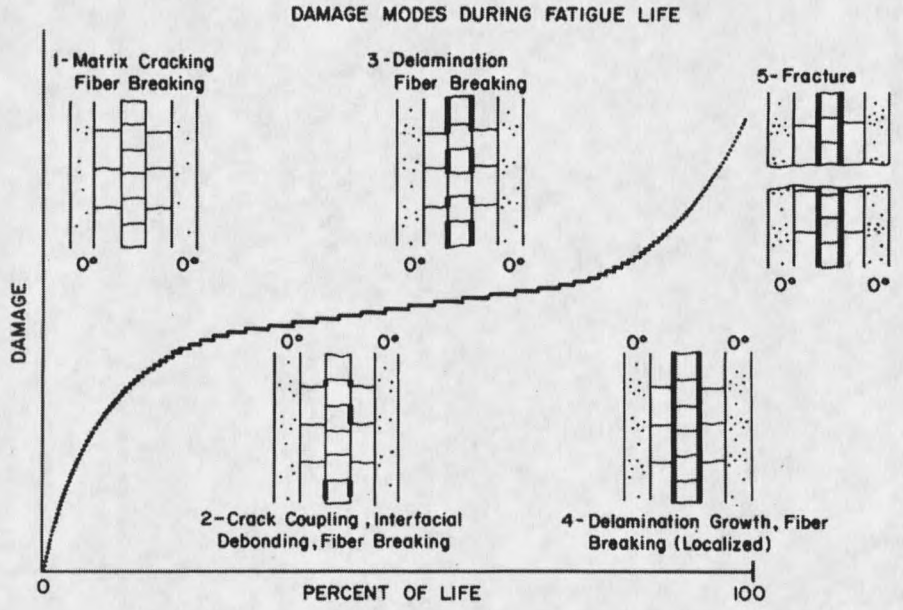


Figure 5.21. Schematic representation of the development of damage during the fatigue life of a multidirectional composite laminate. [51]

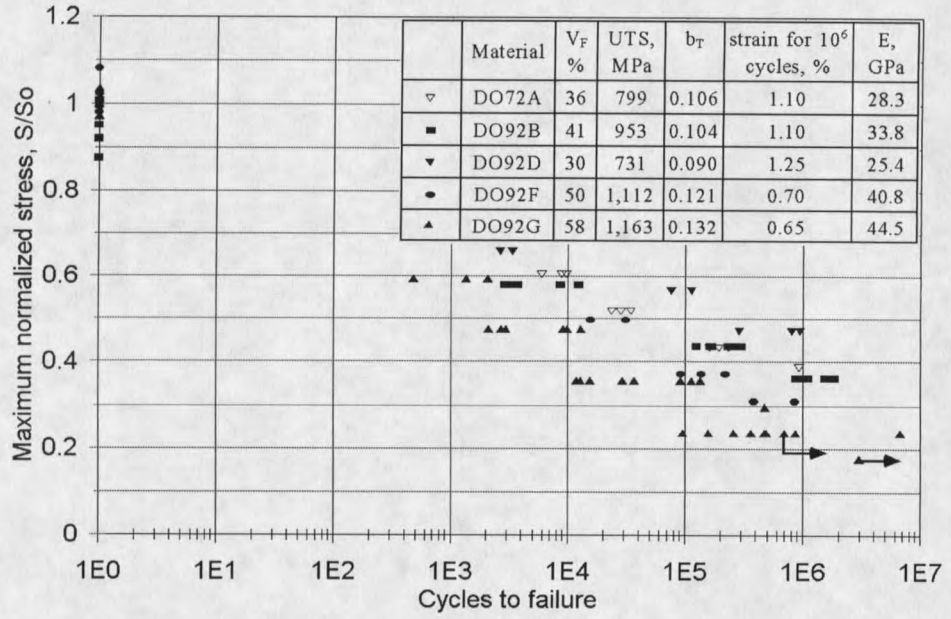
Figures 5.22 to 5.29 show the normalized fatigue data and the initial fatigue strains for the materials listed in Table 5.4. Even though the increasing fiber content raises the static modulus and ultimate tensile strength, the fatigue performance deteriorates significantly on either a normalized (b-value, equation 4.2) or absolute (strain at 10^6 cycles) basis, as the fiber content increases. The latter parameter is the value of maximum initial strain which the material can withstand for 10^6 cycles.

Table 5.3. Summary of fatigue properties for the unidirectional materials tested.

		R = 10			R = 0.1			
Material*	V_F	UCS MPa	b_C	strain for 10^6 cycles, %	UTS, MPa	b_T	strain for 10^6 cycles, %	E GPa
A060	0.41	-315	----	----	579	0.094	0.80	31.4
A130C	0.35	-373	0.062	-0.70	728	0.091	1.10	31.6
A130G	0.55	-423	----	-----	1,203	0.133	0.70	44.4
A260A	0.35	-440	----	-----	776	0.090	1.11	31.1
CM1701	0.38	-573	0.084	-0.93	796	0.126	0.64	30.5
DO72A	0.36	-560	0.075	-1.11	799	0.106	1.04	28.3
DO92B	0.41	-675	----	-----	908	0.104	1.03	33.8
DO92D	0.30	-540	----	-----	731	0.090	1.25	25.4
DO92F	0.50	-679	----	-----	1,112	0.121	0.70	40.8
DO92G	0.58	-692	0.085	-0.97	1,163	0.132	0.60	44.5
D155B	0.39	-653	0.077	-1.10	854	0.102	1.12	31.5
D155C	0.51	-794	----	-----	1,187	0.120	0.90	38.9
D155G	0.59	-765	0.057	-1.00	1,314	0.138	0.64	47.0
D155H	0.49	-755	----	-----	1,121	0.099	1.07	38.3
D155J	0.58	-776	----	-----	1,142	0.108	0.80	47.9
D155K	0.33	-551	----	----	861	0.114	0.98	28.1

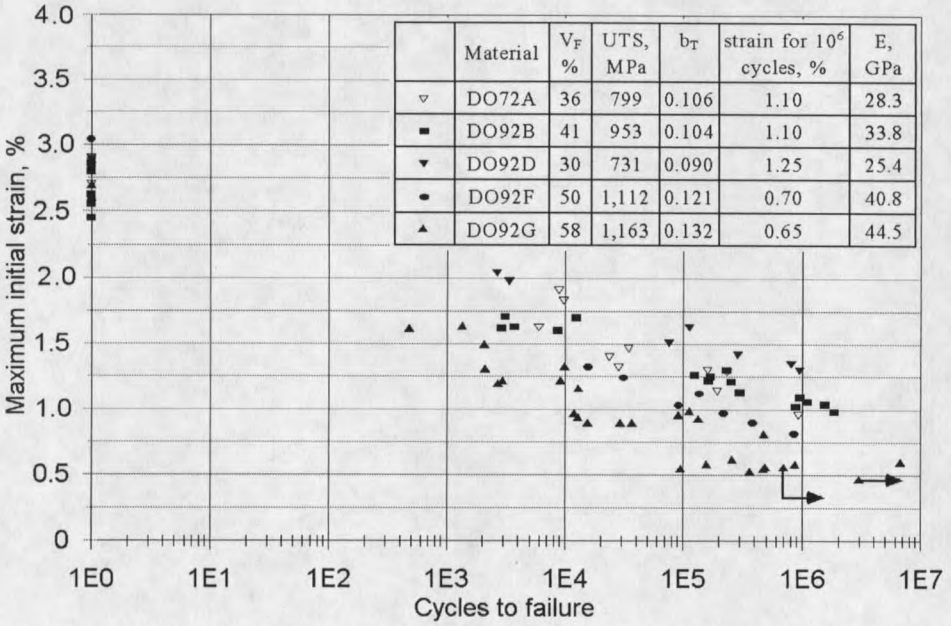
* Reinforcing fabric designation followed by a letter designation where more than one fiber content was tested for that fabric (see Appendix A for more details).

In all cases, the 10^6 cycle strain was less than 1 percent for $V_F > 0.50$. Materials D155H and D155J had the stitching thread removed from the gage length prior to RTM manufacturing, which caused an 10^6 cycle strain improvement from 0.64 to 0.80 percent strain at a fiber volume fraction of 0.58. The tensile strength of the D155J (no stitching) was lower than D155G, which probably resulted from some minor strand misalignment and/or the strength variation noted earlier for the D155 fabrics.



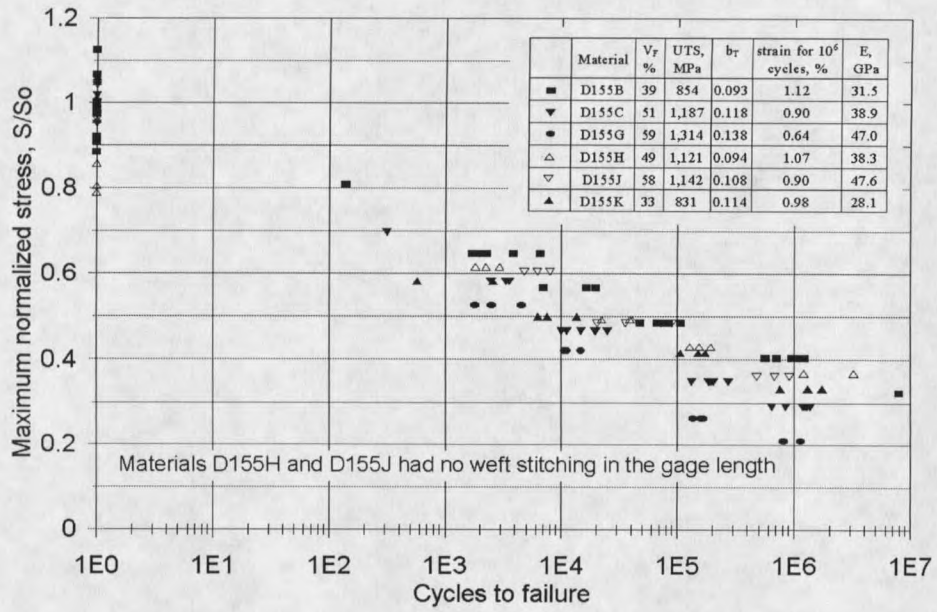
	Material	V_F %	UTS, MPa	b_T	strain for 10^6 cycles, %	E, GPa
▽	DO72A	36	799	0.106	1.10	28.3
■	DO92B	41	953	0.104	1.10	33.8
▼	DO92D	30	731	0.090	1.25	25.4
●	DO92F	50	1,112	0.121	0.70	40.8
▲	DO92G	58	1,163	0.132	0.65	44.5

Figure 5.22. Normalized fatigue data for fabrics D072 and D092, R = 0.1.



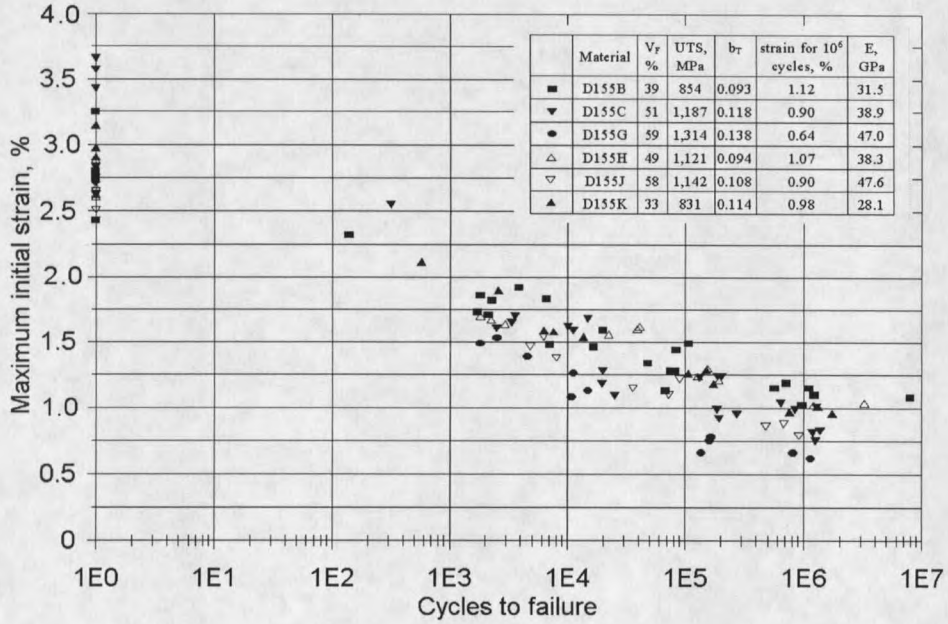
	Material	V_F %	UTS, MPa	b_T	strain for 10^6 cycles, %	E, GPa
▽	DO72A	36	799	0.106	1.10	28.3
■	DO92B	41	953	0.104	1.10	33.8
▼	DO92D	30	731	0.090	1.25	25.4
●	DO92F	50	1,112	0.121	0.70	40.8
▲	DO92G	58	1,163	0.132	0.65	44.5

Figure 5.23. Maximum initial fatigue strain data for fabrics D072 and D092, R = 0.1.



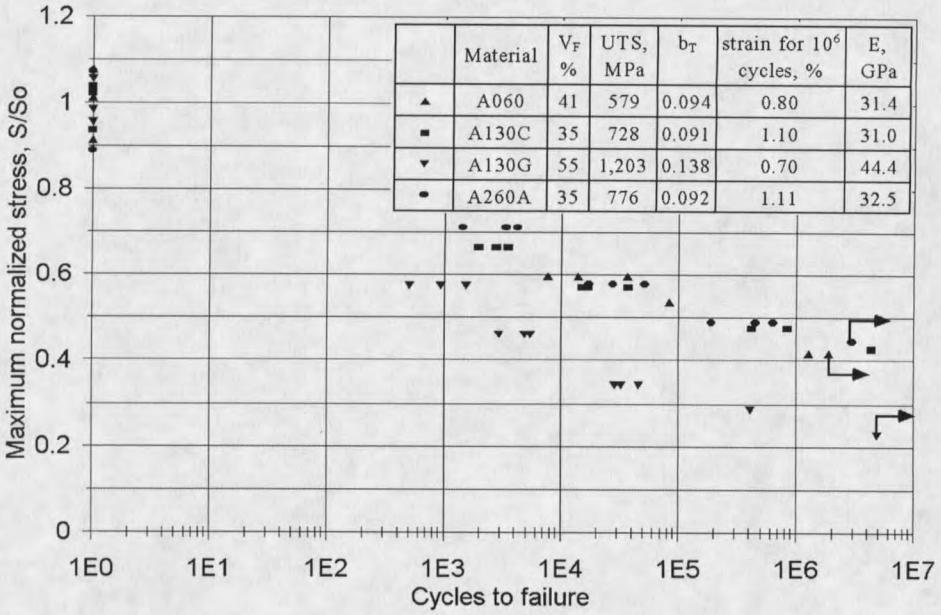
	Material	V_f %	UTS, MPa	b_T	strain for 10^6 cycles, %	E, GPa
■	D155B	39	854	0.093	1.12	31.5
▼	D155C	51	1,187	0.118	0.90	38.9
●	D155G	59	1,314	0.138	0.64	47.0
△	D155H	49	1,121	0.094	1.07	38.3
▽	D155J	58	1,142	0.108	0.90	47.6
▲	D155K	33	831	0.114	0.98	28.1

Figure 5.24. Normalized fatigue data for D155 fabrics (with and without stitching), R = 0.1.



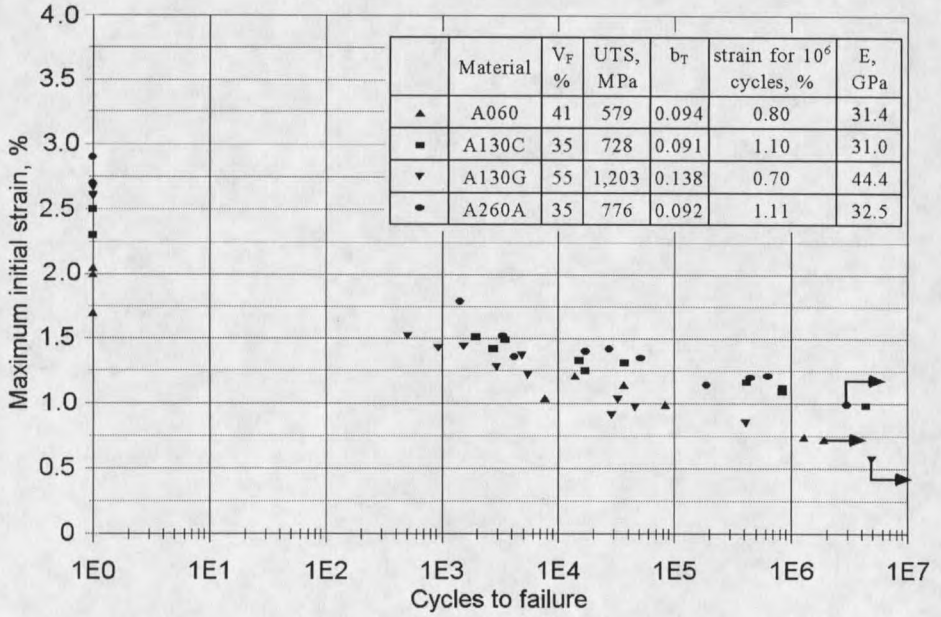
	Material	V_f %	UTS, MPa	b_T	strain for 10^6 cycles, %	E, GPa
■	D155B	39	854	0.093	1.12	31.5
▼	D155C	51	1,187	0.118	0.90	38.9
●	D155G	59	1,314	0.138	0.64	47.0
△	D155H	49	1,121	0.094	1.07	38.3
▽	D155J	58	1,142	0.108	0.90	47.6
▲	D155K	33	831	0.114	0.98	28.1

Figure 5.25. Maximum initial fatigue strain for D155 fabrics (with and without stitching), R = 0.1.



	Material	V_F %	UTS, MPa	b_T	strain for 10^6 cycles, %	E, GPa
▲	A060	41	579	0.094	0.80	31.4
■	A130C	35	728	0.091	1.10	31.0
▼	A130G	55	1,203	0.138	0.70	44.4
●	A260A	35	776	0.092	1.11	32.5

Figure 5.26. Normalized fatigue data for woven fabrics (A060, A130 and A260), R = 0.1.

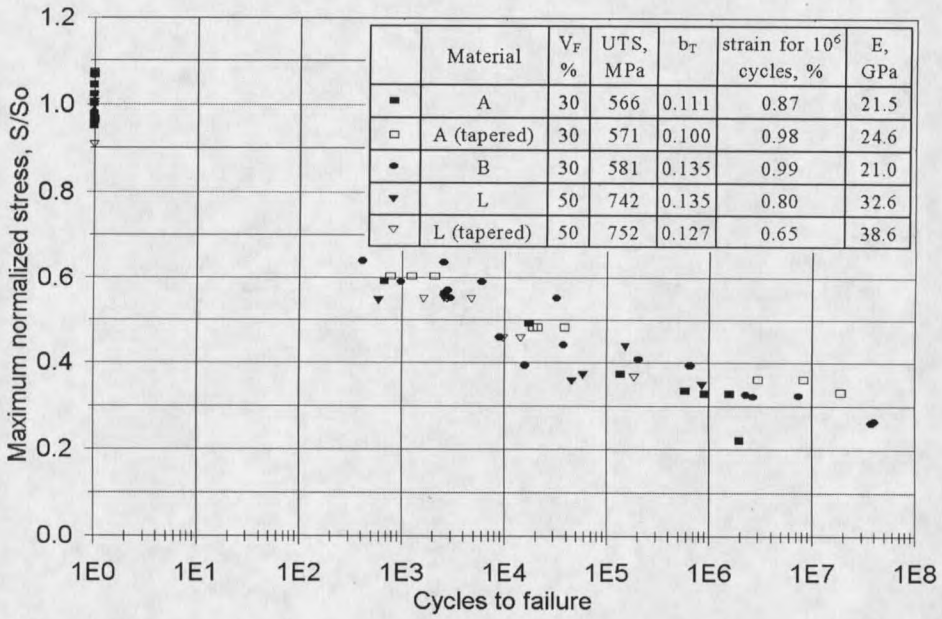


	Material	V_F %	UTS, MPa	b_T	strain for 10^6 cycles, %	E, GPa
▲	A060	41	579	0.094	0.80	31.4
■	A130C	35	728	0.091	1.10	31.0
▼	A130G	55	1,203	0.138	0.70	44.4
●	A260A	35	776	0.092	1.11	32.5

Figure 5.27. Maximum initial fatigue strain data for woven fabrics (A060, A130 and A260), R = 0.1.

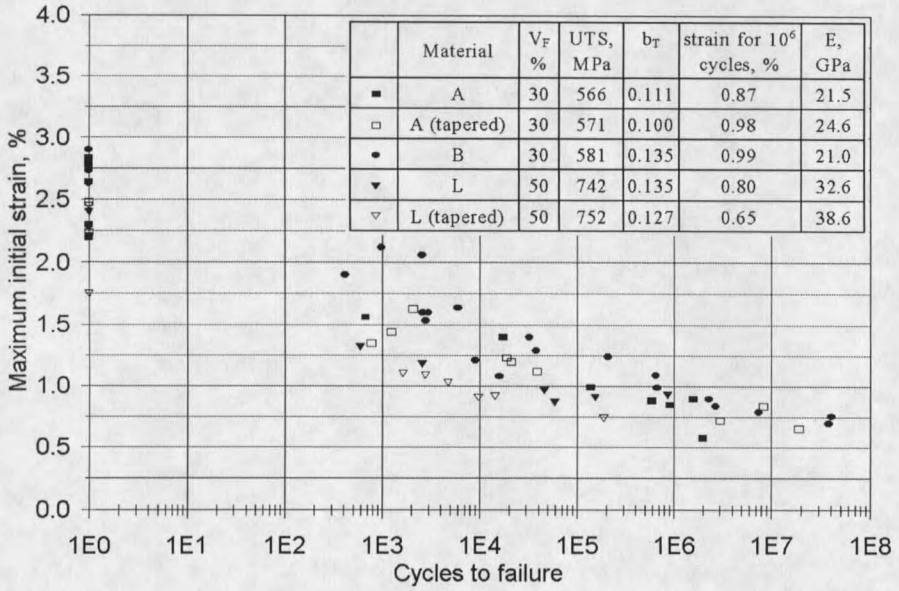
Figures 5.28 and 5.29 show the fatigue data for the standard and the thickness tapered unidirectional coupons for materials A, B and L (database material designations). These materials had some fiber misalignment away from the 0° load direction (up to 4°), which provided a lower static strength and reduced fatigue lifetimes but showed similar fatigue trends as the other unidirectional materials. The tapering reduced the amount of damage present in the coupon ends (hydraulically clamped areas), which improved the failure mode and the fatigue lifetime. Materials A and L had resin rich regions on the outside surfaces which, when thickness tapered, reduced the composite thickness without removing a representative amount of fiber, resulting in an overall longitudinal modulus increase.

Table 5.4 and Figure 5.30 give the tensile and compressive ultimate strains and the normalized fiber strength (UTS / V_F); dividing by V_F gives the stress per unit area of glass fiber, ignoring the matrix. The impregnated D155 strand average strength was 2,750 MPa, while the D155 composites averaged 2,220 MPa, which is a strength reduction of 19 percent; this reduction is probably due to the interaction with other strands and stitching, along with increased matrix cracking. The lighter weight A060 had a low tensile ultimate strain of 1.9 percent and a UTS/V_F ratio of 1,412 MPa, which indicated load carrying problems in the composite. Further inspection of the material determined that the weaving weft and thermoplastic bead were the same that were used for the heavier woven fabrics, giving a great out of plane distortion relative to the tow diameter.



	Material	V_F %	UTS, MPa	b_T	strain for 10^6 cycles, %	E, GPa
■	A	30	566	0.111	0.87	21.5
□	A (tapered)	30	571	0.100	0.98	24.6
●	B	30	581	0.135	0.99	21.0
▼	L	50	742	0.135	0.80	32.6
▽	L (tapered)	50	752	0.127	0.65	38.6

Figure 5.28. Normalized fatigue data for industrial materials A, B and L (with and without thickness tapering), R = 0.1.



	Material	V_F %	UTS, MPa	b_T	strain for 10^6 cycles, %	E, GPa
■	A	30	566	0.111	0.87	21.5
□	A (tapered)	30	571	0.100	0.98	24.6
●	B	30	581	0.135	0.99	21.0
▼	L	50	742	0.135	0.80	32.6
▽	L (tapered)	50	752	0.127	0.65	38.6

Figure 5.29. Maximum initial fatigue strain data for industrial materials A, B and L (with and without thickness tapering), R = 0.1.

Table 5.4. Summary of static properties for the unidirectional materials tested.

Material	V_F	UCS MPa	Compressive failure strain, %	UTS, MPa	Tensile failure strain, %	E GPa	UTS / V_F MPa
A060	0.41	-315	-1.0	579	1.8	31.4	1412
A130C	0.35	-373	-1.4	728	2.4	31.0	2080
A130G	0.55	-423	-1.1	1203	2.7	44.4	2187
A260A	0.35	-440	-1.4	776	2.5	31.1	2217
CM1701	0.38	-573	-1.9	796	2.6	30.5	2095
DO72A	0.36	-560	-2.0	799	2.8	28.3	2219
DO92B	0.41	-675	-2.0	908	2.7	33.8	2214
DO92D	0.30	-540	-2.1	731	2.9	25.4	2437
DO92F	0.50	-679	-1.7	1112	2.7	40.8	2224
DO92G	0.58	-692	-2.0	1163	2.6	44.5	2005
D155B	0.39	-653	-2.2	854	2.7	31.5	2190
D155C	0.51	-794	-2.0	1187	3.1	38.9	2327
D155G	0.59	-765	-1.6	1314	2.8	47.0	2227
D155H	0.49	-755	-2.0	1121	2.9	38.3	2288
D155J	0.58	-776	-1.6	1142	2.4	47.6	1969
D155K	0.33	-551	-2.0	861	3.1	28.1	2609

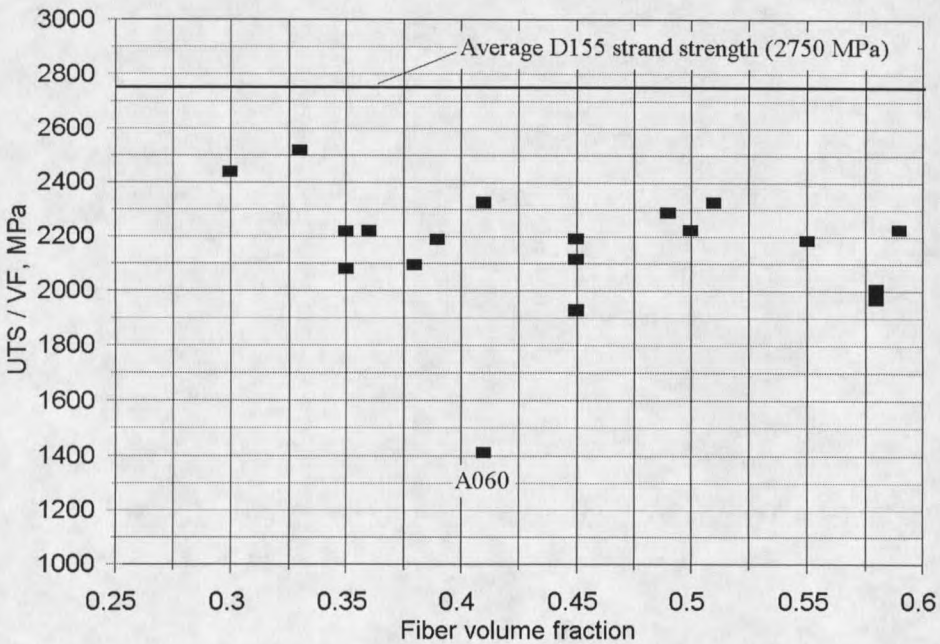


Figure 5.30. Fiber tensile strength (UTS/V_F) versus fiber content for unidirectional materials.

The thermoplastic bead was coating approximately 5 to 7 mm of the A060 strand every 30 mm, which did not bond to the matrix material and reduced the performance of the composite.

Figure 5.31 details the ultimate compressive stress versus the fiber volume fraction. The fabrics with the well aligned fibers form an increasing trend with V_F, while the woven fabrics (A060, A130 and A260) all fall significantly below this performance. Figure 5.32 shows the compressive failure strain versus the fiber volume fraction. As the fiber content increases, the compressive strain to failure decreases. The increasing compressive strength of the D155 fabric with V_F is more than offset by the increasing modulus, so the ultimate strain to failure decreases significantly with increasing V_F. The woven fabrics have a low ultimate compressive strain which does not significantly change over the fiber volume fraction range of 0.30 to 0.60.

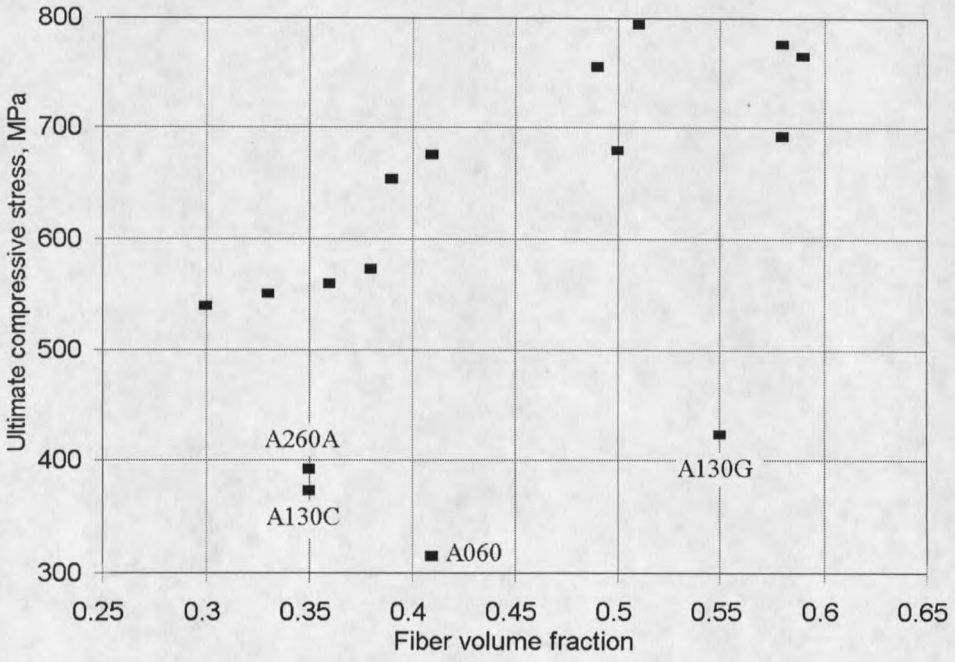


Figure 5.31. Ultimate compressive stress versus fiber volume for unidirectional materials.

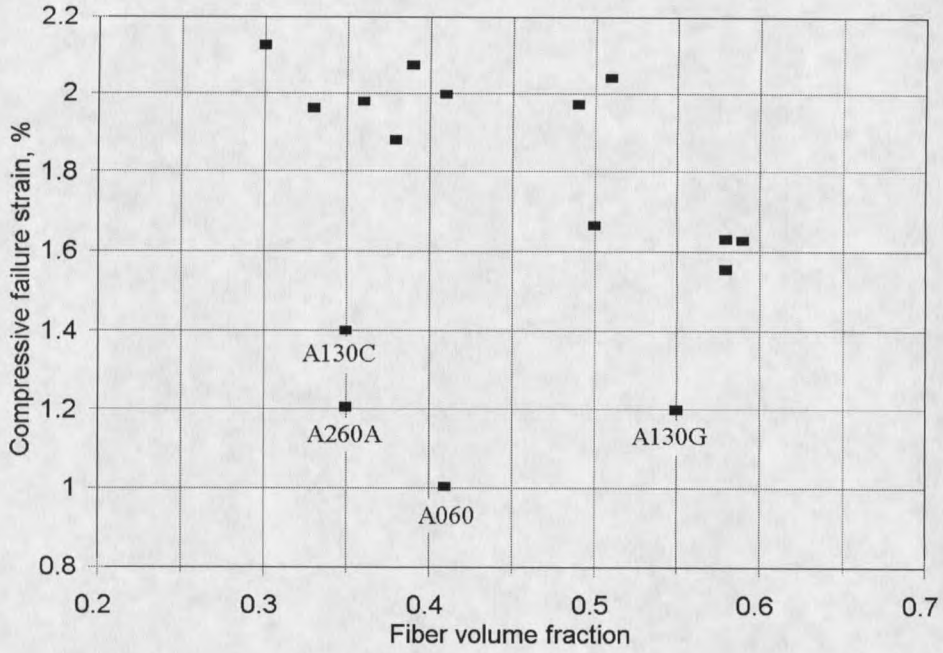


Figure 5.32. Compressive failure strain versus fiber volume for unidirectional materials.

Figure 5.33 shows the tensile million-cycle strain (R=0.1) versus fiber content. As the fiber content is increased, the million-cycle strain decreases. Thus, there is a significant transition to increased fatigue sensitivity in the fiber content range shown. Both the woven and the stitched fabrics are converging to the same strain at fiber volume fractions greater than 0.55. The D155H and D155J materials, which had the weft stitching removed, show the same strain reduction behavior with fiber content as the other unidirectional materials, but the transition occurs at a higher V_F, and their overall strain performance was significantly higher than the stitched or woven fabrics (shifted to the right in Figure 5.33). Figure 5.34 shows the fatigue coefficient, b (R=0.1), changing with fiber content, again with the non-stitched materials performing better. As noted earlier (Figure 5.5), the number of fiber contacts also increase in the range of fiber volume

fraction from 0.3 to 0.4, which may partially explain this trend.

Figure 5.35 shows the normalized compression (R=10) data for the various unidirectional materials. Except for the woven A130C material, the stitched fabric materials showed some ultimate compressive strength increase with increasing fiber content, but the strain at one million cycles was relatively unchanged (-0.97 to -1.11 percent strain) for this group of materials.

The tensile behavior for the fiber strands compared with that of the composites are shown in Figure 5.36. The strands show better performance (as expected) than the composites, apparently due to a smaller volume and a lack of interaction with matrix cracks and other plies. The composites have a fatigue strain performance of approximately 50 percent of the strand strain, depending on V_F; a similar ratio exists in the static tensile data at N = 1. The D155H and D155J materials have a strain performance slightly higher than the other composites, but few points were tested past 10^6 cycles to determine if this performance holds at higher cycles. The lower V_F composites are following a similar trend (b-value) as the strand data, and there appears to be a change in the slope of the trend line in the 10^7 to 10^8 cycle range. More composite data in this cycle range is required to determine if the slope is changing enough to attain a fatigue limit, or whether it is simply following a power law trend.

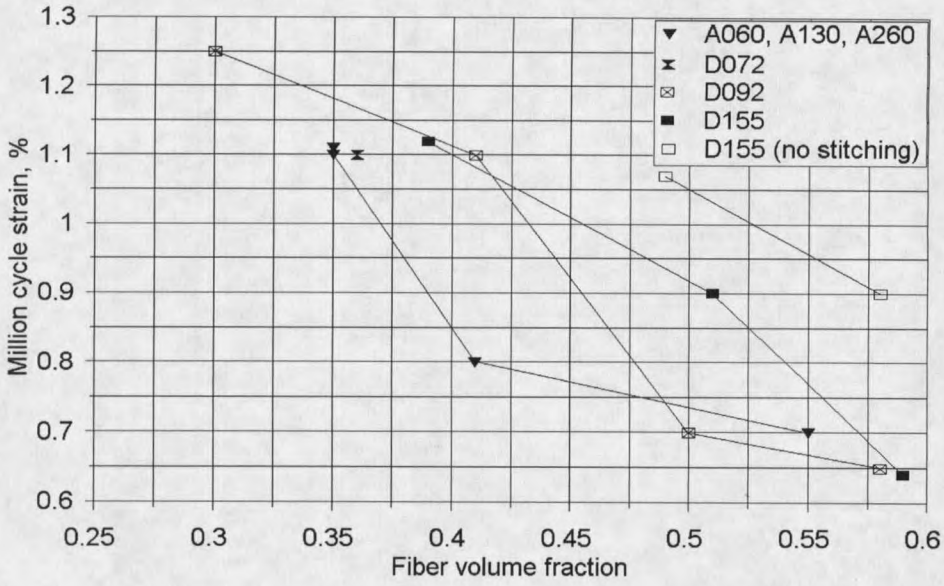


Figure 5.33. Million cycle tensile strain versus fiber volume for unidirectional materials, R=0.1.

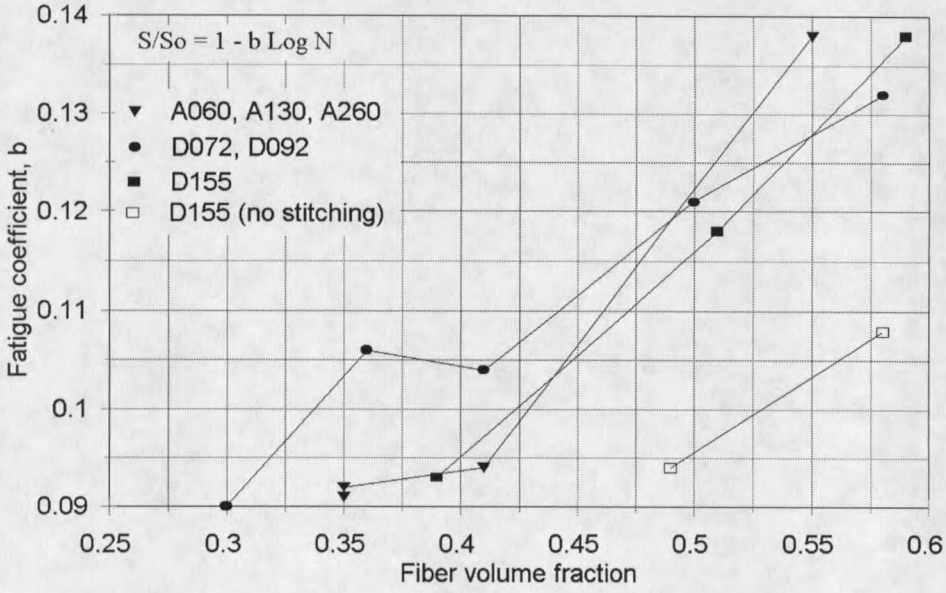
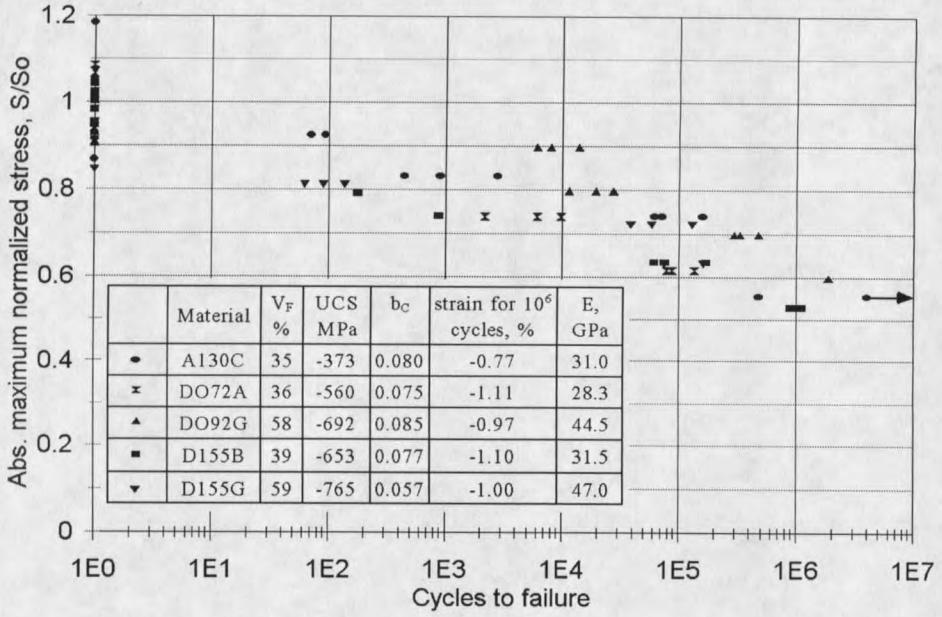


Figure 5.34. Tensile fatigue coefficient, b, versus fiber volume for unidirectional materials.



	Material	V_F %	UCS MPa	b_C	strain for 10^6 cycles, %	E, GPa
•	A130C	35	-373	0.080	-0.77	31.0
x	DO72A	36	-560	0.075	-1.11	28.3
▲	DO92G	58	-692	0.085	-0.97	44.5
■	D155B	39	-653	0.077	-1.10	31.5
▼	D155G	59	-765	0.057	-1.00	47.0

Figure 5.35. Normalized compressive fatigue data for various unidirectional materials, R = 10.

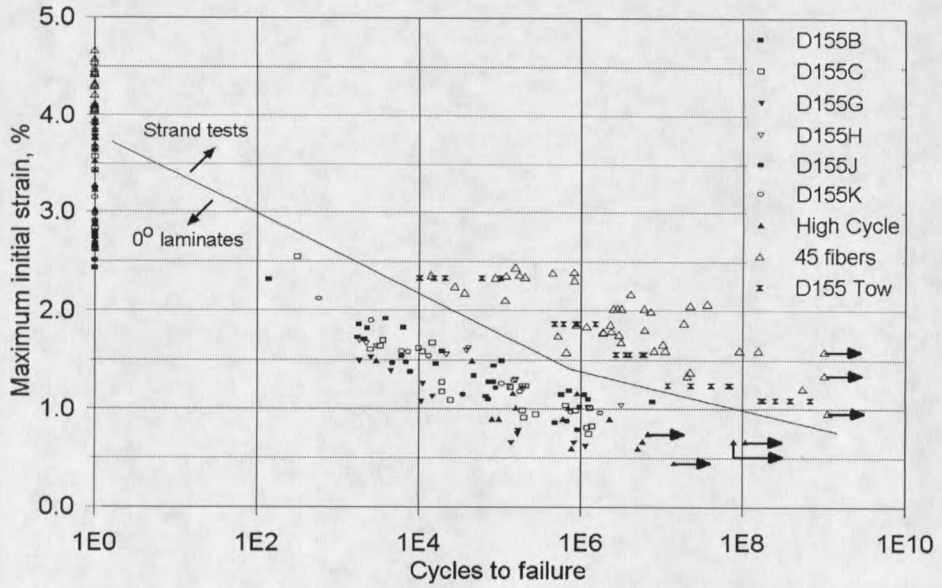


Figure 5.36. Comparison of maximum initial fatigue strain data for various unidirectional materials and impregnated strand tests, R = 0.1.

±45° Fabrics

Three different ±45° stitched fabrics at multiple fiber contents were fatigue tested: DB120, DB240 and DB400; the data are summarized in Table 5.5 (these tests were conducted with the load in the 0° direction). The ±45° materials are expected to behave differently from the 0° materials because they are matrix dominated. The ±45° materials fail by the growth of matrix cracks parallel to the fibers of each ply, followed by the interlaminar separation of the plies. The DB120 fabric is the same ±45° fabric used in the construction of the CDB200 triax fabric; the DB240 fabric uses the same glass strand that is used in the D155 and A130 fabrics. Additional static and fatigue tests were performed on materials using orientated D155 fabric, in a $(\pm 45°)_3$ composite using different matrix materials. Due to difficulties in maintaining a ±45° lay-up with the DB120 and DB240 fabrics, the D155 fabric was used to control the fiber angles so that any variability seen would not be due to the fiber orientation.

Figure 5.32 shows the normalized maximum stress diagram for the materials constructed with the DB120 fabrics under tension-tension (R=0.1) and compression-compression (R=10) fatigue loading. The DB240 and DB400 fabrics showed similar normalized stress trends. Figure 5.37 includes fatigue data from material CH20, which consisted of the DB120 fabric stitched to a glass mat, and the 3M-SP250 prepreg data. Figures 5.38, 5.39 and 5.40 show the maximum initial strains for these ±45° composites; generally, the compressive (R=10) fatigue strain is higher than the tensile (R=0.1) strain (as expected). An interesting observation about these two figures is that the prepreg

Table 5.5. Summary of the ±45° materials tested

		R = 10			R = 0.1			
Material	V_F %	UCS, MPa	b_c	strain for 10^6 cycles, %	UTS, MPa	b_T	strain for 10^6 cycles, %	E GPa
DB120 fabrics								
CH20	25	-230	----	----	133	0.118	0.38	10.9
CH5	28	-190	0.105	-0.85	139	0.123	0.54	8.5
CH4	40	-171	0.112	-0.48	155	0.124	0.48	11.4
CH9	49	-174	0.106	-0.67	151	0.133	0.51	10.3
DB240 fabrics								
CH10	33	-163	0.126	-0.64	120	0.108	0.58	8.1
CH	45	-178	0.105	-0.50	145	0.104	0.46	13.6
CH11	54	-189	0.106	-0.58	134	0.114	0.38	13.4
DB400 fabrics								
CH8	39	-146	0.151	-0.35	93	0.113	0.38	10.0
CH9	49	-174	0.106	-0.67	151	0.133	0.51	10.3
3M-SP250 Prepreg								
PP45	54	-160	----	----	155	0.101	0.34	17.9
Angle plies manufactured with D155 fabric and different matrix materials								
±45 P	38	-138	0.089	-0.65	107	0.109	0.40	9.79
±45V2	36	-149	0.085	-0.71	136	0.119	0.45	10.3
±45P2	40	-160	----	----	96	0.109	0.35	11.4
±45 V	40	-154	----	----	121	0.110	0.40	10.7
90 P	38	-123	0.062	-1.00	27	0.083	0.20	7.34
90V2	38	-171	----	----	54	0.107	0.21	8.85
90 V	40	-167	----	----	49	0.108	0.18	10.3
90 E2	38	-152	----	----	40	0.110	0.18	7.28
Matrix Abbreviations: E2 -Epoxy (SC14), P -Ortho-polyester (COR63AX051), P2 -Iso-polyester (COR75AQ010), V-Vinyl ester (Derakane 411C), V2 -Vinyl ester (Derakane 8084)								

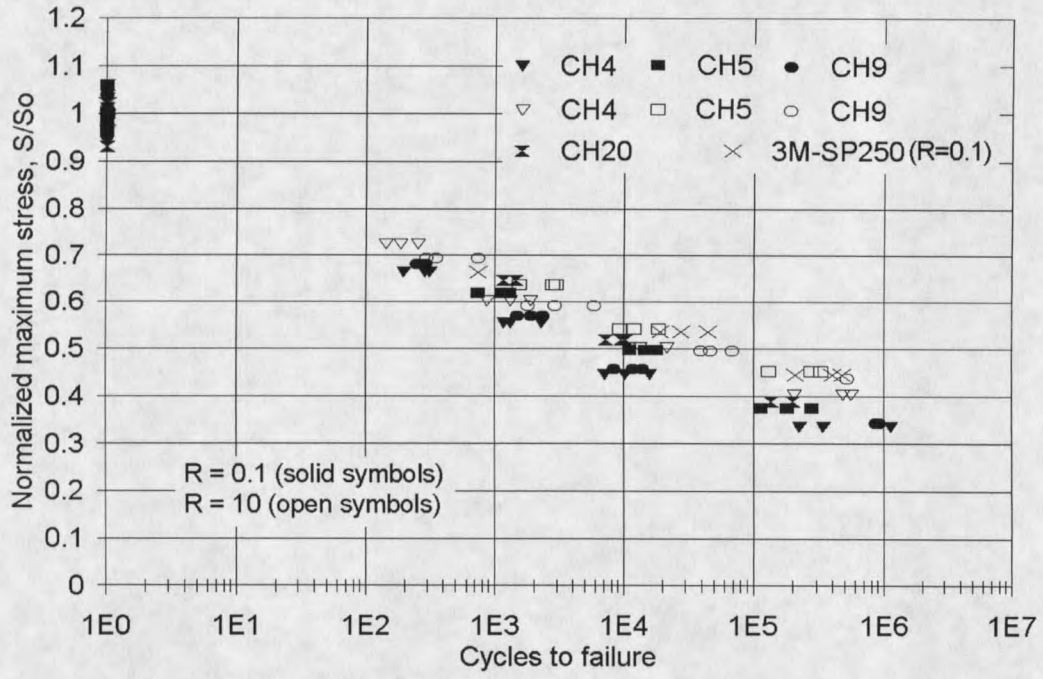


Figure 5.37. Normalized Fatigue SN data for materials with DB120 ±45 fabric (R=0.1 and 10).

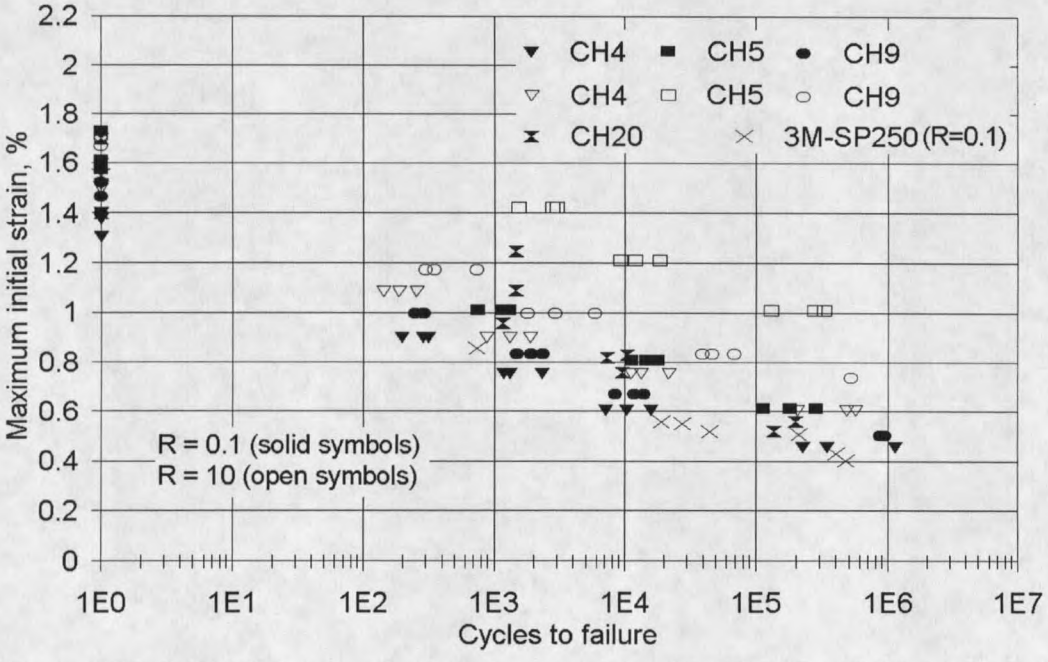


Figure 5.38. Initial fatigue strain data for materials with DB120 ±45 fabric (R=0.1 and 10).

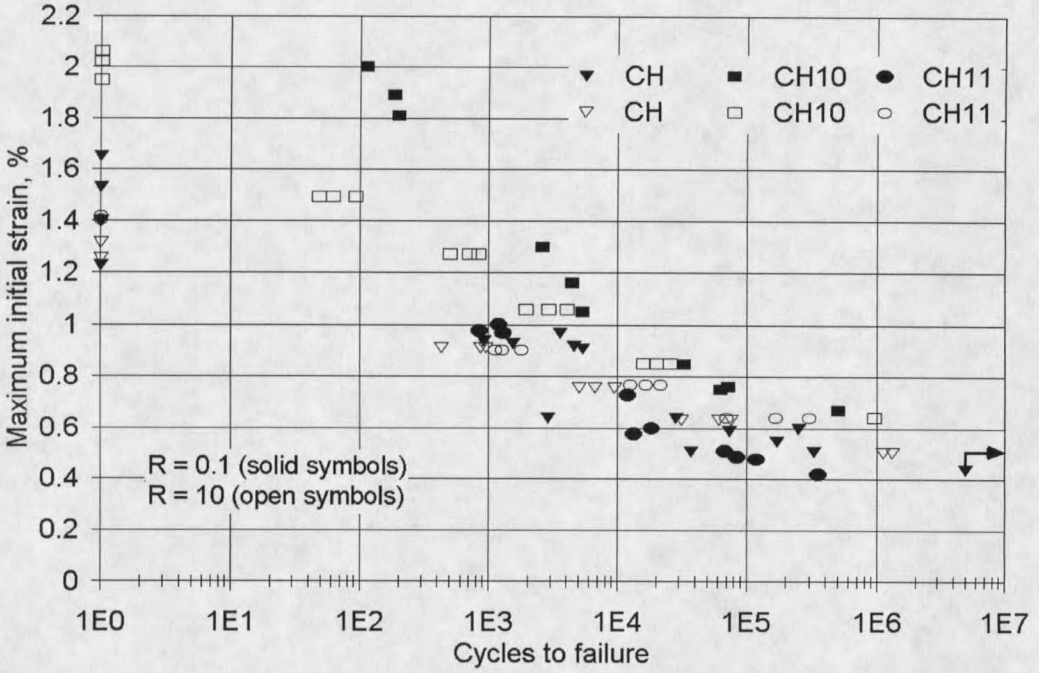


Figure 5.39. Initial fatigue strain data for materials with DB240 ±45 fabric (R=0.1 and 10).

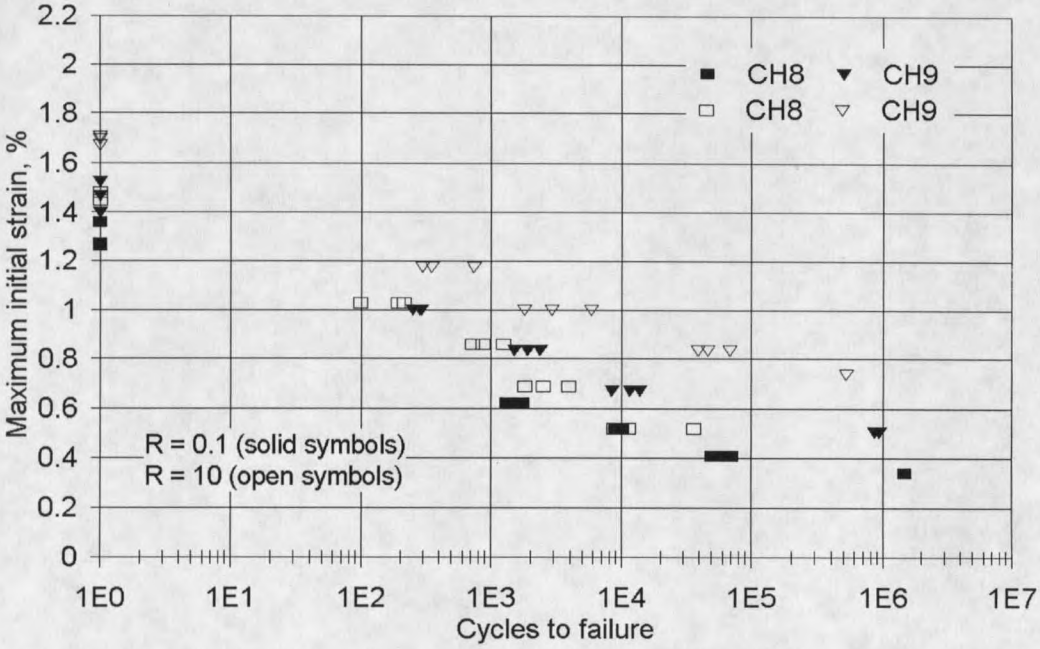
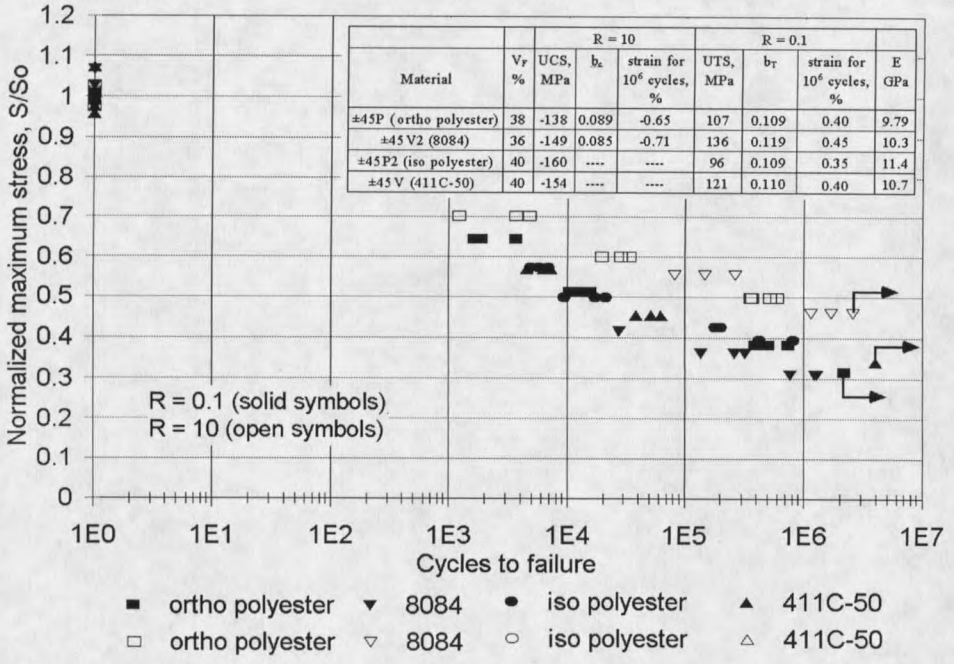


Figure 5.40. Initial fatigue strain data for materials with DB400 ±45 fabric (R=0.1 and 10).



Material	V_F %	R = 10 UCS, MPa	R = 10 b_c	R = 10 strain for 10^6 cycles, %	R = 0.1 UTS, MPa	R = 0.1 b_T	R = 0.1 strain for 10^6 cycles, %	E GPa
±45P (ortho polyester)	38	-138	0.089	-0.65	107	0.109	0.40	9.79
±45 V2 (8084)	36	-149	0.085	-0.71	136	0.119	0.45	10.3
±45P2 (iso polyester)	40	-160	----	----	96	0.109	0.35	11.4
±45 V (411C-50)	40	-154	----	----	121	0.110	0.40	10.7

Figure 5.41. Normalized fatigue SN data for ±45 composites constructed with D155 fabric and different matrix materials (R=0.1 and 10).

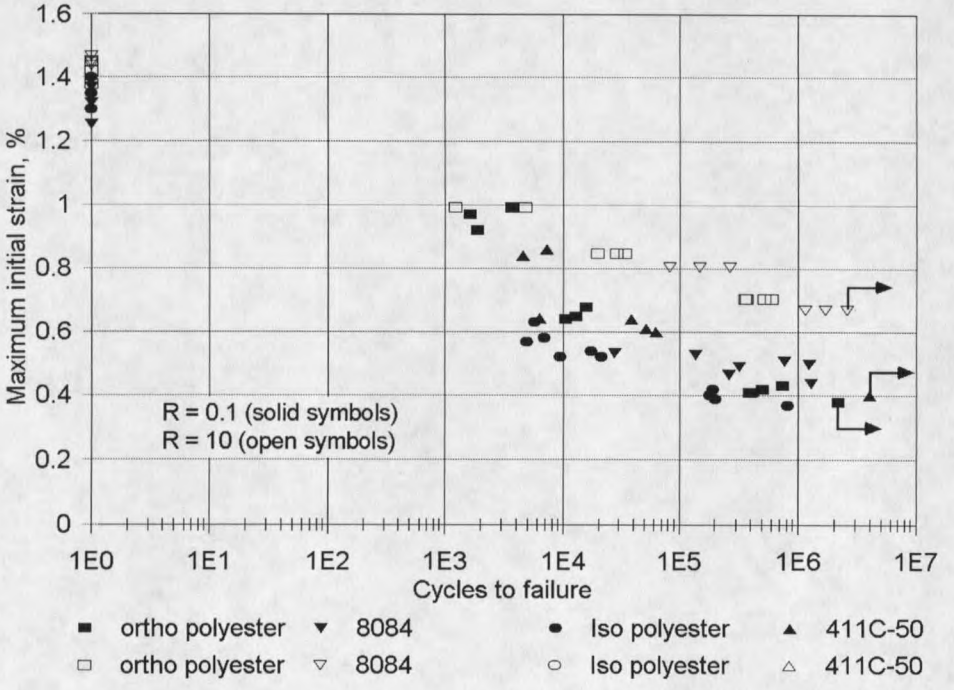


Figure 5.42. Initial fatigue strain data for ±45 composites constructed with D155 fabric and different matrix materials (R=0.1 and 10).

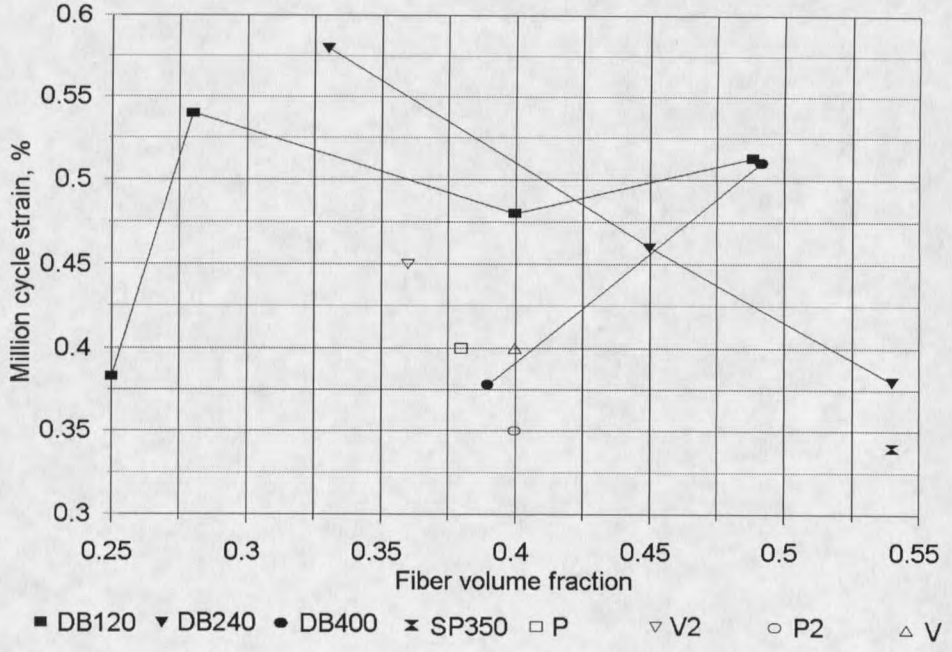


Figure 5.43. Million cycle strain versus fiber volume fraction for ±45 materials.

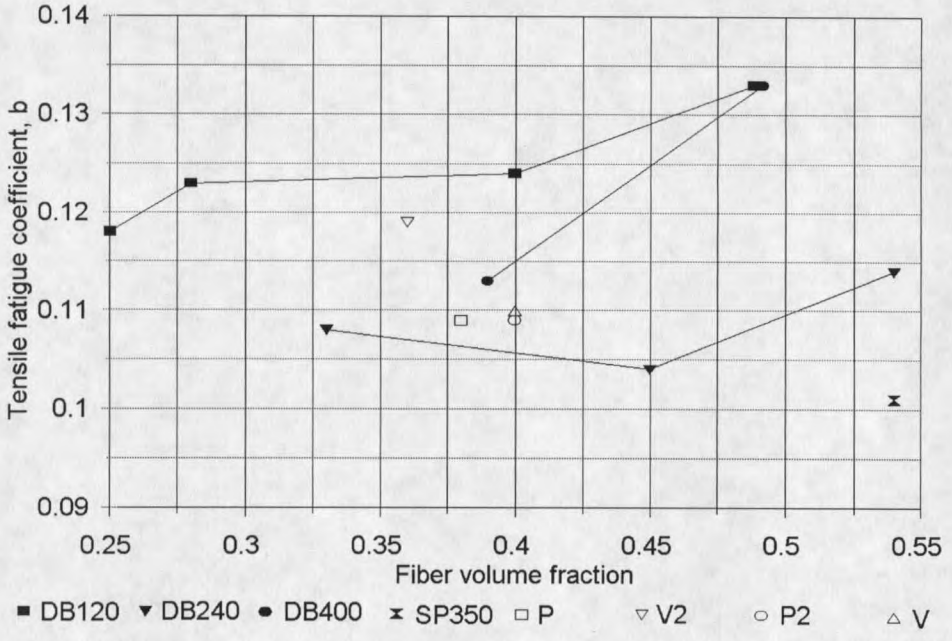


Figure 5.44. Tensile fatigue coefficient, b, versus fiber volume fraction for ±45 materials.

material shows higher than average normalized stress behavior, while performing below average in fatigue strain.

The DB120 fabric provided a higher static strength for a specific fiber content than the DB240 or DB400. Above a fiber volume fraction of approximately 0.45, the tensile strength and modulus of these composites start to decrease with increasing fiber content; a reason for this has not been determined, but may be associated with an increase in micro-porosity within the strands. Thinner plies have been reported to have a higher fatigue resistance due to reduced resin thickness and interlaminar stresses [52-56].

Figures 5.41 and 5.42 show the fatigue data for the D155 constructed ±45° materials using four different resins. Despite the matrix dominated properties of the ±45° materials, there is no significant fatigue difference in the performance of the different resins under R=0.1 or 10 fatigue loading. The results are similar to the results of the 90° materials tests, also listed in Table 5.5

Figure 5.43 details the million cycle tensile strain versus the fiber volume fraction, and Figure 5.44 shows the tensile fatigue coefficient, b, versus the fiber volume fraction. No consistent fatigue trends with fiber volume content are evident for the ±45° laminates.

Materials With Varying Amounts of ±45° and 0° Plies

The ±45° and 0° fabrics were assembled in different combinations to obtain different percentages of 0° plies in the composites. The design of structures like turbine blades or I-beams require a material with a high shear strength and modulus for the web and a material with a high axial strength and modulus for the main spar caps and flanges.

Higher ±45° content provides higher shear properties, while high 0° content provides high axial properties. While these are the main drivers in the engineering of laminates, all the materials must have adequate fatigue resistance at the strain levels imposed in service.

Fatigue Trends

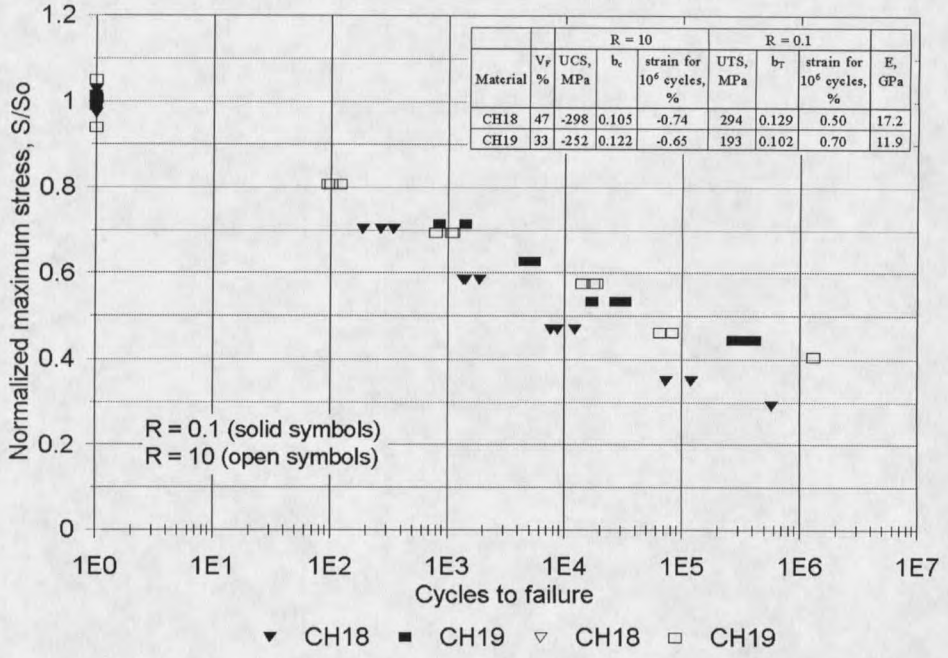
Figures 5.45 through 5.56 detail the fatigue resistance in terms of normalized maximum stress and the maximum initial strain for the materials with 16, 24, 28, 39, 50 and 55 to 63 percent 0° plies at R=0.1 and 10; these materials also differ in overall fiber content as noted. Materials with 16 percent 0° (Figure 5.46) behave similar to the ±45° fabrics previously discussed, with the compressive fatigue strains being at or better than the tensile fatigue strains. At 24 percent 0° (Figure 5.48) the tensile fatigue strains are higher than the compressive strains for most of the fatigue trend and converge around 10^6 cycles. For materials with increasing amounts of 0° material (28, 39 and 50 percent), the difference in initial fatigue strain performance between tensile (R=0.1) or compressive (R=10) fatigue at 10^6 cycles becomes smaller, and at 55 to 63 percent 0° (Figures 5.55 and 5.56), the fatigue trends of the materials show a reduced amount of scatter. These figures show the FF materials (FFA, FFB, FFC, FFD and FFF) which all had the same fabrics, but with different lay-ups, to study the effect of ply stacking sequence. There were no statistical differences between the materials or their failure modes with these fabrics and a fiber volume fraction of 0.38. This may not be observed if significant flaws were introduced, [57] studying carbon fiber composites with 0°, ±45°, and 90° plies with through thickness holes did find a difference of fatigue properties with stacking sequence.

Table 5.6. Summary of materials with 16 to 63 percent 0's.

		R = 10			R = 0.1			
Material (% 0's)	V_F %	UCS, MPa	b_c	strain for 10^6 cycles, %	UTS, MPa	b_T	strain for 10^6 cycles, %	E, GPa
16% 0's (D092 0° and DB240 ±45°)								
CH19	33	-252	0.122	-0.65	193	0.102	0.70	11.9
CH18	47	-298	0.105	-0.74	294	0.129	0.50	17.2
24% 0's (D155 0° and DB240 ±45°)								
CH3	36	-318	0.127	-0.60	336	0.112	0.64	16.8
CH2	41	-342	0.110	-0.70	362	0.127	0.65	16.7
CH13	48	-385	0.107	-0.60	423	0.145	0.48	23.2
28% 0's (D092 0° and DB120 ±45°)								
CH15	32	-345	0.100	-1.02	309	0.103	0.85	14.8
CH16	40	-309	0.085	-0.80	360	0.129	0.68	18.5
CH17	48	-301	0.079	-0.94	359	0.139	0.40	17.6
39% 0's (D155 0° and DB120 ±45°)								
CH23	32	-448	0.106	-0.90	394	0.140	0.40	18.5
CH12	34	-451	0.092	-1.15	398	0.099	0.94	17.4
CH14	44	-412	0.081	-1.00	517	0.134	0.75	21.0
CH6	49	-408	0.100	-0.80	502	0.139	0.50	21.5
50% 0's (various triax materials)								
R	31	-330	----	----	441	0.104	0.98	16.5
AA	35	-348	0.081	-0.95	452	0.140	0.50	18.8
N	36	-318	0.096	-0.70	468	0.140	0.46	19.3
AA4	37	-449	----	----	377	0.105	0.67	20.4
M	38	-286	----	----	516	0.141	0.40	20.7
AA3	51	-284	----	----	478	0.140	0.40	25.2
55 to 63% 0's (D100, D155, A130 0° and DB120 ±45°)								
CC (55)	39	-459	----	----	561	0.121	0.80	21.7
FFA (56)	38	-553	----	----	716	0.123	0.80	24.2
FFB (56)	38	-506	----	----	621	0.119	0.80	23.4
FFC (56)	38	-499	----	----	624	0.121	0.79	22.9
FFD (56)	38	-542	----	----	636	0.120	0.83	23.1
FFF (56)	38	-596	----	----	664	0.123	0.80	23.9
BB (62)	42	-308	----	----	725	0.131	0.80	25.2
CC2 (63)	45	-527	----	----	715	0.118	0.79	26.6
CC3 (63)	45	-541	----	----	682	0.112	0.85	26.3

Table 5.7. Summary of Materials with 69 to 85 percent 0° plies.

		R = 10			R = 0.1			
Material (% 0's)	V_F %	UCS, MPa	b_c	strain for 10^6 cycles, %	UTS, MPa	b_T	strain for 10^6 cycles, %	E, GPa
P (69)	40	-466	0.094	-0.66	667	0.134	0.48	22.5
DD22 (70)	30	-389	----	----	549	0.100	1.13	19.6
DD24 (70)	39	-511	----	----	730	0.115	1.05	23.9
DD6 (72)	31	-505	0.071	-1.40	605	0.100	1.15	21.1
DD11(72)	31	-319	0.090	-0.70	592	0.100	1.20	20.0
DD14 (72)	35	-428	----	----	728	0.133	0.60	25.1
DD5V2 (72)	35	-605	0.064	-1.66	787	0.102	1.39	22.3
DD5E (72)	36	-521	0.056	-1.42	674	0.102	1.10	23.6
DD5P (72)	36	-574	0.072	-1.35	661	0.101	1.16	24.2
DD5V (72)	36	-530	0.057	-1.48	675	0.102	1.11	23.7
DD5 (72)	38	-534	----	----	724	0.104	1.15	25.2
DD2 (72)	42	-581	0.079	-1.15	752	0.110	0.95	27.0
DD2A (72)	42	----	----	----	986	0.122	0.94	28.0
DD8 (72)	42	-582	----	----	778	0.102	0.90	27.1
DD12 (72)	43	-302	----	----	723	0.114	0.85	26.4
DD4 (72)	50	-541	----	----	886	0.136	0.55	31.0
DD13 (72)	50	-314	0.094	-0.45	821	0.130	0.80	29.5
DD7 (72)	54	-581	0.072	-1.03	832	0.147	0.40	32.0
DD9 (72)	54	-556	----	----	907	0.137	0.46	34.6
DD10 (72)	62	-552	0.052	-0.90	956	0.143	0.35	42.5
DD20 (73)	34	-313	----	----	587	0.137	0.50	22.2
DD20A (73)	37	----	----	----	639	0.142	0.50	25.3
DD (76)	49	-788	----	----	910	0.135	0.60	31.3
GG (84)	40	-628	----	----	970	0.116	1.10	28.0
X (85)	35	-438	0.070	-1.00	612	0.091	1.05	25.4
Y (85)	39	-454	0.059	-1.00	626	0.102	0.97	25.0



		R = 10			R = 0.1			
Material	V_F %	UCS, MPa	b_c	strain for 10^6 cycles, %	UTS, MPa	b_T	strain for 10^6 cycles, %	E, GPa
CH18	47	-298	0.105	-0.74	294	0.129	0.50	17.2
CH19	33	-252	0.122	-0.65	193	0.102	0.70	11.9

Figure 5.45. Normalized S-N fatigue data for materials with 16 percent 0° plies, $[\pm 45/0/\pm 45]_S$ layup with D092 and DB240 fabrics, R=0.1 and 10.

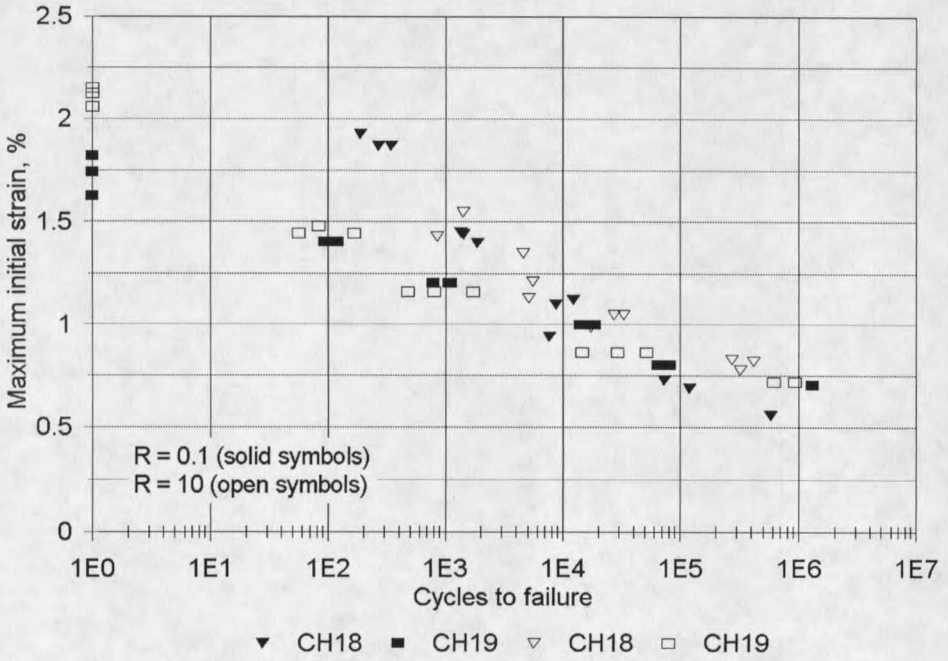
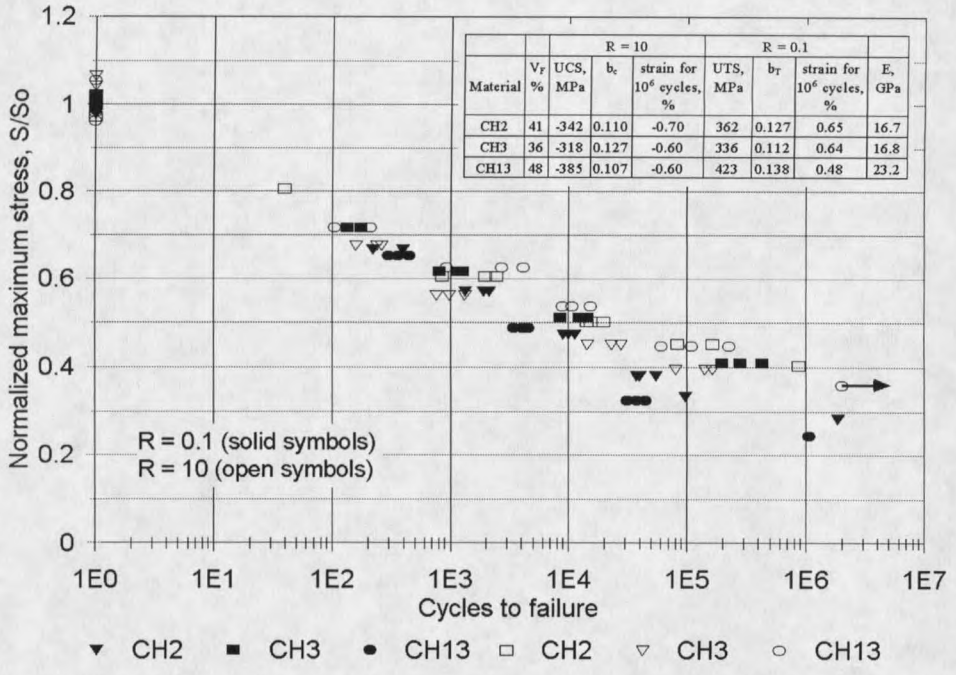


Figure 5.46. Maximum initial fatigue strain data for materials with 16 percent 0° plies, $[\pm 45/0/\pm 45]_S$ layup with D092 and DB240 fabrics, R=0.1 and 10.



Material	V_F %	R = 10 UCS, MPa	b_c	R = 10 strain for 10^6 cycles, %	R = 0.1 UTS, MPa	b_T	R = 0.1 strain for 10^6 cycles, %	E, GPa
CH2	41	-342	0.110	-0.70	362	0.127	0.65	16.7
CH3	36	-318	0.127	-0.60	336	0.112	0.64	16.8
CH13	48	-385	0.107	-0.60	423	0.138	0.48	23.2

Figure 5.47. Normalized S-N fatigue data for materials with 24 percent 0° plies, $[\pm 45/0/\pm 45]_S$ layup with D155 and DB240 fabrics, R=0.1 and 10.

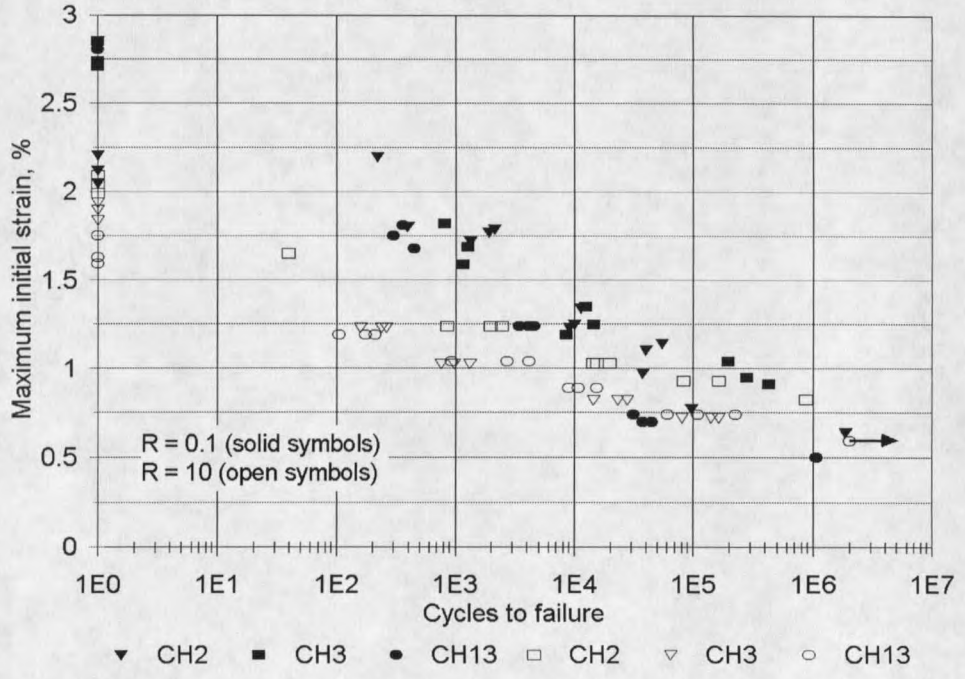
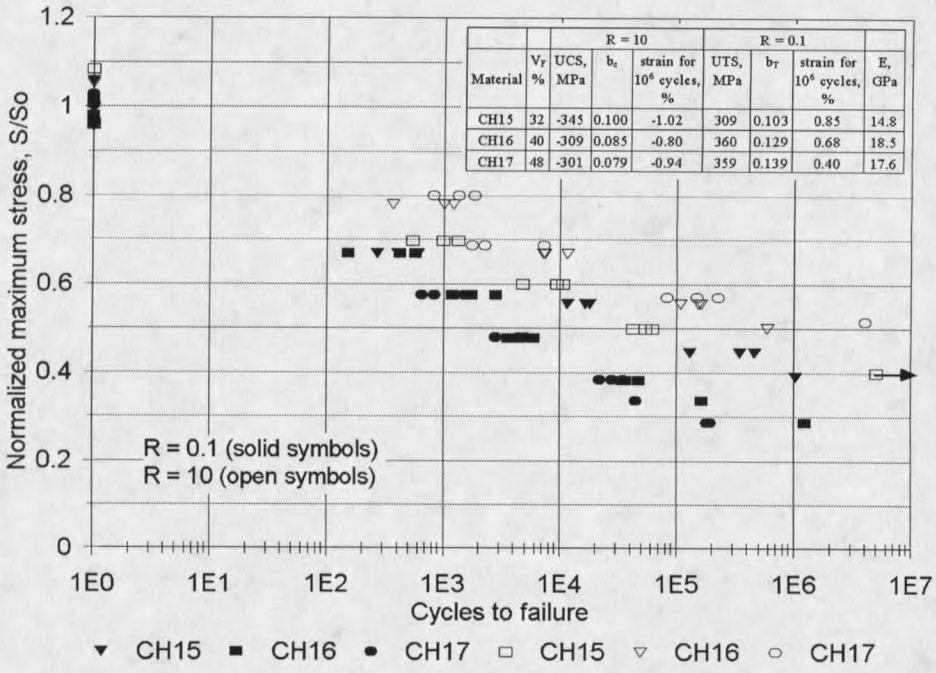


Figure 5.48. Maximum initial fatigue strain data for materials with 24 percent 0° plies, $[\pm 45/0/\pm 45]_S$ layup with D155 and DB240 fabrics, R=0.1 and 10.



Material	V_f %	R = 10 UCS, MPa	b_c	R = 10 strain for 10^6 cycles, %	R = 0.1 UTS, MPa	b_T	R = 0.1 strain for 10^6 cycles, %	E, GPa
CH15	32	-345	0.100	-1.02	309	0.103	0.85	14.8
CH16	40	-309	0.085	-0.80	360	0.129	0.68	18.5
CH17	48	-301	0.079	-0.94	359	0.139	0.40	17.6

Figure 5.49. Normalized S-N fatigue data for materials with 28 percent 0° plies, $[\pm 45/0/\pm 45]_S$ layup with D092 and DB120 fabrics, R=0.1 and 10.

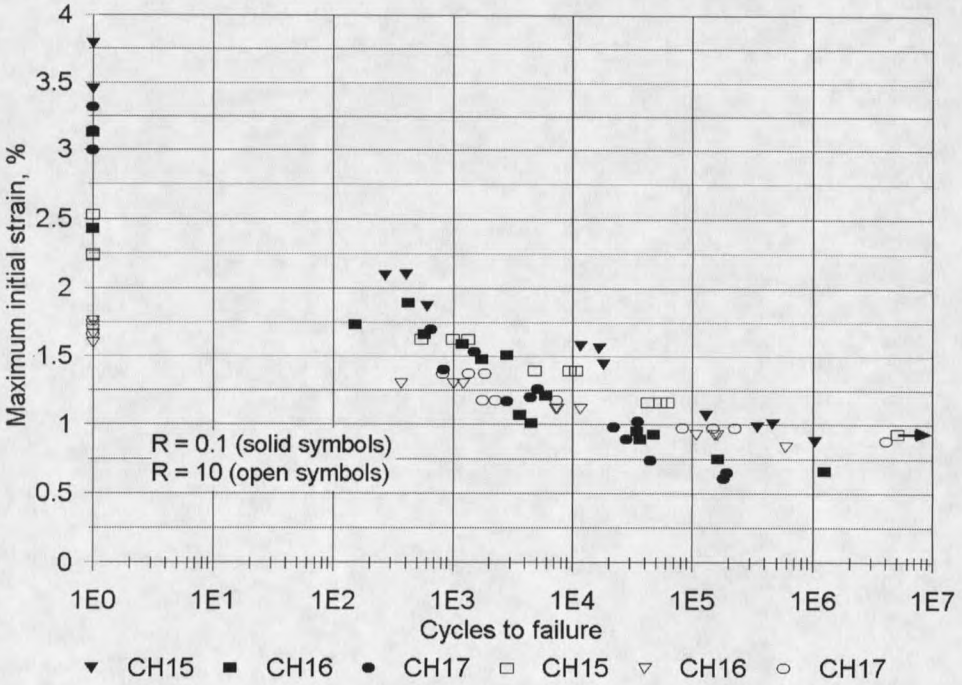
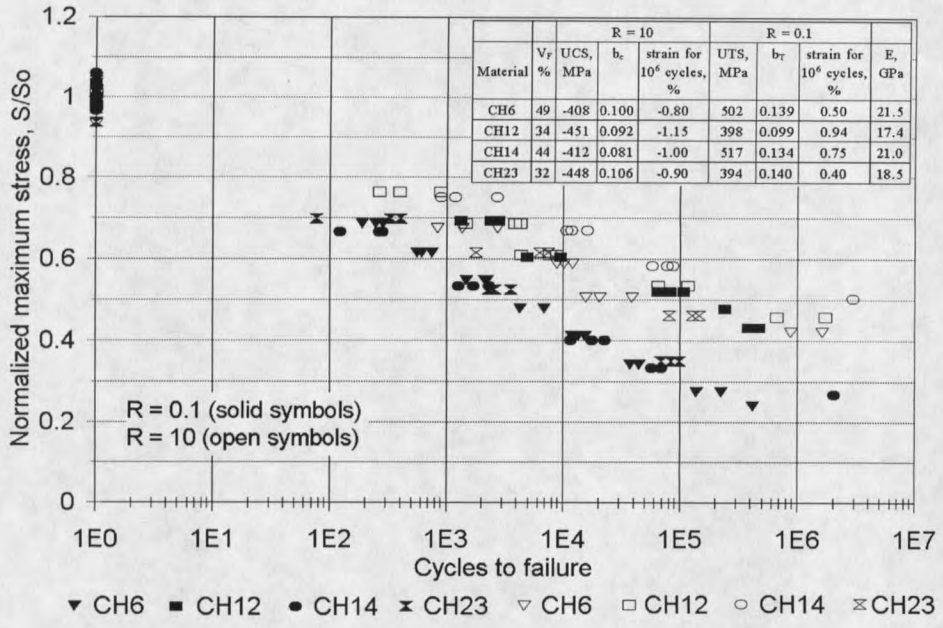


Figure 5.50. Maximum initial fatigue strain data for materials with 28 percent 0° plies, $[\pm 45/0/\pm 45]_S$ layup with D092 and DB120 fabrics, R=0.1 and 10.



		R = 10			R = 0.1			
Material	V_F %	UCS, MPa	b_c	strain for 10^6 cycles, %	UTS, MPa	b_T	strain for 10^6 cycles, %	E, GPa
CH6	49	-408	0.100	-0.80	502	0.139	0.50	21.5
CH12	34	-451	0.092	-1.15	398	0.099	0.94	17.4
CH14	44	-412	0.081	-1.00	517	0.134	0.75	21.0
CH23	32	-448	0.106	-0.90	394	0.140	0.40	18.5

Figure 5.51. Normalized S-N fatigue data for materials with 39 percent 0° plies, $[\pm 45/0/\pm 45]_S$ layup with D155 and DB120 fabrics, R=0.1 and 10.

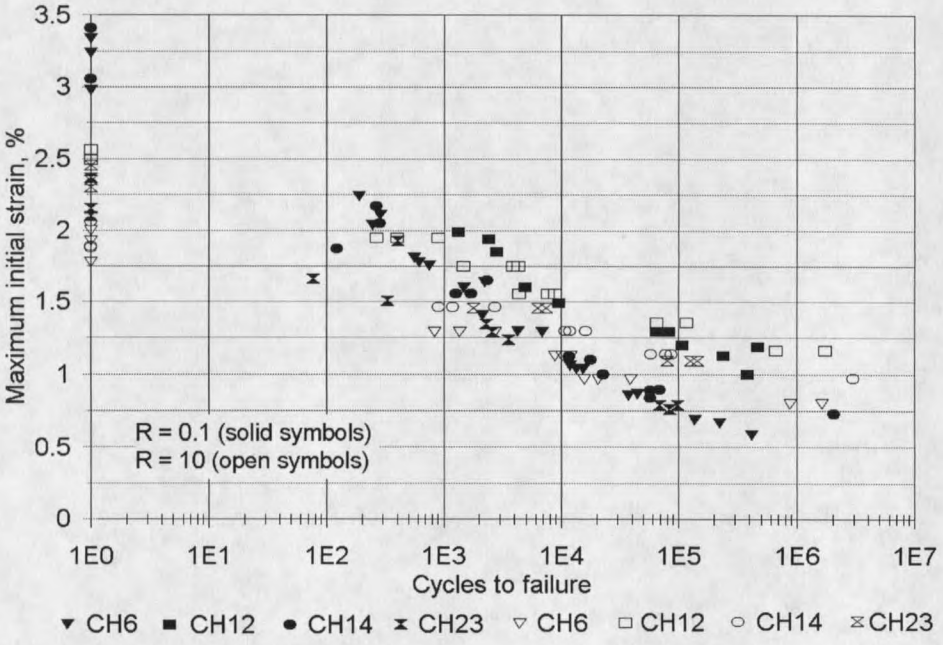
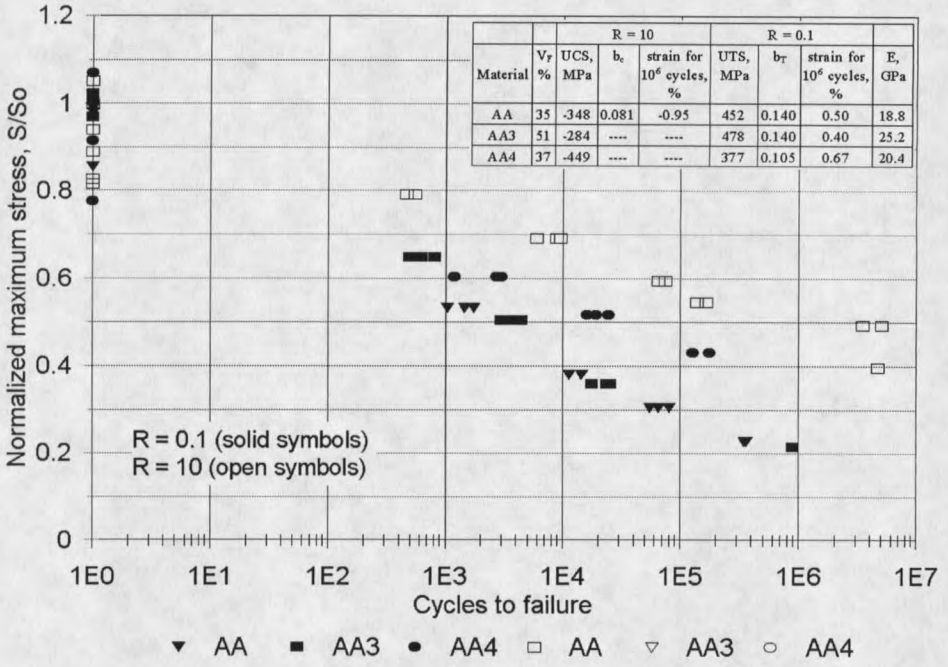


Figure 5.52. Maximum initial fatigue strain data for materials with 39 percent 0° plies, $[\pm 45/0/\pm 45]_S$ layup with D155 and DB120 fabrics, R=0.1 and 10.



Material	V_F %	R = 10 UCS, MPa	b_c	R = 10 strain for 10^6 cycles, %	R = 0.1 UTS, MPa	b_T	R = 0.1 strain for 10^6 cycles, %	E, GPa
AA	35	-348	0.081	-0.95	452	0.140	0.50	18.8
AA3	51	-284	----	----	478	0.140	0.40	25.2
AA4	37	-449	----	----	377	0.105	0.67	20.4

Figure 5.53. Normalized S-N fatigue data for materials with 50 percent 0° plies, $[\pm 45/0/]_N$ layup with stitched triax fabrics, R=0.1 and 10.

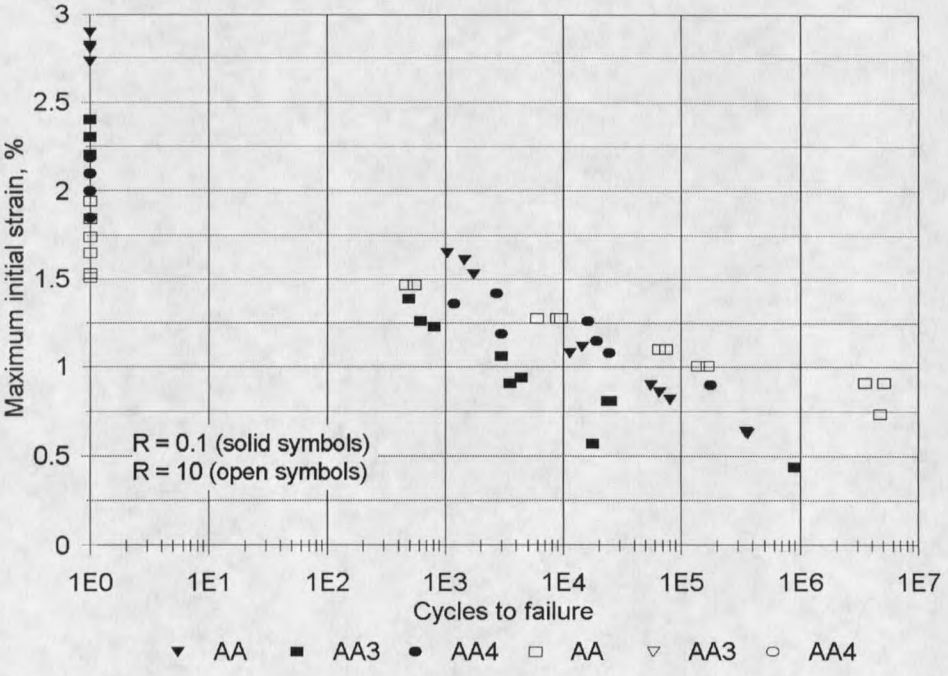


Figure 5.54. Maximum initial fatigue strain data for materials with 50 percent 0° plies, $[\pm 45/0]_N$ layup with triax fabrics, R=0.1 and 10.

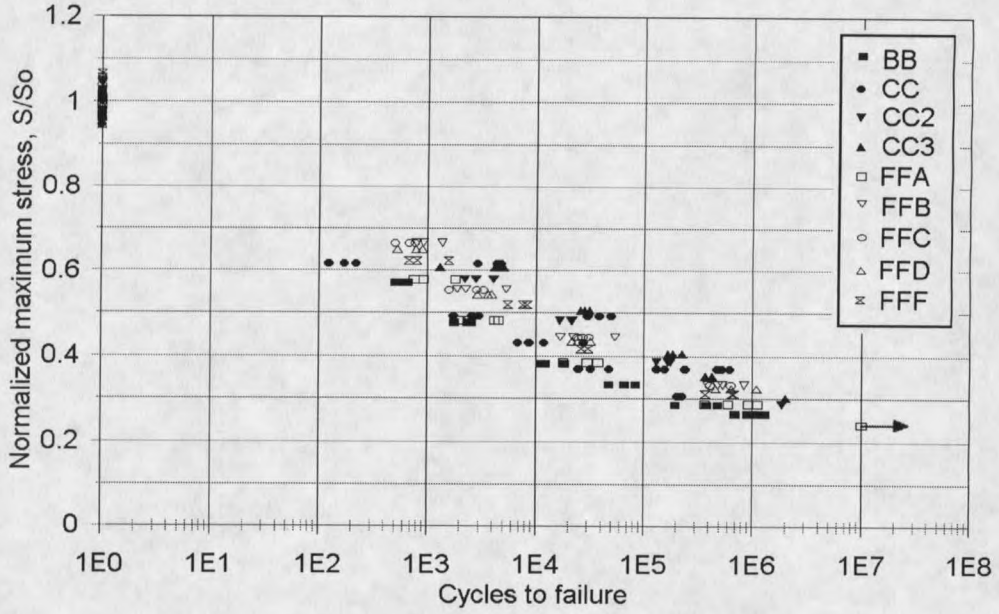


Figure 5.55. Normalized S-N fatigue data for materials with 55 to 63 percent 0° plies, R=0.1.

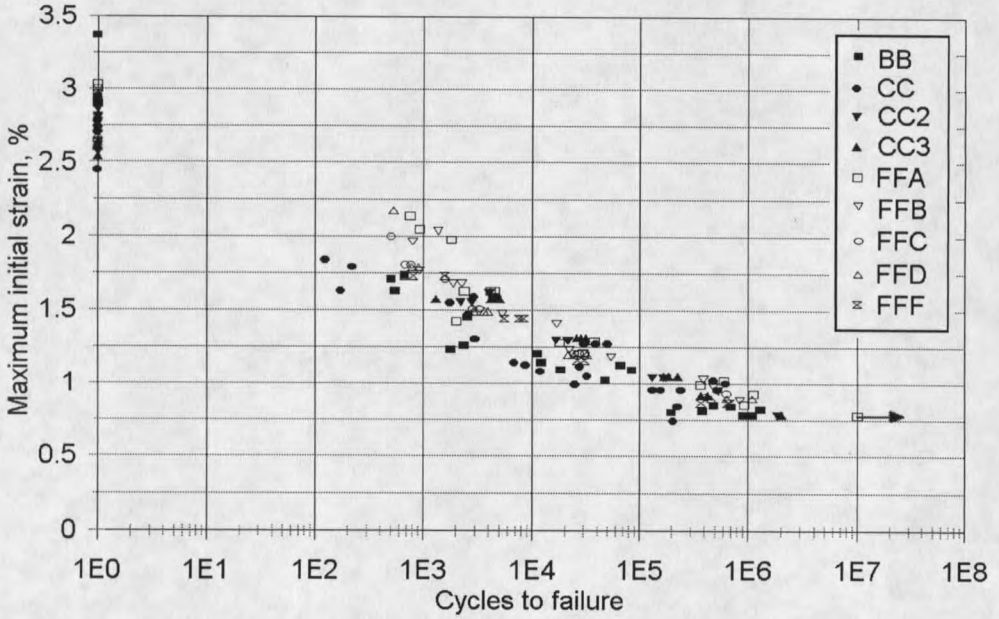


Figure 5.56. Maximum initial fatigue strain data for materials with 55 to 63 percent 0° plies, R=0.1.

Figure 5.57 details the million cycle tensile strain data versus the fiber volume fraction for the materials with 19 to 63 percent 0° plies. As the fiber content increases, the million cycle strain falls, except for materials BB, CC, CC2, CC3 and the FF series, which remain almost constant. These materials show a million cycle strain insensitivity over the fiber volume fraction range of 0.36 to 0.45; higher fiber contents have not yet been tested. The tensile (R=0.1) fatigue coefficient, b, versus the fiber volume fraction is shown in Figure 5.58. As the fiber content increases, the tensile fatigue coefficient increases, again except for materials CC, CC2, CC3 and the FF series. The lay-up of these materials are summarized in Table 5.8 and the improved fatigue behavior may be due to the use of a lighter more uniform fabric with less stitching (D100 fabric 0°) and more plies.

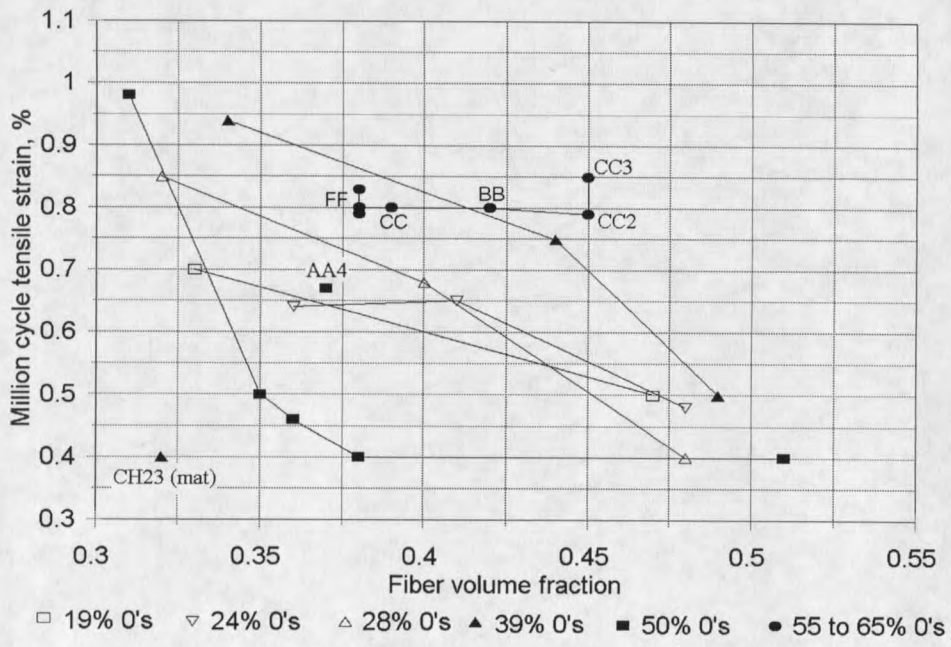


Figure 5.57. Million cycle tensile strain data versus fiber volume fraction for materials with 19 to 63 percent 0° plies, R=0.1.

Figure 5.59 shows the normalized S-N fatigue data (R = 0.1 and 10) for some of the materials with 72 to 85 percent 0° plies. The material lifetime scatter is similar to the materials with less than 55 percent 0° plies and the compressive fatigue behavior is better than the tensile behavior. The reason for the materials with 55 to 63 percent 0° plies having a less scatter in fatigue (R=0.1 and 10) than all the other materials tested has not been determined.

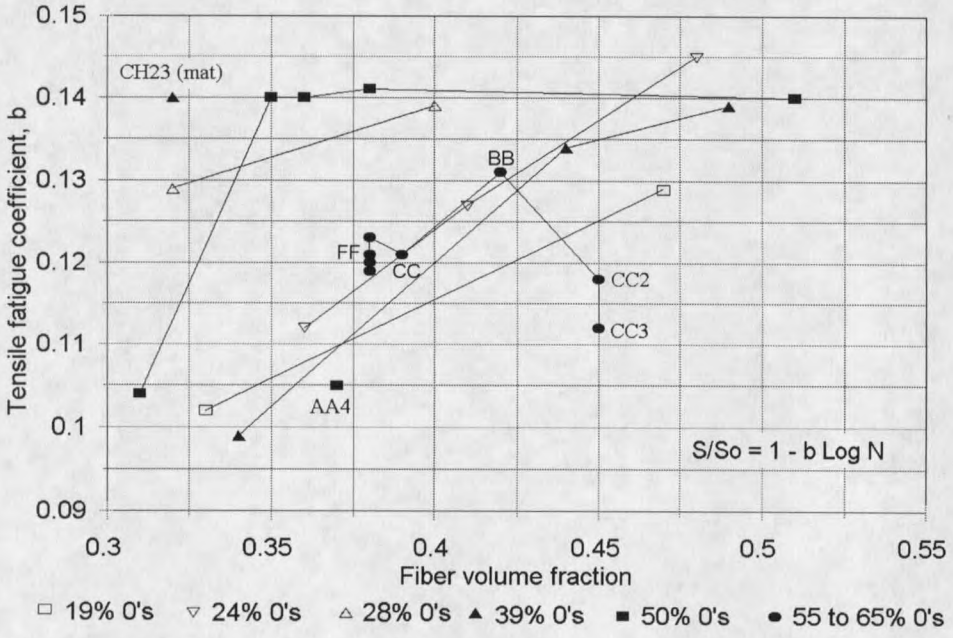


Figure 5.58. Tensile fatigue coefficient, b, versus fiber volume fraction for materials with 19 to 63 percent 0° plies, R=0.1.

Table 5.8. Lay-up summaries for materials with 55 to 63 percent 0° plies.

Material	V_F, %	Ply Configuration	Matrix	Fabric Description
BB	42	$[\pm 45/0_2/+45]_S$	P	0's-A130 (62%), 45's-DB120
CC	39	$[\pm 45/0_2/+45]_S$	P	0's-D100 (55%), 45's-DB120
CC2	45	$[\pm 45/0_3/+45]_S$	P	0's-D100 (63%), 45's-DB120
CC3	45	$[0/\pm 45/0_2/+45]_S$	P	0's-D100 (63%), 45's-DB120
FFA	38	$[\pm 45/0/0/\pm 45]_S$	P	0's-D155 (56%), 45's-DB120 (44%)
FFB	38	$[0/\pm 45/0/\pm 45]_S$	P	
FFC	38	$[0/\pm 45/\pm 45/0]_S$	P	
FFD	38	$[0/0/\pm 45/\pm 45]_S$	P	
FFF	38	$[\pm 45/\pm 45/0/0]_S$	P	

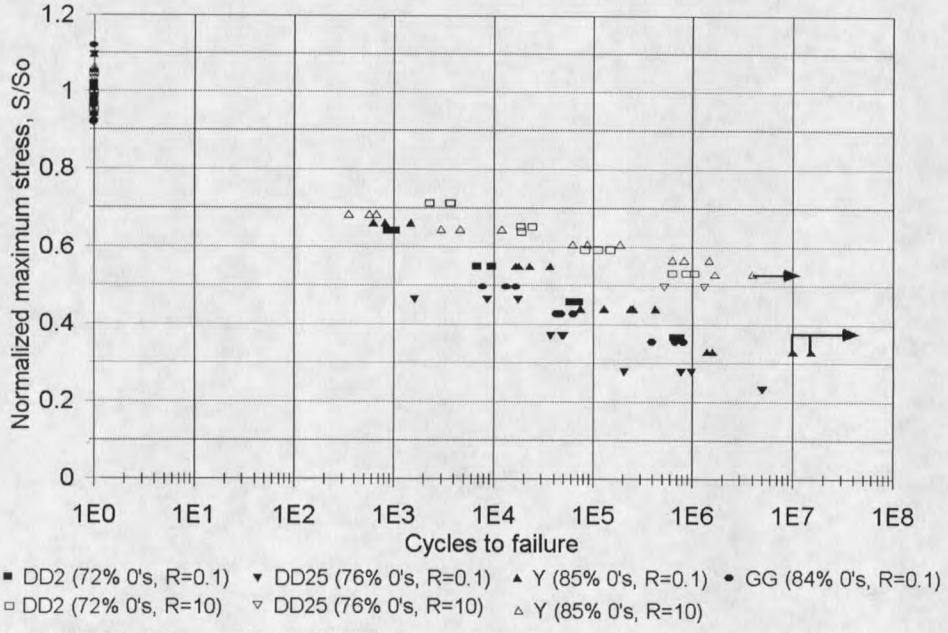


Figure 5.59. Normalized S-N fatigue data for materials with 72 to 85 percent 0° plies.

Effect of R Value

Figures 5.60 and 5.61 shows stress and strain S-N data for R values of 0.1, 10, and -1.0 for material DD5P. The compressive one-cycle strength is typically lower than the tensile strength, but the fatigue coefficient, b, is also lower (less fatigue sensitive), so the R = 0.1 and 10 data sets usually cross at some point as the stress decreases. The reversed loading (tension - compression) case, R = -1, tends to follow below the stresses for the lowest of the other curves, being dominated by compression at higher stresses (shorter lifetimes) and tension at lower stresses (longer lifetimes). The corresponding one million cycle maximum initial strain values for R = 0.1, 10, and -1.0 are 1.15%, 1.30%, and 0.62%, respectively. The strain value is usually the lowest for R = -1.0, while the fatigue coefficient, b, for this case is poorly defined because the failure mode shifts from compression to tension dominated. Thus, these data are markedly nonlinear.

Comparison of Materials

Figure 5.62 gives the tensile fatigue strain based S-N data for a broad sampling of the database, including both MSU and industry fabricated materials. The results show a very broad range of performance, varying from the best observed fiberglass response (b = 0.10, 10^6 cycle ε = 1.2%), evident for many materials, to much poorer performance. The one million cycle strain varies down to about 0.4% for the poorest materials, and b increases to about 0.14 for these same materials. The consequences of the poorer materials relative to the best materials are lifetimes of over 100 times shorter and stresses and strains reduced to as low as one-third of the values for typical material DD5 in the

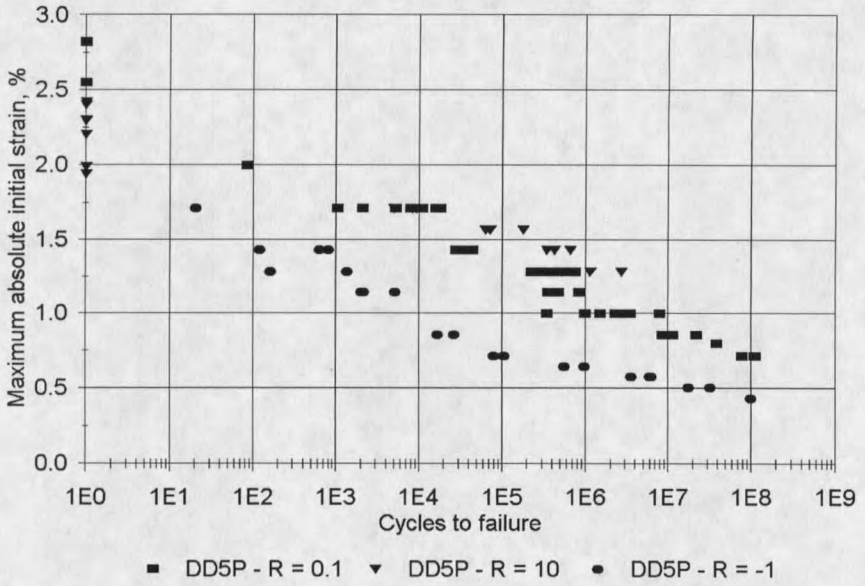


Figure 5.60. Maximum fatigue strain versus cycles for material DD5P, R = 0.1, 10 and -1.

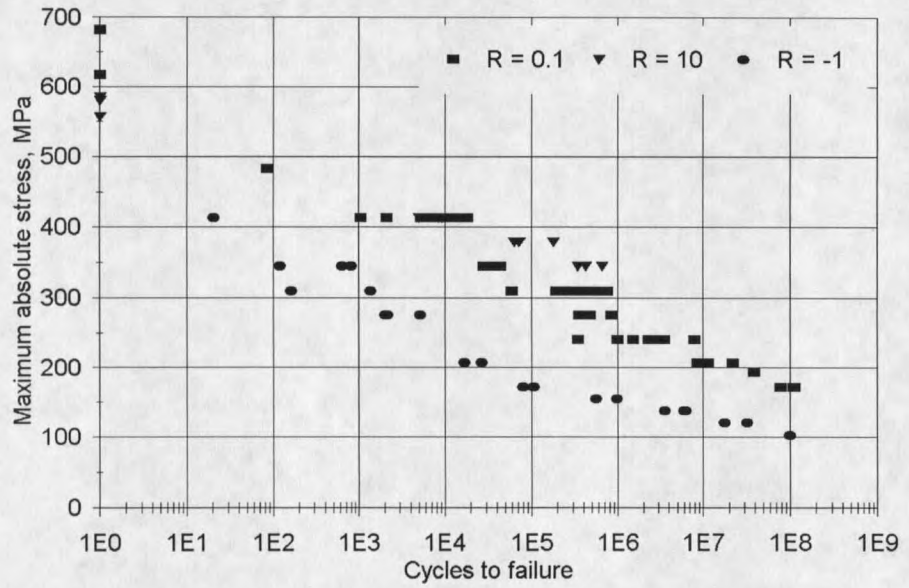


Figure 5.61. Maximum fatigue stress versus cycles for material DD5P, R = 0.1, 10 and -1.

Figure 5.63 gives a simplified representation of the normalized maximum stress mid-stress range. This materials difference could represent a factor of three in wind turbine blade weight if the entire blade length were tensile fatigue dominated in design (which is unlikely). data in terms of "best" and "worst" normalized S-N performance under tensile loading. While fatigue limits have not been rigorously established, failures have not been observed at maximum stresses below $S/S_0 = 0.15$ in the database, which extends to between 10^7 and 10^8 cycles for several materials. This figure should not be interpreted to indicate that $S/S_0 = 0.15$ represents a fatigue limit out to any cycle range. Rather, it indicates that even the poorest performing materials (containing significant 0° fibers) do not fail at stresses below this value over the cycle range tested. Materials with few or no fibers in the 0° direction often fail at much lower strains than those of the "worst" materials in Figure 5.62, as discussed earlier, but still with S/So > 0.15.

Figures 5.64, 5.65, and 5.66 give corresponding results for the overall database at R = 10 and -1.0., with the -1 data normalized by the compressive strength in Figure 5.65 and the tensile strength in Figure 5.66. There is considerably less variation in fatigue performance between different materials under compressive loading (R = 10), as compared to tensile fatigue (R = 0.1). The compressive fatigue response is actually slightly better than the best tensile fatigue performance, with b values generally in the 0.07 to 0.10 range. The reversed loading performance, as noted earlier, is slightly worse than the lowest (lowest stresses on the S-N curve) of the tensile and compressive fatigue data sets. At worst, the strains under reversed loading are around 0.40% at one million cycles, with the best performance around 0.70%. Table 5.9 compares these values for several materials.

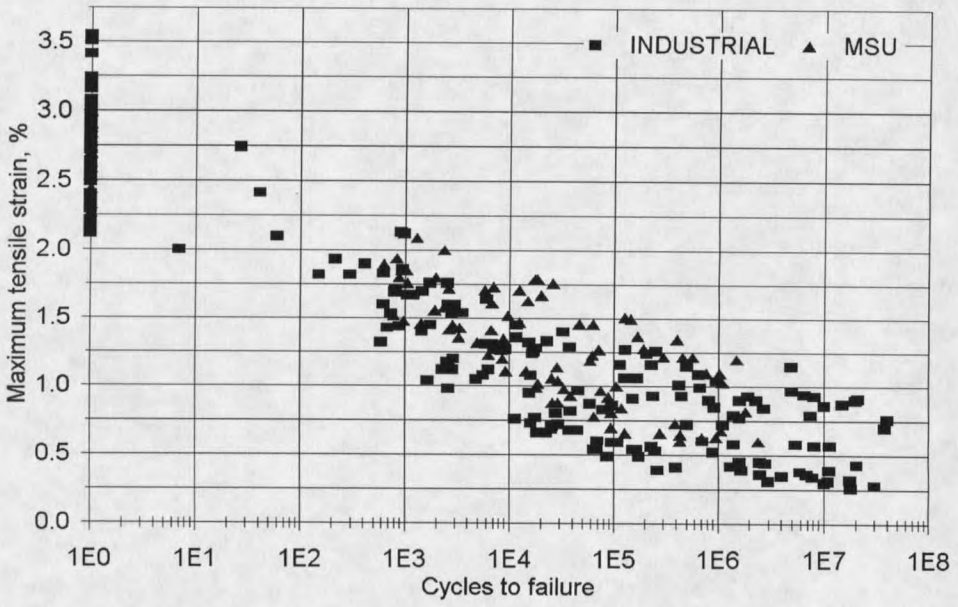


Figure 5.62. Tensile fatigue data for various MSU and industrial materials, R = 0.1.

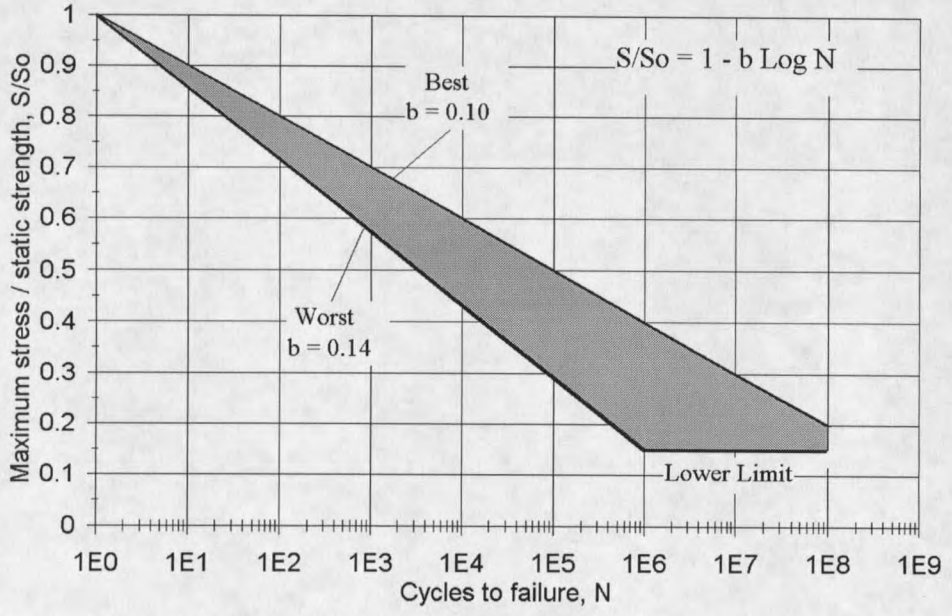


Figure 5.63. Extremes of normalized S-N tensile fatigue data (R = 0.1) for fiberglass laminates with at least 25 percent of the fiber in the 0° direction.

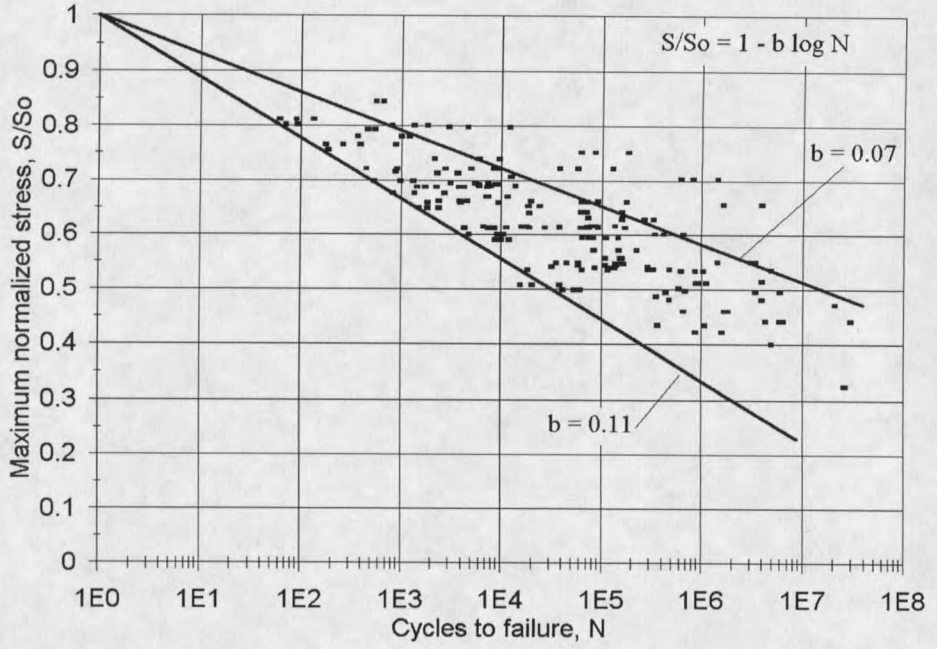


Figure 5.64. Normalized compressive fatigue data for standard coupons with 25 percent or greater percent 0° fibers, R = 10.

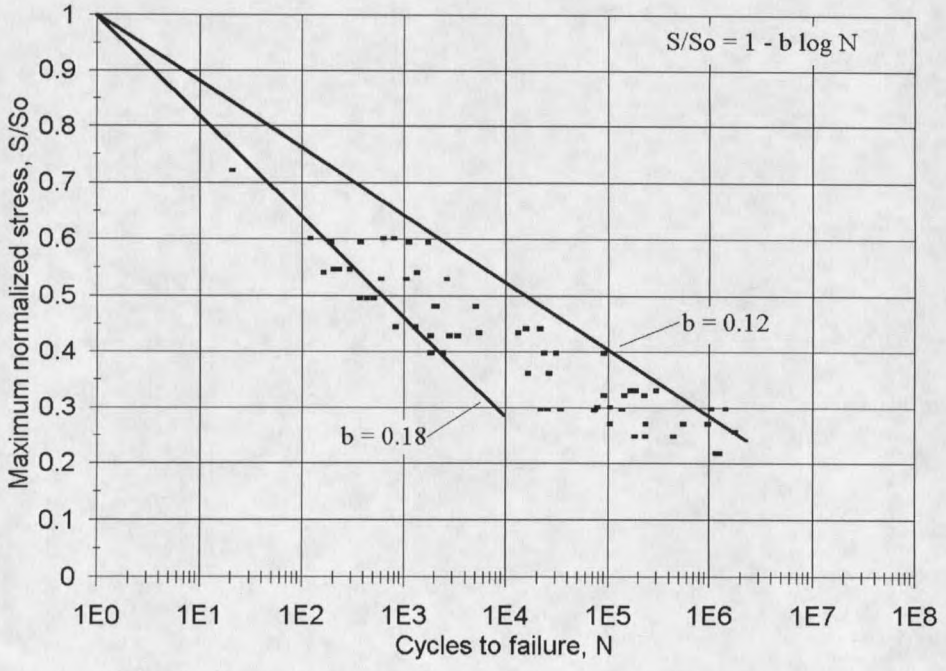


Figure 5.65. Reversed loading fatigue data normalized by the compressive strength for materials with 25 percent or greater percent 0° fibers, R = -1.

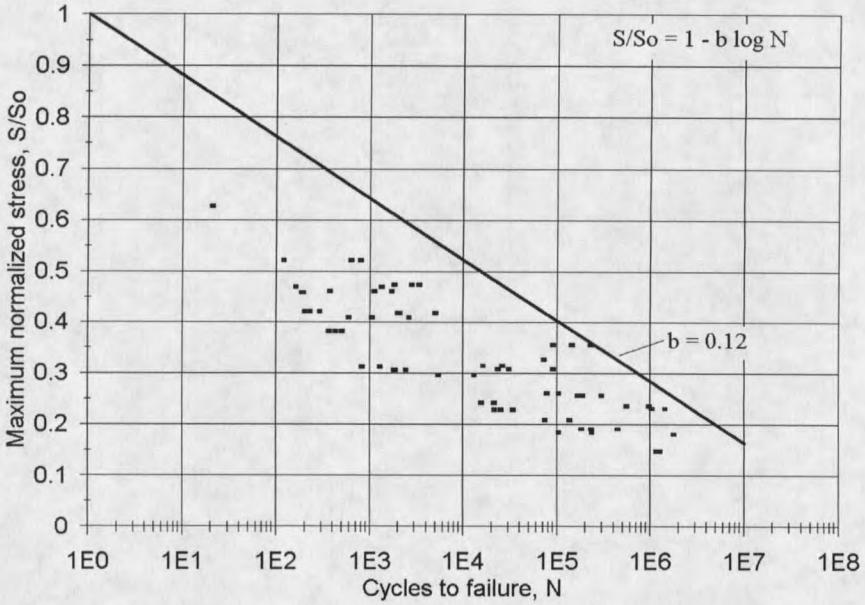


Figure 5.66. reversed loading fatigue data normalized by the tensile strength for materials with 25 percent or greater 0° fibers, R = -1.

Table 5.9. Summary of fatigue results: tensile (R = 0.1), compressive (R = 10) and reversed loading (R = -1).

			R = 0.1		R = 10		R = -1		
Material	V_F %	% 0^o	b_T	strain for 10^6 cycles, %	b_C	strain for 10^6 cycles, %	b_R	strain for 10^6 cycles, %	E, GPa
H	37	70	0.114	0.52	0.100	-0.72	0.136	0.45	24.0
N	38	50	0.140	0.46	0.096	-0.70	0.135	0.30	19.3
P	40	48	0.134	0.48	0.099	-0.66	0.133	0.42	22.5
AA	35	50	0.140	0.50	0.081	-0.95	0.139	0.40	18.8
EEAV	49	70	0.100	0.75	0.077	-1.30	0.068	0.70	28.2
DD4	48	72	0.136	0.55	----	----	0.123	0.50	31.0
DD5E	36	72	0.110	1.20	0.056	-1.42	0.123	0.66	23.6
DD5P	36	72	0.101	1.16	0.072	-1.35	0.135	0.62	24.2
DD5V2	35	72	0.102	1.39	0.064	-1.66	0.117	0.68	22.3
DD11	31	72	0.100	1.20	0.090	-0.70	0.095	0.60	20.0
45D155*	38	0	0.109	0.40	0.089	-0.65	0.148	0.25	9.79
*Material 45D155 was a ±45° composite									

The stitched fabrics used in this study were expected to behave more like uniform layer composites common in materials such as prepreg laminates, which show a fatigue coefficient, b, of about 0.10 at R=0.1 [60]. However, early results in this study with the Triax fabrics showed trends following the "worst" behavior in Figure 5.63 [3]. The Triax fabrics vary in detail, but have ±45° strands stitched against the 0° strands. Detailed experimental study of these materials showed that the 0° strands failed at these stitch points [3]. A very detailed finite element model for the individual strands with cracked matrix found the apparent cause of this problem: if there is no layer of resin matrix between the strands, matrix cracks along the 45° strands will produce significant stress concentrations in the 0° load-bearing strands. Results reported in References 3, 4, and 58 showed that the Triax reinforced materials failed under tensile fatigue loading shortly after the ±45° layers failed, giving it the worst behavior. In general, it is expected that a composite will be designed to fail in a "fiber dominated" mode, where the trend, b, is the same as for the 0° material alone. Here, the combination of glass fiber properties and tightly stitched fabrics resulted in composite failure soon after matrix failure, a behavior which is "matrix dominated". Since matrix failure in 45° layers occurred at lower strains than for fiber failure, this produced poor composite performance in tensile fatigue.

Unfortunately, this matrix dominated response is not limited to Triax reinforcements. Additional tests [7] have shown similar behavior under some conditions with separate 0° and ±45° layers, and even with 0° unidirectional stitched fabric composites without any ±45° material. Figure 5.67 shows the database trends for several materials at R=0.1, but broken into several groups. The top group (denoted with the solid triangles in the figure) behaves like the "best" materials, with b close to 0.1. The middle

group (denoted by an open triangle) behaves like the "worst" materials, with b close to 0.14. The lower group of materials (denoted by a solid square) are ±45 laminates containing no 0° layers. Just as determined for Triax laminates earlier, Figure 5.67 indicates that the poorly performing laminates with 0° layers fail close to the "worst" line in Figure 5.62, because they fail shortly after the ±45° layers reach their failure condition. Thus, the "worst" line in Figure 5.62 appears to originate from matrix failure in the ±45° layers, where present. Unidirectional laminates with only 0° layers which show "worst" behavior (at high V_f) appear to fail shortly after the fabric stitching debonds. In general, the trends with V_F for laminates with 0° and ±45° material are similar to those for the unidirectional materials (Figures 5.33 and 5.34), but the transitions to greater fatigue sensitivity occur at slightly lower values of V_F when ±45° material is present.

Tensile S-N data for the DD series of structural materials (72% 0°, 28% ±45°) at various overall fiber contents are given in Figure 5.68. The trends are clear: at fiber volume fractions below 0.42 the data follow the "best" line in Figure 5.62, b = 0.10; at higher fiber contents the data approach the "worst" condition, b = 0.14. Thus, there is a transition with increasing fiber content from "best" to "worst" fiberglass behavior in tensile fatigue. The strains at 10^6 cycles shown in the insert on Figure 5.68, follow a similar trend, from around 1.0 to 1.2% at lower fiber content to 0.6 to 0.7% at higher fiber content. Even though the increasing fiber content raises the static modulus and ultimate tensile strength, the fatigue performance deteriorates significantly on either a normalized (b) or absolute (strain at 10^6 cycles) basis. Figure 5.69 shows the tensile and compressive fatigue coefficient, b, versus the fiber volume fraction for most of the DD series with D155 stitched fabrics and A130 woven fabrics.

The data are also interesting when plotted as the million-cycle initial maximum strain which can be withstood in tensile fatigue. Figure 5.70 gives the million-cycle strain plotted against the percent 0° layers for low and high fiber volume fraction ranges. At high fiber contents, where b approaches the "worst" value close to 0.14, the million-cycle strain is about 0.5% for the ±45° laminates alone, and for all laminates containing 0° and ±45° layers, rising slightly for the pure unidirectional (0°) laminates. This is consistent with the view that the "worst" behavior corresponds to laminate failure when the ±45° layers or matrix regions fail (all layers are at the same strain). This is matrix-dominated behavior, since the laminate fails shortly after matrix cracks form in the ±45° layers. Compression and reversed loading trends are detailed in Reference 2.

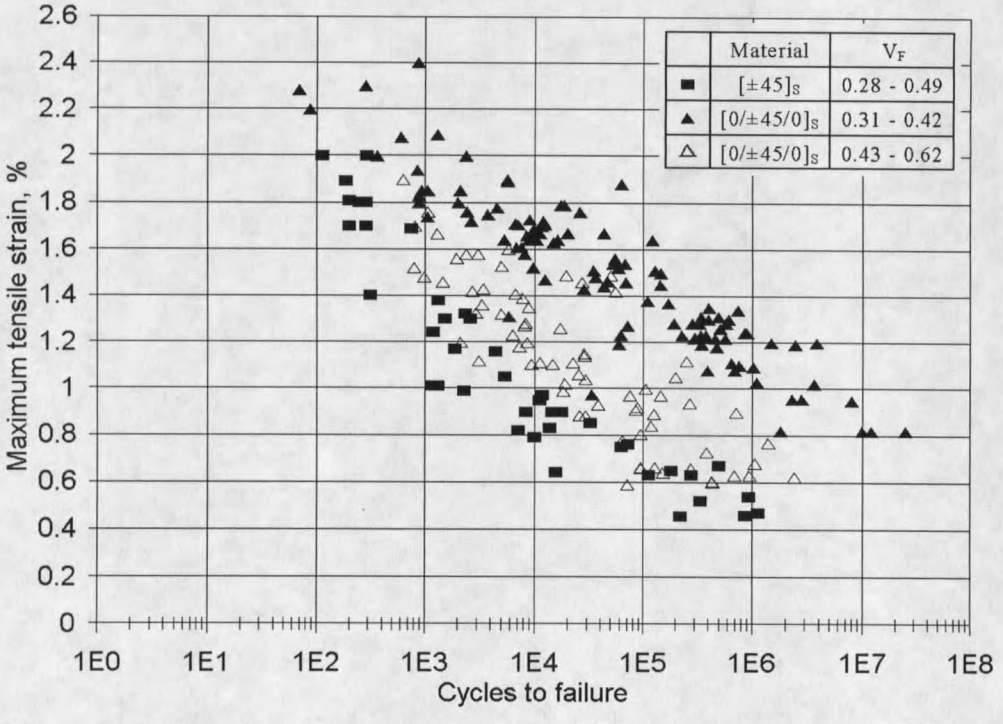
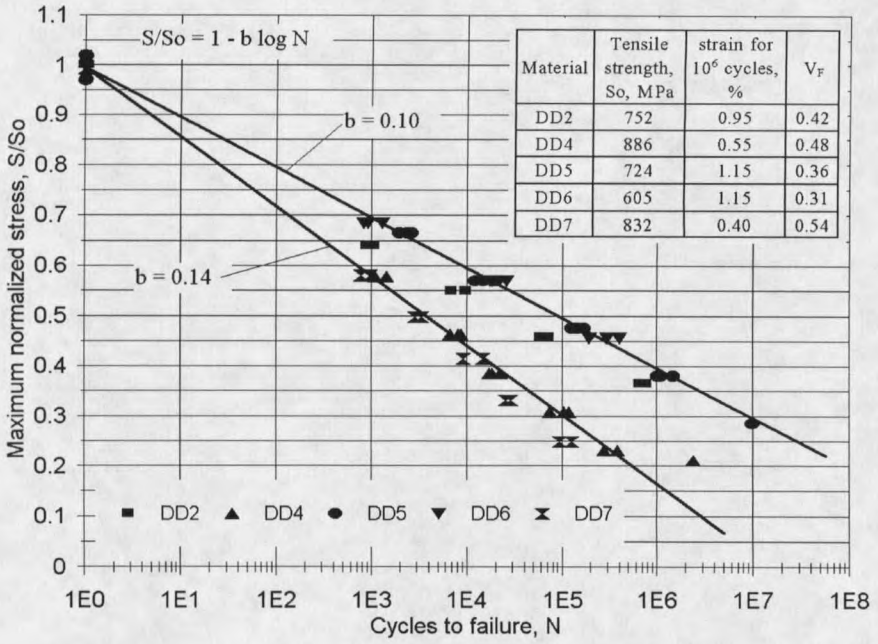


Figure 5.67. Strain fatigue data for $[\pm 45]_S$ and $[0/\pm 45/0]_S$ materials, R=0.1.



Material	Tensile strength, So, MPa	strain for 10^6 cycles, %	V_F
DD2	752	0.95	0.42
DD4	886	0.55	0.48
DD5	724	1.15	0.36
DD6	605	1.15	0.31
DD7	832	0.40	0.54

Figure 5.68. Effect of fiber content on the normalized S-N data, R=0.1, for DD materials $[0/\pm45/0]_S$.

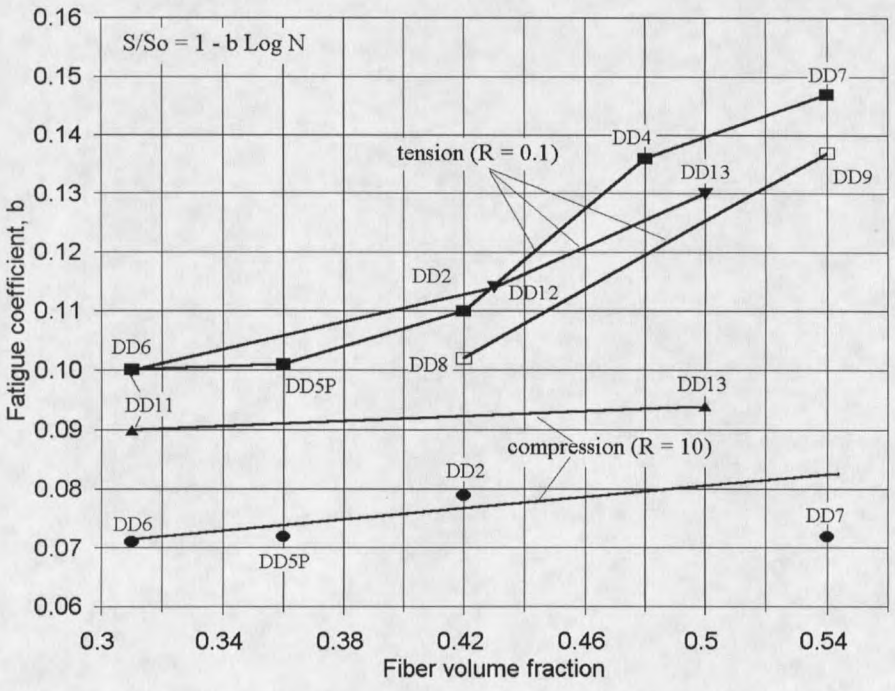


Figure 5.69. Fiber content versus fatigue sensitivity coefficient, b, for DD materials.

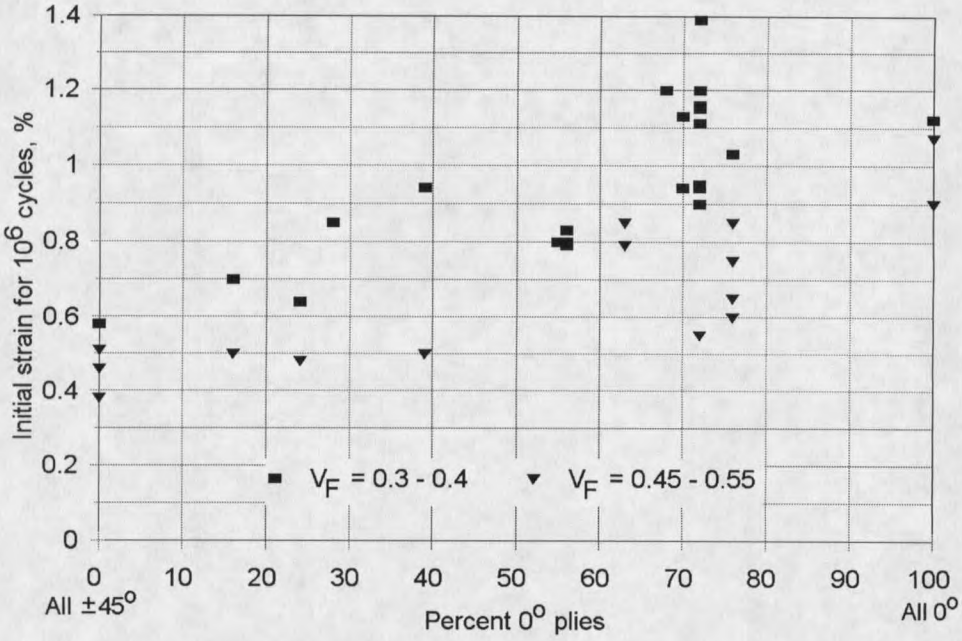


Figure 5.70. Initial strain for 10^6 cycles (R = 0.1) versus percent 0° plies, D155, CH and DD materials.

Failure Modes

Figures 5.71 to 5.83 show photographs of typical failed specimens for a variety of materials and loading conditions. Failure modes for all tests in the database were compared, and, for the most part, few strong trends were evident. This section describes the main differences seen in failure modes.

Testing of unidirectional materials of fiberglass in tensile fatigue is difficult, as noted earlier. Figure 5.71 compares failures of unidirectional Material A tested in the standard tabbed configuration and the tapered thickness configuration (Figure 2.6). The failure is much improved for the tapered specimen, with the brooming-type of separation as compared with failure under the tabs for the standard specimen. However, differences in the tensile fatigue results for the two cases were not significant. Figures 5.72 to5.74

show typical failures for unidirectional RTM materials with two fabrics and low vs high fiber content. The A130 fabric failures show a clear association with the bead over which they are woven, particularly in compression. The D155 fabric based materials show no effect of the stitching in the failure patterns; axial splitting is evident at high fiber content in compression.

Figures 5.76 through 5.81 show materials varying from low to high percent 0° layers at different fiber contents. The 0° layers include both woven (A130) and stitched (D155) fabrics. Other weights of these types of fabric show similar failures. The tensile static and fatigue failures become less localized, with more specimen-long brooming as the fiber content increases. The bead effects evident in the unidirectional A130 materials are also evident when ±45° layers are added. Cracking and delamination at tapered-width specimen shoulders (described in Figure 4.6) is more prominent, even at low cycles, as the percent of 0° layers increases. The typical structural materials such as DD5 (Figure 5.80 and 5.81) show severe shoulder delamination, but failure zones (failed 0° strands) can be seen in the gage section prior to failure at low stresses. At high fiber contents (Figure 5.82), the failures tend to localize in the gage section, with less shoulder damage. The D155 fabric with stitching removed (Figure 5.83) behaves similarly. Shoulder damage starts as splits parallel to the 0° fibers at the break between cut and uncut 0° material, with interply delamination then developing at higher loads or cycles. Specimens which fail away from the shoulder area are preferred, since there is no possible effect of specimen geometry on the test. However, for many materials, this has been impossible to achieve for all specimens in a series of S-N tests.

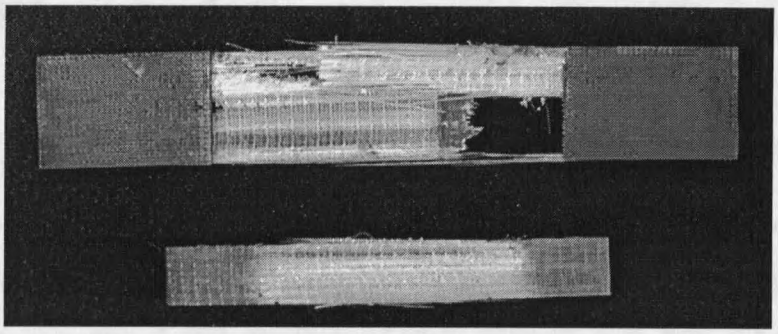


Figure 5.71. Comparison of tensile fatigue test coupons, unidirectional Material A (V_F = 30%). Standard test coupon (top) and thickness tapered coupon (bottom).

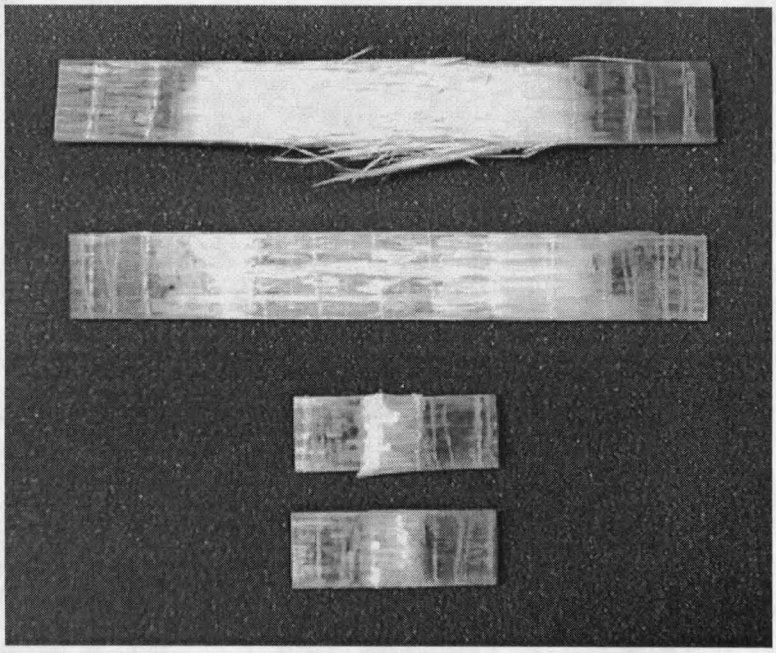


Figure 5.72. Unidirectional materials based on A130 fabric (Material A130C, V_F = 35%). From top to bottom: static tensile coupon; tensile fatigue (R = 0.1, 345 MPa); static compression, and compression fatigue (R = 10, 276 MPa)

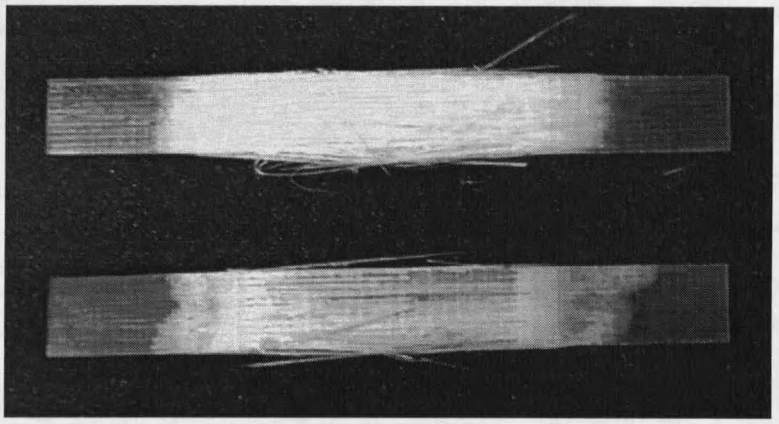


Figure 5.73. Unidirectional low fiber content materials based on D155 fabric (Material D155B, $V_F = 39\%$). Static coupon (top), tensile fatigue R = 0.1, 345 MPa (bottom).

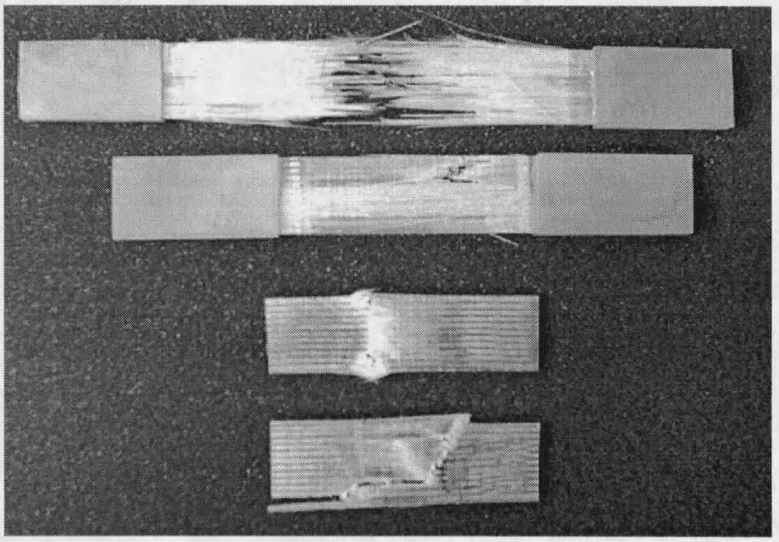


Figure 5.74. Unidirectional high fiber content materials based on D155 fabric (Material D155G, $V_F = 59\%$). From top to bottom: tensile fatigue, R = 0.1 coupons tested at 552 and 276 MPa; static compression and compression fatigue (R = 10, 483 MPa).

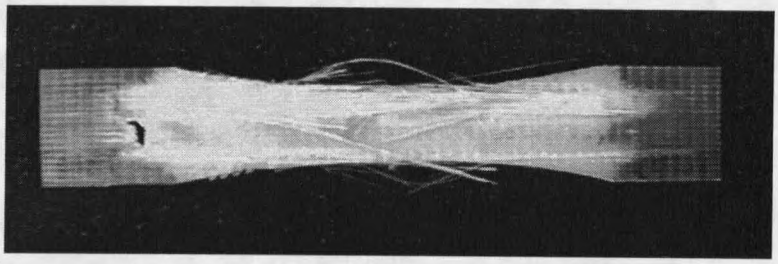


Figure 5.75. Material GG ($V_F = 40\%$) with 84% 0° in the loading direction showing heavy brooming upon failure, tensile fatigue (R = 0.1, 345 MPa).

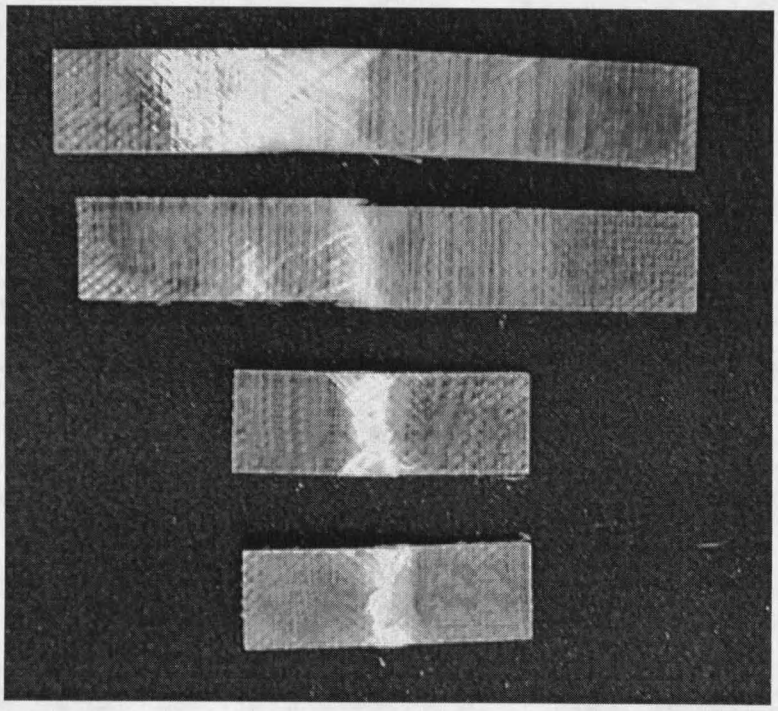


Figure 5.76. Material CH9, ($V_F = 49\%$, all ±45 layers). From top to bottom: static tensile coupon, tensile fatigue, (R = 0.1, 86 MPa); static compression and compression fatigue (R = 10, 86 MPa).

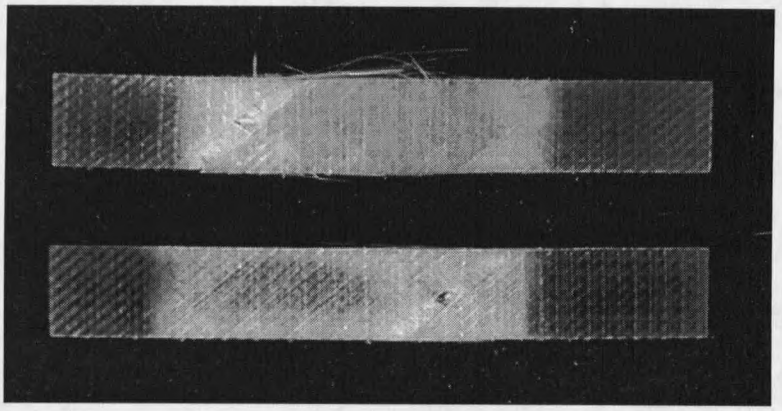


Figure 5.77. Low fiber content, low percent 0's. Material CH3 (V_F = 36%, 24% 0's). Static tension coupon (top) and tensile fatigue (R = 0.1, 72 MPa).

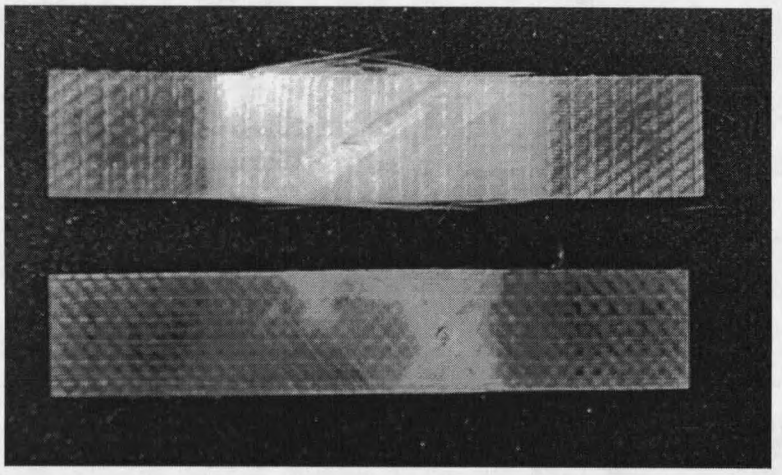


Figure 5.78. High fiber content, low percent 0's. Material CH13 (V_F = 48%, 24% 0's). Static tensile coupon (top) and tensile fatigue (R = 0.1, 172 MPa).

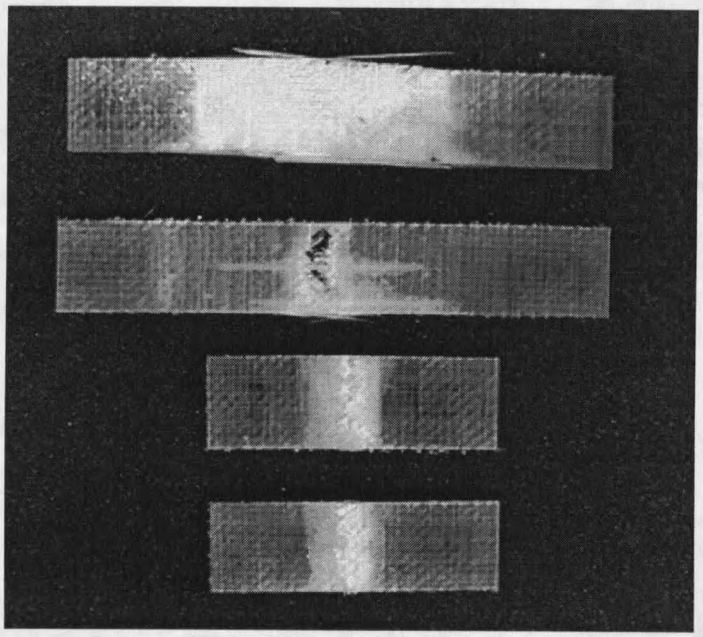


Figure 5.79.Moderate fiber content and percent 0's. Material CH14 (V_F = 44%, 39% 0's). From top to bottom: static tensile coupon; tensile fatigue (R = 0.1 172 MPa); static compression; and compression fatigue (R = 10, 241 MPa).

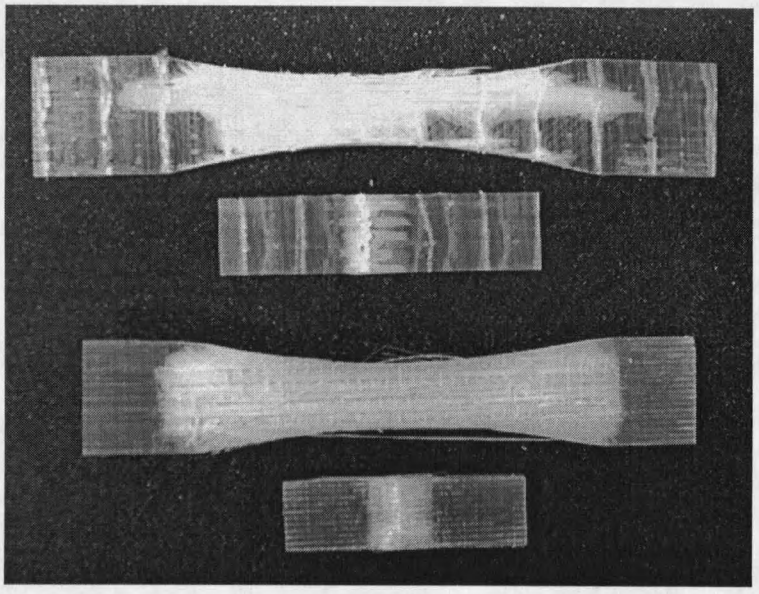


Figure 5.80. Standard structural material at low fiber content, 72% 0's. From top to bottom: Material DD11 (A130 fabric 0's, V_F = 31%); tensile fatigue (R = 0.1, 276 MPa); compression fatigue (R = 10, 172 MPa); and Material DD6 (D155 fabric 0's, V_F = 31%); tensile fatigue (R = 0.1, 276 MPa); and compression fatigue (R = 10, 379 MPa).

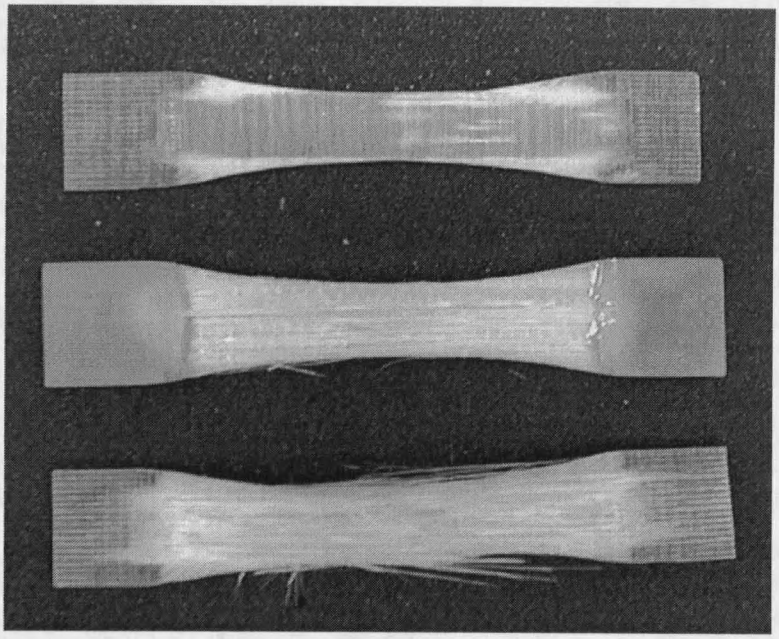


Figure 5.81. Standard structural material with 72% 0's, (Material DD5, $V_F = 38\%$). From top to bottom: static tension, tension fatigue (R = 0.1) 310 MPa and 276 MPa.

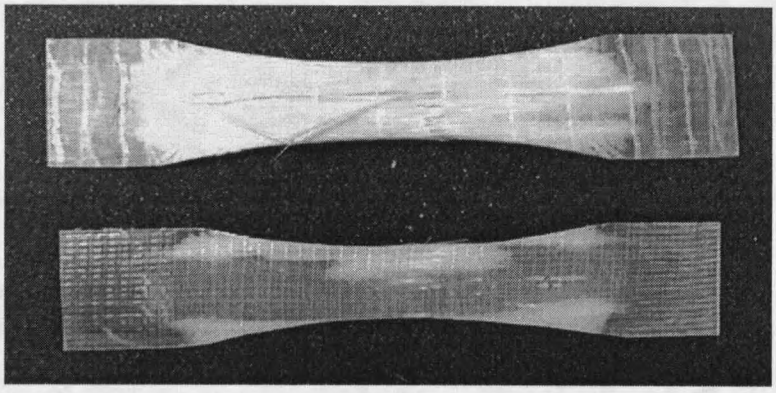


Figure 5.82. Standard structural material at moderate fiber content, Material DD12 (71% A130 0° fabric, $V_F = 43\%$), (top) tensile fatigue (R = 0.1, 241 MPa) and DD5 (72% D155 0° fabric, $V_F = 38\%$) tensile fatigue (R = 0.1, 345 MPa).

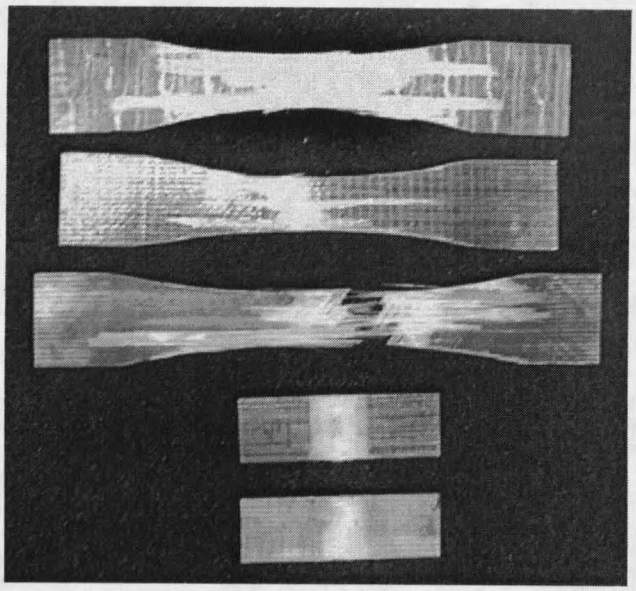


Figure 5.83. Standard structural materials at higher fiber content, from top to bottom: Material DD13 (71% A130 fabric, $V_F = 50\%$), tensile fatigue (R = 0.1, 345 MPa); Material DD7 (72% D155 fabric, $V_F = 54\%$), tensile fatigue (R = 0.1, 207 MPa); Material DD9 (72% D155 fabric, stitching removed, $V_F = 54\%$), tensile fatigue (R = 0.1, 207 MPa); Material DD7 static compression, and compression fatigue (R = 10, 345 MPa).

Compressive failures are very similar for static and fatigue tests, with a symmetrical splaying-out of the layers from the unconstrained specimen surfaces. Little damage is evident in the compressive specimens prior to sudden failure. The A130 fabric based materials often show independent delamination of strands at failure in compression (Figure 5.80). The thermoplastic-coated bead over which strands are woven is evident in this figure.

Fabric Architecture Effects

These results indicate a similar trend for all stranded E-glass fabric reinforced

laminates toward a steeper S-N curve (higher b) as the fiber content increases, with the presence of off-axis (± 45°) layers shifting this transition to lower fiber contents. Fabrics with an effectively high fiber content inherent in the fabric construction, Triax materials with 0° and ±45° strands stitched tightly together, show poor fatigue resistance over the entire fiber content range studied.

The problem of finding a fabric for structural areas with good fatigue properties, good compressive strength, and a high percentage of warp unidirectionals has led in several directions, but has not been solved at this writing. One type of fabric available from Owens Corning Knytex is warp unidirectionals similar to D155, produced by stitching strands to a light mat material (CM1701). D155 in weft unidirectional provides a good balance of properties at fiber contents below 42 percent, but is not produced as a warp unidirectional. The CM1701fabric was tested at 38 percent fiber volume fraction with the results showing disappointing tensile (R=0.1) fatigue results, with b = 0.126 and the million cycle strain at 0.64 percent.

Figures 5.84, 5.85 and 5.86 show photographs of the fabrics used in this study. Figure 5.84 shows the unidirectional stitches and adhesively bonded fabrics. The D072, D092, D155 and UC1018V fabrics had "good" fatigue behaviors (R = 0.1 and 10) up to a fiber volume fraction of approximately 0.40. At higher fiber contents the fatigue performance shifted towards the "worst" behavior shown in Figure 5.63. The A1010 and CM1701A fabrics performed below expectations and provided poor fatigue behavior, especially the A1010 fabric with loose stitching. Microscope specimens of these two materials revealed large and continuous matrix cracks around the stitching. It is believed

that the stitching provided a path for the cracks to develop and easily debond the fiber strands causing delamination and eventual failure.

Figure 5.85 details the woven unidirectional fabrics and three ±45° fabrics which were tested. The A060 fabric was poorly constructed with a weaving thread and thermoplastic bead which was more suited for heavier fabrics. The right hand side of the A060 fabric photograph shows thermoplastic adhesive from other beads on the fabric roll. This thermoplastic bead material did not bond well to the matrix materials and was a starter location for cracking. The A130 and A260 fabrics performed similar to the D155 stitched fabric in tension fatigue (R=0.1), but due to the pre-buckled geometry, had a ultimate compressive strength of less than 50 percent of the D155 fabrics. The DB120 fabric provided a higher static strength for a specific fiber content than the other fabrics. The DBM1204B fabric (not shown) was the DB120 stitched to a glass mat, which showed poor fatigue behavior as the other fabrics containing a mat.

Figure 5.86 shows the two Triax fabrics, front and back faces. The CDB-200 fabric showed consistently poor fatigue performance at all fiber contents, while the TV-3400 showed better fatigue performance. The TV-3400 fabric had less stitching and had a weight which was twice as heavy as the CDB-200 fabric. Additional tests on higher fiber volumes need to be performed on this Triax.

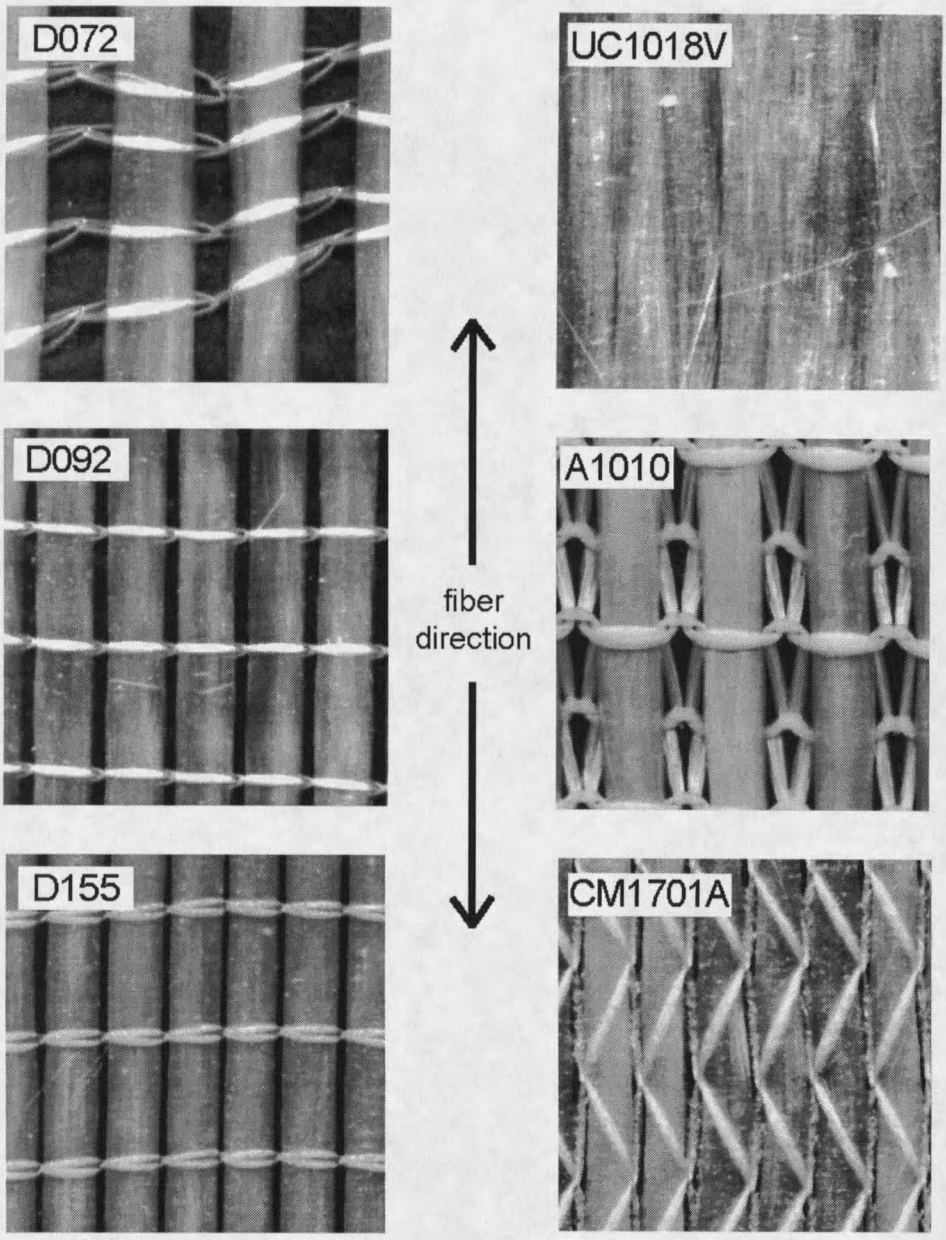


Figure 5.84. Photographs of unidirectional stitched and adhesively bonded fabrics.

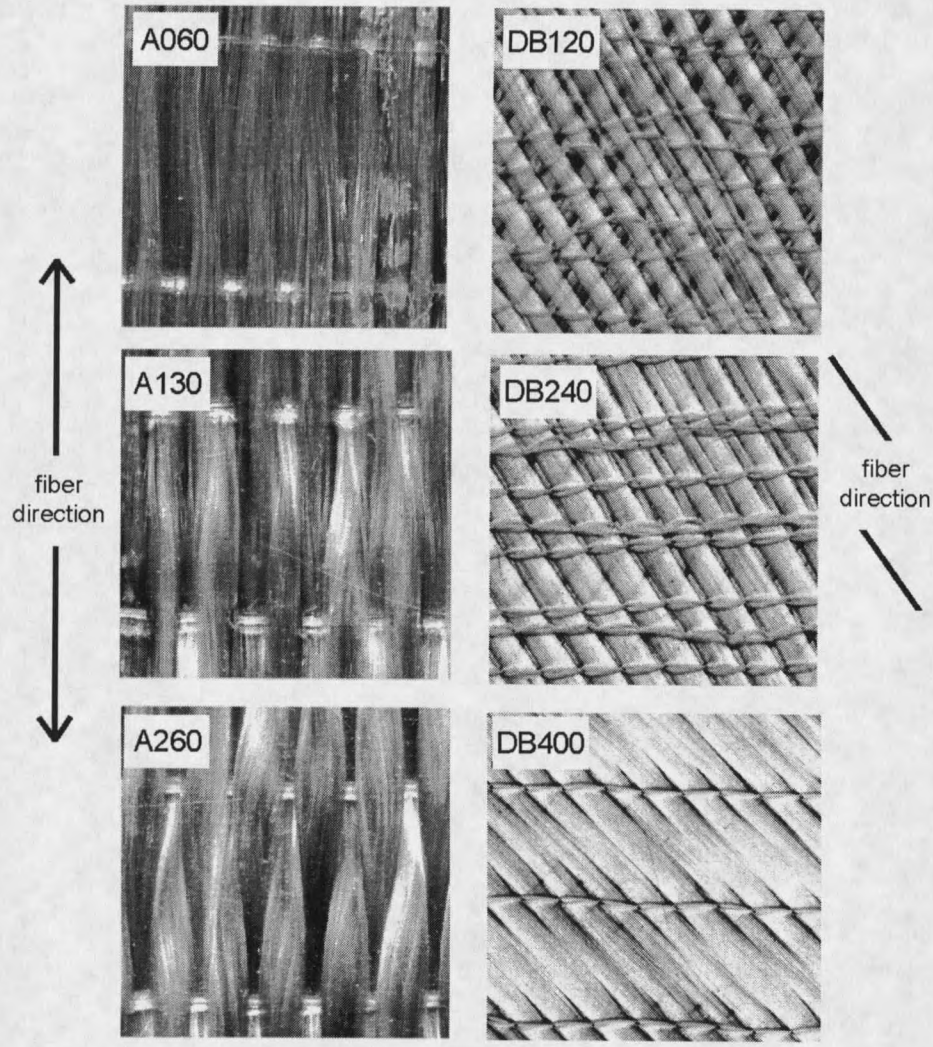


Figure 5.85. Photographs of woven unidirectional and stitched ±45° fabrics.

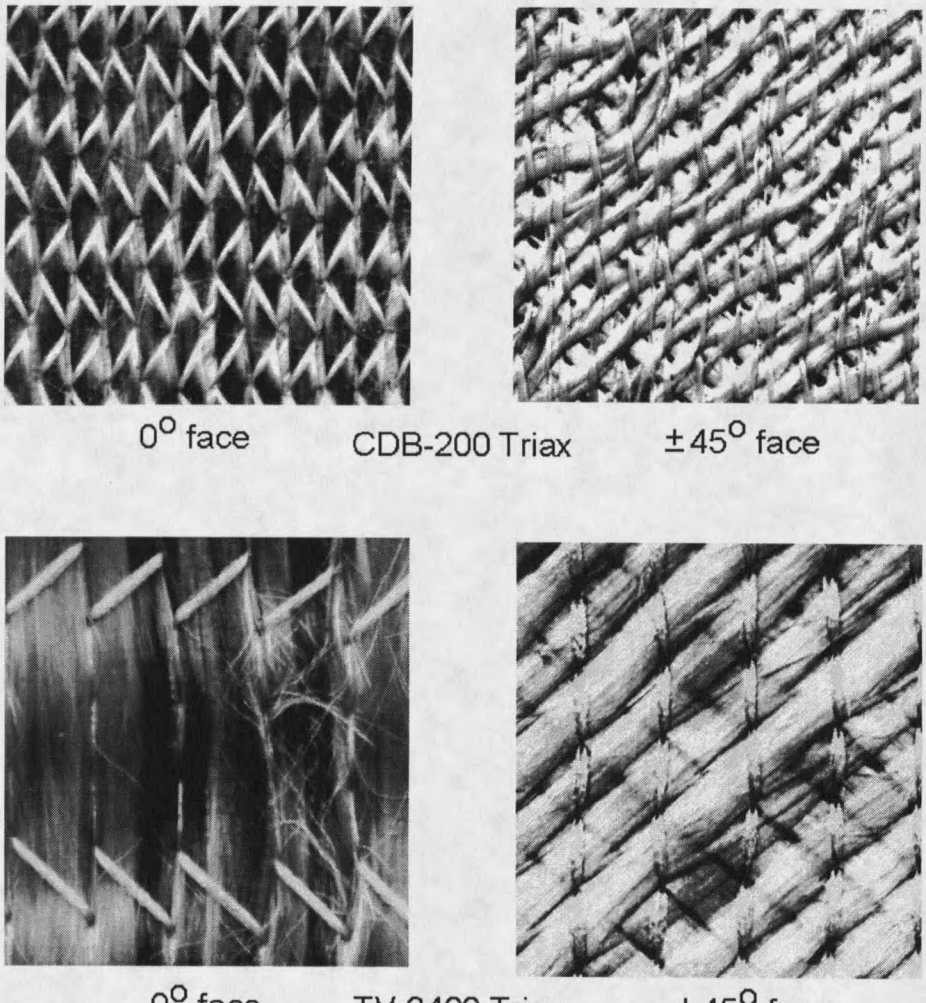


Figure 5.86. Photographs of stitched Triax fabrics.

Conclusions

The tensile fatigue (R = 0.1) performance of glass fibers and unidirectional strands is a property inherent in the fiber reinforcement. Smaller fiber strands gave the best tensile fatigue performance. The high cycle strand fatigue data suggest a leveling off of the S-N trend between 10^8 and 10^9 cycles, but more high cycle data are needed to establish this observation. No clear fatigue limit was observed. With fabrics containing stitching or weaving, this fatigue performance decreases to a fatigue coefficient of approximately 0.10 for lower fiber volume fractions, with a significant increase in sensitivity to around 0.14 for high fiber contents, where fatigue appears to be associated with stitching and matrix cracking.

The Triax material, based on CDB200 fabric with 0° and ±45° layers stitched together, shows poor performance even at low overall fiber contents; similar data for several other Triax materials are given in References 4 and 5, and in the database. The DD materials, with separate 0° and ±45° layers, show a transition from good to poor resistance as the fiber content increases, with the transition centered around 42 percent fiber by volume; this transition is at a slightly lower fiber content than with all 0° materials. When the stitching is manually removed from the D155, 0° fabric, the trend to increasing b with fiber content is shifted to still higher fiber contents, so that good fatigue resistance is now observed above 50 percent fiber by volume. The D155 materials with stitching removed are difficult to handle, and show fiber wash problems during matrix infiltration. Literature values [60, 61] for E-glass/epoxy prepreg laminates with a very uniform distribution of fibers in each layer show a b-value close to 0.10 at 50 to 60

percent fiber by volume, demonstrating that much of the fatigue problem in tension is related to the stranded fabrics.

It has been reported consistently in the course of this study [3, 4, 7] and in the European database [58] that changes in the matrix material have minimal effects on the static and fatigue properties of standard coupons. This has been explored under very well controlled conditions with the RTM process for materials DD5E, DD5P, DD5V, and other ±45° and 90° composites for epoxy, polyester, and vinyl ester matrices at the same fiber content and with other parameters held constant. All the data suggests that there is no significant difference in the fatigue performance of these composites using different matrix materials under dry, room temperature conditions. The main matrix effects occur in delamination resistance and environmental resistance, as reported in Reference 17.

CHAPTER 6

BALANCED ANGLE PLY LAMINATES

Background Information

To reduce the number of design variables, plies in most composites are orientated at either 0°, 90° or ±45°; however, other orientations may provide optimum properties in some applications. Furthermore, the ±45° fabrics used in this study had very poorly controlled orientation due to inaccuracies in the original fabric, or fiber movement either in handling or during the resin transfer molding process. Thus, a study of the effects of orientation on fatigue properties was performed. The initial study concentrated on balanced angle ply composites with angles of ±30°, ±40°, ±45°, ±50° and ±60°, which was later expanded to include ±10°, ±20°, ±70°, ±80° and 90° laminates.

Most of the materials in the database with ±45° plies used the Owens Corning Knytex DB120 fabric. The DB120 fabric, as well as the heavier DB240 fabric, has fiber tows that are loosely stitched together and can be easily stretched during handling and composite manufacture, which alters the fiber orientation angles. The ±45° fiber orientation of the fabric could be easily changed by approximately ±6° to ±10° by handling (fabric unrolling). The angle orientation change from ±45° had been noticed in all the MSU manufactured laminates and the industrial supplied materials included in the DOE/MSU composite material database [2]. The actual ply angles of the 0°/±45° and

±45° laminates listed in the database were measured following matrix digestion, and are summarized in Table 6.1. Most of the industrial materials involved an Owens Corning triaxial fabric (0°/±45°), CDB200, which is a 0° fabric (D092), stitched to a ±45° fabric (DB120).

Table 6.1. Measured angles of 0/±45 and ±45 materials listed in the database.

Material	Measured Angles	Average Measured ± Angles
F	[-55/48/0/-53/48/0/-49/47/0/-50/53/0]	49°/-52°
G	[0/-50/50/0/-50/51/0/-50/52/0/-50/53]	52°/-50°
H	[45/-43/0/50/-47/0/43/-47/0/0/49/-47/0/50/-46/0/44/-48]	47°/-46°
J	[0/47/-47/0/50/-46/0/45/-47/45/-46/0/46/-45/0/51/-42/0]	47°/-46°
M	[43/-49/0/43/-43/0/45/-46/0/37/-44/0]	42°/-46°
N	[42/-49/0/42/-50/0/42/-51/0/42/-48/0]	42°/-50°
P	[0/45/-42/Mat/0/0/Mat/40/-42/0]	43°/-42°
R	[0/33/-42/0/37/-39/0/49/-34/0/37/-42]	39°/-39°
T	[0/-53/54/0/-53/53/0/-54/53/0/-52/51]	53°/-53°
U	[0/42/-41/0/42/-42/0/43/-41/0/42/-42]	42°/-42°
V	[0/45/-46/0/45/-44/0/45/-45/0/46/-45]	45°/-45°
W	[55/-48/0/55/-48/0/56/-48/0/55/-48/0]	55°/-48°
X	[0/0/M/-51/50/0/0]	50°/-51°
Y	[0/0/M/35/-53/0/0]	35°/-53°
DB120	[42/-51]	42°/-51°
DB240	[42/-51]	42°/-51°
DB400	[40/-51]	40°/-51°

It was very difficult to prevent the original fiber orientations from changing during typical manufacturing operations. Careful fabric cutting, handling and RTM injection limited the maximum fiber misalignment of the DB120 fabric to approximately -3° deviation from the +45° ply and an average of +6° from the -45° ply giving an overall fabric orientation of [+42°/-51°]. This was the typical fiber orientation found in the MSU manufactured materials listed in the database dealing with the ±45° Knytex fabrics. The construction of larger, non-flat or more complex composite shapes would cause further difficulty with fabric handling during construction. Part of the fiber orientation problem is the physical tension force required as the fabric is spooled on and off of the fabric storage roll. This tension, and the loose structural stitching, allows for easier fiber reorientation, with biasing towards the fabric rolling (tension) direction. It should be noted that in high technology applications (prepreg or filament winding) such as aerospace, a fiber orientation tolerance of ±0.5° to ±1° is common.

Although this study involved balanced lay-ups, with equal numbers of +θ and -θ plies, more research is required to study the effects of unbalanced lay-ups, which would better represent the actual composites.

The balanced angle-ply composites were manufactured using six plies of the Owens Corning, Knytex D155 fabric and the CoRezyn 63-AX-051 orthothalic polyester resin. The D155 unidirectional fabric was easily manipulated into the various ply angles and the general D155 zero degree properties were well understood and documented in the database. A balanced laminate $(\pm\theta°)_N$, rather than a balanced symmetric laminate $(\pm\theta°)_S$ was used to more accurately represent the MSU manufactured materials listed in the

database. A symmetric eight-ply laminate would have two plies with the same orientation in the center. The double center ply would matrix crack in both plies at once creating a matrix crack two plies in width, compared with the single-ply cracks in typical laminates. Thus, the unsymmetric case was chosen to avoid larger matrix cracks.

General angle-ply data are summarized in the database and are also shown in Table 6.2, for the static strength, longitudinal modulus and major Poisson's ratio, which are values that could be calculated by standard laminate analysis techniques. Very limited angle ply fatigue data (R = 0.1) are available elsewhere [61-64], with all these data being at a high enough testing frequency (17 to 30 Hz) which may have forced thermal, rather

Table 6.2. Properties of MSU manufactured (RTM) fiberglass materials with balanced angle plies.

		R = 10			R = 0.1				
Angle	V_F %	UCS MPa	b_C	strain for 10^6 cycles, %	UTS, MPa	b_T	strain for 10^6 cycles, %	E, GPa	ν_{XY}
$[0]_5$	39	-653	0.077	-1.10	854	0.093	1.12	31.5	0.32
$[\pm 10°]_3$	38	-384	----	-----	277	0.068	0.62	27.9	0.38
$[\pm 20°]_3$	39	-287	----	-----	268	0.079	0.55	24.2	0.56
$[\pm 30°]_3$	40	-176	0.065	-0.48	186	0.098	0.43	17.7	0.67
$[\pm 40°]_3$	40	-132	0.095	-0.50	144	0.109	0.41	11.4	0.62
$[\pm 45°]_3$	38	-138	0.089	-0.65	107	0.109	0.40	9.79	0.57
$[\pm 50°]_3$	39	-138	0.085	-0.78	65	0.092	0.38	8.62	0.51
$[\pm 60°]_3$	40	-141	0.081	-0.94	37	0.074	0.25	7.65	0.35
$[\pm 70°]_3$	40	-136	----	-----	27	0.076	0.19	7.24	0.21
$[\pm 80°]_3$	38	-153	----	-----	26	0.087	0.17	7.16	0.10
$[\pm 90°]_3$	38	-123	0.062	-1.07	26	0.081	0.19	7.24	0.09
All R = 10 test coupons were 25 mm wide and had a 13 mm gage length.									

than mechanical fatigue failures. Other available data are limited to only ±45° angles [65, 66], again with most of the data being potential thermal failures. Reference [6] reported R = 0.1 tension fatigue tests on ±45° laminates at 6 Hz. A few high stress cycled coupons in this reference were probably thermal influenced, but the rest of the lower stressed data appear consistent with the database trends. The European FACT Database has a few dozen fatigue data points for ±10°, ±30° and ±45° at various R values [59] and different matrix materials, but not enough data are available to reach any general conclusions about trends.

Testing Methods

The testing of composites with off-axis plies involves two associated problems with the composite coupon geometry: the width and gage length. The coupon width part of the problem involves interlaminar stresses, specifically τ_{XZ}, for [+θ/-θ] ply laminates under uniaxial tension at the free edges, which can initiate cracks and delaminations that will propagate inward, towards the coupon center, until the coupon fails. Literature [67 to 75] indicates that the high interlaminar stresses (τ_{XZ}, τ_{XY}, σ_{ZZ}) could be treated as an edge effect and that the magnitude of these stresses reduces to laminate theory predicted values within one to two composite thicknesses away from the edges. Reference 76 reported that the failure of laminates with ply orientations less than approximately 35° to 40° is initiated at the free edges as a result of high interlaminar shear strains, but the failure of laminates with angles greater than approximately 40° were not sensitive to test coupon edge effects. A good discussion of edge effect stresses can be found in reference 75. The

effect of test coupon width was not studied and the width was kept constant, 25 mm, for all the static and fatigue tests.

Testing problems associated with the coupon gage length deal with restricting the fibers from rotating as the laminate is stressed. If the gage length is too short, the fibers will be continuously clamped at both ends of the coupon, which increases the internal stresses in the composite [69, 77, 78] and decreases the apparent strength and fatigue life. This was shown in the initial series of ±10° test coupons in the database which had a 100 mm gage length (fibers at both ends were clamped) that averaged 5,500 fatigue cycles at a maximum stress of 172 MPa and R = 0.1. When the gage length was increased to 160 mm, which prevented fibers from being clamped at both ends, the average number of cycles to failure increased to 185,000 cycles at the same stress level and R value. A listing of the gage lengths used in this study is shown in Table 6.3. The compression tests, in order to prevent buckling, required a short gage length which prevented the fiber ends from being free for all angles except the ±70°, ±80°and 90°coupons. In this study, all compression tests used the same 25 mm wide test coupon with a gage length of 13 mm. These results may not be representative of larger test coupons or structures.

Table 6.3. Tension and compression test coupon gage lengths.

Angle	Tensile gage length, mm	Compressive gage length, mm
±10°	160 and 100	13 mm
±20° to 90°	100	

Results and Discussion

The tensile stress-strain diagrams are shown in Figures 6.1 through 6.3 for the angle ply laminates. For the tensile strain values listed in these figures, a clip-on extensometer was used during the tests. Figure 6.1 shows the tensile behavior of the ±10°, ±20°, ±30°, and ±33° laminates. The ±10° and ±20° laminates show linear behavior to failure (brittle behavior), failing when the first matrix crack appears. The ±30° laminates start to show some non-linear behavior as the specimen remains intact with matrix cracks in all plies until sufficient delamination occurs to cause complete separation. The ±33° laminate was tested to better define the angular region where the more nonlinear material behavior begins. Figure 6.2 shows the tensile stress strain behavior of the ±40°, ±45°, and ±50° laminates. All three of these laminates showed extensive non-linear behavior as lamina cracking and delaminations formed and grew until coupon failure. It should be noted that the neat polyester matrix had a tensile strain to failure of only 2%. Reference 62 determined that the onset of damage in the ±45° laminates was due to lamina cracking and not interlaminar shear, as was the case found with the ±10°to ±30° laminates. The ±45° laminate, after onset of cracking, continues to sustain load and continued to form cracks all over the coupon until interlaminar crack growth started and continued until the final coupon failure.

Figure 6.3 details the stress-strain behavior of the ±60°, ±70°, ±80°, and 90° laminates, which showed little non-linear behavior and all had a strain to failure of less than 0.6%, which was much less than the failure strain of the neat polyester matrix. This weak behavior is associated with stress concentrations around the fibers, and voids, which

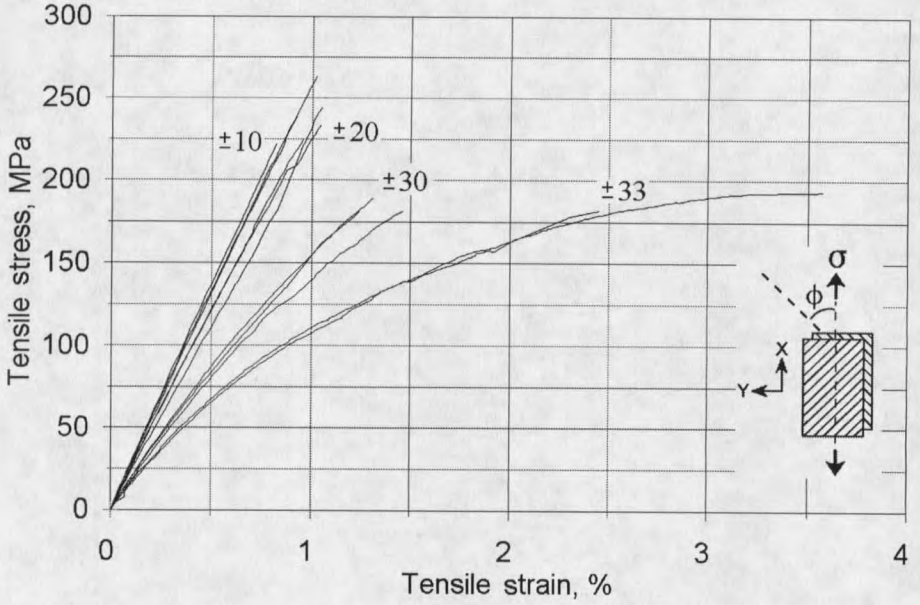


Figure 6.1. Tensile stress - strain curves for balanced ±10°, ±20°, ±30°, and ±33° angle ply laminates (D155 fabric, $V_F = 0.39$).

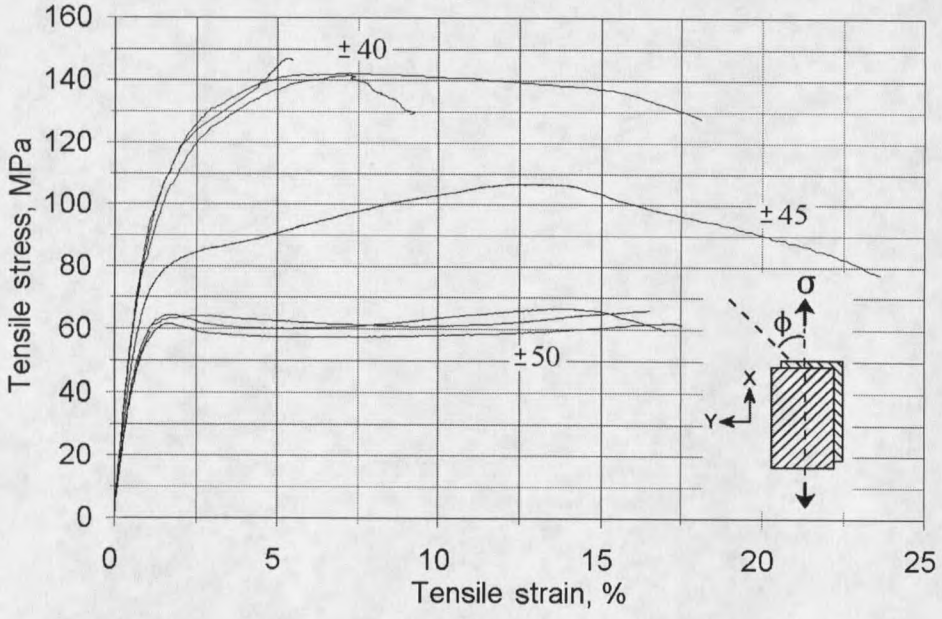


Figure 6.2. Tensile stress - strain curves for balanced ±40°, ±45°, and ±50° angle ply laminates (D155 fabric, $V_F = 0.39$).

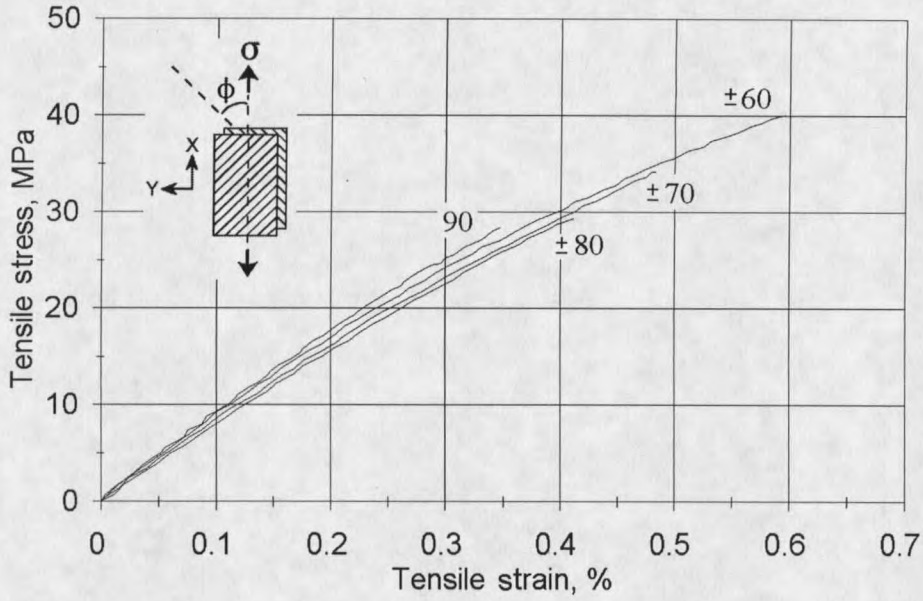


Figure 6.3. Tensile stress - strain curves for balanced ±60°, ±70°, ±80° and 90° angle ply laminates (D155 fabric, $V_F = 0.39$).

lower the transverse composite strength and strain to failure relative to the neat resin [79].

Figure 6.4 summarizes the average tensile static failure strain versus laminate ply angle. The strain to failure peaked with the ±45° laminate which could be classified as having a ductile material behavior, while the other laminates outside of the ±35° to ±50° range resemble brittle materials. Except for the overall magnitude of strain to failure, this figure is consistent with the one generated by Reference 62.

Compression stress-strain diagrams were generated for these laminates using an 18 mm gage length with bonded back-to-back strain gages (BLH FAE-25-35-S13EL-G) which had a 6.35 mm strain grid gage length. The longer coupon gage length was necessary to allow for the placement of the strain gages far enough away from the influence of the gripped coupon ends. The angle ply test coupon widths averaged 25.37

mm (S.D.= 0.21 mm) and the thickness averaged 3.08 mm (S.D.= 0.08 mm) for all of the coupons shown in the compression stress-strain diagrams. The stress-strain diagrams are truncated where the strain gages bifurcated, which was immediately followed by coupon failure.

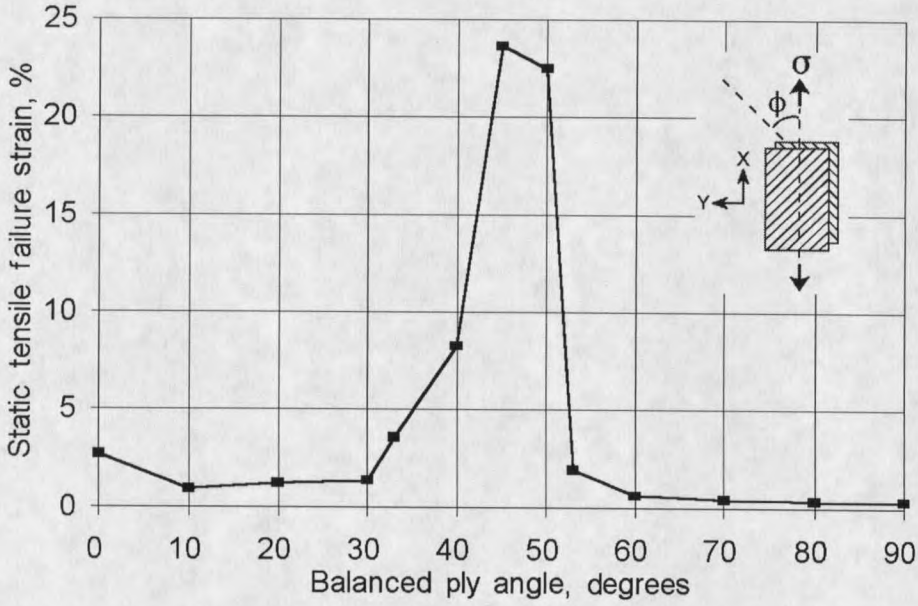


Figure 6.4. Ultimate tensile failure strain versus balanced ply angle.

The compression stress strain diagrams for ±10°, ±20°, ±30°, and ±40° are shown in Figure 6.5. As was the case in the tensile curves, the compressive ±10° and ±20° coupons show little non-linear behavior, and the ±30° and ±40° curves show an increasing amount of non-linear behavior. Since both strain gages are indicating the same strain, it must be inferred that the coupon, under the axial compressive stress, is barreling outward, rather than buckling to produce the nonlinear stress-strain behavior shown. This

same behavior is seen in Figure 6.6 with the ±50°, ±60°, ±70°, ±80°, and 90° laminates. The strain to failure and amount of non-linear behavior decreases as the angle is increased to 90°, as the mode of failure changes from barrelling to through-thickness shearing. The average calculated compressive strength versus ply angle is listed in Table 6.2 and the ultimate strain is shown in Figure 6.7. The minimum failure strain occurs at approximately ±30° while the maximum is at 0° and ±80°.

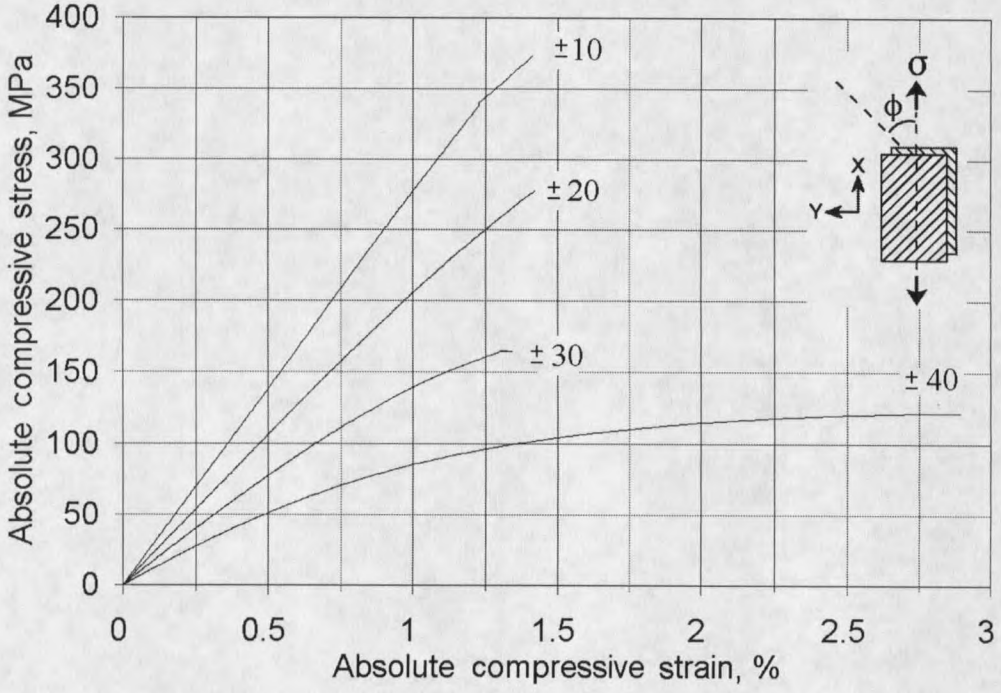


Figure 6.5. Compressive stress - strain curves for balanced ±10°, ±20°, ±30° and ±40° angle ply laminates (D155 fabric, $V_F = 0.39$, 25 mm test coupon width with a 18 mm gage length and unsupported edges).

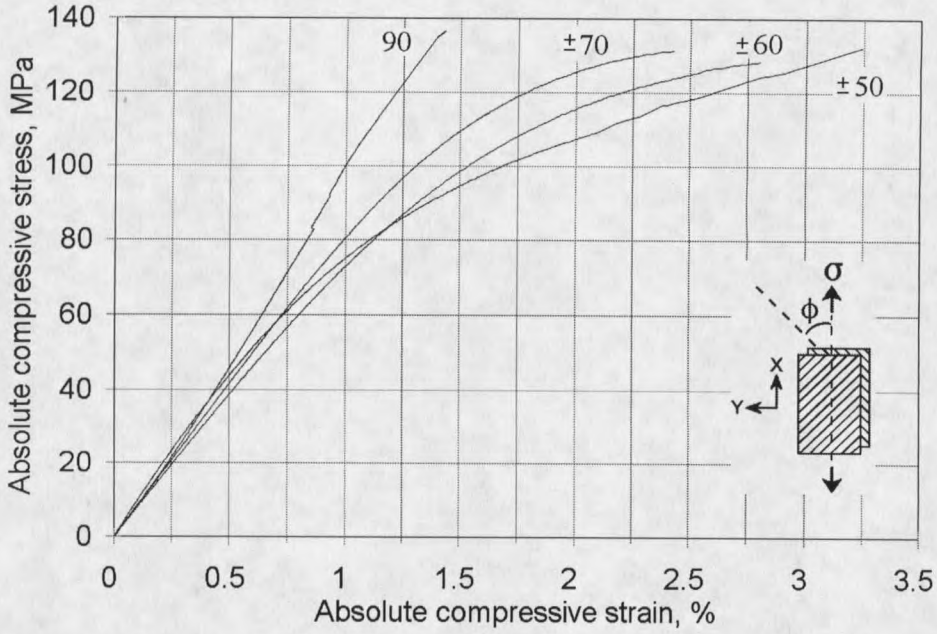


Figure 6.6. Compressive stress - strain curves for balanced ±50°, ±60°, ±70° and 90° angle ply laminates (D155 fabric, $V_F = 0.39$, 25 mm test coupon width with a 18 mm gage length and unsupported faces).

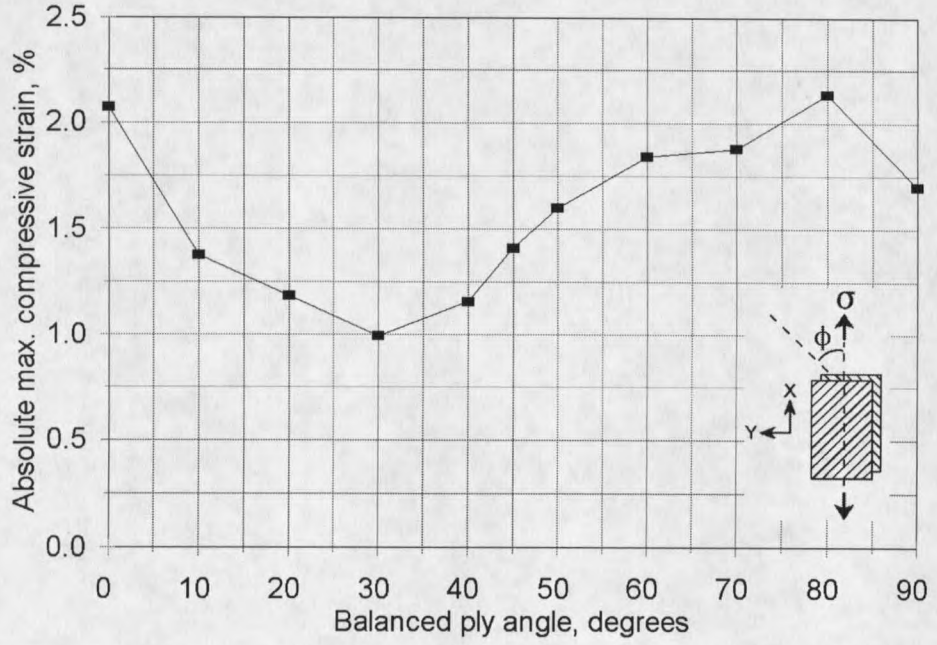


Figure 6.7. Calculated average ultimate compressive failure strain versus ply angle.

Laminate Analysis Predicted Properties

From the generated stress-strain diagrams, the load-direction modulus (E_X) was calculated and is shown in Figure 6.8 along with the laminate theory predicted values. These laminate theory calculations, as well as subsequent laminate analysis, used the property values listed in Table 6.4, which were taken from the database [2] and adjusted for fiber volume content, 0.39 versus the listed 0.45 using the formulae listed in the database. At least one coupon from each angle lay-up was tested with a 0°/90° strain gage to measure the major Poisson's ratio (υ_{XY}) which is shown with the predicted values in Figure 6.9. The predicted Poisson's ratios fall a little lower than of the measured values, which was the same result found in reference 22. (Reference 80 stated that the predicted value of the major Poisson's ratio is critically dependant on the value of the shear modulus used in the calculations and was probably the source of the variability seen.) Since only one test coupon per angle was tested, the variability of this parameter is unknown. The equations used a predicted shear modulus calculated from measured values using simulated shear tests (ASTM D3518) and Iosipescu V-notched shear coupons (ASTM D5379) reported in the database, and the variability of the measured value is probably the source of the over-prediction.

The calculated value of the shear modulus (G_{XY}) versus the ply angle is shown in Figure 6.10 for the angle ply laminates. As expected, the maximum shear modulus occurs at ±45°. Figure 6.11 shows the laminate analysis of the longitudinal stress (σ_{XX}), the transverse stress (σ_{YY}) and the in-plane shear stress (τ_{XY}) versus ply angle. All these stresses have been normalized with respect to the average tensile stress (σ_X) in the

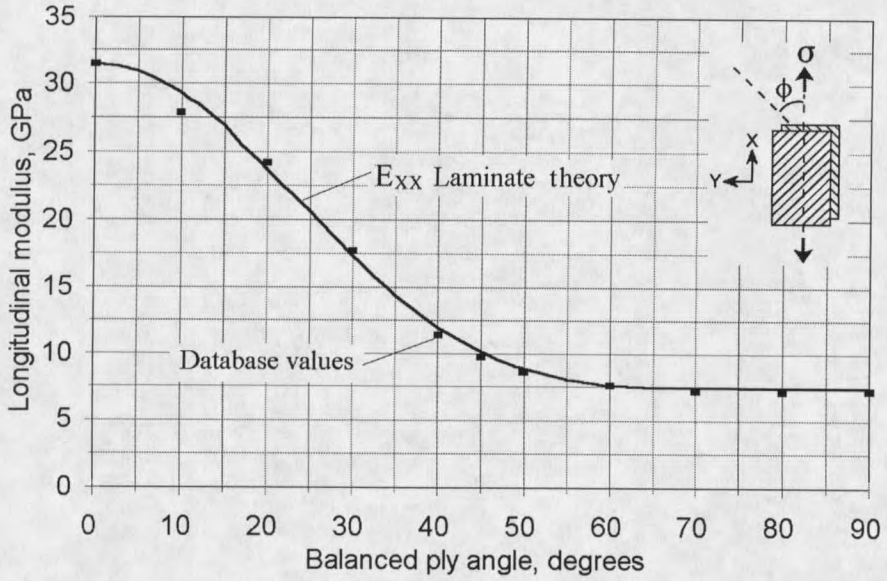
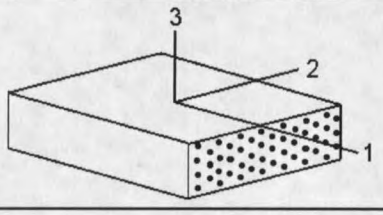


Figure 6.8. Longitudinal elastic modulus versus laminate theory predicted values (D155 fabric, $V_F = 0.39$).

Table 6.4. Ply properties used in the laminate theory analysis (static) and values used for million cycle fatigue predictions adjusted to a fiber volume fraction of 0.39.

Property	Static values	10^6 cycle fatigue values
Longitudinal Modulus, (E_{11})	31.5 GPa	31.5 GPa
Transverse Modulus, (E_{22})	7.42 GPa	7.42 GPa
Shear Modulus, (G_{12})	3.53 GPa	3.53 GPa
Major Poisson's Ratio, (υ_{12})	0.317	0.317
Ultimate Longitudinal Tensile Strain, ($ULTS_{11}$)	2.71 %	1.12 %
Ultimate Transverse Tensile Strain, ($UTTS_{22}$)	0.37 %	0.19 %
Ultimate Tensile Shear Strain, ($UTSS_{12}$)	2.38 %	0.91 %
Ultimate Longitudinal Compressive Strain, ($ULCS_{11}$)	-2.07 %	-1.10 %
Ultimate Transverse Compressive Strain, ($UTCS_{22}$)	-1.67 %	-1.07 %
Ultimate Compressive Shear Strain, ($UCSS_{12}$)	-2.38 %	-0.91 %
		

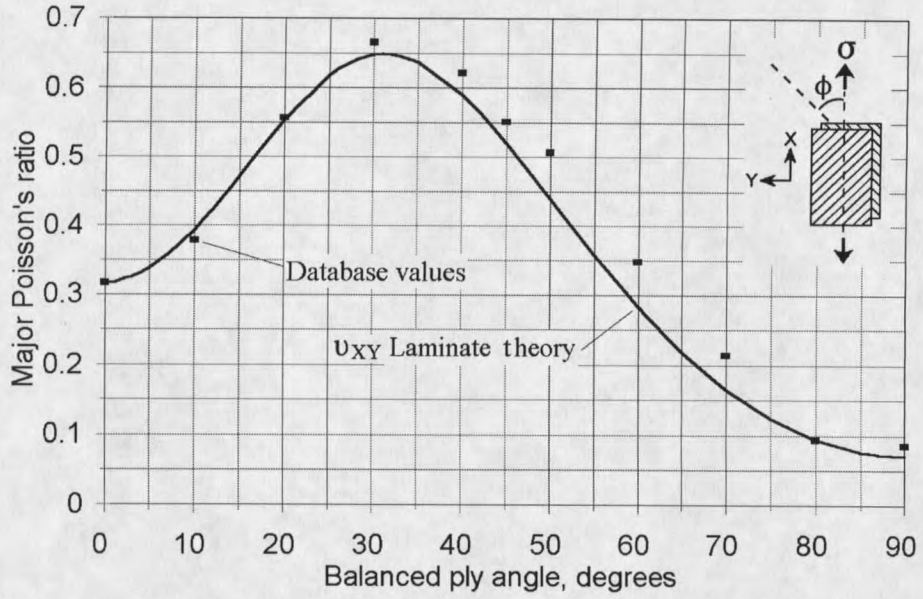


Figure 6.9. Major Poisson's ratio versus laminate theory predicted values (D155 fabric, $V_F = 0.39$).

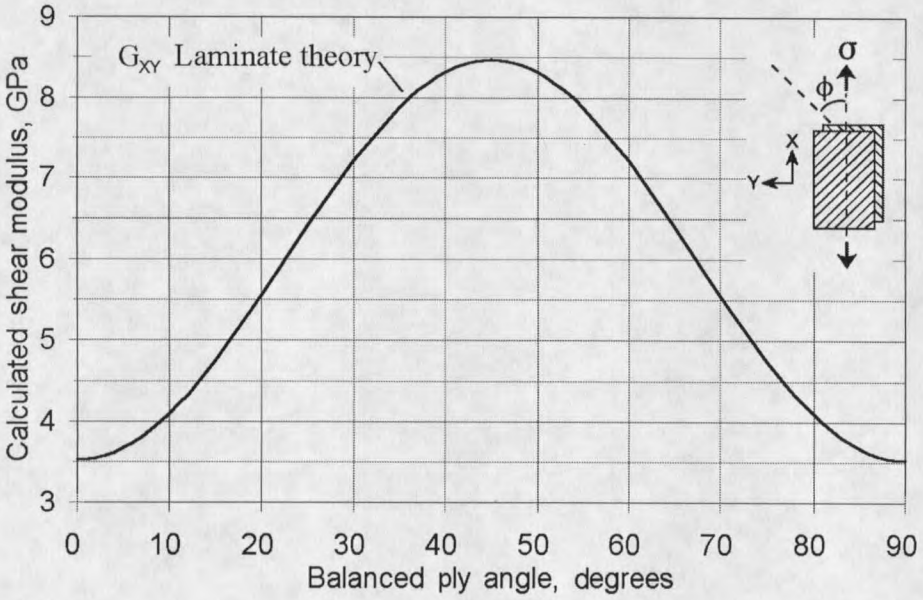


Figure 6.10. Calculated shear modulus versus balanced ply angle (D155 fabric, $V_F = 0.39$).

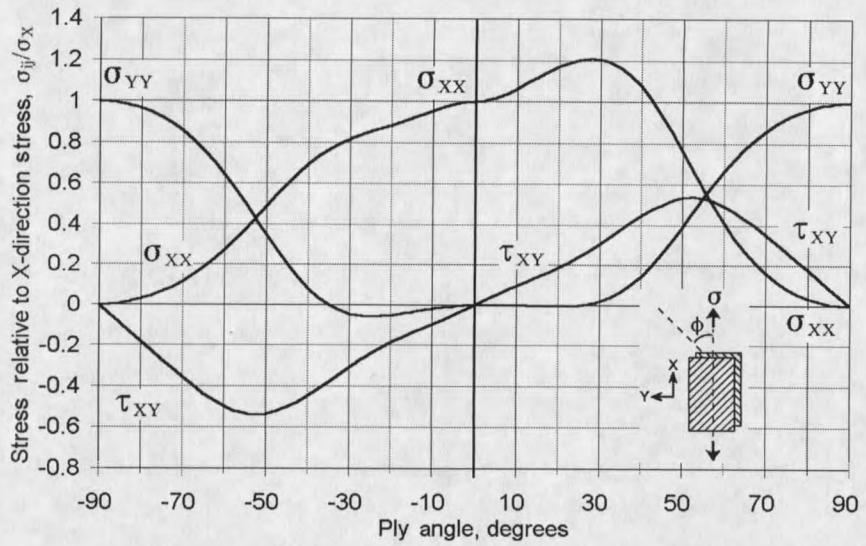


Figure 6.11. In - plane laminate stresses versus balanced ply angle ($\pm[\theta]_3$ laminate with D155 fabric, $V_F = 0.39$).

X-direction. Interesting observations of these stresses include: the maximum longitudinal stress is equal to 1.21 (σ_X) at 28°; the transverse stress has a minimum stress of -0.0046 (σ_X) at 20° and -0.057 (σ_X) at -25°, which is due to Possion contraction; and the shear stresses have a maximum and minimum value of ±0.539 (σ_X) at ±52°. There is also no tensile strain perpendicular to the fibers for fiber orientations less than ±28°, which is also the angle at which the longitudinal tensile stress starts to decrease. As expected, the magnitude of the shear stress is exactly ±0.500 (σ_X) at ±45° and is independent of the material type.

Using laminate analysis to predict the tensile and compressive strength of a laminate requires accurate strengths in the 0° and 90° directions of the plies. With these ply strength data to work from, the maximum strain failure criterion, maximum stress failure criterion or the quadratic failure criterion can be used to predict the strengths of the angle ply laminates. A more detailed discussion of these commonly used criteria can be found in Reference 75; the criteria are summarized in Equations 6.1 to 6.3.

Maximum Stress Failure Criterion

$$\sigma_{X_{FAILURE}} \geq \frac{\sigma_{LU}}{\cos^2\theta};$$

$$\sigma_{X_{FAILURE}} \geq \frac{\sigma_{TU}}{\sin^2\theta}; \qquad 6.1$$

$$\sigma_{X_{FAILURE}} \geq \frac{\tau_{LTU}}{\sin\theta\cos\theta}$$

Maximum Strain Failure Criterion

$$\sigma_{X_{FAILURE}} \geq \frac{\sigma_{LU}}{\cos^2\theta - \nu_{LT}\sin^2\theta};$$

$$\sigma_{X_{FAILURE}} \geq \frac{\sigma_{TU}}{\sin^2\theta - \nu_{LT}\cos^2\theta}; \qquad 6.2$$

$$\sigma_{X_{FAILURE}} \geq \frac{\tau_{LTU}}{\sin\theta\cos\theta}$$

Quadratic Failure Criterion

$$(\sigma)_{FAILURE} = F_1\sigma_{LU} + F_2\sigma_{TU} + F_{11}\sigma_{TU}^2 + 2F_{12}\sigma_{TU}^2 \geq 1; \text{ where}$$

$$F_1 = \frac{1}{X_T} + \frac{1}{X_C} \qquad F_2 = \frac{1}{Y_T} + \frac{1}{Y_C} \qquad 6.3$$

$$F_{11} = \frac{-1}{X_T\ X_C} \qquad F_{22} = \frac{-1}{X_T\ X_C}$$

$$F_{12} = \frac{-1}{2}\sqrt{F_{11}\ F_{22}}$$

$\sigma_{X_{FAILURE}}$ - *X-direction Ultimate failure stress*
σ_{LU} - *Longitudinal ultimate failure stress*
σ_{TU} - *Transverse ultimate failure stress*
τ_{LTU} - *Ultimate shear stress*
ν_{LT} - *Major Poisson's ratio*
X_T - *Longitudinal ultimate tensile strength*
X_C - *Longitudinal ultimate compressive strength*
Y_T - *Transverse ultimate tensile strength*
Y_C - *Transverse ultimate compressive strength*

The maximum strain and maximum stress criteria assume that failure occurs whenever any one component of stress or strain attains a limiting value, independent of the other stress component values. The mode of failure changes as different maximum values are exceeded as the ply angle changes. The major difference between the maximum stress and maximum strain criteria is the presence of a Poisson term in the denominator of the maximum strain criterion; however, the numerators are equivalent. Both the maximum stress and maximum strain criteria lack coupling or interaction effects between the various stress components. The quadratic criterion (which has gone through many revisions as the Tsai-Hill, Tsai-Wu, and Interaction criteria) takes into account the interaction between the stresses to predict failure. Literature tends to suggest that these criteria have a better correlation with experimental data. The quadratic failure theory uses a second order equation which makes no distinction between the positive and negative laminate strengths, which are usually different in magnitude; and does not distinguish between failure mode types. All of these criteria predict first ply failure, and do not consider interlaminar stresses.

Figure 6.12 shows the predicted tensile strengths for a $[\pm\theta^\circ]_3$ laminate. These results show the extreme sensitivity of strength to any misalignment of fibers when the plies are oriented close to 0°. The strength correlation for balanced angle laminates less than ±30° is poor (apparently due to delamination failures described later), while for ply angles greater than ±35°, the predicted strengths are in good agreement with experimental results. All three failure theories are in close agreement with each other, especially for angles greater than ±40°. The compression strength predictions are shown in Figure 6.13. The failure mode predictions from the maximum strain and maximum stress failure criteria are shown in Table 6.5. Reference 61 determined that fiber failure only occurred

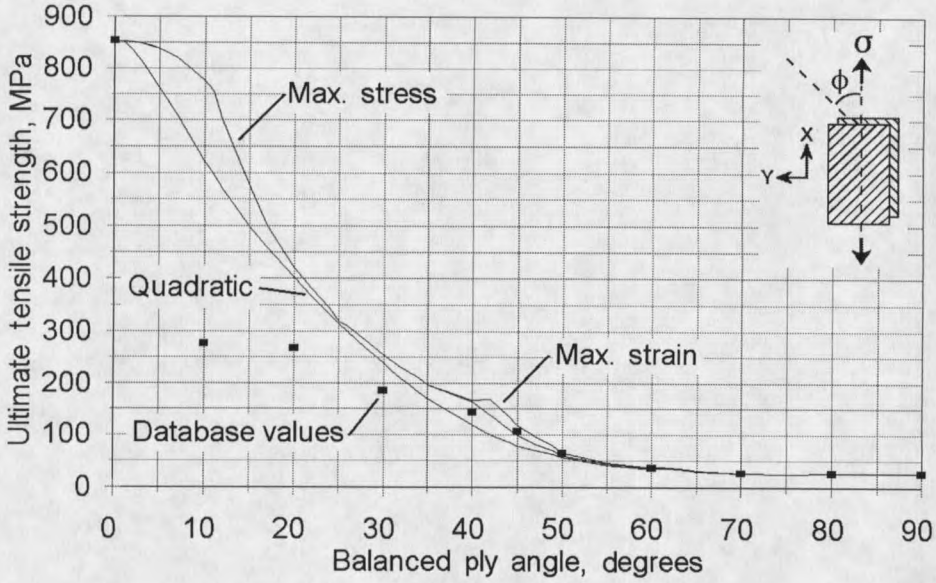


Figure 6.12. Ultimate tensile strength versus balanced ply angle with laminate theory predicted values for first ply failure from the maximum stress, maximum strain and quadratic failure theories.

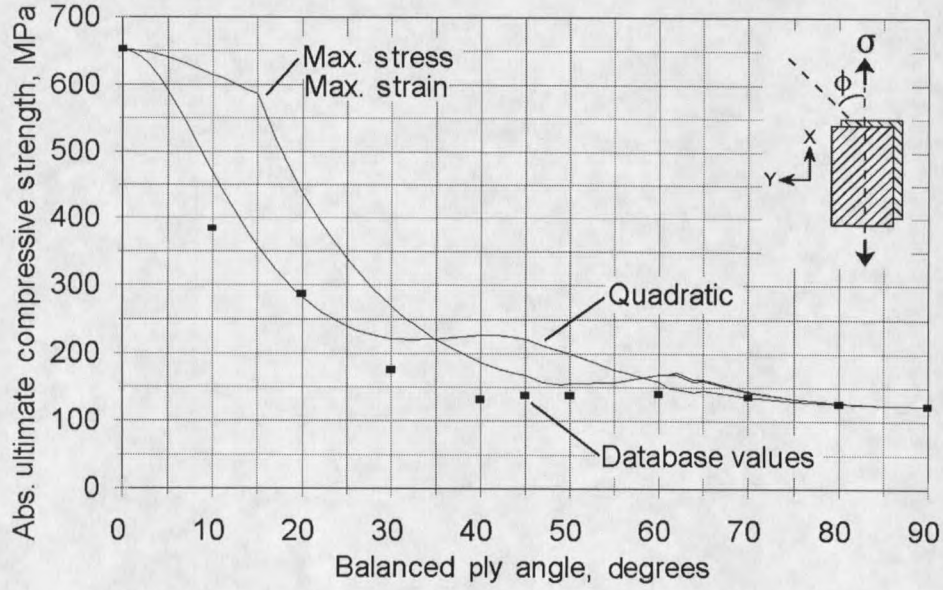


Figure 6.13. Ultimate compressive strength versus balanced ply angle with laminate theory predicted values for first ply failure from the maximum stress, maximum strain and quadratic failure theories.

for fiber angles 0°±2° to the applied stress, whereas the failure criteria predicted fiber failure at angles up to ±9°.

Table 6.5. Failure criterion failure mode predictions for the balanced angle ply laminates with a fiber volume fraction of 0.39.

Criteria	Tension	Compression
Maximum Strain	Fiber tensile - 0° to ±9°	Fiber compression - 0° to 3°
	Resin shear - ±10°to ±43°	Resin shear - ±4°to ±63°
	Resin tensile - ±44° to 90°	Resin compression - ±64° to 90°
Maximum Stress	Fiber tensile - 0° to ±9°	Fiber compression - 0° to 11°
	Resin shear - ±10°to ±41°	Resin shear - ±12°to ±61°
	Resin tensile - ±42° to 90°	Resin compression - ±62° to 90°

Fatigue Testing

A major difficulty with fatigue testing of polymer composites is the material hysteric heating which can cause thermal, rather than a mechanical fatigue failure. The initial (first cycle) hysteresis loop, loaded to a normalized stress of S/So = 0.5 (R = 0), was determined for one of the coupons from each angle ply group, shown in Figure 6.14. The area contained within this hysteresis loop is the energy that has to be dissipated as heat per fatigue cycle at the applied stress is shown in Figure 6.15. This figure shows the same trend as for the ultimate tensile failure strain versus ply angle (Figure 6.4). Due to the amount of hysteresis present in the ±10° to ±52° coupons, the fatigue coupon temperature was aggressively monitored to ensure that a thermal failure did not occur.

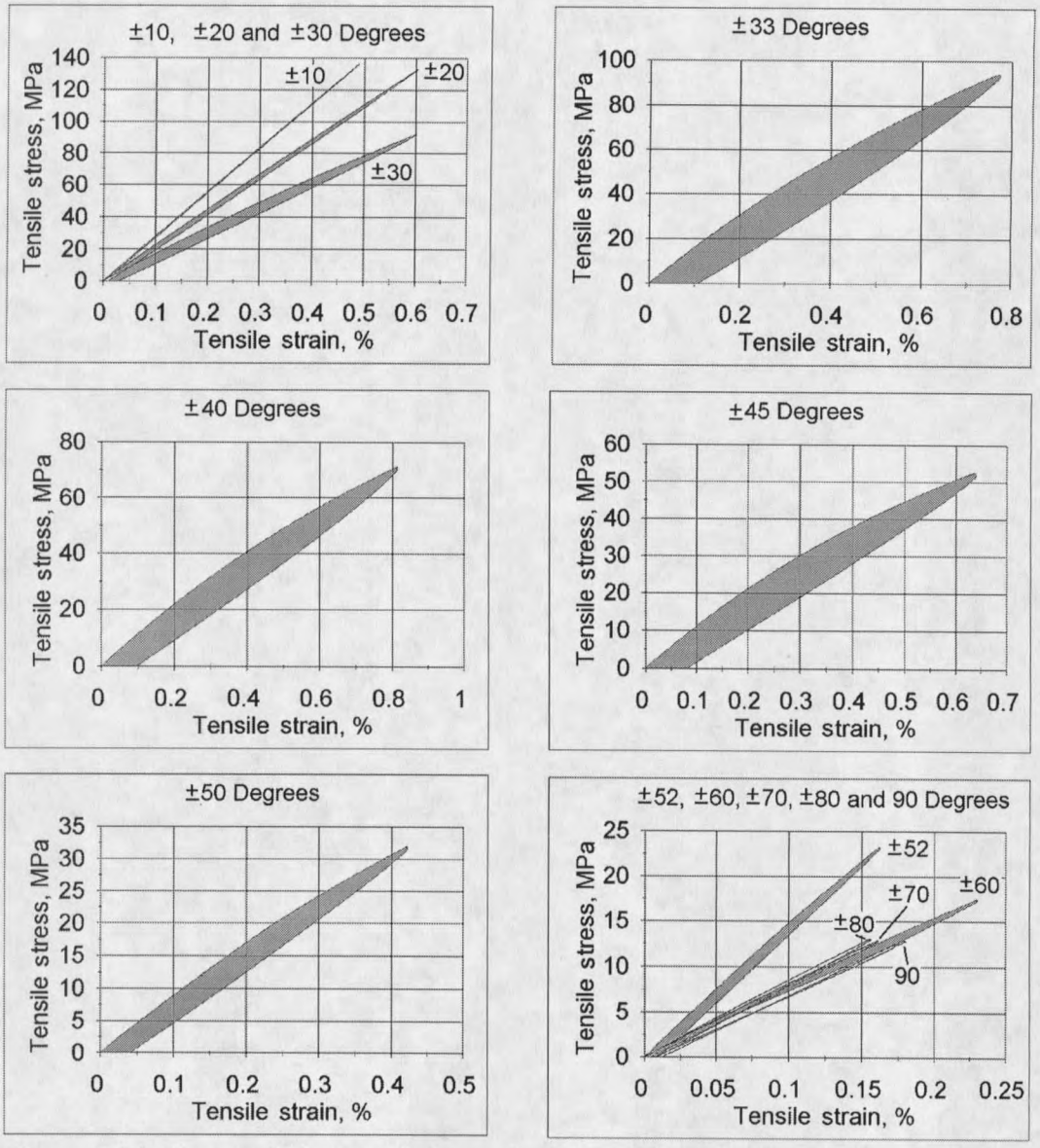


Figure 6.14. First cycle hysteresis loops for balanced angle ply laminates from ±10° to 90°with a maximum stress equal to 50% of the laminates UTS (R=0, D155 fabric, $V_F = 0.39$).

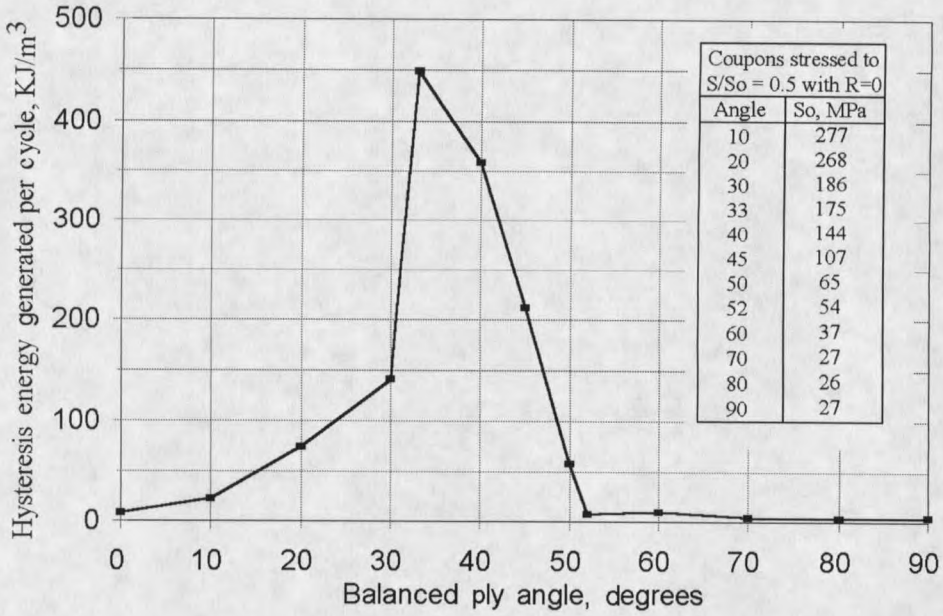


Figure 6.15. Hysteresis energy generated on the first cycle for balanced angle ply laminates from 0° to 90°with a maximum stress equal to 50% of the laminates UTS (R=0, D155 fabric, $V_F = 0.39$).

The amount of hysteric energy dissipated decreases from this first-cycle value as the fatigue test continues. For example, a ±10° coupon after 2,500 cycles (n/N ~ 0.001), at a maximum stress of 139 MPa (S/So = 0.5, R=0.1) had a hysteric energy per cycle of 14 percent of the first cycle value; a ±45° coupon after 2,500 cycles (n/N ~ 0.15), at a stress of 54 MPa (S/So = 0.5, R = 0.1) had a hysteric energy per cycle of 23 percent. As the fatigue test continues, and damage accumulates, the hysteric energy per cycle will start to increase until coupon failure. This increase occurs during the last five to ten percent of the fatigue life.

Tensile fatigue tests at R values of 0.1 gave the results shown in Figures 6.16 through 6.19. The data are also summarized in Table 6.2. All the materials have a

relatively linear tensile fatigue behavior when plotted on a semi-log graph. The tensile fatigue strain for one million cycles versus ply angle is shown in Figure 6.20 along with the laminate analysis predicted first ply (one cycle) cracking where, at angles greater than ±50°, the first ply static cracking strain is approximately twice the failure strain at one million cycles. The figure also shows the laminate analysis predicted million cycle first ply cracking strain which was calculated using the 0°and 90° initial million cycle strain values for the maximum strains in the laminate analysis. The shear strain values used in the analysis were adjusted by taking the maximum Iosipescu (ASTM D5379) shear strain multiplied by a factor of 0.40 (b value reduction of 0.10 x 6 log decades). The values are summarized in Table 6.4. Figure 6.21 summarizes the tensile fatigue coefficient, b, (R = 0.1) versus the ply angle. As the ply angle is increased, the fatigue data trends tend to flatten-out and give lower values of b due to the decrease in ultimate tensile strength. Interlaminar stresses and delamination are probably the cause of the b value increase in the ±20° to ±50° range.

Compression fatigue tests were performed at an R value of 10 for the ±30°, ±40°, ±45°, ±50°, ±60° and 90° lay-ups, summarized in Figures 6.22 and 6.23. The compressive fatigue strain for one million cycles versus ply angle is shown in Figure 6.24 along with the laminate analysis predicted static first ply cracking for the angle laminates tested. The predicted million cycle strains are also shown in the figure and the predicted values do not accurately follow the database values, probably due to the inability of the equations to predict delamination and buckling in the test coupons. The compressive fatigue coefficient, b, (R =10) versus the ply angle is shown in Figure 6.25.

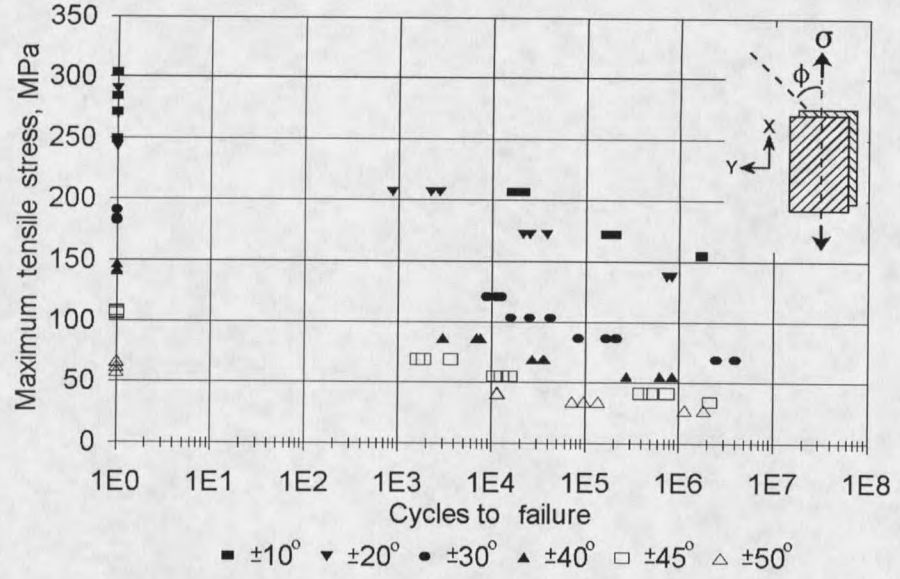


Figure 6.16. Tensile fatigue stress versus cycles to failure data for balanced ±10° to ±50°laminates ($\pm[\theta]_3$ laminates with D155 fabric, V_F = 0.39).

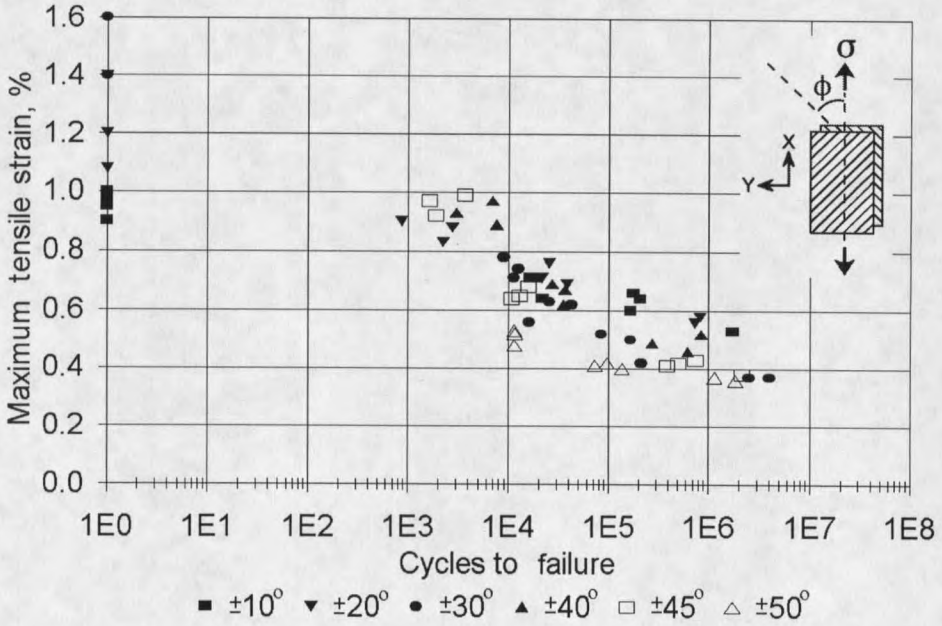


Figure 6.17. Tensile fatigue strain versus cycles to failure data for balanced ±10° to ±50°laminates ($\pm[\theta]_3$ laminate with D155 fabric, V_F = 0.39).

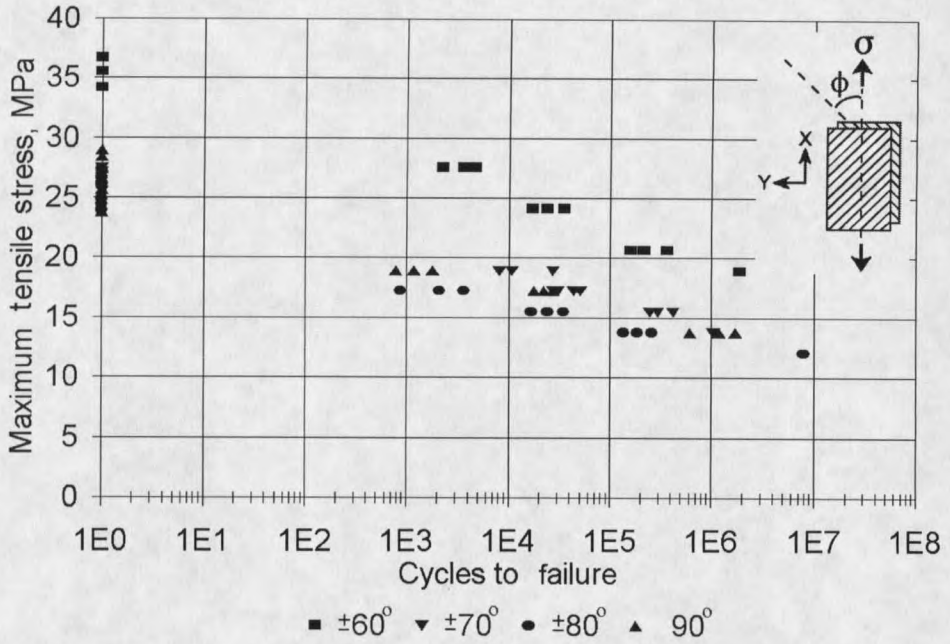


Figure 6.18. Tensile fatigue stress versus cycles to failure data for balanced ±60° to 90°laminates ($\pm[\theta]_3$ laminate with D155 fabric, V_F = 0.39).

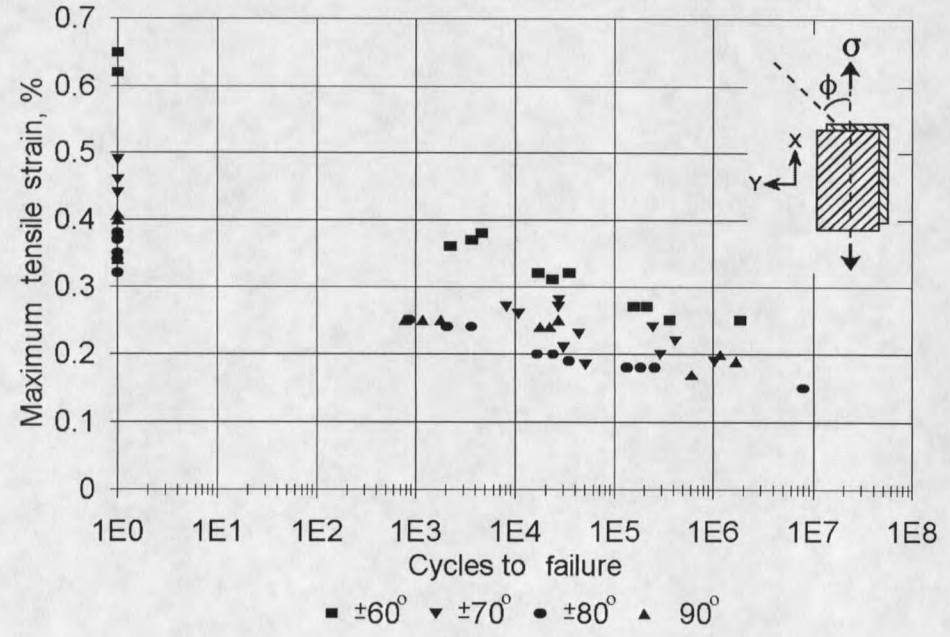


Figure 6.19. Tensile fatigue strain versus cycles to failure data for balanced ±60° to 90°laminates ($\pm[\theta]_3$ laminate with D155 fabric, V_F = 0.39).

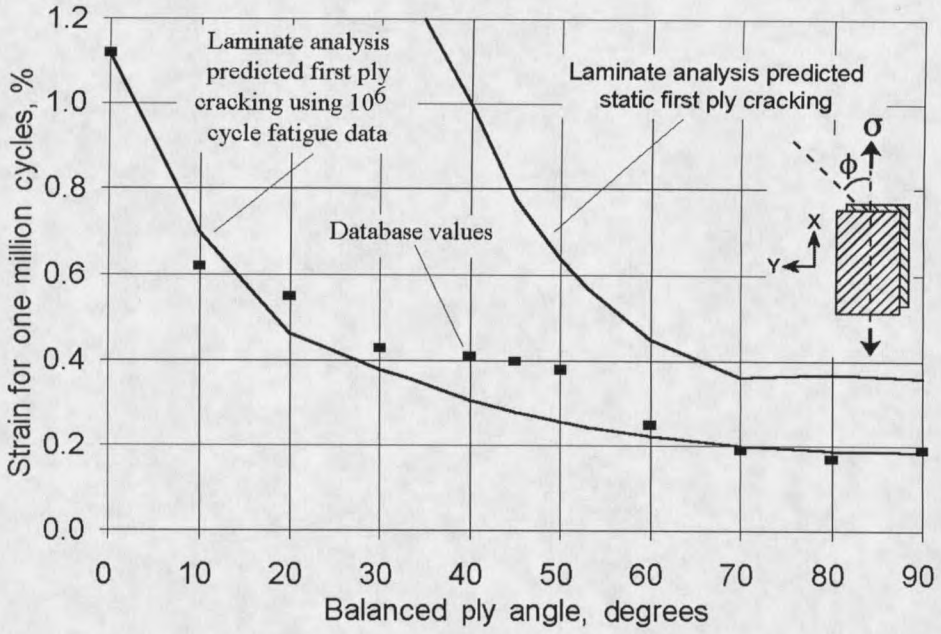


Figure 6.20. One million cycle tensile fatigue failure strain versus balanced ply angle with laminate analysis predicted (maximum stress criterion) first ply static cracking strain and predicted million cycle strain. $(\pm[\theta]_3$ laminate with D155 fabric, $V_F = 0.39$, $R = 0.1)$.

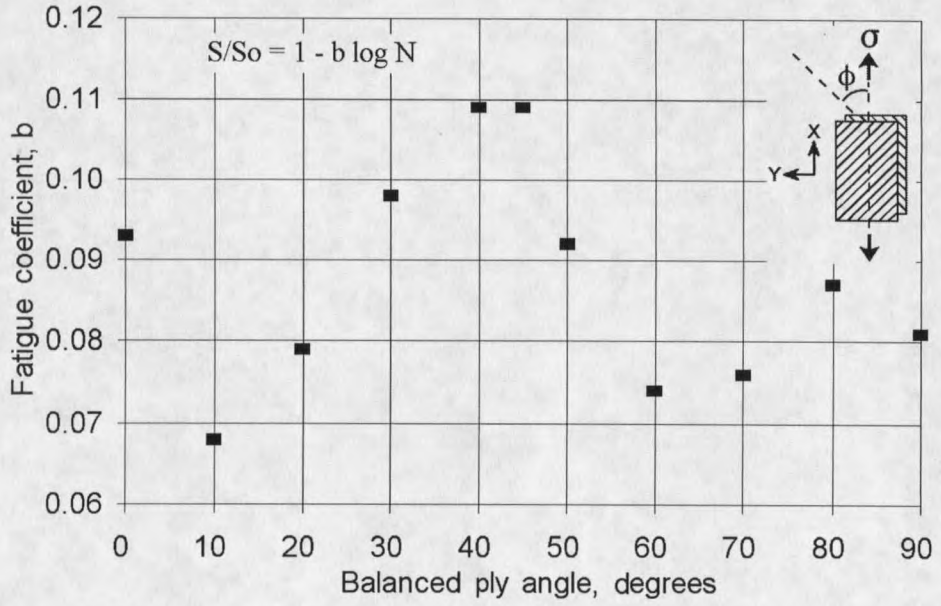


Figure 6.21. Tensile fatigue coefficient, b, versus balanced ply angle $(\pm[\theta]_3$ laminate with D155 fabric, $V_F = 0.39$, $R = 0.1)$.

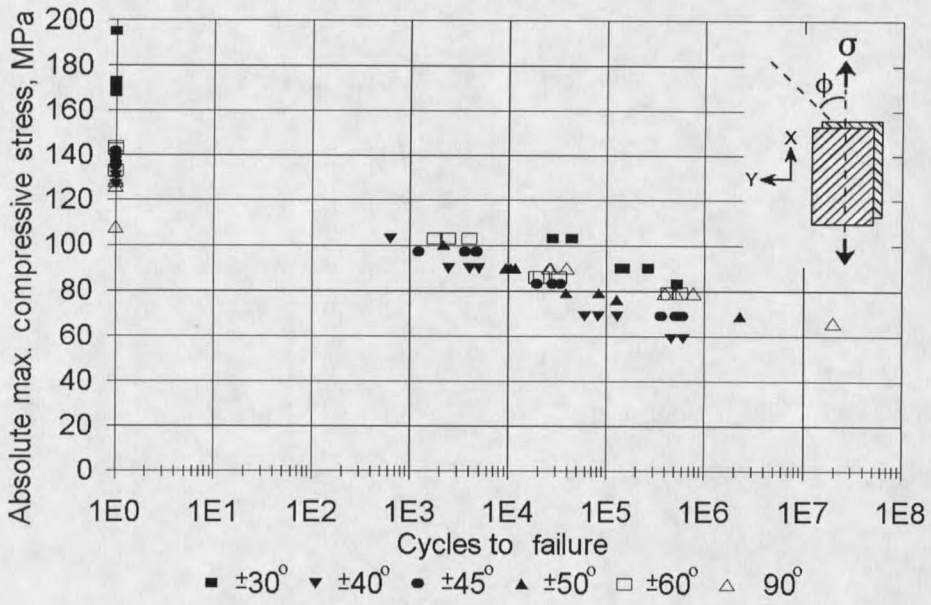


Figure 6.22. Compressive fatigue stress versus cycles to failure data for balanced ±30° to 90°laminates ($\pm[\theta]_3$ laminate with D155 fabric, V_F = 0.39).

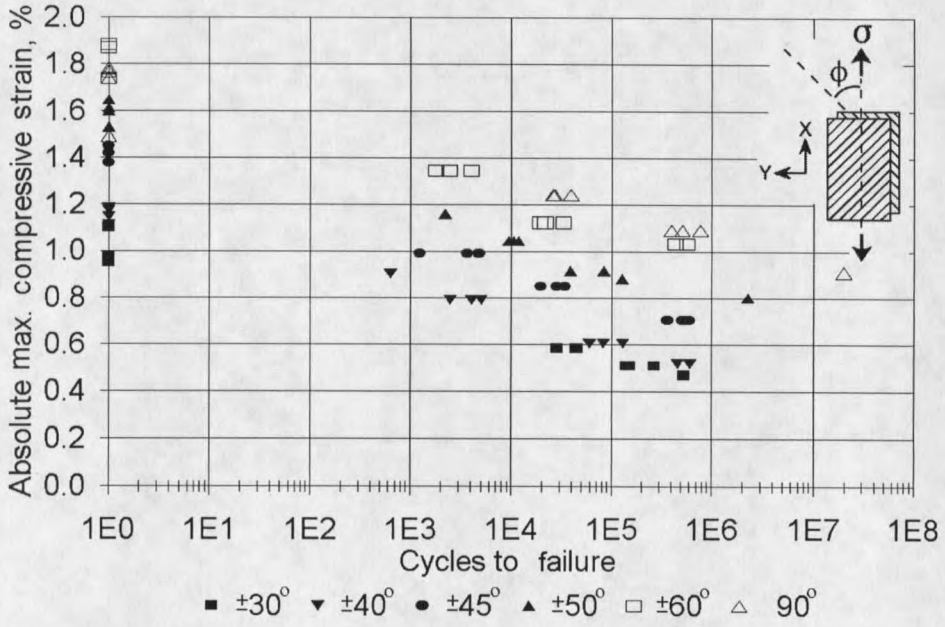


Figure 6.23. Calculated compressive fatigue strain versus cycles to failure data for balanced ±30° to 90°laminates ($\pm[\theta]_3$ laminate with D155 fabric, V_F = 0.39).

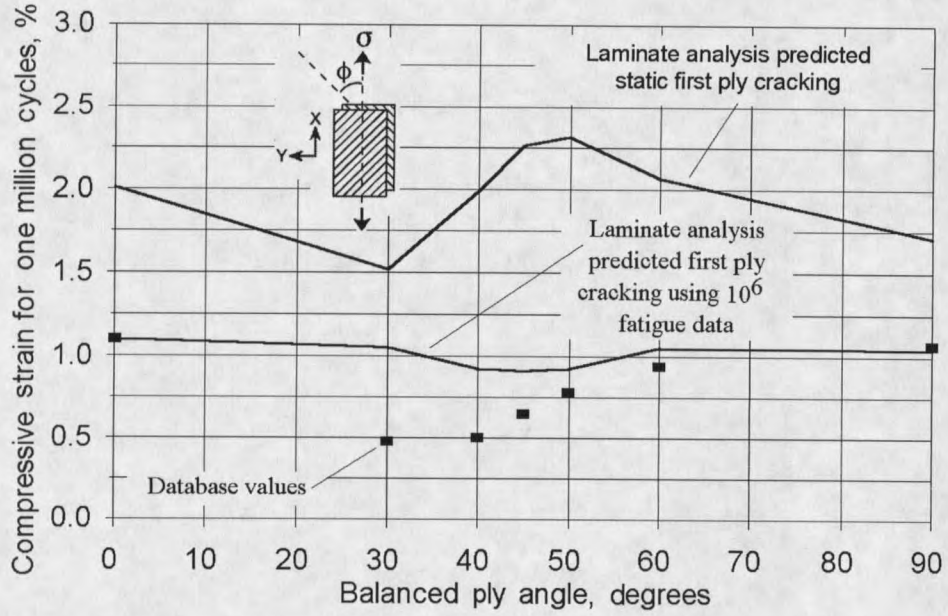


Figure 6.24. One million cycle compressive fatigue strain versus balanced ply angle with laminate analysis predicted (maximum stress criterion) first ply static cracking strain and predicted million cycle fatigue strain ($\pm[\theta]_3$ laminate with D155 fabric, $V_F = 0.39$, R = 10).

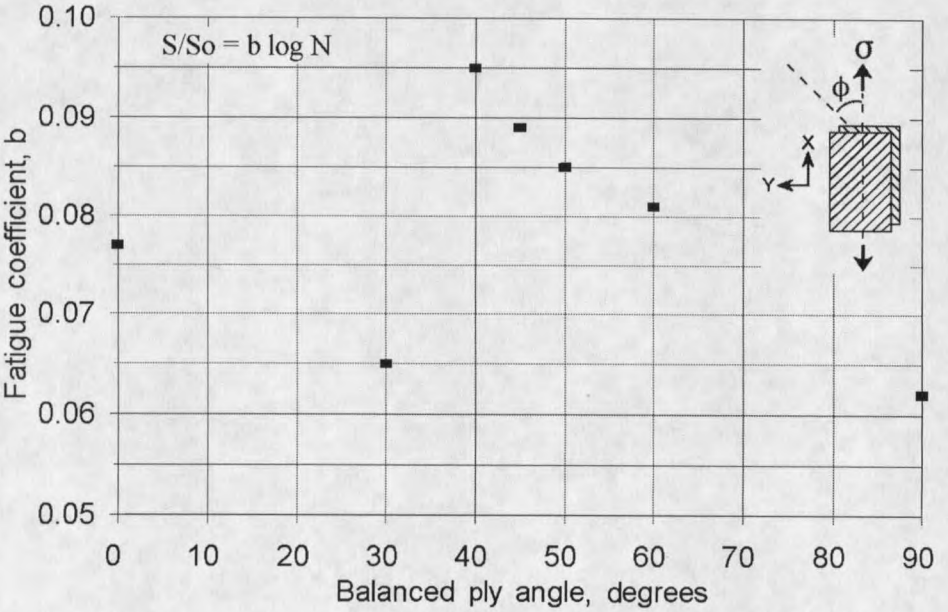


Figure 6.25. Compressive fatigue coefficient, b, versus balanced ply angle ($\pm[\theta]_3$ laminate with D155 fabric, $V_F = 0.39$, R = 10).

Failure modes

Tensile coupon fatigue failures are shown in Figures 6.26 through 6.29 and compressive fatigue failures in Figures 6.30 and 6.31. In all cases, no fiber failure was observed, except for 0°. In the absence of fiber failure, both transverse cracks and delaminations are necessary for complete fracture to occur at most orientations. Reference 61 did not report any fiber failures for fiber angles outside the range of 0°±2°. Matrix cracks and delaminations which formed, grew parallel to the fiber direction and involved the entire ply thickness. The individual failure mode types (as predicted by the maximum strain and maximum stress failure criteria in Table 4) were not as easily seen, due to complex interaction of the cracks and delaminations.

Failed tensile coupons from ±10° to ±30° are shown in Figure 6.26. In all these coupons, the failure started with edge delamination parallel to the fibers and between the D155 tows, and no fiber tow failures were found. The edge delamination grew inwards, between the plies, until failure. As the ply angle was increased, the overall size of the delaminated area decreased. The ±10° and ±30° laminates did not show any internal delamination initiation whereas the ±20° did show delamination initiation at each D155 stitch crossover point as shown in Figure 6.27. These cracks initiated at the stitch crossover point and grew perpendicular to the applied stress and were continuous through the coupon thickness, involving multiple plies. A few of the ±30° test coupons showed a few dozen of these stitch crossover cracks limited to areas within 10 to 15 mm of the gripped ends. Figure 6.26 shows three different ±30° failed coupons, two of which failed from multiple edge delaminations and one from a single delamination failure. Reference 61 reported that for angles less than ±40° the failure mode was delamination, which was

also seen in these tests.

Figure 6.28 shows failed coupons from ±40°, ±45°and ±50°. The delaminations initiated uniformly all over the gage length at stitch crossover points and at the edges. The edge delaminations grew inward approximately 3 to 5 mm before joining with the internally initiated delaminations. Enough damage was generated in these coupons that at failure (unloaded), due to the axial extension, the coupon width had significantly decreased. This decrease was on the order of 0.4 mm for the ±40° coupon, 2 mm for ±45° and 0.5 mm for the ±50° coupon. The delamination in the ±50° coupon also generally grew in one ply direction which completely separated the plies from each other and allowed the three plies in the other orientation to rotate, creating a width offset in the coupon which can be seen in Figure 6.28.

Failed tensile coupons for the ±60°, ±70°, ±80° and 90° are shown in Figure 6.29. The ±60° coupon has a width offset similar to the ±50° failures. This offset was not present in coupons with angles greater than ±60°. As the angle was increased, the number of crack initiation sites was reduced, to the extent that at 90°, the first major crack generally grew parallel to the fibers causing final coupon failure.

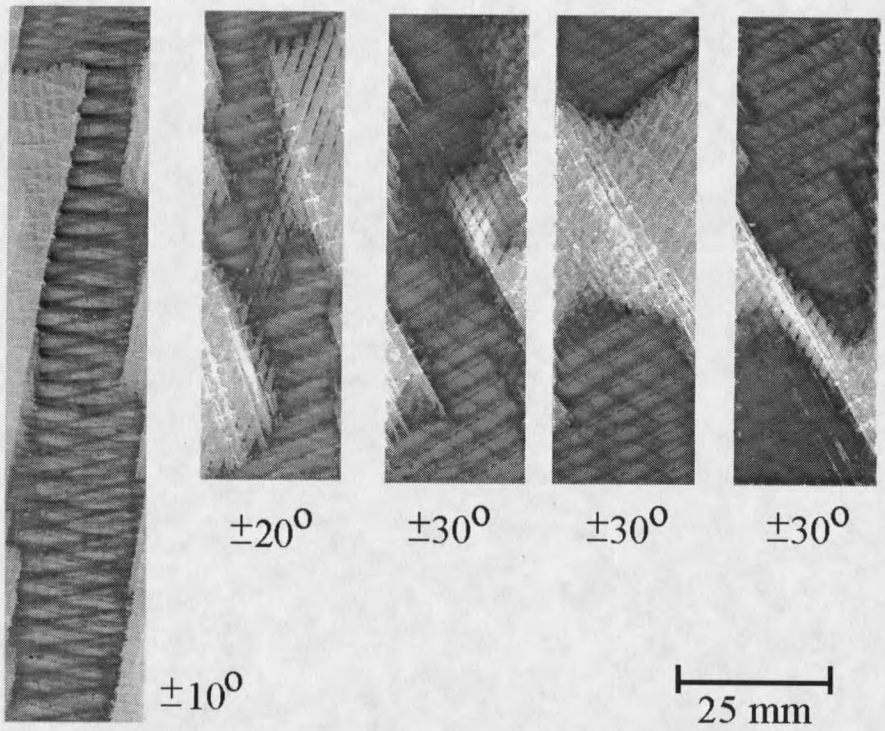


Figure 6.26. Failed tensile fatigue coupons from ±10° to ±30° laminates showing delamination and cracking of plies with edge effects ($\pm[\theta]_3$ laminate with D155 fabric, $V_F = 0.39$).

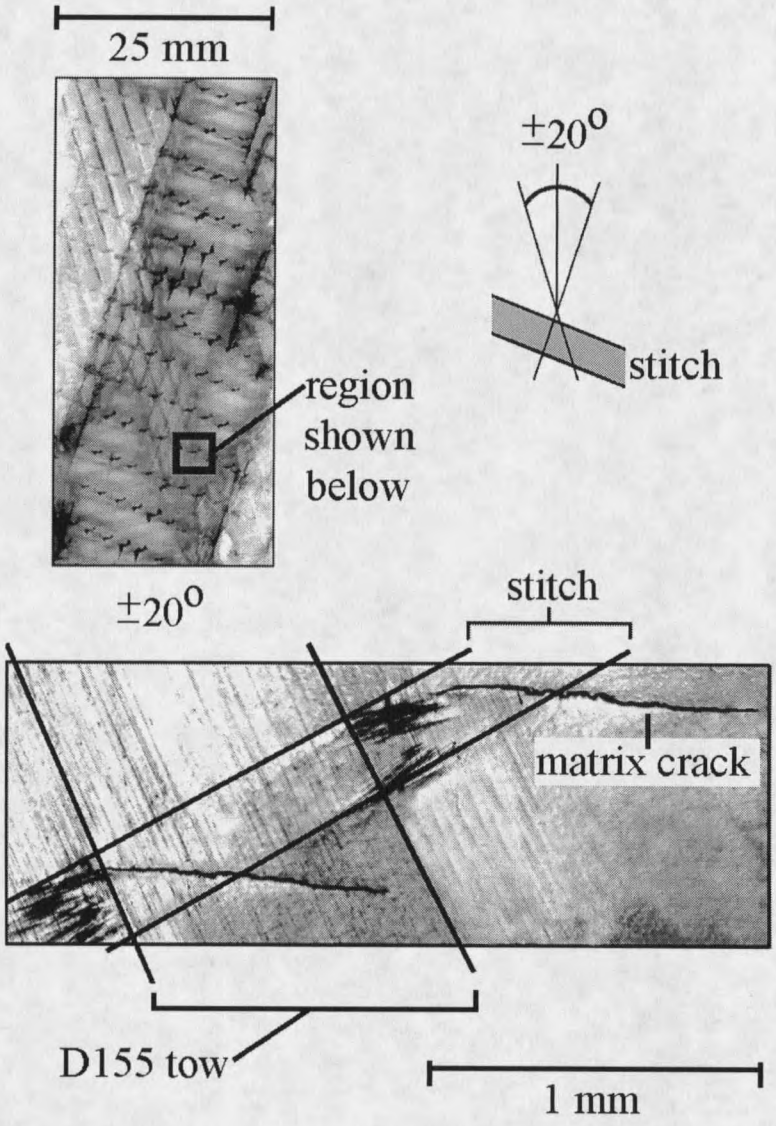


Figure 6.27. Failed tensile fatigue coupon 20D155112, tested at a maximum tensile stress of 172 MPa, R = 0.1, showing crack initiation around the D155 stitching thread-glass tows cross-over points.

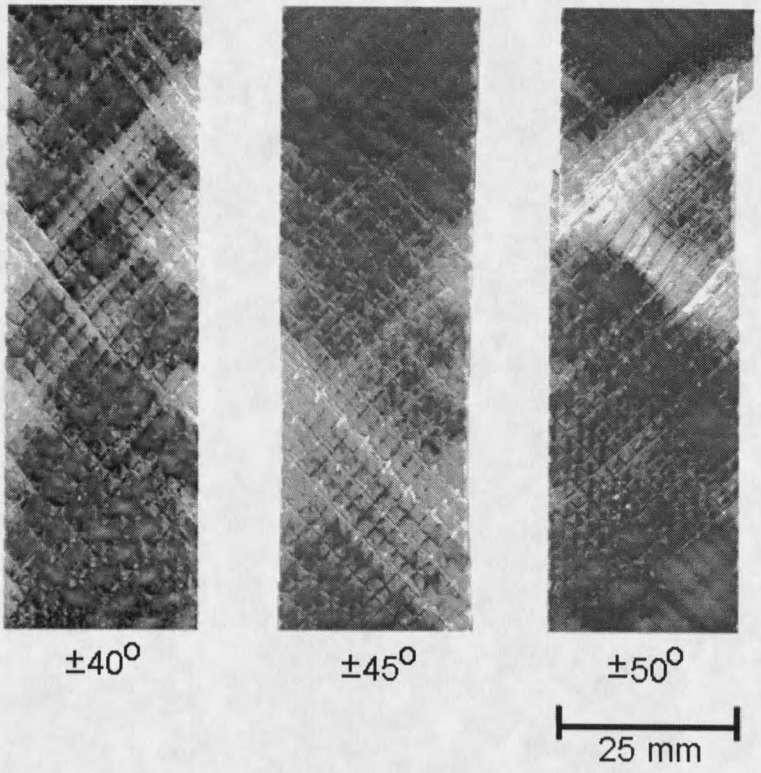


Figure 6.28. Failed tensile fatigue coupons from ±40° to ±45° laminates showing delamination and cracking of plies ($\pm[\theta]_3$ laminate with D155 fabric, $V_F = 0.39$).

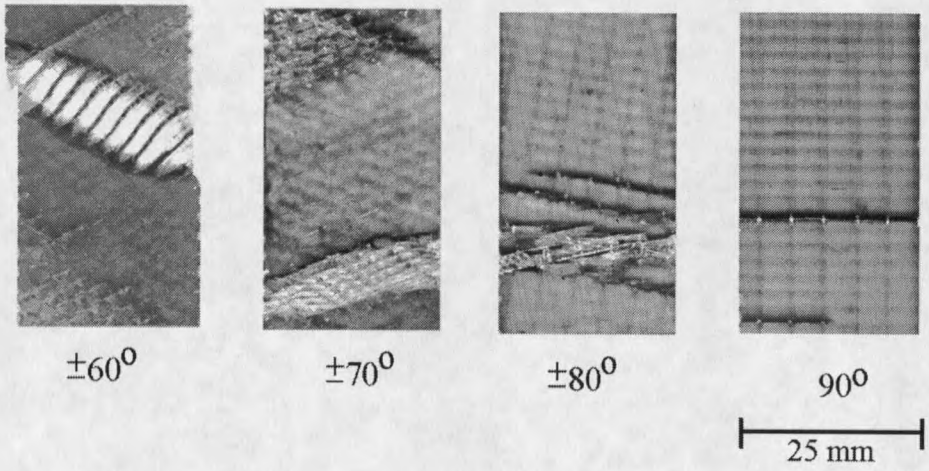


Figure 6.29. Failed tensile fatigue coupons from ±60° to 90° laminates showing cracking of plies ($\pm[\theta]_3$ laminate with D155 fabric, $V_F = 0.39$).

The compressive failures for the ±30°and ±40° laminates are shown in Figure 6.30. The ±30° coupons showed multiple failure modes involving combinations of both shear and material compression. The size of the damage at failure was not limited to the 13 mm gage length in coupons with these ply orientations, which show major shearing in the fiber direction between the D155 tows, producing very clean failure surfaces. In compression fatigue testing, once a delamination formed and grew to a critical size, the coupon catastrophically failed due to buckling. Any instability or nonuniformity in coupon loading was enough to initiate buckling. This, combined with a small gage length, made pre-failure damage observation difficult.

Figure 6.31 shows the compressive fatigue failures for ±50°, ±60°, ±70° and 90° coupons. The size of the failure zone was smaller compared with other angles. The ±70° and 90° coupons show a different type of failure than the other angles, shear failure through the coupon thickness with very little compressive damage or other cracks. Extensive fiber bridging was present in these coupons, which indicates that the shear cracks initiated and grew in the D155 bundles and not between them.

The single cycle (static) tensile coupons are shown in Figures 6.32, 6.33 and 6.34. These tests produced similar failure modes to the fatigued coupons, including the brittle-ductile-brittle transition with θ. The only major difference between the static and fatigued coupons was that no local delaminations were observed around the stitch cross-over points in the ±20° static test coupons, which was observed in the tensile fatigued coupons. The static compressive test coupons are not shown because the static test, combined with a short gage length, crushed the test coupons eliminating any interesting failure features.

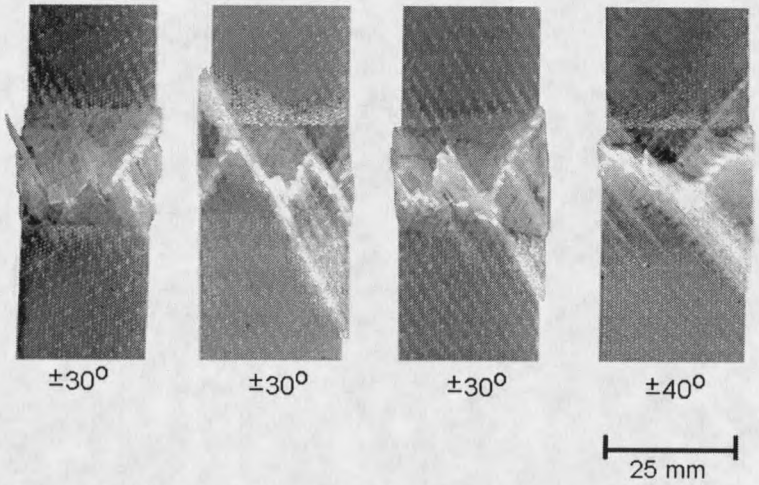


Figure 6.30. Failed compressive fatigue coupons from ±30° to ±40° laminates showing cracking and shearing of plies ($\pm[\theta]_3$ laminate with D155 fabric, $V_F = 0.39$).

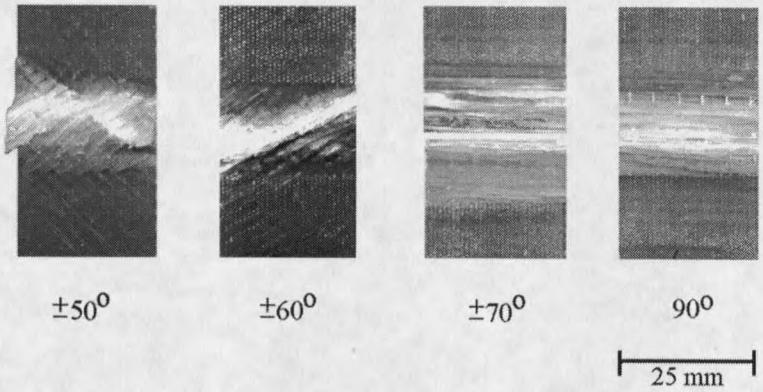


Figure 6.31. Failed compressive fatigue coupons from ±50° to 90° laminates showing cracking and shearing of plies ($\pm[\theta]_3$ laminate with D155 fabric, $V_F = 0.39$).

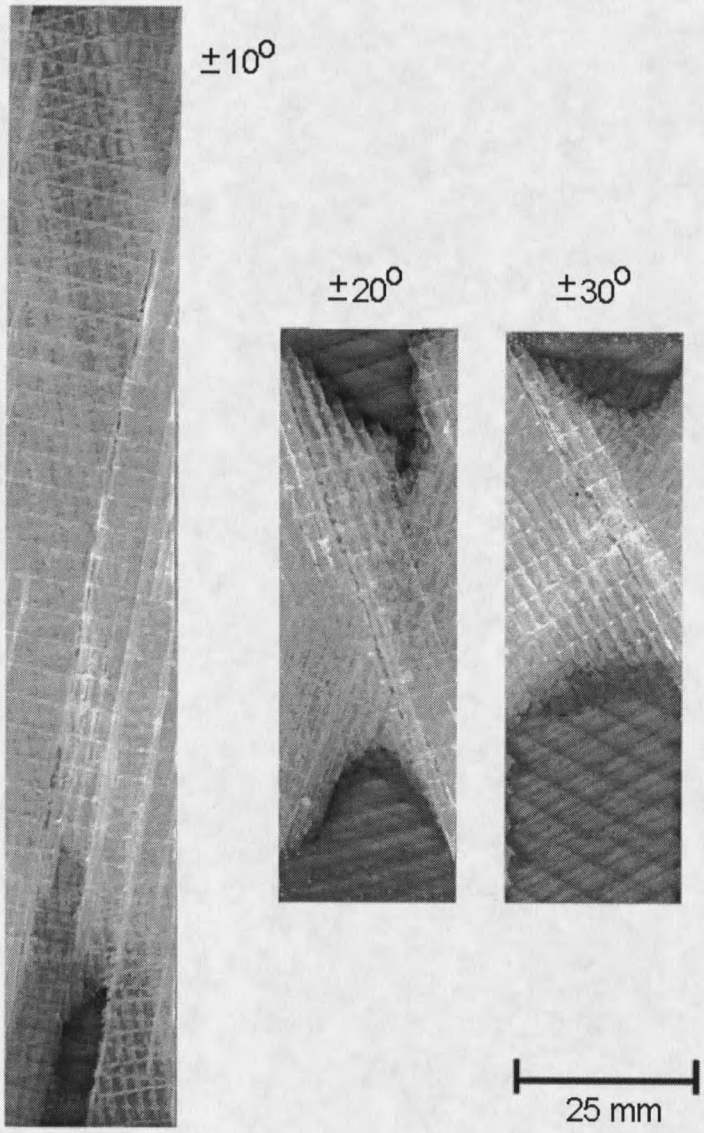


Figure 6.32. Static tensile failure of ±10°, ±20° and ±30° coupons showing lamina cracks parallel to the fiber direction.

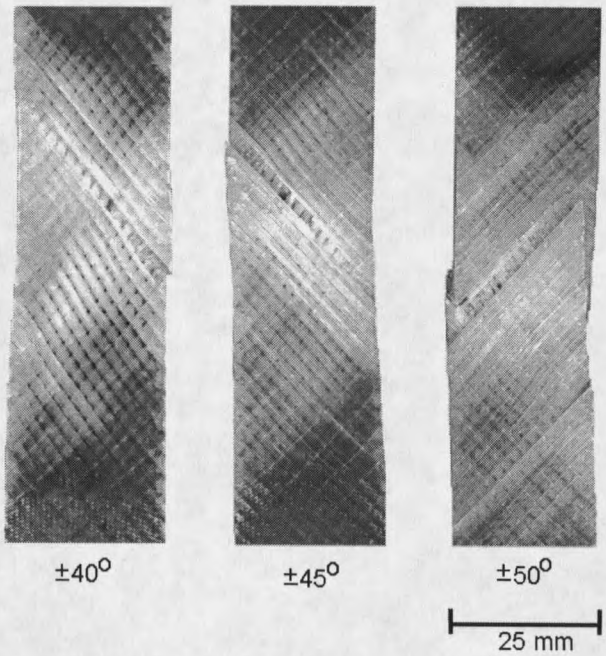


Figure 6.33. Static tensile failure of ±40°, ±45° and ±50° coupons showing lamina cracks parallel to the fiber direction and delaminations causing matrix yielding and fiber movement.

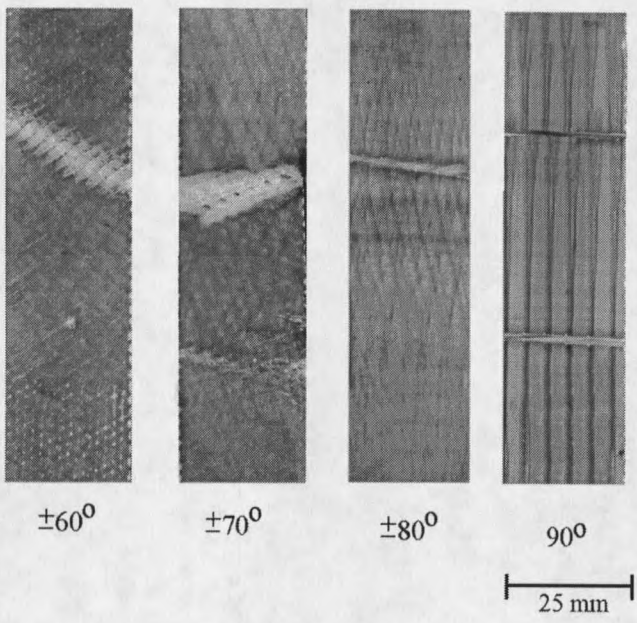


Figure 6.34. Static tensile failure of ±60°, ±70°, ±80°and 90° coupons showing lamina cracks parallel to the fiber direction.

Conclusions for Balanced Ply Laminates

Theoretical predictions using standard accepted laminate analysis techniques agree well for modulus values and for tensile laminate strengths with angles greater than ±40°, but grossly over predict the tensile strength for smaller angles. The over-prediction at low angles is probably due to the interlaminar stresses at the test coupon edges initiating delaminations and premature failure. The compressive strength also agreed well with theory for orientations from ±45° to 90°, over which the compressive strength did not show any angular sensitivity. The maximum stress criterion provided a predicted value closer to the measured strength for all angles.

The fatigue results are summarized in Table 6.2. The commonly observed deviation of the fiber angles in ±45° fabrics does not have a significant effect in the ±40° to ±50° range for tension, with regards to the maximum strain which can be withstood for one million cycles. Both the tensile strength and major Poisson's ratio do significantly change with the angle orientation around ±45°. The calculated compressive strain for one million cycles does show a significant difference (up to 0.15 percent strain) with ply orientations in the ±40° to ±50° range, but with the compressive test geometry (both fiber ends clamped), it was difficult to determine if this was a testing effect or a true material effect.

CHAPTER 7

I-BEAMS

The objective of this study was to apply materials from the database in a typical structural geometry, to validate use of the database in structural design. This intermediate-size structure would also serve as a test bed for exploring improved manufacturing methods and structural design details. Most of this chapter has been published in Reference 2.

The I-beam test specimen was developed as a representative substructural element typical of wind turbine blades [2]. The I-beam test specimen was intended to fulfill the following requirements:

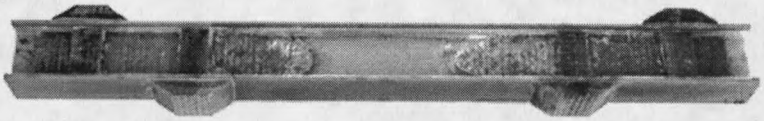
- Allow convenient laboratory testing at maximum forces below 100 kN at frequencies of at least 5 Hz (cycles/second), so that tests could be conducted out to about 10^6 cycles in a few days.
- Allow the inclusion of significant structural details such as ply drops for thickness tapering and adhesive bonding, and flaws such as holes, matrix-rich areas, and fiber misorientation.
- Provide a gage section where the stress conditions are representative of blade stresses (primarily bending stresses).
- Be designed to produce failure in the gage section to allow meaningful comparison with the behavior of the materials in coupon tests.

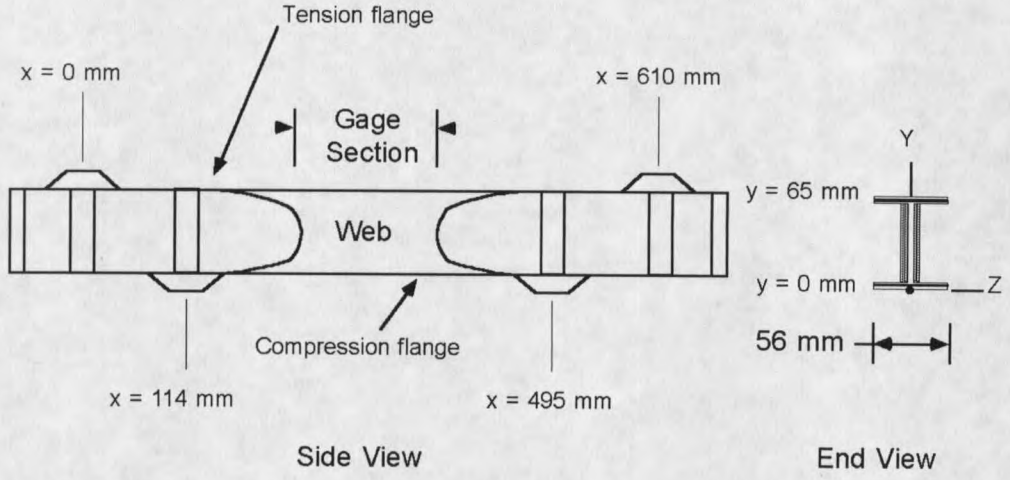
- Be convenient to analyze by finite-element analysis (FEA), and to instrument in tests.
- Allow the incorporation of either MSU manufactured or industry-supplied materials, particularly in the flanges.

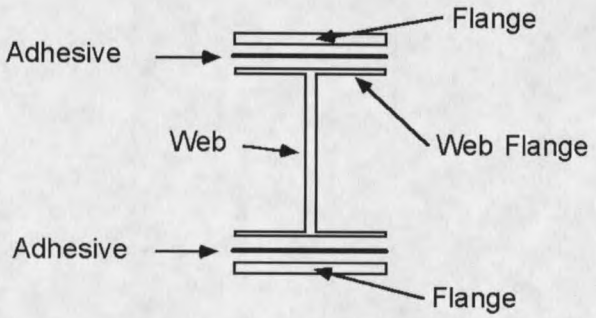
The I-beam configuration was developed and analyzed by Combs [13, 81]. Combs performed an iterative design and analysis process with beams 1 through 5, to develop a beam configuration which fulfilled these objectives. The final beam geometry is shown in Figure 7.1 and the construction techniques are detailed in Chapter 3. For the present study, there were two major design changes from the configuration developed by Combs. The thickness of the web was increased to 5 mm to reduce the possibility of web failures prior to flange failure. For beams numbered 30 and greater, the web was molded by RTM as a single piece, rather than back-to-back bonding of C-channels; this single-piece molding improved dimensional repeatability without the need for sanding the surfaces flat prior to secondary bonding.

Experimental Investigation Of Beam Static and Fatigue Behavior

This section explores the correlation between the coupon fatigue database and material performance in a series of beam structure tests. Static and fatigue tests were performed using several load ranges, with several material variations differing in static and fatigue properties in the flanges and webs. The beams were strain-gaged in each case in order to compare strain-lifetime relationships between the coupon database and the beams. Strains given are from the first few cycles, after which the strain gages failed because of matrix cracks. Appendix B gives detailed results for each beam test.







Beam Gage Section Exploded End View

Figure 7.1 Sketch and photograph of composite I-beam.

The general objective of the beam tests in this section was to compare beam performance with the performance of the flange and web materials in coupon tests, thereby validating use of the coupon database for predicting the static and fatigue performance of structures. The beam materials were divided between triax-based laminates, with relatively poor tensile fatigue performance, and laminates with separate 0° and ±45° layers, with relatively good fatigue performance.

Material and Beam Description

Tables 7.1 to 7.6 give a detailed summary of the materials, conditions, and results of each test. Further details for each test can be found in Appendix B. Beams 6-14, 22, and 23 used CDB200 triax-based flanges, designated as material AA in Table 7.1 and in the database. In this series, flanges were 2.9 mm thick and 53 mm wide. The web used in all of the AA-flanged beams was designated as material CH10 in the database. Material CH10 is 5 mm thick with all ±45° layers of DB240 fabric. We define the materials in more detail in the footnotes for Tables 16-20. This series of tests were performed to determine whether the behavior of beams with AA material flanges (with poor tensile fatigue performance) was consistent with coupon behavior. Material AA has been used in wind turbine blade fabrication, but performs poorly in tensile fatigue because of heavy stitching of the ±45° layers to the 0° layers [2]. (Materials that perform poorly in fatigue are easier to test in a substructure because they require less strain and load transfer to produce the desired central-gage-section failures.) Beams 15, 16, and 17 were further weakened with intentional severe flaws: 13 mm-diameter through-thickness holes in the flanges.

Table 7.1. Static and fatigue data for beams with material AA flanges and material CH10 webs.

Beam	Materials flange / web	Max. / Min. load, kN	Max. / Min. strain, %	Cycles	Failure location
6	AA / CH10	67.08	1.80 / -1.68	1	Compression flange
7	AA / CH10	24.5 / 2.5	0.58 / -0.56	492,147	Tension flange
8	AA / CH10	31.1 / 3.1	0.79 / -0.7	29,051	Tension flange and web
9	AA2 / CH10	59.2	1.78 / -1.8	1	Compression flange
10	AA2 / CH10	40.0 / 4.0	1.07 / -0.97	1,870	Tension flange
11	AA / CH10	40.0 / 4.0	1.08 / -0.96	4,620	Tension flange and web
12	AA / CH10	28.9 / 2.9	0.73 / -0.68	30,290	Tension flange
13	AA / CH10	60.72	2.10 / -1.85	1	Compression flange
14	AA / CH10	24.5 / 2.5	0.59 / -0.58	389,175	Tension flange
15*	AA / CH10	31.1 / 3.1	0.83 / -0.78	2,772	Compression flange
16*	AA / CH10	24.5 / 2.5	0.58 / -0.53	40,448	Tension flange
17*	AA / CH10	46.97	1.3 / -1.08	1	Compression flange
22	AA / CH10	31.1 / 3.1	0.84 / -0.76	36,825	Tension flange
23	AA / CH10	28.9 / 2.9	0.71 / -0.64	119,995	Tension flange
*Beams 15, 16 and 17 had 13 mm diameter holes in the flanges.					

Table 7.2 lists a summary of the tests with beams 18-21 and 24-29. These beams used DD5P material in the flanges, which is a model structural material with about 72% of the fibers in the 0°- direction (x-direction in Figure 1); the remainder of the material is ±45°, as described in the database. With a low fiber volume content of 0.36, material DD5P had a much better tensile fatigue resistance than that of material AA, and is close

Table 7.2. Static and fatigue data for beams with material DD5P flanges and material CH10 webs.

Beam	Materials flange / web	Max. / Min. load, kN	Max. / Min. strain, %	Cycles	Failure Notes
18	DD5P / CH10	62.3 / 6.2	1.42 / -1.34	9,367	Tension flange delamination
19	DD5P / CH10	89.18	1.96 / -1.82	1	Compression flange
20	DD5P / CH10	53.4 / 5.3	1.09 / -1.09	94,391	Tension flange delamination
21	DD5P / CH10	53.4 / 5.3	1.14 / -0.99	23,000	Tension flange
24	DD5P / CH10	88.29	1.93 / -1.77	1	Compression flange
25	DD5P / CH10	62.3 / 6.2	1.43 / -1.31	7,636	Compression flange
26	DD5P / CH10	57.8 / 5.8	1.22 / -1.05	104,407	Compression flange delamination
27	DD5P / CH10	53.4 / 5.3	1.07 / -1.00	243,876	Tension flange delamination
28	DD5P / CH10	44.5 / 4.4	0.86 / -0.85	2,000,000	Tension flange delamination
29	DD5P / CH10	48.9 / 4.9	0.92 / -0.96	815,684	Tension flange delamination

Table 7.3. Fatigue data for beams with material DD5P flanges and material CH3 webs.

Beam	Materials flange / web	Max. / Min. load, kN	Max. / Min. strain, %	Cycles	Failure Notes
30	DD5P / CH3	62.3 / 6.2	1.20 / -1.05	5,741	Web
31	DD5P / CH3	53.4 / 5.3	0.92 / -0.89	2,030,240	Tension flange delamination
32	DD5P / CH3	53.4 / 5.3	0.86 /-0.73	783,153	Load pad, flanges still good
33	DD5P / CH3	53.4/ 5.3	0.94 / -0.93	3,200,000	Web / tension flange delamination

Table 7.4. Static and fatigue data for beams with material DD5P flanges and material CH12 webs.

Beam	Materials Flange / Web	Max. / Min Load, kN	Max. / Min. Strain, %	Cycles	Failure Notes
34	DD5P / CH12	83.26	1.92 / -1.69	1	Compression Flange and Web
35	DD5P / CH12	62.3 / 6.2	1.04 / -1.02	9,771	Web failure

Table 7.5. Fatigue data for beams with material DD5P flanges and material DD5P webs.

Beam	Materials flange / web	Max. / Min. load, kN	Max. / Min. strain, %	Cycles	Failure notes
51	DD5 / DD5	53.4 / 5.3	0.76 / -0.75	3,000,000	Run out
52	DD5 / DD5	62.3 / 6.2	0.93 / -0.89	62,843	Compression flange
53	DD5 / DD5	62.3 / 6.2	0.94 / -0.89	8,700	Web / shear stiffener failure
54	DD5 / DD5	62.3 / 6.2	0.88 / -0.88	2,744,704	Web / shear stiffener failure

Table 7.6. Fatigue data for beams with material DD22 flanges with a balsa wood core, and material CH12 webs.

Beam	Materials flange / web	Max. / Min. load, kN	Max. / Min. strain, %	Cycles	Failure notes
58	DD27 Balsa / CH12	62.3 / 6.2	0.97 / -1.00	230	Compression flange
59	DD27 Balsa / CH12	35.6 / 3.6	0.58 / -0.59	1,000,000	Run out
		44.5 / 4.4	0.75 / -0.75	88,993	Compression flange

to the best obtainable with fiberglass materials [2]. Figure 7.2 compares the coupon test results of tensile fatigue behavior of materials AA and DD5P; Figure 7.3 compares their behavior in compressive fatigue.

The straight lines in these and succeeding figures represent a linear trend on the semi-log plots, following equation 4.2. The implications of a particular assumed trend line (linear on log-log versus linear on semi-log) were discussed in Chapter 5. As noted in Chapter 5, the fatigue coefficient, b, for poor tensile fatigue performance is about 0.14, whereas the best performance is about 0.10.

For the final beam tests in this group (see Tables 7.3 to 7.6) various improved web materials were used (CH3, CH12, and DD5P) to increase the strain capacity in tensile fatigue of the web flange on the tensile side. These web materials include increasing amounts of 0° material. Figure 7.4 compares the tensile fatigue resistance of coupons of the four web materials, CH10, CH3, CH12, and DD5P; these results are discussed in detail in Reference 2.

Studies of Beams with Triax Material Flanges

As previously noted, triax fabric reinforcement produces relatively poor tensile fatigue performance. Figure 7.5 combines the material AA data from Figures 7.2 and 7.3, comparing the tensile and compressive fatigue S-N data. The static tensile strength exceeds the compressive strength, and the stress to produce failure is higher in tension at low cycles. At about a thousand cycles the curves cross, and failure occurs at lower stresses in tension for cycles greater than 1000. Thus, with equal magnitude stresses and strains in both flanges, failure is expected in the beams in compression at low cycles, and tension at high cycles. The 10^6 cycle tensile fatigue strain to failure of the CH10 material used for the web is similar to that for material AA (0.46% for CH10, 0.50% for AA [8]).

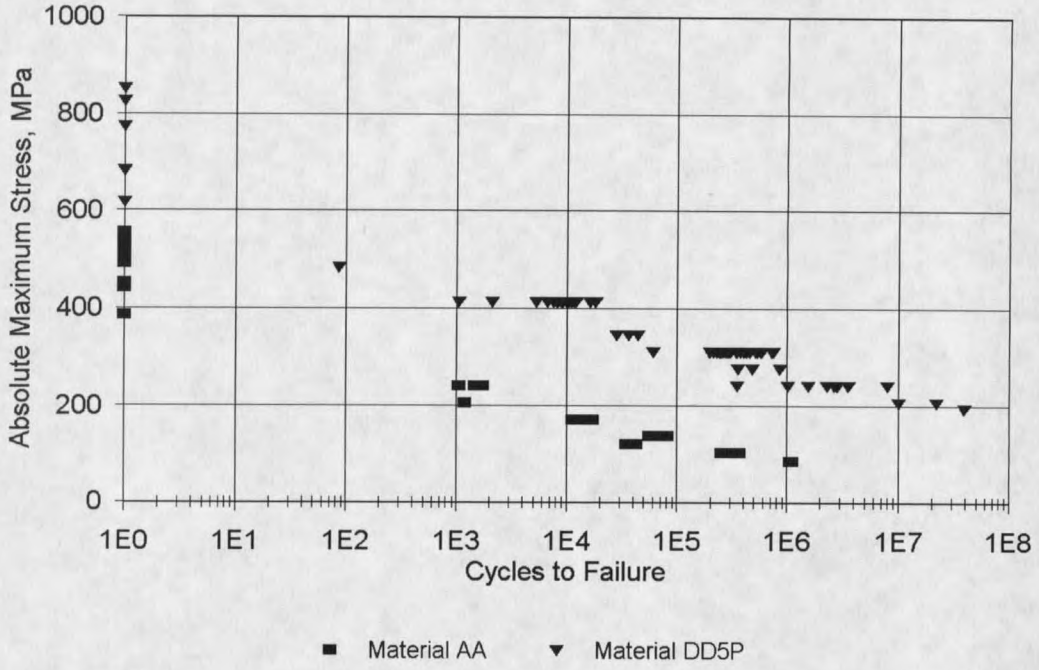


Figure 7.2. Fatigue data for materials AA and DD5P, R = 0.1.

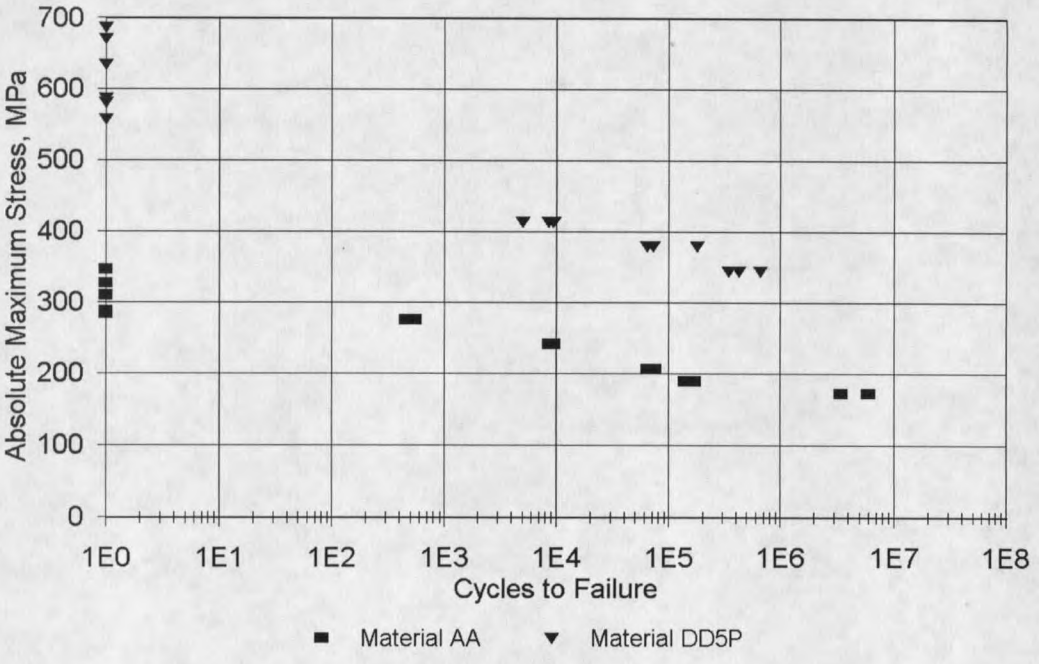


Figure 7.3. Fatigue data for materials AA and DD5P, R = 10.

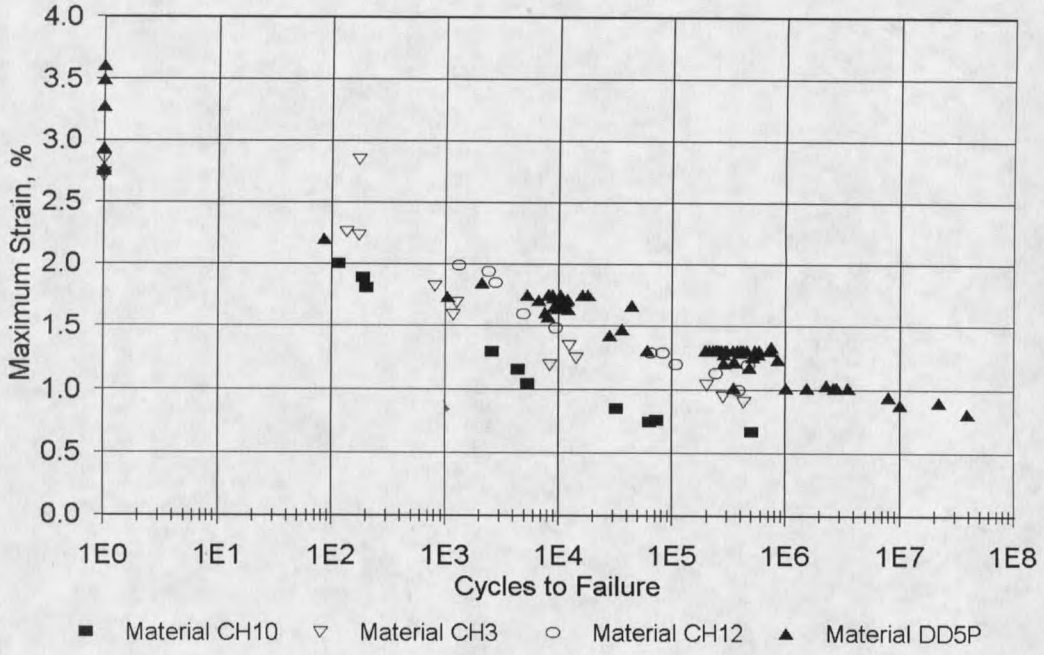


Figure 7.4. Fatigue data for materials CH3, CH10, CH12 and DD5P, R = 0.1.

Thus, failure is expected at about the same time in the tension flange and in the web flange on the tensile side, which see about the same strain levels (because they are bonded together). Appendix B gives details of the materials in the cross section at the beginning of the section on beams with AA material flanges.

Behavior of Beams

Figure 7.6 compares the failure strain conditions for the AA flange beams with the strain-cycles data for the material AA coupons. (The solid square and triangle symbols are the measured initial strains on the tension and compression flanges, respectively; the symbol shown indicates which flange actually failed.) The static beam tests (6, 9, and 13) resulted in compressive flange failures with damage in the web as well (Figure 7.6). The

measured static compressive flange strains at failure cover the range observed for the compressive coupon tests (Figure 7.6, one cycle). Figure 7.7 compares the web material CH10 coupon results with the beam data; the CH10 tensile fatigue strains are, again, similar to the beam failure strains. In order to compare coupon data with web flange strains in the beams, the beam strains are adjusted downward to 0.82 of the measured flange outside surface strains to give the strain at the outside of the web flange (assuming a linear strain variation across the beam depth).

Fatigue tests with beams having the AA material flanges (without holes) for beams 7, 8, 9, 10, 11, 12, and 14. All showed failure on the tension flange. The results in Figure 7.6 show close agreement with the failure strains and cycles for tensile coupons of the same material, tested at R = 0.1 (the same R value as the beam tensile flange). The predicted shift from compressive failure at low cycles to tensile failure at high cycles is observed in the beam results only in the static compression failures compared with tensile fatigue failures; no lifetimes could be produced in fatigue between 1 and 1,000 cycles because of difficulties in controlling tests in the low cycle range. Photographs of failure details are given in the Appendix for most beams, and Figures 7.8 through 7.11 give combined photographs of all flanges in this series as well as several detailed photographs.

The overall results provided in Figures 7.6 and 7.7 validate use of the fatigue coupon database to predict beam structural-element lifetime for tension-dominated failures. References 13 and 81 results showed that the beam strains are accurately predicted by appropriate finite-element analysis, with a reasonable approximation by simple beam theory. Thus, when analyzed appropriately, the results given here confirm

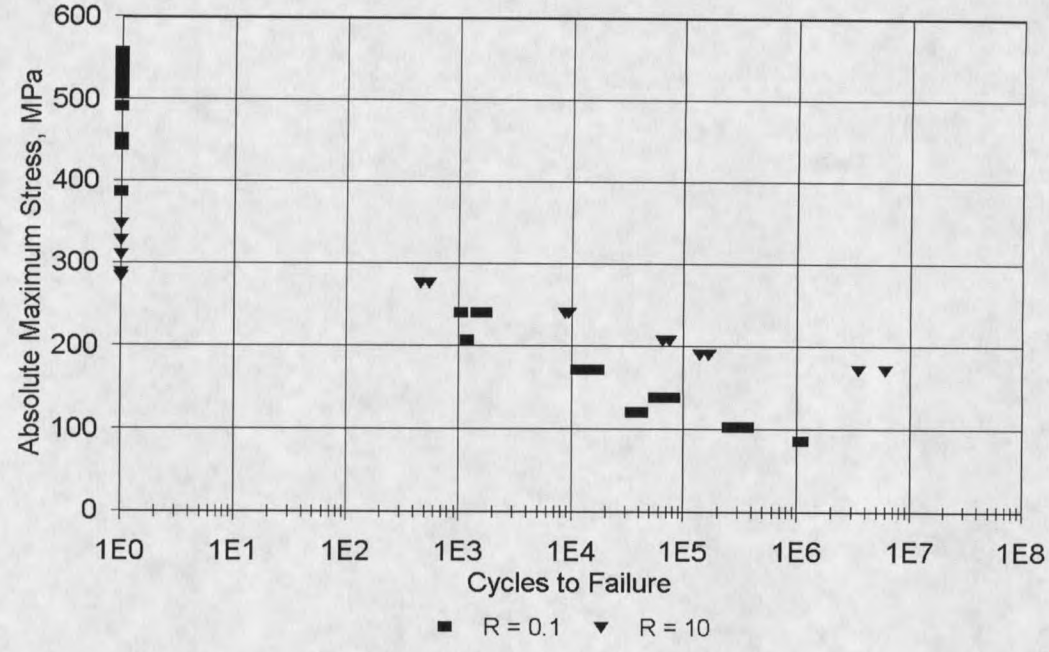


Figure 7.5. Fatigue data for material AA, R = 0.1 and 10.

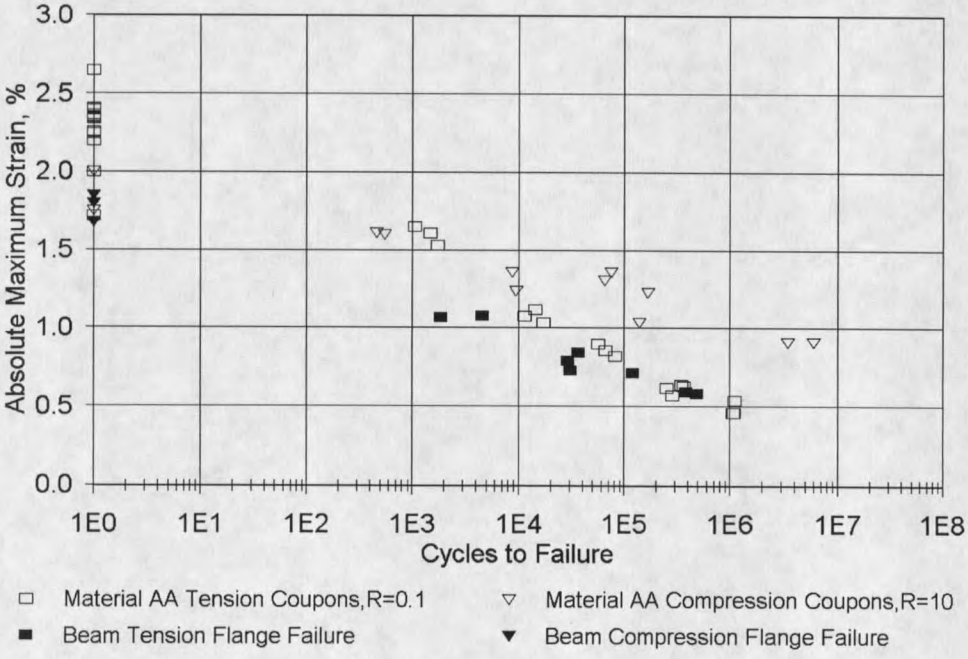


Figure 7.6. Beams 6 - 14, 22 and 23 with material AA flanges and material CH10 web compared with material AA coupon fatigue data.

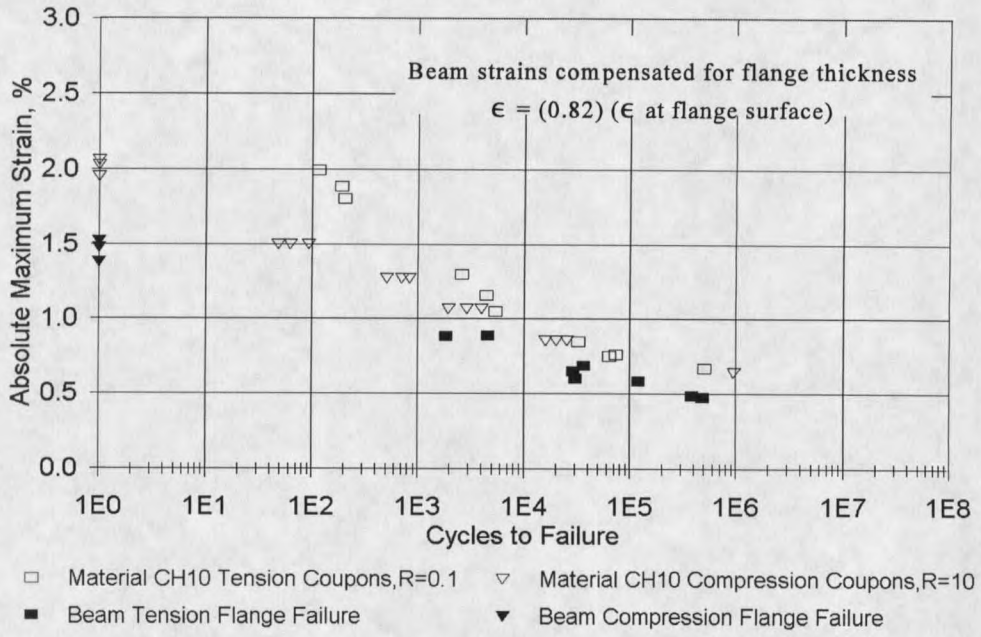
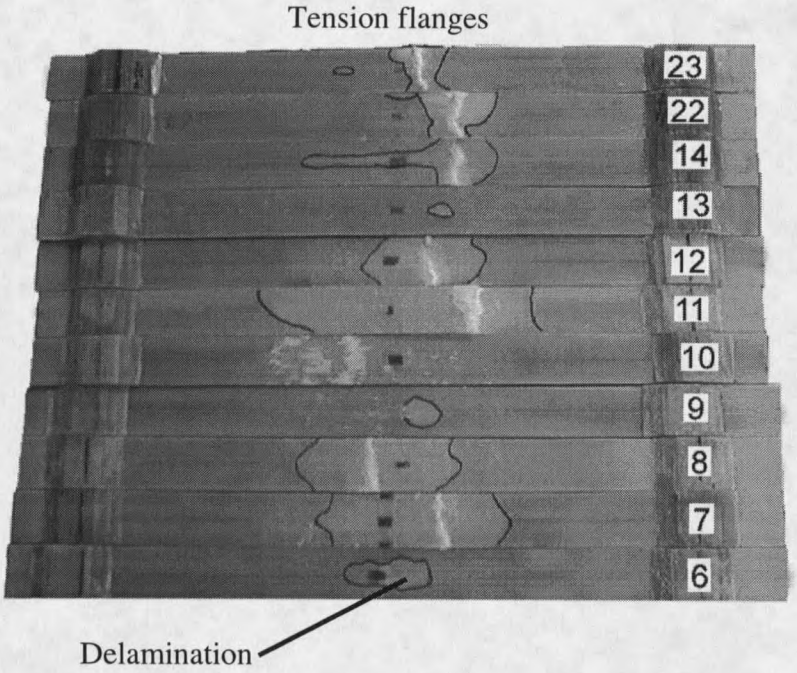


Figure 7.7. Beams 6 - 14, 22 and 23 with material AA flanges and material CH10 web. Compensated for flange thickness compared with material CH10 coupon fatigue data.

that these materials, when fabricated into a structural element similar to a blade, provide the static strength, tensile fatigue lifetime, and failure mode anticipated from simple coupon data. The size, flexural loading, and bonding to the web element do not compromise or complicate the material performance.

These results are for a triax material, which, although representative of blade materials, has poor fatigue resistance. This results in relatively low load transfer and low web loading, which produces flange failures. However, the stress and strain conditions producing beam failure, although lower than in subsequent beams, are more severe than expected in blade service loadings.



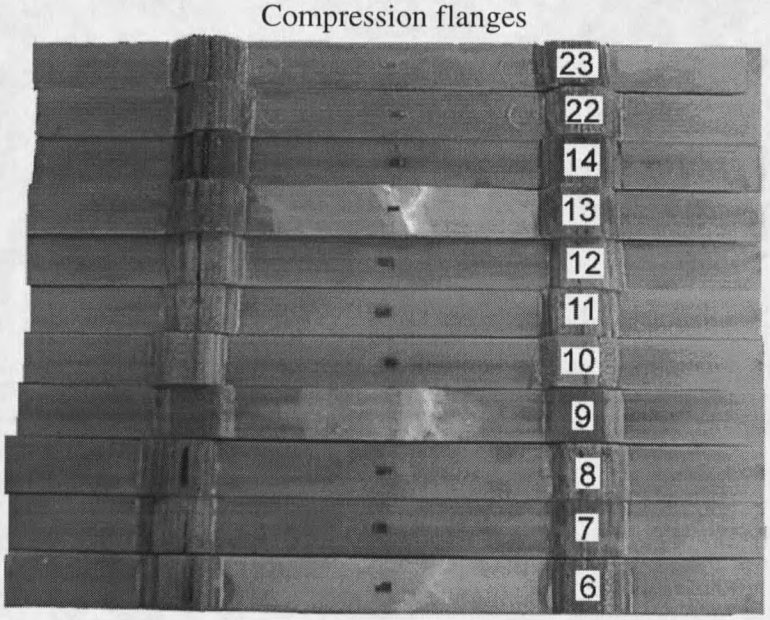


Figure 7.8. Tensile and compressive flanges of failed beams with material AA flanges and material CH10 webs.

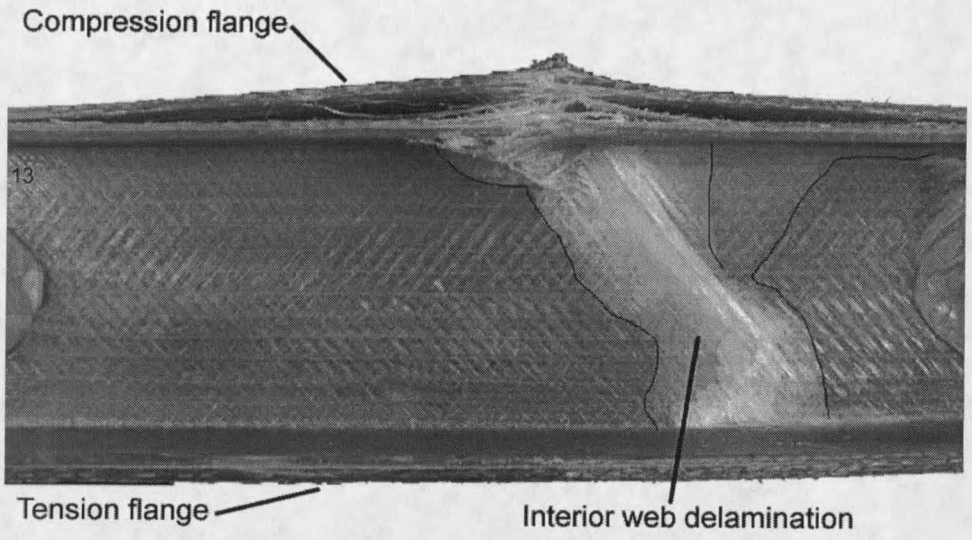


Figure 7.9. Beam 13 static compression flange failure.

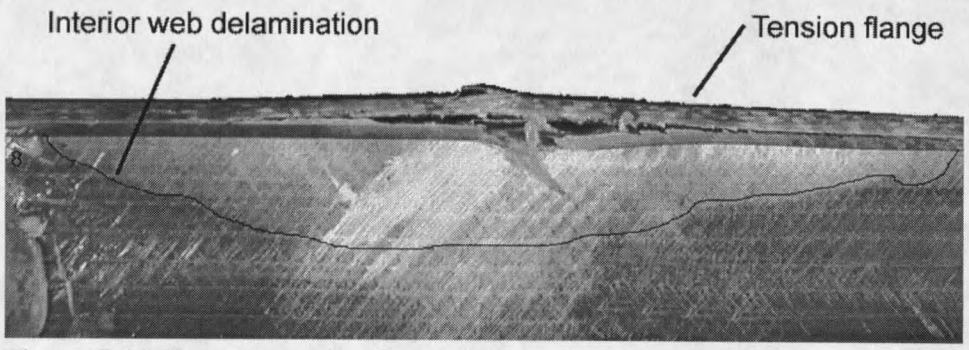


Figure 7.10. Beam 8 tension flange failure.

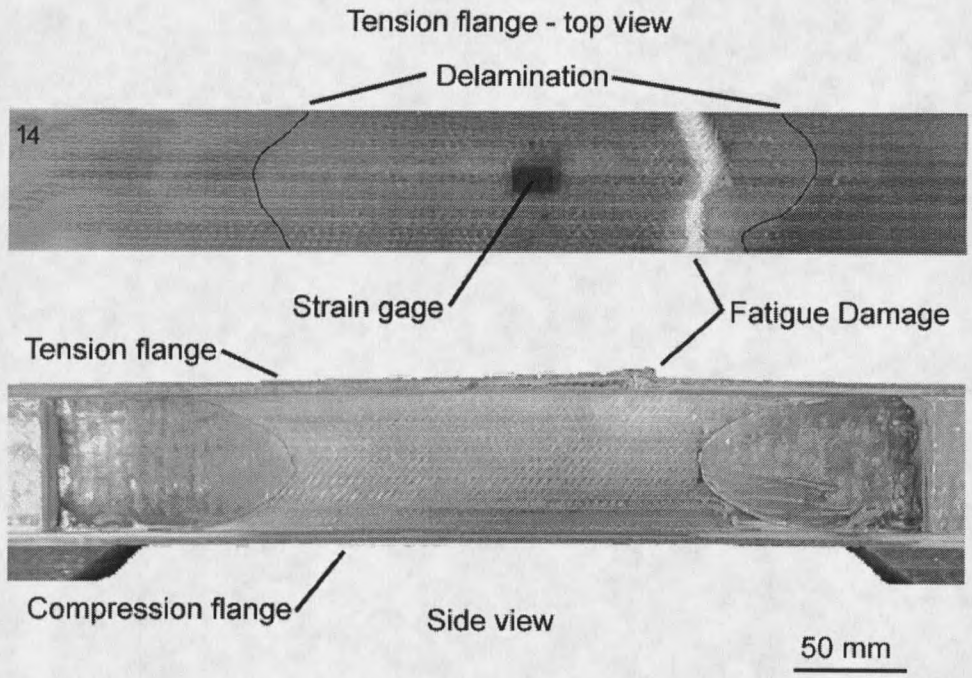


Figure 7.11. Beam 14 tension flange fatigue failure.

Studies of Beams with Improved Flange and Web Materials

This section describes the development of improved materials for the flanges and webs and their application to beams. Flange materials which can withstand more severe fatigue loading tend to produce failure in other modes than flange fracture, such as adhesive failure or web failure adjacent to the flange. Because the flange and web are bonded together, the strains in each are nearly identical at the bonded plane. Thus, the web must withstand the same tensile and compressive fatigue cycling in these areas as do the flanges, while also carrying the shear loads.

Material Development and Coupon Results

It was reported in chapter 5 that the tensile fatigue resistance of triax materials, such as material AA, was very deficient as compared with laminates having separate 0° and ±45° layers [1, 2]. Structural laminates with about 70% 0° material with separate layers were found to behave well in tensile fatigue only at overall fiber volume contents below about 0.42 for laminates containing a high percentage of 0° layers relative to ±45° layers. A complete parametric study of potential structural flange materials is reported in chapter 5, Reference 4 and the database (Appendix A).

For this study, we investigated a similar range of parameters for web materials. The results of the coupon study show that a potential web material must have a relatively high percentage of 0° layers and low overall fiber content to approach the strain capabilities (represented by the 10^6 cycle maximum strain) in tensile fatigue of the structural flange (DD5P) materials. This tends to stiffen the beams significantly, resulting in higher loads and more load-transfer problems to achieve the same flange strains.

Beam Test Results

Table 7.2 describes a series of beams (numbers 18-21 and 24-29) prepared with web material CH10 (all ±45°) and flange material DD5P (72% 0°, 0.36 overall fiber volume content). This flange has excellent fatigue resistance in tension (see Figure 7.2), whereas CH10 is a typical ±45° web material. The flange material coupon results [2] show tension and compression strains for 10^6 cycles of 1.15% and 1.30%, respectively, whereas the values for CH10 are 0.58% in tension and 0.64% in compression. The AA

material 10^6 cycle strains are 0.50% in tension and 0.95% in compression.

Figures 7.12 and 7.13 compare the beam data with flange material and web material coupon data, respectively. All of the failures were predominantly in the web, with some flange interaction. The results in Figure 7.13 show that the web flanges should have already cracked heavily prior to flange failure, and this appeared to be the case (Figure 7.14). Thus, most of these failures were induced in the web flange area, and agree generally with the web coupon data in Figure 7.13. Significant flange-web delamination near the ends of the shear stiffeners was also observed, as shown in Figure 7.15.

The results with web material CH10 were disappointing, in that failures predominantly generated from the web flange area. We decided to test several web materials with strain capability that more nearly approximated the flange material (DD5P), using the flange material itself in the web. Figure 7.4 compares the tensile strains of the four web materials tested in tensile fatigue. Higher 0° material content gives higher tensile fatigue strain capability if the overall fiber content is similar.

Tables 7.3, 7.4 and 7.5, list the results for beams with DD5P flanges and CH3, CH12, and DD5P webs. Figures 7.16 and 7.17 give the DD5P flange/CH3 web results for beams 30-33 compared with flange and web coupon data respectively. All of the beams in this group showed a variety of delamination and web damage. The beam data in Figures 7.16 and 7.17 agree generally with the flange and web coupon data, but failure modes were not simple to interpret.

Beams 34 and 35 included DD5P material flanges and CH12 web material (see Table 7.4 and Figures 7.18 and 7.19). As indicated in Table 7.4, these beams produced

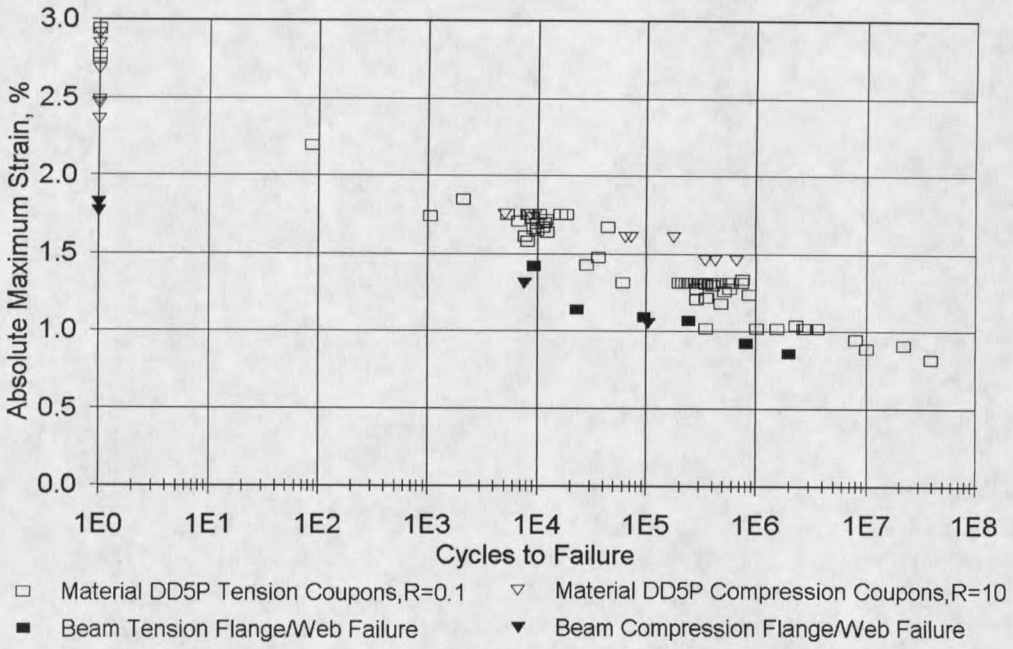


Figure 7.12. Beams 18 - 21 and 24 - 29 with material DD5P flanges and material CH10 web compared with material DD5P coupon fatigue data.

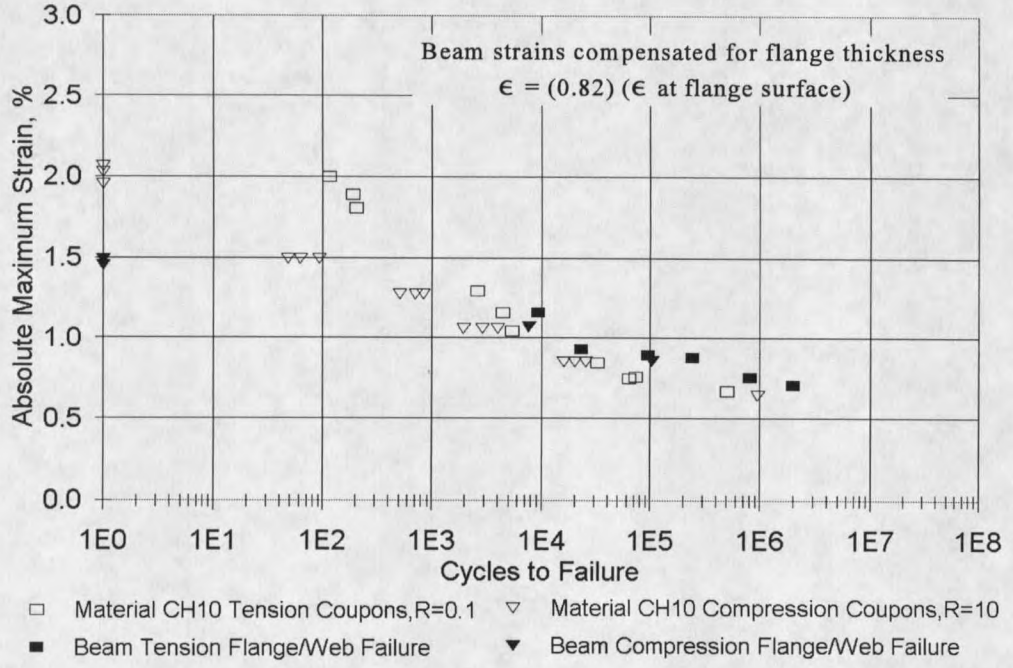


Figure 7.13. Beams 18 - 21 and 24 - 29 with material DD5P flanges and material CH10 web compensated for flange thickness compared with material CH10 coupon fatigue data.

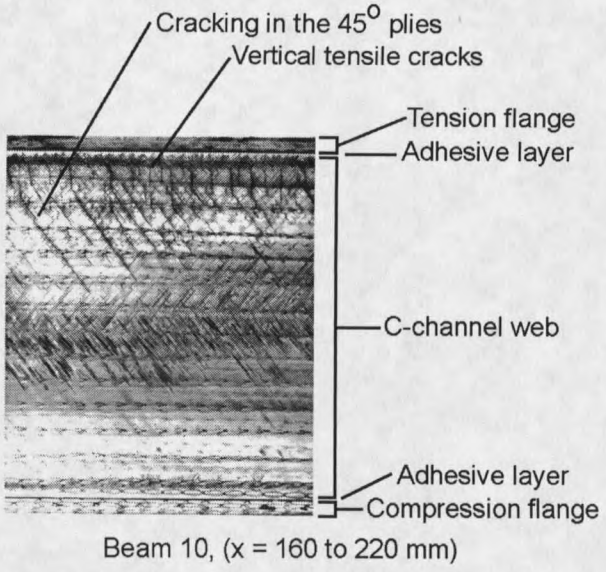


Figure 7.14. Photograph of web from Beam 10 showing extensive cracking of the web near tension flange.

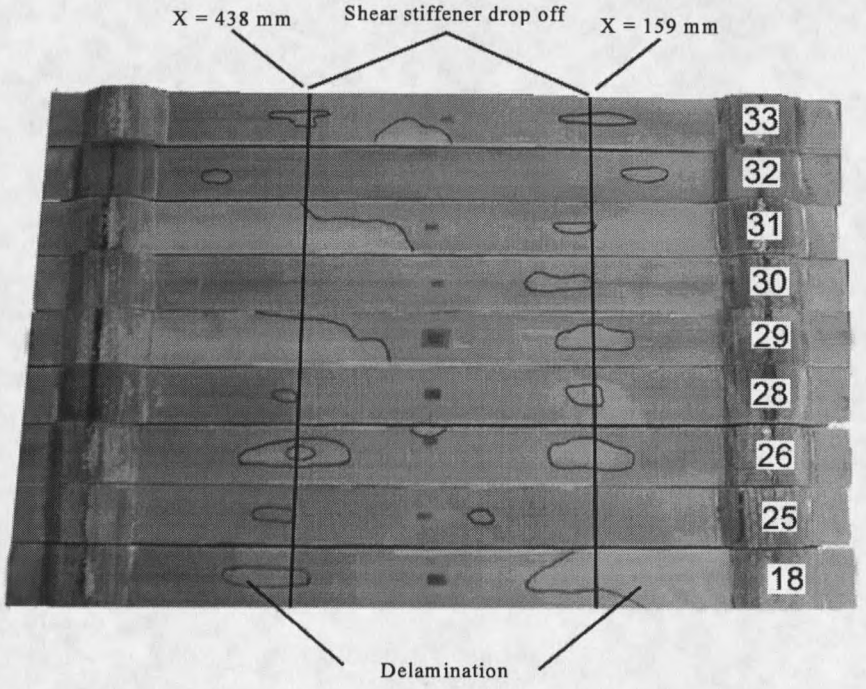


Figure 7.15. Tension flanges of failed beams with material DD5P flanges and material CH3 webs, showing delaminated areas.

delamination failures in the load transfer area of the load pads. The fatigue failure (beam 35) was at a strain well below either set of coupon data, as expected from the load-transfer problems.

Beams with material DD5P in the flanges and web are shown in Table 7.5 and Figure 7.20. The lower cycle results (beams 52 and 53) showed failure in the shear stiffener area (beam 53), which was then increased in thickness, and resulted in beam 52 showing compression flange buckling. Beams 51 and 54 reached close to the coupon data: we stopped the tests with only minor gage section damage; beam 54 eventually failed in the shear stiffener area. Figure 7.21 shows the tension and compression flanges of beams 51 to 54.

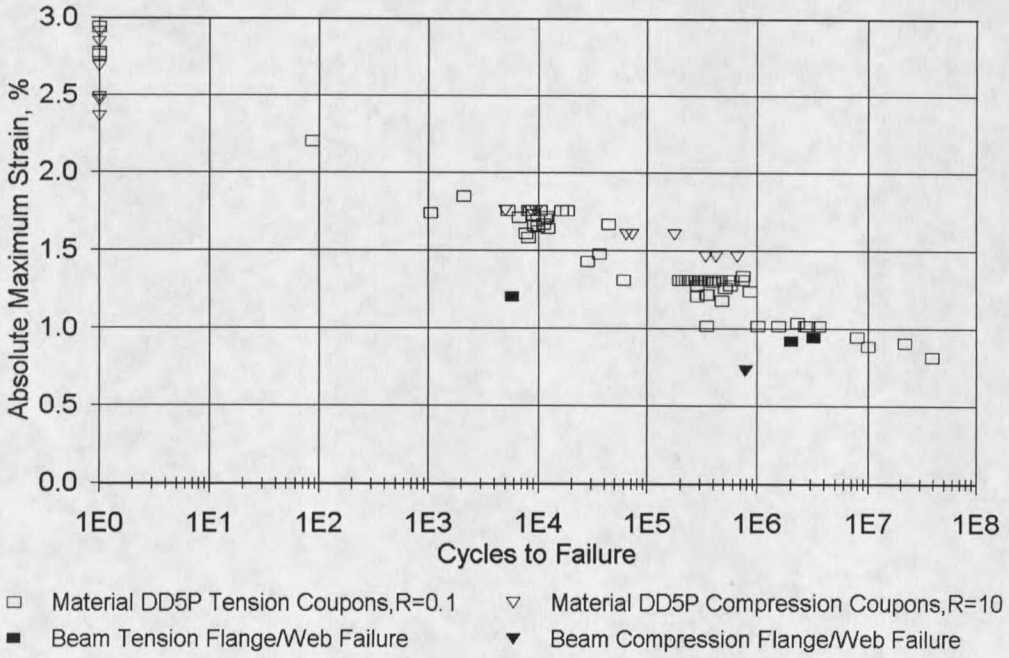


Figure 7.16. Beams 30 - 33 with material DD5P flanges and material CH3 web compared with DD5P coupon fatigue data.

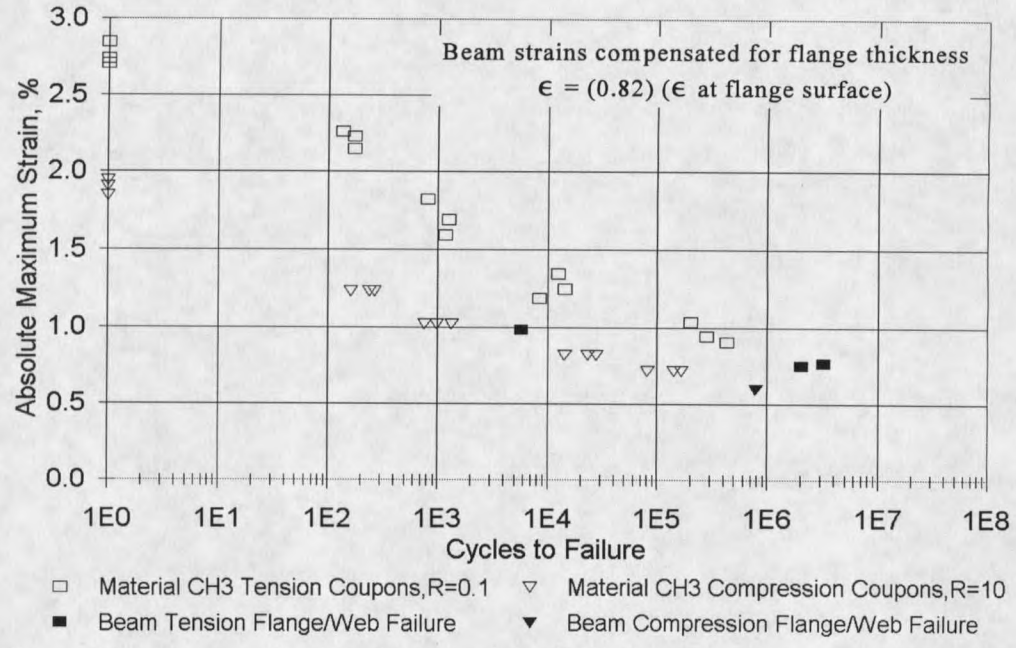


Figure 7.17. Beams 30 - 33 with material DD5P flanges and material CH3 web compensated for flange thickness compared with CH3 coupon fatigue data.

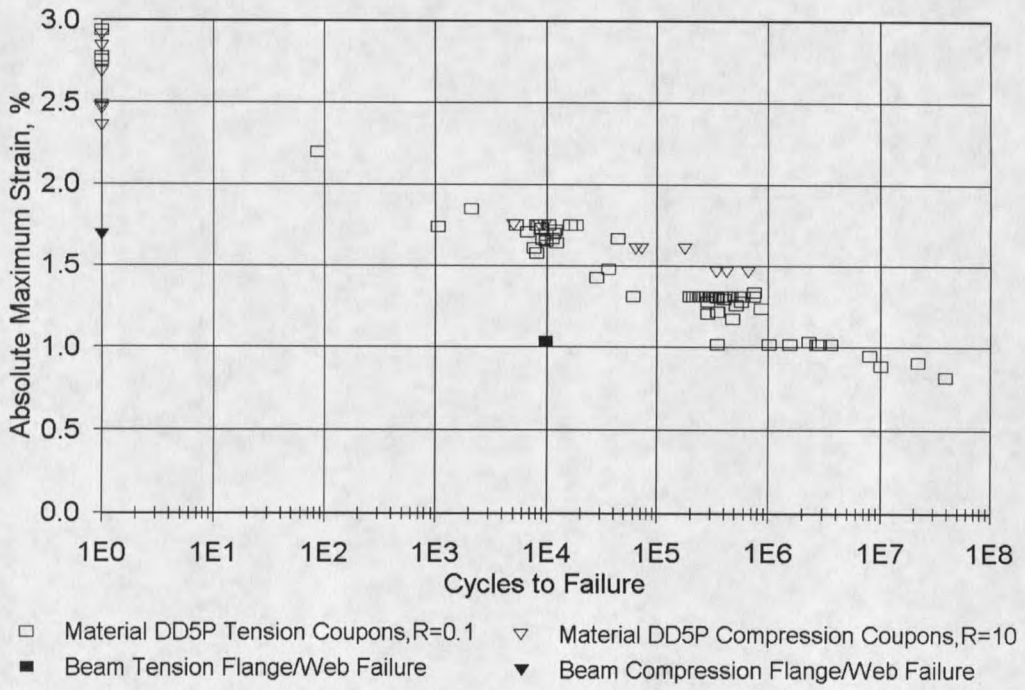


Figure 7.18. Beams 34 and 35 with material DD5P flanges and material CH12 web compared with material DD5P coupon fatigue data.

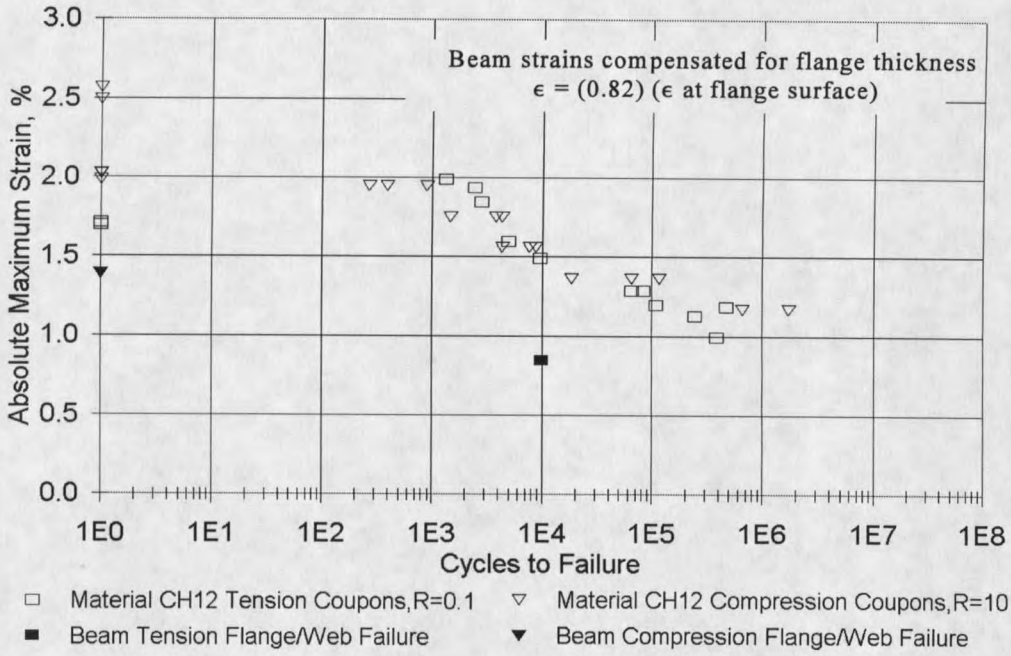


Figure 7.19. Beams 34 and 35 with material DD5P flanges and material CH12 web compensated for flange thickness compared with material CH12 coupon fatigue data.

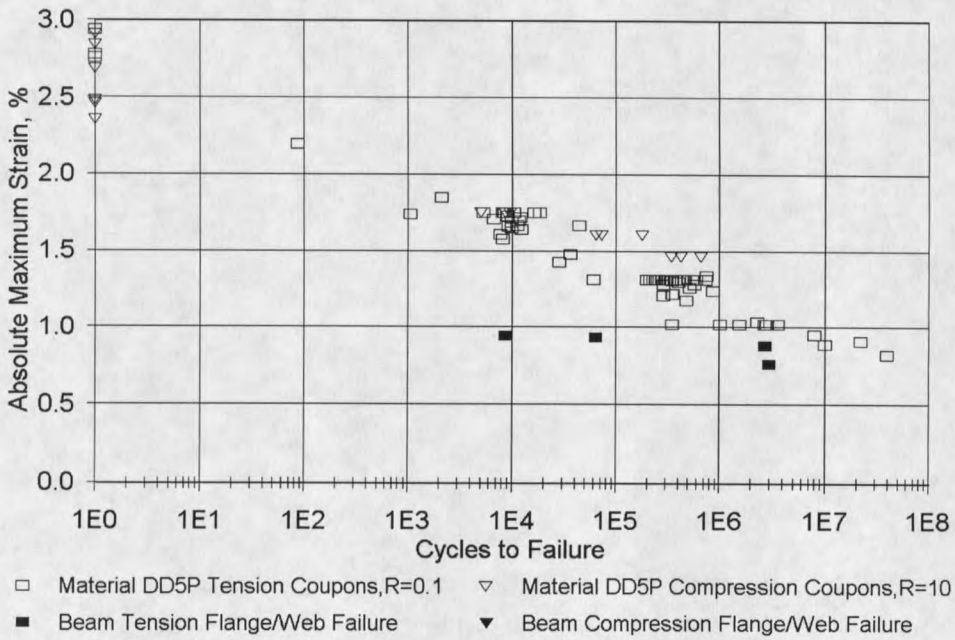


Figure 7.20. Beams 51 - 54 with material DD5P flanges and web compared with material DD5P coupon fatigue data.

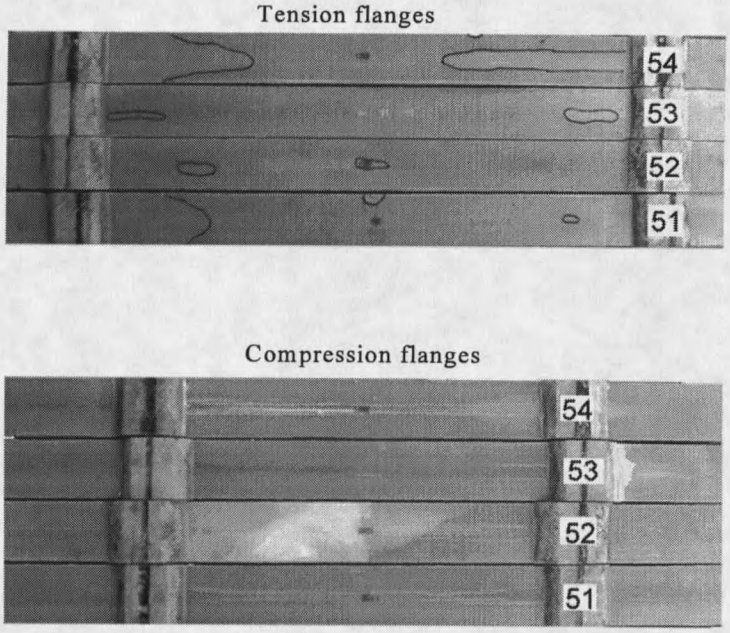


Figure 7.21. Tension and compression flanges of failed beams with material DD5P flanges and webs. Lines indicate delaminated areas.

Conclusions for Beams With Improved Flange and Web Materials

Results for the beams with DD5P material flanges are not as conclusive as those for the AA material flanges. Because these DD5P flanges can withstand strains about twice as great as material AA at 10^6 cycles, and because many of the webs were increased in stiffness over a simple ±45° laminate such as CH10, the load-transfer requirements were increased significantly. Thus, greater demands were put on the web in the web flange area, where the strains were the same as in the flanges. Results for Figures 7.12 and 7.13, for the material DD5P flanges and CH10 (±45°) web, show that the beams survive to a lifetime in the same range as the flange material coupons, exceeding the lifetime of the web material coupons. In most cases, the web material was heavily cracked

prior to failure (Figure 7.14), leading to tensile flange delamination. The finite element stress predictions for the shear stress in this adhesive region are shown in Figures 7.22 to 7.24. These involve a 4-point loading of 17.8 kN [81] and accurately predict the stress concentration location where the tensile flange delamination starts. Figure 7.25 shows a normalized Von Mises stress distribution along the centerline of the tension flange in the adhesive layer. These figures show that there is a stress concentration starting at the location where the shear stiffener tapers from the inner surface of the C-channel. Figure 7.26 shows a section of beam 28, at the start of the tensile flange delamination, showing multiple matrix cracks. Similar agreement between beams and coupons is shown in Figure 7.16 and 7.17, with a web (CH3) containing 24% 0° material. Higher 0° material contents in web materials CH12 and DD5P led to more load-transfer problems; however the beam data do approach the coupon results at lower loads and higher cycles (see Figure 7.20). The load-transfer problems are related to the particular beam design used here, although the web failure adjacent to the flange would be expected in a blade and is a meaningful result. Overall, the beam data with material DD5P flanges are consistent with web and/or flange coupon results in the absence of failures resulting from load introduction problems.

Stiffness Changes

Several of the beams were monitored for stiffness changes. Figure 7.27 gives stiffness change as a function of fractional lifetime for nine beams. Stiffness changes were generally moderate, with the greatest changes associated with delaminations, as

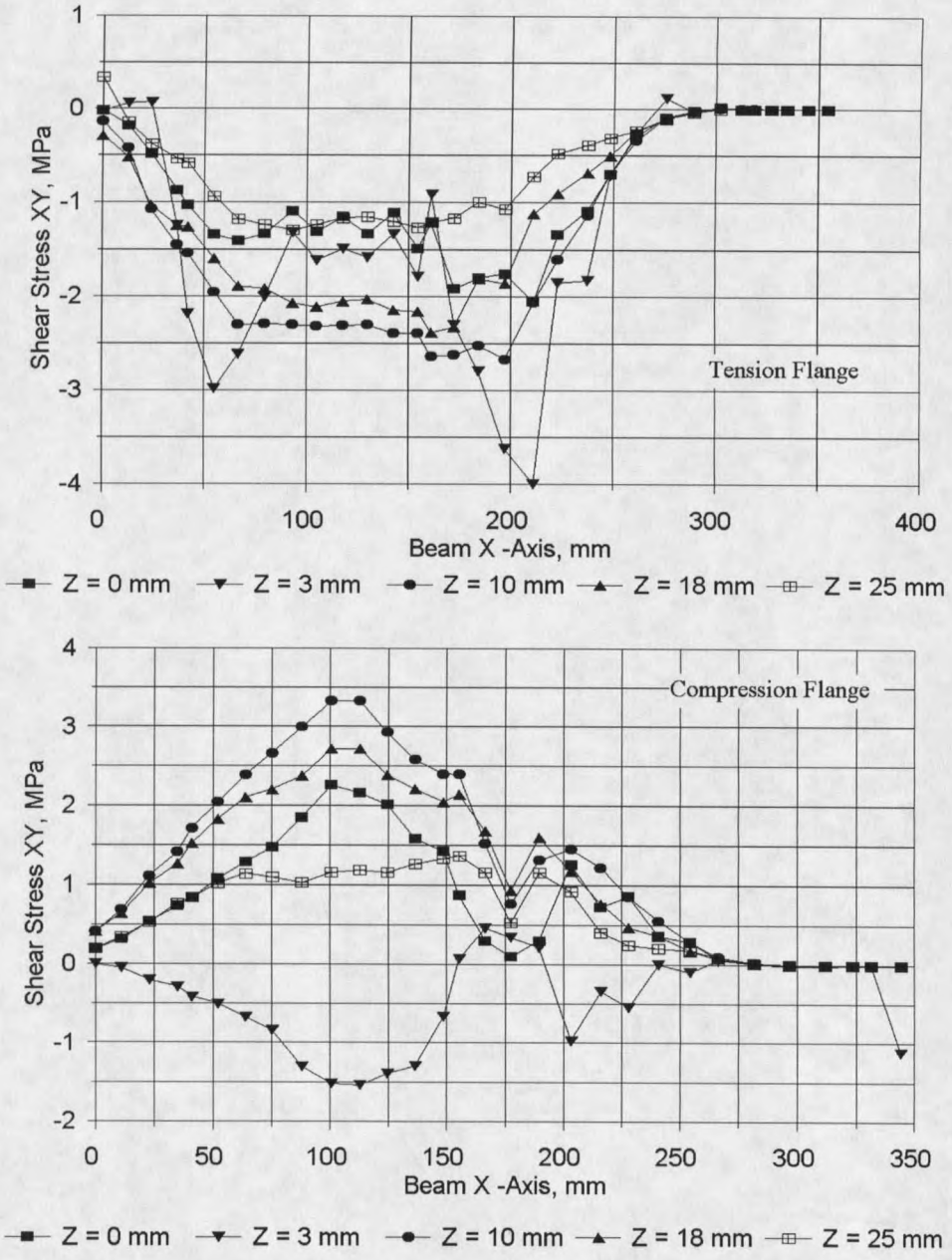
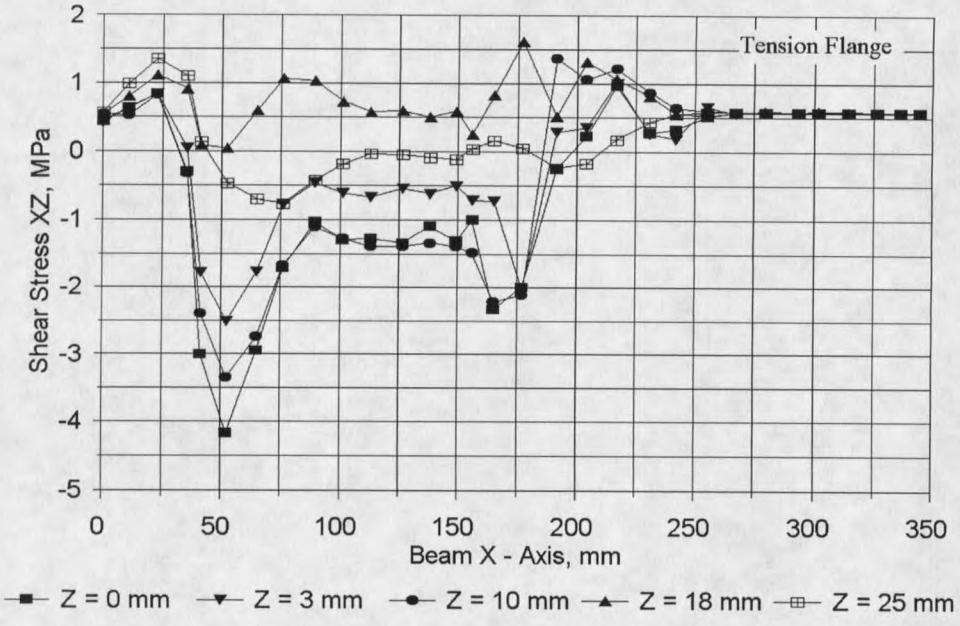


Figure 7.22. Shear stress XY at the adhesive interface of flanges (17.8 kN load).



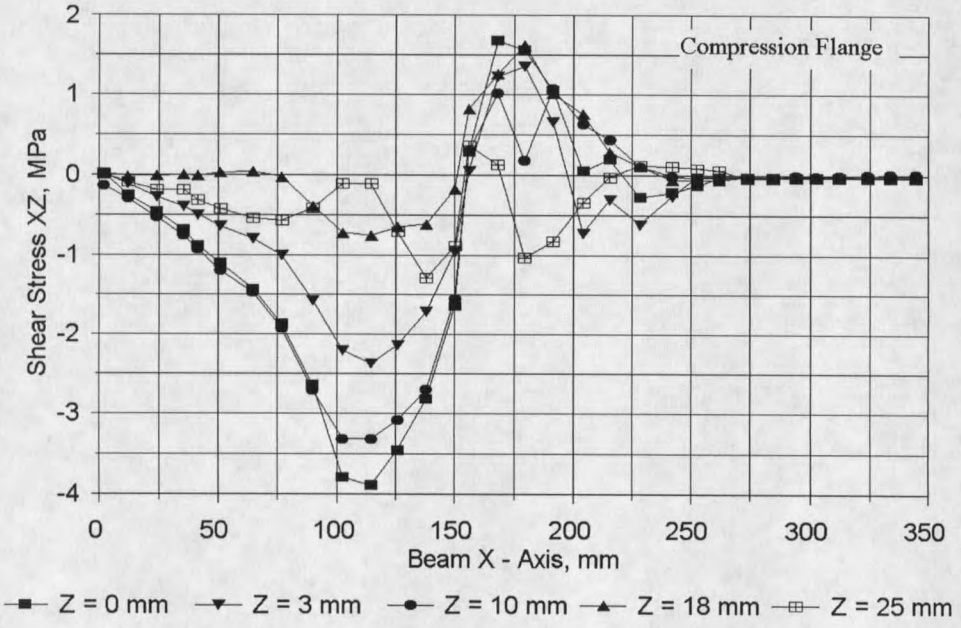


Figure 7.23. Shear stress XZ at the adhesive interface of flanges (17.8 kN load).

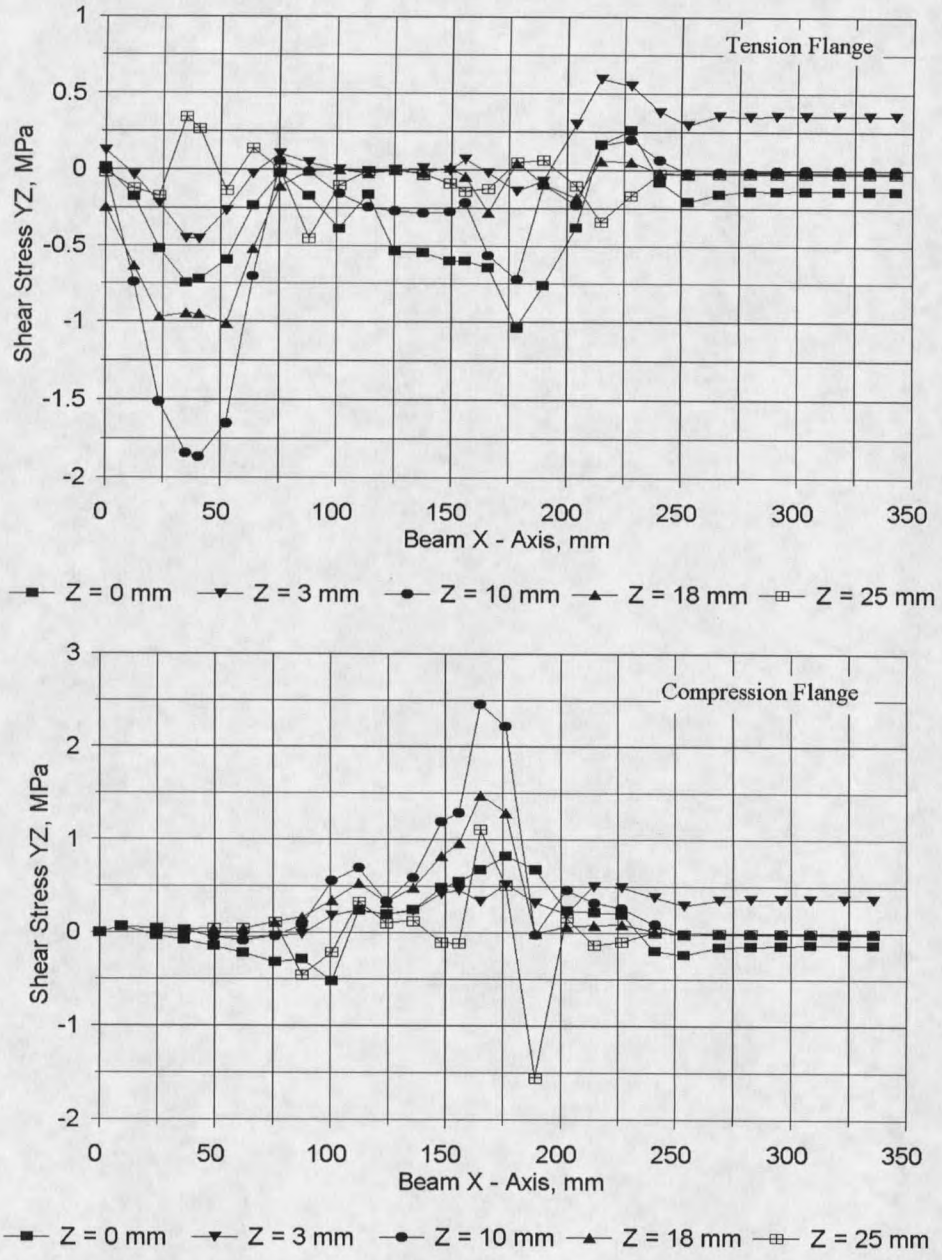


Figure 7.24. Shear stress YZ at the adhesive interface of flanges (17.8 kN load).

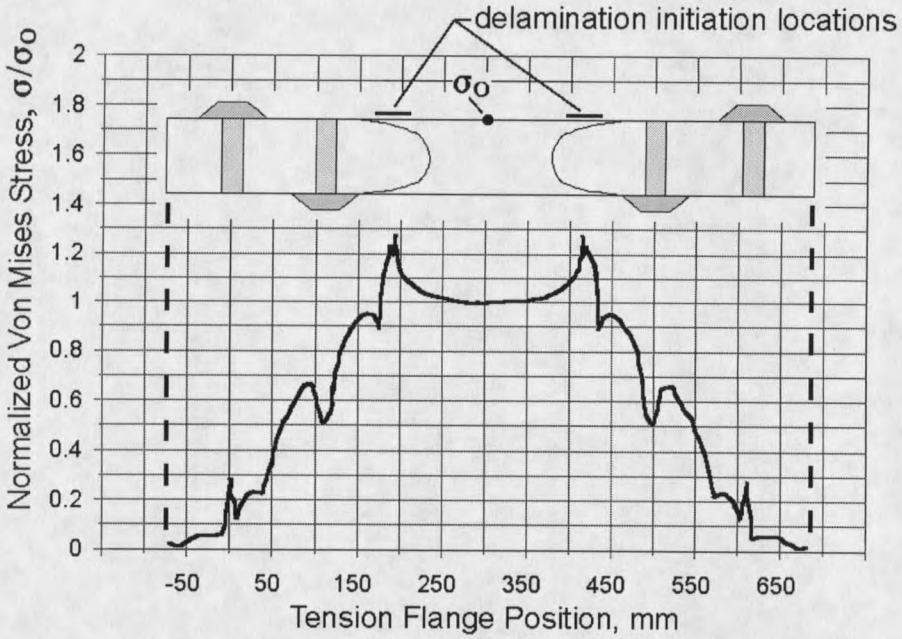


Figure 7.25. Normalized Von Mises stress on the centerline of the beam in the adhesive layer (z = 0)

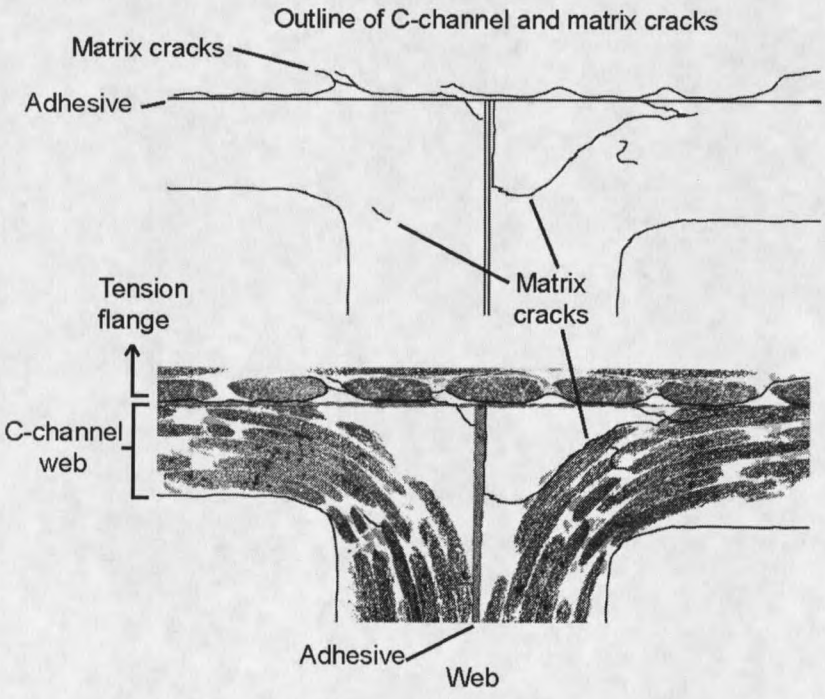


Figure 7.26. Matrix cracking at tensile flange in Beam 28 (x = 178 mm) at delamination initiation location.

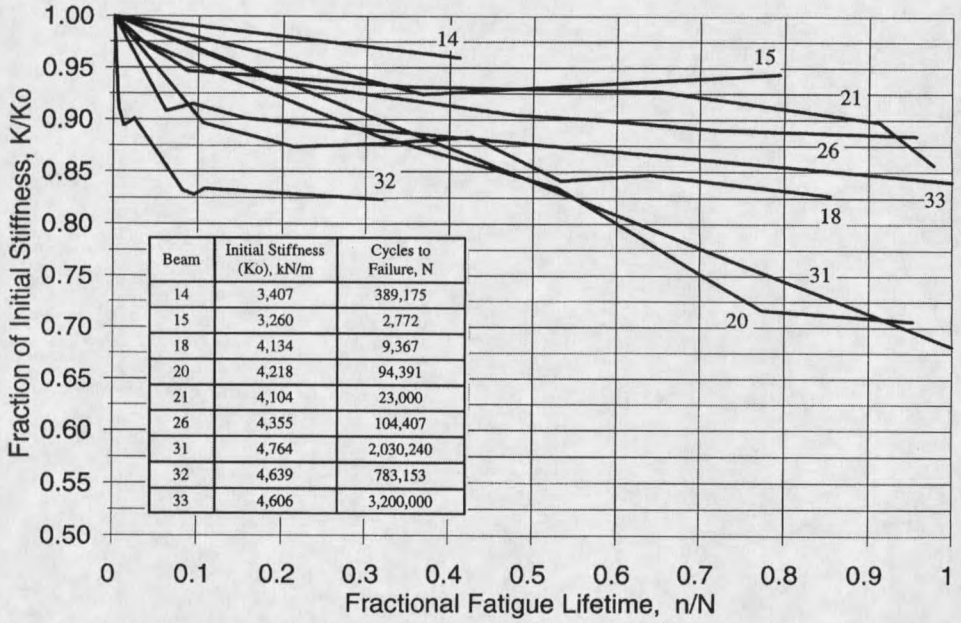
reported in the first section. Material coupon stiffness changes tend to be in the range of 10 to 15 percent until just prior to failure [2]. Changes greater than this are typically the result of structural breakdown as by delamination in the load-transfer area. Strains during fatigue were monitored by special clip gages described in Chapter 2, because bonded strain gages fail with the onset of matrix cracking.

Studies Of Structural Details

Wind turbine blades are comprised of large areas of structure to which the foregoing sections apply. However, they also contain unintentional flaws and necessary structural details such as ply drops and adhesive bonds. The beam test specimen provides a good context in which to consider certain structural details. This section includes results for the effects of severe flaws in the form of through-thickness, 13-mm diameter holes. The coupon data are presented followed by results where the detail is incorporated into beam flanges. Tests with ply drops are described in Reference 13.

Effects of Through-Thickness Holes

Turbine blades are subject to damage and manufacturing flaws, and in some cases may contain bolted connections. Composite materials are relatively insensitive to notches and flaws, but still demonstrate some degree of notch sensitivity in most cases [82, 83]. The most notch-sensitive composites tend to be woven biaxial fabric constructions, with finer weaves giving more notch sensitivity; in the most notch-sensitive cases, or with very large flaws, linear fracture mechanics may be applied for through-thickness flaws [82]. More commonly, stable damage development near flaws is significant, and two parameter models such as the Nuismer-Whitney model are used [83]. Sometimes, a through



Beam	Initial Stiffness (Ko), kN/m	Cycles to Failure, N
14	3,407	389,175
15	3,260	2,772
18	4,134	9,367
20	4,218	94,391
21	4,104	23,000
26	4,355	104,407
31	4,764	2,030,240
32	4,639	783,153
33	4,606	3,200,000

Figure 7.27. Beam stiffness versus lifetime (n: cycles endured; N: cycles to failure).

thickness hole is used in laminate tests, which tends to produce a more severe strength loss than flaws that escape visual inspection. For the carbon-fiber composites that have been investigated, impact damage and resulting delamination tend to be slightly more severe than through-holes in compression.

Coupon Results With Holes

We investigated flaw sensitivity for AA triax material, which, like woven fabrics [84], was expected to exhibit more notch sensitivity than separate ply laminates. Figure 7.28 gives coupon fatigue maximum stress versus cycles to failure (S-N) data for notched and unnotched specimens, where the notch was a central 13-mm diameter through-hole in a 51-mm-wide coupon. The stress plotted in Figure 7.28 is that in the far-field, away from

the notch. Figure 7.29 gives the same data plotted for the net cross-sectional area remaining at the hole, which is about 38-mm wide for the 51-mm overall width notched specimens. The data show moderate notch sensitivity for the static tests. The fatigue trends appear identical when the data are plotted in Figure 7.30 on a normalized basis; the unnotched and notched results are superimposed. These results are typical for those of many fiberglass laminates [1, 2]. In compression, the results are slightly more notch sensitive (see Figure 7.31), but less notch sensitive in reverse loading (see Figure 7.32). However, the reverse-loading case is the most fatigue sensitive for the stresses that produce failure in a given number of cycles. Figures 7.33 and 7.34 show the progression of damage and the damage in failed coupons for the tensile fatigue cases. Figure 7.35 shows local delamination damage for a compression coupon with no hole.

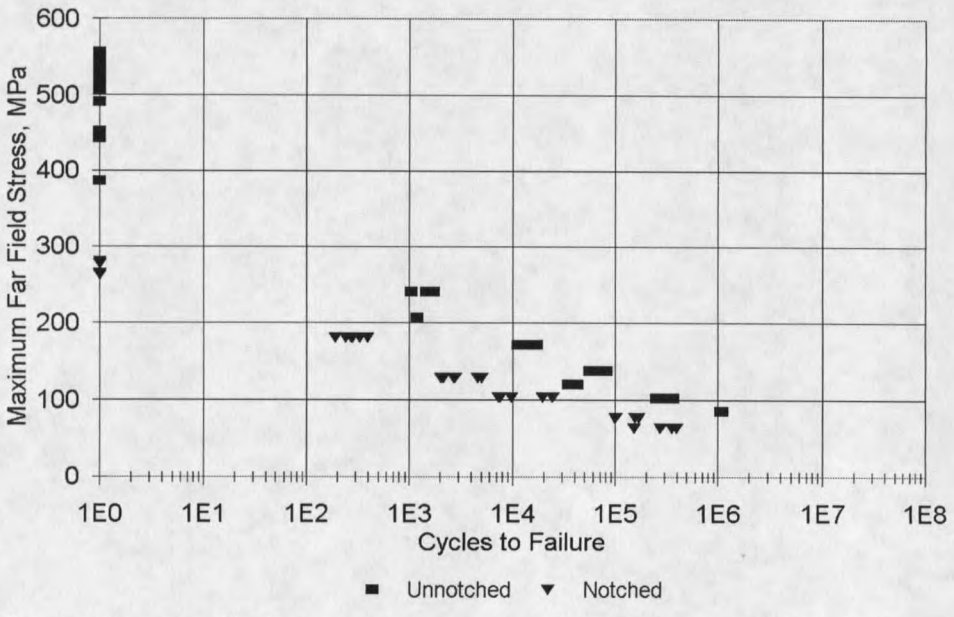


Figure 7.28. Tensile fatigue data for material AA coupons with and without a 13 mm diameter hole, R = 0.1.

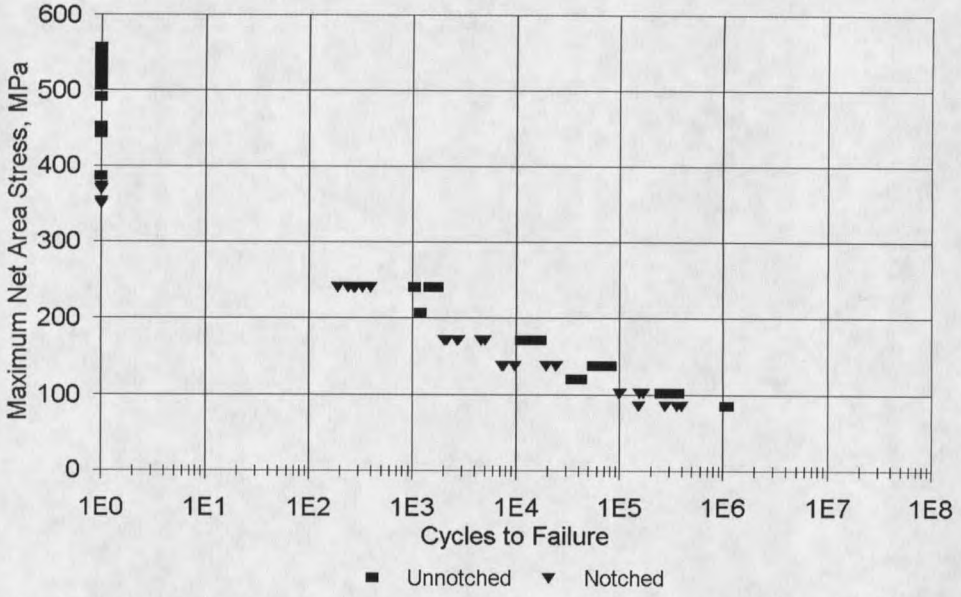


Figure 7.29. Tensile fatigue data for material AA coupons with and without a 13 mm diameter hole, R = 0.1.

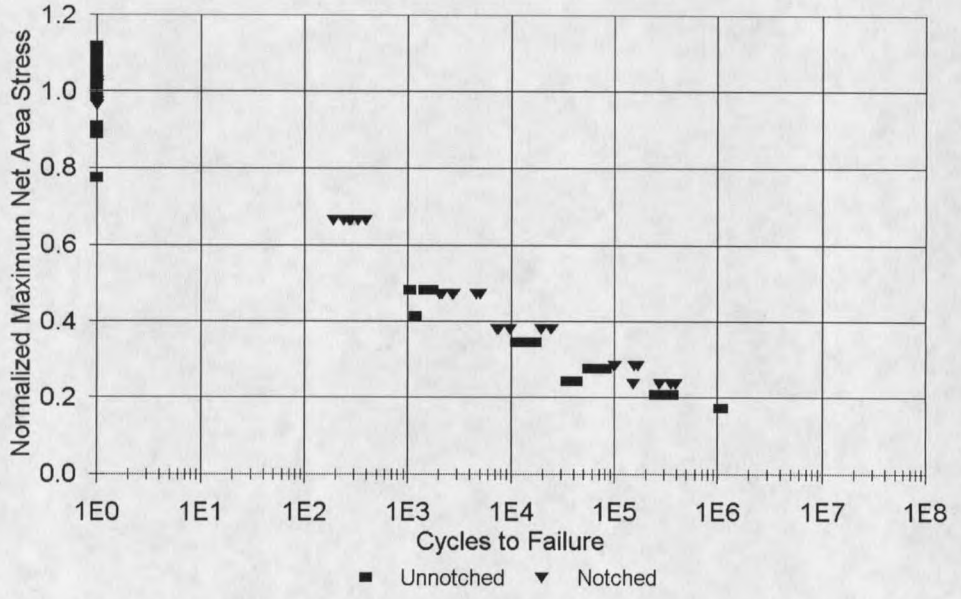


Figure 7.30. Normalized tensile fatigue data for material AA coupons with and without a 13 mm diameter hole, R = 0.1 (stress is divided by the one-cycle strength).

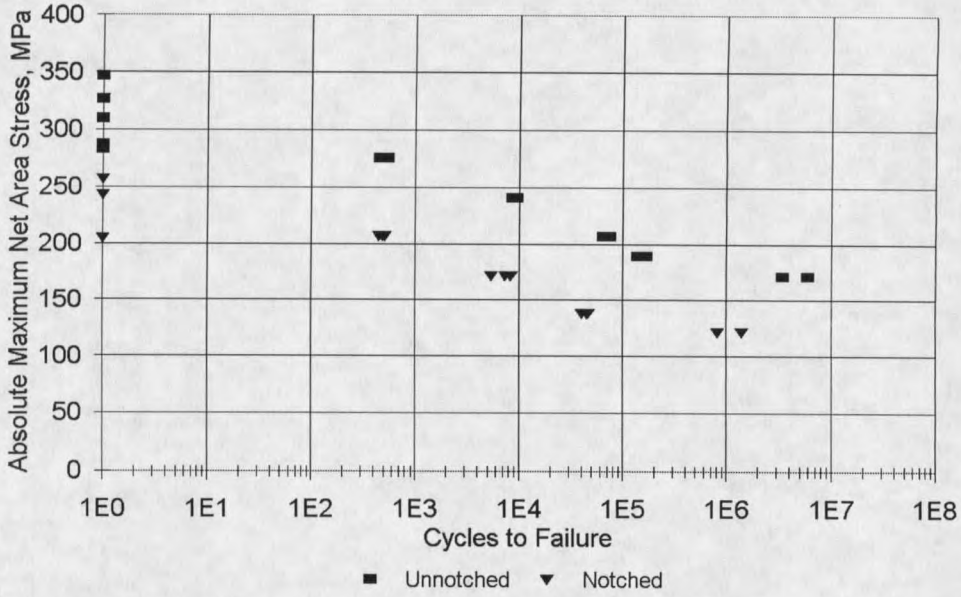


Figure 7.31. Compressive fatigue data for material AA coupons with and without a 13 mm diameter hole, R = 10.

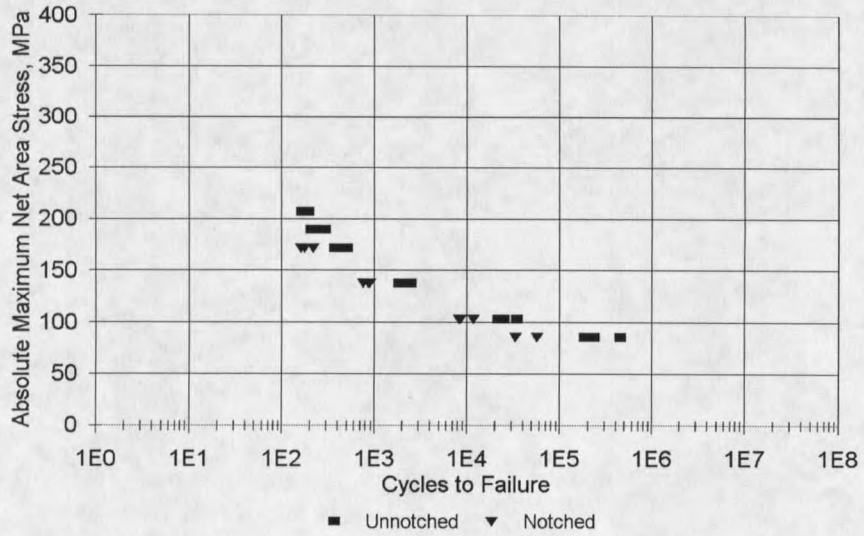


Figure 7.32. Fatigue data for material AA coupons with and without a 13 mm diameter hole, R = -1.

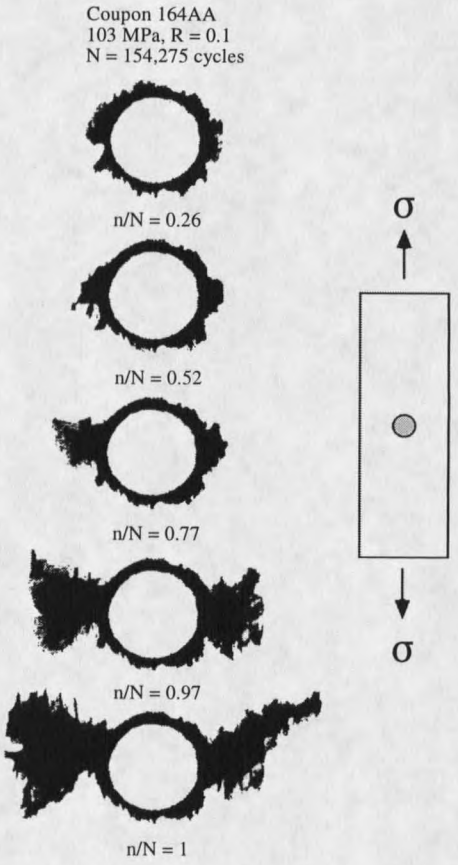


Figure 7.33. Damage around the 13 mm diameter hole versus fatigue lifetime.

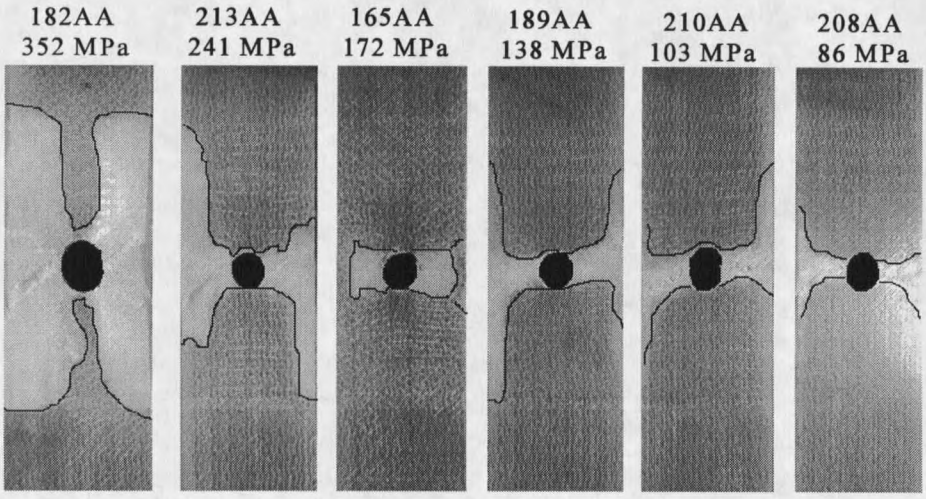


Figure 7.34. Photograph of damage around the 13 mm diameter hole at different stress levels, R = 0.1 (lines indicate damage border).

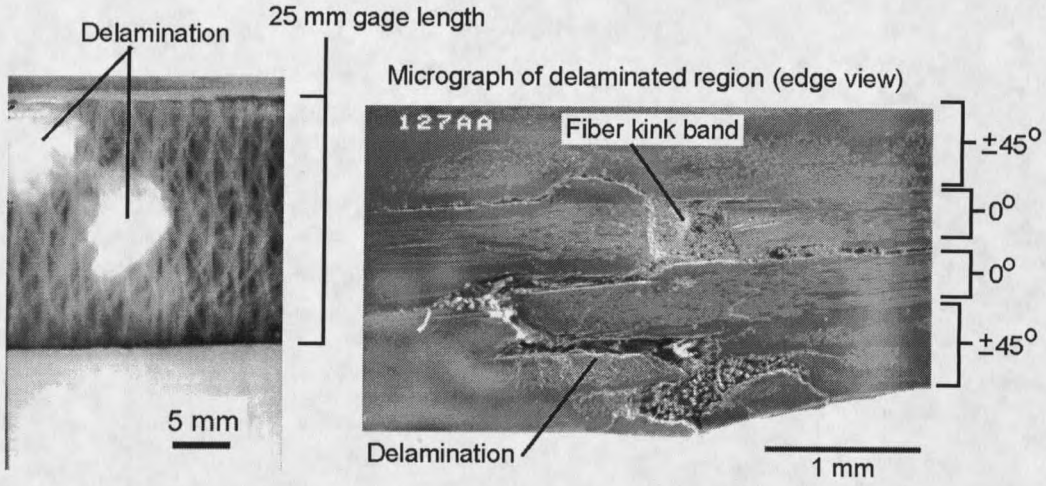


Figure 7.35. Delamination on a compression fatigue coupon (coupon 127AA).

Beam Results With Holes

Three beams with several 13-mm-diameter holes drilled through both tension and compressive flanges (see Table 7.1) were constructed. As expected, Figure 7.36 shows that the holes did reduce the static strength and fatigue life, relative to beams without holes. Figure 7.37 confirms that the beams behave similarly to the coupons containing holes. The static-tested beam (17) and the low-cycle fatigue beam (15) failed in compression, as expected from the coupon data, although at lower stress and higher cycles, the failure shifted to the tensile flange (beam 16). Again this is consistent with the coupon predictions. The mode shift is expected by comparing Figure 7.29 with 7.31. Figure 7.38 shows the details of failed beams with holes and other details as given in Appendix B.

The results of tests in this section for strength, fatigue lifetime and failure mode again show consistent behavior between coupons and beam structures. Severe flaws in the

form of 13-mm-diameter holes produce a moderate-strength reduction in the fatigue life of unflawed coupons. However, the far-field strain to produce failure at 10^6 cycles is still in the 0.4% range, only slightly below that for the unnotched specimens. The unnotched and notched trend lines tend to converge at high cycles in tension, as reported in the literature [13].

Beams Utilizing a Balsa Wood Core

Two beams (58 and 59) were constructed using material DD27 for the flanges and CH12 for the web. Material DD27 is the same as material DD5P with an additional center layer of 6 mm thick balsa wood to increase the moment of inertia of the flange. Both of these beams are detailed in Appendix B. The performance of these flanges was

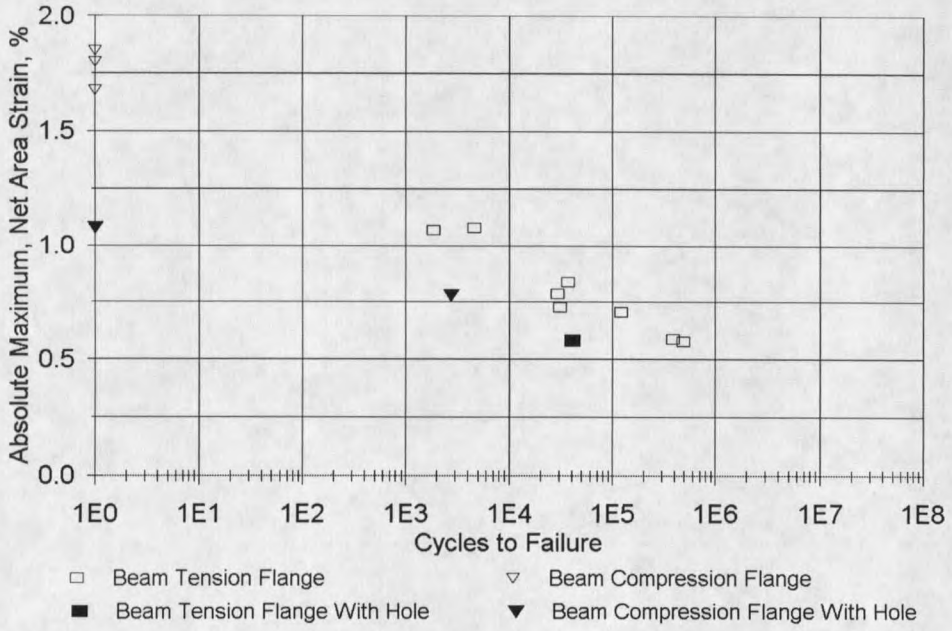


Figure 7.36. Comparison of AA material flange beams without holes to AA beams with 13 mm diameter holes in the flanges.

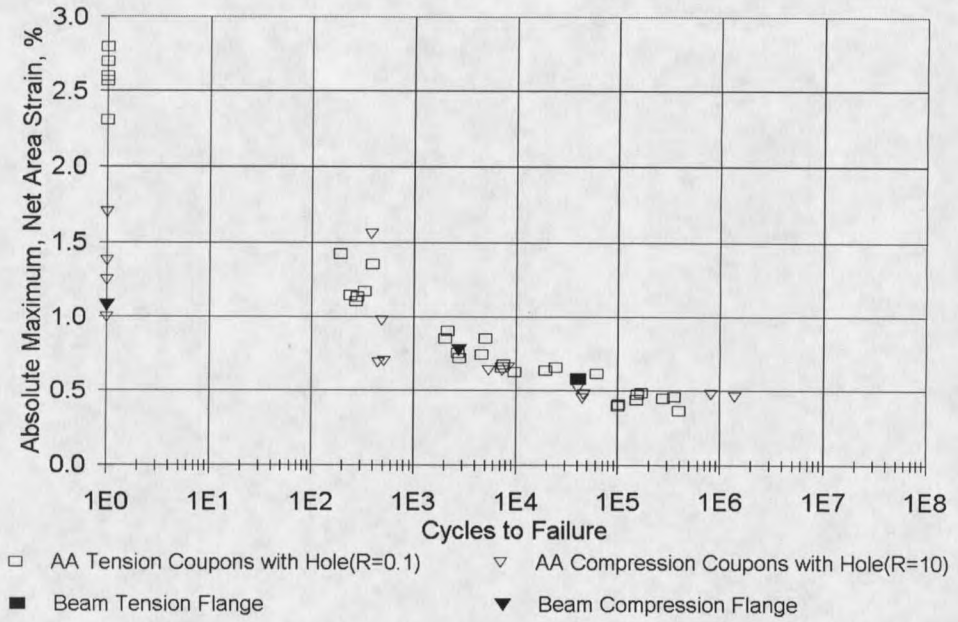
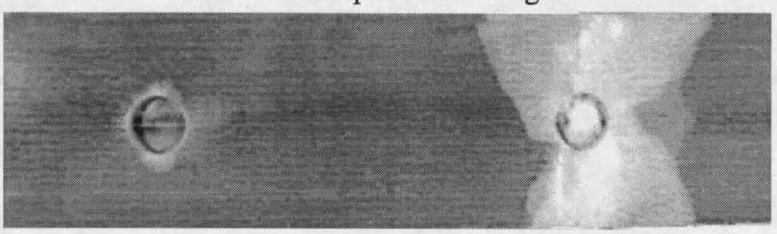


Figure 7.37. Comparison of AA material flange beams with holes to AA material coupons with 13 mm diameter holes.

Beam 15 Compression flange



Beam 15 side view

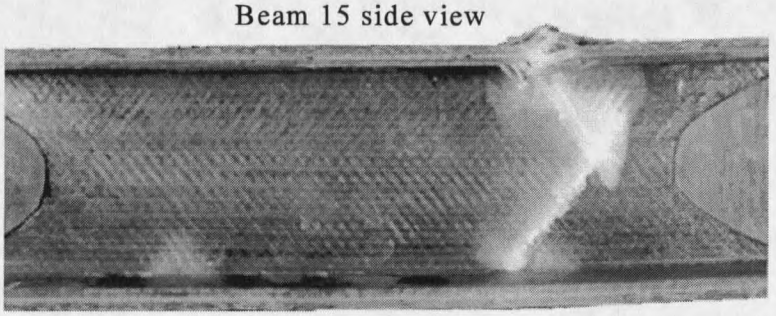


Figure 7.38. Beam 15 with holes, static compression flange failure.

disappointing as the fatigue lifetimes fell well short of the beams previously tested. A possible reason for this performance was the termination of the balsa wood core under the load pads. The termination could have initiated cracks which caused the delamination failures. Further research is required to develop a testing geometry which will prevent this delamination and prevent localized crushing under the load pads.

Conclusions for I-beam Study

The main objective was to develop a beam test specimen representative of wind turbine blade primary substructure to test the validity of using the materials database and current design methodologies for predicting structural strength, stiffness, failure mode, and fatigue lifetime. This objective was met, as the findings show that strength, stiffness, failure mode, and fatigue life can be predicted with acceptable accuracy as long as premature failure does not occur in the load introduction areas. (The specialized load introduction details for the beams are not representative of blades, but the general problem of load transfer at the hub and other special details of blades is of similar concern.)

Tests using the triax (material AA) flanges and ±45° (CH10) web showed good agreement between experimental and predicted results for strength, failure mode, and fatigue lifetime. As predicted, the failure mode shifted from compression at low cycles (only the static, one cycle tests could be conducted experimentally because of the very low cycles) to tensile flange failure at moderate to high cycles and lower loads. The poor tensile fatigue performance of triax fabric in coupons was equally evident in the beam

structures, with good quantitative correlation on lifetimes.

The use of materials with improved fatigue resistance (material DD5P in the flanges) did raise the strain capacity of the beam in fatigue by about a factor of two, as predicted. Failures then shifted to the web flange area, which experienced severe damage, sometimes leading to delamination from the main flange. This failure mode occurred at slightly higher strains than the web material coupons could withstand (materials CH10 and CH3), because the web flange ±45° layers can deteriorate heavily before the beam fails, as compared with failure of the 0° layers in the flange, which produces rapid failure. Further increases in the 0° content of the web (materials CH12 and DD5P) resulted in premature load pad and shear stiffener failures. Although the failure modes were more complex with the material DD5P flanges, making validation of lifetime predictions more difficult, the beam results did fall in the strain and lifetime range predicted by the coupon database.

The final sections of the chapter include results of an ongoing study that uses the beam specimen to explore the effects of flaws and structural details. A 13 mm diameter through-thickness drilled hole has been considered in the composites industry as a very severe type of flaw, worse than most flaws found in service. Coupons with holes showed moderate notch sensitivity in static tests, and similar normalized fatigue trends to unnotched coupons. Beams with holes in both flanges showed results for strength and lifetime that were consistent with the coupon data, again validating the use of coupon data for predicting structural performance.

CHAPTER 8

CYLINDRICAL TUBES

Hollow cylindrical tapered tube geometries were developed for their use in wind turbine blade test sections on a Bergey 10 kW wind turbine (Figure 1.1) at the Rice Ridge Renewable Energy Park near Norris, Montana. The tubes would allow for accelerated fatigue testing of candidate fiberglass materials under actual wind loading conditions. This small, hollow cross-section geometry was selected for its simplicity and because it would develop significant stresses under the loading conditions of a small, 10 kW turbine, while maintaining a wall thickness which was sufficient for commercial reinforcing fabrics. The hollow shape is marginally representative of the hollow cross-section of larger wind turbine blades (like the AOC 15/50, 50 kW machine) and fairly easy to model and manufacture. The geometry of the tube is shown in Figure 8.1 and construction is detailed in Chapter 2. A tapered tube with a varying moment of inertia allowed for a gage section where the maximum bending strains would occur, away from the stress concentrations at the ends. All the measured strains on the tube sections were obtained from this gage section unless otherwise noted. These tubes were tested in both 4-point and cantilever bending geometries.

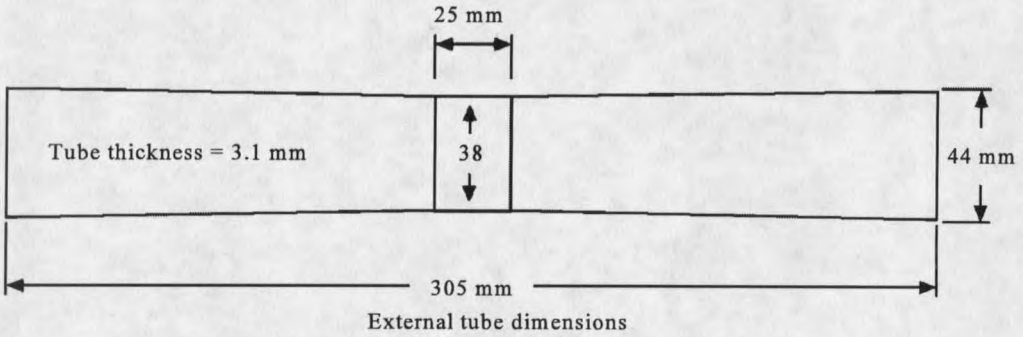


Figure 8.1. Hollow cylindrical tapered tube geometry.

Static 4-Point Bending Tests

The first stage of testing involved static 4-point bending of the tubes in the standard beam testing apparatus, described earlier. The purposes of these preliminary tests was development of the load introduction end fixtures, composite lay-up schedule, and the manufacturing process. The static 4-point bending tests dealing with tubes T110 through T119 are summarized in Table 8.1. Using a relatively thin, hollow cross-section in bending, the resistance to buckling is the limiting static design factor; initiation of failure in these tubes was buckling and delamination of the compression side of the gage section. Different laminate lay-up schedules were performed in an attempt to obtain gage section strength failures prior to buckling. The tubes should produce strains to failure close to those obtained in flat coupons, as did the I-beam tests. The tubes tested in 4-point bending had a 21 cm clear span between two tapered steel mandrels that were adhesively bonded with Hysol EA9309.2NA to the inside surface of the tube.

The first lay-up schedule was a [0/±45/0] lay-up (similar to material DD2) using the D155 and DB120 fabrics. This design gave a wall thickness of 1.9 mm which

corresponded to a fiber volume fraction of 0.44. Tubes T110, T111 and T112 all had very low maximum strains compared with the strains obtained from the coupon tests, indicating that the tube was buckling. Figure 8.2 shows evidence of this buckling in the bending moment versus bending strain diagram for tube T110. The surface damage to Tube T110 is shown in Figure 8.3. This, and subsequent images dealing with the failure surfaces, were obtained by rolling the failed tube section across a digital flatbed scanner, following the scanner sensor movement. This process allowed the entire tube surface to be displayed in one figure. The top and bottom of the figures represent the maximum tensile stress location in the gage section; the maximum compressive stress location (where failure occurred) was in the center of the figure. The right hand side of figures dealing with the cantilever tests was the end with the fixed support.

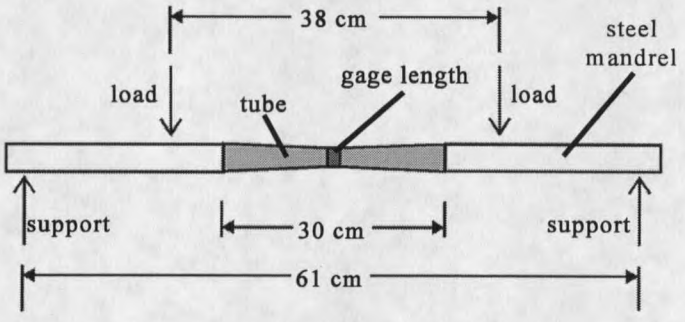
damage was localized in the gage section and it is believed that the evident fiber waviness was the cause of the low failure strains. The other internal plies compressively buckled inward and could be clearly seen by viewing inside the section. The same types of failures were seen with tubes T111 and T112 which are detailed in Figures 8.4 through 8.7. During testing, tube T111 was observed to change from a circular cross-section to an elliptical one prior to catastrophic failure. This tube had better fiber alignment and also reached higher failure strains than tube T110. Figure 8.4 also shows a more nearly linear behavior of the tension and compressive strain gages than tube T110. Tube T112 had some delamination in the outside compressive plies along with a through thickness shear crack, with no other damage on the rest of the tube. The term "shear crack" refers to the evident shear distortion of the fabric across the crack, and the angular direction of the

Figure 8.3 shows delamination of the outside 0° ply with some fiber waviness. The crack. The cause of the through thickness crack is undetermined; this was the only tube that failed in this manner.

Table 8.1. Summary of static four - point bending tests performed on tube sections.

Tube	Fabric lay-up	Wall thickness[1], mm	Maximum strain (tensile/compressive), %	Maximum 4-point bending moment, N-m
T110	[0/±45/0]	1.9 - 2.0	0.49 / -0.60	310
T111			0.85 / -1.30	382
T112			0.48 / -0.50	232
T113	[+45/0_2/-45]	1.9 - 2.0	0.82 / ---	413
T114[2]			--- / -0.92	509
T115			0.51 / -0.32	308
T116	[±45/0_4/∓45]	3.5 - 3.6	2.10 / -1.41	1,551
T117			1.74 / -1.22	1,634
T118			1.92 / -1.98	1,850
T119			2.19 / -1.89	1,930

[1] -Average tube V_F = 0.43 - 0.44. [2] -Tube T114 had a foam core.



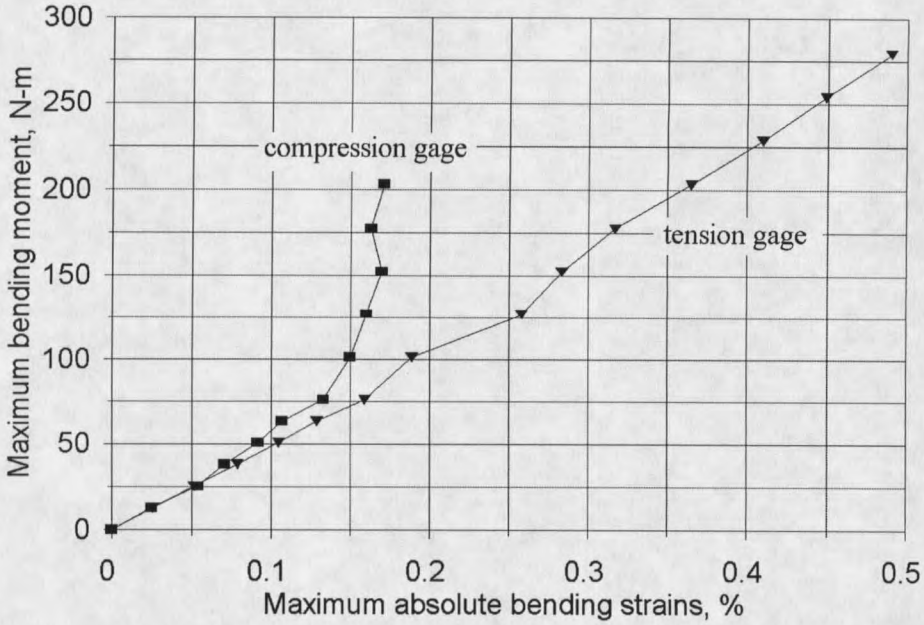


Figure 8.2. Bending moment versus bending strain for T110.

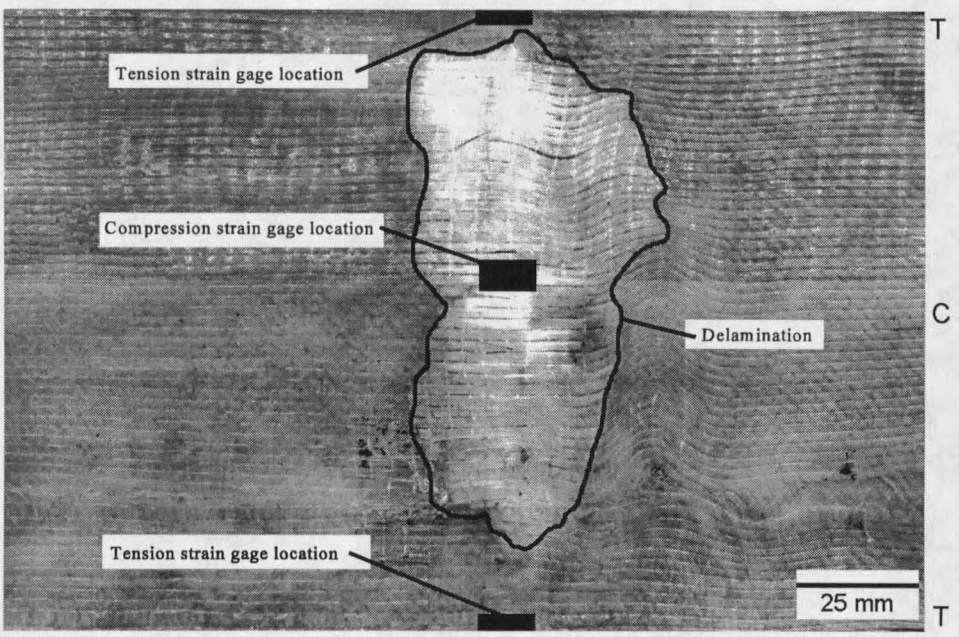


Figure 8.3. T110 failed tube surface.

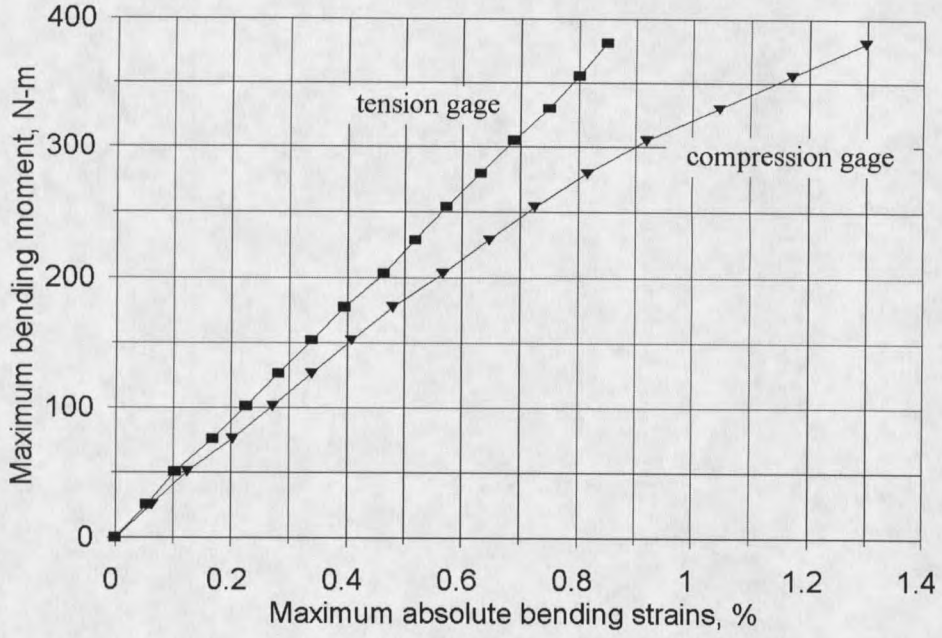


Figure 8.4. Bending moment versus bending strain for T111.

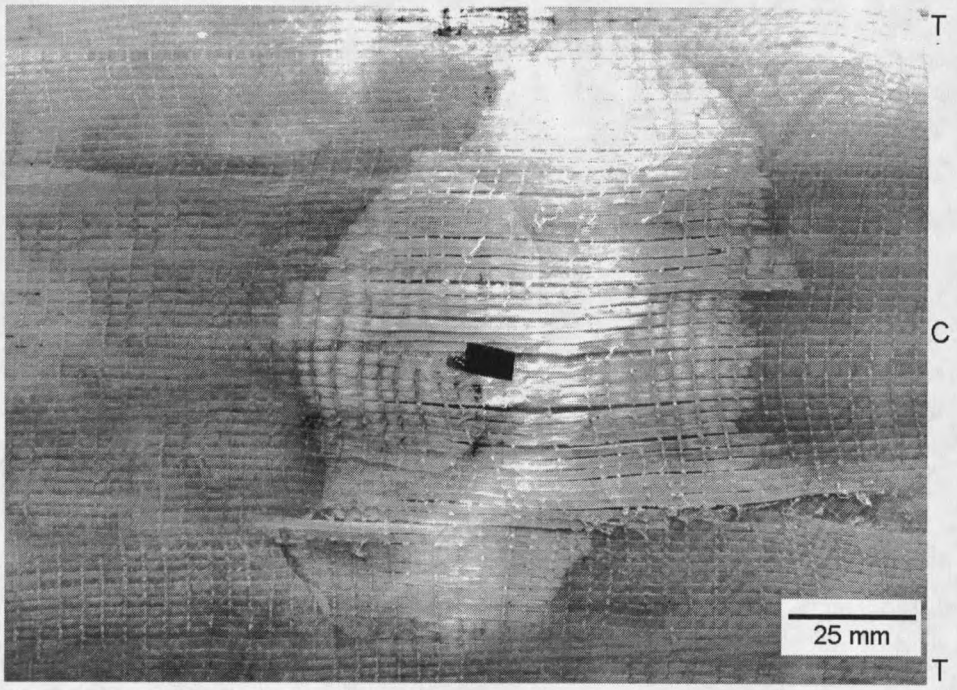


Figure 8.5. T111 failed tube surface.

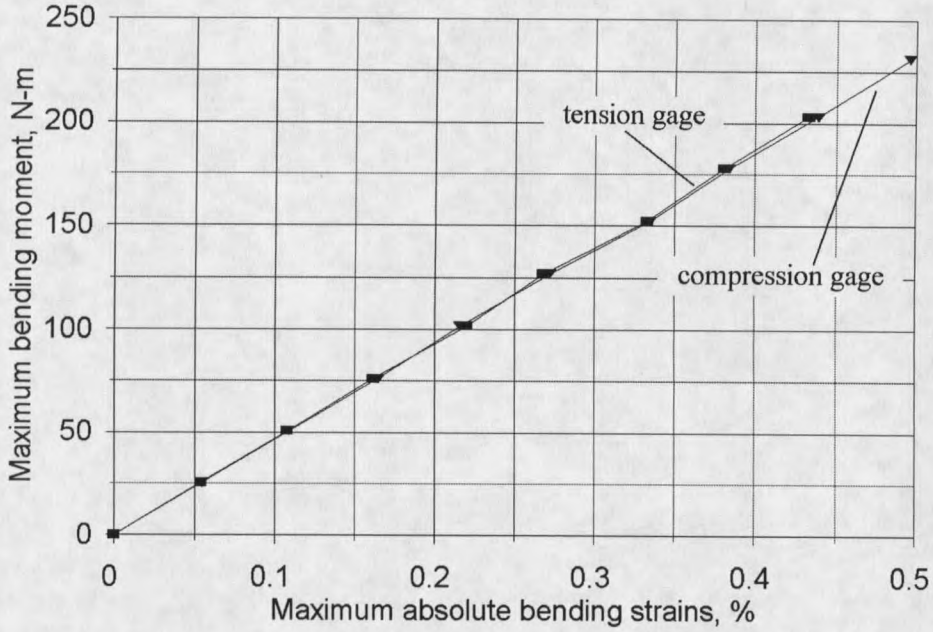


Figure 8.6. Bending moment versus bending strain for T112

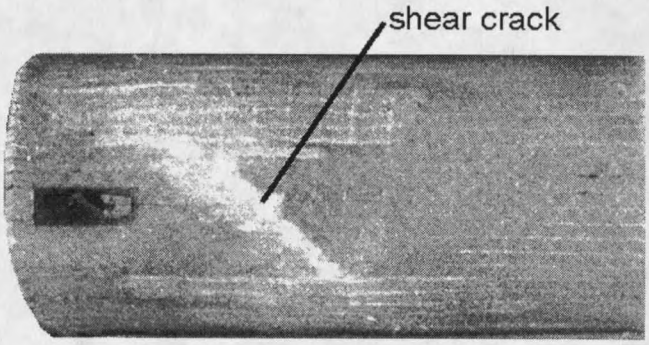


Figure 8.7. T112 failed tube surface.

Tubes T113, T114 and T115 had the orientation of the lay-up reversed which placed the 0° plies in the center of the thickness ([+45/0_2/-45]) as detailed in Figures 8.8 through 8.13. This lay-up was used to determine whether the 45° plies could add lateral

support the 0° plies to increase their buckling resistance. Tubes T113 and T114 had only one strain gage on the gage section and tube T114 had the interior of the tube foamed in with "Great Stuff®" polyurethane foam manufactured by Insta-foam Products (approximate ultimate compressive strength of 80 kPa and modulus of 0.8 MPa and a density of 30 kg/m^3). The foam was used to increase the failure moment of the tube by increasing the buckling resistance, and resulted in a moment capacity increase of approximately 50 percent over the other tubes. Tubes T113 and T115 showed little damage on the surface while tube T114 (with the foam) had massive circumferential delaminations. Figure 8.10 shows the applied bending moment versus the compressive strain for tube T114; the behavior was linear up to 0.8 percent strain when an audible crack was heard during the test. The graph continues non-linearly from this strain; it was not determined if the crack was the foam core delaminating from the interior tube surface

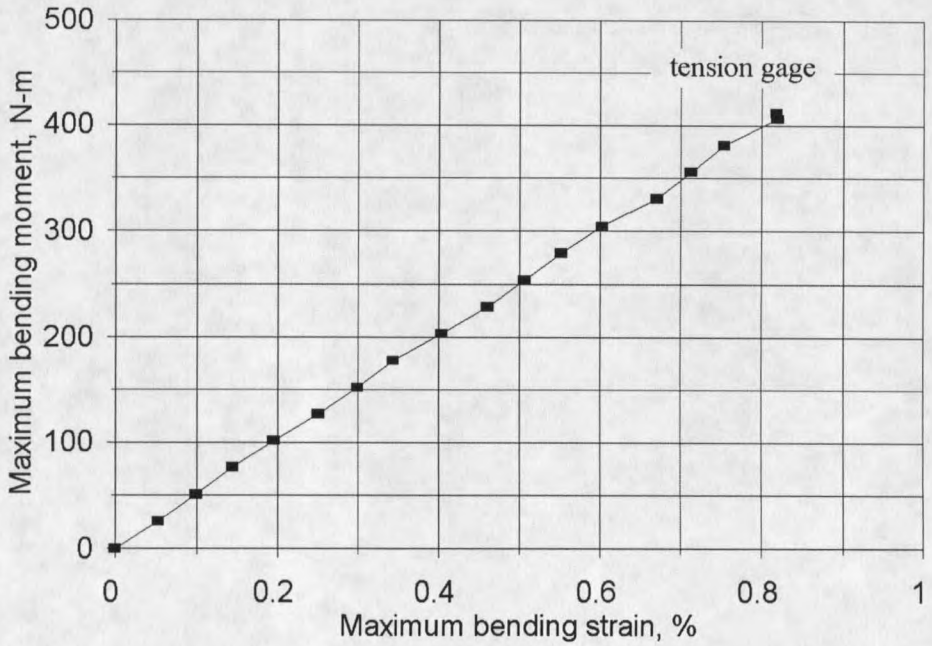


Figure 8.8. Bending moment versus bending strain for Tube T113

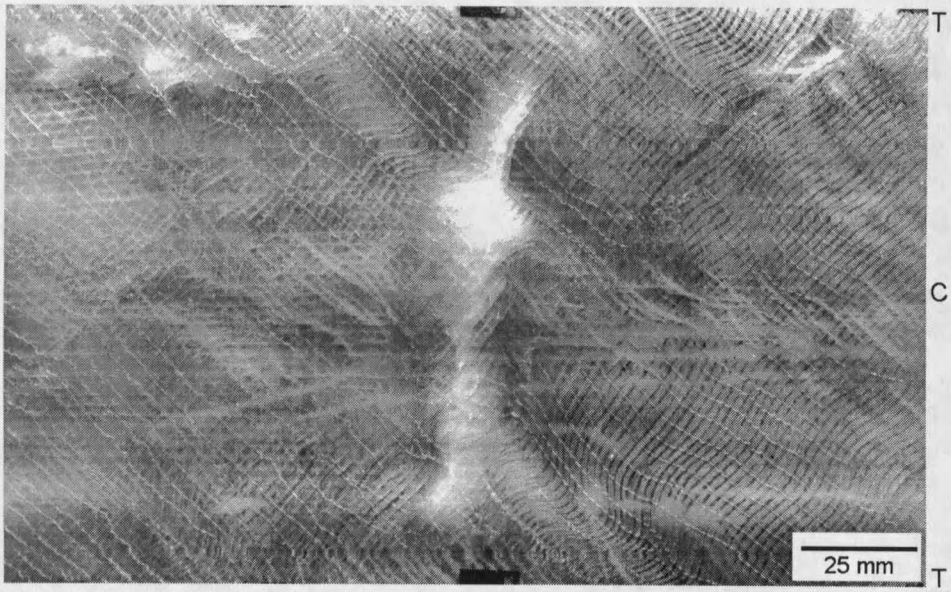


Figure 8.9. T113 failed tube surface.

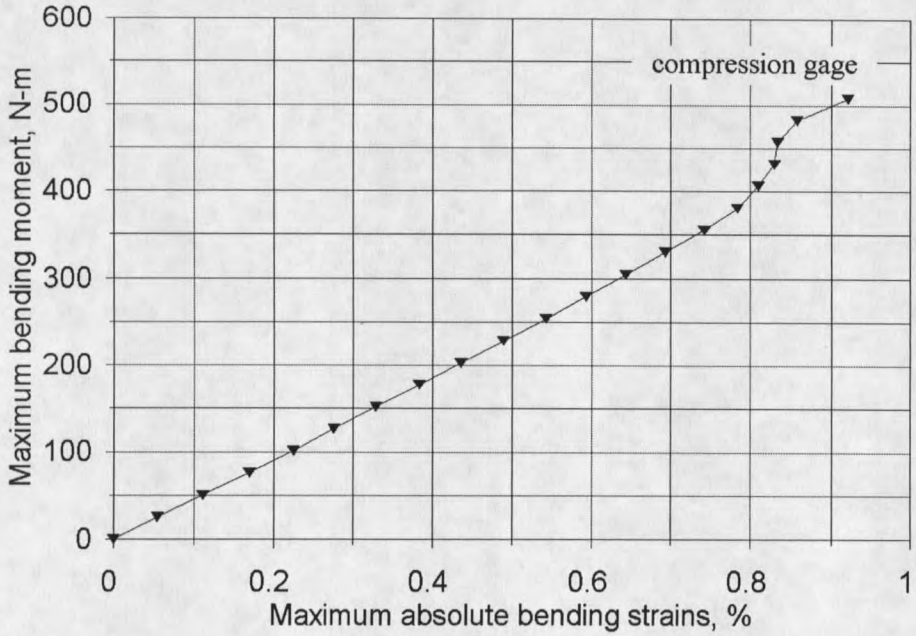


Figure 8.10. Bending moment versus bending strain for T114.

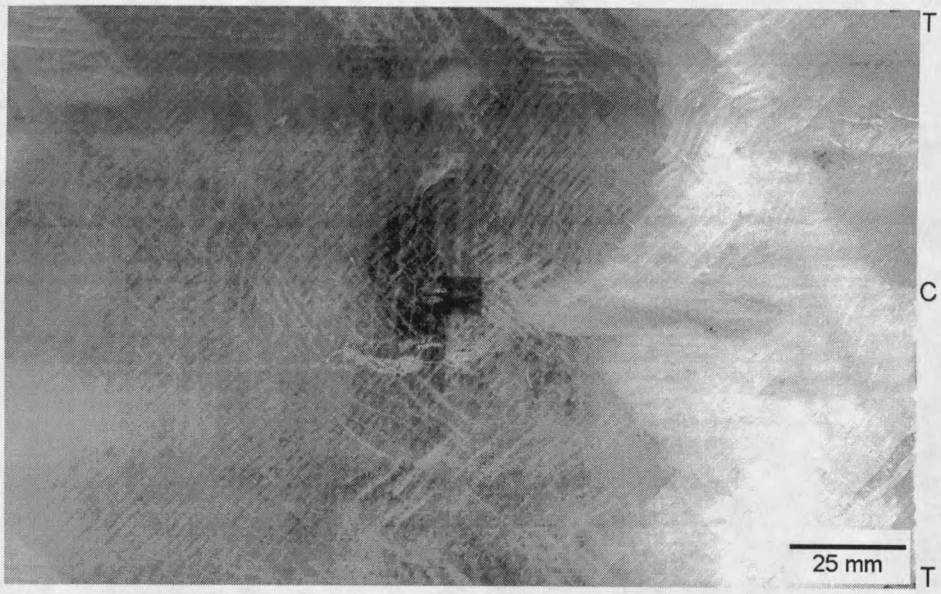


Figure 8.11. T114 failed tube surface.

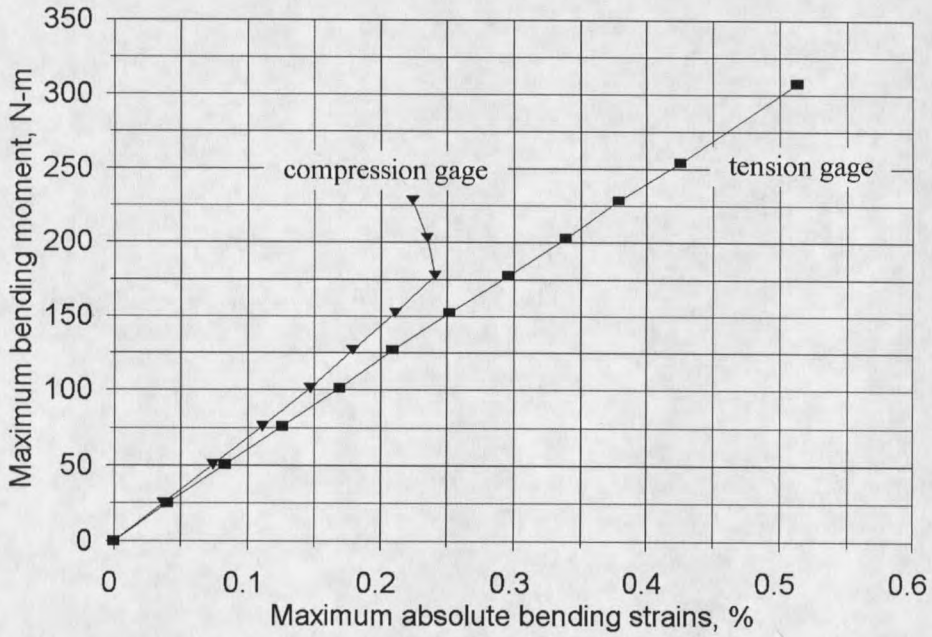


Figure 8.12. Bending moment versus bending strains for T115.

or a delamination between the composite plies. Figure 8.13 details the applied bending moment versus the absolute bending strains for tube T115. The compression gage deviated from a linear behavior early in the test and the failure surface showed little damage around the compression strain gage. The cause of this deviation or the lack of damage at this location was not determined.

The third iteration of the laminate lay-up involved a $[\pm 45/0_4/\pm 45]$ schedule that increased the wall thickness to 3.5 mm while maintaining a fiber volume fraction of 0.43. This lay-up caused an increase in the failure moments and strains in the tubes. Figures 8.14 through 8.20 show the failed tubes and their associated bending moment versus bending strain diagrams. The figures show much larger delaminations than the previous tubes (T110 to T115). Tube T118 had four strain gages located 90° apart from each other and the recorded strains are shown in Figure 8.17. It can be seen from this figure that the bending strains are linear until the compression side of the tube starts to buckle inwards. The strains recorded by strain gages two and four, which should have been on the neutral axis plane of the bending beam, were picking up some minor tensile strains, 0.09% and 0.20% respectively at failure, probably due to the neutral axis shifting towards the compressive side of the tube as the tube changed shape.

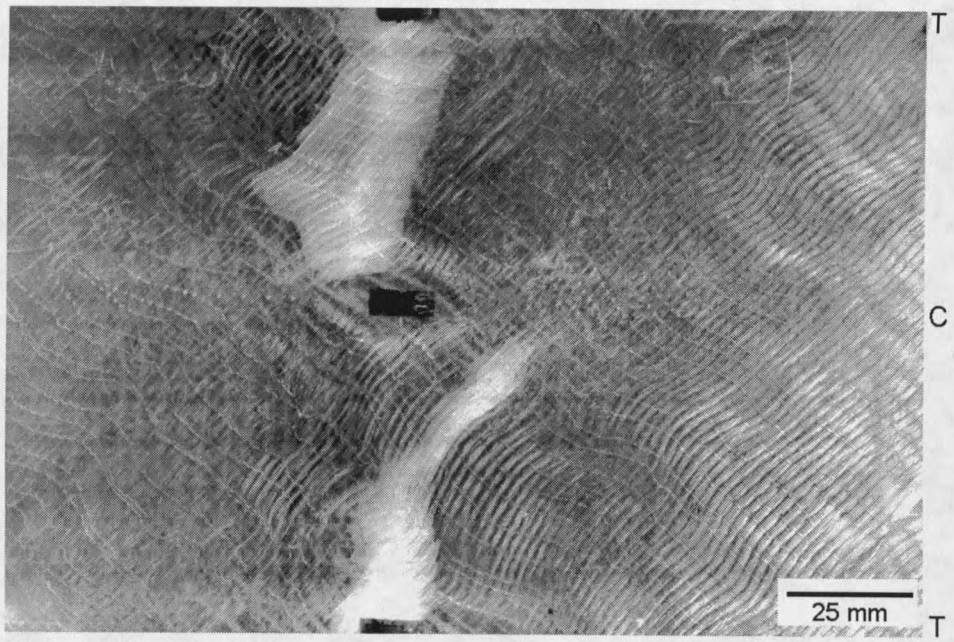


Figure 8.13. T115 failed tube surface.

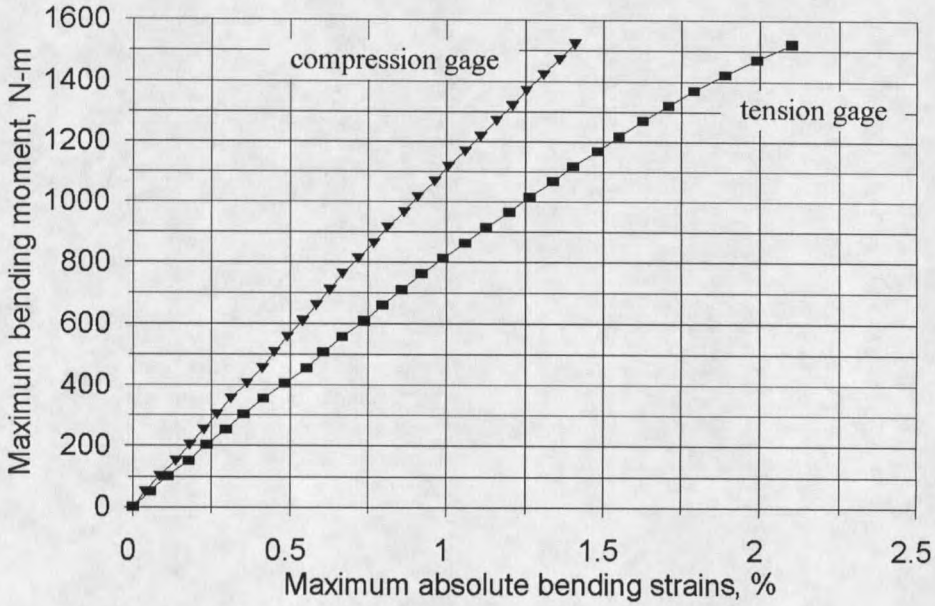


Figure 8.14. Bending moment versus bending strains for T116.

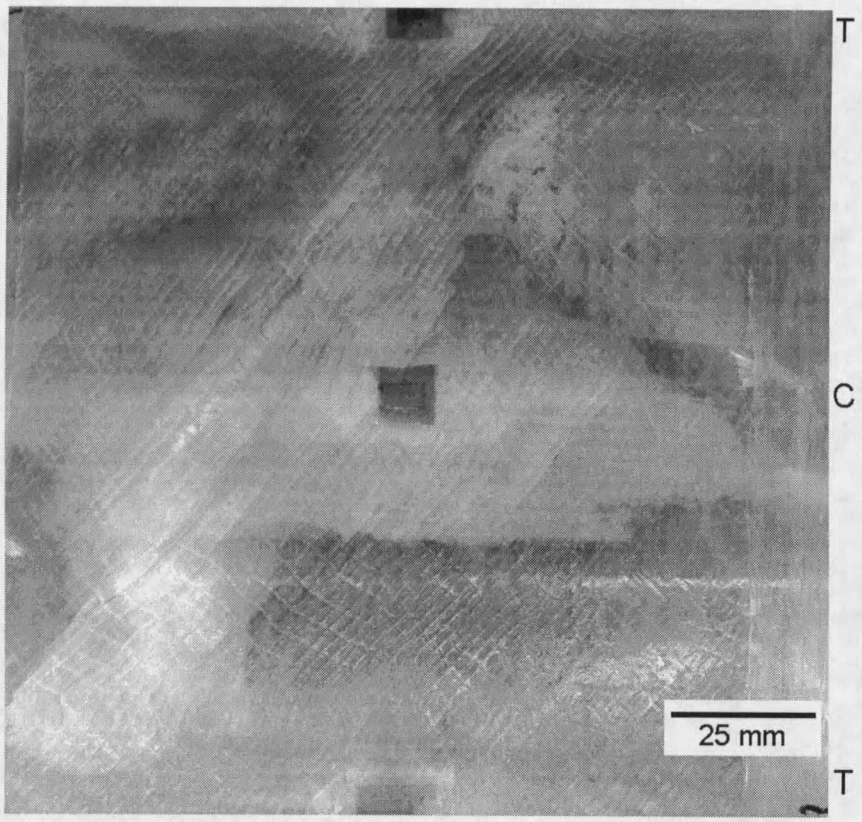


Figure 8.15. T116 failed tube surface.

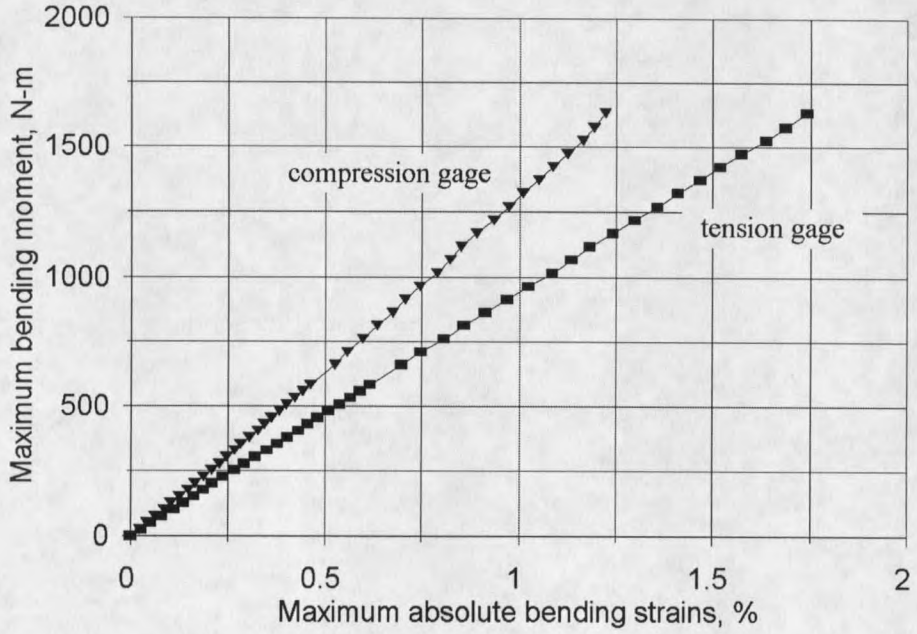


Figure 8.16. Bending moment versus bending strains for T117.

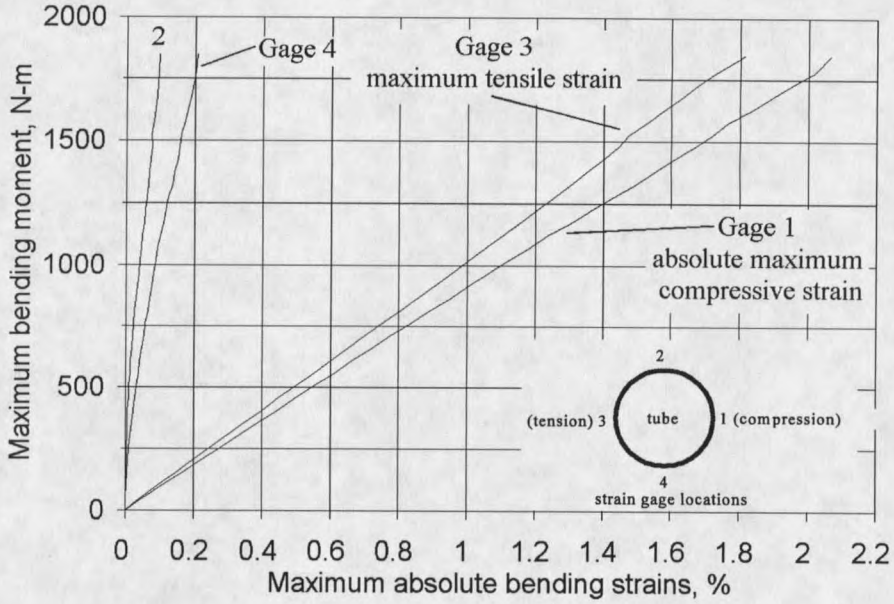


Figure 8.17. Bending moment versus bending strains for T118

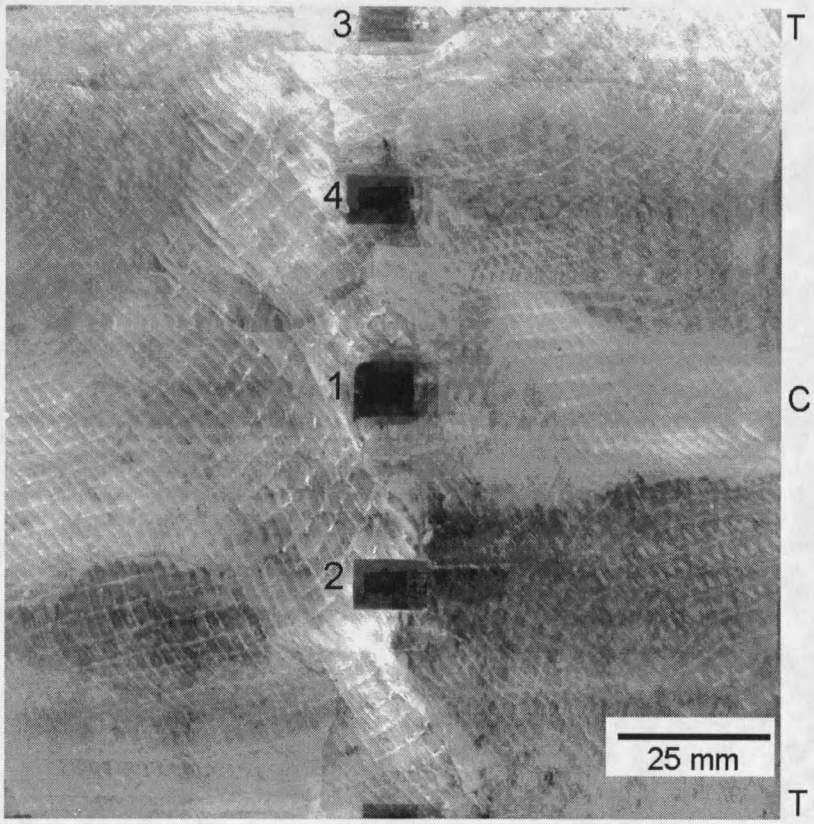


Figure 8.18. T118 failed tube surface.

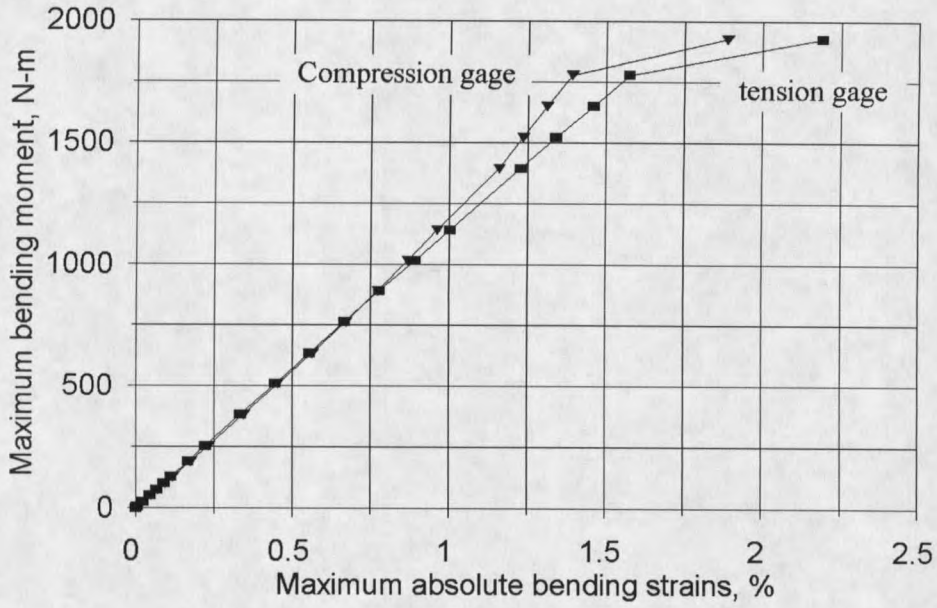


Figure 8.19. Bending moment versus bending strains for T119.

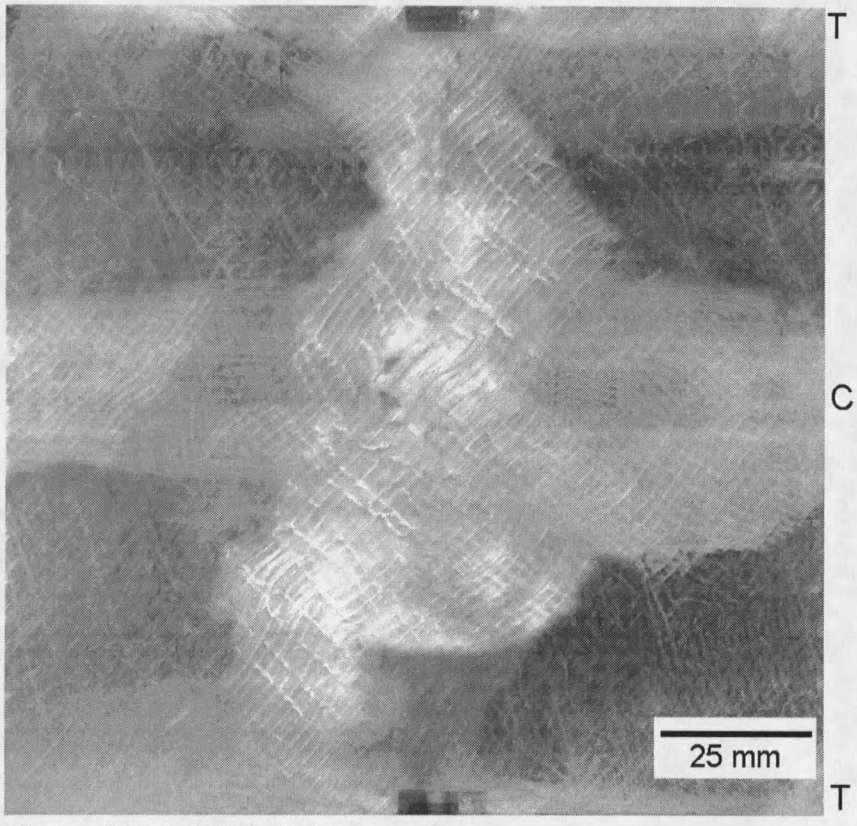
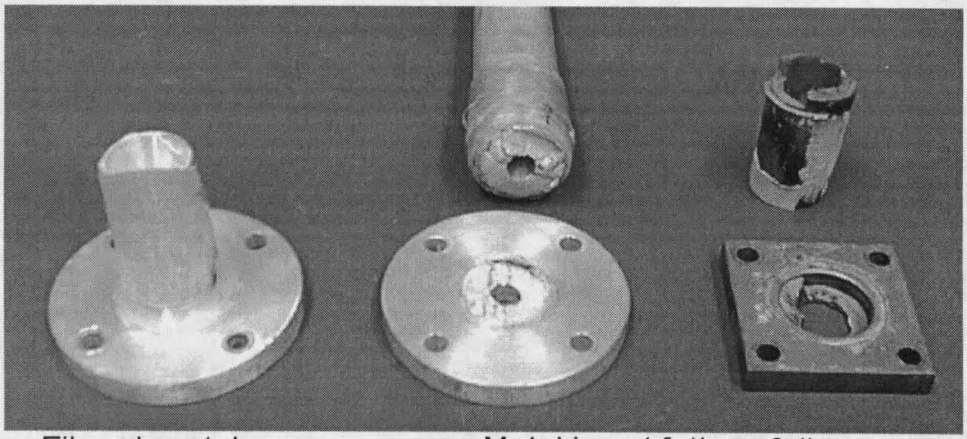


Figure 8.20. T119 failed tube surface.

Static and Fatigue Cantilever Beam Tests

Following the 4-point bending tests, the study turned to fatigue testing and the problems associated with load transfer through the tube section. Various internal, external and combined tube end inserts were studied to transfer the bending loads through the tube section and into the fixed support. Figure 8.21 shows some of the end fatigue failures generated in this research. The final solution was the use of a combined 2024-T3 aluminum internal insert with an external retaining ring, detailed in Chapter 2.



Fiberglass tube pullout

Metal insert fatigue failures (aluminum 6061-T6, steel 4130)

Figure 8.21. Cantilever tube end fixture failures.

A lay-up schedule of $[0/\pm45/0]_S$ (material DD5/DD5P) using the D155 and DB120 fabrics was used for these tubes. This schedule gave a tube wall thickness of 3.1 mm and corresponded to a fiber volume fraction of 0.38 in the gage section. With the tube diameter (38.1 to 25.4 mm) and the distance from the applied cantilever load (46 to 76 cm) changing, the maximum bending stress on the tube varies with position. The normalized maximum bending stress profile on the tube section is detailed in Figure 8.22

and shows that the maximum stress occurred on the inboard side of the gage section nearest the fixed end. The cantilever tests dealing with tubes T120 through T137 are summarized in Table 8.2 along with a diagram of the testing setup.

This series of cantilever bending tests were performed using displacement control at frequencies less than 4 Hz due to the large actuator displacement required (up to 15 cm). Load control was tried, but proved unreliable in this testing application. Figures 8.22 through 8.28 show typical failure surfaces of the tubes. Figures 8.22 through 8.25 show that the failure delamination is predominately in the gage section, extending towards the fixed end of the tube, as was expected from the bending stress distribution. Figure 8.26 shows delaminated 0° material starting under the compressive strain gage; it was not determined whether there was any influence of the surface preparation (light sanding) needed for the strain gage placement. Many of the tubes tested in fatigue initiated some delamination of the surface 0° material on the compression side, and this delamination grew until final failure. During numerous tests, the D155 surface strands were seen to delaminate on the compression side of the tube and buckle off of the surface of the tube, centered around the stitching thread in the D155 fabric. Figures 8.27 and 8.28 show some very localized delamination, and delamination on both sides of the gage length, respectively.

Figure 8.29 shows the bending stress-strain diagram for the static test of tube T122. The compressive failure strain is similar to the failure strains on the I-beams. As the fatigue tests progressed, it was noticed that the end adhesive joints were delaminating from the aluminum fixtures, shown in Figure 8.30. This figure shows cracking of the

adhesive between the aluminum end and the composite tube which extended along the circumference of the aluminum end fitting. Figure 8.31 shows that the cracking initiated and grew between the adhesive layer and the composite. The bonding of the adhesive to the aluminum end appeared intact and functional. This figure is from tube T137 and shows extensive cracking in the composite and at the composite-adhesive interface. Figure 8.32 shows cracking between the 0° D155 and the polyester matrix with most of the cracks along the outside or within the D155 strands.

To investigate the problem of cracking in the adhesive layer, two static axial tensile tests were performed, one with extensive previous bending fatigue cycles on it and one without prior loading. Figures 8.33 and 8.34 show the axial tests. These tests were

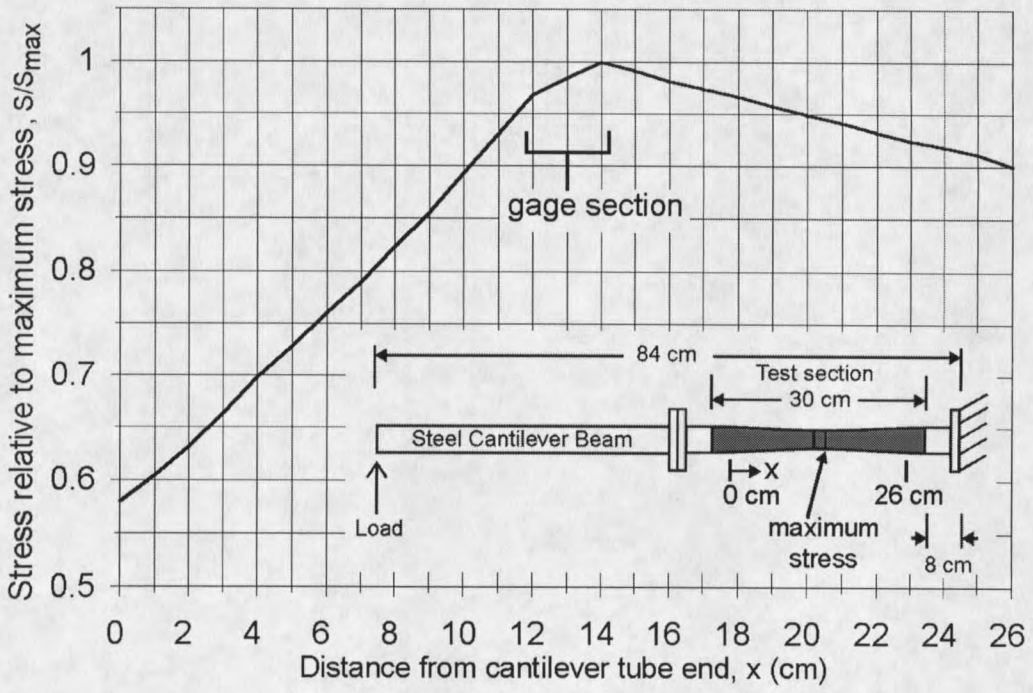
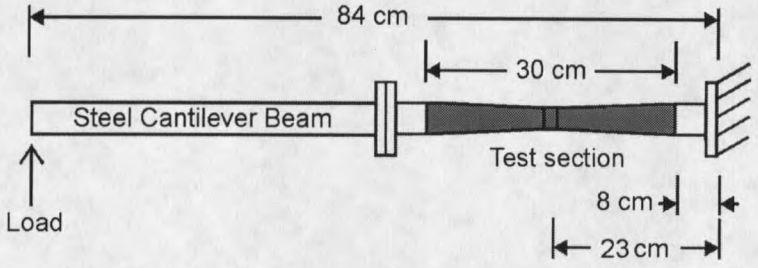


Figure 8.22. Normalized maximum bending stress vs. position on the tube.

Table 8.2. Test summary for tubes T120 through T137.

Tube	Initial stiffness N/m	Maximum strain (tensile/compressive) %	Maximum cantilever bending load, N	Cycles	Comments
T120	279	0.86/-0.92	778	14,213	
T121	225	1.12/-1.37	1,246	1,641	
T122	235	1.66/-1.84	1,850	1	
T123	242	1.86/-1.79	1,966	1	
T124	254	0.78/-0.76	756	250,000 R	End adhesive failure, repaired
	202	0.97/-0.93	756	794,370	
T125	293	0.93/-0.89	756	350,000 R	Steel failed
T126	246	0.94/-0.92	712	29,280	
T127	240	0.83/-0.87	712	200,150 R	End failure
T128	226	1.03/-0.98	667	215,000	
T129	229	0.98/-0.93	578	2,193,960	Fatigue test
		----	1,882	1	Static test
T130	244	0.94/-0.88	601	1,800,000 R	Fatigue and axial test
T131	212	0.95/-0.90	756	177,860	
T132	245	0.83/-0.86	756	2,145,083	
T133	----	0.936	----	1	Axial test
T134	253	0.86/-0.91	712	3,283,749	
T135	240	1.81/-1.78	2,045	1	
T136	227	1.73/-1.88	1,835	1	
T137	215	0.92/-1.01	756	529,919	

All tubes had a lay-up of $(0/\pm45/0)_S$.



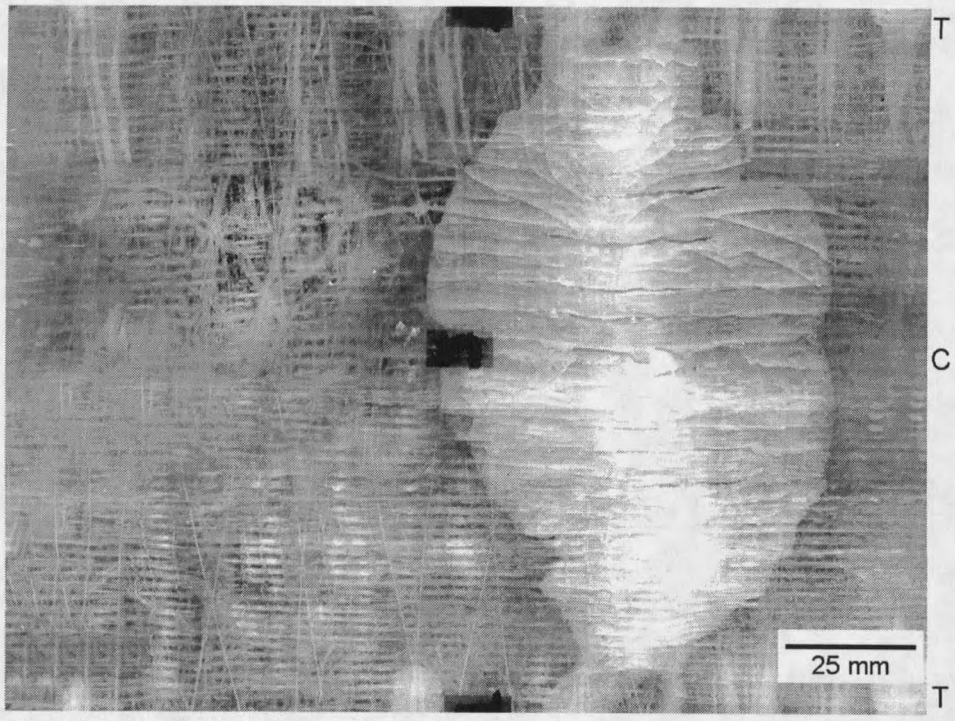


Figure 8.23. T121 failed tube surface.

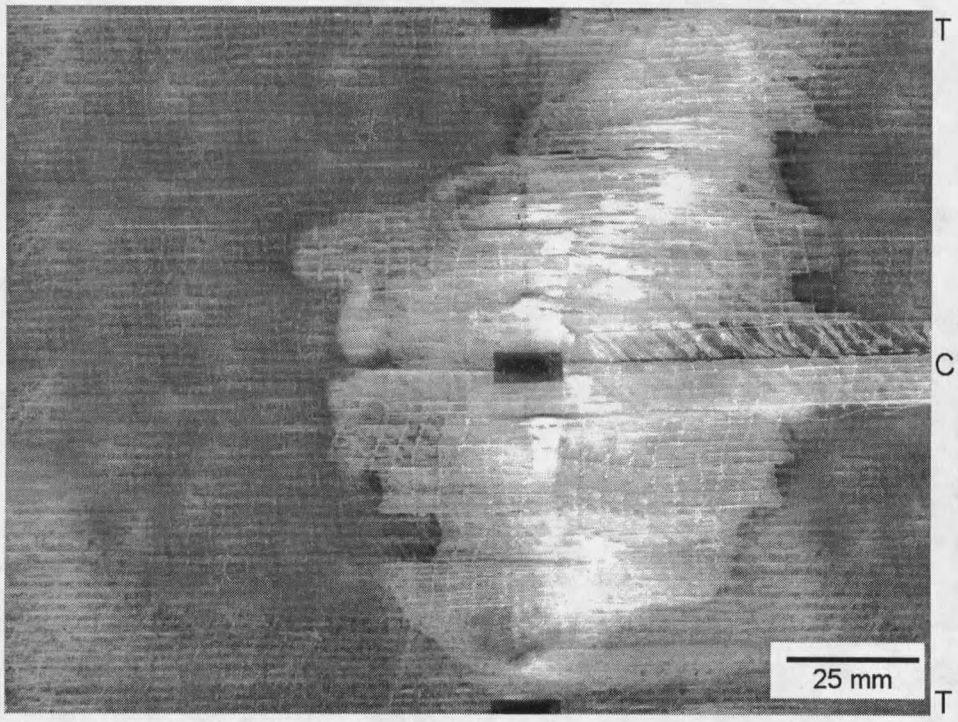


Figure 8.24. T122 failed tube surface.

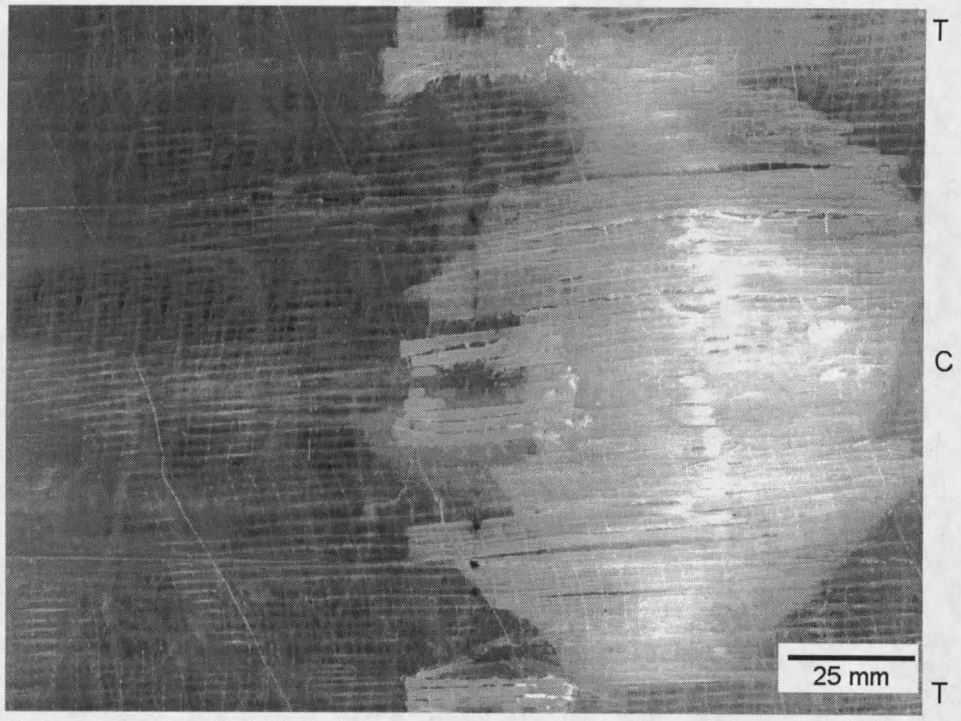


Figure 8.25. T123 failed tube surface.

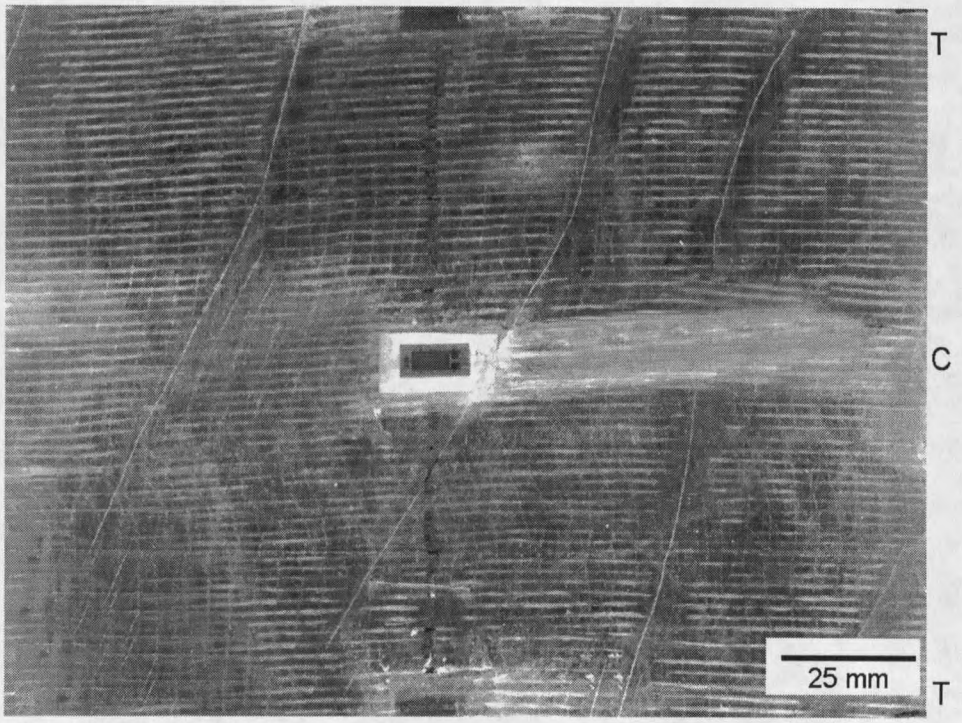


Figure 8.26. T124 failed tube surface.

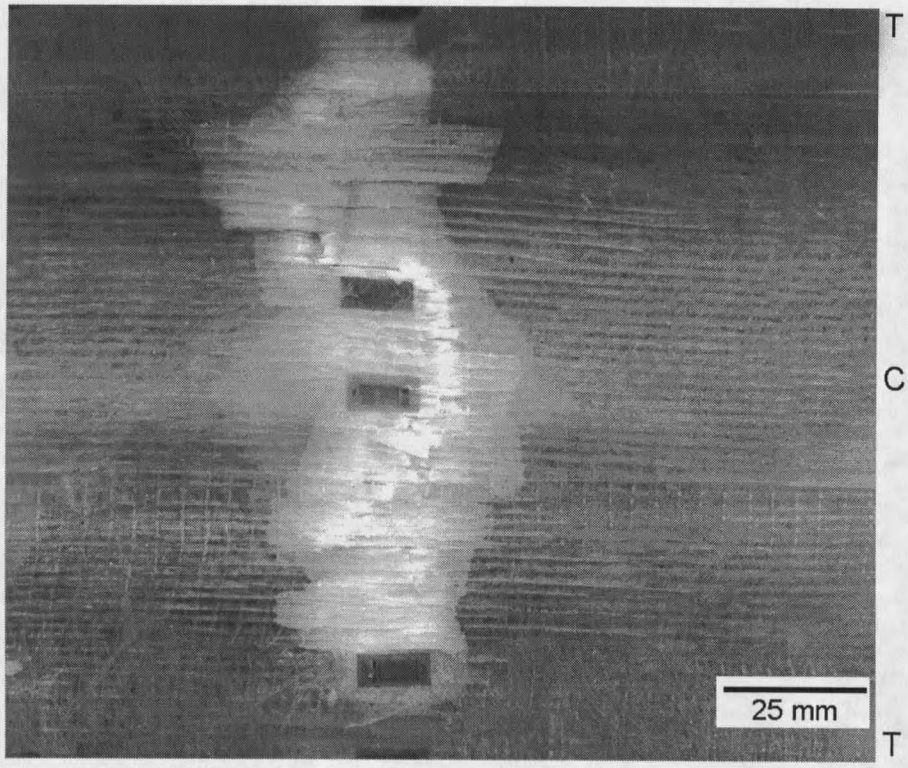


Figure 8.27. T126 failed tube surface.

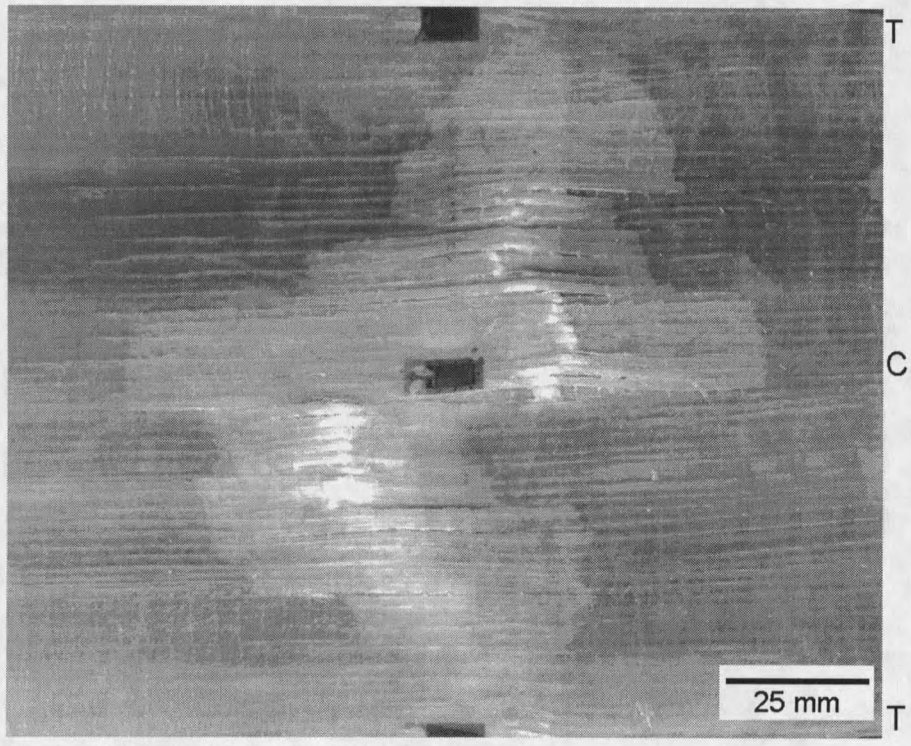


Figure 8.28. T129 failed tube surface.

performed in the Instron 8562 with the extensometer across the gage section of the tube. These two graphs show that the axial strength of the adhesive joint decreases as the tube is fatigued in bending, as was expected. The tube failed between the polyester matrix and the adhesive; no cracks between the adhesive and the aluminum were visible.

Figure 8.35 shows the aluminum end from tube T134, indicating a through thickness fatigue crack in the aluminum end. The presence of this crack and the cracking in the adhesive joint, indicates that further design changes of the aluminum ends may be necessary if a larger number of fatigue cycles are to be applied to the tube sections.

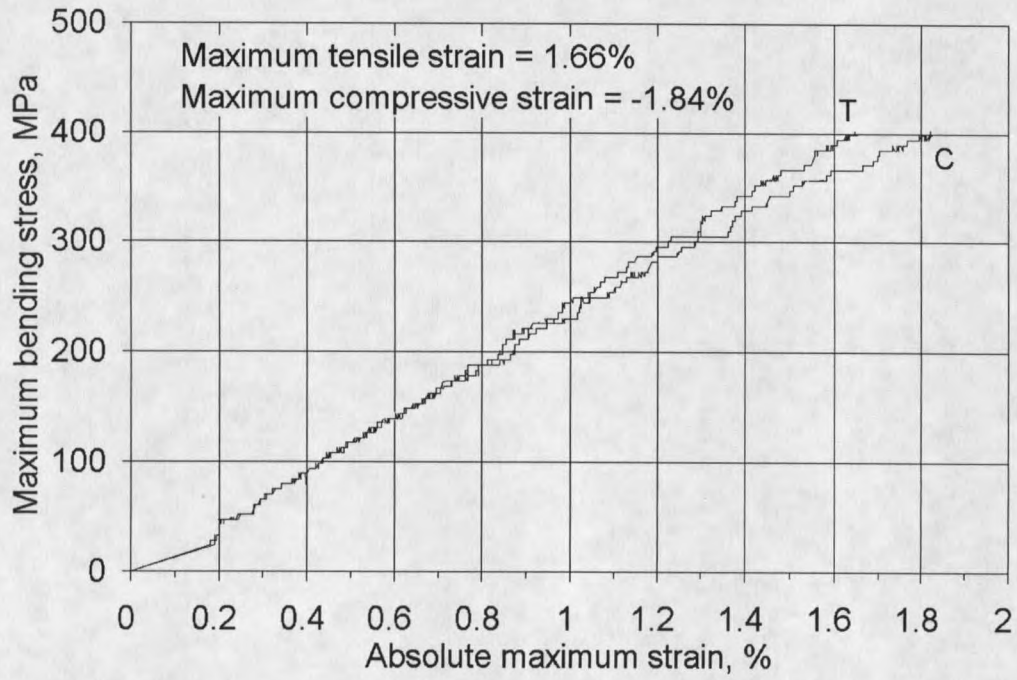


Figure 8.29. Bending stress versus bending strain for T122.

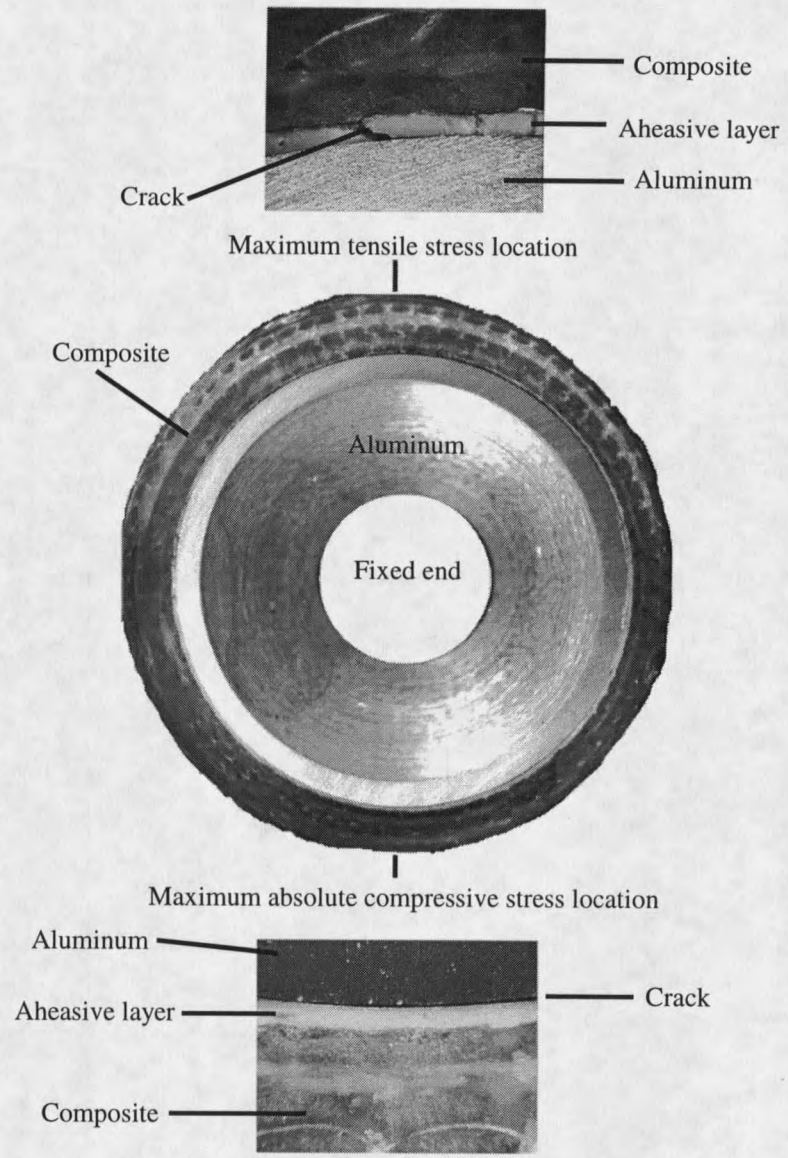


Figure 8.30. Polished end of T130 showing adhesive cracking.

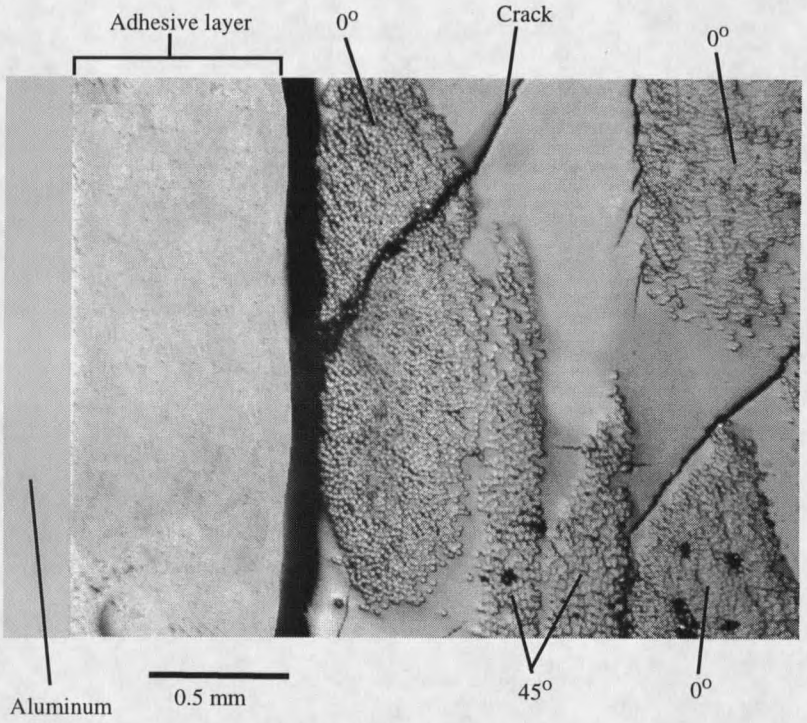


Figure 8.31. T137 fixed end support showing extensive cracking.

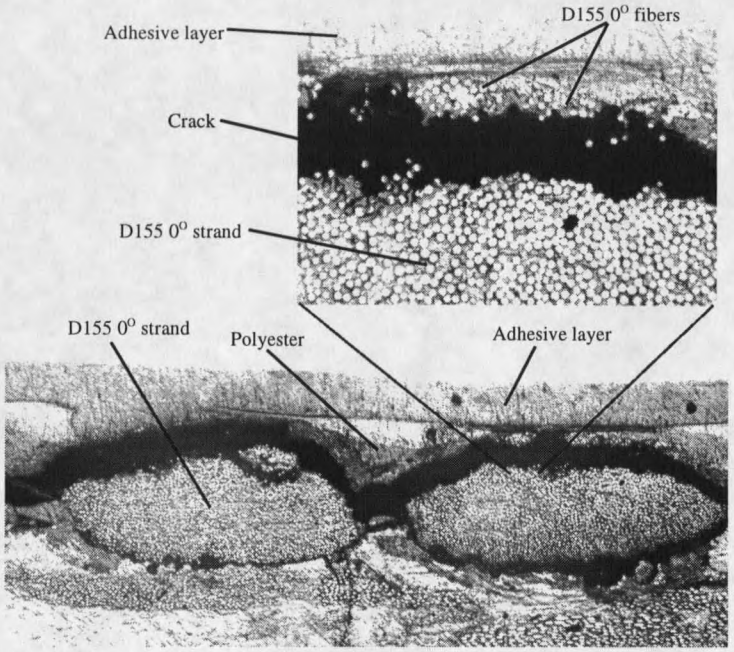


Figure 8.32. T130 fixed end support showing cracking.

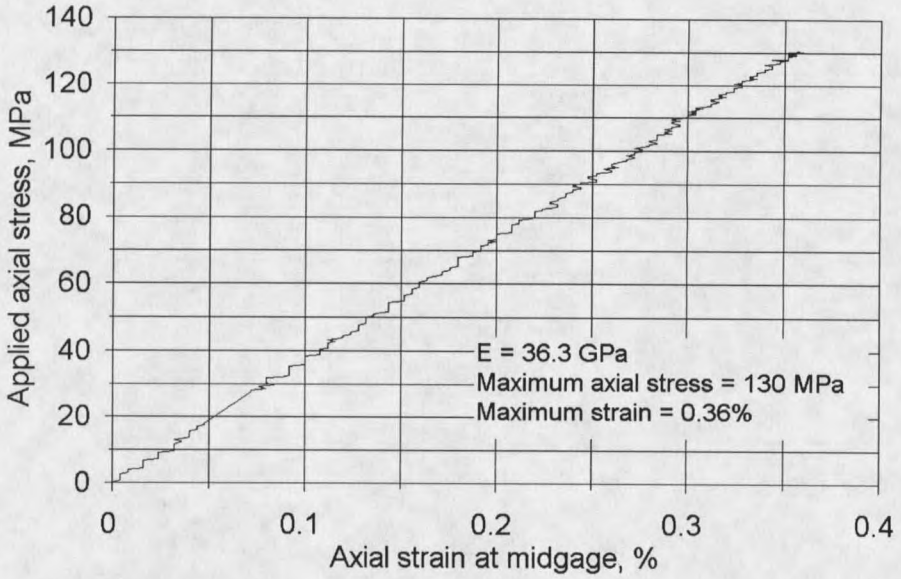


Figure 8.33. Axial stress in the gage length versus axial strain for tube T130 tested in uniaxial tension after 1,800,000 bending fatigue (R=0.1, with a maximum strain of 0.9 %) cycles.

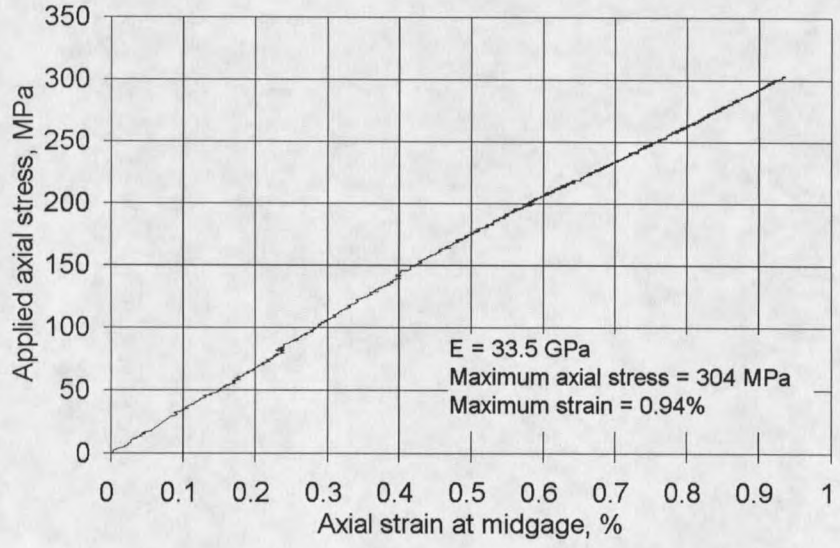


Figure 8.34. Axial stress in the gage section versus axial strain for tube T133, tested in uniaxial tension without prior fatigue testing.

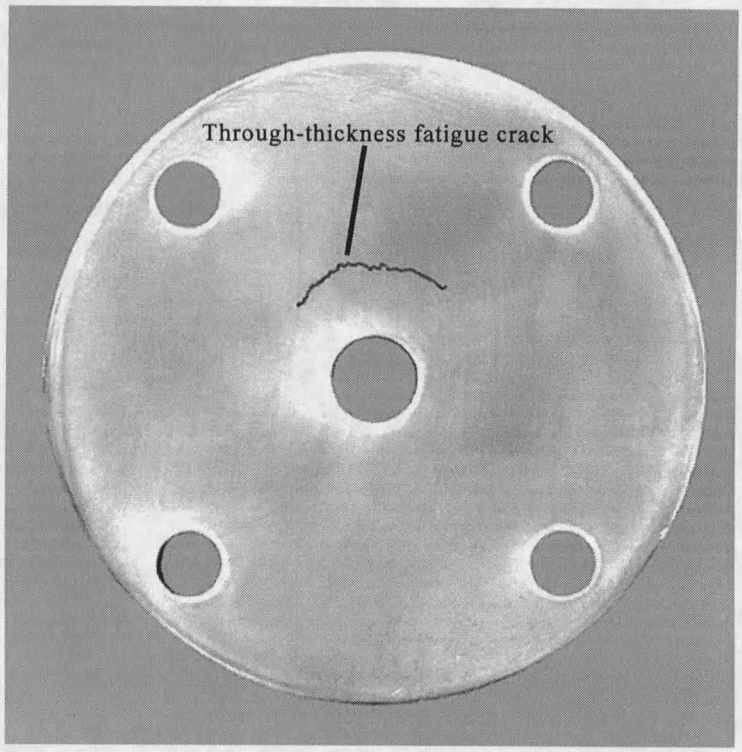


Figure 8.35. Fixed end of tube T134 showing a metal fatigue crack after 3,200,000 cycles.

Comparison with Coupon Tests

The static and fatigue tests were compared with the DD5P material from the database, which is the same lay-up and fiber content as the tubes T120 to T137. These results are presented in Figures 8.36 through 8.40. Figure 8.36 shows the tensile and compressive DD5P test coupons with the tensile and compressive results from the tubes. The static failure strains for the tubes are much less than for the coupons due to the limiting compressive buckling resistance. The maximum static tensile strain is meaningless because, when the tube fails by compression, it fails the entire tube and thus gives a low static tensile strain. None of the tubes failed on the tensile side.

Figure 8.37 details the compressive component of Figure 8.36 and also shows that

all the tube strains are below the DD5P compressive coupon behavior. When these data are normalized by the absolute maximum compressive strain, as shown in Figure 8.38, the behavior of the tubes is accurately predicted by the DD5P coupon tests. These results paralleled the comparisons between the I-beam tests and compression coupons. Higher cycle, lower load fatigue tests would be expected (from coupon data, Figure 8.36) to produce tensile failures; tests have not yet been run in this range.

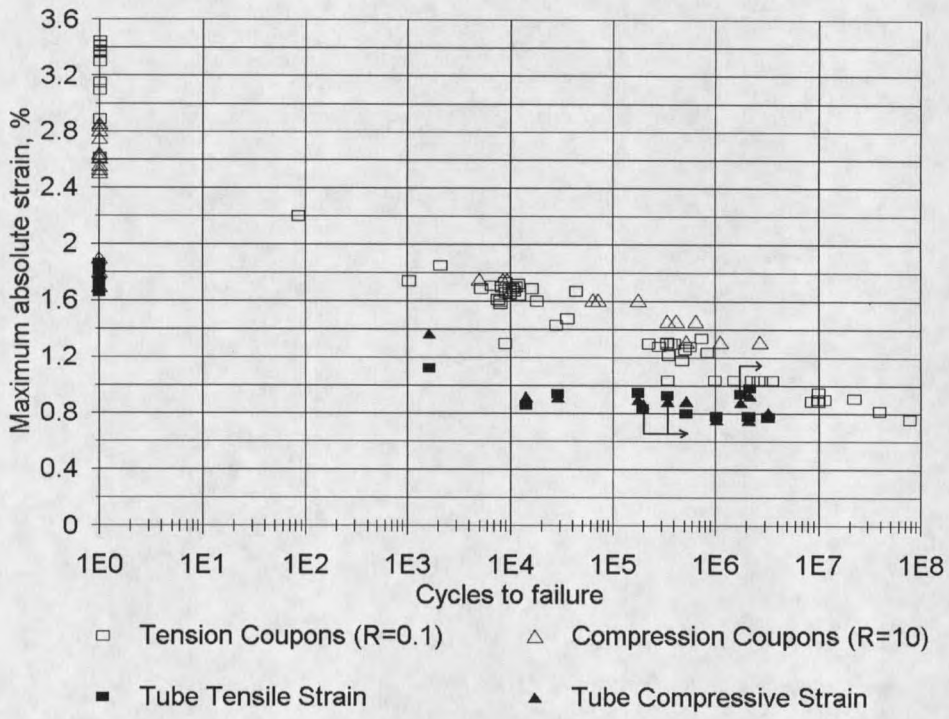


Figure 8.36. Tubes T120 - T137 compared with material DD5P Tensile (R=0.1) and Compressive (R=10) coupons.

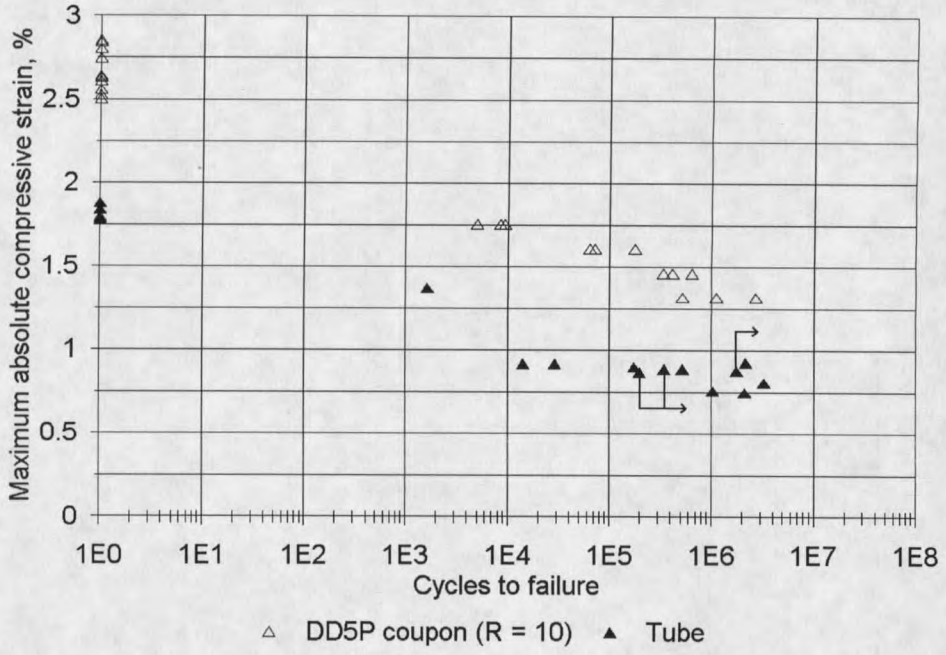


Figure 8.37. Compressive fatigue data for Tubes T120 - T137 compared with material DD5P compressive (R=10) coupons.

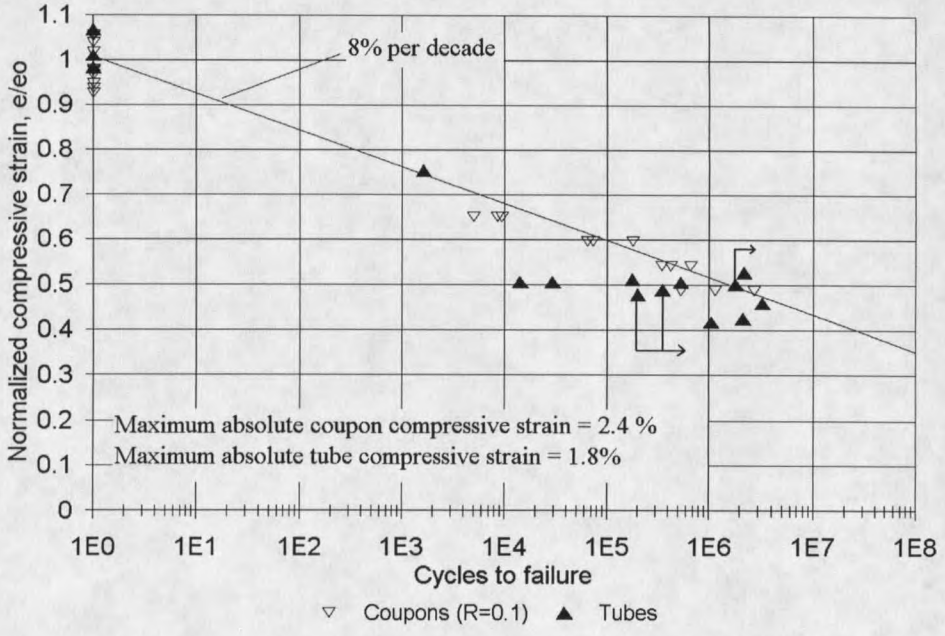


Figure 8.38. Normalized compressive fatigue data for Tubes T120 - T137 compared with material DD5P compressive (R=10) coupons.

Conclusions for Cylindrical Tubes

A hollow cylindrical tapered tube geometry with load transfer connections was developed and tested under both static and fatigue cantilever bending conditions, typical of those found on wind turbine blades. Due to the relatively thin hollow tube geometry, the compressive buckling behavior was the limiting static design parameter and the maximum obtained compressive strain in the tube section was 75 percent of the maximum strain obtained from the database test coupons (which were tested using a 13 mm gage length and unsupported faces). The compressive failure strains of the tubes were similar to those generated by the I-beam tests. Delamination of the test tube from the aluminum ends was a persistent problem, which still has to be addressed to prevent this failure from influencing the lifetime of the tube section under higher cycle fatigue tests.

CHAPTER 9

CONCLUSIONS AND RECOMMENDATIONS

The main motivation of this research has been to develop a fiberglass fatigue database and to validate its use in substructures. As the study developed, it became evident that great differences in fatigue resistance existed as parameters such as fiber content and fabric architecture were varied. The original scope of the thesis was then expanded to locate fatigue problem areas in fiberglass materials and determine their characteristics, specifically dealing with: reinforcement fabric architecture, fiber content, content of fibers orientated in the load direction, matrix material and loading values (tension, compression and reversed loading). The results of this nine-year study are represented in the "DOE/MSU Composite Material Fatigue Database," which currently has over 6000 static and fatigue tests covering 148 different fiberglass materials and numerous R-values (0.1, 10, -1, with some at 0.5, -0.5 and 2). To validate the use of the database in larger structures, selected materials have been incorporated into composite I-beam and hollow tube substructural elements representative of wind turbine blades.

High Cycle Fatigue Behavior of Glass Strands

The behavior of glass strands with 45 and 2000 glass fibers was studied in tensile fatigue (R = 0.1) out to 10^8 to 10^9 cycles. The tensile fatigue behavior of glass fiber is a

fiber dominated property, independent of the matrix or fiber-matrix interface. It is believed that a mechanical wearing or fretting process at the fiber surface, caused by fiber-fiber interaction fiber interaction with other particles at delamination sites, is responsible for the failure of the glass fibers during the fatigue cycling. Locating surface damage on individual fibers generated by the fatigue process was unsuccessful, and it may not be possible to differentiate fatigue induced damage from surface damage present on pristine fibers. Presently, a material fatigue limit has not been found. The 8 to 9 percent per decade linear slope (on a semi-log plot) of the strand tensile fatigue trend line starts to decrease in slope in the 10^8 to 10^9 cycle range, and more data are required to determine if this slope is tapering off enough to constitute a fatigue limit or may just reflect a change in the failure mode. When the data are viewed on a log-log plot, no clear slope change in the 10^8 to 10^9 cycle range is evident.

Reinforcement Fabric Architecture Effects

Detailed conclusions relative to specific fabric types and weights can be found in Chapter 5. There are two general types of glass fabrics available: stitched and woven. Stitched fabrics involve the stitching thread, or weft, to hold the unidirectional fabric together, such as the Owens Corning D155 fabric, so that it may be easily handled during composite manufacture. Individual fiber strands may also be stitched to a mat, veil or a ±45° fabric (triax). The stitching thread can pinch the fiber strand and the strands adjacent to it, causing increased local fiber content and fiber-to-fiber contact within the strands, which decreases the fatigue resistance of the composite. Some of the fabrics

showing relatively good fatigue resistance, such as the D155 fabric, are only available as weft unidirectionals, with the fibers orientated perpendicular to the long direction of the roll, providing only a 1.3 to 2.7 meter fiber length. Wind turbine blades require longer strand lengths and therefore use triax (stitched 0° /±45°) or warp unidirectional woven fabrics. Woven fabrics have delamination problems at the weave cross-over points. Additionally, due to the woven fibers having a small angle away from 0°, their compressive strengths are significantly reduced relative to fabrics with straight strands.

Stitched or woven fabrics restrict the strand movement and produce pinching points periodically along the strands. The only composites which were able to maintain good fatigue resistance at fiber volume fractions greater than 0.5 were fabrics which had the weft stitching thread removed prior to resin transfer molding.

All the unidirectional fabrics tested provided tensile strengths and elastic moduli which were accurately predicted by laminate analysis. The woven fabrics had an ultimate tensile strain of 2.4 to 2.7 percent while the stitched fabrics had a range of 2.6 to 3.1 percent. The A060 fabric produced a low tensile failure strain of 1.8 percent that was explained by the presence of the large thermoplastic-glass weft used to weave the fabric (the same weft used to weave the heavier fabrics). Over a fiber volume fraction range of 0.30 to 0.59, the stitched fabrics provided ultimate compressive strains of -1.6 to -2.1 percent, while the woven fabrics had a range of -1.0 to -1.4 percent strain. This relative difference in failure strains was maintained in fatigue in the million-cycle strain for R=10. There was no significant difference in the fatigue performance between the different ±45° fabrics. The fabrics which were stitched to a mat (CM1701, DBM1204) or

adhesively bonded to a mat (UC1010, UC1018) provided lower static failure strains and poorer fatigue resistance than the materials without the mat at fiber volume fractions greater than 0.40, but had good fatigue resistance at fiber volume fractions less than 0.40 (materials X, Y, and DD25B). Further testing is required to determine if this is a true material behavior or is an interaction of the mat with the other fabrics.

Fiber Content

Increasing the fiber volume fraction of the composite increases the strength and stiffness (modulus), but also tends to decrease the fatigue resistance. A transition from good tensile fatigue resistance to poor resistance occurs as the fiber content increases in the range of 38 to 42 percent fiber by volume for the fabrics tested. The transition occurs at lower fiber contents in multidirectional laminates. As the fiber content increases, the number of fibers (and strands) in direct contact with other fibers increases, as does the local strand fiber content, and this may lead to more rapid fatigue wear-out by increasing the number of fiber breaks in the local pinched area. The presence of a stitch or other discontinuity (weaving weft) increases the severity of this fiber-fiber interaction, due to pinching, and reduces to fatigue resistance.

Content of Fibers in the Loading Direction

Laminates containing 100 percent ±45° plies relative to the load direction had an initial strain for one million cycles of 0.27 to 0.58 percent (R = 0.1), while at high percentages of 0° plies (and low fiber contents), the million-cycle strain reaches the range

of 1.0 to 1.2 percent, the same as for the unidirectional 0° material alone. At lower contents of 0° material (16 to 56 percent) the low fiber volume fraction materials ($V_F <$ 0.37) showed million cycle strain values in tensile fatigue in the 0.7 to 0.8 percent range, somewhat below that for the 0° material alone, but well above the ±45° material alone. At fiber volume fractions less than 0.37, all of the laminates failed in a fiber-dominated mode; in tensile fatigue the major difference was in the static ultimate tensile strain values. The laminates with high 0° content failed around 2.7 to 3.1 percent static ultimate strain, while the laminates with lower 0° material content failed at around 1.8 to 2.2 percent static strain. This difference in failure strain is preserved in fatigue, with similar fiber dominated b coefficients resulting in a lower million-cycle strain at a lower percent 0° material.

Matrix Materials

Six different resin systems, two epoxy, two polyester and two vinyl esters, were tested in ±45°, 90° and $(0/\pm45/0)_S$ laminate configurations. There were no significant differences in the resins tested with the ±45° and 90° laminates under R = 0.1 and 10 conditions. The Derakane 8084 vinyl ester had a slightly increased million-cycle strain (relative to the base polyester) at R = 0.1 and 10, 1.39% and -1.66% versus 1.15% and -1.37%, with the $(0/\pm45/0)_S$ laminate, but there was no improvement in fatigue performance when tested at R = -1. It is believed that the increased resin toughness reduced the amount of damage caused by hydraulic wedge grips, in the gripped ends of the test coupons, which prevented premature fatigue failures. Ongoing environmental-

fatigue sensitivity tests are showing a severe reduction in the $(0/\pm45/0)_S$ laminate compression fatigue properties under hot-wet conditions (50 °C, 1% moisture absorption) of the polyester 63-AX-051. Future tests on the other resin systems are scheduled.

Optimum Laminates for Blade Primary Structure

At this time, the selection of a material for primary blade structure represents a compromise. The best properties derive from fabrics with straight strands such as D155, but these are not widely available with 0° strands in the warp direction of the fabric roll. Thus, the A130 class of woven fabrics, despite a low compressive strength, are the only reasonable choice. These should be used at a fiber volume fraction below 0.42 to obtain the best tensile fatigue properties. The 0° fabric should be combined with at least 25 to 30 percent of a light ±45° fabric, such as DB120, to prevent axial cracking and other problems with all unidirectional material. The choice of matrix is not clear from the fatigue data, but vinyl esters provide improved delamination, heat, and moisture resistance at moderate cost [17].

I-beams

The main objective was to develop a beam test specimen representative of wind turbine blade primary substructure to test the validity of using the materials database and current design methodologies for predicting structural strength, stiffness, failure mode, and fatigue lifetime. This objective was met, as the results show that strength, stiffness, failure mode, and fatigue life can be predicted with acceptable accuracy as long as

premature failure does not occur in the load introduction areas. Tests using the triax (material AA) flanges and ±45° (CH10) web showed good agreement between experimental and predicted results for strength, failure mode, and fatigue lifetime. The use of materials with improved fatigue resistance (material DD5P in the flanges and CH12 in the web) did raise the strain capacity of the beam in fatigue by about a factor of two, which also changed the failure mode from tensile or compression flange failure to a web-flange delamination mode.

Cylindrical Tubes

A cylindrical tapered tube geometry with load transfer connections was developed and tested under both static and fatigue cantilever bending conditions, typical of those found on wind turbine blades. Due to the relatively thin hollow tube geometry, compressive buckling was the limiting static design parameter and the maximum obtained compressive strain in the tube section was 75 percent of the maximum strain obtained from the database test coupons (which were tested using a 13 mm gage length and unsupported faces). The compressive failure strains of the tubes were similar to those generated by the I-beam tests. Delamination of the test tube from the aluminum ends was a persistent problem, which still has to be addressed to prevent this failure from influencing the lifetime of the tube section under higher cycle fatigue tests.

Recommendations

The database needs to be expanded to include other composite laminates at

different R-values and at higher cycles. Fatigue testing of actual composite components could also be performed to ascertain other manufacturing problems or defects which affect the fatigue life of the component. Spectrum loading, more typical of the loadings present on wind turbine blades and other structures, also needs to be addressed.

Other fabric forms should be developed for improved fatigue resistance. Bonded fabrics or fabrics which use different stitching patterns or employ stitching which dissolves into the liquid resin could reduce the number of fiber-fiber contact points. Varying the ply thickness and stacking sequence could also be investigated, as well as fabrics mixed with non-structural filler plies or fiber mats to produce composites with thickness varying fiber volume fractions.

Most of the database has involved testing at room temperature and low humidity; further environmental fatigue testing must be performed to better simulate the actual conditions materials undergo when exposed to the weathering elements. Different resin systems should be investigated for improved delamination and crack resistance, and environmental stability, especially in larger substructures or assemblies.

REFERENCES

1. Mandell, J.F., Reed, R.M. Jr. and Samborsky, D.D., "Fatigue of Fiberglass Wind Turbine Blade Materials," Contractor Report SAND92-7005, Sandia National Laboratories, Albuquerque, NM (1992). [www.Sandia.gov/Library.htm]

2. Mandell, J.F., and Samborsky, "DOE/MSU Composite Material Fatigue Database: Test Methods, Materials, and Analysis," Contractor Report SAND97-3002, Sandia National Laboratories, Albuquerque, NM (1997). [www.Sandia.gov/Library.htm]

3. Mandell, J.F., Reed, R.M., and Samborsky, D.D., "High Cycle Fatigue of Wind Turbine Blade Materials," in SED-Vol 12, *Wind Energy 92*, P.S. Veers, S.M. Hock, eds., ASME, New York, p. 105 (1992).

4. Mandell, J.F., Reed, R.M. Jr., Samborsky, D.D., and Pan, Q., "Fatigue Performance of Wind Turbine Blade Materials," in SED-Vol 14, *Wind Energy 93*, S. Hock, ed., ASME, New York, 191-198. (1993).

5. Mandell, J.F., Creed, R.M. Jr., Pan, Q., Combs, D.W., and Shrinivas, M., "Fatigue of Fiberglass Generic Materials and Substructures" in SED-Vol 15, *Wind Energy 94*, W.D. Musial, S.M. Hock and D.E. Berg, eds., ASME, New York, pp. 207-213 (1994).

6. Mandell, J.F., Combs, D.E., and Samborsky, D.D., "Fatigue of Fiberglass Beam Substructures," *Wind Energy 1995*, W.D. Musial, S.M. Hock, and D.E. Berg, Eds., SED-Vol. 16, ASME, 99 - 106 (1995).

7. Samborsky, D., and Mandell, J.F., "Fatigue Resistant Fiberglass Laminates for Wind Turbine Blades," *Wind Energy 1996*, ASME, 46-51 (1996).

8. Mandell, J.F.; Samborsky, D.D., "MSU/DOE Wind Turbine Blade Composite Material Fatigue Database," (November 1995) available through Dr. Herbert J. Sutherland, Sandia National Laboratories, Albuquerque, NM, 87185. [www.Sandia.gov/Renewable_Energy/wind_energy/homepage.html]

9. Sutherland, H.J., Mandell, J.F., "Application of the U.S. High Cycle Fatigue Data Base to Wind Turbine Blade Lifetime Predictions.," *Wind Energy 1996*, ASME, pp. 85-92. (1996).

10. Mandell, J.F., Samborsky, D.D., and Cairns, D.S., "Advanced Wind Turbine Blade Structure Development Program at Montana State University," *Wind Energy 1997*, ASME/AIAA, 189-196 (1997).

11. Cairns, D. S., Haugen, D. J., Mandell, J. F., and Samborsky, D. D., "Fracture of Skin/Stiffener Intersections in Composite Wind Turbine Structures," *Wind Energy 1998*, ASME/AIAA, pp. 334 - 343. (1998).

12. Mandell, J. F., Samborsky, D. D., Combs, D.W., Scott, M.E., and Cairns, D. S, "Fatigue of Composite Material Beam Elements Representative of Wind Turbine Blade Substructure," NREL Contractor Report SR-500-24379, November 1998. [www.NREL.gov/Publications/]

13. Mandell, J. F., Samborsky, D. D., Scott, M.E., and Cairns, D. S, "Effects of Structural Details on Delamination and fatigue Life of Fiberglass Laminates," *Wind Energy 1998*, ASME/AIAA, pp. 323 - 327. (1998).

14. Samborsky, D. D., Mandell, J. F., and Cairns, D. S, "Selection of Reinforcing Fabrics for Wind Turbine Blades," *Wind Energy 1999*, AIAA-99-0024, ASME/AIAA, (1999).

15. Mandell, John F., Samborsky, Daniel D., Sutherland, Herbert J., "Effects of Materials Parameters and Design Details on the Fatigue of Composite Materials for Wind Turbine Blades," *1999 European Wind Energy Conference*, 1-5 March 1999, Nice, France, pp. 628-633.

16. Mandell, J.F., Samborsky, D.D., Li. Mei, Orozco, Ricardo, and Cairns, D.S., "Selection of Fiberglass Matrix Resins for Increased Toughness and Environmental Resistance in Wind Turbine Blades," *Wind Energy 2000*, AIAA-2000-0057, ASME/AIAA, (to be published).

17. Mandell, J.F., Creed, R.J., Pan, Q., Combs, D.W., and Shrinivas, M., "Fatigue of Fiberglass Generic Materials and Substructures," *Wind Energy 1994*, SED-Vol. 15. ASME, pp. 207-213.

18. Spera, David A., "*Wind Turbine Technology: Fundamental Concepts of Wind Turbine Engineering*," American Society of Mechanical Engineers, ASME Press, 1994.

19. Hedley, C.W., "Mold Filling Parameters in Resin Transfer Molding," Masters Thesis, Dept. of Chem. Engr., Montana State University, (1994).

20. Humbert, D.R., "Modeling of Resin Transfer Molding of Composite Materials With Oriented Unidirectional Plies," Masters Thesis, Dept. of Chem. Engr., Montana State University, (1996).

21. Combs, David W., "Design, Analysis and Testing of a Wind Turbine Blade Substructure," Masters Thesis, Dept. of Mech. Engr. Montana State University, (1994).

22. Hart-Smith, L.J., "Some Observations About Test Specimens and Structural Analysis for Fibrous Composites," *Composite Materials: Testing and Design (9th Volume)*, ASTM STP 1059, S.P. Garbo, Ed., American Society for Testing and Materials, Philadelphia, 1990, pp. 86 - 120.

23. Loveless, H. S., "Specimen Geometry Effects on the Strength of Unidirectional Resin Matrix Composites," *Journal of Testing and Evaluation*, Vol. 1, No. 6, Nov. 1973, pp. 532 - 537.

24. Hojo, M., Sawada, Y.,Miyairi, H., "Influence of Clamping Method on Tensile Properties of Unidirectional CFRP in 0^{o} and 90^{o} directions - Round Robin Activity for International Standardization in Japan," *Composites*, Vol. 25, No. 8, 1994, pp. 786 - 795.

25. Foos, B.C., Wolfe, W.E., Sandhu, R.S., "The Effect of Tab Orientation on the Distribution of Strains in Composite Specimens," *Composite Materials: Testing and Design (10th Volume)*, ASTM STP 1120, G.C. Grimes, Ed., American Society for Testing and Materials, Philadelphia, 1992, pp. 103 - 113.

26. Adams, D.F., Finley, G.A., "Experimental Study of Thickness - Tapered Unidirectional Composite Compression Specimens," *Experimental Mechanics*, December 1996, Vol. 36, No. 4. pp. 345 - 352.

27. Camponeschi, E.T. Jr.,"Compression of Composite Materials: A Review," *Composite Materials: Fatigue and Fracture (3th Volume)*, ASTM STP 1110, T.K. O'Brien, Ed., American Society for Testing and Materials, Philadelphia, 1991, pp. 550 - 578.

28. Wung, E.C.J., Chatterjee, S.N.,"On the Failure Mechanisms in Laminate Compression Specimens and the Measurement of Strength," *Journal of Composite Materials*, Vol. 26, No. 13, 1992, pp.1885 - 1914.

29. Adams, D.F., Lewis, E.Q., "Influence of Specimen Gage Length and Loading Method on the Axial Compressive Strength of a Unidirectional Composite Material," *Experimental Mechanics*, March 1991, pp. 14 - 20.

30. Chawla, K.K., *Composite Materials, Science and Engineering*, Springer-Verlag publishers, 1987, p. 186.

31. Puck, A., "Zur Beanspruchen und Verformung von GFK- Mehrschichtenverbund-Bauelementen," (System Distortion of Stacked Multilayer Glass Fiber Composites) *Kunstoffe*, Vol. 57, 1967, pp. 965-973.

32. Adams, D.F., Doner, D.R., "Transverse Normal Loading of a Unidirectional Composite", *Journal of Composite Materials*, Vol. 1, 1967, p. 152.

33. Glathart, J.L., and Preston, F.W., "The Fatigue Modulus of Glass", *Journal of Applied Physics*, Vol. 17, 1946, pp. 189-195.

34. Wiederhorn, S.M., "Moisture Assisted Crack Growth in Ceramics", *International Journal of Fracture*, Vol. 4, 1968, pp 171 - 177.

35. Michalske, T.A., and Bunker, B.C., "The Fracturing of Glass," *Scientific American*, Dec. 1987, pp. 122 - 129.

36. Chamberlain, D.W., Lloyd, B.R., and Tennent, R.L., "Determination of the Performance of Plastic Laminates at Cryogenic Temperatures", Air Force Materials Laboratory Report ASD-TDR-62-794, Part II, 1964.

37. Cameron, N.M., *Glass Technology*, Vol. 9, 1968, p. 14.

38. Wiederhorn, S.M., "Environmental Stress Corrosion Cracking of Glass," in *Corrosion Fatigue: Chemistry, Mechanics and Microstructure*, National Association of Corrosion Engineers Conference, NACE-2, June 1971, pp. 731-742.

39. LI, Chia-Geng, "Fatigue of Fiber Reinforced Plastics," Masters Thesis, Massachusetts Institute of Technology, February 1983.

40. Trombly, Sharon Elaine, "Glass Fiber Bundles as a Model for the Fatigue Behavior of Fiber Reinforced Composites," Bachelors Thesis, Massachusetts Institute of Technology, June 1983.

41. Mandell, J.F., Huang, D.D., McGarry, F.J., "Tensile Fatigue Performance of Glass Fiber Dominated Composites," Massachusetts Institute of Technology, Research Report R80-4, November 1980.

42. Mandell, J.F., Huang, D.D., McGarry, F.J., "Tensile Fatigue Performance of Glass Fiber Dominated Composites," *Composites Technology Review*, Vol. 3, No. 3, Fall 1981, pp. 96-102.

43. Mandell, J.F., McGarry, F.J., Hsieh, A.J.-Y and LI, C.G., "Tensile Fatigue of Glass and Composites with Conventional and Surface Compressed Fibers," Reinforced Plastics/Composites Institute, SPI, Paper 7-G, 1985.

44. Mandell, J.F., McGarry, F.J., Hsieh, A.J.-Y and LI, C.G., "Tensile Fatigue of Glass and Composites with Conventional and Surface Compressed Fibers," *Polymer Composites*, Vol. 6., 1985, pp. 168-174

45. Dharan, C.K.H., "Fatigue Failure Mechanisms in a Unidirectionally Reinforced Composite Material," *Fatigue of Composite Materials*, ASTM STP 569, ASTM, 1975, pp. 171-188.

46. Dharan, C.K.H., "Fatigue Failure Mechanisms in a Unidirectionally Reinforced Composite Material," *Journal of Material Science*, Vol. 10, pp. 1665 - 1670.

47. Mandell, J.F., Huang, D.D., McGarry, F.J., "Fatigue of Glass and Carbon Fiber reinforced Engineering Thermoplastics," paper 20D in Proceedings of the 35th Annual Conference of the RP/C Institute, Society of the Plastics Industry, New York, 1980.

48. Mandell, J.F., "Fatigue Crack Propagation in Woven and Nonwoven Fiberglass Laminates," *Composites Reliability*, STP 580, ASTM, 1975, pp. 515-527.

49. Sun, C.T., and Yamada, S.E., "Strength Distribution of a Unidirectional Fiber Composite," *Journal of Composite Materials*, Vol. 12 (April 1978), pp. 169-178.

50. Reifsnider, K.L., "Damage and Damage Mechanics (Chapter 2)," *The Fatigue Behavior of Composite Materials*, K.L. Reifsnider, Ed., Elsevier (1990)

51. Herakovich, C.T., "Influence of Layer Thickness on the Strength of Angle-Ply Laminates," *Journal of Composites Materials,* Vol. 16 (May 1982), pp. 216-227.

52. Pagano, N.J., Pipes, B.R., "The Influence of Stacking Strength on Laminate Strength," *Journal of Composites Materials*, Vol. 5 (January 1971), pp. 50-57.

53. Sutherland, L.S., Shenoi, R.A., Lewis, S.M.,"Size and Scale Effects in Composites: I. Literature Review," *Composites Science and Technology*, 59 (1999) pp. 209-220.

54. Sutherland, L.S., Shenoi, R.A., Lewis, S.M.,"Size and Scale Effects in Composites: II. Unidirectional Laminates," *Composites Science and Technology*, 59 (1999) pp. 221-233.

55. Sutherland, L.S., Shenoi, R.A., Lewis, S.M.,"Size and Scale Effects in Composites: III. Woven-Roving Laminates," *Composites Science and Technology*, 59 (1999) pp. 235-251.

56. Ratwani, M.M. and Kan, H.P., "Effect of Stacking Sequence on Damage Propagation and Failure Modes in Composite Laminates," *Damage in Composite Materials*, ASTM STP 775, K.L. Reifsnider, Ed., ASTM, 1982, pp. 211-228.

57. Shrinivas, M., "Three Dimensional Finite Element Analysis of Matrix Cracks in Multidirectional Composite Laminates," Matrers Thesis, Dept. of Chem. Engr., Montana State University (1993).

58. DeSmet, B.J. and Bach, P.W., "DATABASE FACT: Fatigue of Composites for Wind Turbines," ECN-C-94-045, ECN, Petten, the Netherlands (1994).

59. Mandell, J.F., "Fatigue Behavior of Short Fiber Composite Materials," in *The Fatigue Behavior of Composite Materials*, K.L. Reifsnider, ed, Elsevier, 232-237 (1991).

60. Mandell, J.F., *Composite Reliability*, ASTM STP 580, 515 (1980).

61. Hashin, Zvi, Rotem, Assa,"A Fatigue Failure Criterion for Fiber Reinforced Materials," Journal of Composite Materials, Vol. 7. pp.448-464.

62. Rotem, Assa, Hashin, Zvi, "Failure Modes of Angle Ply Laminates," *Journal of Composite Materials*, Vol. 9, pp.191-206.

63. Rotem, Assa, Hashin, Zvi, "Fatigue Failure of Angle Ply Laminates," *AIAA Journal*, Vol. 14, No. 7. pp.868-872.

64. Rotem, Assa, "Fatigue Failure of Multidirectional Laminate," *AIAA Journal*, Vol. 17, No. 3. pp.271-277.

65. A. Brivio et Al, "Consideration on the Fatigue Damage of Specimens Used for Composite Critical Components Qualification," *The Role of the Polymeric Matrix in the Processing and Structural Properties of Composite Materials*, Edited by James Seferis and Luigi Nicolais, Plenum Publishers, 1983, pp. 607 - 615.

66. Sundsrud, Jerry, Davis, J. W., "Fatigue Data on a Variety of Non-Woven Glass Composites for Helicopter Rotor Blades," *Composite Materials: Testing and Design (Fifth Volume)*, ASTM STP 674, S.W. Tsai, Ed., 1979, pp. 137-148.

67. Lagace, P., Brewer, J., and Kassapoglou, C., "The Effect of Thickness on Interlaminar Stresses and Delamination in Straight-Edged Laminates," *Journal of Composites Technology and Research*, Vol. 9, No. 3, 1987, pp. 81-87.

68. N.J. Pagano, "Exact Solutions for Rectangular Bidirectional Composites and Sandwich Plates," *Journal of Composite Materials*, 4 (1), p. 20, 1970.

69. N.J. Pagano and J. Halpin, "Influence of End Constraints in the Testing of Anisotropic Bodies," *Journal of Composite Materials*, 2 (4), p. 18, 1968.

70. J.M. Whitney, "The Effects of Transverse Shear Deformation on the Bending of Laminate Plates," *Journal of Composite Materials*, 3 (4), p. 534, 1969.

71. J.M. Whitney and E.E. Browning, "Free-Edge Delamination of Tensile Coupons," *Journal of Composite Materials*, 6 (2), p. 300, 1972.

72. A.H. Puppo and H.A. Evensen, "Interlaminar Shear in Laminated Composites under Generalized Plane Stress," *Journal of Composite Materials*, 4 (2), p. 204, 1970.

73. R.B. Pipes and N.J. Pagano, "Interlaminar Stresses in Composite Laminates under Uniform Axial Extension," *Journal of Composite Materials*, 4 (4), p. 538, 1970.

74. R.B. Pipes and I.M. Daniel, "Moire Analysis of the Interlaminar Shear Edge Effect in Laminated Composites," *Journal of Composite Materials*, 5 (2), p. 255, 1971.

75. B. Agarwal and L. Broutman, "*Analysis and Performance of Fiber Composites*," 2nd Edition, John Wiley Publisher, 1990, pp. 175 - 183, 245 - 251.

76. Pipes, R. B., Kaminski, B.E., and Pagano, N.J., "Influence of the Free Edge upon the Strength of Angle-Ply Laminates," *Analysis of the Test Methods for High Modulus Fibers and Composites*, ASTM STP 521, ASTM, 1973, pp. 218-228.

77. C.O. Horgan, Journal of Composite Materials, 16, pp. 411-422, 1982.

78. Tarnopol'skii, Yu. M. and Kincis, T. "*Static Test Methods For Composites*", Van Nostrand Reinhold Co. Publishers, 1985, pp. 67-69.

79. Hull, D, Clyne, T.W., *An Introduction to Composite Materials*, 2nd edition, Chapter 4., Cambridge University Press, 1996.

80. P.D. Craig and J. Summerscales, "Poisson's Ratios in Glass Fibre Reinforced Plastics," *Composite Structures,* Vol. 9 (1988), pp 173 - 188.

81. Combs, D.W., "Design, Analysis and Testing of a Wind Turbine Blade Substructure," Masters Thesis, Dept. Of Mechanical Engineering, Montana State University (1995).

82. Mandell, J.F., *Crack Propagation and Fracture of Composites*. Proceedings of the 14th Society of Engineering Sciences, G. C. Sih, ed., Bethlehem, PA., Lehigh University., 1977.

83. Nuismer, R.J.; Whitney, J.M. (1995). *Fracture Mechanics of Composites.* ASTM STP 953, ASTM, Philadelphia. pp. 117-142.

84. Samborsky, D., Wahl, N., Belinky, A., "Fatigue Behavior of Glass Polyester Composites With and Without a Hole," CHE551 Report, Montana State University, May 1994.

APPENDICES

APPENDIX A

DOE/MSU COMPOSITE MATERIAL FATIGUE DATABASE

DOE / MSU COMPOSITE MATERIAL FATIGUE DATABASE
December 1, 1999

This report was prepared as a part of work sponsored by an agency of the U.S. Government. Neither the U.S. Government, nor any agency thereof, nor any of their employees, nor any of their contractors, subcontractors, or their employees, makes any warranty, expressed or implied, or assumes any legal liability or responsibility for the accuracy, completeness, or usefulness of this program, or represents that opinion expressed herein do not necessarily state or reflect those of the U.S. Government, any agency thereof or any of their contractors or subcontractors. The material presented in this publication should not be used or relied upon for any specific application without competent examination and verification of its accuracy, suitability, and applicability by qualified professionals. Reference herein to any specific commercial product or process by trade name, trademark, manufacturer, or otherwise, does not necessarily constitute or imply its endorsement or recommendation.
This December 1, 1999 version of the database supersedes all previous versions.

TABLE OF CONTENTS PAGE

Notes on the use of the DOE/MSU fatigue database 277
Lay-up of Commercially Supplied Fiberglass Materials 282
Lay-up of MSU Manufactured (RTM) Fiberglass Materials 283
Properties of Industrial Materials 289
Longitudinal and Transverse Properties of Unidirectional Materials 290
Properties of MSU Manufactured Materials 293
Properties of R = -1 Tested Materials 297
Properties of High Cycle Materials 298
Material A, $V_F = 0.30$, $[0]_5$ 299
Material B, $V_F = 0.30$, $[0]_5$ 299
Material F, $V_F = 0.36$, $[(\pm 45/0)_3]_S$ 300
Material G, $V_F = 0.36$, $[(0/\pm 45)_3]_S$ 301
Material H, $V_F = 0.39$, $[(\pm 45/0)_3]_S$ 301
Material J, $V_F = 0.43$, $[(0/\pm 45)_3]_S$ 302
Material L, $V_F = 0\ 50$, $[0]_3$ 303
Material M, $V_F = 0.38$, $[0/\pm 45]_4$ 304
Material N, $V_F = 0.36$, $[0/\pm 45]_4$ 304
Material P, $V_F = 0.36$, $[0/\pm 45/M/0]_S$ 305
Material R, $V_F = 0.32$, $[0/\pm 45]_4$ 306
Material T, $V_F = 0.30$, $[0/\pm 45]_5$ 307
Material U, $V_F = 0.29$, $[0/\pm 45]_5$ 307
Material V, $V_F = 0.32$, $[0/\pm 45]_5$ 308
Material W, $V_F = 0.33$, $[0/\pm 45]_5$ 308
Material X, $V_F = 0.35$, $[0_2/M/\pm 45/0_2]$ 309
Material Y, $V_F = 0.39$, $[0_2/M/\pm 45/0_2]$ 310
Material EE, $V_F = 0.54$, $[M/\pm 45/0]_S$ 311
Material EEAV, $V_F = 0.48$, $[M/\pm 45/0]_S$ 312
Material EEAP, $V_F = 0\ 49$, $[M/\pm 45/0]_S$ 313
Material EEBP, $V_F = 0\ 43$, $[M/\pm 45/0]_S$ 313
Material EECP, $V_F = 0\ 49$, $[M/\pm 45/0]_S$ 314
Summary of MSU Manufactured Material Fatigue Tests 315
Material AA, $V_F = 0.35$, $[(\pm 45/0)_3(\mp 45/0)_2]$ 315
Material AA2, $V_F = 0.40$, $[(0/\pm 45)_2]_S$ 323
Material AA3, $V_F = 0.51$, $[(\pm 45/0)_3]_S$ 327
Material AA4, $V_F = 0.38$, $[(\pm 45/0)_2]_S$ 327
Material BB, $V_F = 0.42$, $[\pm 45/0_2/+45]_S$ 327
Material CC, $V_F = 0.39$, $[\pm 45/0_2/+45]_S$ 328
Material CC2, $V_F = 0.45$, $[\pm 45/0_3/+45]_S$ 329
Material CC3, $V_F = 0.45$, $[0/\pm 45/0_2/+45]_S$ 330
Material CH, $V_F = 0.45$, $[(\pm 45)_3]_S$ 330
Material CH2, $V_F = 0.41$, $[\pm 45/0/\pm 45]_S$ 331

Material CH3, $V_F = 0.36$, $[\pm 45/0/\pm 45]_S$ 332
Material CH4, $V_F = 0.40$, $[(\pm 45)_3]_S$ 332
Material CH5, $V_F = 0.28$, $[(\pm 45)_3]_S$ 333
Material CH6, $V_F = 0.49$, $[\pm 45/0/\pm 45]_S$ 335
Material CH7, $V_F = 0.55$, $[(\pm 45)_3]_S$ 335
Material CH8, $V_F = 0.39$, $[(\pm 45)_3]_S$ 336
Material CH9, $V_F = 0.49$, $[(\pm 45)_3]_S$ 337
Material CH10, $V_F = 0.33$, $[(\pm 45)_3]_S$ 337
Material CH11, $V_F = 0.54$, $[(\pm 45)_3]_S$ 338
Material CH12, $V_F = 0.34$, $[\pm 45/0/\pm 45]_S$ 339
Material CH13, $V_F = 0.48$, $[\pm 45/0/\pm 45]_S$ 341
Material CH14, $V_F = 0.44$, $[\pm 45/0/\pm 45]_S$ 342
Material CH15, $V_F = 0.32$, $[\pm 45/0/\pm 45]_S$ 343
Material CH16, $V_F = 0.40$, $[\pm 45/0/\pm 45]_S$ 343
Material CH17, $V_F = 0.48$, $[\pm 45/0/\pm 45]_S$ 344
Material CH18, $V_F = 0.47$, $[\pm 45/0/\pm 45]_S$ 345
Material CH19, $V_F = 0.33$, $[\pm 45/0/\pm 45]_S$ 345
Material CH20, $V_F = 0.25$, $[(\pm 45_3)]_S$ 346
Material CH23, $V_F = 0.32$, $[\pm 45/0/\pm 45]_S$ 346
Material DD, $V_F = 0.49$, $(0/\pm 45/0_3/\pm 45/0)$ 347
Material DD2, $V_F = 0.42$, $(0/\pm 45/0)_S$ 348
Material DD2A, $V_F = 0.42$, $(0/\pm 45/0)_S$ 348
Material DD4, $V_F = 0.50$, $(0/\pm 45/0)_S$ 349
Material DD5, $V_F = 0.38$, $(0/\pm 45/0)_S$ 349
Material DD5E, $V_F = 0.36$, $(0/\pm 45/0)_S$ 350
Material DD5P, $V_F = 0.36$, $(0/\pm 45/0)_S$ 351
Material DD5V, $V_F = 0.36$, $(0/\pm 45/0)_S$ 357
Material DD5V2, $V_F = 0.35$, $(0/\pm 45/0)_S$ 357
Material DD6, $V_F = 0.31$, $(0/\pm 45/0)_S$ 358
Material DD7, $V_F = 0.54$, $(0/\pm 45/0)_S$ 359
Material DD8, $V_F = 0.42$, $(0/\pm 45/0)_S$ 360
Material DD8A, $V_F = 0.42$, $(0/\pm 45/0)_S$ 360
Material DD8B, $V_F = 0.42$, $(0/\pm 45/0)_S$ 360
Material DD9, $V_F = 0.54$, $(0/\pm 45/0)_S$ 360
Material DD10, $V_F = 0.62$, $(0/\pm 45/0)_S$ 361
Material DD11, $V_F = 0.31$, $(0/\pm 45/0)_S$ 361
Material DD11A, $V_F = 0.31$, $(\pm 45/0_4/\mp 45)$ 363
Material DD12, $V_F = 0.43$, $(0/\pm 45/0)_S$ 363
Material DD13, $V_F = 0.50$, $(0/\pm 45/0)_S$ 363
Material DD14, $V_F = 0.35$, $(0/\pm 45/0)_S$ 364
Material DD15, $V_F = 0.25$, $(0/\pm 45/0)_S$ 364
Material DD16, $V_F = 0.36$, $(90/0/\pm 45/0)_S$ 364
Material DD17, $V_F = 0.37/0.52$, $(0/\pm 45/0)_S$ 365

Material DD17A, $V_F = 0.35/0.44$, $(0/\pm45/0)_S$ 365
Material DD18, $V_F = 0.34/0.40$, $(0/\pm45/0)_S$ 366
Material DD18A, $V_F = 0.36/0.43$, $(0/\pm45/0)_S$ 367
Material DD19, $V_F = 0.34/0.47$, $(0/\pm45/0)_S$ 368
Material DD19A, $V_F = 0.36/0.50$, $(0/\pm45/0)_S$ 368
Material DD19B, $V_F = 0.36/0.50$, $(0/\pm45/0)_S$ 369
Material DD20, $V_F = 0.34$, $[0_2/\pm45/0]_S$ 370
Material DD20A, $V_F = 0.37$, $[0_2/\pm45/0]_S$ 370
Material DD22, $V_F = 0.30$, $[0_2/\pm45/0]_S$ 370
Material DD24, $V_F = 0.39$, $(0/\pm45/0_3/\pm45/0)$ 371
Material DD25, $V_F = 0.45$, $(0/\pm45/0)_S$ 371
Material DD25A, $V_F = 0.48$, $(0/\pm45/0)_S$ 372
Material DD25B, $V_F = 0.31$, $(0/\pm45/0)_S$ 372
Material DD25D, $V_F = 0.35/0.45$, $(0/\pm45/0)_S$ 373
Material DD26, $V_F = 0.50$, $(0/\pm45/0)_S$ 373
Material FFA, $V_F = 0.38$, $(\pm45/0/0/\pm45)_S$ 373
Material FFB, $V_F = 0.38$, $(0/\pm45/0/\pm45)_S$ 374
Material FFC, $V_F = 0.38$, $(0/\pm45/\pm45/0)_S$ 375
Material FFD, $V_F = 0.38$, $(0/0/\pm45/\pm45)_S$ 375
Material FFF, $V_F = 0.38$, $(\pm45/\pm45/0/0)_S$ 376
Material GG, $V_F = 0.40$, $(0_2/\pm45/0_2)$ 376
0^O Unidirectional Tests 378
Material A060, $V_F = 0.41$,$[0]_{10}$ 378
Material A130, $V_F = 0.45$, $[0]_8$ 378
Material A130C, $V_F = 0.35$,$[0]_5$ 379
Material A130G, $V_F = 0.55$,$[0]_{14}$ 380
Material A260, $V_F = 0.35$, $[0]_4$ 380
Material CM1701, $V_F = 0.38$, $[0]_6$ 381
Material DO72A, $V_F = 0.36$, $[0]_{10}$ 381
Material DO92, $V_F = 0.45$, $[0]_{10}$ 382
Material DO92B, $V_F = 0.41$,$[0]_8$ 382
Material DO92D, $V_F = 0.30$,$[0]_7$ 383
Material DO92F, $V_F = 0.50$,$[0]_{10}$ 383
Material DO92G, $V_F = 0.58$,$[0]_9$ 384
Material D155, $V_F = 0.45$, $[0]_6$ 385
Material D155B, $V_F = 0.39$,$[0]_5$ 385
Material D155C, $V_F = 0.51$,$[0]_7$ 386
Material D155G, $V_F = 0.59$,$[0]_8$ 387
Material D155H, $V_F = 0.49$,$[0]_7$ 388
Material D155J, $V_F = 0.58$,$[0]_6$ 389
Material D155K, $V_F = 0.33$,$[0]_7$ 389
Material DB120, $V_F = 0.44$,$[0]_{16}$ 390
Material DB240, $V_F = 0.46$,$[0]_8$ 391

Angle Ply Testing 392
Material D155B, $V_F = 0.39,[0]_5$ 392
Material 10D155, $V_F = 0.38,[\pm10]_3$ 392
Material 20D155, $V_F = 0.39,[\pm20]_3$ 392
Material 30D155, $V_F = 0.40,[\pm30]_3$ 393
Material 40D155, $V_F = 0.40,[\pm40]_3$ 393
Material 45D155, $V_F = 0.38,[\pm45]_3$ 394
Material 45D155P2, $V_F = 0.40, [\pm45]_3$ 395
Material 45D155V2, $V_F = 0.39,[\pm45]_3$ 395
Material 45D155V, $V_F = 0.40,[\pm45]_3$ 396
Material 50D155, $V_F = 0.39,[\pm50]_3$ 396
Material 60D155, $V_F = 0.40,[\pm60]_3$ 397
Material 70D155, $V_F = 0.40,[\pm70]_3$ 397
Material 80D155, $V_F = 0.38,[\pm80]_3$ 398
Material 90D155, $V_F = 0.38,[\pm90]_3$ 398
Material 90D155V2, $V_F = 0.38,[\pm90]_3$ 399
Material 90D155V, $V_F = 0.40,[\pm90]_3$ 399
Material 90D155E2, $V_F = 0.38, [\pm90]_3$ 400
MaterialROV1, $V_F = 0.46, (0/90)_4$ 400
MaterialROV2, $V_F = 0.30, (0/90)_4$ 401
Material ROV3, $V_F = 0.40, (0/90)_5$ 401
Material ROV4, $V_F = 0.53, (0/90)_6$ 402
High Cycle Fatigue Database 403
Longitudinal, $V_F = 0.48$ to $0.52, (0)_2$ 403
Transverse, $V_F = 0.38, (90)_4$ 407
Prepreg (3M - 250E) Materials 410
Material PP, $V_F = 0.56, (0)_{15}$ 410
Material PP45, $V_F = 0.54, [(\pm45)_2]_S$ 410
Material PPDD5, $V_F = 0.56, (0_3/\pm45/0_3)_S$ 410
Glass-carbon Hybrids 411
Material DD23, $V_F = 0.45, (0_2/\pm45/0/0_C)_S$ 411
Material CG, $V_F = 0.56, [0_2/0_{2C}/0/0_{2C}/0_2]$ 412
Material CA, $V_F = 0.48, (0)_{12}$ 412
Glass Roving Tests 413
D155 - Strand, 2000 Fibers 413
DB120 - Strand, 750 Fibers 421
OC-990-BC-2385-4093- Strand, 45 Fibers 423
Residual Strength Tests 425
Environmentally Conditioned Tests 429
$[0/\pm45/0]_S$ and $[\pm45]_3$ Laminates 429
DD5P and DD11 Laminates 443
Neat Resin Tests 445
Tests excluded from database due to testing irregularities 446

DOE/MSU Fiberglass Composite Database Introduction

A detailed guide to use of the database and test methods may be found in Reference 2 at the end of this section. Presently there are 22 commercial and 126 Montana State University - Bozeman (MSU) manufactured fiberglass composites which have been fatigue tested for this database. Test methods are outlined in papers listed at the end of this section.

Materials presently in the database include lay-up combinations of 0^o, $\pm 45^o$ and $0^o/\pm 45^o$ fabrics tested in the strongest (longitudinal) and weakest (transverse) directions. The commercial materials were generally hand lay-up and the MSU materials were resin transfer molded (RTM). The database contains results from cyclic fatigue tests using a constant stress amplitude sine waveform with R - values of 0.1 (tension-tension), 10 (compression-compression) and -1 (tension-compression). The high cycle (typically 100 million cycle range), high frequency part of the database has R - values of: 0.1, 0.5, 2, 10, -0.5 and -1. The R - value is defined by:

$$R = \frac{Minimum\ cyclic\ stress}{Maximum\ cyclic\ stress}$$

where tensile stress is treated as a positive value and the compressive stress is negative. Thermal failures of the polymer matrix materials were avoided by using forced air cooling and low testing frequencies, generally less than 20 Hz, with specialized test geometries for higher frequencies. Generally the tension (R = 0.1) coupons used a 100 mm gage length and the compression (R = 10) and reversed (R = -1) coupons used a 13 mm gage length with unsupported edges.

Each test material is given a letter or letter and number designation which uniquely identify the material and individual test coupons. All materials are E - glass fabric reinforced thermoset polymer matrix composites unless otherwise noted. A brief description of the database structure and the description of each composite is given below.

Tables 1 through 8 summarize the materials included in this database by fiber volume fraction (V_F), ply configuration, matrix material and description of the fabric used, including fabric manufacturer. Additional information about the material is listed before the material test summary.

Table 9 summarizes the material properties of industry supplied materials typical of those used in wind turbine blade structures. This summary lists the material, fiber volume fraction, ultimate compressive strength, compressive fatigue sensitivity coefficient (b_C), compressive strain for failure at one million cycles, ultimate tensile strength, tensile fatigue sensitivity coefficient (b_T), tensile strain for failure at 1 million cycles and the initial elastic modulus in the direction tested. The fatigue sensitivity coefficient, b_C and b_T, are taken from a linear curve fit to the normalized semi-log S-N fatigue plots, as S/So = 1 - b Log N, where S is the maximum cyclic stress, So is the one-cycle strength, N is the cycles to failure abd b

is the fatigue coefficient.

Table 10 summarizes the static longitudinal, transverse and simulated shear properties for six fabrics used in the MSU manufactured composites. These properties have been used in hand calculations and standard laminate analysis programs for fiber volume fractions between 44% and 46%. Adjustments for other fiber contents can be found in Reference 2. It should be noted that this table was generated with a coupon testing rate of 0.25 mm/s, which enhanced data acquisition, versus the standard database rate of 13 mm/s.

Tables 11 and 12 summarize the 3-D properties and strengths of a D155 composite for finite element analysis.

Tables 13 through 17 summarize the material properties of the materials manufactured at MSU.

Table 18 summarizes the materials tested at an R value of R = -1.

Table 19 summarizes the data from the high cycle fatigue tests and includes the strain to failure at 1 million cycles and strain to failure at 100 million cycles for longitudinal and transverse directions of a 0° composite.

The individual coupon test results are listed and summarized using eight columns with the following example data structure:

(Col.1)	(Col.2)	(Col.3)	(Col.4)	(Col.5)	(Col.6)	(Col.7)	(Col.8)
TEST & SAMPLE ID #	MAXIMUM STRESS MPa	R	Q Hz	E GPa	e %	CYCLES TO FAIL	NOTES
(Col.1)	(Col.2)	(Col.3)	(Col.4)	(Col.5)	(Col.6)	(Col.7)	(Col.8)
63 102J	561	*	25	23.7	1.60	1	25
70 105J	129	0.1	10	26.2	0.31	11,000,000	25 R
86 101NT	54	0.1	1	8.62	1.34	6,479	25
149 132N	86	-1	5	22.8	0.36	105,505	25
215 125P	-207	10	10	28.0	-0.63	14,121	25

Col. 1: Lists the MSU mechanical test reference number and the test coupon reference label. If the sample ID label is succeeded by the letter T, the material was tested in the transverse direction or ninety degrees to the major zero degree fiber direction.

Col. 2: This column indicates the maximum stress in megapascals (MPa) which was applied to the coupon. A positive number indicates tension while a negative number indicates compression. For a compression test the stress listed as maximum is actually the minimum stress. (English conversion factor is 1 MPa = 145.0326 psi)

Col. 3: Indicates the R - value of the fatigue test. An asterisk indicates a static, single cycle tension or compression test.

Col. 4: Lists the cyclic sine wave frequency (Hz) at which the coupon was tested in fatigue

or, in the case of a static test, the constant displacement ramp rate in millimeters per second (mm/s).

Col. 5: Lists the initial (first cycle) measured elastic modulus (E) of the coupon in the direction tested, in gigapascals (GPa).

Col. 6: Indicates the initial (first cycle) absolute maximum fatigue running strain (e) in percent or the percent strain to failure for a static test.

Col. 7: Indicates the total cycles to failure for the test coupon, where failure is defined as the inability of the test coupon to support the maximum absolute applied fatigue load.

Col. 8: Lists the test coupon width in millimeters (mm) and any other notation for comments.

The notations used in column 8 are summarized below (see Reference 2):

H - Coupon had a 12.7 mm diameter circular hole in the middle of the gage length

R - Run out, coupon has significant fatigue cycles but has not yet failed, test stopped.

Z - Double coupon thickness, two coupons bonded together to increase thickness

- Coupons were post cured at a temperature of 110°C which was higher than the standard curing temperature of 60°C.

±45 - Test coupon was tested with all the fibers orientated in the ±45 direction to obtain shear properties.

ZERO - Test coupon was tested with all fibers orientated in the zero degree load axis. Fabrics were taken apart and orientated in the zero direction.

90 - Test coupon was tested with all the fibers orientated in the 90 degree or transverse to the axis of loading.

tab - Coupon had additional tab material in the gripped area of the composite

tow - A complete glass strand from a particular fabric.

---- - Indicates that a value was unavailable.

Other notations used in the test material summary tables include:

V_F - Fiber volume content of the material in percent

UCS - Ultimate Compressive Strength of the material in MPa

UTS - Ultimate Tensile Strength of the material in MPa

b - fatigue sensitivity coefficient from a linear regression curve fit to the S - N data. Assuming a linear S - N curve on the semi - log plot, yields the equation, $S / S_0 = 1 - b \log N$, where S is the maximum stress, S_0 is the single cycle strength and N is the total cycles to failure.

b_C - Slope of the compressive fatigue (R = 10) trend line on a semi - log graph (compressive fatigue sensitivity coefficient)

b_T - Slope of the tensile fatigue (R = 0.1) trend line on a semi - log graph (tensile fatigue sensitivity coefficient)

b_R - Slope of the reversed loading (R = -1) fatigue trend line on a semi - log graph (completely reversed loading fatigue sensitivity coefficient)

E - Epoxy matrix material is used in the composite
P - Polyester matrix material is used in the composite
V - Vinyl ester matrix material is used in the composite
S.D. - Sample statistical standard deviation

Some of the fatigue data and the testing procedures followed to produce this database were discussed in the following reports:

1. Mandell, J.F., Reed, R.M. Jr. and Samborsky, D.D., "Fatigue of Fiberglass Wind Turbine Blade Materials", Contractor Report SAND92-7005, Sandia National Laboratories, Albuquerque, NM (1992). [www.Sandia.gov/Library.htm]

2. Mandell, J.F., and Samborsky, "DOE/MSU Composite Material Fatigue Database: Test Methods, Materials, and Analysis", Contractor Report SAND97-3002, Sandia National Laboratories, Albuquerque, NM (1997).[www.Sandia.gov/Library.htm]

3. Mandell, J.F., Reed, R.M., and Samborsky, D.D., "High Cycle Fatigue of Wind Turbine Blade Materials," in SED-Vol 12, Wind Energy 92, P.S. Veers, S.M. Hock, eds., ASME, New York, p. 105 (1992).

4. Mandell, J.F., Reed, R.M. Jr., Samborsky, D.D., and Pan, Q., "Fatigue Performance of Wind Turbine Blade Materials," in SED-Vol 14, Wind Energy 93, S. Hock, ed., ASME, New York, 191-198. (1993).

5. Mandell, J.F., Creed, R.M. Jr., Pan, Q., Combs, D.W., and Shrinivas, M., "Fatigue of Fiberglass Generic Materials and Substructures" in SED-Vol 15, Wind Energy 94, W.D. Musial, S.M. Hock and D.E. Berg, eds., ASME, New York, pp. 207-213 (1994).

6. Mandell, J.F., Combs, D.E., and Samborsky, D.D., "Fatigue of Fiberglass Beam Substructures", Wind Energy 1995, W.D. Musial, S.M. Hock, and D.E. Berg, Eds., SED-Vol. 16, ASME, 99 - 106 (1995).

7. Samborsky, D., and Mandell, J.F., "Fatigue Resistant Fiberglass Laminates for Wind Turbine Blades," Wind Energy 1996, ASME, 46-51 (1996).

8. Sutherland, H.J., and Mandell, J.F., "Application of the U.S. High Cycle Fatigue Database To Wind Turbine Blade Lifetime Predictions" Wind Energy 1996, ASME, pp. 78-84 (1996).

9. Mandell, J.F., Samborsky, D.D., and Cairns, D.S., "Advanced Wind Turbine Blade Structure Development Program at Montana State University," Wind Energy 1997, ASME/AIAA, 189-196 (1997).

10. Samborsky, Daniel D., "Fatigue of E-Glass Fiber Reinforced Composite Materials and Substructures," Civil Engineering Masters Thesis, Montana State University, December 1999.

11. Cairns, D.S., Mandell, J.F., Scott, M.E., and Macagnano, J.Z., "Design Considerations for Ply Drops in Composite Wind Turbine Blades" Wind Energy 1997, ASME/AIAA, pp. 197-208. (1997).

12. Cairns, D. S., Haugen, D. J., Mandell, J. F., and Samborsky, D. D., "Fracture of Skin/Stiffener Intersections in Composite Wind Turbine Structures," Wind Energy 1998, ASME/AIAA, pp. 334 - 343. (1998).

13. Mandell, J. F., Samborsky, D. D., Combs, D.W., Scott, M.E., and Cairns, D. S, "Fatigue of Composite Material Beam Elements Representative of Wind Turbine Blade Substructure", NREL Contractor Report SR-500-24379, November 1998.

14. Mandell, J. F., Samborsky, D. D., Scott, M.E., and Cairns, D. S, "Effects of Structural Details on Delamination and fatigue Life of Fiberglass Laminates," Wind Energy 1998, ASME/AIAA, pp. 323 - 327. (1998).

15. Samborsky, D. D., Mandell, J. F., and Cairns, D. S, "Selection of Reinforcing Fabrics for Wind Turbine Blades," Wind Energy 1999, AIAA-99-0024, ASME/AIAA, (1999).

16. Cairns, D.S, McKittrick, L., Rabern, D., Vanluchene, D., Mandell, J.F., "Design and Manufacturing Synthesis of Composite Wind Turbine Blades", Wind Energy 1999, ASME/AIAA, (1999).

17. Mandell, John F., Samborsky, Daniel D., Sutherland, Herbert J., "Effects of Materials Parameters and Design Details on the Fatigue of Composite Materials for Wind Turbine Blades", 1999 European Wind Energy Conference, 1-5 March 1999, Nice, France, pp. 628-633.

18. Mandell, J. F., Samborsky, D. D., Li, Mei, Orozco, Ricardo, and Cairns, D. S, "Selection of Fiberglass Matrix Resins for Increased Toughness and Environmental Resistance in Wind Turbine Blades," Wind Energy 2000, ASME/AIAA, (to be published).

Glass fabrics used in this database were obtained from the following companies:

Brunswick Technologies Inc., 43 Bibber Parkway, Brunswick, Maine, 04011
CollinsCraft Composites Group Inc., 1857 Westminster Hwy. Walhalla, SC, 29691.
Owens Corning Fabrics (Knytex). 1851 South Seguin St., New Braunfels, Texas, 78130.

Table 1. Lay-up of Commercial Fiberglass Materials

Material	V_F,%	Ply Configuration	Matrix	Fabric Description
A	30	$[0]_5$	P	407 g/m^2 0's, A1012, CoRezyn 63-AX-050 polyester
B	30	$[0]_5$	V	407 g/m^2 0's, A1012, Hetron 922L-25 Vinyl ester
F	36	$[(\pm45/0)_3]_S$	P	1,152 g/m^2 Triax (48%- 0's) Center two plies dropped off (6 plies➜ 4 plies), CoRezyn 63-AX-050 polyester resin
G	36	$[(0/\pm45)_3]_S$	P	
H	39	$[(\pm45/0)_3]_S$	P	1,081 g/m^2 Triax (70%- 0's, 30%- ±45's), Hexcel XH120, Center two plies have butt joint (6 plies ➜ 4 plies)
J	43	$[(0/\pm45)_3]_S$	P	
L	50	$[0]_3$	P	0's - A260's
M	38	$[0/\pm45]_4$	V	747 g/m^2 Triax (50%-0's)
N	36	$[0/\pm45]_4$	P	
P	36	$[(0/\pm45)/M/0]_S$	V	747 g/m^2 Triax (0/±45), 203 g/m^2 Mat(M), 0's -A260 (69%-0's)
R	32	$[0/\pm45]_4$	P	0's - DN105, 45 - DB120 (47%-0's)
T	30	$[0/\pm45]_5$	P	Folded edge Triax (CDB200), CoRezyn 63-AX-051 polyester resin
U	29	$[0/\pm45]_5$	P	Cut edge Triax (CDB222), CoRezyn 63-AX-051 polyester resin
V	32	$[0/\pm45]_5$	P	Folded edge Triax (CDB222),CoRezyn 63-AX-051 polyester resin
W	33	$[0/\pm45]_5$	P	Cut edge Triax (CDB200), CoRezyn 63-AX-051 polyester resin
X	35	$[0_2/M/\pm45/0_2]$	P	85%-0's (A260), 10%-±45's (407 g/m^2), 5%-Mat(M) (203 g/m^2)
Y	39	$[0_2/M/\pm45/0_2]$	E	
EE	54	$[M/\pm45/0]_S$	E	65%-0's, 18%- 45's, 17%- Mat
EEAV	48	$[M/\pm45/0]_S$	V	71%-0's, 18%- 45's, 11%- Mat
EEAP	49	$[M/\pm45/0]_S$	P	70%-0's, 19%- 45's, 11%- Mat
EEBP	43	$[M/\pm45/0]_S$	V	57%-0's, 26%- 45's, 17%- Mat
EECP	49	$[M/\pm45/0]_S$	V	65%-0's, 20%- 45's, 15%- Mat
Matrix Abbreviations: E -Epoxy, P -Polyester, V-Vinyl ester Materials EE, EEAV, EEAP, EEBP and EECP were obtained from a production wind turbine blade.				

Table 2. Lay-up of MSU Manufactured (RTM) Fiberglass Materials

Material	V_F %	Ply Configuration	Matrix	Fabric Description
AA	35	$[(\pm 45/0)_3(\mp 45/0)_2]$	P	CDB-200 Triax
AA2	40	$[(0/\pm 45)_2]_S$	P	CDB-200 Triax
AA3	51	$[(\pm 45/0)_3]_S$	P	CDB - 200 Triax
AA4	38	$[(\pm 45/0)_2]_S$	P	TV-3400 Triax (BTI)
BB	42	$[\pm 45/0_2/+45]_S$	P	0's-A130 (62%), 45's-DB120
CC	39	$[\pm 45/0_2/+45]_S$	P	0's-D100 (55%), 45's-DB120
CC2	45	$[\pm 45/0_3/+45]_S$	P	0's-D100 (63%), 45's-DB120
CC3	45	$[0/\pm 45/0_2/+45]_S$	P	0's-D100 (63%), 45's-DB120
CH	45	$[(\pm 45)_3]_S$	P	45's-DB240
CH2	41	$[\pm 45/0/\pm 45]_S$	P	0's-D155 (24%), 45's-DB240
CH3	36	$[\pm 45/0/\pm 45]_S$	P	0's-D155 (24%), 45's-DB240
CH4	40	$[(\pm 45)_3]_S$	P	45's-DB120
CH5	28	$[(\pm 45)_3]_S$	P	45's-DB120
CH6	49	$[\pm 45/0/\pm 45]_S$	P	0's-D155 (39%), 45's-DB120
CH7	55	$[(\pm 45)_3]_S$	P	45's-DB400
CH8	39	$[(\pm 45)_3]_S$	P	45's-DB400
CH9	49	$[(\pm 45)_3]_S$	P	45's-DB120
CH10	33	$[(\pm 45)_3]_S$	P	45's-DB240
CH11	54	$[(\pm 45)_3]_S$	P	45's-DB240
CH12	34	$[\pm 45/0/\pm 45]_S$	P	0's-D155 (39%), 45's-DB120
CH13	48	$[\pm 45/0/\pm 45]_S$	P	0's-D155 (24%), 45's-DB240
CH14	44	$[\pm 45/0/\pm 45]_S$	P	0's-D155 (39%), 45's-DB120
CH15	32	$[\pm 45/0/\pm 45]_S$	P	0's-D092 (28%), 45's-DB120
CH16	40	$[\pm 45/0/\pm 45]_S$	P	0's-D092 (28%), 45's-DB120

Matrix Abbreviations: E -Epoxy (Epon 9410), E2 -Epoxy (SC14), P -Ortho-polyester (COR63AX051), P2 -Iso-polyester (COR75AQ010), V-Vinyl ester (Derakane 411C), V2 -Vinyl ester (Derakane 8084)

Owens Corning Fabrics: A060-206 g/m^2 , A130 - 444 g/m^2 , CM1701 - 587 g/m^2, D072 - 230 g/m^2 , D092 - 310 g/m^2 , D100 - 339 g/m^2 , D155 - 527 g/m^2 , DB120 - 393 g/m^2 , DB240 - 837 g/m^2 , DB400 - 1349 g/m^2 , DBM1204B - 420 g/m^2, CDB200 (Triax) - 759 g/m^2 (uses D092 and DB120 fabrics),
BTI Fabrics - TV3400 (triax) - 1150 g/m^2 ,
CollinsCraft Fabrics - A1010 - 351 g/m^2 , UC1010 - 424 g/m^2 , UC1018/V (polyester veil) - 644 g/m^2 , UC1018/GV (glass veil)- 678 g/m^2

Table 3. Lay-up of MSU Manufactured (RTM) Fiberglass Materials

Material	V_F, %	Ply Configuration	Matrix	Fabric Description
CH17	48	$[\pm 45/0/\pm 45]_S$	P	0's-D092 (28%), 45's-DB120
CH18	47	$[\pm 45/0/\pm 45]_S$	P	0's-D092 (16%), 45's-DB240
CH19	33	$[\pm 45/0/\pm 45]_S$	P	0's-D092 (16%), 45's-DB240
CH20	25	$[(\pm 45_3)]_S$	P	45's-DBM1204B
CH23	32	$[\pm 45/0/\pm 45]_S$	P	0's-D155 (39%), 45's-DBM1204B
DD	49	$(0/\pm 45/0_3/\pm 45/0)$	P	0's-D155 (76%), 45's-DB120
DD2	42	$(0/\pm 45/0)_S$	P	0's-D155 (72%), 45's-DB120
DD2A	42	$(0/\pm 45/0)_S$	P	
DD4	50	$(0/\pm 45/0)_S$	P	
DD5	38	$(0/\pm 45/0)_S$	P	
DD5E	36	$(0/\pm 45/0)_S$	E	
DD5P	36	$(0/\pm 45/0)_S$	P	
DD5V	36	$(0/\pm 45/0)_S$	V	
DD5V2	35	$(0/\pm 45/0)_S$	V2	
DD6	31	$(0/\pm 45/0)_S$	P	
DD7	54	$(0/\pm 45/0)_S$	P	
DD8	42	$(0/\pm 45/0)_S$	P	0's-D155 (72%), 45's-DB120 All fabric weft stitching thread was removed
DD9	54	$(0/\pm 45/0)_S$	P	
DD10	62	$(0/\pm 45/0)_S$	P	
DD8A	42	$(0/\pm 45/0)_S$	P	0's-D155 (no weft stitching thread), DB120
DD8B	42	$(0/\pm 45/0)_S$	P	0's-D155 (no stitching), DB120 (no stitching between +45 and -45 plies)
DD11	31	$(0/\pm 45/0)_S$	P	0's-A130 (68%), 45's-DB120
DD11A	31	$(\pm 45/0_4/\mp 45)$	P	
DD12	43	$(0/\pm 45/0)_S$	P	
DD13	50	$(0/\pm 45/0)_S$	P	
DD14	35	$(0/\pm 45/0)_S$	P	0'S-CM1701 (72%), 45'S-DB120
DD15	25	$(0/\pm 45/0)_S$	P	

Matrix Abbreviations: E -Epoxy (Epon 9410), E2 -Epoxy (SC14), P -Ortho-polyester (COR63AX051), P2 -Iso-polyester (COR75AQ010), V-Vinyl ester (Derakane 411C), V2 -Vinyl ester (Derakane 8084)

Owens Corning Fabrics: A060-206 g/m^2 , A130 - 444 g/m^2 , CM1701 - 587 g/m^2, D072 - 230 g/m^2 , D092 - 310 g/m^2 , D100 - 339 g/m^2 , D155 - 527 g/m^2 , DB120 - 393 g/m^2 , DB240 - 837 g/m^2 , DB400 - 1349 g/m^2 , DBM1204B - 420 g/m^2, CDB200 (Triax) - 759 g/m^2 (uses D092 and DB120 fabrics),
BTI Fabrics - TV3400 (triax) - 1150 g/m^2 ,
CollinsCraft Fabrics - A1010 - 351 g/m^2 , UC1010 - 424 g/m^2 , UC1018/V (polyester veil) - 644 g/m^2 , UC1018/GV (glass veil)- 678 g/m^2

Table 4. Lay-up of MSU Manufactured (RTM) Fiberglass Materials

	V_F, %	Ply Configuration	Matrix	Fabric Description
DD16	36	$(90/0/\pm45/0)_S$	P	0's-D155 (53%), 90's-D155 (26%) 45's-DB120 (21%)
DD17	37/52	$(0/\pm45/0)_S$	P	0's-D155 (72%), 45's-DB120 Has surface indentation (flaw)
DD17A	35/44	$(0/\pm45/0)_S$	P	0's-A130 (68%), 45's-DB120 Has surface indentation (flaw)
DD18	34/40	$(0/\pm45/0)_S$	P	0's-D155 (72%), 45's-DB120 Has center flaw, one 90° (D155) tow
DD18A	36/43	$(0/\pm45/0)_S$	P	0's-D155 (68%), 45's-DB120, Has center flaw, one 90°(D155) tow across width
DD19	34/47	$(0/\pm45/0)_S$	P	0's-D155 (72%), 45's-DB120, Has center flaw, two 90° (D155) tows across width
DD19A	36/50	$(0/\pm45/0)_S$	P	0's-A130 (68%), 45's-DB120, Has center flaw, two 90°(D155) tows across width
DD19B	36/50	$(0/\pm45/0)_S$	P	0's-A130 (68%), 45's-DB120, Has centered 8 mm x 19 mm flaw (two 0°(D155) tows)
DD20	34	$[0_2/\pm45/0]_S$	P	0's - Collins Craft A1010 (73%), 45's -DB120
DD20A	37			
DD22	30	$[0_2/\pm45/0]_S$	P	0's- D092 (70%), 45's- DB120 (30%)
DD23	38	$[0/\pm45/0/0^*]_S$	P	0's - D155, 0*-carbon, 45's DB120
DD24	39	$(0/\pm45/0_3/\pm45/0)$	P	0's - CollinsCraft UC1010V, 45's -DB120 (70% 0's)
DD25	45	$(0/\pm45/0)_S$	P	0's - CollinsCraft UC1018GV, Glass veil, 45's -DB120 (76% 0's)
DD25A	48	$(0/\pm45/0)_S$	P	0's - Collins Craft UC1018V, Polyester veil, 45's -DB120 (76% 0's)
DD25B	31	$(0/\pm45/0)_S$	P	
DD25D	35/45	$(0/\pm45/0)_S$	P	Same as DD25A, Surface Indentation
DD26	50	$(0/\pm45/0)_S$	P	0's - Collins Craft UC1018V, Polyester veil, 45's -DB120, with a different general purpose polyester binder. (76% 0's)

Matrix Abbreviations: E -Epoxy (Epon 9410), E2 -Epoxy (SC14), P -Ortho-polyester (COR63AX051), P2 -Iso-polyester (COR75AQ010), V-Vinyl ester (Derakane 411C), V2 -Vinyl ester (Derakane 8084)

Owens Corning Fabrics: A060-206 g/m^2 , A130 - 444 g/m^2 , CM1701 - 587 g/m^2, D072 - 230 g/m^2 , D092 - 310 g/m^2 , D100 - 339 g/m^2 , D155 - 527 g/m^2 , DB120 - 393 g/m^2 , DB240 - 837 g/m^2 , DB400 - 1349 g/m^2 , DBM1204B - 420 g/m^2, CDB200 (Triax) - 759 g/m^2 (uses D092 and DB120 fabrics), BTI Fabrics - TV3400 (triax) - 1150 g/m^2 ,
CollinsCraft Fabrics - A1010 - 351 g/m^2 , UC1010 - 424 g/m^2 , UC1018/V (polyester veil) - 644 g/m^2 , UC1018/GV (glass veil)- 678 g/m^2

Table 5. Lay-up of MSU Manufactured (RTM) Fiberglass Materials

Material	V_F, %	Ply Configuration	Matrix	Fabric Description
FFA	38	$(\pm 45/0/0/\pm 45)_S$	P	0's-D155 (56%), 45's-DB120 (44%)
FFB	38	$(0/\pm 45/0/\pm 45)_S$	P	
FFC	38	$(0/\pm 45/\pm 45/0)_S$	P	
FFD	38	$(0/0/\pm 45/\pm 45)_S$	P	
FFF	38	$(\pm 45/\pm 45/0/0)_S$	P	
GG	40	$(0_2/\pm 45/0_2)$	P	0's-D155 (84%), 45's-DB120 (16%)
ROV2	30	$(0/90)_4$	P	0/90, 600 g/m^2, balanced construction
ROV3	40	$(0/90)_5$	P	0/90, 814 g/m^2, balanced construction
ROV4	53	$(0/90)_6$	P	0/90, 814 g/m^2, balanced construction

Matrix Abbreviations: E -Epoxy (Epon 9410), E2 -Epoxy (SC14), P -Ortho-polyester (COR63AX051), P2 -Iso-polyester (COR75AQ010), V-Vinyl ester (Derakane 411C), V2 -Vinyl ester (Derakane 8084)

Owens Corning Fabrics: A060-206 g/m^2 , A130 - 444 g/m^2 , CM1701 - 587 g/m^2, D072 - 230 g/m^2 , D092 - 310 g/m^2 , D100 - 339 g/m^2 , D155 - 527 g/m^2 , DB120 - 393 g/m^2 , DB240 - 837 g/m^2 , DB400 - 1349 g/m^2 , DBM1204B - 420 g/m^2, CDB200 (Triax) - 759 g/m^2 (uses D092 and DB120 fabrics),
BTI Fabrics - TV3400 (triax) - 1150 g/m^2 ,
CollinsCraft Fabrics - A1010 - 351 g/m^2 , UC1010 - 424 g/m^2 , UC1018/V (polyester veil) - 644 g/m^2 , UC1018/GV (glass veil)- 678 g/m^2

Table 6. Lay-up of MSU Manufactured (RTM) Unidirectional Fiberglass Materials

Material (fabric)	V_F, %	Ply Configuration	Matrix	Fabric Description
A060	41	$[0]_{10}$	P	0's - A060 (100%)
A130	45	$[0]_8$	P	0's - A130 (100%)
A130C	35	$[0]_5$	P	
A130G	55	$[0]_{14}$	P	
A260	35	$[0]_4$	P	0's - A260 (100%)
CM1701	38	$[0]_6$	P	0's - CM1701A (100%)
DO72A	36	$[0]_{10}$	P	0's - DO72 (100%)
DO92	45	$[0]_{10}$	P	0's - DO92 (100%)
DO92B	41	$[0]_8$	P	
DO92D	30	$[0]_7$	P	
DO92F	50	$[0]_{10}$	P	
DO92G	58	$[0]_9$	P	
D155	45	$[0]_6$	P	0's-D155 (100%)
D155B	39	$[0]_5$	P	
D155C	51	$[0]_7$	P	
D155G	59	$[0]_8$	P	
D155H	49	$[0]_7$	P	0's-D155 (100%) All fabric weft stitching removed
D155J	58	$[0]_6$	P	
D155K	33	$[0]_7$	P	0's-D155 (100%)

Matrix Abbreviations: E -Epoxy (Epon 9410), E2 -Epoxy (SC14), P -Ortho-polyester (COR63AX051), P2 -Iso-polyester (COR75AQ010), V-Vinyl ester (Derakane 411C), V2 -Vinyl ester (Derakane 8084).

Owens Corning Fabrics: A060-206 g/m^2 , A130 - 444 g/m^2 , CM1701 - 587 g/m^2, D072 - 230 g/m^2 , D092 - 310 g/m^2 , D100 - 339 g/m^2 , D155 - 527 g/m^2 , DB120 - 393 g/m^2 , DB240 - 837 g/m^2 , DB400 - 1349 g/m^2 , DBM1204B - 420 g/m^2, CDB200 (Triax) - 759 g/m^2 (uses D092 and DB120 fabrics),
BTI Fabrics - TV3400 (triax) - 1150 g/m^2 ,
CollinsCraft Fabrics - A1010 - 351 g/m^2 , UC1010 - 424 g/m^2 , UC1018/V (polyester veil) - 644 g/m^2 , UC1018/GV (glass veil)- 678 g/m^2

Table 7. Lay-up of MSU Manufactured (RTM) Fiberglass Materials with Symmetric Angle Plies

Material	V_F, %	Ply Configuration	Matrix	Fabric Description
10D155	38	$[\pm 10]_3$	P	D155 (100%) fabric orientated to balanced angles
20D155	39	$[\pm 20]_3$	P	
30D155	40	$[\pm 30]_3$	P	
40D155	40	$[\pm 40]_3$	P	
45D155	38	$[\pm 45]_3$	P	
50D155	39	$[\pm 50]_3$	P	
60D155	40	$[\pm 60]_3$	P	
70D155	40	$[\pm 70]_3$	P	
80D155	38	$[\pm 80]_3$	P	
90D155	38	$[\pm 90]_3$	P	
45D155P2	40	$[\pm 45]_3$	P2	
45D155V2	39	$[\pm 45]_3$	V2	
45D155V	40	$[\pm 45]_3$	V	
90D155V2	38	$[\pm 90]_3$	V2	
90D155V	40	$[\pm 90]_3$	V	
90D155E2	38	$[\pm 90]_3$	E	
Matrix Abbreviations: E -Epoxy (Epon 9410), E2 -Epoxy (SC14), P -Ortho-polyester (COR63AX051), P2 -Iso-polyester (COR75AQ010), V-Vinyl ester (Derakane 411C), V2 -Vinyl ester (Derakane 8084)				

Table 8. Lay-up of MSU High Cycle Materials

Material	V_F, %	Ply Configuration	Matrix	Fabric Description
Longitudinal	48 - 52	$(0)_2$	CoRezyn 63-AX-051 Polyester	0's - D155 (100%)
Transverse	38	$(90)_4$		90's - D100 (100%)

Table 9. Fatigue Summary Properties of Commercial Materials

		R = 10			R = 0.1			
Material	V_F %	UCS, MPa	b_C	strain for 10^6 cycles, %	UTS, MPa	b_T	strain for 10^6 cycles, %	E, GPa
A	30	-313	----	----	566	0.111	0.87	21.5
B	30	-287	----	----	581	0.135	0.99	21.0
F	36	-364	----	----	357	0.130	0.48	17.2
G	36	-258	----	----	361	0.129	0.45	19.3
H	37	-435	0.10	-0.72	513	0.114	0.52	24.0
J	37	-410	----	----	440	0.118	0.52	24.2
L	50	-407	----	----	742	0.135	0.70	33.6
M	38	-286	----	----	516	0.141	0.40	20.7
N	36	-318	0.096	-0.70	468	0.140	0.46	19.3
NT	40	-131	----	----	87	0.100	0.43	8.1
P	40	-466	0.094	-0.66	667	0.134	0.48	22.5
R	31	-330	----	----	441	0.104	0.98	16.5
T	28	-290	----	----	365	0.116	0.65	17.7
U	29	-354	----	----	372	0.138	0.36	21.2
V	32	-379	----	----	374	0.133	0.43	20.0
W	33	-336	----	----	341	0.116	0.64	19.3
X	35	-438	0.070	-1.00	612	0.091	1.05	25.4
XT	35	-159	----	----	43	0.110	0.23	8.3
Y	39	-454	0.059	-1.00	626	0.102	0.97	25.0
YT	39	-107	----	----	34	0.106	0.17	7.0
EE	55	-538	----	----	543	0.132	0.60	31.4
EEAV	49	-645	0.077	-1.30	583	0.100	0.75	28.2
EEAP	48	-729	0.088	-1.25	511	0.101	0.82	29.0
EEBP	43	-417	----	-----	515	0.100	0.75	26.6
EECP	49	-419	-----	-----	526	0.100	0.70	28.3

Table 10. Laminate Analysis Input Properties for E - Glass fabrics used in the MSU RTM composites (static longitudinal, transverse and simulated shear properties).

			Longitudinal Direction									Transverse Direction			
			Elastic Constants				Tension		Compression		Shear	Tension		Compression	
Fabric	lay-up	V_F %	E_L GPa	E_T GPa	υ_{LT}	G_{LT} GPa	UTS_L MPa	ϵ_U %	UCS_L MPa	ϵ_U %	τ_{TU} MPa	UTS_T MPa	ϵ_U %	UCS_T MPa	ϵ_U %
A130	$[0]_8$	45	36.3	8.76	0.32	3.48	858	2.53	-334	-0.92	85.3	33.8	0.39	-93.3	-1.05
D092	$[0]_{10}$	45	35.3	8.76	0.31	4.15	959	2.98	-773	-2.19	141	38.3	0.44	-133	-1.52
D155	$[0]_6$	45	35.0	8.99	0.31	4.10	987	2.83	-746	-2.02	97.7	27.2	0.32	-123	-1.67
DB120*	$[0]_{16}$	44	26.6	7.52	0.39	4.12	610	2.49	-551	-2.08	84.9	24.9	0.33	-114	-2.00
DB240*	$[0]_8$	46	31.0	7.34	0.35	3.74	697	2.67	-528	-1.74	68.7	19.7	0.27	-122	-1.69
0/90ROV*	$[0/90]_7$	46	23.9	23.9	0.26	4.08	382	2.27	-223	-0.93	99.1	382	2.27	-223	-0.93

Notes: All coupons for this Table were tested at 0.25 mm/s, with a 100 mm gage length. Compression tests used a 13 mm gage length with unsupported edges.
E_L - Longitudinal modulus
υ_{LT} - Poisson's ratio
G_{LT} and τ_{TU} - Shear modulus and ultimate shear stress from a simulated shear (±45) ASTM D3518 test.
UTS_L - Ultimate longitudinal tensile strength
ϵ_U - Ultimate tensile strain
UCS_L - Ultimate longitudinal compressive strength
ϵ_U - Ultimate compressive strain. Coupons had a 13 mm gage length.
* DB120 and DB240 fabrics were separated into a +45° and a -45° orientation and then rotated to 0 degrees to form a unidirectional material. The reasoning behind the testing of the DB120 and DB240 fabrics is that the fabric stitching operation causes a noticeable waviness in the fabric. If the properties of straight fiber tows are used to model the ±45 directions, the calculated values would be extremely high than what actually would be present because of this waviness. The 0°/90° ROV material was tested as a balanced 0°/90° fabric.

Table 11. Physical 3-D Constants of Material D155, V_F = 36 and 44%.

Physical Constants of Material D155, V_F = 36%			
Property and test plane	Test Values	Average	s.d.
E_L, GPa (LT plane)	28.1, 27.0, 29.8	28.3	1.4
E_L, GPa (LZ plane)	28.0, 28.3, 27.6	28.0	0.4
E_T, GPa (TZ plane)	8.00, 7.31, 7.93	7.75	0.38
E_Z, GPa (ZX plane)	7.10, 7.65, 7.38	7.38	0.28
NU_{LT}	0.329, 0.320, 0.301	0.32	0.01
NU_{LZ}	0.305, 0.338, 0.331	0.33	0.02
NU_{TZ}	0.466, 0.395, 0.449	0.44	0.04
G_{LT}, GPa	3.31, 3.35, 3.23	3.30	0.06
G_{LZ}, GPa	3.03, 2.72, 2.70	2.82	0.19
G_{TZ}, GPa	2.78, 3.12, 1.76	2.55	0.71
Physical Constants of Material D155, V_F = 44%			
Property and test plane	Test Values	Average	s.d.
E_L, GPa (LT plane)	31.9, 35.4, 33.6	33.6	1.8
E_L, GPa (LZ plane)	34.5, 34.3, 34.5	34.4	0.1
E_T, GPa (TZ plane)	8.14, 8.96, 7.52	8.21	0.72
E_Z, GPa (ZX plane)	7.58, 8.00, 8.00	7.86	0.24
NU_{LT}	0.289, 0.291, 0.290	0.29	0.01
NU_{LZ}	0.302, 0.314, 0.308	0.31	0.01
NU_{TZ}	0.373, 0.371, 0.366	0.37	0.01
G_{LT}, GPa	5.76, 3.94, 3.74	4.48	1.11
G_{LZ}, GPa	3.88, 4.40, 3.07	3.78	0.67
G_{TZ}, GPa	2.96, 2.70, 2.20	2.62	0.39
Shear properties determined by V-notched beam (ASTM 5379)			

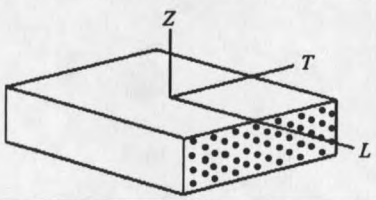


Table 12. Physical 3-D Strengths of Material D155, V_F = 36 and 44%.

Strengths of Material D155, V_F = 36%			
Property and test plane	Test Values	Average	s.d.
UTS_L, MPa (LT plane)	891, 814, 883, 838	856	37
UTS_L, MPa (LZ plane)	679, 672, 685, 646	671	17
UTS_T, MPa (TZ plane)	26.6, 36.0, 30.4, 32.9, 29.0	31.0	3.6
UTS_Z, MPa (ZT plane)	21.7, 18.7, 20.4, 18.1	19.7	1.6
UTS_Z, MPa (ZL plane)	19.4, 17.7, 22.3, 17.1, 15.2	18.4	2.7
τ_{LT}, MPa	95.1, 82.1, 78.8	85.3	8.7
τ_{LZ}, MPa	79.6, 77.3, 77.1, 63.2	74.3	7.5
τ_{TZ}, MPa	19.9, 17.6, 12.0	16.5	4.0
Strengths of Material D155, V_F = 44%			
Property and test plane	Test Values	Average	s.d.
UTS_L, MPa (LT plane)	991, 1000, 1045	1,012	29
UTS_L, MPa (LZ plane)	881, 855, 896	877	21
UTS_T, MPa (TZ plane)	33.3, 29.3, 28.6, 32.1, 29.7	30.6	2.0
UTS_Z, MPa (ZT plane)	12.0, 13.4, 13.4, 12.3	12.8	0.7
τ_{LT}, MPa	67.5, 79.1, 73.1	73.2	5.8
τ_{LZ}, MPa	75.0, 66.2, 70.8	70.7	4.4
τ_{TZ}, MPa	13.6, 17.0, 20.1	16.9	3.3
Shear properties determined by V-notched beam (ASTM 5379)			

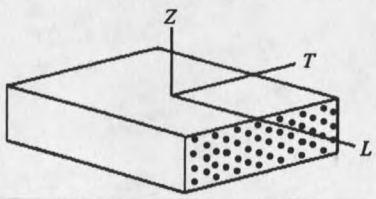


Table 13. Fatigue Summary Properties of MSU (RTM) Manufactured Materials

		R = 10			R = 0.1			
Material	V_F %	UCS, MPa	b_c	strain for 10^6 cycles, %	UTS, MPa	b_T	strain for 10^6 cycles, %	E, GPa
AA	35	-348	0.081	-0.95	452	0.140	0.50	18.8
AA3	51	-284	----	----	478	0.140	0.40	25.2
AA4	37	-449	----	----	377	0.105	0.67	20.4
BB	42	-308	----	----	725	0.131	0.80	25.2
BBT	42	-248	----	----	105	----	----	11.7
CC	39	-459	----	----	561	0.121	0.80	21.7
CC2	45	-527	----	----	715	0.118	0.79	26.6
CC3	45	-541	----	----	682	0.112	0.85	26.3
CH	45	-178	0.105	-0.50	145	0.104	0.46	13.6
CH2	41	-342	0.110	-0.70	362	0.127	0.65	16.7
CH3	36	-318	0.127	-0.60	336	0.112	0.64	16.8
CH4	40	-171	0.112	-0.48	155	0.124	0.48	11.4
CH5	28	-190	0.105	-0.85	139	0.123	0.54	8.5
CH6	49	-408	0.100	-0.80	502	0.139	0.50	21.5
CH7	55	-168	0.113	-0.30	114	0.110	0.27	17.0
CH8	39	-146	0.151	-0.35	93	0.113	0.38	10.0
CH9	49	-174	0.106	-0.67	151	0.133	0.51	10.3
CH10	33	-163	0.126	-0.64	120	0.108	0.58	8.1
CH11	54	-189	0.106	-0.58	134	0.114	0.38	13.4
CH12	34	-451	0.092	-1.15	398	0.099	0.94	17.4
CH13	48	-385	0.107	-0.60	423	0.138	0.48	23.2
CH14	44	-412	0.081	-1.00	517	0.134	0.75	21.0

Table 14. Fatigue Summary Properties of MSU (RTM) Manufactured Materials

		R = 10			R = 0.1			
Material	V_F %	UCS, MPa	b_C	strain for 10^6 cycles, %	UTS, MPa	b_T	strain for 10^6 cycles, %	E, GPa
CH15	32	-345	0.100	-1.02	309	0.103	0.85	14.8
CH16	40	-309	0.085	-0.80	360	0.129	0.68	18.5
CH17	48	-301	0.079	-0.94	359	0.139	0.40	17.6
CH18	47	-298	0.105	-0.74	294	0.129	0.50	17.2
CH19	33	-252	0.122	-0.65	193	0.102	0.70	11.9
CH20	25	-230	----	----	133	0.118	0.38	10.9
CH23	32	-448	0.106	-0.90	394	0.140	0.40	18.5
DD	49	-788	----	----	910	0.135	0.60	31.3
DD2	42	-581	0.079	-1.15	752	0.110	0.95	27.0
DD2A	42	----	----	----	986	0.122	0.94	28.0
DD4	50	-541	----	----	886	0.136	0.55	31.0
DD5	38	-534	----	----	724	0.104	1.15	25.2
DD5E	36	-521	0.056	-1.42	674	0.110	1.20	23.6
DD5P	36	-574	0.072	-1.35	661	0.101	1.16	24.2
DD5PT	36	-148	----	----	66	0.100	0.30	8.80
DD5V	36	-530	0.057	-1.48	675	0.102	1.11	23.7
DD5V2	35	-605	0.064	-1.66	787	0.102	1.39	22.3
DD6	31	-505	0.071	-1.40	605	0.100	1.15	21.1
DD7	54	-581	0.072	-1.03	832	0.147	0.40	32.0
DD8	42	-582	----	----	778	0.102	0.90	27.1
DD9	54	-556	----	----	907	0.137	0.46	34.6
DD10	62	-552	0.053	-0.90	956	0.143	0.35	42.5
DD11	31	-319	0.090	-0.70	592	0.100	1.20	20.0
DD11A	31	-350	----	----	604	----	----	19.5
DD12	43	-302	----	----	723	0.114	0.85	26.4
DD13	50	-314	0.094	-0.45	821	0.130	0.80	29.5

Table 15. Fatigue Summary Properties of MSU (RTM) Manufactured Materials

		R = 10			R = 0.1			
Material	V_F,%	UCS MPa	b_C	strain for 10^6 cycles, %	UTS, MPa	b_T	strain for 10^6 cycles, %	E, GPa
DD14	35	-428	----	----	728	0.133	0.60	25.1
DD15	25	-428	----	----	----	----	----	----
DD16	36	-418	----	----	672	0.120	0.103	18.2
DD17	37/52	-420	0.082	-0.96	782	0.148	0.45	22.3
DD17A	35/44	-265	0.074	-0.63	646	0.121	0.80	23.4
DD18	34/40	-508	----	----	730	0.116	1.00	22.6
DD18A	36/43	-325	----	----	700	0.120	0.90	22.7
DD19	34/47	-375	0.073	-0.96	710	0.129	0.75	22.0
DD19A	36/50	-293	0.079	-0.66	651	0.140	0.60	23.2
DD19B	36/50	----	----	----	694	0.134	0.70	24.5
DD20	34	-313	----	----	587	0.137	0.50	22.2
DD20A	37	----	----	----	639	0.140	0.55	25.5
DD22	30	-389	----	----	549	0.100	1.13	19.6
DD23	38	-494	----	----	647	0.092	1.05	27.4
DD24	39	-511	----	----	730	0.115	0.94	23.9
DD25	45	-483	----	----	743	0.126	0.65	28.1
DD25A	48	-629	----	----	783	0.121	0.75	28.5
DD25B	31	-419	----	----	514	0.102	1.03	19.3
DD25D	35/45	----	----	----	478	0.123	0.58	22.0
DD26	50	-567	0.082	-0.96	853	0.121	0.85	30.0
FFA	38	-553	----	----	716	0.123	0.80	24.2
FFB	38	-506	----	----	621	0.112	0.80	23.4
FFC	38	-499	----	----	624	0.121	0.79	22.9
FFD	38	-542	----	----	636	0.120	0.83	23.1
FFF	38	-596	----	----	664	0.123	0.80	23.9
GG	40	-628	----	----	970	0.116	1.10	28.0
ROV2	30	-244	----	----	362	0.110	0.72	21.5
ROV3	40	-203	----	----	422	0.120	0.65	20.9
ROV4	43	-314	----	----	505	0.150	0.35	26.7

Table 16. Fatigue Summary Properties of MSU (RTM) Manufactured Unidirectional Materials

		R = 10			R = 0.1			
Material	V_F %	UCS MPa	b_C	strain for 10^6 cycles, %	UTS, MPa	b_T	strain for 10^6 cycles, %	E, GPa
A060	41	-315	----	----	579	0.094	0.80	31.4
A130C	35	-373	0.062	-0.70	728	0.091	1.10	31.6
A130G	55	-423	----	-----	1,203	0.133	0.70	44.4
A260A	35	-440	----	-----	776	0.090	1.11	31.1
CM1701	38	-573	0.084	-0.93	796	0.126	0.64	30.5
DO72A	36	-560	0.075	-1.11	799	0.106	1.04	28.3
DO92B	41	-675	----	-----	908	0.104	1.03	33.8
DO92D	30	-540	----	-----	731	0.090	1.25	25.4
DO92F	50	-679	----	-----	1,112	0.121	0.70	40.8
DO92G	58	-692	0.085	-0.97	1,163	0.132	0.60	44.5
D155B	39	-653	0.077	-1.10	854	0.102	1.12	31.5
D155C	51	-794	----	-----	1,187	0.120	0.90	38.9
D155G	59	-765	0.057	-1.00	1,314	0.138	0.64	47.0
D155H	49	-755	----	-----	1,121	0.099	1.07	38.3
D155J	58	-776	----	-----	1,142	0.108	0.80	47.9
D155K	33	-551	----	----	861	0.114	0.98	28.1

Table 17. Fatigue Summary Properties of MSU Manufactured (RTM) Fiberglass Materials with Symmetric Angle Plies

		R = 10			R = 0.1				
Angle of D155 fabric	V_F%	UCS MPa	b_C	strain for 10^6 cycles, %	UTS, MPa	b_T	strain for 10^6 cycles, %	E, GPa	ν_{XY}
D155B (0)	39	-653	0.077	-1.10	854	0.093	1.12	31.5	0.32
±10	38	-384	----	-----	277	0.068	0.62	27.9	0.38
±20	39	-287	----	-----	268	0.079	0.55	24.2	0.56
±30	40	-176	0.065	-0.48	186	0.098	0.43	17.7	0.67
±40	40	-132	0.095	-0.50	144	0.109	0.41	11.4	0.62
±45	38	-138	0.089	-0.65	107	0.109	0.40	9.79	0.57
±50	39	-138	0.085	-0.78	65	0.092	0.38	8.62	0.51
±60	40	-141	0.081	-0.94	37	0.074	0.25	7.65	0.35
±70	40	-136	----	-----	27	0.076	0.19	7.24	0.21
±80	38	-153	----	-----	26	0.087	0.17	7.16	0.10
90	38	-123	0.062	-1.07	26	0.081	0.19	7.24	0.09
±45V2	36	-149	0.085	-0.71	136	0.119	0.45	10.3	0.57
±45P2	40	-160	----	----	96	0.109	0.35	11.4	0.56
±45V	40	-154	----	----	121	0.110	0.40	10.7	----
90V2	38	-171	----	----	54	0.107	0.21	8.85	----
90V	40	-167	----	----	49	0.108	0.18	10.3	----
90E2	38	-152	----	----	40	0.110	0.18	7.28	----

Matrix Abbreviations: E -Epoxy (Epon 9410), E2 -Epoxy (SC14), P -Ortho-polyester (COR63AX051), P2 -Iso-polyester (COR75AQ010), V-Vinyl ester (Derakane 411C), V2 -Vinyl ester (Derakane 8084).
All R = 10 test coupons were 25 mm wide with a 13 mm gage length and unsupported edges.

Table 18. Fatigue Summary Properties of R = -1 Tested Materials

Material	V_F, %	b_R,[1]	strain for 10^6 cycles, %	E, GPa
H	37	0.092	0.42	24.0
N	38	0.123	0.30	21.0
P	40	0.106	0.41	28.9
EEAV	48	0.100	0.70	28.2
AA	35	0.134	0.40	18.8
DD4	48	0.125	0.50	31.0
DD5E	36	0.109	0.65	23.6
DD5P	36	0.117	0.57	24.2
DD5V2	35	0.117	0.68	22.3
DD11	31	0.095	0.60	20.0
45D155	38	0.148	0.25	9.79

[1] No static test values were used in the linear regression curve fit.
All test coupons were 25 mm wide with a 13 mm gage length and unsupported edges.

Table 19. Fatigue Summary Properties of High Cycle Materials

Material	R	V_F %	UTS, MPa	UCS, MPa	strain for 10^6 cycles, %	strain for 10^8 cycles, %	E, GPa
$[0]_2$	0.1	52[1]	1470	----	0.90	0.67	46.2
	0.5	48	1357	----	1.36	1.00	39.2
	-1	52	1390	-584	0.55	0.40	39.2
	10	48	----	-789	-0.90	-0.80	35.7
	2	52	----	-789	-1.3	-1.20	35.4
	-0.5	48	1470	-716	0.65	0.52	40.2
$[90]_4$	0.1	38	21	----	0.14	0.12	8.62
	0.5		22	----	0.16	0.13	8.70
	-1		18	----	0.08	0.07	8.80
	10		----	-117	-0.70	-0.62	9.00
	2		----	-116	-0.95	-0.80	9.00
DD5P $(0/\pm45/0)_S$	0.1	36	661	-574	1.15	0.73	23.6
	0.5				1.30	1.06	
	-1				0.62	0.45	

[1] The $[0]_2$, R = 0.1 test coupons were thickness tapered, which increased the fiber volume in the gage length to 67%

SUMMARY OF COMMERCIAL MATERIAL FATIGUE TESTS

MATERIAL A

Lay-up = $[0]_5$, $V_F = 0.30$, Ave. thickness = 3.68 mm, S.D. = 0.13 mm, Polyester

TEST & SAMPLE ID #		MAX. STRESS MPa	R	Q Hz	E GPa	e %	CYCLES TO FAIL	WIDTH (mm) and Notes
5	105A	125	0.1	10	----	----	1,996,768	25 tab
6	108A	190	0.1	5	----	----	593,319	25 tab
7	110A	335	0.1	1	----	----	674	25 tab
23	111A	279	0.1	5	20.0	1.40	17,700	50 tab
25	112A	212	0.1	10	22.3	----	138,596	50 tab
30	121A	591	*	13	22.4	2.83	1	25 tab
31	120A	567	*	13	19.9	2.82	1	25 tab
32	119A	538	*	13	20.4	2.64	1	25 tab
36	114A	186	0.1	10	21.0	0.90	1,612,585	50 tab
37	113A	186	0.1	10	22.6	0.85	920,132	50 tab
97	137A	548	*	6	22.0	2.20	1	25 tab
98	136A	579	*	6	23.2	2.30	1	25 tab
180	138A	-323	*	6	----	----	1	25 tab
181	139A	-319	*	6	----	----	1	25 tab
182	140A	-298	*	6	----	----	1	25 tab
The following tensile coupons in this material were thickness tapered (versus standard ASTM D3039)								
2914	301A	551	*	13	----	----	1	25 tab
2915	309A	552	*	13	----	----	1	25 tab
2916	303A	611	*	13	----	----	1	25 tab
2917	305A	345	0.1	2	22.8	1.63	2,080	25 tab
2918	304A	345	0.1	2	25.8	1.44	1,244	25 tab
2919	308A	345	0.1	2	25.8	1.35	779	25 tab
2920	306A	276	0.1	4	22.4	1.23	19,034	25 tab
2921	311A	276	0.1	4	24.0	1.12	38,474	25 tab
2922	307A	190	0.1	12	23.8	0.66	18,865,901	25 tab
2923	310A	207	0.1	12	28.9	0.72	3,000,000	25 R tab
2924	312A	276	0.1	5	22.2	1.20	21,100	25 tab
2925	316A	207	0.1	12	----	----	8,266,515	25 tab

MATERIAL B

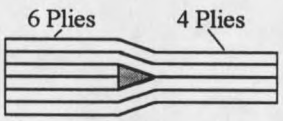
Lay-up = $[0]_5$, $V_F = 0.30$, Ave. thickness = 3.45 mm, S.D. = 0.26 mm, Vinylester

9	103B	370	0.1	1	21.8	2.06	2,584	25 tab
12	108B	267	0.1	5	22.5	1.21	9,173	25 tab
13	109B	328	0.1	5	20.9	1.60	2,640	25 tab
15	111B	387	0.1	0.1	18.6	1.82	7	25 tab
16	112B	256	0.1	5	20.1	1.29	38,133	25 tab
17	113B	332	0.1	5	21.4	1.53	2,841	25 tab
18	114B	372	0.1	1	19.5	1.90	415	25 tab
20	116B	321	0.1	5	19.2	1.6	3,008	25 tab
21	107B	321	0.1	4	22.6	1.4	32,640	25 tab
22	117B	229	0.1	10	----	----	655,147	50 tab
24	118B	343	0.1	1	16.3	2.12	981	50 tab
26	119B	571	*	13	22.3	2.63	1	25 tab

TEST & SAMPLE ID #		MAX. STRESS MPa	R	Q Hz	E GPa	e %	CYCLES TO FAIL	WIDTH (mm) and Notes
27	123B	622	*	13	21.4	2.73	1	25 tab
28	124B	571	*	13	21.2	2.76	1	25 tab
29	125B	582	*	13	22.8	2.77	1	25 tab
33	120B	229	0.1	10	21.2	1.08	16,156	50 tab
34	121B	237	0.1	5	19.2	1.24	206,864	50 tab
35	122B	229	0.1	10	23.1	0.99	671,330	50 tab
38	126B	190	0.1	10	20.8	0.90	2,310,849	50 tab
39	129B	154	0.1	15	19.9	0.76	40,000,000	50 R tab
40	130B	188	0.1	10	22.6	0.79	7,475,243	50 tab
56	135B	187	0.1	10	22.3	0.84	2,720,584	25 tab
57	133B	152	0.1	15	21.7	0.70	37,906,456	25 R tab
58	127B	619	*	25	22.4	2.90	1	25 tab
61	137B	568	*	25	20.3	2.79	1	25 tab
64	138B	245	*	25	----	----	1	25 tab
66	138B	343	0.1	1	20.9	1.64	6,085	25 tab
99	128B	560	*	6	19.9	2.82	1	25 tab
100	131B	559	*	6	24.4	2.29	1	25 tab
183	139B	-265	*	6	----	----	1	25 tab
184	140B	-283	*	6	----	----	1	25 tab
185	141B	-278	*	6	----	----	1	25 tab
186	142B	-303	*	6	----	----	1	25 tab
187	143B	-307	*	6	----	----	1	25 tab

MATERIAL F

Lay-up = $[(\pm 45/0)_3]_S$, $V_F = 0.36$, Had two center triax plies dropped, Ave. thickness = 4.88 mm (thin), 7.24 mm (thick), S.D. = 0.13 mm (thin) 0.16 mm (thick), Polyester. Maximum stress and strain recorded on smallest cross sectional area.

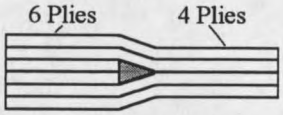


41	105F	370	*	13	17.8	2.80	1	25 tab
44	106F	363	*	13	14.6	2.55	1	25 tab
45	108F	339	*	13	19.2	2.37	1	25 tab
47	109F	195	0.1	5	----	----	2,689	25 tab
49	101F	102	0.1	5	----	----	95,101	50 tab
51	104F	78	0.1	10	----	----	1,615,838	50 tab
53	103F	78	0.1	10	----	----	2,487,507	50 tab
55	111F	102	0.1	10	----	----	108,029	25 tab
188	119F	-373	*	6	----	----	1	25 tab
189	120F	-364	*	6	----	----	1	25 tab
190	121F	-340	*	6	----	----	1	25 tab
191	122F	-378	*	6	----	----	1	25 tab

TEST & SAMPLE ID #		MAX. STRESS MPa	R	Q Hz	E GPa	e %	CYCLES TO FAIL	WIDTH (mm) and Notes

MATERIAL G

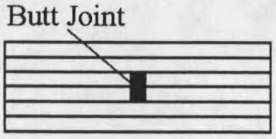
Lay-up = $[(0/\pm45)_3]_S$, $V_F = 0.36$, Has two center triax plies dropped, Ave. thickness = 4.83 mm (thin), 7.26 mm (thick), S.D. = 0.13 mm (thin) 0.17 mm (thick). Polyester matrix. Maximum stress, strain and modulus were recorded on smallest cross sectional area.



42	105G	397	*	13	15.9	2.49	1	25 tab
43	106G	366	*	13	16.4	2.71	1	25 tab
46	108G	332	*	25	----	----	1	25 tab
48	107G	190	0.1	5	----	----	2,637	25 tab
50	101G	103	0.1	10	----	----	69,052	50 tab
52	102G	77	0.1	10	----	----	1,669,945	50 tab
54	109G	103	0.1	10	----	----	65,372	25 tab
67	110G	78	0.1	10	17.8	0.43	11,160,358	25 tab
107	104G	352	*	6	19.6	1.50	1	25 tab
108	105G	358	*	6	20.4	1.75	1	25 tab
Tests 1925 - 1927 used the smaller cross sectional area with no joint.								
1925	200G	-266	*	13	----	----	1	25 tab
1926	201G	-228	*	13	----	----	1	25 tab
1927	202G	-280	*	13	----	----	1	25 tab

MATERIAL H

Lay-up = $[(\pm45/0)_3]_S$, $V_F = 0.39$, Ave. thickness = 6.58 mm, S.D. = 0.4 mm, Had two center triax plies cut to simulate a butt joint. Polyester matrix. Stress, strain and modulus were recorded the on average cross sectional area, no reduction multiplier was used to account for the center cut plies.

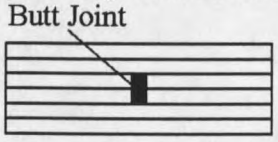


59	101H	429	*	25	25.8	2.24	1	25 tab
60	102H	597	*	25	18.8	2.42	1	25 tab
69	104H	172	0.1	5	25.2	0.68	45,360	25 tab
Tests 71, 72, 73 and 74 did not have a joint in the test gage section								
71	106H	485	*	5	24.6	2.1+	1	25 tab
72	107H	592	*	6	----	----	1	25 tab
73	108H	531	*	6	----	----	1	25 tab
74	109H	598	*	6	----	----	1	25 tab
Test 75 is a transverse test								
75	110HT	47	*	6	----	----	1	25 tab
76	105H	86	0.1	10	28.2	0.30	10,000,000	25 R tab
89	111H	87	0.1	15	23.4	0.43	20,500,167	25 tab
91	113H	207	0.1	1	27.2	0.73	16,137	25 tab
92	114H	131	0.1	10	24.0	0.60	69,425	25 tab
95	115H	162	0.1	10	20.8	0.76	11,417	25 tab
144	121H	103	-1	5	25.0	0.41	1,824,012	25 tab

TEST & SAMPLE ID #		MAX. STRESS MPa	R	Q Hz	E GPa	e %	CYCLES TO FAIL	WIDTH (mm) and Notes
147	122H	138	-1	5	25.2	0.55	21,713	25 tab
148	117H	138	-1	5	23.2	0.59	15,930	25 tab
192	116H	-431	*	6	----	----	1	25 tab
193	117H	-425	*	6	----	----	1	25 tab
Tests 221 and 222 involved coupons with a center 13 mm diameter hole, net section stresses and no joint.								
221	117H	-352	*	13	----	----	1	50 H tab
222	119H	-207	10	5	----	----	2,400	50 HR tab
235	123H	-138	10	15	25.8	-0.51	19,996	25 tab
Tests 236, 238, 240, 241, 243, 244, 245, 246, 247, 248, 249, 250, 251, 252, 253 do not have a joint								
236	126H	-138	10	20	24.5	-0.38	4,385,009	25 R tab
238	120H	-207	10	15	27.7	----	91,656	25 tab
239	116H	-138	10	15	24.5	----	6,000,000	25 R tab
240	119H	-138	10	20	23.5	-0.58	30,000,000	25 R tab
241	133H	138	0.1	15	----	----	1,401,491	25 tab
242	137H	138	0.1	15	----	----	5,420,000	25 R tab
243	136H	172	0.1	10	----	----	502,598	25 tab
244	131H	172	0.1	10	----	----	1,104,989	25 tab
245	132H	207	0.1	10	24.8	0.86	96,327	25 tab
246	135H	207	0.1	10	25.0	0.83	79,610	25 tab
247	130H	241	0.1	10	25.7	0.95	15,703	25 tab
248	139H	276	0.1	5	23.2	1.20	2,921	25 tab
249	143H	276	0.1	5	27.7	1.04	1,668	25 tab
250	140H	345	0.1	5	23.4	1.53	742	25 tab
251	138H	-207	10	15	26.8	-0.76	4,578	25 tab
252	141H	-207	10	15	24.6	-0.85	3,918	25 tab
253	149H	138	0.1	20	23.8	0.57	8,222,998	25 tab
254	150H	138	0.1	15	----	----	11,500,000	25 R tab
Tests 258, 259 and 260 do not have a joint								
258	118H	707	*	6	24.2	----	1	25 tab
259	150H	734	*	6	27.7	----	1	25 tab
260	151H	744	*	6	28.8	----	1	25 tab
269	125H	446	*	6	24.2	----	1	25 tab
270	128H	438	*	6	25.0	----	1	25 tab
4773	305H	103	-1	4	----	----	530,122	25
4774	302H	103	-1	4	----	----	379,953	25
4775	303H	138	-1	2	----	----	31,448	25

MATERIAL J

Lay-up = $[(0/\pm45)_3]_S$, $V_F = 0.43$, Ave. thickness = 6.63 mm, S.D. = 0.52 mm, Polyester, Stress and strain recorded on average cross sectional area, no multiplier was used to account for the center cut plies.



62	101J	475	*	25	27.0	2.83	1	25 tab
63	102J	398	*	25	23.7	2.60	1	25 tab
68	104J	172	0.1	5	22.8	0.77	17,882	25 tab

TEST & SAMPLE ID #		MAX. STRESS MPa	R	Q Hz	E GPa	e %	CYCLES TO FAIL	WIDTH (mm) and Notes
70	105J	86	0.1	10	26.2	0.31	11,000,000	25 R tab
81	106J	65	0.1	15	22.6	0.26	18,000,000	25 R tab
82	107J	75	0.1	15	27.3	0.28	30,300,000	25 R tab
93	108J	124	0.1	10	23.1	0.54	153,500	25 R tab
127	110J	103	0.1	15	24.2	0.42	1,460,000	25 tab
194	111J	-403	*	6	----	----	1	25 tab
195	112J	-417	*	6	----	----	1	25 tab
Tests 220 and 223 involved coupons with a center 13 mm diameter hole, net section stresses and no joint.								
220	113J	-226	*	3	----	----	1	50 H tab
223	114J	-138	10	10	----	----	6,500,000	50 HR tab
Tests 261, 262, 263 do not have a joint								
261	140J	723	*	6	26.3	----	1	25 tab
262	141J	711	*	6	25.7	----	1	25 tab
263	142J	689	*	6	24.2	----	1	25 tab
268	115J	446	*	6	24.5	----	1	25 tab

MATERIAL L

Lay-up = $[0]_3$, $V_F = 0.50$, Ave. thickness = 2.46 mm, S.D. = 0.26 mm, Polyester

77	101L	410	0.1	1	35.4	1.18	2,580	25 tab
78	103L	406	0.1	1	30.9	1.32	593	25 tab
79	102L	276	0.1	5	31.5	0.87	59,081	25 tab
80	104L	266	0.1	5	29.0	0.97	45,848	25 tab
83	109L	325	0.1	10	34.5	0.91	153,402	25 tab
84	127L	259	0.1	10	32.4	0.93	856,066	25 tab
101	117L	740	*	6	30.8	2.40	1	25 tab
102	119L	745	*	6	36.6	2.21	1	25 tab
196	122L	-325	*	6	----	----	1	25 tab
197	123L	-332	*	6	----	----	1	25 tab
198	125L	-328	*	6	----	----	1	25 tab
199	126L	-351	*	6	----	----	1	25 tab
231	126L	-361	*	6	----	----	1	50 tab
232	127L	-444	*	6	----	----	1	50 tab
233	128L	-416	*	6	----	----	1	50 tab
The following tensile coupons in this material were thickness tapered (versus standard ASTM D3039)								
2926	130L	807	*	13	37.4	2.20	1	25 tab
2927	134L	767	*	13	31.9	2.45	1	25 tab
2928	133L	683	*	13	39.6	1.75	1	25 tab
2929	131L	414	0.1	2	39.4	1.10	1,651	25 tab
2930	106L	414	0.1	2	40.0	1.09	2,814	25 tab
2931	125L	414	0.1	2	43.3	1.03	4,755	25 tab
2932	111L	345	0.1	4	38.5	0.92	14,578	25 tab
2933	135L	345	0.1	4	39.1	0.91	9,731	25 tab
2934	129L	276	0.1	10	38.4	0.74	187,213	25 tab

TEST & SAMPLE ID #		MAX. STRESS MPa	R	Q Hz	E GPa	e %	CYCLES TO FAIL	WIDTH (mm) and Notes
MATERIAL M								
Lay-up = $[0/\pm45]_4$, V_F = 0.38, Ave. thickness = 3.10 mm, S.D. = 0.10 mm, Vinylester								
129	101M	69	0.1	15	21.4	0.32	17,764,694	50 tab
130	102M	76	0.1	15	21.0	0.36	6,899,599	50 tab
131	104M	525	*	60	21.0	2.62	1	50 tab
132	113M	507	*	60	20.2	2.90	1	50 tab
133	112M	138	0.1	10	21.6	0.66	18,650	50 tab
134	106M	138	0.1	10	21.2	0.66	22,360	50 tab
135	109M	207	0.1	5	19.3	1.12	2,319	50 tab
136	103M	207	0.1	5	19.1	1.12	2,855	50 tab
137	114M	276	0.1	5	20.1	1.43	687	50 tab
138	105M	276	0.1	5	19.2	1.44	879	50 tab
139	115M	103	0.1	15	21.0	0.49	86,249	50 tab
140	107M	103	0.1	15	20.9	0.49	174,168	50 tab
141	118M	86	0.1	15	20.5	0.41	397,000	50 tab
142	110M	86	0.1	15	22.4	0.39	266,000	50 tab
143	108M	76	0.1	15	21.4	0.36	2,498,512	50 tab
200	124M	-275	*	6	----	----	1	25 tab
201	123M	-295	*	6	----	----	1	25 tab
202	122M	-289	*	6	----	----	1	25 tab
203	125M	-284	*	6	----	----	1	25 tab
228	126M	-267	*	3	----	----	1	50 tab
229	127M	-291	*	6	----	----	1	50 tab
230	128M	-301	*	6	----	----	1	50 tab
MATERIAL N								
Lay-up = $[0/\pm45]_4$, V_F = 0.36, Ave. thickness = 3.23 mm, S.D. = 0.08 mm, Polyester								
Tests 85, 86, 87, 88, 96, 105, 106, 109, 110, 114, 3054 were transverse tests								
85	111NT	86	*	6	----	3.28	1	25 tab
86	101NT	54	0.1	1	8.62	1.34	6,479	25 tab
87	102NT	68	0.1	1	7.86	1.70	470	50 tab
88	104NT	35	0.1	5	8.55	0.45	511,047	50 tab
96	103NT	21	0.1	15	9.10	0.23	34,000,000	50 R tab
103	011N	482	*	6	20.9	2.97	1	25 tab
104	012N	468	*	6	20.9	2.84	1	25 tab
105	113NT	87	*	6	6.90	3.82	1	25 tab
106	114NT	90	*	6	9.17	2.29	1	25 tab
109	111NT	54	0.1	1	8.83	1.15	7,950	50 tab
110	112NT	68	0.1	1	6.69	1.42	711	50 tab
111	117N	388	0.1	1	17.0	2.74	27	25 tab
112	116N	276	0.1	1	18.2	1.63	626	25 tab
113	120N	276	0.1	5	17.3	1.70	811	25 tab
114	114NT	35	0.1	15	8.20	0.42	1,634,579	50 tab
115	118N	207	0.1	5	19.2	1.08	5,684	25 tab
116	119N	207	0.1	5	19.7	1.05	4,871	25 tab
117	010N	138	0.1	10	20.1	0.73	25,371	50 tab

TEST & SAMPLE ID #		MAX. STRESS MPa	R	Q Hz	E GPa	e %	CYCLES TO FAIL	WIDTH (mm) and Notes
118	009N	138	0.1	10	19.5	0.71	25,781	50 tab
119	129N	138	0.1	10	20.4	0.69	37,597	50 tab
120	128N	138	0.1	10	19.2	0.72	29,230	50 tab
121	131N	103	0.1	15	18.4	0.56	231,826	50 tab
122	130N	86	0.1	15	19.8	0.42	1,336,695	50 tab
123	006N	345	0.1	1	19.2	1.82	150	50 tab
124	126N	76	0.1	15	19.7	0.39	1,648,137	50 tab
125	008N	69	0.1	15	19.9	0.34	7,825,000	50 tab
126	121N	103	0.1	15	19.0	0.54	165,980	50 tab
128	127N	69	0.1	15	19.3	0.35	4,005,593	50 tab
145	116N	462	*	60	20.2	2.81	1	50 tab
146	117N	459	*	60	18.9	2.75	1	50 tab
For reversed and compression loading, a gage length of 38 mm was used.								
149	132N	86	-1	5	22.8	0.36	105,505	50 tab
150	133N	86	-1	10	21.5	0.38	240,528	50 tab
151	134N	138	-1	5	21.5	0.61	5,570	50 tab
152	137N	138	-1	5	24.6	0.56	13,337	50 tab
153	135N	69	-1	15	21.9	0.29	1,189,053	50 tab
154	136N	69	-1	15	23.4	0.29	1,282,726	50 tab
155	138N	-138	10	15	23.5	-0.61	1,098,374	50 tab
156	139N	-103	10	20	23.5	-0.44	26,707,000	50 R tab
158	145N	-103	10	20	25.6	-0.41	25,738,868	50 tab
159	140N	-138	10	15	23.5	-0.60	367,505	50 tab
160	143N	-172	10	10	25.0	-0.69	292,181	50 tab
161	142N	-172	10	10	23.7	-0.74	32,227	50 tab
208	151N	-318	*	13	----	----	1	25 tab
209	152N	-334	*	13	----	----	1	25 tab
210	153N	-301	*	13	----	----	1	25 tab
3054	201NT	-131	*	13	----	----	1	25 tab

MATERIAL P

Lay-up = $[0/\pm45/M/0]_S$, $V_F = 0.36$, Ave. thickness = 3.78 mm, S.D. = 0.23 mm, Vinylester

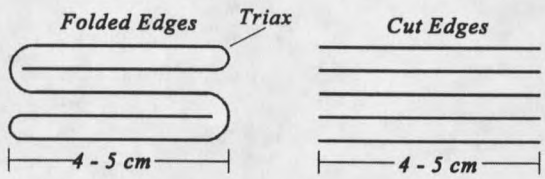
163	108P	612	*	60	28.1	2.73	1	25 tab
164	107P	716	*	60	26.8	2.89	1	25 tab
165	105P	103	0.1	15	23.3	0.44	2,808,490	50 tab
166	108P	103	0.1	15	27.8	0.38	5,985,000	50 tab
168	101P	276	0.1	5	22.1	1.27	7,251	50 tab
169	103P	276	0.1	5	24.6	1.12	6,354	50 tab
170	102P	207	0.1	10	26.1	0.82	38,469	50 tab
171	106P	207	0.1	10	26.3	0.80	28,198	50 tab
172	107P	345	0.1	5	25.9	1.40	1,467	50 tab
173	104P	345	0.1	5	24.0	1.45	1,773	50 tab
174	111P	414	0.1	5	19.0	2.22	296	50 tab
175	112P	138	0.1	15	26.9	0.52	900,000	50 tab
176	126P	674	*	60	28.8	2.60	1	25 tab
177	115P	414	0.1	5	29.1	0.93	216	50 tab
178	113P	138	0.1	15	23.4	0.60	715,000	50 tab
179	116P	76	-1	20	29.2	0.26	15,000,000	50 R tab

TEST & SAMPLE ID #		MAX. STRESS MPa	R	Q Hz	E GPa	e %	CYCLES TO FAIL	WIDTH (mm) and Notes
For reversed and compression loading, a gage length of 38 mm was used.								
204	132P	-288	*	6	----	----	1	25 tab
205	133P	-333	*	6	----	----	1	25 tab
206	136P	-319	*	6	----	----	1	25 tab
207	137P	-343	*	6	----	----	1	25 tab
211	120P	138	-1	10	29.4	0.44	139,604	50 tab
212	123P	207	-1	5	29.5	0.70	938	50 tab
213	121P	207	-1	5	27.2	0.74	1,320	50 tab
214	122P	138	-1	10	28.3	0.46	76,483	50 tab
215	125P	-207	10	10	28.0	-0.63	14,121	50 tab
216	124P	-138	10	20	30.9	-0.40	6,000,000	50 R tab
217	119P	-207	10	10	30.4	-0.63	21,177	50 tab
218	117P	-172	10	20	25.0	-0.82	1,094,359	50 tab
219	118P	-172	10	20	31.4	-0.51	8,020,000	50 R tab
224	119P	-138	10	20	----	----	1,189,000	50 R tab
225	130P	-396	*	3	----	----	1	50 tab
226	131P	-477	*	6	----	----	1	50 tab
227	132P	-526	*	6	----	----	1	50 tab
MATERIAL R								
Lay-up = $[0/\pm45]_4$, $V_F = 0.32$, Ave. thickness = 3.56 mm, S.D. = 0.07 mm, Polyester								
255	101R	412	*	6	16.6	2.50	1	25 tab
256	102R	427	*	6	16.6	2.63	1	25 tab
257	107R	138	0.1	15	17.0	0.31	7,842,000	50 tab
264	105R	276	0.1	5	14.8	2.13	925	50 tab
265	111R	483	*	6	17.7	3.41	1	50 tab
266	108R	207	0.1	10	16.3	1.31	6,967	50 tab
267	104R	207	0.1	10	16.9	1.31	6,035	50 tab
270	109R	138	0.1	15	16.0	0.93	8,170,168	50 tab
271	103R	138	0.1	15	15.7	0.90	820,153	50 tab
272	112R	172	0.1	15	17.1	----	972,000	50 tab
273	106R	190	0.1	10	----	----	230,233	50 tab
274	110R	190	0.1	10	----	----	115,056	50 tab
276	114R	190	0.1	15	----	----	4,932,613	50 tab
277	118R	345	0.1	1	17.4	2.52	60	50 tab
278	117R	345	0.1	1	----	----	41	50 tab
279	125R	276	0.1	2	----	----	1,072	50 tab
280	126R	207	0.1	7	----	----	17,096	50 tab
281	119R	190	0.1	10	----	----	505,551	50 tab
282	124R	155	0.1	15	----	----	1,942,442	50 tab
284	120R	436	*	6	----	----	1	50 tab
285	121R	426	*	6	----	----	1	50 tab
1928	200R	-287	*	13	----	----	1	25 tab
1929	201R	-297	*	13	----	----	1	25 tab
1930	202R	-286	*	13	----	----	1	25 tab
3080	403R	-317	*	13	----	----	1	25 tab
3081	402R	-321	*	13	----	----	1	25 tab
3082	401R	-353	*	13	----	----	1	25 tab

TEST & SAMPLE ID #		MAX. STRESS MPa	R	Q Hz	E GPa	e %	CYCLES TO FAIL	WIDTH (mm) and Notes
4460	405R	207	0.1	4	----	----	10,713	50 tab
4461	406R	207	0.1	4	----	----	202,846	50 tab
4462	407R	207	0.1	4	----	----	35,270	50 tab
4463	408R	207	0.1	4	----	----	43,407	50 tab
4464	409R	190	0.1	4	----	----	473,815	50 tab
4465	410R	190	0.1	4	----	----	519,652	50 tab
4466	411R	276	0.1	2	----	----	2,473	50 tab

MATERIAL T

Lay-up = $[0/\pm45]_5$, $V_F = 0.30$, Ave. thickness = 4.34 mm, S.D. = 0.22 mm, Polyester. Materials T, U, V and W involved folded fabric edges (T and U) and cut fabric edges to study test coupon edge effects.



1306	T1	366	*	6	----	----	1	50 tab
1307	T2	145	0.1	15	----	----	64,333	50 tab
1308	T3	100	0.1	15	----	----	701,345	50 tab
1309	T5	86	0.1	15	----	----	2,069,625	50 tab
1310	T6	101	0.1	15	----	----	1,731,348	50 tab
1311	T7	145	0.1	10	----	----	56,979	50 tab
1312	T8	107	0.1	15	----	----	615,110	50 tab
1313	T9	369	*	6	----	----	1	50 tab
1916	T200	252	*	13	17.7	3.47	1	25 tab
1917	T201	-313	*	13	----	----	1	25 tab
1918	T202	-267	*	13	----	----	1	25 tab

MATERIAL U

Lay-up = $[0/\pm45]_5$, $V_F = 0.29$, Ave. thickness = 4.55 mm, S.D. = 0.18 mm, Polyester. Materials T, U, V and W involved folded fabric edges (T and U) and cut fabric edges to study test coupon edge effects.

1314	U1	336	*	6	----	----	1	50 tab
1315	U2	138	0.1	--	----	----	14,573	50 tab
1316	U3	102	0.1	--	----	----	114,237	50 tab
1317	U4	86	0.1	15	----	----	400,500	50 tab
1318	U5	69	0.1	15	----	----	2,278,230	50 tab
1319	U6	102	0.1	15	----	----	178,679	50 tab
1320	U7	69	0.1	10	----	----	2,422,608	50 tab
1321	U8	138	0.1	10	----	----	16,591	50 tab
1322	U9	421	*	6	----	----	1	50 tab
1931	U200	416	*	13	21.2	2.51	1	25 tab
1932	U201	-364	*	13	----	----	1	25 tab
1933	U202	-345	*	13	----	----	1	25 tab

TEST & SAMPLE ID #		MAX. STRESS MPa	R	Q Hz	E GPa	e %	CYCLES TO FAIL	WIDTH (mm) and Notes
MATERIAL V								
Lay-up = $[0/\pm45]_5$, V_F = 0.32, Ave. thickness = 3.33 mm, S.D. = 0.30 mm, Polyester. Materials T, U, V and W involved folded fabric edges (T and U) and cut fabric edges to study test coupon edge effects.								
1323	V1	460	*	6	----	----	1	50 tab
1324	V2	489	*	6	----	----	1	50 tab
1325	V3	138	0.1	5	----	----	28,861	50 tab
1326	V4	138	0.1	5	----	----	35,501	50 tab
1327	V5	172	0.1	1	----	----	11,273	50 tab
1328	V6	172	0.1	1	----	----	12,339	50 tab
1329	V7	103	0.1	10	----	----	123,370	50 tab
1330	V8	103	0.1	10	----	----	111,873	50 tab
1331	V9	86	0.1	15	----	----	950,987	50 tab
1332	V10	86	0.1	15	----	----	871,319	50 tab
1333	V11	69	0.1	15	----	----	7,871,024	50 tab
1334	V15	86	0.1	15	----	----	848,378	50 tab
1335	V16	86	0.1	15	----	----	791,827	50 tab
1336	V17	103	0.1	10	----	----	222,481	50 tab
1337	V18	172	0.1	1	----	----	11,370	50 tab
1338	V20	138	0.1	5	----	----	23,829	50 tab
1339	V27	382	*	6	18.5	----	1	25 tab
1340	V30	377	*	6	19.7	----	1	25 tab
1341	V31	393	*	6	20.1	----	1	25 tab
1919	V200	-363	*	13	----	----	1	25 tab
1920	V201	-392	*	13	----	----	1	25 tab
1921	V202	-383	*	13	----	----	1	25 tab
MATERIAL W								
Lay-up = $[0/\pm45]_5$, V_F = 0.33, Ave. thickness = 3.43 mm, S.D. = 0.07 mm, Polyester. Materials T, U, V and W involved folded fabric edges (T and U) and cut fabric edges to study test coupon edge effects.								
1342	W1	172	0.1	2	19.0	----	25,839	50 tab
1343	W2	172	0.1	2	19.1	----	30,040	50 tab
1344	W5	138	0.1	10	----	----	311,392	50 tab
1345	W6	138	0.1	10	----	----	154,745	50 tab
1346	W7	103	0.1	15	----	----	5,040,762	50 tab
1347	W8	359	*	6	----	----	1	50 tab
1348	W9	435	*	6	----	----	1	50 tab
1349	W10	121	0.1	10	----	----	502,900	50 tab
1350	W11	121	0.1	10	----	----	1,071,927	50 tab
1351	W12	103	0.1	15	----	----	3,464,238	50 tab
1352	W13	86	0.1	15	----	----	27,537,000	50 R tab
1922	W200	-302	*	13	----	----	1	25 tab
1923	W201	-355	*	13	----	----	1	25 tab
1924	W202	-351	*	13	----	----	1	25 tab

TEST & SAMPLE ID #		MAX. STRESS MPa	R	Q Hz	E GPa	e %	CYCLES TO FAIL	WIDTH (mm) and Notes
MATERIAL X								
Lay-up = $[0_2/M/\pm45/0_2]$, $V_F = 0.35$, Ave. thickness = 4.52 mm, S.D. = 0.24 mm, Polyester								
304	107X	624	*	13	25.6	2.59	1	25 tab
305	102X	595	*	13	23.7	2.51	1	25 tab
306	103X	617	*	13	24.6	2.97	1	25 tab
309	112X	276	0.1	10	23.0	1.26	255,862	25 tab
310	105X	414	0.1	5	25.5	1.76	1,753	25 tab
311	106X	414	0.1	5	23.0	1.86	953	25 tab
312	104X	345	0.1	5	25.9	1.32	15,414	25 tab
313	108X	345	0.1	5	25.2	1.36	11,550	25 tab
314	101X	241	0.1	20	25.4	0.94	6,492,710	25 tab
315	109X	276	0.1	10	26.3	1.06	127,309	25 tab
Tests 316 - 320, 328, 330 - 335, 337, 363, 485 - 489, 1837, 1838 were transverse tests								
316	116XT	39	*	13	7.7	0.83	1	25 tab
317	118XT	45	*	13	7.6	0.72	1	25 tab
318	117XT	43	*	13	7.9	0.92	1	25 tab
319	119XT	28	0.1	2	9.0	0.28	1,083	25 tab
320	124XT	21	0.1	15	8.3	0.24	50,606	25 tab
321	110X	241	0.1	20	25.0	0.97	5,000,000	25 R tab
322	114X	241	0.1	20	26.0	0.91	21,000,000	25 R tab
323	113X	241	0.1	20	26.7	0.90	20,000,000	25 R tab
327	151X	-241	10	10	27.4	-0.84	3,175,600	25 tab
328	126XT	19	0.1	15	9.1	0.25	614,730	50 tab
329	142X	-207	10	25	26.3	-0.68	21,000,000	25 R tab
330	130XT	19	0.1	10	8.6	0.27	436,440	50 tab
331	132XT	17	0.1	20	8.3	0.21	785,700	50 R tab
332	128XT	17	0.1	20	8.5	0.23	1,132,780	50 R tab
333	134XT	28	0.1	2	8.3	0.37	2,074	50 tab
334	129XT	28	0.1	2	8.4	0.34	1,545	50 tab
335	135XT	17	0.1	20	7.3	0.24	897,103	50 tab
336	144X	-241	10	10	26.7	-0.94	3,500,000	25 R tab
337	133XT	14	0.1	15	8.0	0.19	10,377,400	50 tab
363	131XT	14	0.1	15	8.0	0.17	11,247,700	50 tab
378	159X	-435	*	13	25.0	-1.74	1	25 Z
379	158X	-430	*	13	26.8	-1.70	1	25 Z
380	165X	-450	*	13	26.1	-1.98	1	25 Z
381	161X	-310	10	2	23.4	-1.41	12,455	25 Z
382	164X	-310	10	2	25.7	-1.37	12,865	25 Z
383	157X	-276	10	5	24.8	-1.20	271,161	25 Z
384	160X	-276	10	5	24.2	-1.07	333,581	25 Z
385	156X	-276	10	10	25.9	-1.10	161,397	25 Z
386	162X	-241	10	10	26.1	-0.93	1,472,970	25 Z
482	139X	414	0.1	5	25.6	1.67	1,223	25 tab
483	152X	345	0.1	5	25.7	1.45	11,786	25 tab
484	153X	276	0.1	10	26.6	1.06	169,031	25 tab
485	136XT	24	0.1	5	9.3	0.26	21,745	50 tab
486	123XT	24	0.1	5	9.0	0.25	15,040	50 tab
487	125XT	47	*	13	10.1	0.52	1	25 tab

TEST & SAMPLE ID #		MAX. STRESS MPa	R	Q Hz	E GPa	e %	CYCLES TO FAIL	WIDTH (mm) and Notes
488	120XT	24	0.1	5	10.1	0.24	18,858	25 tab
489	121XT	19	0.1	10	9.5	0.22	587,181	25 tab
705	177X	-310	10	2	24.5	1.39	14,129	25 tab
1837	201XT	-170	*	13	----	----	1	25 tab
1838	127XT	-149	*	13	----	----	1	25 tab
MATERIAL Y								
Lay-up = $[0_2/M/\pm45/0_2]$, $V_F = 0.39$, Ave. thickness = 4.62 mm, S.D. = 0.48 mm, Epoxy								
286	111Y	583	*	100	23.1	2.72	1	25 tab
287	117Y	591	*	100	21.3	3.12	1	25 tab
288	105Y	611	*	100	22.5	2.91	1	25 tab
289	112Y	276	0.1	25	27.4	0.53	251,141	25 tab
290	108Y	207	0.1	25	24.4	0.79	1,412,113	25 tab
291	118Y	345	0.1	15	23.6	1.33	23,109	25 tab
292	113Y	345	0.1	15	25.9	1.28	18,000	25 tab
293	104Y	345	0.1	15	23.9	1.24	16,762	25 tab
294	116Y	414	0.1	4	27.2	1.83	628	25 tab
295	106Y	276	0.1	25	25.1	1.11	73,530	25 tab
296	102Y	414	0.1	4	22.4	1.71	821	25 tab
297	107Y	276	0.1	25	20.8	1.27	128,578	25 tab
298	115Y	276	0.1	25	20.4	0.93	237,864	25 tab
299	119Y	207	0.1	25	25.9	0.77	1,607,127	25 tab
300	114Y	661	*	13	24.3	2.80	1	25 tab
301	110Y	687	*	13	28.1	2.54	1	25 tab
302	109Y	620	*	13	24.2	2.56	1	25 tab
303	101Y	207	0.1	15	25.3	0.87	15,000,000	25 R tab
481	170Y	-276	10	5	24.3	1.13	62,517	25 tab
490	125Y	414	0.1	4	29.7	1.70	1,486	25 tab
491	121Y	345	0.1	5	29.7	1.54	36,812	25 tab
493	123Y	276	0.1	5	28.7	1.01	423,059	25 tab
494	127Y	207	0.1	15	26.6	0.86	10,000,000	25 R tab
Tests 495 - 512, 1839 - 1841 were transverse tests								
495	141YT	29	*	13	7.7	0.67	1	50 tab
496	145YT	29	*	13	7.5	0.79	1	50 tab
497	146YT	30	*	13	6.8	0.85	1	50 tab
498	152YT	21	0.1	2	7.1	0.48	4,103	50 tab
499	144YT	21	0.1	2	7.0	0.41	2,716	50 tab
500	147YT	17	0.1	10	6.5	0.34	26,513	50 tab
501	143YT	17	0.1	10	7.5	0.29	47,049	50 tab
502	140YT	24	0.1	1	7.2	1.35	208	50 tab
503	151YT	24	0.1	1	7.1	1.22	277	50 tab
504	148YT	14	0.1	15	6.9	0.25	252,205	50 tab
505	142YT	14	0.1	15	6.3	0.22	432,161	50 tab
506	149YT	14	0.1	15	6.9	0.20	657,472	50 tab
507	157YT	24	0.1	1	7.2	1.37	173	50 tab
508	153YT	21	0.1	2	6.6	0.37	2,033	50 tab
509	155YT	17	0.1	10	6.6	0.26	31,204	50 tab
510	159YT	33	*	13	7.6	----	1	50 tab

TEST & SAMPLE ID #		MAX. STRESS MPa	R	Q Hz	E GPa	e %	CYCLES TO FAIL	WIDTH (mm) and Notes
511	161YT	32	*	13	7.5	----	1	50 tab
512	160YT	35	*	13	7.5	----	1	50 tab
543	168Y	-391	*	13	----	----	1	25
544	181Y	-389	*	13	----	----	1	25
545	176Y	-341	*	13	----	----	1	25
546	171Y	-369	*	13	----	----	1	25
547	172Y	-276	10	10	----	----	87,235	25
548	167Y	-310	10	5	----	----	354	25
549	166Y	-241	10	20	21.5	1.18	4,000,000	25 R
581	170Y	-276	10	5	24.3	1.13	62,517	25
686	193Y	-329	*	13	----	----	1	25 Z
687	182Y	-359	*	13	----	----	1	25 Z
688	184Y	-355	*	13	----	----	1	25 Z
689	178Y	-310	10	2	----	----	568	25 Z
690	197Y	-293	10	2	----	----	12,145	25 Z
691	200Y	-293	10	5	----	----	3,011	25 Z
692	190Y	-293	10	2	----	----	4,652	25 Z
693	187Y	-310	10	2	----	----	672	25 Z
694	199Y	-276	10	10	----	----	187,512	25 Z
695	196Y	-483	*	25	----	----	1	25
696	193Y	-450	*	25	----	----	1	25
697	192Y	-431	*	25	----	----	1	25
699	201Y	-258	10	15	----	----	632,624	25
701	173Y	-258	10	15	23.9	-1.09	833,939	25
702	169Y	-258	10	15	26.3	-0.98	1,477,548	25
706	195Y	-241	10	20	----	----	1,672,575	25
1839	201YT	-95	*	13	----	----	1	25 tab
1840	202YT	-116	*	13	----	----	1	25 tab
1841	203YT	-112	*	13	----	----	1	25 tab

MATERIAL EE

Lay-up = $[M/\pm45/0]_S$, $V_F = 0.54$, Ave. thickness = 3.53 mm, S.D. = 0.10 mm, Epoxy, Coupons taken from a pultruded blade section.

1178	EE101	565	*	13	28.8	2.23	1	20 tab
1179	EE102	546	*	13	34.5	1.76	1	20 tab
1180	EE103	518	*	13	30.7	1.78	1	20 tab
1181	EE104	345	0.1	2	32.1	1.14	570	20 tab
1182	EE112	310	0.1	4	29.2	1.07	1,085	20 tab
1183	EE105	276	0.1	5	30.1	0.93	4,076	20 tab
1184	EE111	207	0.1	10	32.8	0.65	34,583	20 tab
1185	EE110	138	0.1	20	33.2	0.43	1,857,630	20 tab
1186	EE107	345	0.1	2	----	----	402	13 tab
1187	EE109	276	0.1	5	----	----	2,936	13 tab
1188	EE108	310	0.1	5	----	----	2,033	13 tab
1189	EE106	207	0.1	10	----	----	23,385	13 tab
1190	EE119	310	0.1	5	----	----	1,840	13 tab
1191	EE121	276	0.1	5	----	----	2,377	13 tab
1192	EE114	207	0.1	10	----	----	58,110	13 tab

TEST & SAMPLE ID #		MAX. STRESS MPa	R	Q Hz	E GPa	e %	CYCLES TO FAIL	WIDTH (mm) and Notes
1193	EE115	172	0.1	15	----	----	496,094	13 tab
1194	EE120	172	0.1	15	----	----	287,688	13 tab
1195	EE125	241	0.1	5	----	----	10,021	13 tab
1196	EE126	241	0.1	5	----	----	8,786	13 tab
1197	EE116	172	0.1	20	----	----	224,138	13 tab
1198	EE128	-546	*	13	----	----	1	13 tab
1199	EE129	-550	*	13	----	----	1	13 tab
1200	EE113	138	0.1	20	----	----	3,804,099	13 tab
1201	EE131	-519	*	13	----	----	1	13 tab
1202	EE118	138	0.1	20	----	----	4,622,485	13 tab
1203	EE128	510	*	13	----	----	1	13 tab

MATERIAL EEAV

Lay-up = $[M/\pm45/0]_S$, $V_F = 0.48$, Ave. thickness = 3.36 mm, S.D. = 0.24 mm, Vinyl ester, Coupons taken from a pultruded blade section.

2716	EEAV105	619	*	13	29.0	2.47	1	20
2717	EEAV106	559	*	13	26.3	2.31	1	20
2718	EEAV101	569	*	13	26.6	2.33	1	20
2719	EEAV107	345	0.1	2	29.0	1.30	1,836	20
2720	EEAV109	345	0.1	2	28.1	1.31	3,260	20
2721	EEAV103	276	0.1	5	27.7	1.01	27,047	20
2722	EEAV108	276	0.1	5	29.2	1.01	43,424	20
2723	EEAV102	207	0.1	12	27.2	0.79	2,414,147	20
2724	EEAV144	207	0.1	20	28.6	0.74	1,366,767	20
2725	EEAV143	345	0.1	4	28.9	1.29	2,811	20
2726	EEAV145	276	0.1	5	29.8	1.00	35,462	20
2737	EEAV114	-657	*	13	----	----	1	25
2738	EEAV125	-666	*	13	----	----	1	25
2739	EEAV110	-614	*	13	----	----	1	25
2746	EEAV124	-448	10	5	----	----	7,498	25
2747	EEAV126	-448	10	5	----	----	5,539	25
2748	EEAV111	-448	10	5	----	----	3,169	25
2749	EEAV115	-345	10	20	----	----	5,000,000	25 R
2750	EEAV113	-396	10	12	----	----	93,149	25
2751	EEAV112	-396	10	12	----	----	38,280	25
2752	EEAV117	-396	10	12	----	----	72,451	25
2753	EEAV116	207	-1	5	----	----	145,367	25
2754	EEAV122	207	-1	10	----	----	231,003	25
2755	EEAV123	276	-1	2	----	----	1,866	25
2756	EEAV121	276	-1	2	----	----	3,412	25
2757	EEAV120	276	-1	2	----	----	2,875	25
2758	EEAV119	207	-1	5	----	----	92,539	25
2759	EEAV118	190	-1	10	----	----	74,105	25
Tests 2760 - 2765 were transverse tests								
2760	EEAV204T	76	*	13	15.9	0.48	1	25
2761	EEAV203T	81	*	13	14.6	0.63	1	25
2762	EEAV201T	86	*	13	14.2	0.71	1	25
2763	EEAV205T	-195	*	13	----	----	1	25

TEST & SAMPLE ID #		MAX. STRESS MPa	R	Q Hz	E GPa	e %	CYCLES TO FAIL	WIDTH (mm) and Notes
2764	EEAV206T	-197	*	13	----	----	1	25
2765	EEAV207T	-192	*	13	----	----	1	25

MATERIAL EEAP

Lay-up = $[M/\pm45/0]_S$, $V_F = 0.49$, Ave. thickness = 3.64 mm, S.D. = 0.10 mm, Polyester, Coupons taken from a pultruded blade section.

2797	EEAP101	505	*	13	29.5	2.0	1	20
2798	EEAP106	501	*	13	27.8	2.1	1	20
2799	EEAP109	529	*	13	30.2	2.0	1	20
2800	EEAP112	345	0.1	2	30.0	1.15	1,958	20
2801	EEAP102	345	0.1	2	27.0	1.20	890	20
2802	EEAP108	345	0.1	2	29.1	1.24	573	20
2803	EEAP111	276	0.1	4	31.2	0.90	9,912	20
2804	EEAP105	276	0.1	5	27.6	1.04	17,575	20
2805	EEAP104	276	0.1	5	29.2	1.03	15,403	20
2806	EEAP103	207	0.1	15	28.8	0.74	1,596,779	20
2807	EEAP110	207	0.1	15	28.3	0.73	2,483,304	20
2809	EEAP122	-716	*	13	----	----	1	25
2810	EEAP119	-750	*	13	----	----	1	25
2811	EEAP125	-721	*	13	----	----	1	25
2812	EEAP123	-448	10	4	----	----	6,703	25
2813	EEAP121	-448	10	4	----	----	16,229	25
2814	EEAP124	-448	10	4	----	----	18,158	25
2815	EEAP118	-396	10	10	----	----	110,507	25
2816	EEAP116	-396	10	10	----	----	140,415	25
2817	EEAP115	-362	10	10	----	----	696,647	25
2818	EEAP120	-396	10	10	----	----	59,096	25
2819	EEAP130	-362	15	15	----	----	1,445,447	25

MATERIAL EEBP

Lay-up = $[M/\pm45/0]_S$, $V_F = 0.43$, Ave. thickness = 2.90 mm, S.D. = 0.04 mm, Vinyl ester, Coupons taken from a pultruded blade section.

2727	EEB103	512	*	13	27.8	2.1	1	20
2728	EEB101	513	*	13	27.5	2.3	1	20
2729	EEB102	520	*	13	27.5	2.2	1	20
2730	EEB105	276	0.1	5	24.6	1.21	8,392	20
2731	EEB108	276	0.1	5	25.2	1.22	11,375	20
2732	EEB106	345	0.1	2	27.5	1.40	504	20
2733	EEB107	345	0.1	2	26.1	1.44	358	20
2734	EEB109	207	0.1	10	26.8	0.81	365,195	20
2735	EEB104	207	0.1	12	27.5	0.80	462,172	20
2736	EEB141	276	0.1	4	25.8	1.20	12,141	20
2740	EEB125	-412	*	13	----	----	1	25
2741	EEB126	-449	*	13	----	----	1	25
2742	EEB112	-390	*	13	----	----	1	25

TEST & SAMPLE ID #		MAX. STRESS MPa	R	Q Hz	E GPa	e %	CYCLES TO FAIL	WIDTH (mm) and Notes
MATERIAL EECP								
Lay-up = $[M/\pm45/0]_S$, $V_F = 0.49$, Ave. thickness = 2.48 mm, S.D. = 0.10 mm, Vinyl ester, Coupons taken from a pultruded blade section.								
2703	EEC123	546	*	13	27.4	2.4	1	20
2704	EEC122	505	*	13	29.8	2.1	1	20
2705	EEC132	526	*	13	27.9	2.2	1	20
2706	EEC133	345	0.1	2	29.5	1.35	257	20
2707	EEC128	345	0.1	2	27.5	1.41	149	20
2708	EEC131	345	0.1	2	28.6	1.49	86	20
2709	EEC126	276	0.1	4	28.4	1.07	5,070	20
2710	EEC125	276	0.1	4	28.9	1.04	2,474	20
2711	EEC130	276	0.1	4	27.3	1.08	3,114	20
2712	EEC118	207	0.1	10	28.0	0.77	285,157	20
2713	EEC120	207	0.1	10	29.0	0.77	141,150	20
2714	EEC129	207	0.1	10	29.4	0.76	159,441	20
2715	EEC127	172	0.1	20	27.1	0.68	1,293,553	20
2743	EEC136	-434	*	13	----	----	1	25
2744	EEC101	-436	*	13	----	----	1	25
2745	EEC143	-387	*	13	----	----	1	25

SUMMARY OF MSU MANUFACTURED MATERIAL FATIGUE TESTS

MATERIAL AA

Lay-up = $[(\pm 45/0)_2, (\pm 45/0), (\pm 45/0)_2]$, $V_F = 0.35$, Ave. thickness = 4.37 mm, S.D. = 0.11 mm, CoRezyn 63-AX-051 Polyester

TEST & SAMPLE ID #		MAX. STRESS MPa	R	Q Hz	E GPa	e %	CYCLES TO FAIL	WIDTH (mm) and Notes
339	101AA	443	*	13	17.3	2.73	1	25 tab
340	102AA	453	*	13	16.7	2.90	1	25 tab
341	103AA	448	*	13	17.0	2.82	1	25 tab
342	104AA	387	*	13	16.7	2.81	1	25 tab
343	110AA	241	0.1	5	16.9	1.53	1,741	25 tab
344	111AA	241	0.1	5	17.5	1.61	1,459	25 tab
345	106AA	172	0.1	10	17.9	1.08	11,293	25 tab
346	108AA	172	0.1	10	16.8	1.12	14,316	25 tab
347	109AA	103	0.1	20	17.0	0.63	366,798	25 tab
348	105AA	138	0.1	15	18.1	0.82	81,207	25 tab
349	107AA	241	0.1	15	17.3	1.65	1,051	25 tab
350	112AA	103	0.1	20	16.8	0.64	352,093	25 tab
351	116AA	138	0.1	20	16.7	0.90	55,485	25 tab
352	113AA	138	0.1	15	16.9	0.86	65,926	25 tab
353	123AA	-288	*	13	17.1	-1.06	1	25 tab
354	129AA	-284	*	13	18.4	-1.02	1	25 tab
355	119AA	-310	*	13	19.2	-0.90	1	25 tab
356	122AA	-138	10	15	20.1	-0.68	4,658,000	25 R tab
357	126AA	-241	10	5	18.8	-1.36	8,700	25 tab
358	118AA	-241	10	5	19.9	-1.24	9,419	25 tab
359	128AA	-207	10	10	19.2	-1.31	64,783	25 tab
360	127AA	-207	10	10	19.3	-1.36	75,000	25 tab
361	121AA	-172	10	15	20.0	-0.91	5,000,000	25 R tab
362	124AA	-172	10	10	18.2	-0.91	3,477,199	25 tab
364	134AA	-327	*	13	19.4	-1.75	1	25 Z tab
365	133AA	-347	*	13	17.7	-2.00	1	25 Z tab
366	137AA	-366	*	13	19.1	----	1	25 Z tab
367	132AA	-276	10	3	19.6	-1.60	547	25 Z tab
368	131AA	-276	10	3	18.3	-1.61	462	25 Z tab
369	135AA	-241	10	5	----	----	5,973	25 Z tab
370	125AA	-190	10	10	18.3	-1.23	167,058	25 Z tab
371	120AA	-190	10	10	18.4	-1.04	139,700	25 ZR tab
The following coupons with a 13 mm diameter hole are listed using the NET area stress. These coupons (excluding the "#" tests) had an average hole diameter of 13.00 mm and a standard deviation of 0.40 mm.								
372	141AA	207	0.1	13	18.3	0.83	1,200	50 HR tab
373	130AA	-190	10	5	----	----	151,283	25 Z tab
374	143AA	164	0.1	20	17.8	0.75	4,000	50 RH tab
375	145AA	121	0.1	5	19.7	0.48	42,000	50 RH tab
376	146AA	121	0.1	10	18.8	0.49	34,500	50 RH tab
377	144AA	103	0.1	15	19.7	0.40	97,692	50 H tab
387	150AA	444	*	13	19.4	2.04	1	25
388	152AA	468	*	13	17.9	2.47	1	25

TEST & SAMPLE ID #		MAX. STRESS MPa	R	Q Hz	E GPa	e %	CYCLES TO FAIL	WIDTH (mm) and Notes
Tests listed with a "#" indicate coupons post cured at 120 °C rather than the standard 60 °C. The average hole diameter for the tests with a "#" was 12.86 mm with a standard deviation of 0.41 mm.								
389	153AA	373	*	13	19.7	2.70	1	50 H#
390	161AA	369	*	13	20.5	2.80	1	50 H#
391	160AA	370	*	13	21.6	2.60	1	50 H#
392	159AA	241	0.1	2	19.8	1.18	328	50 H#
393	157AA	241	0.1	2	20.9	1.11	270	50 H#
394	156AA	172	0.1	5	19.7	0.86	5,032	50 H#
395	155AA	172	0.1	5	20.4	0.75	4,620	50 H#
396	158AA	138	0.1	5	20.2	0.64	19,409	50 H#
397	154AA	138	0.1	5	20.3	0.66	24,375	50 H#
398	163AA	103	0.1	15	21.3	0.49	168,606	50 H#
399	164AA	103	0.1	15	21.2	0.48	154,275	50 H#
400	167AA	241	0.1	2	17.4	1.36	392	50 H#
401	165AA	172	0.1	5	17.9	0.91	2,163	50 H#
402	182AA	352	*	13	----	----	1	50 H
403	181AA	350	*	13	18.7	2.31	1	50 H
404	168AA	353	*	13	18.3	2.57	1	50 H
405	169AA	103	0.1	15	20.2	0.41	100,806	50 H
406	166AA	172	0.1	2	18.8	0.86	2,030	50 H
407	184AA	241	0.1	2	19.7	1.14	280	50 H
408	183AA	86	0.1	20	18.9	0.46	355,500	50 H
Tests involving compression or reversed loading used a 25 mm gage length								
409	170AA	-205	*	13	19.8	-1.38	1	50 H
410	185AA	86	0.1	20	18.3	0.37	395,450	50 H
411	173AA	-257	*	13	20.8	-1.30	1	50 HZ
412	175AA	-257	*	13	19.5	-1.25	1	50 HZ
413	178AA	-243	*	13	20.0	-1.23	1	50 HZ
414	176AA	-207	10	2	19.9	-0.98	483	50 HZ
415	180AA	-138	10	5	19.0	-0.52	39,859	50 HZ
416	188AA	103	0.1	20	18.9	0.57	289,500	25 tab
417	185AA	103	0.1	25	16.6	0.62	252,137	25 tab
418	162AA	86	0.1	20	22.6	0.44	152,641	50 H#
419	190AA	138	0.1	5	17.2	0.68	7,527	50 H
420	189AA	138	0.1	5	17.3	0.66	7,294	50 H
421	192AA	-207	10	2	19.4	-0.70	508	50 HZ
422	196AA	-138	10	5	20.8	-0.45	45,064	50 HZ
423	187AA	86	0.1	10	19.8	0.46	1,097,890	25 tab
424	197AA	86	0.1	15	16.5	0.54	1,110,190	25 tab
425	171AA	-207	10	10	18.7	-1.08	59,130	25 Z
426	191AA	-207	10	2	19.8	-0.69	446	50 HZ
427	193AA	-138	10	5	20.0	-0.48	45,833	50 HZ
428	194AA	-172	10	5	18.3	-0.66	8,338	50 HZ
429	202AA	-371	*	13	17.9	-2.41	1	25 Z
430	203AA	-327	*	13	19.0	-2.20	1	25 Z
431	195AA	-172	10	10	18.6	-0.64	5,439	50 HZ
432	204AA	-190	10	10	18.1	-1.05	172,910	25 Z
433	200AA	-121	10	10	19.2	-0.46	1,400,699	50 HZ

TEST & SAMPLE ID #		MAX. STRESS MPa	R	Q Hz	E GPa	e %	CYCLES TO FAIL	WIDTH (mm) and Notes
434	186AA	86	0.1	20	19.2	0.46	1,063,690	25 tab
435	205AA	-190	10	25	16.9	-1.11	240,000	25 Z
436	198AA	-121	10	15	15.2	-0.48	820,290	50 HZ
437	187AA	172	0.1	10	16.6	1.04	17,149	25 tab
438	209AA	241	0.1	2	16.9	1.43	187	50 H
439	210AA	103	0.1	15	16.7	0.62	61,628	50 H
440	207AA	172	0.1	10	18.1	0.72	2,757	50 H
441	211AA	172	0.1	5	18.9	0.76	2,700	50 H
442	206AA	138	0.1	5	17.8	0.63	9,650	50 H
443	208AA	86	0.1	15	17.9	0.45	276,248	50 H
444	213AA	241	0.1	2	18.6	1.15	237	50 H
445	218AA	-276	10	1	18.1	-1.56	380	25 Z
446	238AA	-241	10	5	18.6	-1.29	11,145	25 Z
447	199AA	-172	10	5	21.3	-0.64	7,345	50 HZ
449	240AA	207	-1	1	19.0	1.38	195	25 Z
450	230AA	207	-1	1	20.8	1.22	191	25 Z
451	239AA	190	-1	2	17.9	1.27	296	25 Z
452	232AA	172	-1	1	17.4	1.07	509	25 Z
453	221AA	172	-1	1	18.3	1.01	438	25 Z
454	216AA	138	-1	1	19.0	0.78	1,850	25 Z
455	217AA	138	-1	1	17.3	0.86	2,493	25 Z
456	241AA	190	-1	1	17.9	1.40	232	25 Z
457	136AA	138	-1	1	----	----	1,897	25 Z tab
458	224AA	138	-1	1	19.6	0.51	753	50 HZ
459	231AA	86	-1	1	21.8	0.28	33,341	50 HZ
460	222AA	172	-1	1	16.3	0.71	160	50 HZ
461	228AA	172	-1	1	21.7	0.58	218	50 HZ
462	227AA	172	-1	1	22.7	0.55	176	50 HZ
463	229AA	138	-1	1	19.7	0.49	860	50 HZ
464	225AA	138	-1	1	20.5	0.50	891	50 HZ
465	223AA	103	-1	1	20.1	0.39	8,513	50 HZ
466	236AA	103	-1	1	19.7	0.37	8,262	50 HZ
467	235AA	86	-1	1	22.0	0.29	33,347	50 HZ
468	237AA	103	-1	1	19.1	0.34	11,756	50 HZ
469	242AA	207	-1	1	19.0	1.20	168	25 Z tab
470	226AA	190	-1	1	18.0	1.17	208	25 Z tab
471	242AA	172	-1	1	18.4	1.08	376	25 Z tab
472	220AA	103	-1	1	18.6	0.58	25,488	25 Z tab
473	219AA	103	-1	1	18.8	0.57	21,992	25 Z tab
474	234AA	86	-1	2	19.2	0.32	56,945	50 HZ
475	233AA	121	10	10	20.5	0.57	10,000	50 HZR
476	274AA	-190	10	15	18.5	-1.23	153,542	25 Z tab
477	115AA	86	-1	5	18.8	0.45	456,549	25 tab
478	117AA	86	-1	5	17.4	0.49	187,649	25 tab
479	269AA	86	-1	5	20.5	0.44	236,152	25
480	271AA	103	-1	2	18.5	0.56	34,956	25
Tests 513 - 527 involved a gage length of 76 mm (strain rate effect tests).								
513	275AA	506	*	13	22.8	2.25	1	25

TEST & SAMPLE ID #		MAX. STRESS MPa	R	Q Hz	E GPa	e %	CYCLES TO FAIL	WIDTH (mm) and Notes
514	276AA	510	*	13	21.6	2.36	1	25
515	277AA	518	*	13	22.1	2.35	1	25
516	278AA	524	*	13	22.5	2.34	1	25
517	279AA	517	*	13	21.9	2.37	1	25
518	280AA	552	*	13	23.0	2.40	1	25
519	281AA	530	*	13	23.5	2.26	1	25
520	282AA	540	*	13	22.4	2.41	1	25
521	283AA	491	*	13	22.4	2.20	1	25
522	284AA	557	*	13	23.7	2.35	1	25
523	285AA	536	*	13	22.8	2.35	1	25
524	286AA	542	*	13	23.3	2.32	1	25
525	287AA	506	*	13	24.0	2.10	1	25
526	288AA	512	*	13	21.4	2.39	1	25
527	289AA	507	*	13	23.0	2.21	1	25
Tests 528 - 542 involved a gage length of 38 mm and a coupon width of 13 mm (strain rate effect tests).								
528	296AA	476	*	6	21.1	2.24	1	13
529	301AA	511	*	6	22.6	2.27	1	13
530	293AA	479	*	6	21.9	2.19	1	13
531	299AA	579	*	6	23.7	2.75	1	13
532	298AA	501	*	6	22.3	2.25	1	13
533	304AA	500	*	6	22.7	2.21	1	13
534	297AA	554	*	6	25.9	2.29	1	13
535	290AA	526	*	6	22.1	2.39	1	13
536	303AA	513	*	6	23.7	2.17	1	13
537	295AA	543	*	6	23.7	2.30	1	13
538	291AA	498	*	6	23.2	2.14	1	13
539	300AA	484	*	6	24.0	2.02	1	13
540	292AA	478	*	6	23.2	2.05	1	13
541	294AA	517	*	6	22.1	2.33	1	13
542	302AA	538	*	6	23.2	2.10	1	13
Tests 550 - 565 involved a gage length of 114 mm and a coupon width of 38 mm (strain rate effect tests).								
550	306AA	551	*	19	22.0	2.60	1	38
551	310AA	537	*	19	20.8	2.59	1	38
552	314AA	539	*	19	21.2	2.54	1	38
553	312AA	578	*	19	23.9	2.43	1	38
554	307AA	534	*	19	22.4	2.39	1	38
555	318AA	539	*	19	21.4	2.52	1	38
556	316AA	530	*	19	21.9	2.42	1	38
557	320AA	509	*	19	22.3	2.28	1	38
558	308AA	584	*	19	22.8	2.56	1	38
559	315AA	541	*	19	23.0	2.35	1	38
560	305AA	559	*	19	23.0	2.43	1	38
561	311AA	548	*	19	21.5	2.54	1	38
562	319AA	555	*	19	21.4	2.59	1	38
563	313AA	519	*	19	21.2	2.45	1	38
564	309AA	552	*	19	22.6	2.45	1	38
565	336AA	529	*	19	20.8	2.54	1	38
Tests 566 - 580 involved a gage length of 152 mm and a coupon width of 50 mm (strain rate effect tests).								

TEST & SAMPLE ID #		MAX. STRESS MPa	R	Q Hz	E GPa	e %	CYCLES TO FAIL	WIDTH (mm) and Notes
566	324AA	533	*	25	21.0	2.54	1	50
567	329AA	540	*	25	20.7	2.62	1	50
568	334AA	547	*	25	20.8	2.63	1	50
569	322AA	557	*	25	21.6	2.58	1	50
570	333AA	550	*	25	21.5	2.55	1	50
571	331AA	511	*	25	21.1	2.42	1	50
572	327AA	544	*	25	22.0	2.47	1	50
573	325AA	514	*	25	22.4	2.29	1	50
574	330AA	523	*	25	21.8	2.40	1	50
575	321AA	546	*	25	21.8	2.50	1	50
576	332AA	548	*	25	22.1	2.48	1	50
577	326AA	528	*	25	20.8	2.50	1	50
578	323AA	561	*	25	23.4	2.39	1	50
579	337AA	518	*	25	21.9	2.37	1	50
580	335AA	550	*	25	21.8	2.53	1	50
Tests 581 - 595 involved a gage length of 19 mm and a coupon width of 6 mm (strain rate effect tests).								
581	338AA	517	*	3	----	----	1	6
582	339AA	503	*	3	----	----	1	6
583	340AA	468	*	3	----	----	1	6
584	341AA	490	*	3	----	----	1	6
585	342AA	546	*	3	----	----	1	6
586	343AA	508	*	3	----	----	1	6
587	344AA	559	*	3	----	----	1	6
588	345AA	569	*	3	----	----	1	6
589	346AA	539	*	3	----	----	1	6
590	347AA	535	*	3	----	----	1	6
591	348AA	524	*	3	----	----	1	6
592	349AA	473	*	3	----	----	1	6
593	350AA	555	*	3	----	----	1	6
594	351AA	571	*	3	----	----	1	6
595	352AA	498	*	3	----	----	1	6
Tests 596 - 610 involved a gage length of 38 mm and a coupon width of 13 mm (strain rate effect tests).								
596	353AA	481	*	6	----	----	1	13
597	354AA	575	*	6	----	----	1	13
598	355AA	519	*	6	----	----	1	13
599	356AA	506	*	6	----	----	1	13
600	357AA	568	*	6	----	----	1	13
601	358AA	508	*	6	----	----	1	13
602	359AA	573	*	6	----	----	1	13
603	360AA	482	*	6	----	----	1	13
604	361AA	532	*	6	----	----	1	13
605	362AA	491	*	6	----	----	1	13
606	363AA	519	*	6	----	----	1	13
607	364AA	522	*	6	----	----	1	13
608	365AA	497	*	6	----	----	1	13
609	366AA	490	*	6	----	----	1	13
610	367AA	528	*	6	----	----	1	13
Tests 611 - 625 involved a gage length of 57 mm and a coupon width of 19 mm (strain rate effect tests).								

TEST & SAMPLE ID #		MAX. STRESS MPa	R	Q Hz	E GPa	e %	CYCLES TO FAIL	WIDTH (mm) and Notes
611	368AA	556	*	10	----	----	1	19
612	369AA	528	*	10	----	----	1	19
613	370AA	536	*	10	----	----	1	19
614	371AA	565	*	10	----	----	1	19
615	372AA	483	*	10	----	----	1	19
616	373AA	528	*	10	----	----	1	19
617	374AA	544	*	10	----	----	1	19
618	375AA	547	*	10	----	----	1	19
619	376AA	561	*	10	----	----	1	19
620	377AA	506	*	10	----	----	1	19
621	378AA	559	*	10	----	----	1	19
622	379AA	563	*	10	----	----	1	19
623	380AA	532	*	10	----	----	1	19
624	381AA	543	*	10	----	----	1	19
625	382AA	530	*	10	----	----	1	19
Tests 626 - 640 involved a gage length of 95 mm and a coupon width of 32 mm (strain rate effect tests).								
626	383AA	539	*	16	----	----	1	32
627	384AA	572	*	16	----	----	1	32
628	385AA	549	*	16	----	----	1	32
629	386AA	508	*	16	----	----	1	32
630	387AA	554	*	16	----	----	1	32
631	388AA	533	*	16	----	----	1	32
632	389AA	555	*	16	----	----	1	32
633	390AA	526	*	16	----	----	1	32
634	391AA	503	*	16	----	----	1	32
635	392AA	520	*	16	----	----	1	32
636	393AA	525	*	16	----	----	1	32
637	394AA	497	*	16	----	----	1	32
638	395AA	527	*	16	----	----	1	32
639	396AA	511	*	16	----	----	1	32
640	397AA	519	*	16	----	----	1	32
Tests 641 - 655 involved a gage length of 114 mm and a coupon width of 38 mm (strain rate effect tests).								
641	398AA	525	*	19	----	----	1	38
642	399AA	509	*	19	----	----	1	38
643	400AA	555	*	19	----	----	1	38
644	401AA	553	*	19	----	----	1	38
645	402AA	544	*	19	----	----	1	38
646	403AA	491	*	19	----	----	1	38
647	404AA	521	*	19	----	----	1	38
648	405AA	514	*	19	----	----	1	38
649	406AA	532	*	19	----	----	1	38
650	407AA	513	*	19	----	----	1	38
651	408AA	527	*	19	----	----	1	38
652	409AA	542	*	19	----	----	1	38
653	410AA	492	*	19	----	----	1	38
654	411AA	522	*	19	----	----	1	38
655	412AA	477	*	19	----	----	1	38
Tests 656 - 670 involved a gage length of 10 mm and a coupon width of 3 mm (strain rate effect tests).								

TEST & SAMPLE ID #		MAX. STRESS MPa	R	Q Hz	E GPa	e %	CYCLES TO FAIL	WIDTH (mm) and Notes
656	413AA	380	*	2	----	----	1	3
657	414AA	468	*	2	----	----	1	3
658	415AA	389	*	2	----	----	1	3
659	416AA	357	*	2	----	----	1	3
660	417AA	365	*	2	----	----	1	3
661	418AA	448	*	2	----	----	1	3
662	419AA	378	*	2	----	----	1	3
663	420AA	476	*	2	----	----	1	3
664	421AA	456	*	2	----	----	1	3
665	422AA	384	*	2	----	----	1	3
666	423AA	354	*	2	----	----	1	3
667	424AA	441	*	2	----	----	1	3
668	425AA	394	*	2	----	----	1	3
669	426AA	437	*	2	----	----	1	3
670	427AA	386	*	2	----	----	1	3
Tests 671 - 685 involved a gage length of 133 mm and a coupon width of 44 mm (strain rate effect tests).								
671	428AA	537	*	22	----	----	1	44
672	429AA	528	*	22	----	----	1	44
673	430AA	503	*	22	----	----	1	44
674	431AA	540	*	22	----	----	1	44
675	432AA	520	*	22	----	----	1	44
676	433AA	546	*	22	----	----	1	44
677	434AA	535	*	22	----	----	1	44
678	435AA	546	*	22	----	----	1	44
679	436AA	559	*	22	----	----	1	44
680	437AA	525	*	22	----	----	1	44
681	438AA	547	*	22	----	----	1	44
682	439AA	533	*	22	----	----	1	44
683	440AA	523	*	22	----	----	1	44
684	441AA	520	*	22	----	----	1	44
685	442AA	552	*	22	----	----	1	44
Tests 707 - 716 involved a gage length of 10 mm and a coupon width of 3 mm (strain rate effect tests).								
707	464AA	-323	*	2	----	----	1	3
708	465AA	-371	*	2	----	----	1	3
709	466AA	-311	*	2	----	----	1	3
710	467AA	-313	*	2	----	----	1	3
711	468AA	-330	*	2	----	----	1	3
712	469AA	-305	*	2	----	----	1	3
713	470AA	-319	*	2	----	----	1	3
714	471AA	-304	*	2	----	----	1	3
715	472AA	-326	*	2	----	----	1	3
716	473AA	-334	*	2	----	----	1	3
Tests 717 - 726 involved a gage length of 76 mm and a coupon width of 25 mm (strain rate effect tests).								
717	474AA	-311	*	13	----	----	1	25
718	475AA	-313	*	13	----	----	1	25
719	476AA	-311	*	13	----	----	1	25
720	477AA	-302	*	13	----	----	1	25
721	478AA	-307	*	13	----	----	1	25

TEST & SAMPLE ID #		MAX. STRESS MPa	R	Q Hz	E GPa	e %	CYCLES TO FAIL	WIDTH (mm) and Notes
722	479AA	-306	*	13	----	----	1	25
723	480AA	-302	*	13	----	----	1	25
724	481AA	-320	*	13	----	----	1	25
725	482AA	-316	*	13	----	----	1	25
726	483AA	-313	*	13	----	----	1	25
Tests 727 - 746 involved a gage length of 57 mm and a coupon width of 19 mm (strain rate effect tests).								
727	484AA	-321	*	10	----	----	1	19
728	485AA	-334	*	10	----	----	1	19
729	486AA	-333	*	10	----	----	1	19
730	487AA	-329	*	10	----	----	1	19
731	488AA	-337	*	10	----	----	1	19
732	489AA	-314	*	10	----	----	1	19
733	490AA	-325	*	10	----	----	1	19
734	491AA	-322	*	10	----	----	1	19
735	492AA	-331	*	10	----	----	1	19
736	493AA	-323	*	10	----	----	1	19
737	494AA	-320	*	10	----	----	1	19
738	495AA	-318	*	10	----	----	1	19
739	496AA	-316	*	10	----	----	1	19
740	497AA	-331	*	10	----	----	1	19
741	498AA	-323	*	10	----	----	1	19
742	499AA	-332	*	10	----	----	1	19
743	500AA	-327	*	10	----	----	1	19
744	501AA	-313	*	10	----	----	1	19
745	502AA	-322	*	10	----	----	1	19
746	503AA	-320	*	10	----	----	1	19
Tests 747 - 756 involved a gage length of 19 mm and a coupon width of 13 mm (strain rate effect tests).								
747	504AA	-358	*	6	----	----	1	13
748	505AA	-330	*	6	----	----	1	13
749	506AA	-347	*	6	----	----	1	13
750	507AA	-335	*	6	----	----	1	13
751	508AA	-351	*	6	----	----	1	13
752	509AA	-353	*	6	----	----	1	13
753	510AA	-355	*	6	----	----	1	13
754	511AA	-329	*	6	----	----	1	13
755	512AA	-339	*	6	----	----	1	13
756	513AA	-354	*	6	----	----	1	13
Tests 757 - 766 involved a gage length of 133 mm and a coupon width of 44 mm (strain rate effect tests).								
757	514AA	-264	*	22	----	----	1	44
758	515AA	-262	*	22	----	----	1	44
759	516AA	-265	*	22	----	----	1	44
760	517AA	-263	*	22	----	----	1	44
761	518AA	-267	*	22	----	----	1	44
762	519AA	-273	*	22	----	----	1	44
763	520AA	-266	*	22	----	----	1	44
764	521AA	-264	*	22	----	----	1	44
765	522AA	-269	*	22	----	----	1	44
766	523AA	-266	*	22	----	----	1	44

TEST & SAMPLE ID #		MAX. STRESS MPa	R	Q Hz	E GPa	e %	CYCLES TO FAIL	WIDTH (mm) and Notes
Tests 1233 - 1242 involved a gage length of 152 mm and a coupon width of 50 mm (strain rate effect tests).								
1233	443AA	-254	*	25	----	----	1	50
1234	444AA	-250	*	25	----	----	1	50
1235	445AA	-250	*	25	----	----	1	50
1236	446AA	-250	*	13	----	----	1	50
1237	447AA	-249	*	25	----	----	1	50
1238	448AA	-251	*	25	----	----	1	50
1239	449AA	-252	*	25	----	----	1	50
1240	450AA	-256	*	25	----	----	1	50
1241	451AA	-249	*	25	----	----	1	50
1242	452AA	-250	*	25	----	----	1	50
Tests 1243 - 1253 involved a gage length of 19 mm and a coupon width of 6 mm (strain rate effect tests).								
1243	453AA	-374	*	13	----	----	1	6
1244	454AA	-356	*	13	----	----	1	6
1245	455AA	-368	*	13	----	----	1	6
1246	456AA	-375	*	13	----	----	1	6
1247	457AA	-390	*	13	----	----	1	6
1248	458AA	-366	*	13	----	----	1	6
1249	459AA	-356	*	13	----	----	1	6
1250	460AA	-366	*	13	----	----	1	6
1251	461AA	-380	*	13	----	----	1	6
1252	462AA	-364	*	13	----	----	1	6
1253	463AA	-372	*	13	----	----	1	6

MATERIAL AA2

Lay-up = $[(0/\pm45)_2]_S$, $V_F = 0.39$, Ave. thickness = 2.63 mm, S.D. = 0.07 mm, CoRezyn 63-AX-051 Polyester

Tests 767 - 776 involved a gage length of 152 mm and a coupon width of 50 mm (strain rate effect tests).								
767	524AA2	-298	*	25	----	----	1	50
768	525AA2	-298	*	25	----	----	1	50
769	526AA2	-301	*	25	----	----	1	50
770	527AA2	-312	*	25	----	----	1	50
771	528AA2	-315	*	25	----	----	1	50
772	529AA2	-294	*	25	----	----	1	50
773	530AA2	-300	*	25	----	----	1	50
774	531AA2	-298	*	25	----	----	1	50
775	532AA2	-305	*	25	----	----	1	50
776	533AA2	-319	*	25	----	----	1	50
Tests 777 - 786 involved a gage length of 76 mm and a coupon width of 25 mm (strain rate effect tests).								
777	534AA2	-308	*	13	----	----	1	25
778	535AA2	-315	*	13	----	----	1	25
779	536AA2	-315	*	13	----	----	1	25
780	537AA2	-307	*	13	----	----	1	25
781	538AA2	-317	*	13	----	----	1	25
782	539AA2	-328	*	13	----	----	1	25
783	540AA2	-313	*	13	----	----	1	25
784	541AA2	-313	*	13	----	----	1	25
785	542AA2	-322	*	13	----	----	1	25

TEST & SAMPLE ID #		MAX. STRESS MPa	R	Q Hz	E GPa	e %	CYCLES TO FAIL	WIDTH (mm) and Notes
786	543AA2	-322	*	13	----	----	1	25
Tests 787 - 796 involved a gage length of 38 mm and a coupon width of 12 mm (strain rate effect tests).								
787	544AA2	-315	*	6	----	----	1	13
788	545AA2	-337	*	6	----	----	1	13
789	546AA2	-327	*	6	----	----	1	13
790	547AA2	-300	*	6	----	----	1	13
791	548AA2	-330	*	6	----	----	1	13
792	549AA2	-324	*	6	----	----	1	13
793	550AA2	-340	*	6	----	----	1	13
794	551AA2	-298	*	6	----	----	1	13
795	552AA2	-305	*	6	----	----	1	13
796	553AA2	-309	*	6	----	----	1	13
Tests 797 - 806 involved a gage length of 114 mm and a coupon width of 38 mm (strain rate effect tests).								
797	554AA2	-310	*	19	----	----	1	38
798	555AA2	-317	*	19	----	----	1	38
799	556AA2	-289	*	19	----	----	1	38
800	557AA2	-293	*	19	----	----	1	38
801	558AA2	-299	*	19	----	----	1	38
802	559AA2	-295	*	19	----	----	1	38
803	560AA2	-296	*	19	----	----	1	38
804	561AA2	-312	*	19	----	----	1	38
805	562AA2	-301	*	19	----	----	1	38
806	563AA2	-282	*	19	----	----	1	38
Tests 807 - 827 involved a gage length of 57 mm and a coupon width of 19 mm (strain rate effect tests).								
807	564AA2	-311	*	10	----	----	1	19
808	565AA2	-290	*	10	----	----	1	19
809	566AA2	-286	*	10	----	----	1	19
810	567AA2	-282	*	10	----	----	1	19
811	568AA2	-286	*	10	----	----	1	19
812	569AA2	-282	*	10	----	----	1	19
813	570AA2	-314	*	10	----	----	1	19
814	571AA2	-276	*	10	----	----	1	19
815	572AA2	-275	*	10	----	----	1	19
816	573AA2	-276	*	10	----	----	1	19
817	574AA2	-287	*	10	----	----	1	19
818	575AA2	-266	*	10	----	----	1	19
819	576AA2	-314	*	10	----	----	1	19
820	577AA2	-252	*	10	----	----	1	19
821	578AA2	-288	*	10	----	----	1	19
822	579AA2	-297	*	10	----	----	1	19
823	580AA2	-318	*	10	----	----	1	19
824	581AA2	-278	*	10	----	----	1	19
825	582AA2	-281	*	10	----	----	1	19
826	583AA2	-302	*	10	----	----	1	19
827	584AA2	-310	*	10	----	----	1	19
Tests 828 - 837 involved a gage length of 19 mm and a coupon width of 6 mm (strain rate effect tests).								
828	585AA2	-209	*	13	----	----	1	6
829	586AA2	-230	*	13	----	----	1	6

TEST & SAMPLE ID #		MAX. STRESS MPa	R	Q Hz	E GPa	e %	CYCLES TO FAIL	WIDTH (mm) and Notes
830	587AA2	-215	*	13	----	----	1	6
831	588AA2	-213	*	13	----	----	1	6
832	589AA2	-221	*	13	----	----	1	6
833	590AA2	-211	*	13	----	----	1	6
834	591AA2	-226	*	13	----	----	1	6
835	592AA2	-244	*	13	----	----	1	6
836	593AA2	-216	*	13	----	----	1	6
837	594AA2	-221	*	13	----	----	1	6
Tests 838 - 847 involved a gage length of 13 mm and a coupon width of 4 mm (strain rate effect tests).								
838	595AA2	-281	*	2	----	----	1	4
839	596AA2	-239	*	2	----	----	1	4
840	597AA2	-252	*	2	----	----	1	4
841	598AA2	-271	*	2	----	----	1	4
842	599AA2	-222	*	2	----	----	1	4
843	600AA2	-235	*	2	----	----	1	4
844	601AA2	-236	*	2	----	----	1	4
845	602AA2	-241	*	2	----	----	1	4
846	603AA2	-260	*	2	----	----	1	4
847	604AA2	-232	*	2	----	----	1	4
Tests 848 - 857 involved a gage length of 95 mm and a coupon width of 32 mm (strain rate effect tests).								
848	605AA2	-318	*	16	----	----	1	32
849	606AA2	-293	*	16	----	----	1	32
850	607AA2	-281	*	16	----	----	1	32
851	608AA2	-275	*	16	----	----	1	32
852	609AA2	-272	*	16	----	----	1	32
853	610AA2	-283	*	16	----	----	1	32
854	611AA2	-320	*	16	----	----	1	32
855	612AA2	-262	*	16	----	----	1	32
856	613AA2	-304	*	16	----	----	1	32
857	614AA2	-303	*	16	----	----	1	32
Tests 858 - 867 involved a gage length of 133 mm and a coupon width of 44 mm (strain rate effect tests).								
858	615AA2	-268	*	22	----	----	1	44
859	616AA2	-304	*	22	----	----	1	44
860	617AA2	-322	*	22	----	----	1	44
861	618AA2	-294	*	22	----	----	1	44
862	619AA2	-306	*	22	----	----	1	44
863	620AA2	-269	*	22	----	----	1	44
864	621AA2	-283	*	22	----	----	1	44
865	622AA2	-309	*	22	----	----	1	44
866	623AA2	-305	*	22	----	----	1	44
867	624AA2	-317	*	22	----	----	1	44
868	625AA2	423	*	22	----	----	1	25
869	630AA2	448	*	22	----	----	1	25
Tests 870 - 877 involved a gage length of 76 mm and a coupon width of 25 mm (standard test).								
870	626AA2	517	*	13	23.0	2.67	1	25
871	627AA2	462	*	13	23.2	2.10	1	25
872	628AA2	494	*	13	22.7	2.18	1	25
873	629AA2	463	*	13	22.1	2.10	1	25

TEST & SAMPLE ID #		MAX. STRESS MPa	R	Q Hz	E GPa	e %	CYCLES TO FAIL	WIDTH (mm) and Notes
877	630AA2	430	*	13	21.1	2.04	1	25
Tests 879 - 888 involved a gage length of 76 mm and a coupon width of 25 mm (strain rate effect tests).								
879	631AA2	478	*	13	----	----	1	25
880	632AA2	478	*	13	----	----	1	25
881	633AA2	431	*	13	----	----	1	25
882	634AA2	489	*	13	----	----	1	25
883	635AA2	563	*	13	----	----	1	25
884	636AA2	420	*	13	----	----	1	25
885	637AA2	529	*	13	----	----	1	25
886	638AA2	524	*	13	----	----	1	25
887	639AA2	448	*	13	----	----	1	25
888	640AA2	446	*	13	----	----	1	25
Tests 890 - 906 involved a gage length of 38 mm and a coupon width of 13 mm (strain rate effect tests).								
890	642AA2	506	*	6	----	----	1	13
891	643AA2	486	*	6	----	----	1	13
892	644AA2	494	*	6	----	----	1	13
893	645AA2	494	*	6	----	----	1	13
895	647AA2	462	*	6	----	----	1	13
896	648AA2	437	*	6	----	----	1	13
897	649AA2	439	*	6	----	----	1	13
898	650AA2	506	*	6	----	----	1	13
900	652AA2	428	*	6	----	----	1	13
901	653AA2	469	*	6	----	----	1	13
902	654AA2	479	*	6	----	----	1	13
903	655AA2	472	*	6	----	----	1	13
904	656AA2	509	*	6	----	----	1	13
905	657AA2	474	*	6	----	----	1	13
906	658AA2	451	*	6	----	----	1	13
Tests 907 - 916 involved a gage length of 95 mm and a coupon width of 32 mm (strain rate effect tests).								
907	659AA2	-297	*	16	----	----	1	32
908	660AA2	-297	*	16	----	----	1	32
909	661AA2	-295	*	16	----	----	1	32
910	662AA2	-297	*	16	----	----	1	32
911	663AA2	-299	*	16	----	----	1	32
912	664AA2	-290	*	16	----	----	1	32
913	665AA2	-303	*	16	----	----	1	32
914	666AA2	-292	*	16	----	----	1	32
915	667AA2	-294	*	16	----	----	1	32
916	668AA2	-296	*	16	----	----	1	32
Tests 917 - 926 involved a gage length of 114 mm and a coupon width of 38 mm (strain rate effect tests).								
917	669AA2	-277	*	19	----	----	1	38
918	670AA2	-279	*	19	----	----	1	38
919	671AA2	-282	*	19	----	----	1	38
920	672AA2	-281	*	19	----	----	1	38
921	673AA2	-283	*	19	----	----	1	38
922	674AA2	-278	*	19	----	----	1	38
923	675AA2	-287	*	19	----	----	1	38
924	676AA2	-276	*	19	----	----	1	38

TEST & SAMPLE ID #		MAX. STRESS MPa	R	Q Hz	E GPa	e %	CYCLES TO FAIL	WIDTH (mm) and Notes
925	677AA2	-281	*	19	----	----	1	38
926	678AA2	-276	*	19	----	----	1	38

MATERIAL AA3

Lay-up = $[(\pm 45/0)_3,]_S$, $V_F = 0.51$, Ave. thickness = 3.45 mm, S.D. = 0.15 mm, CoRezyn 63-AX-051 Polyester

2367	AA3104	482	*	0.5	23.7	2.3	1	25
2368	AA3110	463	*	0.5	25.2	2.4	1	25
2369	AA3109	489	*	0.5	25.3	2.2	1	25
2370	AA3106	241	0.1	4	26.5	0.91	3,572	25
2371	AA3113	241	0.1	4	25.8	0.94	4,447	25
2372	AA3111	241	0.1	4	22.7	1.06	2,986	25
2373	AA3114	172	0.1	8	23.9	0.81	25,183	25
2374	AA3108	172	0.1	8	29.5	0.57	17,683	25
2375	AA3102	172	0.1	8	23.4	0.81	23,753	25
2376	AA3107	103	0.1	15	25.2	0.44	900,000	25R
2377	AA3115	310	0.1	2	26.5	1.39	493	25
2378	AA3112	310	0.1	2	24.7	1.26	626	25
2379	AA3103	310	0.1	2	25.2	1.23	812	25
2627	AA3301	-340	*	13	----	----	1	25
2628	AA3302	-283	*	13	----	----	1	25
2629	AA3303	-280	*	13	----	----	1	25
2630	AA3304	-233	*	13	----	----	1	25

MATERIAL AA4

Lay-up = $[(\pm 45/0)_2,]_S$, $V_F = 0.37$, Ave. thickness = 5.12 mm, S.D. = 0.13 mm, CoRezyn 63-AX-051 Polyester

3513	AA4104	310	*	13	22.0	2	1	25
3514	AA4101	427	*	13	21.9	2.10	1	25
3515	AA4102	365	*	13	21.4	1.85	1	25
3516	AA4107	404	*	13	20.5	2.19	1	25
3517	AA4109	241	0.1	2	18.3	1.36	1,203	25
3518	AA4113	241	0.1	2	21.2	1.19	3,002	25
3519	AA4111	241	0.1	2	19.5	1.42	2,752	25
3520	AA4110	207	0.1	4	22.0	1.08	24,288	25
3521	AA4112	207	0.1	4	19.1	1.15	19,180	25
3522	AA4116	207	0.1	4	18.5	1.26	15,966	25
3523	AA4120	172	0.1	5	20.5	0.90	179,566	25
3524	AA4118	172	0.1	5	----	----	127,836	25
3829	AA4136	-413	*	13	----	----	1	25
3830	AA4133	-442	*	13	----	----	1	25
3831	AA4131	-493	*	13	----	----	1	25

MATERIAL BB

Lay-up = $[\pm 45/0_2/+45]_S$, $V_F = 0.42$, Ave. thickness = 2.67 mm, S.D. = 0.06 mm, CoRezyn 63-AX-051 Polyester

927	BB101	734	*	13	23.9	3.37	1	25

TEST & SAMPLE ID #		MAX. STRESS MPa	R	Q Hz	E GPa	e %	CYCLES TO FAIL	WIDTH (mm) and Notes
928	BB102	728	*	13	24.8	2.94	1	25
929	BB103	735	*	13	24.8	3.37	1	25
930	BB113	703	*	13	25.9	2.91	1	25 tab
931	BB109	414	0.1	2	25.4	1.63	550	25 tab
932	BB119	414	0.1	2	23.8	1.74	673	25 tab
933	BB118	414	0.1	2	25.0	1.71	512	25 tab
934	BB117	345	0.1	5	26.5	1.23	1,810	25 tab
935	BB124	345	0.1	5	27.3	1.26	2,415	25 tab
936	BB115	345	0.1	5	23.8	1.45	2,585	25 tab
937	BB123	276	0.1	10	26.8	1.09	18,755	25 tab
938	BB112	276	0.1	10	24.1	1.14	12,437	25 tab
939	BB114	276	0.1	10	25.2	1.20	11,302	25 tab
940	BB110	207	0.1	15	26.3	0.85	494,149	25 tab
941	BB116	207	0.1	15	25.8	0.80	197,629	25 tab
942	BB111	207	0.1	15	25.8	0.81	390,137	25 tab
943	BB108	241	0.1	15	24.6	1.12	66,612	25 tab
944	BB121	241	0.1	15	24.3	1.02	47,939	25 tab
945	BB107	241	0.1	15	24.3	1.09	84,343	25 tab
946	BB122	193	0.1	20	25.2	0.78	1,100,000	25 tab
947	BB106	193	0.1	20	25.2	0.78	921,400	25 tab
948	BB120	193	0.1	20	25.6	0.82	1,320,150	25 tab
949	BB113T	101	*	13	11.3	1.00	1	25 tab
950	BB112T	104	*	13	11.3	0.94	1	25 tab
951	BB111T	111	*	13	11.3	0.99	1	25 tab
952	BB120T	-225	*	13	12.5	1.81	1	25
953	BB128T	-229	*	13	11.2	1.86	1	25
954	BB127T	-244	*	13	12.2	1.99	1	25
955	BB135T	-294	*	13	----	----	1	25
956	BB141	-325	*	13	----	----	1	25
957	BB143	-291	*	13	----	----	1	25
958	BB105	193	0.1	15	26.0	0.84	707,401	25 tab

MATERIAL CC

Lay-up = $[\pm 45/0_2/+45]_S$, $V_F = 0.39$, Ave. thickness = 2.44 mm, S.D. = 0.07 mm, CoRezyn 63-AX-051 Polyester

959	CC105	574	*	13	21.0	2.74	1	25
960	CC107	562	*	13	21.1	2.70	1	25
961	CC102	574	*	13	20.6	2.78	1	25
962	CC119	345	0.1	2	22.5	1.63	174	25 tab
963	CC108	345	0.1	2	21.0	1.84	124	25 tab
964	CC121	345	0.1	2	21.7	1.79	223	25 tab
965	CC118	276	0.1	4	21.9	1.55	1,787	25 tab
966	CC113	276	0.1	4	23.3	1.47	2,637	25 tab
967	CC104	276	0.1	4	21.2	1.30	3,029	25 tab
968	CC116	241	0.1	10	21.6	1.12	8,838	25 tab
969	CC117	241	0.1	10	23.3	1.14	6,956	25 tab
970	CC103	241	0.1	10	22.3	1.08	12,015	25 tab
971	CC112	207	0.1	15	21.9	0.99	25,203	25 tab

TEST & SAMPLE ID #		MAX. STRESS MPa	R	Q Hz	E GPa	e %	CYCLES TO FAIL	WIDTH (mm) and Notes
972	CC120	207	0.1	15	21.9	1.02	48,080	25 tab
973	CC124	207	0.1	15	21.6	1.05	32,670	25 tab
974	CC106	172	0.1	10	21.8	0.84	228,453	25 tab
975	CC114	172	0.1	15	23.2	0.74	205,864	25 tab
976	CC110	241	0.1	10	----	----	27,772	25 tab
977	CC115	207	0.1	10	----	----	158,287	25 tab
978	CC123	207	0.1	15	----	----	133,440	25 tab
979	CC109	207	0.1	15	----	----	243,962	25 tab
980	CC137	207	0.1	15	----	----	531,499	25
981	CC135	207	0.1	15	20.7	1.00	631,495	25
982	CC130	207	0.1	15	20.2	1.02	486,225	25
983	CC134	276	0.1	10	----	----	50,289	25
984	CC131	276	0.1	10	----	----	30,467	25
985	CC133	276	0.1	10	----	----	38,977	25
986	CC132	345	0.1	2	----	----	2,979	25
987	CC143	345	0.1	2	----	----	4,476	25
988	CC144	345	0.1	2	----	----	4,807	25
989	CC142	531	*	13	----	----	1	25
990	CC140	562	*	13	----	----	1	25
3052	CC160	-475	*	13	----	----	1	25
3053	CC161	-442	*	13	----	----	1	25

MATERIAL CC2

Lay-up = $[\pm 45/0_3/+45]_S$, $V_F = 0.45$, Ave. thickness = 2.69 mm, S.D. = 0.03 mm, CoRezyn 63-AX-051 Polyester

991	CC2101	746	*	13	27.0	2.78	1	25
992	CC2103	730	*	13	26.9	2.86	1	25
993	CC2102	701	*	13	27.0	2.81	1	25
994	CC2105	414	0.1	5	25.6	1.62	4,104	25
995	CC2106	276	0.1	15	----	----	168,303	25
996	CC2116	276	0.1	10	----	----	132,591	25
997	CC2108	276	0.1	10	----	----	176,536	25
998	CC2111	414	0.1	15	----	----	2,231	25
999	CC2113	414	0.1	4	----	----	2,820	25
1000	CC2107	345	0.1	10	----	----	21,413	25
1001	CC2117	345	0.1	10	----	----	16,914	25
1002	CC2110	345	0.1	10	----	----	21,965	25
1003	CC2109	207	0.1	20	----	----	1,873,767	25
1004	CC2115	683	*	13	----	----	1	25
1005	CC2114	695	*	13	----	----	1	25
1006	CC2112	735	*	13	----	----	1	25
1842	CC2201	-555	*	13	----	----	1	25
1843	CC2202	-500	*	13	----	----	1	25
1844	CC2119	-526	*	13	----	----	1	25

TEST & SAMPLE ID #		MAX. STRESS MPa	R	Q Hz	E GPa	e %	CYCLES TO FAIL	WIDTH (mm) and Notes
MATERIAL CC3								
Lay-up = $[0/\pm45/0_2/+45]_S$, V_F = 0.45, Ave. thickness = 2.74 mm, S.D. = 0.06 mm, CoRezyn 63-AX-051 Polyester								
1007	CC3101	690	*	0.5	26.1	2.64	1	25
1008	CC3102	657	*	0.5	25.8	2.54	1	25
1009	CC3103	700	*	0.5	26.9	2.60	1	25
1010	CC3107	414	0.1	5	----	----	1,324	25
1011	CC3104	414	0.1	5	----	----	5,122	25
1012	CC3105	414	0.1	5	----	----	4,241	25
1013	CC3108	276	0.1	10	----	----	186,787	25
1014	CC3106	276	0.1	10	----	----	226,915	25
1015	CC3109	276	0.1	10	----	----	169,059	25
1016	CC3111	414	0.1	5	----	----	4,469	25
1017	CC3110	345	0.1	5	----	----	26,235	25
1018	CC3113	345	0.1	5	----	----	31,512	25
1019	CC3112	345	0.1	5	----	----	28,465	25
1020	CC3121	241	0.1	15	----	----	371,472	25
1021	CC3120	241	0.1	20	----	----	428,636	25
1022	CC3124	207	0.1	15	----	----	2,016,665	25
1848	CC3200	-570	*	13	----	----	1	25
1849	CC3201	-539	*	13	----	----	1	25
1850	CC3202	-513	*	13	----	----	1	25
MATERIAL CH								
Lay-up = $[(\pm45)_3]_S$, V_F = 0.45, Ave. thickness = 3.86 mm, S.D. = 0.04 mm, CoRezyn 63-AX-051 Polyester								
1254	CH108	135	*	13	15.4	1.2	1	25
1255	CH119	162	*	13	13.7	1.7	1	25
1256	CH112	139	*	13	12.8	1.5	1	25
1257	CH111	103	0.1	2	13.4	0.97	3,591	25
1258	CH105	103	0.1	2	12.3	0.93	1,545	25
1259	CH116	86	0.1	5	13.5	0.64	2,886	25
1260	CH109	69	0.1	5	13.5	0.51	37,378	25
1261	CH117	52	0.1	15	11.7	0.44	5,000,000	25 R
1262	CH114	103	0.1	2	13.6	0.94	920	25
1263	CH113	86	0.1	4	14.1	0.91	5,340	25
1264	CH107	86	0.1	4	14.3	0.92	4,604	25
1265	CH104	69	0.1	5	13.8	0.59	73,763	25
1266	CH106	69	0.1	5	14.3	0.64	28,432	25
1267	CH128	137	*	13	13.7	1.4	1	25
1268	CH125	62	0.1	10	14.1	0.51	327,862	25
1269	CH126	62	0.1	10	13.0	0.60	250,000	25
1270	CH110	62	0.1	10	14.0	0.55	171,332	25
1271	CH131	-190	*	0.1	----	----	1	25
1272	CH141	-179	*	0.1	----	----	1	25
1273	CH152	-171	*	0.1	----	----	1	25

TEST & SAMPLE ID #		MAX. STRESS MPa	R	Q Hz	E GPa	e %	CYCLES TO FAIL	WIDTH (mm) and Notes
1274	CH137	-124	10	2	----	----	433	25
1275	CH134	-124	10	2	----	----	870	25
1276	CH136	-86	10	5	----	----	61,185	25
1277	CH138	-86	10	10	----	----	31,317	25
1278	CH139	-69	10	20	----	----	1,317,352	25
1279	CH145	-103	10	5	----	----	5,030	25
1280	CH144	-103	10	5	----	----	9,428	25
1281	CH152	-124	10	2	----	----	956	25
1282	CH132	-103	10	5	----	----	6,653	25
1283	CH133	-69	10	20	----	----	1,125,335	25
1284	CH135	-86	10	10	----	----	76,452	25
1372a	CH146	-171	*	13	----	----	1	25

MATERIAL CH2

Lay-up = $[(\pm 45/0/\pm 45)]_S$, V_F = 0.41, Ave. thickness = 3.78 mm, S.D. = 0.10 mm, CoRezyn 63-AX-051 Polyester

1349	CH2116	354	*	13	16.0	2.21	1	25
1350	CH2101	365	*	13	17.2	2.12	1	25
1351	CH2107	367	*	13	17.9	2.05	1	25
1352	CH2103	241	0.1	2	16.4	1.80	396	25
1356	CH2112	241	0.1	2	16.2	2.20	221	25
1357	CH2109	207	0.1	4	16.6	1.79	2,148	25
1358	CH2115	207	0.1	4	16.5	1.77	1,917	25
1359	CH2113	172	0.1	5	15.9	1.34	11,276	25
1360	CH2106	138	0.1	5	16.7	1.10	40,073	25
1361	CH2111	103	0.1	20	17.2	0.64	1,855,170	25
1362	CH2117	207	0.1	2	16.8	1.72	1,342	25
1363	CH2114	172	0.1	4	17.0	1.25	9,910	25
1364	CH2105	172	0.1	4	17.4	1.23	8,987	25
1365	CH2110	138	0.1	10	14.8	1.14	54,659	25
1366	CH2108	138	0.1	5	16.9	0.97	37,586	25
1367	CH2102	121	0.1	10	18.0	0.77	97,564	25
1368	CH2149T	117	*	13	12.4	2.64	1	25
1369	CH2104	370	*	13	16.5	2.85	1	25
1370	CH2146T	134	*	13	12.6	----	1	25
1371	CH2147T	122	*	13	12.3	----	1	25
1372	CH2129	-342	*	13	----	----	1	25
1373	CH2130	-333	*	13	----	----	1	25
1374	CH2128	-350	*	13	----	----	1	25
1375	CH2146T	-171	*	13	----	----	1	25
1376	CH2127	-276	10	2	----	----	39	25
1377	CH2156	-207	10	2	----	----	848	25
1378	CH2126	-207	10	2	----	----	1,972	25
1379	CH2118	-207	10	2	----	----	2,458	25
1380	CH2141	-172	10	5	----	----	19,691	25
1381	CH2122	-172	10	5	----	----	15,420	25
1382	CH2119	-138	10	20	----	----	871,785	25

TEST & SAMPLE ID #		MAX. STRESS MPa	R	Q Hz	E GPa	e %	CYCLES TO FAIL	WIDTH (mm) and Notes
1383	CH2121	-172	10	5	----	----	14,149	25
1384	CH2133	-155	10	10	----	----	166,026	25
1385	CH2125	-155	10	15	----	----	83,700	25

MATERIAL CH3

Lay-up = $[(\pm 45/0/\pm 45)]_S$, V_F = 0.36, Ave. thickness = 4.19 mm, S.D. = 0.07 mm, CoRezyn 63-AX-051 Polyester

1386	CH3105	-326	*	13	----	----	1	25
1387	CH3117	-319	*	13	----	----	1	25
1388	CH3111	-309	*	13	----	----	1	25
1389	CH3106	-207	10	2	----	----	238	25
1390	CH3109	-207	10	2	----	----	159	25
1391	CH3110	-172	10	5	----	----	1,331	25
1392	CH3115	-172	10	4	----	----	760	25
1393	CH3108	-138	10	5	----	----	23,189	25
1394	CH3102	-138	10	5	----	----	14,301	25
1395	CH3103	-207	10	2	----	----	264	25
1396	CH3104	-172	10	4	----	----	982	25
1397	CH3107	-138	10	10	----	----	27,750	25
1398	CH3101	-121	10	15	----	----	141,901	25
1399	CH3112	-121	10	15	----	----	81,244	25
1400	CH3118	-121	10	20	----	----	164,715	25
1472	CH3124	333	*	13	17.3	2.71	1	25
1473	CH3135	340	*	13	16.5	2.85	1	25
1474	CH3131	336	*	13	16.1	2.74	1	25
1475	CH3125	241	0.1	2	16.6	2.23	173	25
1476	CH3132	241	0.1	2	16.1	2.85	174	25
1477	CH3136	241	0.1	2	15.9	2.26	134	25
1478	CH3122	207	0.1	2	16.8	1.59	1,166	25
1479	CH3134	207	0.1	2	17.0	1.69	1,270	25
1480	CH3128	207	0.1	2	15.6	1.82	814	25
1481	CH3119	172	0.1	5	17.8	1.19	8,478	25
1482	CH3129	172	0.1	4	16.6	1.35	12,387	25
1483	CH3123	172	0.1	5	18.3	1.25	14,410	25
1484	CH3126	138	0.1	10	17.2	0.95	282,621	25
1485	CH3121	138	0.1	5	15.7	1.04	200,174	25
1486	CH3130	138	0.1	10	18.1	0.91	429,020	25

MATERIAL CH4

Lay-up = $[(\pm 45)_3]_S$, V_F = 0.40, Ave. thickness = 2.92 mm, S.D. = 0.08 mm, CoRezyn 63-AX-051 Polyester

1445	CH4123	-173	*	13	----	----	1	25
1446	CH4133	-171	*	13	----	----	1	25
1447	CH4129	-173	*	13	----	----	1	25
1448	CH4140	-124	10	2	----	----	144	25
1449	CH4134	-124	10	1	----	----	188	25

TEST & SAMPLE ID #		MAX. STRESS MPa	R	Q Hz	E GPa	e %	CYCLES TO FAIL	WIDTH (mm) and Notes
1450	CH4141	-124	10	1	----	----	256	25
1451	CH4137	-103	10	2	----	----	1,313	25
1452	CH4142	-103	10	2	----	----	1,883	25
1453	CH4126	-103	10	2	----	----	873	25
1454	CH4128	-86	10	5	----	----	21,748	25
1455	CH4130	-86	10	5	----	----	13,364	25
1456	CH4131	-86	10	4	----	----	11,200	25
1457	CH4125	-69	10	15	----	----	206,018	25
1458	CH4135	-69	10	10	----	----	564,767	25
1459	CH4122	-69	10	15	----	----	485,632	25
1509	CH4106	160	*	13	11.0	6.41	1	25
1510	CH4114	157	*	13	11.2	5.15	1	25
1511	CH4115	149	*	13	11.4	6.35	1	25
1512	CH4117	103	0.1	2	11.4	1.70	198	25
1513	CH4107	103	0.1	2	11.0	1.80	287	25
1514	CH4110	103	0.1	2	12.4	1.40	314	25
1515	CH4118	86	0.1	4	11.7	1.38	1,319	25
1516	CH4111	86	0.1	2	12.1	0.99	2,311	25
1517	CH4113	86	0.1	4	10.9	1.24	1,186	25
1518	CH4102	69	0.1	10	11.2	0.82	7,072	25
1519	CH4119	69	0.1	10	10.7	0.79	10,172	25
1520	CH4103	69	0.1	10	12.2	0.64	15,843	25
1521	CH4101	52	0.1	20	11.1	0.52	342,135	25
1522	CH4116	52	0.1	20	----	----	224,519	25
1523	CH4104	52	0.1	20	12.2	0.47	1,136,938	25

MATERIAL CH5

Lay-up = $[(\pm 45)_3]_S$, $V_F = 0.28$, Ave. thickness = 3.05 mm, S.D. = 0.09 mm, CoRezyn 63-AX-051 Polyester

1460	CH5126	-190	*	13	----	----	1	25
1461	CH5123	-190	*	13	----	----	1	25
1462	CH5119	-190	*	13	----	----	1	25
1463	CH5127	-86	10	10	----	----	131,302	25
1464	CH5128	-121	10	2	----	----	1,548	25
1465	CH5129	-121	10	2	----	----	2,777	25
1466	CH5125	-121	10	2	----	----	2,989	25
1467	CH5118	-103	10	4	----	----	12,027	25
1468	CH5120	-103	10	5	----	----	9,130	25
1469	CH5121	-103	10	5	----	----	18,621	25
1470	CH5122	-86	10	15	----	----	329,191	25
1471	CH5124	-86	10	15	----	----	277,202	25
1524	CH5112	147	*	13	9.8	4.12	1	25
1525	CH5103	134	*	13	7.5	----	1	25
1526	CH5105	137	*	13	9.0	----	1	25
1527	CH5115	86	0.1	2	8.3	----	1,140	25
1528	CH5101	86	0.1	2	8.3	----	1,310	25
1529	CH5106	86	0.1	2	8.1	1.69	749	25
1530	CH5102	69	0.1	4	8.1	0.95	11,184	25

TEST & SAMPLE ID #		MAX. STRESS MPa	R	Q Hz	E GPa	e %	CYCLES TO FAIL	WIDTH (mm) and Notes
1531	CH5113	69	0.1	5	8.8	0.90	17,929	25
1532	CH5104	69	0.1	4	9.0	0.90	14,588	25
1533	CH5114	52	0.1	15	8.7	0.63	113,426	25
1534	CH5107	52	0.1	12	8.5	0.63	282,007	25
1535	CH5111	52	0.1	10	8.3	0.65	181,712	25
Tests 3557 - 3583 involved a gage length of 13 mm (strain rate effect tests).								
3557	CH5121	-194	*	0.025	----	----	1	25 tab
3558	CH5144	-202	*	0.025	----	----	1	25 tab
3559	CH5142	-189	*	0.025	----	----	1	25 tab
3560	CH5122	-214	*	0.254	----	----	1	25 tab
3561	CH5123	-207	*	0.254	----	----	1	25 tab
3562	CH5135	-213	*	0.254	----	----	1	25 tab
3563	CH5145	-213	*	2.54	----	----	1	25 tab
3564	CH5147	-206	*	2.54	----	----	1	25 tab
3565	CH5146	-219	*	2.54	----	----	1	25 tab
3566	CH5148	-230	*	6.35	----	----	1	25 tab
3567	CH5124	-225	*	6.35	----	----	1	25 tab
3568	CH5133	-216	*	6.35	----	----	1	25 tab
3569	CH5140	-223	*	12.7	----	----	1	25 tab
3570	CH5141	-225	*	12.7	----	----	1	25 tab
3571	CH5143	-243	*	12.7	----	----	1	25 tab
3572	CH5118	-227	*	19.1	----	----	1	25 tab
3573	CH5125	-224	*	19.1	----	----	1	25 tab
3574	CH5132	-207	*	19.1	----	----	1	25 tab
3575	CH5120	-242	*	25.4	----	----	1	25 tab
3576	CH5136	-242	*	25.4	----	----	1	25 tab
3577	CH5137	-211	*	25.4	----	----	1	25 tab
3578	CH5138	-223	*	63.5	----	----	1	25 tab
3579	CH5139	-238	*	63.5	----	----	1	25 tab
3580	CH5116	-215	*	63.5	----	----	1	25 tab
3581	CH5136	-241	*	127	----	----	1	25 tab
3582	CH5126	-239	*	127	----	----	1	25 tab
3583	CH5127	-228	*	127	----	----	1	25 tab
Tests 3557 - 3583 involved a gage length of 100 mm (strain rate effect tests).								
3584	CH5105	120	*	0.025	----	----	1	25 tab
3585	CH5114	120	*	0.025	----	----	1	25 tab
3586	CH5111	120	*	0.025	----	----	1	25 tab
3587	CH5112	125	*	0.254	----	----	1	25 tab
3588	CH5110	126	*	0.254	----	----	1	25 tab
3589	CH5109	126	*	0.254	----	----	1	25 tab
3590	CH5107	126	*	2.54	----	----	1	25 tab
3591	CH5108	137	*	2.54	----	----	1	25 tab
3592	CH5102	131	*	2.54	----	----	1	25 tab
3593	CH5103	137	*	12.7	----	----	1	25 tab
3594	CH5113	135	*	12.7	----	----	1	25 tab
3595	CH5106	136	*	12.7	----	----	1	25 tab
3596	CH5101	137	*	63.5	----	----	1	25 tab
3597	CH5104	142	*	63.5	----	----	1	25 tab

TEST & SAMPLE ID #		MAX. STRESS MPa	R	Q Hz	E GPa	e %	CYCLES TO FAIL	WIDTH (mm) and Notes
3598	CH5114	131	*	63.5	----	----	1	25 tab

MATERIAL CH6

Lay-up = [±45/0/±45]s, V_F = 0.49, Ave. thickness = 2.26 mm, S.D. = 0.09 mm, CoRezyn 63-AX-051 Polyester

1416	CH6106	-413	*	13	----	----	1	25
1417	CH6114	-381	*	13	----	----	1	25
1418	CH6105	-428	*	13	----	----	1	25
1419	CH6103	-207	10	5	----	----	15,707	25
1420	CH6117	-207	10	10	----	----	20,605	25
1421	CH6107	-207	10	5	----	----	38,711	25
1422	CH6101	-241	10	4	----	----	10,088	25
1423	CH6112	-241	10	4	----	----	11,950	25
1424	CH6102	-241	10	4	----	----	8,842	25
1425	CH6109	-276	10	2	----	----	2,727	25
1426	CH6110	-276	10	2	----	----	1,373	25
1427	CH6119	-276	10	2	----	----	840	25
1428	CH6104	-172	10	20	----	----	880,742	25
1429	CH6118	-172	10	20	----	----	1,628,900	25
1487	CH6123	510	*	13	22.5	3.34	1	25
1488	CH6128	500	*	13	21.6	2.98	1	25
1489	CH6133	495	*	13	22.9	3.24	1	25
1490	CH6140	345	0.1	2	20.9	2.11	284	25
1491	CH6127	345	0.1	2	20.0	2.24	189	25
1492	CH6134	345	0.1	2	21.2	2.04	246	25
1493	CH6139	310	0.1	2	20.3	1.81	561	25
1494	CH6124	310	0.1	2	20.9	1.76	758	25
1495	CH6138	310	0.1	2	20.5	1.78	619	25
1496	CH6130	276	0.1	4	20.3	1.64	2,224	25
1497	CH6131	276	0.1	4	21.1	1.60	1,490	25
1498	CH6125	276	0.1	4	22.4	1.41	2,153	25
1499	CH6126	241	0.1	5	21.8	1.30	4,278	25
1500	CH6129	241	0.1	10	21.0	1.29	6,877	25
1501	CH6135	207	0.1	10	23.0	1.04	13,309	25
1502	CH6132	207	0.1	5	22.1	1.04	15,150	25
1503	CH6141	207	0.1	5	22.4	1.06	11,807	25
1504	CH6122	172	0.1	5	21.7	0.87	44,634	25
1505	CH6136	172	0.1	10	22.1	0.86	37,335	25
1506	CH6137	138	0.1	10	22.5	0.67	224,743	25
1507	CH6142	138	0.1	10	21.1	0.69	138,170	25
1508	CH6148	121	0.1	20	20.5	0.59	419,563	25

MATERIAL CH7

Lay-up = $[(\pm 45)_3]$s, V_F = 0.55, Ave. thickness = 3.86 mm, S.D. = 0.05 mm, CoRezyn 63-AX-051 Polyester

1401	CH7110	-174	*	13	----	----	1	25
1402	CH7114	-164	*	13	----	----	1	25

TEST & SAMPLE ID #		MAX. STRESS MPa	R	Q Hz	E GPa	e %	CYCLES TO FAIL	WIDTH (mm) and Notes
1403	CH7109	-165	*	13	----	----	1	25
1404	CH7107	-103	10	2	----	----	1,918	25
1405	CH7102	-103	10	2	----	----	1,763	25
1406	CH7106	-103	10	2	----	----	3,055	25
1407	CH7108	-86	10	5	----	----	16,492	25
1408	CH7104	-86	10	5	----	----	20,747	25
1409	CH7111	-86	10	5	----	----	15,719	25
1410	CH7150	-69	10	20	----	----	96,260	25
1411	CH7112	-69	10	20	----	----	278,521	25
1412	CH7101	-69	10	15	----	----	167,393	25
1413	CH7122	112	*	13	13.8	1.75	1	25
1414	CH7126	107	*	13	15.4	----	1	25
1415	CH7128	113	*	13	15.4	----	1	25
1536	CH7115	115	*	13	15.7	4.80	1	25
1537	CH7117	116	*	13	17.9	----	1	25
1538	CH7127	112	*	13	18.6	----	1	25
1539	CH7125	69	0.1	5	16.3	0.55	4,943	25
1540	CH7120	69	0.1	5	17.2	0.49	3,145	25
1541	CH7119	69	0.1	5	17.5	0.49	3,797	25
1542	CH7121	52	0.1	10	17.8	0.32	92,285	25
1543	CH7116	52	0.1	10	16.5	0.34	62,832	25
1544	CH7123	52	0.1	10	15.2	0.34	116,214	25
1545	CH7130	83	0.1	2	19.0	0.70	418	25
1546	CH7118	83	0.1	2	18.2	0.57	521	25

MATERIAL CH8

Lay-up = $[(\pm 45)_3]s$, $V_F = 0.39$, Ave. thickness = 5.89 mm, S.D. = 0.12 mm, CoRezyn 63-AX-051 Polyester

1430	CH8141	-145	*	13	----	----	1	25
1431	CH8128	-145	*	13	----	----	1	25
1432	CH8122	-148	*	13	----	----	1	25
1433	CH8136	-103	10	4	----	----	191	25
1434	CH8126	-103	10	2	----	----	99	25
1435	CH8125	-103	10	2	----	----	215	25
1436	CH8129	-86	10	2	----	----	1,242	25
1437	CH8121	-86	10	2	----	----	862	25
1438	CH8127	-86	10	2	----	----	719	25
1439	CH8130	-69	10	4	----	----	2,509	25
1440	CH8139	-69	10	4	----	----	3,894	25
1441	CH8135	-69	10	4	----	----	1,784	25
1442	CH8124	-52	10	5	----	----	11,312	25
1443	CH8123	-52	10	5	----	----	8,752	25
1444	CH8132	-52	10	5	----	----	36,219	25
1547	CH8107	91	*	13	9.4	5.86	1	25
1548	CH8104	97	*	13	9.8	6.70	1	25
1549	CH8118	90	*	13	11.9	7.43	1	25
1550	CH8116	52	0.1	4	9.0	0.61	8,968	25
1551	CH8102	52	0.1	4	10.0	0.60	9,804	25

TEST & SAMPLE ID #		MAX. STRESS MPa	R	Q Hz	E GPa	e %	CYCLES TO FAIL	WIDTH (mm) and Notes
1552	CH8106	52	0.1	5	8.6	0.65	10,105	25
1553	CH8105	62	0.1	2	12.4	0.60	1,756	25
1554	CH8113	62	0.1	2	9.5	0.90	1,333	25
1555	CH8119	62	0.1	2	9.2	0.82	1,691	25
1556	CH8115	41	0.1	10	10.7	0.42	59,831	25
1557	CH8114	41	0.1	10	11.1	0.40	50,912	25
1558	CH8103	41	0.1	10	9.4	0.43	70,962	25
1559	CH8101	34	0.1	15	9.3	0.37	1,480,988	25

MATERIAL CH9

Lay-up = $[(\pm 45)_3]s$, $V_F = 0.49$, Ave. thickness = 2.13 mm, S.D. = 0.07 mm, CoRezyn 63-AX-051 Polyester

1560	CH9106	157	*	13	10.4	7.70	1	25
1561	CH9113	144	*	13	10.1	5.17	1	25
1562	CH9105	151	*	13	10.6	9.15	1	25
1563	CH9110	103	0.1	2	10.0	1.80	250	25
1564	CH9101	103	0.1	2	10.6	1.70	285	25
1565	CH9114	103	0.1	2	10.8	2.00	294	25
1566	CH9108	86	0.1	2	10.1	1.30	1,503	25
1567	CH9112	86	0.1	2	10.8	1.17	1,901	25
1568	CH9103	86	0.1	2	10.4	1.32	2,357	25
1569	CH9107	69	0.1	5	9.7	0.97	11,702	25
1570	CH9109	52	0.1	20	11.5	0.46	868,713	25
1571	CH9102	69	0.1	5	8.1	0.90	8,369	25
1572	CH9115	69	0.1	5	10.3	0.83	13,987	25
1573	CH9116	52	0.1	15	10.1	0.54	937,400	25
1643	CH9144	-172	*	13	----	----	1	25
1644	CH9136	-176	*	13	----	----	1	25
1645	CH9133	-175	*	13	----	----	1	25
1646	CH9132	-121	10	2	----	----	299	25
1647	CH9137	-121	10	4	----	----	738	25
1648	CH9145	-121	10	2	----	----	352	25
1649	CH9143	-103	10	4	----	----	5,842	25
1650	CH9140	-103	10	4	----	----	1,801	25
1651	CH9134	-103	10	2	----	----	2,917	25
1652	CH9130	-86	10	10	----	----	68,643	25
1653	CH9138	-86	10	10	----	----	39,626	25
1654	CH9131	-86	10	5	----	----	46,815	25
1655	CH9141	-76	10	10	----	----	522,908	25

MATERIAL CH10

Lay-up = $[(\pm 45)_3]s$, $V_F = 0.33$, Ave. thickness = 5.56 mm, S.D. = 0.08 mm, CoRezyn 63-AX-051 Polyester

1574	CH10114	124	*	13	7.6	7.17	1	25
1575	CH10105	122	*	13	7.4	6.42	1	25
1576	CH10115	116	*	13	7.7	8.12	1	25
1577	CH10113	69	0.1	4	8.1	1.16	4,432	25

TEST & SAMPLE ID #		MAX. STRESS MPa	R	Q Hz	E GPa	e %	CYCLES TO FAIL	WIDTH (mm) and Notes
1578	CH10119	69	0.1	4	7.9	1.30	2,609	25
1579	CH10110	69	0.1	2	8.3	1.05	5,331	25
1580	CH10109	86	0.1	1	8.2	1.81	201	25
1581	CH10104	86	0.1	1	7.3	2.00	114	25
1582	CH10118	86	0.1	1	7.8	1.89	187	25
1583	CH10117	52	0.1	5	8.5	0.67	506,181	25
1584	CH10103	59	0.1	5	9.2	0.76	72,644	25
1585	CH10108	59	0.1	5	9.1	0.75	63,552	25
1586	CH10121	59	0.1	4	8.0	0.85	32,735	25
The compression gage length for the CH10 coupons was 19 mm instead of the standard 13 mm due to hydraulic grip space restrictions (grip heads would impact with a 13 mm gage length).								
1668	CH10153	-167	*	13	----	----	1	25
1669	CH10132	-158	*	13	----	----	1	25
1670	CH10142	-164	*	13	----	----	1	25
1671	CH10130	-121	10	1	----	----	93	25
1672	CH10149	-121	10	1	----	----	48	25
1673	CH10151	-121	10	1	----	----	62	25
1674	CH10139	-103	10	1	----	----	510	25
1675	CH10146	-103	10	1	----	----	843	25
1676	CH10133	-103	10	1	----	----	709	25
1677	CH10138	-86	10	2	----	----	2,914	25
1678	CH10131	-86	10	2	----	----	3,996	25
1679	CH10155	-86	10	2	----	----	1,948	25
1680	CH10135	-69	10	5	----	----	25,535	25
1681	CH10144	-69	10	5	----	----	15,850	25
1682	CH10134	-69	10	5	----	----	20,095	25
1683	CH10145	-52	10	15	----	----	948,262	25

MATERIAL CH11

Lay-up = $[(\pm 45)_3]s$, $V_F = 0.54$, Ave. thickness = 2.41 mm, S.D. = 0.05 mm, CoRezyn 63-AX-051 Polyester

1587	CH11114	128	*	13	13.0	6.78	1	25
1588	CH11111	143	*	13	13.0	6.00	1	25
1589	CH11105	132	*	13	13.0	----	1	25
1590	CH11113	86	0.1	4	14.0	0.98	861	25
1591	CH11109	86	0.1	4	13.8	1.00	1,207	25
1592	CH11101	86	0.1	4	13.1	0.97	1,310	25
1593	CH11102	69	0.1	4	15.2	0.58	13,430	25
1594	CH11107	69	0.1	4	14.0	0.60	18,411	25
1595	CH11106	69	0.1	4	12.0	0.73	11,934	25
1596	CH11103	59	0.1	12	14.0	0.49	85,334	25
1597	CH11104	59	0.1	15	13.6	0.48	120,347	25
1598	CH11110	59	0.1	15	12.8	0.51	68,035	25
1599	CH11112	52	0.1	15	13.0	0.42	356,380	25
1656	CH11120	-190	*	13	----	----	1	25
1657	CH11129	-188	*	13	----	----	1	25
1658	CH11125	-188	*	13	----	----	1	25
1659	CH11116	-121	10	2	----	----	1,285	25

TEST & SAMPLE ID #		MAX. STRESS MPa	R	Q Hz	E GPa	e %	CYCLES TO FAIL	WIDTH (mm) and Notes
1660	CH11115	-121	10	2	----	----	1,821	25
1661	CH11118	-121	10	2	----	----	1,122	25
1662	CH11124	-103	10	5	----	----	16,602	25
1663	CH11123	-103	10	5	----	----	12,602	25
1664	CH11121	-103	10	5	----	----	21,683	25
1665	CH11117	-86	10	10	----	----	71,004	25
1666	CH11128	-86	10	12	----	----	168,236	25
1667	CH11126	-86	10	10	----	----	302,383	25

MATERIAL CH12

Lay-up = [±45/0/±45]s, V_F = 0.34, Ave. thickness = 3.00 mm, S.D. = 0.10 mm, CoRezyn 63-AX-051 Polyester

1600	CH12114	391	*	13	15.8	5.49	1	25
1601	CH12109	412	*	13	18.0	6.82	1	25
1602	CH12116	393	*	13	16.0	5.92	1	25
1603	CH12121	276	0.1	2	11.4	1.94	2,415	25
1604	CH12108	276	0.1	2	17.7	1.99	1,325	25
1605	CH12118	276	0.1	2	17.9	1.85	2,803	25
1606	CH12102	207	0.1	10	18.6	1.20	108,802	25
1607	CH12101	207	0.1	10	18.6	1.29	65,123	25
1608	CH12117	207	0.1	10	18.2	1.29	82,951	25
1609	CH12107	190	0.1	10	18.8	1.13	244,866	25
1610	CH12119	172	0.1	15	16.3	1.19	476,154	25
1611	CH12106	241	0.1	4	17.9	1.49	9,523	25
1612	CH12105	241	0.1	4	17.5	1.60	4,914	25
1613	CH12120	172	0.1	10	18.7	1.00	389,771	25
1684	CH12143	-442	*	13	----	----	1	25
1685	CH12144	-455	*	13	----	----	1	25
1686	CH12133	-455	*	13	----	----	1	25
1687	CH12123	-276	10	4	----	----	4,326	25
1688	CH12135	-276	10	2	----	----	7,611	25
1689	CH12124	-276	10	4	----	----	8,723	25
1693	CH12137	-241	10	15	----	----	116,437	25
1694	CH12129	-207	10	15	18.9	-1.09	1,712,433	25
1695	CH12126	-207	10	15	----	----	663,181	25
1696	CH12131	-310	10	2	----	----	4,295	25
1697	CH12140	-310	10	2	----	----	3,815	25
1698	CH12127	-310	10	2	----	----	1,465	25
1699	CH12128	-241	10	10	----	----	64,663	25
1700	CH12146	-345	10	1	----	----	887	25
1701	CH12144	-345	10	1	----	----	266	25
1702	CH12145	-345	10	1	----	----	394	25
Tests 3199 - 3219 involved a gage length of 100 mm (coupon width effect tests).								
3199	CH1225	331	*	13	----	----	1	51
3200	CH1226	317	*	13	----	----	1	51
3201	CH1227	295	*	13	----	----	1	51
3202	CH1231	321	*	13	----	----	1	38
3203	CH1232	316	*	13	----	----	1	38

TEST & SAMPLE ID #		MAX. STRESS MPa	R	Q Hz	E GPa	e %	CYCLES TO FAIL	WIDTH (mm) and Notes
3204	CH1233	299	*	13	----	----	1	38
3205	CH1234	308	*	13	----	----	1	32
3206	CH1235	304	*	13	----	----	1	32
3207	CH1236	310	*	13	----	----	1	32
3208	CH1237	304	*	13	----	----	1	25
3209	CH1238	304	*	13	----	----	1	25
3210	CH1239	301	*	13	----	----	1	25
3211	CH1240	306	*	13	----	----	1	19
3212	CH1241	297	*	13	----	----	1	19
3213	CH1242	309	*	13	----	----	1	19
3214	CH1243	287	*	13	----	----	1	13
3215	CH1244	273	*	13	----	----	1	13
3216	CH1245	278	*	13	----	----	1	13
3217	CH1246	251	*	13	----	----	1	6
3218	CH1247	255	*	13	----	----	1	6
3219	CH1248	219	*	13	----	----	1	6
Tests 3220 - 3243 involved a gage length of 13 mm (coupon width effect tests).								
3220	CH12121	-312	*	13	----	----	1	51
3221	CH12122	-323	*	13	----	----	1	51
3222	CH12123	-330	*	13	----	----	1	51
3223	CH12124	-333	*	13	----	----	1	44
3224	CH12125	-288	*	13	----	----	1	44
3225	CH12126	-335	*	13	----	----	1	44
3226	CH12127	-336	*	13	----	----	1	38
3227	CH12128	-397	*	13	----	----	1	38
3228	CH12129	-401	*	13	----	----	1	38
3229	CH1210	-384	*	13	----	----	1	32
3230	CH1211	-401	*	13	----	----	1	32
3231	CH1212	-382	*	13	----	----	1	32
3232	CH1213	-359	*	13	----	----	1	25
3233	CH1214	-358	*	13	----	----	1	25
3234	CH1215	-352	*	13	----	----	1	25
3235	CH1216	-356	*	13	----	----	1	19
3236	CH1217	-351	*	13	----	----	1	19
3237	CH1218	-354	*	13	----	----	1	19
3238	CH1219	-354	*	13	----	----	1	13
3239	CH1220	-328	*	13	----	----	1	13
3240	CH1221	-334	*	13	----	----	1	13
3241	CH1222	-308	*	13	----	----	1	6
3242	CH1223	-352	*	13	----	----	1	6
3243	CH1224	-299	*	13	----	----	1	6
Tests 3301 - 3318 involved a gage length of 100 mm (strain rate effect tests).								
3301	CH12001	366	*	0.025	----	----	1	25
3302	CH12002	328	*	0.025	----	----	1	25
3303	CH12003	345	*	0.025	----	----	1	25
3304	CH12004	387	*	0.25	----	----	1	25
3305	CH12005	388	*	0.25	----	----	1	25
3306	CH12006	379	*	0.25	----	----	1	25

TEST & SAMPLE ID #		MAX. STRESS MPa	R	Q Hz	E GPa	e %	CYCLES TO FAIL	WIDTH (mm) and Notes
3307	CH12007	430	*	2.54	----	----	1	25
3308	CC12008	413	*	2.54	----	----	1	25
3309	CH12009	419	*	2.54	----	----	1	25
3310	CH12010	440	*	25	----	----	1	25
3311	CH12011	420	*	25	----	----	1	25
3312	CH12012	443	*	25	----	----	1	25
3313	CH12013	455	*	64	----	----	1	25
3314	CH12014	480	*	64	----	----	1	25
3315	CH12015	472	*	64	----	----	1	25
3316	CH12016	437	*	127	----	----	1	25
3317	CH12017	485	*	127	----	----	1	25
3318	CH12018	484	*	127	----	----	1	25
Tests 3319 - 3336 involved a gage length of 13 mm (strain rate effect tests).								
3319	CH12025	-408	*	0.025	----	----	1	25
3320	CH12026	-444	*	0.025	----	----	1	25
3321	CH12027	-377	*	0.025	----	----	1	25
3322	CH12028	-415	*	0.25	----	----	1	25
3323	CH12029	-426	*	0.25	----	----	1	25
3324	CH12030	-443	*	0.25	----	----	1	25
3325	CH12031	-447	*	2.54	----	----	1	25
3326	CH12032	-468	*	2.54	----	----	1	25
3327	CH12033	-424	*	2.54	----	----	1	25
3232	CH12013	-359	*	13	----	----	1	25
3233	CH12014	-358	*	13	----	----	1	25
3234	CH12015	-352	*	13	----	----	1	25
3328	CH12034	-482	*	25	----	----	1	25
3329	CH12035	-500	*	25	----	----	1	25
3330	CH12036	-492	*	25	----	----	1	25
3331	CH12037	-438	*	64	----	----	1	25
3332	CH12038	-402	*	64	----	----	1	25
3333	CH12039	-402	*	64	----	----	1	25
3334	CH12040	-455	*	127	----	----	1	25
3335	CH12041	-449	*	127	----	----	1	25
3336	CH12042	-454	*	127	----	----	1	25

MATERIAL CH13

Lay-up = [±45/0/±45]s, V_F = 0.48, Ave. thickness = 3.28 mm, S.D. = 0.05 mm, CoRezyn 63-AX-051 Polyester

1614	CH13113	428	*	13	23.0	----	1	25
1615	CH13108	420	*	13	23.2	----	1	25
1616	CH13107	420	*	13	22.6	2.81	1	25
1617	CH13104	276	0.1	2	22.5	1.68	449	25
1618	CH13114	276	0.1	1	24.4	1.75	301	25
1619	CH13111	276	0.1	1	23.5	1.81	363	25
1620	CH13103	207	0.1	4	23.2	1.24	4,078	25
1621	CH13109	207	0.1	4	23.0	1.24	3,466	25
1622	CH13106	207	0.1	4	23.3	1.24	4,587	25
1623	CH13112	138	0.1	10	23.2	0.70	37,685	25

TEST & SAMPLE ID #		MAX. STRESS MPa	R	Q Hz	E GPa	e %	CYCLES TO FAIL	WIDTH (mm) and Notes
1624	CH13102	138	0.1	5	23.1	0.74	31,299	25
1625	CH13105	138	0.1	5	23.8	0.70	44,571	25
1626	CH13101	103	0.1	20	23.2	0.50	1,067,315	25
1703	CH13127	-406	*	13	----	----	1	25
1704	CH13128	-378	*	13	----	----	1	25
1705	CH13126	-370	*	13	----	----	1	25
1706	CH13125	-241	10	2	----	----	933	25
1707	CH13121	-241	10	2	----	----	2,759	25
1708	CH13115	-241	10	4	----	----	4,163	25
1709	CH13116	-207	10	10	----	----	8,887	25
1710	CH13123	-138	10	15	----	----	2,000,000	25 R
1711	CH13119	-207	10	10	----	----	10,738	25
1712	CH13120	-207	10	10	----	----	15,164	25
1713	CH13122	-172	10	15	----	----	109,685	25
1714	CH13118	-172	10	10	----	----	61,058	25
1715	CH13124	-172	10	10	----	----	228,268	25
1716	CH13117	-276	10	1	----	----	174	25
1717	CH13110	-276	10	1	----	----	104	25
1718	CH13140	-276	10	1	----	----	212	25

MATERIAL CH14

Lay-up = [±45/0/±45]s, $V_F = 0.44$, Ave. thickness = 2.49 mm, S.D. = 0.09 mm, CoRezyn 63-AX-051 Polyester

1627	CH14112	548	*	13	23.0	3.06	1	25
1628	CH14106	499	*	13	21.3	3.41	1	25
1629	CH14105	504	*	13	22.5	3.69	1	25
1630	CH14104	345	0.1	1	20.6	2.05	283	25
1631	CH14103	345	0.1	1	22.1	1.87	121	25
1632	CH14116	345	0.1	2	21.0	2.17	266	25
1633	CH14107	276	0.1	4	19.7	1.65	2,344	25
1634	CH14110	276	0.1	4	20.0	1.56	1,280	25
1635	CH14113	276	0.1	4	21.2	1.56	1,709	25
1636	CH14118	207	0.1	10	20.1	1.12	11,600	25
1637	CH14119	207	0.1	10	21.6	1.10	17,423	25
1638	CH14102	207	0.1	10	21.4	1.00	22,579	25
1639	CH14115	138	0.1	20	19.8	0.73	2,054,772	25
1640	CH14120	172	0.1	10	17.7	0.90	69,782	25
1641	CH14111	172	0.1	10	21.7	0.89	57,256	25
1642	CH14101	172	0.1	10	22.7	0.84	57,107	25
1719	CH14134	-398	*	13	----	----	1	25
1720	CH14124	-401	*	13	----	----	1	25
1721	CH14123	-437	*	13	----	----	1	25
1722	CH14139	-310	10	2	----	----	903	25
1723	CH14140	-310	10	2	----	----	2,756	25
1724	CH14129	-310	10	2	----	----	1,188	25
1725	CH14133	-276	10	5	----	----	10,716	25
1726	CH14125	-276	10	4	----	----	16,008	25
1727	CH14128	-276	10	5	----	----	11,756	25

TEST & SAMPLE ID #		MAX. STRESS MPa	R	Q Hz	E GPa	e %	CYCLES TO FAIL	WIDTH (mm) and Notes
1728	CH14131	-241	10	10	----	----	58,134	25
1729	CH14132	-241	10	5	----	----	86,421	25
1730	CH14130	-241	10	10	----	----	78,283	25
1731	CH14126	-207	10	20	----	----	3,000,000	25 R

MATERIAL CH15

Lay-up = [±45/0/±45]s, V_F = 0.32, Ave. thickness = 2.51 mm, S.D. = 0.11 mm, CoRezyn 63-AX-051 Polyester

1732	CH15139	-332	*	13	----	----	1	25
1733	CH15138	-374	*	13	----	----	1	25
1734	CH15128	-331	*	13	----	----	1	25
1735	CH15142	-241	10	2	----	----	996	25
1736	CH15143	-241	10	2	----	----	542	25
1737	CH15147	-241	10	2	----	----	1,345	25
1738	CH15141	-207	10	4	----	----	4,825	25
1739	CH15123	-207	10	4	----	----	9,366	25
1740	CH15122	-207	10	5	----	----	10,507	25
1741	CH15145	-172	10	5	----	----	61,865	25
1742	CH15144	-172	10	10	----	----	54,046	25
1743	CH15137	-172	10	10	----	----	41,806	25
1744	CH15136	-138	10	20	----	----	5,000,000	25 R
1800	CH15105	327	*	13	14.0	3.45	1	25
1801	CH15121	308	*	13	15.3	----	1	25
1802	CH15114	296	*	13	15.2	3.79	1	25
1803	CH15118	207	0.1	2	13.6	2.10	403	25
1804	CH15116	207	0.1	2	15.0	1.87	608	25
1805	CH15113	207	0.1	2	14.3	2.09	270	25
1806	CH15115	172	0.1	4	14.5	1.44	18,054	25
1807	CH15117	172	0.1	4	13.4	1.56	16,456	25
1808	CH15104	172	0.1	4	15.0	1.58	11,511	25
1889	CH15103	138	0.1	10	15.7	1.07	132,279	25
1810	CH15106	138	0.1	10	16.4	0.99	350,007	25
1811	CH15102	138	0.1	10	15.3	1.01	465,775	25
1812	CH15101	121	0.1	12	15.4	0.88	1,029,975	25

MATERIAL CH16

Lay-up = $[\pm 45/0/\pm 45]_S$, V_F = 0.40, Ave. thickness = 2.36 mm, S.D. = 0.06 mm, CoRezyn 63-AX-051 Polyester

1745	CH16136	-325	*	13	----	----	1	25
1746	CH16122	-295	*	13	----	----	1	25
1747	CH16133	-307	*	13	----	----	1	25
1748	CH16123	-241	10	1	----	----	371	25
1749	CH16129	-241	10	2	----	----	1,216	25
1750	CH16138	-241	10	1	----	----	1,010	25
1751	CH16124	-207	10	4	----	----	7,458	25
1752	CH16130	-207	10	4	----	----	11,541	25
1753	CH16128	-207	10	4	----	----	7,137	25

TEST & SAMPLE ID #		MAX. STRESS MPa	R	Q Hz	E GPa	e %	CYCLES TO FAIL	WIDTH (mm) and Notes
1754	CH16139	-172	10	5	----	----	162,300	25
1755	CH16132	-172	10	12	----	----	109,008	25
1756	CH16135	-172	10	10	----	----	155,530	25
1757	CH16120	-155	10	15	----	----	596,803	25
1813	CH16102	366	*	13	19.4	3.13	1	25
1814	CH16104	362	*	13	17.1	----	1	25
1815	CH16105	353	*	13	18.3	2.43	1	25
1816	CH16101	241	0.1	1	18.8	1.73	151	25
1817	CH16115	241	0.1	1	18.3	1.89	421	25
1818	CH16118	241	0.1	1	19.9	1.66	580	25
1819	CH16106	207	0.1	2	18.5	1.51	2,805	25
1820	CH16112	207	0.1	2	19.0	1.48	1,746	25
1821	CH16116	207	0.1	2	17.9	1.59	1,203	25
1822	CH16119	172	0.1	4	17.3	1.21	5,928	25
1823	CH16103	172	0.1	4	20.8	1.07	3,595	25
1824	CH16109	172	0.1	4	21.6	1.01	4,508	25
1825	CH16107	138	0.1	5	17.5	0.89	36,647	25
1826	CH16110	138	0.1	5	17.7	0.93	47,119	25
1827	CH16108	138	0.1	5	16.3	0.95	34,528	25
1828	CH16113	121	0.1	10	18.2	0.75	163,247	25
1829	CH16140	103	0.1	15	17.1	0.66	1,247,001	25

MATERIAL CH17

Lay-up = [±45/0/±45]s, V_F = 0.48, Ave. thickness = 1.96 mm, S.D. = 0.09 mm, CoRezyn 63-AX-051 Polyester

1758	CH17130	-303	*	13	----	----	1	25
1759	CH17142	-309	*	13	----	----	1	25
1760	CH17144	-292	*	13	----	----	1	25
1761	CH17154	-241	10	2	----	----	822	25
1762	CH17123	-241	10	2	----	----	1,359	25
1763	CH17125	-241	10	2	----	----	1,847	25
1764	CH17141	-207	10	5	----	----	2,279	25
1765	CH17138	-207	10	4	----	----	1,767	25
1766	CH17140	-207	10	4	----	----	7,278	25
1767	CH17124	-172	10	5	----	----	227,223	25
1768	CH17134	-172	10	15	----	----	149,828	25
1769	CH17146	-172	10	10	----	----	83,725	25
1770	CH17137	-155	10	20	----	----	4,030,851	25
1901	CH17201	363	*	13	16.0	4.28	1	25
1902	CH17217	345	*	13	17.7	3.14	1	25
1903	CH17202	369	*	13	18.1	3.32	1	25
1904	CH17205	207	0.1	2	18.0	1.53	1,521	25
1905	CH17209	207	0.1	2	18.6	1.40	841	25
1906	CH17212	207	0.1	2	15.7	1.70	657	25
1907	CH17213	172	0.1	4	18.0	1.20	4,396	25
1908	CH17206	172	0.1	5	18.7	1.17	2,826	25
1909	CH17216	172	0.1	5	17.1	1.26	5,024	25
1910	CH17214	138	0.1	5	17.6	0.89	28,190	25

TEST & SAMPLE ID #		MAX. STRESS MPa	R	Q Hz	E GPa	e %	CYCLES TO FAIL	WIDTH (mm) and Notes
1911	CH17210	138	0.1	5	16.6	1.02	34,959	25
1912	CH17203	138	0.1	5	17.4	0.98	21,682	25
1913	CH17208	121	0.1	5	18.7	0.74	44,730	25
1914	CH17207	103	0.1	5	18.5	0.61	183,268	25
1915	CH17215	103	0.1	5	17.2	0.65	196,692	25

MATERIAL CH18

Lay-up = [±45/0/±45]s, V_F = 0.47, Ave. thickness = 3.10 mm, S.D. = 0.05 mm, CoRezyn 63-AX-051 Polyester

1771	CH18125	-300	*	13	----	----	1	25
1772	CH18127	-280	*	13	----	----	1	25
1773	CH18129	-313	*	13	----	----	1	25
1774	CH18124	-241	10	1	----	----	120	25
1775	CH18121	-241	10	1	----	----	99	25
1776	CH18120	-241	10	1	----	----	94	25
1777	CH18122	-207	10	2	----	----	1,077	25
1778	CH18123	-207	10	2	----	----	783	25
1779	CH18138	-207	10	2	----	----	1,103	25
1780	CH18118	-172	10	4	----	----	17,383	25
1781	CH18117	-172	10	5	----	----	14,090	25
1782	CH18136	-172	10	10	----	----	18,452	25
1783	CH18128	-138	10	15	----	----	64,880	25
1784	CH18119	-138	10	10	----	----	82,563	25
1785	CH18126	-121	10	15	----	----	1,295,428	25
1872	CH18214	286	*	13	14.0	3.24	1	25
1873	CH18203	302	*	13	17.5	2.98	1	25
1874	CH18212	295	*	13	17.0	3.10	1	25
1875	CH18202	207	0.1	2	17.1	1.87	343	25
1876	CH18208	207	0.1	2	16.1	1.93	187	25
1877	CH18205	207	0.1	2	17.5	1.87	269	25
1878	CH18206	172	0.1	4	17.6	1.45	1,360	25
1879	CH18209	172	0.1	4	18.1	1.44	1,424	25
1880	CH18207	172	0.1	4	17.7	1.40	1,875	25
1881	CH18211	138	0.1	4	15.8	1.12	12,279	25
1882	CH18201	138	0.1	5	20.3	0.94	7,623	25
1883	CH18220	138	0.1	4	17.7	1.10	8,671	25
1884	CH18204	103	0.1	5	17.7	0.69	119,853	25
1885	CH18210	103	0.1	5	17.3	0.73	73,139	25
1886	CH18213	86	0.1	10	17.4	0.56	585,178	25

MATERIAL CH19

Lay-up = [±45/0/±45]s, V_F = 0.33, Ave. thickness = 4.60 mm, S.D. = 0.19 mm, CoRezyn 63-AX-051 Polyester

1786	CH19142	-256	*	13	----	----	1	25
1787	CH19128	-253	*	13	----	----	1	25
1788	CH19127	-245	*	13	----	----	1	25
1789	CH19147	-172	10	1	----	----	167	25

TEST & SAMPLE ID #		MAX. STRESS MPa	R	Q Hz	E GPa	e %	CYCLES TO FAIL	WIDTH (mm) and Notes
1790	CH19134	-176	10	1	----	----	82	25
1791	CH19136	-172	10	1	----	----	56	25
1792	CH19125	-138	10	2	----	----	476	25
1793	CH19141	-138	10	1	----	----	801	25
1794	CH19132	-138	10	1	----	----	1,702	25
1795	CH19143	-103	10	4	----	----	28,708	25
1796	CH19122	-103	10	5	----	----	14,379	25
1797	CH19137	-103	10	10	----	----	51,234	25
1798	CH19130	-86	10	10	----	----	928,343	25
1799	CH19120	-86	10	15	----	----	622,350	25
1887	CH19201	192	*	13	11.7	3.88	1	25
1888	CH19210	196	*	13	10.8	3.85	1	25
1889	CH19207	191	*	13	11.6	3.87	1	25
1890	CH19202	121	0.1	4	12.3	1.21	5,507	25
1891	CH19214	121	0.1	2	12.1	1.35	4,586	25
1892	CH19206	121	0.1	2	11.9	1.13	5,100	25
1893	CH19209	103	0.1	5	12.3	1.05	32,613	25
1894	CH19204	103	0.1	5	12.7	0.99	17,152	25
1895	CH19203	86	0.1	10	11.7	0.78	324,779	25
1896	CH19205	103	0.1	5	11.7	1.05	27,183	25
1897	CH19208	86	0.1	10	11.2	0.83	278,576	25
1898	CH19220	86	0.1	12	12.2	0.82	423,198	25
1899	CH19211	138	0.1	1	12.0	1.43	850	25
1900	CH19212	138	0.1	1	11.7	1.55	1,414	25

MATERIAL CH20

Lay-up = $[(\pm 45)_3]s$, $V_F = 0.25$, Ave. thickness = 3.76 mm, S.D. = 0.15 mm, CoRezyn 63-AX-051 Polyester

3003	CH20116	136	*	13	10.9	1.60	1	25
3004	CH20121	141	*	13	10.2	1.40	1	25
3005	CH20115	124	*	13	10.6	1.70	1	25
3006	CH20101	51.7	0.1	12	12.0	0.52	136,994	25
3007	CH20107	86	0.1	2	10.5	1.09	1,458	25
3008	CH20105	86	0.1	2	11.9	0.96	1,169	25
3009	CH20106	86	0.1	2	10.0	1.25	1,456	25
3010	CH20119	69.0	0.1	4	11.3	0.76	9,530	25
3011	CH20113	51.7	0.1	4	10.4	0.56	199,855	25
3012	CH20110	69.0	0.1	5	10.6	0.83	10,324	25
3013	CH20114	69.0	0.1	4	10.4	0.82	7,214	25
3014	CH20131	-232	*	13	----	----	1	25
3015	CH20130	-233	*	13	----	----	1	25
3016	CH20132	-224	*	13	----	----	1	25

MATERIAL CH23

Lay-up = $[\pm 45/0/\pm 45]s$, $V_F = 0.32$, Ave. thickness = 2.95 mm, S.D. = 0.13 mm, CoRezyn 63-AX-051 Polyester

3017	CH23111	410	*	13	20.0	2.15	1	25

TEST & SAMPLE ID #		MAX. STRESS MPa	R	Q Hz	E GPa	e %	CYCLES TO FAIL	WIDTH (mm) and Notes
3018	CH23112	369	*	13	17.0	2.37	1	25
3019	CH23103	402	*	13	20.6	2.10	1	25
3020	CH23104	276	0.1	2	21.2	1.51	331	25
3021	CH23118	207	0.1	4	17.2	1.35	2,311	25
3022	CH23119	207	0.1	4	17.8	1.29	2,596	25
3023	CH23110	207	0.1	4	18.3	1.24	3,577	25
3024	CH23114	138	0.1	5	19.5	0.76	84,094	25
3025	CH23106	138	0.1	5	18.2	0.79	69,137	25
3026	CH23147	-207	10	5	----	----	147,440	25
3027	CH23141	-207	10	5	----	----	81,067	25
3028	CH23160	-444	*	13	----	----	1	25
3029	CH23148	-464	*	13	----	----	1	25
3030	CH23144	-435	*	13	----	----	1	25
3031	CH23168	-276	10	4	----	----	7,443	25
3032	CH23143	-276	10	4	----	----	1,786	25
3033	CH23161	-276	10	4	----	----	6,288	25
3034	CH23143	-207	10	10	----	----	128,233	25
3035	CH23121	276	0.1	1	21.4	1.66	77	25
3036	CH23109	276	0.1	2	18.4	1.93	403	25
3037	CH23115	138	0.1	10	18.1	0.79	98,304	25

MATERIAL DD

Lay-up = $[0/\pm45/0_3/\pm45/0]$, $V_F = 0.49$, Ave. thickness = 2.67 mm, S.D. = 0.07 mm,
CoRezyn 63-AX-051 Polyester

1023	DD101	903	*	13	31.9	2.84	1	22
1024	DD103	893	*	13	29.0	3.07	1	22
1025	DD102	934	*	13	30.6	3.10	1	22
1026	DD112	552	0.1	2	31.4	1.76	1,065	22
1027	DD114	552	0.1	2	32.3	1.70	807	22
1028	DD108	552	0.1	2	28.9	1.90	631	22
1029	DD118	483	0.1	5	30.5	1.58	3,044	22
1030	DD113	483	0.1	5	30.9	1.56	1,937	22
1031	DD117	483	0.1	5	30.5	1.58	2,377	22
1032	DD116	414	0.1	5	31.3	1.32	4,997	22
1033	DD119	414	0.1	5	32.4	1.27	8,143	22
1034	DD115	345	0.1	5	32.4	1.06	25,503	22
1035	DD104	345	0.1	5	30.1	1.14	28,657	22
1036	DD110	276	0.1	15	35.2	0.78	64,373	22
1037	DD111	276	0.1	15	29.7	0.92	87,936	22
1038	DD106	207	0.1	15	32.7	0.63	704,401	22
1039	DD109	207	0.1	15	30.6	0.68	1,062,397	22
1040	DD107	207	0.1	20	32.6	0.63	947,447	22
1835	DD105	-781	*	13	----	----	1	25
1836	DD201	-795	*	13	----	----	1	25

TEST & SAMPLE ID #		MAX. STRESS MPa	R	Q Hz	E GPa	e %	CYCLES TO FAIL	WIDTH (mm) and Notes
MATERIAL DD2								
Lay-up = $[0/\pm45/0]_S$, V_F = 0.42, Ave. thickness = 2.64 mm, S.D. = 0.07 mm, CoRezyn 63-AX-051 Polyester								
1043	DD2106	767	*	13	28.6	2.70	1	22
1044	DD2102	757	*	13	30.0	2.53	1	25
1045	DD2114	731	*	13	25.7	2.90	1	22
1046	DD2105	414	0.1	5	27.2	1.52	9,691	25
1047	DD2113	414	0.1	5	25.9	1.61	6,904	22
1048	DD2107	483	0.1	4	27.9	1.80	883	22
1049	DD2117	483	0.1	4	26.1	1.85	1,055	22
1050	DD2108	276	0.1	15	25.2	1.10	766,525	22
1051	DD2110	345	0.1	15	27.2	1.27	71,702	22
1052	DD2111	345	0.1	20	28.9	1.19	59,123	22
1053	DD2109	345	0.1	15	27.9	1.23	62,149	22
1060	DD2115	276	0.1	15	24.7	1.11	655,028	22
1078	DD2116	276	0.1	20	25.5	1.08	697,390	22
1285	DD2171	-579	*	13	----	----	1	25
1286	DD2164	-609	*	13	----	----	1	25
1287	DD2170	-554	*	13	----	----	1	25
1288	DD2163	-414	10	2	----	----	2,311	25
1289	DD2169	-414	10	5	----	----	3,675	25
1290	DD2168	-379	10	5	----	----	24,450	25
1291	DD2167	-379	10	5	----	----	18,781	25
1292	DD2152	-345	10	15	----	----	82,800	25
1293	DD2153	-372	10	10	----	----	19,205	25
1294	DD2161	-310	10	20	----	----	636,142	25
1295	DD2158	-310	10	20	----	----	868,215	25
1296	DD2173	-345	10	15	----	----	111,458	25
1297	DD2176	-414	10	5	----	----	3,775	25
1298	DD2162	-345	10	10	----	----	147,520	25
1299	DD2165	-310	10	20	----	----	1,054,781	25
MATERIAL DD2A								
Lay-up = $[0/\pm45/0]_S$, V_F = 0.42, Ave. thickness = 2.61 mm, S.D. = 0.12 mm, CoRezyn 63-AX-051 Polyester Due to variations of ultimate strengths with the D155 fabrics (roll-to-roll), a second batch of coupons were manufactured and tested.								
4037	DD2A200	345	0.1	5	28.3	1.29	124,809	22 tab
4038	DD2A201	345	0.1	4	29.1	1.33	126,545	22 tab
4039	DD2A202	345	0.1	4	28.5	1.28	153,886	22 tab
4040	DD2A204	1,015	*	13	31.5	3.2	1	22 tab
4041	DD2A205	944	*	13	26.9	3.5	1	22 tab
4042	DD2A207	998	*	13	29.4	3.4	1	22 tab
4043	DD2A206	276	0.1	10	27.2	1.02	1,490,033	22 tab
4044	DD2A208	276	0.1	8	28.7	0.99	564,480	22 tab
4864	DD2A212	276	0.1	8	28.6	1.00	1,849,488	25 tab

TEST & SAMPLE ID #		MAX. STRESS MPa	R	Q Hz	E GPa	e %	CYCLES TO FAIL	WIDTH (mm) and Notes
MATERIAL DD4								
Lay-up = $[0/\pm45/0]_S$, V_F = 0.50, Ave. thickness = 2.36 mm, S.D. = 0.07 mm, CoRezyn 63-AX-051 Polyester								
1061	DD4108	276	0.1	15	27.7	1.00	106,008	22
1062	DD4103	276	0.1	15	28.6	0.97	74,777	22
1063	DD4102	414	0.1	5	29.3	1.41	6,714	22
1064	DD4113	414	0.1	5	32.2	1.28	8,257	22
1065	DD4109	414	0.1	5	30.7	1.35	8,821	22
1066	DD4117	903	*	13	27.9	3.30	1	22
1067	DD4101	901	*	13	31.0	2.91	1	22
1068	DD4114	880	*	13	29.4	2.99	1	22
1069	DD4110	517	0.1	4	35.5	1.46	1,438	22
1070	DD4120	517	0.1	4	----	----	1,284	22
1071	DD4104	345	0.1	10	33.9	1.02	18,821	22
1072	DD4111	345	0.1	10	34.8	0.99	18,293	22
1073	DD4106	345	0.1	10	----	----	22,542	22
1074	DD4118	276	0.1	15	32.7	0.84	118,241	22
1075	DD4115	207	0.1	15	31.6	0.66	278,835	22
1076	DD4116	207	0.1	20	28.3	0.73	386,766	22
1077	DD4105	193	0.1	20	----	----	2,426,414	22
1304	DD4130	-515	*	13	----	----	1	25
1305	DD4131	-519	*	13	----	----	1	25
3083	DD4163	-590	*	13	----	----	1	25
3084	DD4156	-514	*	13	----	----	1	25
3085	DD4151	-566	*	13	----	----	1	25
3105	DD4191	345	-1	2	----	----	972	25
3106	DD4160	345	-1	2	----	----	793	25
3107	DD4165	345	-1	2	----	----	1,436	25
3108	DD4106	861	*	--	----	----	1	25
3109	DD4158	207	-1	5	----	----	83,385	25
3110	DD4157	276	-1	4	----	----	13,351	25
3111	DD4167	276	-1	4	----	----	17,873	25
3112	DD4159	276	-1	4	----	----	9,178	25
3113	DD4150	172	-1	8	----	----	218,504	25
3114	DD4162	207	-1	5	----	----	47,671	25 tab
3115	DD4152	207	-1	4	----	----	63,270	25 tab
3116	DD4161	138	-1	12	----	----	2,000,000	25 R tab
MATERIAL DD5								
Lay-up = $[0/\pm45/0]_S$, V_F = 0.38, Ave. thickness = 2.97 mm, S.D. = 0.06 mm, CoRezyn 63-AX-051 Polyester								
1079	DD5113	703	*	13	26.6	2.78	1	22
1080	DD5108	740	*	13	23.8	3.10	1	22
1081	DD5112	729	*	13	23.7	3.08	1	22
1082	DD5109	207	0.1	20	25.2	0.82	1,820,826	22 R
1083	DD5107	483	0.1	2	24.1	2.00	2,386	22
1084	DD5116	483	0.1	2	27.9	1.72	2,650	22

TEST & SAMPLE ID #		MAX. STRESS MPa	R	Q Hz	E GPa	e %	CYCLES TO FAIL	WIDTH (mm) and Notes
1085	DD5106	483	0.1	2	26.8	1.80	1,996	22
1086	DD5119	414	0.1	5	24.7	1.67	20,246	22
1087	DD5117	276	0.1	20	24.1	1.20	1,500,000	22 R
1088	DD5104	414	0.1	15	25.4	1.63	14,980	22
1089	DD5102	414	0.1	15	28.1	1.47	12,469	22
1090	DD5118	276	0.1	20	26.7	1.03	1,103,247	22
1091	DD5114	345	0.1	15	22.9	1.51	127,898	22
1092	DD5103	345	0.1	15	23.0	1.50	145,581	22
1093	DD5105	345	0.1	15	25.2	1.37	169,754	22
1094	DD5115	276	0.1	20	----	----	1,033,583	22
1302	DD5130	-553	*	13	----	----	1	25
1303	DD5131	-514	*	13	----	----	1	25
1835	DD5105	-781	*	13	----	----	1	25
1836	DD5201	-795	*	13	----	----	1	25

MATERIAL DD5E

Lay-up = $[0/\pm45/0]_S$, $V_F = 0.36$, Ave. thickness = 3.10 mm, S.D. = 0.07 mm, Epon 9410 Epoxy

1859	DD5E406	680	*	13	22.8	2.98	1	22
1860	DD5E403	662	*	13	22.8	2.90	1	22
1861	DD5E408	682	*	13	24.4	2.80	1	22
1940	DD5E419	-528	*	13	27.2	----	1	25
1942	DD5E415	-531	*	13	27.2	----	1	25
1943	DD5E418	-503	*	13	25.3	----	1	25
1962	DD5E424	-345	10	10	----	----	334,460	25
1963	DD5E424	-345	10	5	----	----	1,176,784	25
1964	DD5E420	-379	10	4	----	----	85,056	25
1965	DD5E426	-379	10	4	----	----	59,318	25
1966	DD5E422	-379	10	4	----	----	143,526	25
1967	DD5E416	-414	10	2	----	----	5,232	25
1968	DD5E425	-414	10	2	----	----	7,541	25
1970	DD5E421	-345	10	10	----	----	1,740,718	25 R
1971	DD5E428	-414	10	4	----	----	3,855	25
1982	DD5E411	276	0.1	10	23.3	1.19	348,038	22 tab
1983	DD5E409	276	0.1	10	21.5	1.31	498,494	22 tab
1984	DD5E401	276	0.1	10	23.9	1.24	899,308	22 tab
1985	DD5E412	345	0.1	5	23.4	1.51	34,642	22 tab
1986	DD5E405	345	0.1	5	22.3	1.54	67,480	22 tab
1987	DD5E410	414	0.1	2	22.7	1.83	878	22 tab
1988	DD5E414	414	0.1	2	24.4	1.76	2,429	22
1989	DD5E407	345	0.1	5	22.7	1.54	52,731	22
1990	DD5E402	483	0.1	1	21.8	2.28	69	22 tab
1991	DD5E413	241	0.1	15	21.6	1.19	2,441,330	22
2986	DD5E251	310	-1	2	----	----	1,387	25
2987	DD5E261	310	-1	2	----	----	380	25
2988	DD5E254	310	-1	2	----	----	1,130	25
2989	DD5E252	207	-1	4	----	----	23,990	25
2990	DD5E259	207	-1	4	----	----	31,172	25

TEST & SAMPLE ID #		MAX. STRESS MPa	R	Q Hz	E GPa	e %	CYCLES TO FAIL	WIDTH (mm) and Notes
2991	DD5E252	207	-1	4	----	----	92,394	25
2992	DD5E260	172	-1	5	----	----	191,803	25
2993	DD5E258	276	-1	2	----	----	1,072	25
2994	DD5E256	276	-1	2	----	----	601	25
2995	DD5E257	276	-1	2	----	----	2,665	25
2996	DD5E262	155	-1	10	----	----	1,060,993	25
2997	DD5E263	172	-1	10	----	----	168,947	25
2998	DD5E250	172	-1	10	----	----	305,106	25
2999	DD5E270	155	-1	12	----	----	1,463,729	25
3000	DD5E286T	76	*	13	7.31	1.04	1	25
3001	DD5E281T	73	*	13	8.76	0.84	1	25
3002	DD5E280T	64	*	13	7.24	0.89	1	25

MATERIAL DD5P

Lay-up = $[0/\pm45/0]_S$, $V_F = 0.36$, Ave. thickness = 3.02 mm, S.D. = 0.08 mm, CoRezyn 63-AX-051 Polyester

1853	DD5P206	683	*	13	23.6	2.94	1	22
1854	DD5P209	682	*	13	24.7	2.76	1	22
1855	DD5P214	617	*	13	22.3	2.78	1	22
1871	DD5P201	241	0.1	15	25.7	0.95	8,000,000	22 R
1937	DD5P221	-581	*	13	26.3	----	1	25
1938	DD5P228	-557	*	13	25.0	----	1	25
1939	DD5P219	-586	*	13	25.2	----	1	25
1953	DD5P215	-414	10	2	----	----	5,041	25
1954	DD5P224	-414	10	2	----	----	9,422	25
1955	DD5P218	-414	10	2	----	----	8,491	25
1956	DD5P223	-379	10	5	----	----	178,704	25
1957	DD5P225	-379	10	5	----	----	63,853	25
1958	DD5P216	-379	10	4	----	----	72,641	25
1959	DD5P217	-345	10	10	----	----	344,570	25
1960	DD5P226	-345	10	10	----	----	424,220	25
1961	DD5P227	-345	10	15	----	----	661,103	25
1973	DD5P207	483	0.1	1	24.3	2.20	86	22 tab
1974	DD5P205	414	0.1	2	23.5	1.85	2,102	22 tab
1975	DD5P208	414	0.1	2	24.3	1.74	1,045	22 tab
1976	DD5P212	345	0.1	4	23.9	1.48	36,290	22 tab
1977	DD5P204	345	0.1	5	23.5	1.67	43,703	22 tab
1978	DD5P203	345	0.1	5	24.4	1.43	28,269	22
1979	DD5P210	276	0.1	10	22.7	1.24	857,025	22
1980	DD5P211	276	0.1	10	23.0	1.22	357,553	22 tab
1981	DD5P213	276	0.1	10	21.3	1.18	481,129	22 tab
2965	DD5P255	414	-1	2	----	----	21	25
2966	DD5P259	345	-1	2	----	----	634	25
2967	DD5P260	345	-1	1	----	----	121	25
2968	DD5P251	345	-1	2	----	----	810	25
2969	DD5P250	310	-1	2	----	----	1,360	25
2970	DD5P254	310	-1	1	----	----	163	25
2971	DD5P252	276	-1	2	----	----	5,179	25

TEST & SAMPLE ID #		MAX. STRESS MPa	R	Q Hz	E GPa	e %	CYCLES TO FAIL	WIDTH (mm) and Notes
2972	DD5P253	276	-1	2	----	----	2,038	25
2973	DD5P257	276	-1	2	----	----	2,131	25
2974	DD5P256	207	-1	4	----	----	16,718	25
2975	DD5P261	207	-1	4	----	----	26,796	25
2976	DD5P258	155	-1	10	----	----	986,000	25 R
2977	DD5P262	172	-1	5	----	----	106,267	25
2978	DD5P257	172	-1	4	----	----	79,563	25
2979	DD5P162	155	-1	10	----	----	561,486	25
2980	DD5P263T	53	*	13	8.96	0.59	1	25
2981	DD5P264T	54	*	13	8.83	0.61	1	25
2982	DD5P265T	56	*	13	8.89	0.63	1	25
2983	DD5P269T	-170	*	13	----	----	1	25
2984	DD5P267T	-153	*	13	----	----	1	25
2985	DD5P266T	-163	*	13	----	----	1	25
Tests 3150 - 3180 involved a gage length of 13 mm (width effect tests).								
3150	DD5P001	-591	*	13	----	----	1	51
3151	DD5P002	-662	*	13	----	----	1	51
3152	DD5P003	-674	*	13	----	----	1	51
3153	DD5P004	-622	*	13	----	----	1	51
3154	DD5P005	-624	*	13	----	----	1	44
3155	DD5P006	-616	*	13	----	----	1	44
3156	DD5P007	-671	*	13	----	----	1	44
3157	DD5P008	-649	*	13	----	----	1	44
3158	DD5P009	-597	*	13	----	----	1	38
3159	DD5P010	-604	*	13	----	----	1	38
3160	DD5P011	-638	*	13	----	----	1	38
3161	DD5P012	-695	*	13	----	----	1	38
3162	DD5P013	-649	*	13	----	----	1	32
3163	DD5P014	-648	*	13	----	----	1	32
3164	DD5P015	-666	*	13	----	----	1	32
3165	DD5P016	-650	*	13	----	----	1	32
3166	DD5P061	-687	*	13	----	----	1	25
3167	DD5P062	-634	*	13	----	----	1	25
3168	DD5P063	-671	*	13	----	----	1	25
3169	DD5P021	-588	*	13	----	----	1	19
3170	DD5P022	-580	*	13	----	----	1	19
3171	DD5P023	-630	*	13	----	----	1	19
3172	DD5P024	-610	*	13	----	----	1	19
3173	DD5P025	-614	*	13	----	----	1	13
3174	DD5P026	-550	*	13	----	----	1	13
3175	DD5P027	-581	*	13	----	----	1	13
3176	DD5P028	-607	*	13	----	----	1	13
3177	DD5P029	-495	*	13	----	----	1	6
3178	DD5P030	-549	*	13	----	----	1	6
3179	DD5P031	-539	*	13	----	----	1	6
3180	DD5P032	-519	*	13	----	----	1	6
Tests 3181 - 3198 involved a gage length of 100 mm (width effect tests).								
3181	DD5P28	853	*	13	----	----	1	38

TEST & SAMPLE ID #		MAX. STRESS MPa	R	Q Hz	E GPa	e %	CYCLES TO FAIL	WIDTH (mm) and Notes
3182	DD5P29	861	*	13	----	----	1	38
3183	DD5P30	825	*	13	----	----	1	38
3184	DD5P31	824	*	13	----	----	1	32
3185	DD5P32	843	*	13	----	----	1	32
3186	DD5P33	840	*	13	----	----	1	32
3187	DD5P13	852	*	13	----	----	1	25
3188	DD5P14	774	*	13	----	----	1	25
3189	DD5P15	825	*	13	----	----	1	25
3190	DD5P037	787	*	13	----	----	1	19
3191	DD5P038	814	*	13	----	----	1	19
3192	DD5P039	792	*	13	----	----	1	19
3193	DD5P040	737	*	13	----	----	1	13
3194	DD5P041	792	*	13	----	----	1	13
3195	DD5P042	683	*	13	----	----	1	13
3196	DD5P043	536	*	13	----	----	1	6
3197	DD5P044	526	*	13	----	----	1	6
3198	DD5P045	537	*	13	----	----	1	6
Tests 3244 - 3276 involved a gage length of 13 mm (strain rate effect tests).								
3244	DD5P17	-502	*	0.0025	----	----	1	25
3245	DD5P18	-492	*	0.0025	----	----	1	25
3246	DD5P19	-497	*	0.0025	----	----	1	25
3247	DD5P40	-582	*	0.025	----	----	1	25
3248	DD5P41	-591	*	0.025	----	----	1	25
3249	DD5P42	-528	*	0.025	----	----	1	25
3250	DD5P43	-626	*	0.25	----	----	1	25
3251	DD5P44	-592	*	0.25	----	----	1	25
3252	DD5P45	-547	*	0.25	----	----	1	25
3253	DD5P46	-585	*	1.27	----	----	1	25
3254	DD5P47	-578	*	1.27	----	----	1	25
3255	DD5P48	-577	*	1.27	----	----	1	25
3256	DD5P49	-588	*	2.54	----	----	1	25
3257	DD5P50	-628	*	2.54	----	----	1	25
3258	DD5P51	-581	*	2.54	----	----	1	25
3259	DD5P52	-653	*	6.35	----	----	1	25
3260	DD5P53	-624	*	6.35	----	----	1	25
3261	DD5P54	-674	*	6.35	----	----	1	25
3262	DD5P55	-671	*	13	----	----	1	25
3263	DD5P56	-662	*	13	----	----	1	25
3264	DD5P57	-656	*	13	----	----	1	25
3265	DD5P58	-697	*	19	----	----	1	25
3266	DD5P59	-689	*	19	----	----	1	25
3267	DD5P60	-676	*	19	----	----	1	25
3268	DD5P61	-678	*	25	----	----	1	25
3269	DD5P62	-692	*	25	----	----	1	25
3270	DD5P63	-675	*	25	----	----	1	25
3271	DD5P64	-692	*	64	----	----	1	25
3272	DD5P65	-671	*	64	----	----	1	25
3273	DD5P66	-709	*	64	----	----	1	25

TEST & SAMPLE ID #		MAX. STRESS MPa	R	Q Hz	E GPa	e %	CYCLES TO FAIL	WIDTH (mm) and Notes
3274	DD5P67	-697	*	127	----	----	1	25
3275	DD5P68	-704	*	127	----	----	1	25
3276	DD5P69	-665	*	127	----	----	1	25
Tests 3277 - 3300 involved a gage length of 100 mm (strain rate effect tests).								
3277	DD5P1	552	*	0.0025	----	----	1	25
3278	DD5P2	592	*	0.0025	----	----	1	25
3279	DD5P3	585	*	0.0025	----	----	1	25
3280	DD5P4	624	*	0.025	----	----	1	25
3281	DD5P5	614	*	0.025	----	----	1	25
3282	DD5P6	610	*	0.025	----	----	1	25
3283	DD5P7	730	*	0.25	----	----	1	25
3284	DD5P8	722	*	0.25	----	----	1	25
3285	DD5P9	705	*	0.25	----	----	1	25
3286	DD5P10	748	*	2.54	----	----	1	25
3287	DD5P11	736	*	2.54	----	----	1	25
3288	DD5P12	757	*	2.54	----	----	1	25
3289	DD5P13	852	*	13	----	----	1	25
3290	DD5P14	834	*	13	----	----	1	25
3291	DD5P15	825	*	13	----	----	1	25
3292	DD5P16	763	*	25	----	----	1	25
3293	DD5P17	778	*	25	----	----	1	25
3294	DD5P18	841	*	25	----	----	1	25
3295	DD5P19	810	*	64	----	----	1	25
3296	DD5P20	919	*	64	----	----	1	25
3297	DD5P21	876	*	64	----	----	1	25
3298	DD5P22	916	*	127	----	----	1	25
3299	DD5P23	903	*	127	----	----	1	25
3300	DD5P24	895	*	127	----	----	1	25
Tests 3455 - 3533 involved different coupon geometries (standard and mini-coupon) and frequencies.								
3455	DD5P550	414	0.1	2	26.7	1.58	8,157	22
3456	DD5P520	414	0.1	2	26.6	1.64	12,185	22
3457	DD5P524	414	0.1	2	23.6	1.70	11,533	22
3458	DD5P511	414	0.1	2	23.6	1.71	6,716	22
3459	DD5P555	414	0.1	2	24.2	1.72	12,041	22
3460	DD5P510	414	0.1	2	26.0	1.61	7,640	22
3461	DD5P501	414	0.1	2	23.5	1.67	11,085	22
3462	DD5P551	414	0.1	2	25.3	1.65	9,930	22
3463	DD5P533	414	0.1	2	25.3	1.66	9,191	22
3464	DD5P517	414	0.1	2	24.2	1.73	9,067	22
3465	DD5P542	310	0.1	10	25.9	1.26	514,201	22
3466	DD5P508	310	0.1	10	23.1	1.28	285,386	22
3467	DD5P521	310	0.1	10	23.6	1.22	351,717	22
3468	DD5P560	310	0.1	10	24.0	1.31	345,652	22
3469	DD5P519	310	0.1	10	24.3	1.34	749,084	22
3470	DD5P544	310	0.1	10	24.3	1.28	579,002	22 tab
3471	DD5P504	414	0.1	2	23.5	1.69	9,912	22 tab
3472	DD5P564	414	0.1	2	----	----	16,271	22 tab
3473	DD5P503	414	0.1	2	----	----	5,305	22 tab

TEST & SAMPLE ID #		MAX. STRESS MPa	R	Q Hz	E GPa	e %	CYCLES TO FAIL	WIDTH (mm) and Notes
3474	DD5P515	414	0.1	2	----	----	10,499	22 tab
3475	DD5P525	310	0.1	10	----	----	342,738	22 tab
3476	DD5P540	310	0.1	10	----	----	228,420	22 tab
3477	DD5P506	310	0.1	10	----	----	376,933	22 tab
3478	DD5P541	414	0.1	2	----	----	8,883	22 tab
3479	DD5P502	310	0.1	10	24.6	1.30	403,000	22 tab
3498	DD5P605	241	0.1	30	----	----	2,820,426	8 tab
3499	DD5P601	207	0.1	40	----	0.89	10,027,337	8 tab
3500	DD5P602	241	0.1	20	----	----	1,548,025	8 tab
3501	DD5P601	241	0.1	25	----	----	348,666	8 tab
3502	DD5P606	241	0.1	20	----	----	1,016,251	8 tab
3503	DD5P614	241	0.1	25	23.6	1.04	2,312,896	8 tab
3525	DD5P612	207	0.1	40	----	0.91	22,002,386	8 tab
3525	DD5P603	193	0.1	45	23.6	0.82	39,082,107	8 tab
3526	DD5P610	414	0.1	2	----	----	8,123	8 tab
3527	DD5P604	414	0.1	2	----	----	18,264	8 tab
3528	DD5P613	414	0.1	2	----	----	8,358	8 tab
3529	DD5P643	241	0.1	10	----	----	2,668,144	8 tab
3532	DD5P628	241	0.1	10	----	----	2,823,516	8 tab
3533	DD5P599	241	0.1	10	----	----	3,554,421	8 tab
Tests 3534 - 3556 were run at different frequencies to study thermal and mechanical effects.								
3534	DD5P635	310	0.1	10	----	----	594,298	8 tab
3535	DD5P634	310	0.1	10	----	----	537,593	8 tab
3536	DD5P631	310	0.1	10	----	----	252,317	8 tab
3537	DD5P637	310	0.1	10	----	----	296,456	8 tab
3538	DD5P636	310	0.1	10	----	----	275,551	8 tab
3539	DD5P627	310	0.1	10	----	----	261,531	8 tab
3540	DD5P638	310	0.1	5	----	----	379,674	8 tab
3541	DD5P629	310	0.1	5	----	----	240,098	8 tab
3542	DD5P642	310	0.1	5	----	----	458,684	8 tab
3543	DD5P570	310	0.1	2	----	----	304,764	8 tab
3544	DD5P571	310	0.1	2	----	----	227,372	8 tab
3545	DD5P563	310	0.1	2	----	----	247,249	8 tab
3546	DD5P633	310	0.1	20	----	----	404,285	8 tab
3547	DD5P622	310	0.1	20	----	----	432,281	8 tab
3548	DD5P630	310	0.1	20	----	----	731,478	8 tab
3549	DD5P620	310	0.1	2	----	----	196,929	8 tab
3550	DD5P623	310	0.1	30	----	----	59,971	8 tab
3554	DD5P509	310	0.1	1	25.6	1.21	284,133	22 tab
3555	DD5P580	310	0.1	1	----	----	213,190	22 tab
3556	DD5P581	310	0.1	1	----	----	198,210	22 tab
3850	DD5P624T	-145	*	13	----	----	1	25
3851	DD5P633T	-142	*	13	----	----	1	25
3852	DD5P625T	-158	*	13	----	----	1	25
3853	DD5P601T	67	*	13	9.21	1.33	1	25
3854	DD5P602T	65	*	13	8.84	1.28	1	25
3855	DD5P603T	66	*	13	9.31	1.35	1	25
3856	DD5P604T	24	0.1	10	8.46	0.29	3,846,149	25

TEST & SAMPLE ID #		MAX. STRESS MPa	R	Q Hz	E GPa	e %	CYCLES TO FAIL	WIDTH (mm) and Notes
3857	DD5P605T	31	0.1	5	8.62	0.45	160,829	25
3858	DD5P606T	31	0.1	5	8.33	0.48	84,821	25
3859	DD5P607T	35	0.1	5	9.20	0.57	39,239	25
3860	DD5P608T	31	0.1	5	8.61	0.50	105,856	25
3861	DD5P609T	28	0.1	5	8.33	0.33	329,077	25
3862	DD5P610T	35	0.1	5	8.67	0.54	25,383	25
3863	DD5P611T	35	0.1	5	8.63	0.65	39,867	25
3864	DD5P617T	38	0.1	2	8.73	1.10	4,765	25
3865	DD5P612T	38	0.1	2	9.05	1.09	10,816	25
3866	DD5P615T	41	0.1	2	8.93	1.25	7,778	25
3867	DD5P614T	28	0.1	5	9.37	0.32	4,025,994	25
3868	DD5P616T	28	0.1	7	8.84	0.34	930,682	25
3869	DD5P613T	38	0.1	4	8.40	----	9,712	25
3982	DD5P661	207	0.1	25	----	----	8,672,644	8 tab
3983	DD5P632	207	0.1	25	----	----	9,754,976	8 tab
3984	DD5P660	207	0.1	25	----	----	11,452,158	8 tab
3985	DD5P664	172	0.1	60	----	----	112,139,744	8 R tab
3986	DD5P641	172	0.1	60	----	----	78,244,896	8 tab
3987	DD5P639	172	0.1	60	----	----	110,000,000	8 R tab
3988	DD5P674	138	-1	15	----	----	6,276,710	8 tab
3989	DD5P670	138	-1	15	----	----	3,601,668	8 tab
3990	DD5P671	138	-1	15	----	----	6,071,355	8 tab
4016	DD5P662	103	-1	30	----	----	100,000,000	8 R tab
4017	DD5P677	121	-1	15	----	----	18,077,742	8 tab
4018	DD5P690	121	-1	15	----	----	32,308,210	8 tab
4120	DD5P666	241	0.5	40	----	----	100,000,000	8 R tab
4121	DD5P675	379	0.5	10	----	----	438,618	8 tab
4122	DD5P672	379	0.5	10	----	----	610,270	8 tab
4123	DD5P667	379	0.5	10	----	----	297,323	8 tab
4124	DD5P673	310	0.5	30	----	----	13,320,248	8 tab
4125	DD5P669	310	0.5	40	----	----	3,809,795	8 tab
4126	DD5P640	310	0.5	40	----	----	8,730,709	8 tab
4127	DD5P665	276	0.5	40	----	----	30,480,698	8 tab
4128	DD5P676	276	0.5	40	----	----	26,841,282	8 tab
4129	DD5P700	276	0.5	50	----	----	47,918,327	8 tab
4222	DD5P751	-470	*	13	----	----	1	8
4223	DD5P752	-481	*	13	----	----	1	8
4224	DD5P750	-556	*	13	----	----	1	8
4225	DD5P753	-533	*	13	----	----	1	8
4230	DD5P712	742	*	13	----	----	1	8
4231	DD5P754	770	*	13	----	----	1	8
4232	DD5P756	750	*	13	----	----	1	8
4233	DD5P757	752	*	13	----	----	1	8
4859	DD59801	-310	10	10	----	----	2,747,477	25
4860	DD5P802	-310	10	10	----	----	1,143,005	25
4861	DD5P803	-310	10	10	----	----	531,709	25

TEST & SAMPLE ID #		MAX. STRESS MPa	R	Q Hz	E GPa	e %	CYCLES TO FAIL	WIDTH (mm) and Notes
MATERIAL DD5V								
Lay-up = $[0/\pm45/0]_S$, V_F = 0.36, Ave. thickness = 3.05 mm, S.D. = 0.09 mm, Derakane 411-C-50 Vinyl ester								
1856	DD5V311	688	*	13	23.4	3.00	1	22
1857	DD5V308	672	*	13	22.5	3.39	1	22
1858	DD5V303	664	*	13	21.7	3.10	1	22
1862	DD5V309	483	0.1	2	22.5	2.30	283	22
1863	DD5V306	414	0.1	4	22.1	1.89	5,751	22
1864	DD5V301	414	0.1	2	28.3	1.66	8,529	22
1865	DD5V302	276	0.1	10	25.8	1.08	392,541	22
1866	DD5V312	345	0.1	5	22.9	1.56	54,570	22
1867	DD5V313	345	0.1	5	24.3	1.46	68,513	22
1868	DD5V314	345	0.1	5	24.2	1.52	58,782	22
1869	DD5V310	241	0.1	15	23.4	1.02	3,673,144	22
1870	DD5V350	276	0.1	5	23.0	1.30	618,125	22
1934	DD5V315	-519	*	13	----	----	1	25
1935	DD5V318	-533	*	13	----	----	1	25
1936	DD5V316	-538	*	13	----	----	1	25
1944	DD5V329	-414	10	5	----	----	9,981	25
1945	DD5V317	-414	10	4	----	----	18,310	25
1946	DD5V327	-414	10	5	----	----	11,920	25
1947	DD5V325	-345	10	10	----	----	1,462,167	25
1948	DD5V325	-345	10	20	----	----	943,258	25
1949	DD5V319	-379	10	5	----	----	179,421	25
1950	DD5V324	-379	10	5	----	----	84,516	25
1951	DD5V322	-379	10	5	----	----	73,591	25
1952	DD5V321	-379	10	5	----	----	107,610	25
1972	DD5V304	345	0.1	5	23.9	1.44	42,916	22 tab
MATERIAL DD5V2								
Lay-up = $[0/\pm45/0]_S$, V_F = 0.35, Ave. thickness = 3.18 mm, S.D. = 0.09 mm, Derakane 8084 Epoxy Vinyl ester								
4367	DD5V2101	276	0.1	10	----	----	3,326,186	22 tab
4368	DD5V2102	414	0.1	4	21.4	1.94	20,070	22 tab
4369	DD5V2103	414	0.1	3	22.9	1.89	35,015	22 tab
4370	DD5V2114	345	0.1	5	21.6	1.61	454,290	22 tab
4371	DD5V2110	345	0.1	5	23.2	1.53	228,519	22 tab
4372	DD5V2112	345	0.1	5	22.2	1.62	375,206	22 tab
4373	DD5V2113	414	0.1	4	----	----	18,445	22 tab
4374	DD5V2109	798	*	13	22.2	3.4	1	22 tab
4375	DD5V2108	757	*	13	21.0	3.3	1	22 tab
4376	DD5V2111	807	*	13	24.1	3.3	1	22 tab
4377	DD5V2115	276	*	7	22.5	1.25	3,738,875	22 tab
4378	DD5V2150	-629	*	13	----	----	1	25
4379	DD5V2153	-597	*	13	----	----	1	25
4380	DD5V2156	-588	*	13	----	----	1	25
4381	DD5V2157	-414	10	6	----	----	366,453	25

TEST & SAMPLE ID #		MAX. STRESS MPa	R	Q Hz	E GPa	e %	CYCLES TO FAIL	WIDTH (mm) and Notes
4382	DD5V2151	-414	10	6	----	----	122,340	25
4383	DD5V2158	-414	10	5	----	----	63,740	25
4384	DD5V2155	-448	10	2	----	----	4,337	25
4385	DD5V2152	-448	10	3	----	----	11,119	25
4386	DD5V2154	-448	10	3	----	----	12,549	25
4387	DD5V2170	-379	10	5	----	----	783,925	25
4388	DD5V2160	-379	10	6	----	----	91,821	25
4389	DD5V2161	345	-1	1	----	----	765	25
4390	DD5V2162	345	-1	1	----	----	549	25
4391	DD5V2168	345	-1	1	----	----	984	25
4392	DD5V2167	310	-1	2	----	----	1,675	25
4393	DD5V2166	310	-1	1	----	----	1,463	25
4394	DD5V2165	310	-1	2	----	----	3,443	25
4395	DD5V2164	207	-1	5	----	----	46,477	25
4396	DD5V2164	172	-1	5	----	----	471,449	25
4397	DD5V2172	172	-1	5	----	----	342,089	25
4398	DD5V2174	172	-1	6	----	----	941,295	25

MATERIAL DD6

Lay-up = $[0/\pm45/0]_S$, $V_F = 0.31$, Ave. thickness = 3.53 mm, S.D. = 0.05 mm, CoRezyn 63-AX-051 Polyester

1095	DD6116	602	*	13	20.9	2.88	1	22
1096	DD6104	609	*	13	22.6	2.69	1	22
1097	DD6106	603	*	13	23.8	2.53	1	22
1098	DD6101	414	0.1	5	22.3	1.85	928	22
1099	DD6108	414	0.1	2	21.4	1.94	841	22
1100	DD6111	414	0.1	2	19.8	2.09	1,302	22
1101	DD6113	345	0.1	5	19.3	1.79	17,421	22
1102	DD6103	345	0.1	10	19.5	1.76	26,109	22
1103	DD6112	345	0.1	10	19.2	1.79	18,696	22
1104	DD6102	276	0.1	15	21.5	1.28	193,637	22
1105	DD6110	276	0.1	10	20.4	1.35	406,267	22
1106	DD6107	276	0.1	15	22.7	1.22	300,000	22 R
1121	DD6121	-447	*	13	----	----	1	25
1122	DD6150	-448	*	13	----	----	1	25
1126	DD6126	-447	*	13	----	----	1	25
1127	DD6143	-448	*	13	----	----	1	25
1128	DD6130	-449	*	13	----	----	1	25
1129	DD6128	-460	*	13	----	----	1	25
1140	DD6118	-276	10	15	----	----	1,918,022	25
1142	DD6125	-276	10	20	----	----	1,223,779	25
1145	DD6124	-345	10	10	----	----	54,759	25
1146	DD6123	-345	10	15	----	----	35,062	25
1153	DD6109	-379	10	10	----	----	15,355	25
1154	DD6114	-379	10	10	----	----	10,750	25
1158	DD6133	-345	10	10	----	----	42,786	25
1159	DD6132	-310	10	15	----	----	423,811	25
1160	DD6105	-379	10	5	----	----	9,779	25

TEST & SAMPLE ID #		MAX. STRESS MPa	R	Q Hz	E GPa	e %	CYCLES TO FAIL	WIDTH (mm) and Notes
1161	DD6131	-310	10	15	----	----	324,531	25
1166	DD6141	-475	*	13	----	----	1	25
1167	DD6139	-310	10	20	----	----	284,644	25
1170	DD6115	-276	10	20	----	----	2,012,851	25
1171	DD6130	-414	10	4	----	----	1,883	25
1172	DD6148	-414	10	4	----	----	2,341	25
1300	DD6143	-510	*	13	----	----	1	25
1301	DD6145	-529	*	13	----	----	1	25

MATERIAL DD7

Lay-up = $[0/\pm45/0]_S$, $V_F = 0.54$, Ave. thickness = 2.11 mm, S.D. = 0.06 mm, CoRezyn 63-AX-051 Polyester

1107	DD7105	837	*	13	36.5	2.80	1	22
1108	DD7113	824	*	13	30.7	2.69	1	22
1109	DD7107	826	*	13	30.3	2.73	1	22
1110	DD7112	839	*	13	32.4	2.59	1	22
1111	DD7108	483	0.1	2	32.5	1.48	978	22
1112	DD7103	483	0.1	2	32.4	1.52	784	22
1113	DD7111	414	0.1	5	28.9	1.43	3,379	22
1114	DD7110	414	0.1	5	----	----	2,916	22
1115	DD7106	345	0.1	10	----	----	9,304	22
1116	DD7109	345	0.1	10	----	----	14,481	22
1117	DD7104	276	0.1	10	----	----	29,331	22
1118	DD7114	276	0.1	10	----	----	25,746	22
1119	DD7102	207	0.1	20	----	----	127,887	22
1120	DD7115	207	0.1	20	----	----	94,292	22
1143	DD7131	-276	10	20	----	----	2,761,322	25
1144	DD7129	-310	10	20	----	----	4,919,032	25
1147	DD7124	-577	*	13	----	----	1	25
1148	DD7133	-605	*	13	----	----	1	25
1149	DD7118	-562	*	13	----	----	1	25
1155	DD7101	-379	10	10	----	----	45,445	25
1156	DD7131	-379	10	10	----	----	66,177	25
1157	DD7132	-379	10	10	----	----	52,848	25
1163	DD7122	-345	10	10	----	----	928,436	25
1164	DD7128	-345	10	15	----	----	511,438	25
1165	DD7133	-448	10	4	----	----	843	25
1168	DD7140	-345	10	20	----	----	781,113	25
1169	DD7130	-448	10	4	----	----	1,307	25
1173	DD7117	-414	10	5	----	----	10,902	25
1174	DD7119	-414	10	5	----	----	8,454	25
1175	DD7137	-310	10	20	----	----	5,322,151	25

TEST & SAMPLE ID #		MAX. STRESS MPa	R	Q Hz	E GPa	e %	CYCLES TO FAIL	WIDTH (mm) and Notes
MATERIAL DD8								
Lay-up = $[0/\pm45/0]_S$, $V_F = 0.42$, Ave. thickness = 2.67 mm, S.D. = 0.06 mm, CoRezyn 63-AX-051 Polyester Material is the same as DD2 except that all the fabric stitching (D155 and DB120) was removed.								
1204	DD8105	483	0.1	4	----	----	12,460	22
1206	DD8106	483	0.1	4	----	----	7,139	22
1207	DD8109	414	0.1	10	22.0	1.88	63,076	22
1209	DD8102	414	0.1	10	----	----	46,816	22
1210	DD8101	345	0.1	10	----	----	298,339	22
1211	DD8111	345	0.1	15	----	----	567,522	22
1212	DD8103	483	0.1	4	22.9	1.31	5,846	22
1213	DD8104	276	0.1	15	----	----	33,425	22 R
1214	DD8121	345	0.1	10	----	----	462,481	22
1215	DD8108	741	*	13	30.3	2.44	1	22
1216	DD8115	698	*	13	30.8	2.27	1	22
1217	DD8120	818	*	13	28.3	2.33	1	22
1218	DD8117	856	*	13	28.1	2.44	1	22
1833	DD8112	-587	*	13	----	----	1	25
1834	DD8143	-576	*	13	----	----	1	25
MATERIAL DD8A								
Lay-up = $[0/\pm45/0]_S$, $V_F = 0.42$, Ave. thickness = 2.61 mm, S.D. = 0.08 mm, CoRezyn 63-AX-051 Polyester Stitching was removed from the D155 fabric. The DB120 fabric was not altered								
4031	DD8A103	345	0.1	5	31.3	1.15	475,424	22 tab
4032	DD8A105	345	0.1	5	29.4	1.22	385,518	22 tab
4033	DD8A104	345	0.1	5	28.7	1.27	321,056	22 tab
MATERIAL DD8B								
Lay-up = $[0/\pm45/0]_S$, $V_F = 0.42$, Ave. thickness = 2.64 mm, S.D. = 0.09 mm, CoRezyn 63-AX-051 Polyester Stitching was removed from the D155 fabric. The DB120 stitch which stitches the +45 to the -45 ply was removed. Each +45 and -45 ply still had their individual ply stitch intact.								
4034	DD8B102	345	0.1	5	26.0	1.29	366,371	22 tab
4035	DD8B105	345	0.1	5	24.7	1.37	244,659	22 tab
4036	DD8B104	345	0.1	5	27.8	1.22	199,990	22 tab
MATERIAL DD9								
Lay-up = $[0/\pm45/0]_S$, $V_F = 0.54$, Ave. thickness = 2.03 mm, S.D. = 0.04 mm, CoRezyn 63-AX-051 Polyester Material is the same as DD7 except that all the fabric stitching (D155 and DB120) was removed.								
1219	DD9101	414	0.1	10	34.5	1.20	8,603	22
1220	DD9109	483	0.1	5	33.9	1.42	2,695	22
1221	DD9116	414	0.1	5	33.8	1.23	6,359	22
1223	DD9103	345	0.1	10	33.2	1.04	29,276	22
1224	DD9104	207	0.1	15	34.6	0.60	432,809	22
1226	DD9107	944	*	13	----	----	1	22

TEST & SAMPLE ID #		MAX. STRESS MPa	R	Q Hz	E GPa	e %	CYCLES TO FAIL	WIDTH (mm) and Notes
1227	DD9109	903	*	13	----	----	1	22
1228	DD9110	873	*	13	----	----	1	22
1229	DD9114	483	0.1	4	35.6	1.36	3,294	22
1230	DD9113	345	0.1	10	36.8	0.93	38,377	22
1231	DD9106	276	0.1	10	----	----	94,262	22
1232	DD9113	207	0.1	10	----	----	432,480	22
1830	DD9200	-513	*	13	----	----	1	25
1831	DD9202	-603	*	13	----	----	1	25
1832	DD9201	-552	*	13	----	----	1	25

MATERIAL DD10

Lay-up = $[0/\pm45/0]_S$, $V_F = 0.62$, Ave. thickness = 1.73 mm, S.D. = 0.08 mm, CoRezyn 63-AX-051 Polyester
Material had all the fabric stitching (D155 and DB120) removed.

2820	DD10110	1,045	*	13	42.8	2.45	1	22
2821	DD10109	888	*	13	42.6	2.08	1	22
2822	DD10108	935	*	13	39.1	2.40	1	22
2823	DD10107	483	0.1	4	43.0	1.12	3,132	22
2824	DD10105	483	0.1	4	40.0	1.20	2,128	22
2825	DD10102	414	0.1	5	42.6	1.18	7,291	22
2826	DD10101	414	0.1	5	43.7	1.11	11,251	22
2827	DD10103	276	0.1	10	43.7	0.59	72,116	22
2828	DD10104	276	0.1	10	43.2	0.66	94,297	22
2829	DD10106	276	0.1	10	44.6	0.64	152,411	22
2866	DD10127	-525	*	13	----	----	1	25
2867	DD10121	-557	*	13	----	----	1	25
2868	DD10125	-607	*	13	----	----	1	25
2869	DD10124	-362	10	20	----	----	10,000,000	25 R
2870	DD10122	-414	10	2	----	----	266	25
2871	DD10123	-379	10	12	----	----	798,311	25
2872	DD10128	-379	10	12	----	----	576,424	25
2873	DD10126	-379	10	12	----	----	1,678,467	25
2874	DD10130	-518	*	13	----	----	1	25 Z
2875	DD10131	-553	*	13	----	----	1	25 Z
2963	DD10401	-379	10	12	----	----	844,707	has stitch
2964	DD10402	-379	10	12	----	----	553,651	has stitch

MATERIAL DD11

Lay-up = $[0/\pm45/0]_S$, $V_F = 0.31$, Ave. thickness = 3.19 mm, S.D. = 0.07 mm, CoRezyn 63-AX-051 Polyester

2853	DD11101	543	*	13	20.1	2.70	1	22
2854	DD11110	642	*	13	19.3	3.20	1	22
2855	DD11102	589	*	13	18.8	3.13	1	22
2856	DD11103	276	0.1	5	21.7	1.28	328,394	22
2857	DD11104	276	0.1	5	20.0	1.45	144,473	22
2858	DD11105	414	0.1	1	19.9	2.08	602	22
2859	DD11107	414	0.1	1	17.4	2.40	859	22

TEST & SAMPLE ID #		MAX. STRESS MPa	R	Q Hz	E GPa	e %	CYCLES TO FAIL	WIDTH (mm) and Notes
2860	DD11108	414	0.1	1	21.0	2.00	359	22
2861	DD11109	345	0.1	2	19.0	1.90	5,733	22
2862	DD11106	345	0.1	2	20.3	1.78	4,560	22
2863	DD11114	241	0.1	12	20.7	1.20	3,880,803	22
2864	DD11111	276	0.1	5	20.1	1.38	109,080	22
2865	DD11118	345	0.1	2	20.8	1.75	3,741	22
2876	DD11128	-331	*	13	----	----	1	25
2877	DD11129	-314	*	13	----	----	1	25
2878	DD11120	-310	*	13	----	----	1	25
2879	DD11125	-241	10	1	----	----	189	25
2880	DD11127	-207	10	2	----	----	2,411	25
2881	DD11122	-207	10	2	----	----	1,882	25
2882	DD11121	-207	10	2	----	----	1,530	25
2883	DD11124	-172	10	10	----	----	137,454	25
2884	DD11126	-172	10	10	----	----	87,211	25
2885	DD11123	-172	10	10	----	----	123,600	25
2886	DD11131	-155	10	12	----	----	356,114	25
3992	DD11T309	35	0.1	1	7.84	1.47	21	25
3993	DD11T308	21	0.1	4	----	----	69,027	25
3994	DD11T310	21	0.1	5	8.00	0.25	112,343	25
3995	DD11T315	21	0.1	5	7.94	0.26	104,931	25
3996	DD11T313	17	0.1	10	7.62	0.22	4,000,000	25 R
3997	DD11T312	24	0.1	5	8.19	0.30	24,784	25
3998	DD11T301	24	0.1	4	7.41	0.31	10,054	25
3999	DD11T305	24	0.1	4	7.65	0.31	8,202	25
4000	DD11T311	42	*	13	7.43	0.68	1	25
4001	DD11T307	43	*	13	8.32	0.53	1	25
4002	DD11T306	34	*	13	7.64	0.46	1	25
4325	DD11224	103	-1	5	----	----	1,695,591	25
4322	DD11227	138	-1	5	----	----	79,076	25
4323	DD11221	103	-1	5	----	----	1,767,448	25
4328	DD11213	138	-1	5	----	----	40,380	25
4329	DD11219	138	-1	5	----	----	118,395	25
4330	DD11210	138	-1	5	----	----	32,677	25
4331	DD11212	121	-1	5	----	----	269,627	25
4332	DD11215	121	-1	5	----	----	406,842	25
4333	DD11214	121	-1	5	----	----	464,001	25
4334	DD11223	103	-1	5	----	----	2,148,180	25
4336	DD11225	172	-1	5	----	----	9,734	25
4337	DD11220	172	-1	5	----	----	11,680	25
4338	DD11217	172	-1	3	----	----	6,888	25
4339	DD11218	207	-1	1	----	----	1,144	25
4340	DD11211	207	-1	1	----	----	987	25
4341	DD11216	207	-1	1	----	----	2,953	25
4365	DD11244	138	-1	10	----	----	1,023,726	25
4366	DD11240	138	-1	10	----	----	8,000,000	25 R

TEST & SAMPLE ID #		MAX. STRESS MPa	R	Q Hz	E GPa	e %	CYCLES TO FAIL	WIDTH (mm) and Notes
MATERIAL DD11A								
Lay-up = $(\pm 45/0_4/\mp 45)$, $V_F = 0.31$, Ave. thickness = 3.38 mm, S.D. = 0.14 mm, CoRezyn 63-AX-051 Polyester								
2953	DD11A102	-309	*	13	----	----	1	25
2954	DD11A101	-413	*	13	----	----	1	25
2955	DD11A106	-327	*	13	----	----	1	25
3931	DD11A112	629	*	13	18.3	3.40	1	25
3932	DD11A110	595	*	13	20.4	2.93	1	25
3933	DD11A111	589	*	13	19.9	3.03	1	25
MATERIAL DD12								
Lay-up = $[0/\pm 45/0]_S$, $V_F = 0.43$, Ave. thickness = 2.40 mm, S.D. = 0.11 mm, CoRezyn 63-AX-051 Polyester								
2842	DD12108	708	*	13	26.0	2.71	1	22
2843	DD12110	731	*	13	26.7	2.73	1	22
2844	DD12112	729	*	13	26.7	2.74	1	22
2845	DD12103	414	0.1	2	26.4	1.53	4,967	22
2846	DD12107	276	0.1	12	29.3	0.94	272,993	22
2847	DD12109	276	0.1	12	24.6	1.12	252,590	22
2848	DD12104	241	0.1	12	26.3	0.90	721,943	22
2849	DD12111	345	0.1	5	24.7	1.46	27,280	22
2850	DD12106	345	0.1	5	25.8	1.42	55,126	22
2851	DD12105	345	0.1	5	26.6	1.49	50,100	22
2852	DD12101	276	0.1	5	27.0	1.05	199,436	22
2897	DD12132	-339	*	13	----	----	1	25
2898	DD12131	-273	*	13	----	----	1	25
2899	DD12130	-293	*	13	----	----	1	25
MATERIAL DD13								
Lay-up = $[0/\pm 45/0]_S$, $V_F = 0.50$, Ave. thickness = 2.13 mm, S.D. = 0.12 mm, CoRezyn 63-AX-051 Polyester								
2830	DD13111	855	*	13	29.6	2.89	1	22
2831	DD13110	799	*	13	30.4	2.63	1	22
2832	DD13113	809	*	13	32.9	2.56	1	22
2833	DD13101	414	0.1	4	26.2	1.60	5,769	22
2834	DD13102	414	0.1	4	29.0	1.39	7,805	22
2835	DD13107	345	0.1	5	29.3	1.26	17,253	22
2836	DD13108	207	0.1	12	27.6	0.77	1,397,049	22
2837	DD13106	345	0.1	5	31.2	1.15	28,437	22
2838	DD13105	345	0.1	5	26.9	1.49	19,323	22
2839	DD13113	276	0.1	10	28.9	0.97	145,120	22
2840	DD13114	276	0.1	10	30.2	0.91	85,412	22
2841	DD13115	276	0.1	10	31.7	0.89	124,822	22
2887	DD13129	-319	*	13	----	----	1	25
2888	DD13122	-311	*	13	----	----	1	25
2889	DD13124	-312	*	13	----	----	1	25
2890	DD13130	-207	10	2	----	----	1,870	25

TEST & SAMPLE ID #		MAX. STRESS MPa	R	Q Hz	E GPa	e %	CYCLES TO FAIL	WIDTH (mm) and Notes
2891	DD13123	-207	10	2	----	----	9,529	25
2892	DD13127	-207	10	2	----	----	4,017	25
2893	DD13120	-172	10	10	----	----	59,117	25
2894	DD13131	-172	10	10	----	----	35,801	25
2895	DD13128	-172	10	12	----	----	45,057	25
2896	DD13126	-155	10	10	----	----	443,122	25

MATERIAL DD14

Lay-up = $[0/\pm45/0]_S$, $V_F = 0.35$, Ave. thickness = 2.71 mm, S.D. = 0.07 mm, CoRezyn 63-AX-051 Polyester

2956	DD14301	-452	*	13	----	----	1	25
2957	DD14303	-385	*	13	----	----	1	25
2958	DD14302	-447	*	13	----	----	1	25
4064	DD14112	794	*	13	25.7	3.11	1	22 tab
4065	DD14106	754	*	13	25.5	3.05	1	22 tab
4066	DD14105	637	*	13	23.3	2.80	1	22 tab
4067	DD14111	345	0.1	2	25.4	1.48	5,851	22 tab
4068	DD14107	345	0.1	2	26.0	1.38	8,812	22 tab
4069	DD14109	345	0.1	2	24.1	1.56	6,090	22 tab
4070	DD14104	276	0.1	6	23.9	1.09	26,391	22 tab
4071	DD14103	276	0.1	5	25.7	1.13	25,357	22 tab
4072	DD14102	207	0.1	10	25.4	0.78	432,261	22 tab
4073	DD14101	276	0.1	5	25.5	1.20	47,275	22 tab
4074	DD14110	207	0.1	10	25.1	0.85	513,840	22 tab
4075	DD14108	207	0.1	10	26.0	0.80	210,479	22 tab

MATERIAL DD15

Lay-up = $[0/\pm45/0]_S$, $V_F = 0.25$, Ave. thickness = 3.13 mm, S.D. = 0.18 mm, CoRezyn 63-AX-051 Polyester

2959	DD15302	-435	*	13	----	----	1	25
2960	DD15301	-411	*	13	----	----	1	25
2961	DD15303	-471	*	13	----	----	1	25

MATERIAL DD16

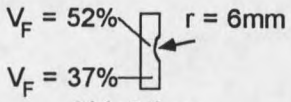
Lay-up = $[90/0/\pm45/0]_S$, $V_F = 0.36$, Ave. thickness = 4.62 mm, S.D. = 0.07 mm, CoRezyn 63-AX-051 Polyester
This material is similar to the DD5P coupons except for an additional 90 ply on the outside.
These additional 90 plies were NOT included in the cross sectional area / stress calculations, nominal thickness was taken as 3.175 mm. (So actual true testing stress is 0.68 multiplied by the stress listed.) See the residual strength section of this database for additional tests.

3650	DD16102	414	0.1	2	17.1	1.83	32,965	25
3654	DD16108	310	0.1	10	18.1	1.26	844,744	25
3655	DD16101	310	0.1	10	18.9	1.24	274,618	25
3656	DD16103	310	0.1	10	18.2	1.27	658,704	25
3657	DD16106	310	0.1	10	18.6	1.30	523,116	25
Test 3690 and 3691 had four additional 90 plies on the outside over a 25 mm length.								
3690	DD16200	310	0.1	10	----	----	560,000	25 R

TEST & SAMPLE ID #		MAX. STRESS MPa	R	Q Hz	E GPa	e %	CYCLES TO FAIL	WIDTH (mm) and Notes
3691	DD16202	310	0.1	10	----	----	396,989	25
3832	DD16150	-394	*	13	----	----	1	25
3833	DD16151	-406	*	13	----	----	1	25
3834	DD16152	-454	*	13	----	----	1	25

MATERIAL DD17

Lay-up = $[0/\pm45/0]_S$, V_F = 0.37, 0.52 , Ave. thickness = 2.90 mm, 2.09 mm (indentation) S.D. = 0.05 mm, 0.07 mm (indentation), CoRezyn 63-AX-051 Polyester. This material had a surface indentation to locally raise the V_F. The listed stress does NOT take into account the indentation. (the average stress increase due to this indentation = 1.39)

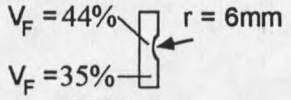


Side View

3694	DD17104	445	0.1	2	----	----	1,317	25 tab
3696	DD17106	448	0.1	2	----	----	1,210	25 tab
3697	DD17107	333	0.1	2	----	----	8,591	25 tab
3698	DD17108	328	0.1	2	----	----	7,151	25 tab
3699	DD17109	165	0.1	10	----	----	198,817	25 tab
3700	DD17110	111	0.1	12	----	----	889,958	25 tab
3701	DD17111	108	0.1	12	----	----	2,048,532	25 tab
3702	DD17112	165	0.1	12	----	----	218,200	25 tab
3703	DD17101	787	*	13	----	----	1	25 tab
3704	DD17102	784	*	13	----	----	1	25 tab
3705	DD17103	775	*	13	----	----	1	25 tab
3706	DD17118	166	0.1	10	----	----	225,558	25 tab
3707	DD17118	334	0.1	2	----	----	5,342	25 tab
3950	DD17211	-394	*	13	----	----	1	25 Z
3951	DD17213	-427	*	13	----	----	1	25 Z
3952	DD17210	-440	*	13	----	----	1	25 Z
3953	DD17206	-276	10	4	----	----	8,751	25 Z
3954	DD17202	-276	10	4	----	----	21,582	25 Z
3955	DD17208	-276	10	3	----	----	4,910	25 Z
3956	DD17207	-207	10	20	----	----	1,184,170	25 Z
3957	DD17214	-207	10	20	----	----	5,357,313	25 Z
3958	DD17209	-207	10	20	----	----	890,895	25 Z

MATERIAL DD17A

Lay-up = $[0/\pm45/0]_S$, V_F = 0.35, 0.44, Ave. thickness = 2.83 mm, 2.29 mm (indentation) S.D. = 0.15 mm, 0.06 mm (indentation), CoRezyn 63-AX-051 Polyester. This material has a surface indentation to raise the V_F. The listed stress does NOT take into account the indentation. (the average stress increase due to this indentation = 1.24)

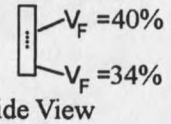


Side View

TEST & SAMPLE ID #		MAX. STRESS MPa	R	Q Hz	E GPa	e %	CYCLES TO FAIL	WIDTH (mm) and Notes
3875	DD17A127	414	0.1	2	24.3	1.87	870	25
3876	DD17A106	414	0.1	2	24.5	1.88	993	25
3877	DD17A116	414	0.1	2	22.5	2.10	440	25 R
3878	DD17A112	345	0.1	4	23.1	1.65	1,637	25
3879	DD17A103	345	0.1	4	26.1	1.52	7,677	25
3880	DD17A113	345	0.1	4	23.2	1.60	3,156	25
3881	DD17A102	345	0.1	4	23.8	1.52	2,866	25
3882	DD17A109	276	0.1	5	22.4	1.30	23,820	25
3883	DD17A101	276	0.1	4	22.1	1.33	52,327	25
3884	DD17A107	276	0.1	4	22.1	1.29	15,558	25
3885	DD17A111	207	0.1	5	23.2	0.97	385,099	25
3886	DD17A128	207	0.1	5	24.3	0.92	186,232	25
3887	DD17A110	207	0.1	5	22.6	0.96	119,502	25
3888	DD17A122	207	0.1	5	25.5	0.97	170,000	25 R
3889	DD17A125	681	*	13	23.2	3.05	1	25
3890	DD17A121	621	*	13	22.5	3.01	1	25
3891	DD17A120	636	*	13	24.3	2.92	1	25
3892	DD17A123	207	0.1	5	23.0	0.96	584,702	25 tab
3893	DD17A104	276	0.1	2	25.2	1.18	65,356	25 tab
3894	DD17A108	190	0.1	8	22.6	0.86	843,279	25 tab
3895	DD17A119	190	0.1	8	21.1	0.94	510,998	25 tab
3896	DD17A117	172	0.1	8	22.9	0.80	6,125,824	25 tab
3897	DD17A115	345	0.1	2	24.3	1.64	2,414	25 tab
3898	DD17A126	345	0.1	3	22.5	1.70	12,349	25 tab
3899	DD17A114	276	0.1	4	23.6	1.20	43,591	25 tab
3959	DD17A209	-207	10	2	----	----	118	25 Z
3960	DD17A214	-207	10	4	----	----	584	25 Z
3961	DD17A215	-207	10	2	----	----	506	25 Z
3962	DD17A210	-138	10	10	----	----	1,496,838	25 Z
3963	DD17A208	-138	10	25	----	----	20,000,000	25 Z R
3964	DD17A221	-138	10	15	----	----	499,160	25 Z
3965	DD17A213	-297	*	13	----	----	1	25 Z
3966	DD17A216	-243	*	13	----	----	1	25 Z
3967	DD17A217	-255	*	13	----	----	1	25 Z
3968	DD17A218	-138	10	10	----	----	1,296,088	25 Z

MATERIAL DD18

Lay-up = $[0/\pm45/0]_S$, V_F = 0.34, 0.40, Ave. thickness = 3.35 mm, S.D. = 0.07 mm, CoRezyn 63-AX-051 Polyester. This material has a mid-laminate 90 degree D155 ply, 4 mm long and across the width of the coupon, to locally raise the V_F.



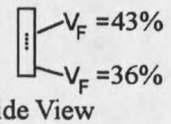
Side View

3722	DD18107	241	0.1	10	21.2	1.12	268,555	25
3723	DD18112	241	0.1	10	22.5	1.15	328,011	25
3724	DD18111	241	0.1	10	21.5	1.24	463,110	25

TEST & SAMPLE ID #		MAX. STRESS MPa	R	Q Hz	E GPa	e %	CYCLES TO FAIL	WIDTH (mm) and Notes
3725	DD18110	414	0.1	2	24.6	1.91	12,899	25
3726	DD18109	414	0.1	2	22.8	1.99	10,402	25
3727	DD18108	414	0.1	2	22.9	2.05	8,310	25
3728	DD18105	345	0.1	5	23.0	1.66	49,566	25
3729	DD18104	345	0.1	5	23.7	1.47	25,373	25
3730	DD18106	345	0.1	5	22.1	1.48	45,228	25
3731	DD18103	754	*	13	22.3	3.40	1	25
3732	DD18102	708	*	13	21.8	3.30	1	25
3733	DD18101	727	*	13	22.2	----	1	25
3734	DD18140	207	0.1	12	23.3	0.90	2,661,881	25
3835	DD18150	-575	*	13	----	----	1	25
3836	DD18151	-466	*	13	----	----	1	25
3837	DD18152	-484	*	13	----	----	1	25

MATERIAL DD18A

Lay-up = $[0/\pm45/0]_S$, V_F = 0.36, 0.43, Ave. thickness = 2.78 mm, S.D. = 0.08 mm, CoRezyn 63-AX-051 Polyester. This material has a mid-laminate 90 degree D155 ply, 4 mm long and across the width of the coupon, to locally raise the V_F.



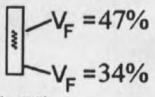
Side View

3900	DD18A115	190	0.1	10	21.0	0.95	1,750,000	25 R tab
3901	DD18A112	414	0.1	2	22.2	2.13	913	25 tab
3902	DD18A101	345	0.1	4	21.5	1.79	5,846	25 tab
3903	DD18A108	276	0.1	5	23.1	1.18	78,800	25 tab
3904	DD18A104	414	0.1	2	22.6	1.96	1,508	25 tab
3905	DD18A113	414	0.1	2	21.7	2.00	815	25 tab
3906	DD18A106	207	0.1	8	22.0	1.15	654,689	25 tab
3907	DD18A110	345	0.1	4	22.3	1.67	3,418	25 tab
3908	DD18A114	345	0.1	3	24.3	1.55	8,292	25 tab
3909	DD18A105	276	0.1	5	24.4	1.22	65,338	25 tab
3910	DD18A103	276	0.1	5	22.5	1.29	67,612	25 tab
3911	DD18A102	207	0.1	8	23.2	0.99	3,000,000	25 R tab
3913	DD18A150	716	*	13	23.1	3.20	1	25 tab
3914	DD18A151	716	*	13	23.3	3.07	1	25 tab
3915	DD18A152	667	*	13	23.3	3.06	1	25 tab
3941	DD18A140	-320	*	13	----	----	1	25
3942	DD18A111	-338	*	13	----	----	1	25
3943	DD18A141	-318	*	13	----	----	1	25

TEST & SAMPLE ID #	MAX. STRESS MPa	R	Q Hz	E GPa	e %	CYCLES TO FAIL	WIDTH (mm) and Notes

MATERIAL DD19

Lay-up = $[0/\pm45/0]_S$, V_F = 0.34, 0.47, Ave. thickness = 3.39 mm, S.D. = 0.11 mm, CoRezyn 63-AX-051 Polyester. This material has two mid-laminate 90 degree plies, 4 mm long and across the width of the coupon, to locally raise the V_F.

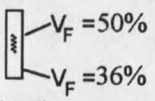


Side View

3710	DD19107	414	0.1	2	22.0	2.17	2,235	25
3711	DD19106	241	0.1	8	21.8	1.23	57,266	25
3712	DD19109	241	0.1	5	21.4	1.24	92,441	25
3713	DD19108	241	0.1	5	21.8	1.20	77,008	25
3714	DD19111	155	0.1	12	22.6	0.75	1,354,001	25
3715	DD19110	155	0.1	12	24.3	0.68	955,238	25
3716	DD19101	155	0.1	12	20.5	0.83	3,104,534	25
3717	DD19112	345	0.1	2	----	----	9,055	25
3718	DD19119	345	0.1	1	----	----	8,722	25
3719	DD19105	716	*	13	21.2	3.4	1	25
3720	DD19104	706	*	13	21.5	3.3	1	25
3721	DD19103	707	*	13	22.4	3.2	1	25
3838	DD19120	-400	*	13	----	----	1	25
3839	DD19121	-332	*	13	----	----	1	25
3840	DD19126	-392	*	13	----	----	1	25
3944	DD19124	-207	10	10	----	----	93,523	25
3945	DD19125	-207	10	15	----	----	3,000,000	25
3946	DD19127	-276	10	10	----	----	27,769	25
3947	DD19122	-276	10	5	----	----	1,397	25
3948	DD19123	-276	10	5	----	----	18,564	25
3949	DD19131	-241	10	5	----	----	5,710	25

MATERIAL DD19A

Lay-up = $[0/\pm45/0]_S$, V_F = 0.36, 0.50, Ave. thickness = 2.78 mm, S.D. = 0.03 mm, CoRezyn 63-AX-051 Polyester. This material has two mid-laminate 90 degree plies, 4 mm wide, to locally raise the V_F.



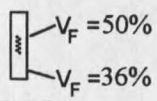
Side View

3916	DD19A140	207	0.1	7	23.7	0.88	31,090	25 tab
3917	DD19A117	138	0.1	6	23.9	0.58	1,250,000	25 R tab
3918	DD19A118	345	0.1	2	24.0	1.50	877	25 tab
3919	DD19A106	345	0.1	2	24.6	1.61	1,088	25 tab
3920	DD19A128	345	0.1	2	21.9	1.69	1,590	25 tab
3921	DD19A127	276	0.1	4	22.4	1.34	8,594	25 tab
3922	DD19A121	276	0.1	4	22.8	1.35	31,283	25 tab
3923	DD19A122	276	0.1	5	23.5	1.36	11,012	25 tab

TEST & SAMPLE ID #		MAX. STRESS MPa	R	Q Hz	E GPa	e %	CYCLES TO FAIL	WIDTH (mm) and Notes
3924	DD19A111	207	0.1	7	23.4	0.96	108,773	25 tab
3925	DD19A116	207	0.1	7	22.2	1.11	72,092	25 tab
3926	DD19A119	172	0.1	8	23.9	0.83	143,171	25 tab
3927	DD19A110	646	*	13	23.3	3.01	1	25 tab
3928	DD19A114	647	*	13	21.8	3.18	1	25 tab
3929	DD19A115	661	*	13	22.6	3.0	1	25 tab
3930	DD19A126	172	0.1	5	----	----	95,294	25 tab
3931	DD19A113	-328	*	13	----	----	1	25
3932	DD19A124	-299	*	13	----	----	1	25
3933	DD19A123	-252	*	13	----	----	1	25
3934	DD19A109	-172	10	10	----	----	88,437	25
3935	DD19A102	-138	10	10	----	----	4,312,570	25
3936	DD19A103	-138	10	20	----	----	12,000,000	25 R
3937	DD19A104	-172	10	10	----	----	62,730	25
3940	DD19A101	-172	10	10	----	----	124,618	25
3972	DD19AT107	69	*	13	11.1	0.64	1	25
3973	DD19AT102	68	*	13	9.74	0.71	1	25
3974	DD19AT101	68	*	13	9.60	0.74	1	25
3975	DD19AT106	17	0.1	20	11.2	0.16	4,000,000	25 R
3976	DD19AT104	38	0.1	2	10.5	0.37	13,061	25
3977	DD19AT103	35	0.1	4	10.7	0.34	39,706	25
3978	DD19AT110	35	0.1	4	10.1	0.34	85,033	25
3979	DD19AT109	28	0.1	12	10.5	0.26	930,960	25
3980	DD19AT108	28	0.1	12	10.8	0.26	2,571,689	25
3981	DD19AT105	28	0.1	15	11.8	0.24	2,461,981	25

MATERIAL DD19B

Lay-up = $[0/\pm45/0]_S$, V_F = 0.35, 0.44, Ave. thickness = 2.78 mm, S.D. = 0.07 mm, CoRezyn 63-AX-051 Polyester, This material had two 8 mm x 19 mm internal (between center 0° plies and centered side-to-side) D155 fabric patches to raise the V_F without any test coupon edge effects.



Side View

4003	DD19B117	276	0.1	4	24.1	1.09	27,705	25 tab
4004	DD19B113	276	0.1	4	22.7	1.25	50,000	25 R tab
4005	DD19B109	276	0.1	4	22.2	1.20	18,014	25 tab
4006	DD19B110	276	0.1	4	26.2	1.13	10,666	25 tab
4007	DD19B105	241	0.1	4	25.8	1.03	46,870	25 tab
4008	DD19B115	207	0.1	5	25.3	0.88	123,726	25 tab
4009	DD19B112	207	0.1	7	26.4	0.78	711,185	25 tab
4010	DD19B114	241	0.1	4	23.8	1.07	17,022	25 tab
4011	DD19B111	241	0.1	4	22.5	1.15	62,757	25 tab
4012	DD19B101	697	*	13	26.1	2.94	1	25 tab
4013	DD19B106	693	*	13	25.3	2.87	1	25 tab
4014	DD19B107	691	*	13	23.8	3.02	1	25 tab

TEST & SAMPLE ID #		MAX. STRESS MPa	R	Q Hz	E GPa	e %	CYCLES TO FAIL	WIDTH (mm) and Notes
4015	DD19B119	207	0.1	6	24.4	0.80	377,162	25 tab

MATERIAL DD20

Lay-up = $[0_2/\pm45/0]_S$, V_F = 0.34, Ave. thickness = 2.89 mm, S.D. = 0.04 mm, CoRezyn 63-AX-051 Polyester.

4019	DD20101	584	*	13	22.6	2.8	1	22 tab
4020	DD20105	582	*	13	23.1	2.6	1	22 tab
4021	DD20108	594	*	13	23.2	2.8	1	22 tab
4022	DD20103	310	0.1	2	22.6	1.55	8,408	22 tab
4023	DD20102	310	0.1	4	22.0	1.58	4,899	22 tab
4024	DD20109	310	0.1	4	22.9	1.46	5,860	22 tab
4025	DD20104	207	0.1	5	23.3	0.96	27,916	22 tab
4026	DD20106	172	0.1	10	21.7	0.83	87,234	22 tab
4027	DD20112	172	0.1	5	20.0	0.89	65,250	22 tab
4028	DD20111	138	0.1	7	22.8	0.63	484,310	22 tab
4029	DD20110	138	0.1	7	21.2	0.69	459,000	22 tab
4030	DD20107	138	0.1	7	20.9	0.70	362,971	22 tab
4206	DD20143	-337	*	13	----	----	1	25
4207	DD20142	-313	*	13	----	----	1	25
4208	DD20141	-294	*	13	----	----	1	25
4209	DD20140	-308	*	13	----	----	1	25

MATERIAL DD20A

Lay-up = $[0_2/\pm45/0]_S$, V_F = 0.37, Ave. thickness = 2.66 mm, S.D. = 0.07 mm, CoRezyn 63-AX-051 Polyester.

4054	DD20A112	653	*	13	25.7	2.69	1	22 tab
4055	DD20A110	645	*	13	24.5	2.76	1	22 tab
4056	DD20A108	619	*	13	24.3	2.64	1	22 tab
4057	DD20A104	310	0.1	3	26.7	1.35	5,006	22 tab
4058	DD20A102	310	0.1	3	25.4	1.35	6,014	22 tab
4059	DD20A109	310	0.1	3	25.6	1.41	5,207	22 tab
4060	DD20A106	207	0.1	8	25.0	0.83	38,386	22 tab
4061	DD20A111	207	0.1	8	26.4	0.80	24,080	22 tab
4062	DD20A107	207	0.1	8	25.2	0.88	44,850	22 tab
4063	DD20A101	138	0.1	12	24.1	0.60	1,209,687	22 tab
4076	DD20A103	172	0.1	10	----	----	46,058	22 tab

MATERIAL DD22

Lay-up = $[0_2/\pm45/0]_S$, V_F = 0.37, Ave. thickness = 2.86 mm, S.D. = 0.12 mm, CoRezyn 63-AX-051 Polyester.

4045	DD22112	564	*	13	21.0	2.8	1	22 tab
4046	DD22103	551	*	13	19.5	2.86	1	22 tab
4047	DD22109	533	*	13	21.1	2.61	1	22 tab
4048	DD22110	207	0.1	5	20.3	1.06	1,873,215	22 tab
4049	DD22104	276	0.1	4	18.2	1.67	62,055	22 tab
4050	DD22106	276	0.1	3	19.2	1.61	88,185	22 tab
4051	DD22102	276	0.1	3	19.5	1.54	58,843	22 tab

TEST & SAMPLE ID #		MAX. STRESS MPa	R	Q Hz	E GPa	e %	CYCLES TO FAIL	WIDTH (mm) and Notes
4052	DD22105	241	0.1	4	18.4	1.27	384,914	22 tab
4053	DD22111	241	0.1	10	19.3	1.25	960,823	22 tab
4210	DD22140	-372	*	13	----	----	1	25
4211	DD22141	-416	*	13	----	----	1	25
4212	DD22142	-398	*	13	----	----	1	25
4213	DD22143	-370	*	13	----	----	1	25

MATERIAL DD24

Lay-up = $[0/\pm45/0_3/\pm45/0]$, $V_F = 0.39$, Ave. thickness = 2.59 mm, S.D. = 0.07 mm, CoRezyn 63-AX-051 Polyester

4130	DD24124	345	0.1	8	----	----	40,767	22 tab
4131	DD24131	345	0.1	8	22.5	1.53	17,433	22 tab
4132	DD24129	345	0.1	8	24.7	1.50	20,925	22 tab
4133	DD24125	276	0.1	8	21.8	1.31	190,571	22 tab
4134	DD24130	241	0.1	12	22.9	1.08	696,493	22 tab
4135	DD24128	241	0.1	12	23.3	1.12	314,716	22 tab
4136	DD24115	746	*	13	25.9	2.9	1	22 tab
4137	DD24117	704	*	13	----	----	1	22 tab
4138	DD24114	739	*	13	26.8	2.9	1	22 tab
4139	DD24127	207	0.1	12	23.6	0.88	5,000,000	22 R tab
4164	DD24106	-528	*	13	----	----	1	25
4165	DD24105	-537	*	13	----	----	1	25
4166	DD24104	-500	*	13	----	----	1	25
4167	DD24107	-477	*	13	----	----	1	25

MATERIAL DD25

Lay-up = $[0/\pm45/0]_S$, $V_F = 0.45$, Ave. thickness = 2.89 mm, S.D. = 0.14 mm, Glass Veil, CoRezyn 63-AX-051 Polyester

4140	DD25102	814	*	13	28.4	3.0	1	22 tab
4141	DD25105	682	*	13	28.0	3.1	1	22 tab
4142	DD25108	733	*	13	27.2	2.7	1	22 tab
4143	DD25109	345	0.1	7	27.7	1.42	1,621	22 tab
4144	DD25106	207	0.1	10	29.2	0.73	205,450	22 tab
4145	DD25107	172	0.1	12	26.0	0.67	5,000,000	22 R tab
4146	DD25101	276	0.1	5	25.7	1.10	37,442	22 tab
4147	DD25110	276	0.1	5	29.3	0.99	50,003	22 tab
4148	DD25111	276	0.1	5	29.7	1.01	48,799	22 tab
4149	DD25114	207	0.1	12	30.4	0.68	778,703	22 tab
4150	DD25104	345	0.1	2	27.0	1.37	8,578	22 tab
4151	DD25113	345	0.1	2	28.8	1.22	17,706	22 tab
4152	DD25103	207	0.1	8	27.7	0.78	982,766	22 tab
4160	DD25130	-498	*	13	----	----	1	25
4161	DD25131	-505	*	13	----	----	1	25
4162	DD25132	-464	*	13	----	----	1	25
4163	DD25133	-465	*	13	----	----	1	25

TEST & SAMPLE ID #		MAX. STRESS MPa	R	Q Hz	E GPa	e %	CYCLES TO FAIL	WIDTH (mm) and Notes
4173	DD25132	-241	10	15	----	----	1,322,357	25
4174	DD25136	-241	10	15	----	----	524,658	25

MATERIAL DD25A

Lay-up = $[0/\pm45/0]_S$, $V_F = 0.48$, Ave. thickness = 2.67 mm, S.D. = 0.08 mm, Polyester Veil, CoRezyn 63-AX-051 Polyester

4153	DD25A113	790	*	13	27.6	3.0	1	22 tab
4154	DD25A112	780	*	13	28.8	2.8	1	22 tab
4155	DD25A111	778	*	13	27.3	2.9	1	22 tab
4183	DD25A101	207	0.1	10	28.0	0.74	1,015,979	22 tab
4184	DD25A108	241	0.1	10	27.7	0.86	503,924	22 tab
4185	DD25A104	241	0.1	10	27.7	0.91	740,566	22 tab
4186	DD25A109	241	0.1	12	----	----	1,178,054	22 tab
4187	DD25A106	276	0.1	10	28.6	1.01	135,192	22 tab
4188	DD25A110	276	0.1	4	29.5	0.97	146,154	22 tab
4189	DD25A102	276	0.1	4	29.5	0.99	253,259	22 tab
4190	DD25A103	345	0.1	4	29.5	1.23	20,249	22 tab
4191	DD25A107	345	0.1	4	28.5	1.24	44,823	22 tab
4192	DD25A105	345	0.1	4	29.3	1.20	44,578	22 tab
4218	DD25A160	-679	*	13	----	----	1	25
4219	DD25A161	-657	*	13	----	----	1	25
4220	DD25A163	-608	*	13	----	----	1	25
4221	DD25A162	-570	*	13	----	----	1	25

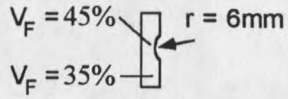
MATERIAL DD25B

Lay-up = $[0/\pm45/0]_S$, $V_F = 0.31$, Ave. thickness = 4.27 mm, S.D. = 0.06 mm, Polyester Veil, CoRezyn 63-AX-051 Polyester

4156	DD25B104	486	*	13	18.2	2.7	1	22 tab
4157	DD25B103	540	*	13	19.7	2.9	1	22 tab
4158	DD25B111	516	*	13	19.0	2.8	1	22 tab
4159	DD25B102	207	0.1	10	20.2	1.07	1,200,000	22 R tab
4168	DD25B130	-437	*	13	----	----	1	25
4169	DD25B131	-363	*	13	----	----	1	25
4170	DD25B132	-453	*	13	----	----	1	25
4171	DD25B133	-422	*	13	----	----	1	25
4175	DD25B110	241	0.1	5	----	----	118,550	22 tab
4176	DD25B108	241	0.1	10	18.5	1.38	178,659	22 tab
4177	DD25B112	241	0.1	10	17.5	1.46	70,464	22 tab
4178	DD25B107	276	0.1	4	20.1	1.41	49,497	22 tab
4179	DD25B106	276	0.1	4	19.1	1.48	17,956	22 tab
4180	DD25B105	276	0.1	4	19.3	1.52	41,266	22 tab
4182	DD25B109	310	0.1	2	21.2	1.54	5,663	22 tab

MATERIAL DD25D

Lay-up = $[0/\pm45/0]_S$, V_F = 0.35, 0.45, Ave. thickness = 3.96 mm, 2.55 mm (indentation) S.D. = 0.09 mm, 0.06 mm (indentation), Polyester veil, CoRezyn 63-AX-051 Polyester. This material has a surface indentation to raise the V_F. The listed stress does NOT take into account the indentation. (the average stress increase due to this indentation = 1.55)



4234	DD25D102	516	*	13	25.5	2.15	1	25
4235	DD25D101	179	0.1	5	23.1	1.17	110,424	25
4236	DD25D110	181	0.1	4	25.0	0.94	180,832	25
4237	DD25D112	155	0.1	7	22.0	0.83	584,489	25
4238	DD25D111	155	0.1	8	----	----	252,968	25
4239	DD25D108	176	0.1	4	----	----	66,875	25
4240	DD25D105	153	0.1	8	----	----	182,727	25
4241	DD25D104	156	0.1	5	----	----	347,113	25
4242	DD25D107	180	0.1	5	----	----	159,308	25
4243	DD25D117	451	*	13	----	----	1	25
4244	DD25D118	467	*	13	----	----	1	25

MATERIAL DD26

Lay-up = $[0/\pm45/0]_S$, V_F = 0.50, Ave. thickness = 2.61 mm, S.D. = 0.10 mm, CoRezyn 63-AX-051 Polyester. Same fabric as DD25, but with a different binder used for general purpose polyester resins.

4245	DD26116	849	*	13	32.0	2.65	1	22 tab
4246	DD26101	808	*	13	30.4	2.70	1	22 tab
4247	DD26110	902	*	13	29.6	3.05	1	22 tab
4248	DD26115	414	0.1	4	32.4	1.45	10,628	22 tab
4249	DD26114	414	0.1	4	28.8	1.53	13,112	22 tab
4250	DD26111	414	0.1	4	29.0	1.45	9,883	22 tab
4251	DD26112	345	0.1	8	28.8	1.25	39,204	22 tab
4252	DD26113	345	0.1	8	30.1	1.20	44,872	22 tab
4253	DD26104	241	0.1	12	30.1	0.80	780,507	22 tab
4254	DD26103	345	0.1	5	30.7	1.24	92,698	22 tab
4255	DD26107	241	0.1	12	28.1	0.90	609,415	22 tab
4256	DD26105	241	0.1	10	29.6	0.83	2,019,100	22 tab
4257	DD26106	241	0.1	10	30.5	0.83	1,568,929	22 tab
4258	DD26126	-563	*	13	----	----	1	25
4259	DD26127	-593	*	13	----	----	1	25
4260	DD26125	-519	*	13	----	----	1	25
4261	DD26129	-594	*	13	----	----	1	25
4262	DD26124	-310	10	10	----	----	103,105	25
4263	DD26120	-241	10	12	----	----	20,000,000	25 R
4264	DD26130	-276	10	12	----	----	2,851,058	25
4264	DD26121	-276	10	12	----	----	2,185,867	25
4265	DD26122	-276	10	12	----	----	1,343,877	25
2466	DD26132	-276	10	12	----	----	363,720	25 R

MATERIAL FFA

TEST & SAMPLE ID #		MAX. STRESS MPa	R	Q Hz	E GPa	e %	CYCLES TO FAIL	WIDTH (mm) and Notes
Lay-up = $[\pm 45/0/0/\pm 45]_S$, V_F =0.38, Ave. thickness = 3.78 mm, S.D. = 0.07 mm, CoRezyn 63-AX-051 Polyester. The FFA, FFB, FFC, FFD and FFF materials involved the same fabrics with the lay-up orientation changed to investigate ply sequence fatigue differences.								
3337	FFA104	721	*	13	24.3	3.00	1	25
3338	FFA112	717	*	13	23.6	3.03	1	25
3339	FFA106	710	*	13	24.8	2.90	1	25
3340	FFA109	414	0.1	2	23.6	1.98	1,832	25
3341	FFA102	414	0.1	2	23.8	2.14	757	25
3342	FFA114	414	0.1	2	25.0	2.05	926	25
3343	FFA111	345	0.1	4	24.9	1.63	4,233	25
3344	FFA118	276	0.1	4	25.9	1.21	30,201	25
3345	FFA115	345	0.1	2	24.8	1.63	4,642	25
3346	FFA107	276	0.1	4	24.3	1.29	37,675	25
3347	FFA113	345	0.1	2	24.9	1.63	2,420	25
3348	FFA105	276	0.1	4	23.6	1.28	18,064	25
3349	FFA103	172	0.1	10	23.9	0.78	10,000,000	25 R
3350	FFA110	207	0.1	10	23.7	0.93	1,123,713	25
3351	FFA116	207	0.1	12	23.7	0.99	372,007	25
3352	FFA117	207	0.1	12	22.8	1.02	612,692	25
3370	FFA153	207	0.1	12	----	----	926,563	25
3371	FFA108	345	0.1	2	----	----	2,039	25
Tests 3373 - 3377 were run at 20 Hz to observe thermal failures								
3373	FFA160	207	0.1	20	----	----	42,809	25
3374	FFA155	345	0.1	20	----	----	820	25
3375	FFA152	276	0.1	20	----	----	5,899	25
3376	FFA151	172	0.1	20	----	----	157,623	25
3377	FFA154	138	0.1	20	----	----	5,000,000	25
3424	FFA150	-557	*	13	----	----	1	25
3425	FFA152	-558	*	13	----	----	1	25
3426	FFA151	-544	*	13	----	----	1	25

MATERIAL FFB

Lay-up = $[0/\pm 45/0/\pm 45/0]_S$, V_F =0.38, Ave. thickness = 3.81 mm, S.D. = 0.05 mm, CoRezyn 63-AX-051 Polyester. The FFA, FFB, FFC, FFD and FFF materials involved the same fabrics with the lay-up orientation changed to investigate ply orientation fatigue differences.

3353	FFB136	599	*	13	24.1	3	1	25
3354	FFB132	607	*	13	23.4	2.9	1	25
3355	FFB138	657	*	13	24.9	2.8	1	25
3356	FFB128	414	0.1	2	23.6	1.97	803	25
3357	FFB141	414	0.1	2	23.9	2.04	1,391	25
3358	FFB134	345	0.1	2	23.4	1.68	2,293	25
3359	FFB130	345	0.1	2	23.4	1.68	1.909	25
3360	FFB142	276	0.1	4	22.3	1.41	16,986	25
3361	FFB140	276	0.1	2	24.4	1.23	22,313	25
3362	FFB131	207	0.1	12	23.3	0.98	486,273	25
3363	FFB127	207	0.1	12	21.0	1.03	393,660	25

TEST & SAMPLE ID #		MAX. STRESS MPa	R	Q Hz	E GPa	e %	CYCLES TO FAIL	WIDTH (mm) and Notes
3364	FFB139	207	0.1	12	23.6	0.95	540,700	25
Tests 3365 - 3368 were notched on the edges to reduce the stress concentration at the grips.								
3365	FFB137	276	0.1	4	----	----	54,111	15
3366	FFB133	207	0.1	12	----	----	849,853	15
3367	FFB129	414	0.1	1	----	----	925	15
3368	FFB125	345	0.1	2	----	----	5,420	15
3369	FFB135	635	*	13	----	----	1	25
3427	FFB114	-517	*	13	----	----	1	25
3428	FFB109	-507	*	13	----	----	1	25
3429	FFB115	-495	*	13	----	----	1	25

MATERIAL FFC

Lay-up = $[0/\pm45/\pm45/0]_S$, V_F =0.38, Ave. thickness = 3.81 mm, S.D. = 0.05 mm, CoRezyn 63-AX-051 Polyester. The FFA, FFB, FFC, FFD and FFF materials involved the same fabrics with the lay-up orientation changed to investigate ply orientation fatigue differences.

3378	FFC117	648	*	13	23.6	2.90	1	25
3379	FFC111	620	*	13	----	----	1	6
3380	FFC104	604	*	13	----	----	1	6
3381	FFC114	414	0.1	1	23.1	2.00	508	25
3382	FFC110	414	0.1	1	----	----	692	25
3383	FFC107	345	0.1	2	22.6	1.71	1,621	25
3384	FFC108	345	0.1	2	----	----	3,371	25
3385	FFC109	276	0.1	4	----	----	31,551	25
3386	FFC118	276	0.1	4	----	----	24,762	25
3387	FFC103	414	0.1	1	----	----	788	25
3388	FFC115	345	0.1	2	----	----	2,895	25
3389	FFC105	276	0.1	4	----	----	27,395	25
3390	FFC101	207	0.1	12	----	----	417,819	25
3391	FFC112	207	0.1	12	----	----	414,180	25
3392	FFC113	207	0.1	21	22.4	0.93	649,406	25
3430	FFC134	-517	*	13	----	----	1	25
3431	FFC128	-476	*	13	----	----	1	25
3432	FFC136	-505	*	13	----	----	1	25

MATERIAL FFD

Lay-up = $[0/0/\pm45/\pm45]_S$, V_F =0.38, Ave. thickness = 3.83 mm, S.D. = 0.04 mm, CoRezyn 63-AX-051 Polyester. The FFA, FFB, FFC, FFD and FFF materials involved the same fabrics with the lay-up orientation changed to investigate ply orientation fatigue differences.

3393	FFD112	676	*	13	24.0	2.90	1	25
3394	FFD106	630	*	13	----	----	1	25
3395	FFD107	602	*	13	----	----	1	25
3396	FFD110	414	0.1	2	22.2	2.18	533	25
3397	FFD111	414	0.1	2	----	----	793	6
3398	FFD104	414	0.1	2	----	----	912	6
3399	FFD102	345	0.1	2	----	----	3,683	6

TEST & SAMPLE ID #		MAX. STRESS MPa	R	Q Hz	E GPa	e %	CYCLES TO FAIL	WIDTH (mm) and Notes
3400	FFD105	345	0.1	2	----	----	2,923	6
3401	FFD114	345	0.1	2	----	----	3,993	6
3402	FFD115	276	0.1	4	----	----	24,441	6
3403	FFD116	276	0.1	4	----	----	32,380	6
3404	FFD101	276	0.1	4	----	----	21,567	6
3405	FFD103	207	0.1	12	----	----	1,099,442	6
3406	FFD117	207	0.1	12	----	----	466,758	6
3407	FFD104	207	0.1	12	----	----	650,603	6
3433	FFD133	-547	*	13	----	----	1	25
3434	FFD141	-549	*	13	----	----	1	25
3435	FFD138	-530	*	13	----	----	1	25

MATERIAL FFF

Lay-up = $[\pm45/\pm45/0/0]_S$, V_F =0.38, Ave. thickness = 3.77 mm, S.D. = 0.05 mm, CoRezyn 63-AX-051 Polyester. The FFA, FFB, FFC, FFD and FFF materials involved the same fabrics with the lay-up orientation changed to investigate ply orientation fatigue differences.

3408	FFF110	640	*	13	----	----	1	6
3409	FFF106	643	*	13	----	----	1	6
3410	FFF122	708	*	13	----	----	1	25
3411	FFF108	414	0.1	1	----	----	683	6
3412	FFF107	414	0.1	1	----	----	810	6
3413	FFF114	414	0.1	2	----	----	1,587	6
3415	FFF112	345	0.1	2	----	----	7,694	6
3416	FFF117	345	0.1	2	----	----	5,602	6
3417	FFF113	345	0.1	2	----	----	8,381	6
3418	FFF115	276	0.1	4	----	----	30,596	6
3419	FFF109	276	0.1	5	----	----	30,569	6
3420	FFF132	276	0.1	5	----	----	26,561	6
3421	FFF116	207	0.1	12	----	----	374,533	6
3422	FFF111	207	0.1	12	----	----	665,573	6
3423	FFF143	207	0.1	20	----	----	684,496	6
3436	FFF125	-605	*	13	----	----	1	25
3437	FFF134	-627	*	13	----	----	1	25
3438	FFF129	-555	*	13	----	----	1	25

MATERIAL GG

Lay-up = $[0_2/\pm45/0_2]$, V_F =0.40, Ave. thickness = 2.46 mm, S.D. = 0.10 mm, CoRezyn 63-AX-051 Polyester.

3439	GG110	1087	*	13	----	----	1	22
3440	GG104	933	*	13	27.8	3.4	1	22
3441	GG102	891	*	13	27.3	3.3	1	22
3442	GG107	483	0.1	2	28.3	2.00	16,881	22
3443	GG106	483	0.1	2	29.0	2.01	7,897	22
3444	GG101	414	0.1	2	27.6	1.68	47,335	22
3445	GG105	414	0.1	4	27.3	1.73	62,970	22
3446	GG108	345	0.1	5	27.1	1.35	390,948	22

TEST & SAMPLE ID #		MAX. STRESS MPa	R	Q Hz	E GPa	e %	CYCLES TO FAIL	WIDTH (mm) and Notes
3447	GG109	345	0.1	5	28.4	1.26	680,831	22
3448	GG103	345	0.1	5	28.5	1.31	814,868	22
3449	GG116	483	0.1	2	28.4	1.97	13,403	22
3450	GG117	414	0.1	2	28.3	1.66	42,910	22
3451	GG130	-623	*	13	----	----	1	25
3452	GG131	-644	*	13	----	----	1	25
3453	GG132	-617	*	13	----	----	1	25
3454	GG118	980	*	13	28.5	3.44	1	22

0^{o} UNIDIRECTIONAL TESTS

Materials A130, D092A, D155A, DB120A and DB240A were tested in the longitudinal (0°), transverse (90°) and (±45°) fiber directions for material properties. Fabrics DB120A and DB240A were unstitched into +45° and -45° plies, rotated to the 0°direction and tested as a unidirectional fabric. In the notes column, ZERO indicates a unidirectional 0° test, 90 indicates a transverse test and ±45 indicates a simulated shear test (ASTM D3518). These tests are summarized in Table 10.

MATERIAL A060

Lay-up = $[0]_{10}$, $V_F = 0.41$, Ave. thickness = 1.76 mm, S.D. = 0.10 mm, CoRezyn 63-AX-051 Polyester

TEST & SAMPLE ID #		MAX. STRESS MPa	R	Q Hz	E GPa	e %	CYCLES TO FAIL	WIDTH (mm) and Notes
3038	A060104	-317	*	13	----	----	1	25
3039	A060106	-278	*	13	----	----	1	25
3040	A060101	-219	*	13	----	----	1	25
3041	A060119	-440	*	13	----	----	1	25 Z
3042	A060120	-322	*	13	----	----	1	25 Z
3068	A060117	624	*	13	31.4	2.00	1	25
3069	A060113	586	*	13	29.4	2.05	1	25
3070	A060114	529	*	13	32.0	1.70	1	25
3071	A060116	345	0.1	5	27.6	1.21	13,952	25
3072	A060118	345	0.1	5	33.9	1.04	7,687	25
3073	A060110	241	0.1	12	31.8	0.72	1,900,000	25 R
3074	A060118	241	0.1	12	32.5	0.74	1,284,494	25
3075	A060111	345	0.1	5	32.5	1.14	36,913	25
3076	A060115	310	0.1	10	31.4	0.99	84,367	25

MATERIAL A130

Lay-up = $[0]_8$, $V_F = 0.45$, Ave. thickness = 2.62 mm, S.D. = 0.04 mm, CoRezyn 63-AX-051 Polyester
Tests 2036 - 2054 in this section were done for Table 10.Compression tests involved a 13 mm gage length.

2036	A13001	840	*	0.25	38.8	2.20	1	ZERO
2037	A13002	852	*	0.25	38.4	2.80	1	ZERO
2038	A13003	881	*	0.25	37.5	2.60	1	ZERO
2039	A13004	81	*	0.25	11.2	----	1	±45
2040	A13005	87	*	0.25	11.4	----	1	±45
2041	A13006	88	*	0.25	11.4	----	1	±45
2042	A13007	-300	*	0.25	29.1	----	1	ZERO
2043	A13008	-337	*	0.25	28.4	----	1	ZERO
2044	A13009	-364	*	0.25	32.1	----	1	ZERO
2045	A13010	-91	*	0.25	11.9	----	1	±45
2046	A13011	-85	*	0.25	11.9	----	1	±45
2047	A13012	-90	*	0.25	10.6	----	1	±45
2048	A13013	-98	*	0.25	7.79	----	1	90
2049	A13014	-89	*	0.25	6.69	----	1	90
2050	A13015	-93	*	0.25	8.27	----	1	90
2051	A13016	34	*	0.25	8.48	0.37	1	90
2052	A13017	34	*	0.25	9.03	0.36	1	90
2053	A13050	900	*	0.25	35.3	2.71	1	ZERO

TEST & SAMPLE ID #		MAX. STRESS MPa	R	Q Hz	E GPa	e %	CYCLES TO FAIL	WIDTH (mm) and Notes
2054	A13051	92	*	0.25	11.0	----	1	±45
MATERIAL A130C								
Lay-up = $[0]_6$, $V_F = 0.35$, Ave. thickness = 2.97 mm, S.D. = 0.12 mm, CoRezyn 63-AX-051 Polyester,								
2415	A130C110	682	*	13	29.9	2.30	1	25
2416	A130C112	756	*	13	30.2	2.50	1	25
2417	A130C113	745	*	13	29.9	2.50	1	25
2418	A130C104	414	0.1	5	31.0	1.33	15,268	25
2419	A130C109	414	0.1	5	33.1	1.25	17,020	25
2420	A130C106	483	0.1	2	34.1	1.42	2,781	25
2421	A130C108	483	0.1	2	32.0	1.51	1,986	25
2422	A130C102	345	0.1	8	29.8	1.16	425,772	25
2423	A130C103	483	0.1	2	32.5	1.49	3,521	25
2424	A130C111	414	0.1	5	31.5	1.31	37,072	25
2425	A130C101	345	0.1	10	33.9	1.12	854,215	25
2426	A130C118	310	0.1	10	31.6	0.98	4,377,528	25
2427	A130C119	345	0.1	10	31.6	1.09	841,256	25
2631	A130C301	-356	*	3	----	----	1	25
2632	A130C302	-347	*	3	----	----	1	25
2633	A130C303	-394	*	3	----	----	1	25
2634	A130C304	-324	*	3	----	----	1	25
2900	A130C144	-207	10	12	----	----	484,312	25
2901	A130C141	-207	10	12	----	----	4,000,000	25 R
2902	A130C148	-276	10	5	----	----	161,152	25
2903	A130C145	-442	*	13	----	----	1	25
2904	A130C146	-345	10	1	----	----	94	25
2905	A130C143	-310	10	2	----	----	2,799	25
2906	A130C149	-310	10	2	----	----	916	25
2907	A130C147	-310	10	2	----	----	452	25
2908	A130C142	-276	10	10	----	----	71,475	25
2909	A130C149	-345	10	1	----	----	71	25
2910	A130C151	-276	10	10	----	----	62,465	25
Tests 3077 - 3079 were manufactured with epoxy to see if this increased the compressive strength								
3077	A130C103E	-287	*	13	----	----	1	25 Epoxy
3078	A130C102E	-262	*	13	----	----	1	25 Epoxy
3079	A130C301E	-296	*	13	----	----	1	25 Epoxy
Tests 5727 - 5738 involved trying to remove the weaving stitch prior to RTM to improve the compressive strength properties.								
Tests 5727 were the control coupons								
5727	A130C401	-349	*	13	----	----	1	25
5728	A130C402	-385	*	13	----	----	1	25
5729	A130C403	-371	*	13	----	----	1	25
5730	A130C404	-330	*	13	----	----	1	25
Tests 5731 - 5734 had the thermoplastic bead burned off, but the glass stitching thread remained								
5731	A130C405	-395	*	13	----	----	1	25
5732	A130C406	-466	*	13	----	----	1	25
5733	A130C407	-545	*	13	----	----	1	25
5734	A130C408	-509	*	13	----	----	1	25

TEST & SAMPLE ID #		MAX. STRESS MPa	R	Q Hz	E GPa	e %	CYCLES TO FAIL	WIDTH (mm) and Notes
Tests 5735 - 5738 had the thermoplastic bead burned off and the glass stitching thread removed								
5735	A130C409	-515	*	13	----	----	1	25
5736	A130C410	-483	*	13	----	----	1	25
5737	A130C411	-477	*	13	----	----	1	25
5738	A130C412	-509	*	13	----	----	1	25
MATERIAL A130G								
Lay-up = $[0]_{14}$, $V_F = 0.55$, Ave. thickness = 4.38 mm, S.D. = 0.12 mm, CoRezyn 63-AX-051 Polyester								
2401	A130G113	1186	*	13	45.3	2.61	1	25
2402	A130G103	1150	*	13	43.7	2.60	1	25
2403	A130G109	1272	*	13	47.6	2.67	1	25
2404	A130G114	690	0.1	2	48.0	1.43	938	25
2405	A130G108	690	0.1	2	45.2	1.52	507	25
2406	A130G112	690	0.1	2	48.3	1.44	1,546	25
2407	A130G107	552	0.1	4	45.0	1.22	5,452	25
2408	A130G110	552	0.1	4	43.2	1.28	2,952	25
2409	A130G105	552	0.1	4	40.0	1.37	4,864	25
2410	A130G101	414	0.1	5	42.4	0.97	45,710	25
2411	A130G102	414	0.1	5	40.0	1.03	32,282	25
2412	A130G115	276	0.1	15	46.9	0.57	4,847,670	25 R
2413	A130G104	414	0.1	4	45.5	0.91	28,621	25
2114	A130G106	345	0.1	8	40.5	0.85	413,627	25
2635	A130G301	-488	*	3	----	----	1	25
2636	A130G302	-414	*	3	----	----	1	25
2637	A130G303	-369	*	3	----	----	1	25
2638	A130G304	-422	*	3	----	----	1	25
MATERIAL A260								
Lay-up = $[0]_4$, $V_F = 0.35$, Ave. thickness = 3.71 mm, S.D. = 0.13 mm, CoRezyn 63-AX-051 Polyester								
3086	A260109	-396	*	13	----	----	1	25
3087	A260118	-357	*	13	----	----	1	25
3088	A260105	-540	*	13	----	----	1	25
3089	A260102	-422	*	13	----	----	1	25
3090	A260108	-460	*	13	----	----	1	25
3091	A260120	-470	*	13	----	----	1	25
3092	A260124	833	*	13	31.2	2.70	1	25
3093	A260122	690	*	13	23.4	2.90	1	25
3094	A260126	805	*	13	27.3	2.90	1	25
3095	A260127	345	0.1	5	29.9	0.99	3,000,000	25 R
3096	A260123	448	0.1	5	29.0	1.35	51,850	25
3097	A260125	448	0.1	8	32.1	1.42	27,702	25
3098	A260128	448	0.1	5	28.5	1.40	17,163	25
3099	A260121	379	0.1	10	31.9	1.14	191,959	25
3100	A260133	552	0.1	2	35.9	1.36	4,207	25
3101	A260120	552	0.1	2	32.5	1.79	1,448	25
3102	A260130	552	0.1	2	36.4	1.52	3,348	25

TEST & SAMPLE ID #		MAX. STRESS MPa	R	Q Hz	E GPa	e %	CYCLES TO FAIL	WIDTH (mm) and Notes
3103	A260132	379	0.1	10	32.1	1.21	640,153	25
3104	A260134	379	0.1	10	34.3	1.20	455,258	25

MATERIAL CM1701A

Lay-up = $[0]_6$, $V_F = 0.38$, Ave. thickness = 3.20 mm, S.D. = 0.10 mm, CoRezyn 63-AX-051 Polyester

2911	CMA101	-604	*	13	----	----	1	25
2912	CMA102	-573	*	13	----	----	1	25
2913	CMA103	-542	*	13	----	----	1	25
2935	CMA116	874	*	13	32.4	2.70	1	25
2936	CMA113	784	*	13	28.6	2.75	1	25
2937	CMA107	730	*	13	29.2	2.50	1	25
2938	CMA112	483	0.1	2	29.8	1.63	784	25
2939	CMA106	483	0.1	2	38.3	1.29	1,940	25
2940	CMA105	483	0.1	2	33.2	1.46	1,574	25
2941	CMA111	414	0.1	5	29.3	1.54	17,955	25
2943	CMA110	414	0.1	4	26.8	1.60	6,418	25
2945	CMA117	345	0.1	5	28.0	1.19	26,217	25
2946	CMA108	345	0.1	5	32.3	1.00	38,086	25
2947	CMA114	276	0.1	10	28.8	0.89	81,998	25
2948	CMA119	276	0.1	10	29.1	0.92	117,831	25
2911	CMA101	-604	*	13	----	----	1	25
2912	CMA102	-573	*	13	----	----	1	25
2913	CMA103	-542	*	13	----	----	1	25
2949	CMA121	-345	10	4	----	----	42,588	25
2950	CMA125	-345	10	4	----	----	13,272	25
2951	CMA127	-345	10	4	----	----	80,669	25
2952	CMA123	-310	10	10	----	----	105,995	25
2953	CMA132	-310	10	12	----	----	532,367	25
2962	CMA134	-310	10	10	----	----	460,941	25

MATERIAL D072A

Lay-up = $[0]_{10}$, $V_F = 0.36$, Ave. thickness = 3.30 mm, S.D. = 0.05 mm, CoRezyn 63-AX-051 Polyester

3043	D072A118	-608	*	13	----	----	1	25
3044	D072A123	-562	*	13	----	----	1	25
3045	D072A122	-508	*	13	----	----	1	25
3046	D072A120	-345	10	5	----	----	87,741	25
3047	D072A119	-414	10	3	----	----	9,757	25
3048	D072A117	-414	10	4	----	----	2,192	25
3049	D072A116	-345	10	5	----	----	79,404	25
3050	D072A121	-414	10	4	----	----	6,097	25
3051	D072A115	-345	10	5	----	----	136,908	25
3055	D072A110	812	*	13	28.3	2.87	1	25
3056	D072A109	789	*	13	29.3	2.70	1	25
3057	D072A108	796	*	13	27.8	2.90	1	25
3058	D072A107	483	0.1	4	26.8	1.83	9,586	25
3059	D072A106	483	0.1	4	26.7	1.91	8,838	25

TEST & SAMPLE ID #		MAX. STRESS MPa	R	Q Hz	E GPa	e %	CYCLES TO FAIL	WIDTH (mm) and Notes
3060	D072A105	310	0.1	10	28.2	0.96	929,460	25
3061	D072A101	483	0.1	4	31.7	1.63	5,993	25
3062	D072A102	345	0.1	5	27.7	1.14	195,791	25
3063	D072A111	414	0.1	5	31.3	1.32	28,168	25
3064	D072A112	414	0.1	5	26.9	1.47	34,247	25
3065	D072A121	414	0.1	5	28.4	1.40	23,522	25
3066	D072A118	345	0.1	10	26.3	1.30	162,352	25
3067	D072A123	345	0.1	10	27.7	1.29	237,010	25

MATERIAL D092

Lay-up = $[0]_{10}$, $V_F = 0.46$, Ave. thickness = 3.10 mm, S.D. = 0.07 mm, CoRezyn 63-AX-051 Polyester
Tests 1992 - 2013 in this section were done for Table 10.Compression tests involved a 13 mm gage length.

1992	D09201	929	*	0.25	35.1	2.82	1	ZERO
1993	D09202	926	*	0.25	36.8	2.87	1	ZERO
1994	D09203	911	*	0.25	34.3	3.14	1	ZERO
1995	D09204	134	*	0.25	12.2	----	1	±45
1996	D09205	37	*	0.25	10.1	0.35	1	90
1997	D09208	-761	*	0.25	28.4	-2.6	1	ZERO
1998	D09209	-745	*	0.25	30.6	-2.4	1	ZERO
1999	D09210	-783	*	0.25	31.8	-2.5	1	ZERO
2000	D09211	-130	*	0.25	12.3	----	1	±45
2001	D09212	-129	*	0.25	10.9	----	1	±45
2002	D09213	-130	*	0.25	11.1	----	1	±45
2003	D09214	-141	*	0.25	7.38	-1.91	1	90
2004	D09215	40	*	0.25	7.10	0.56	1	90
2005	D09216	-130	*	0.25	7.65	-1.91	1	90
2006	D09217	150	*	0.25	9.44	----	1	±45
2007	D09250	-816	*	0.25	32.5	-1.63	1	ZERO
2008	D09251	-758	*	0.25	31.4	-1.47	1	ZERO
2009	D09252	-127	*	0.25	6.62	-1.92	1	90
2010	D09253	-129	*	0.25	14.2	----	1	±45
2011	D09254	1041	*	0.25	34.9	3.09	1	ZERO
2012	D09255	140	*	0.25	12.5	----	1	±45
2013	D09256	38	*	0.25	9.79	0.37	1	90

MATERIAL D092B

Lay-up = $[0]_9$, $V_F = 0.41$, Ave. thickness = 2.76 mm, S.D. = 0.12 mm, CoRezyn 63-AX-051 Polyester

2144	D092B105	994	*	13	35.6	2.80	1	25 tab
2145	D092B104	907	*	13	32.9	2.86	1	25 tab
2146	D092B106	959	*	13	34.7	2.80	1	25 tab
2147	D092B107	552	0.1	4	36.1	1.60	8,610	25 tab
2148	D092B109	552	0.1	4	32.9	1.70	12,301	25 tab
2149	D092B110	414	0.1	15	36.8	1.13	302,338	25
2150	D092B103	414	0.1	15	32.6	1.21	259,952	25
2151	D092B111	414	0.1	15	31.9	1.30	236,479	25
2152	D092B108	345	0.1	15	33.9	1.04	1,557,555	25

TEST & SAMPLE ID #		MAX. STRESS MPa	R	Q Hz	E GPa	e %	CYCLES TO FAIL	WIDTH (mm) and Notes
2153	D092B101	345	0.1	15	32.0	1.09	957,554	25
2154	D092B102	345	0.1	15	35.7	0.98	1,847,878	25
2380	D092B230	878	*	13	33.4	2.62	1	25
2381	D092B208	875	*	13	34.3	2.55	1	25
2382	D092B204	834	*	13	34.1	2.45	1	25
2383	D092B216	552	0.1	4	34.0	1.62	2,914	25
2384	D092B210	552	0.1	4	32.2	1.71	3,142	25
2385	D092B201	552	0.1	4	33.9	1.63	3,756	25
2386	D092B213	414	0.1	10	32.9	1.26	126,113	25
2387	D092B203	414	0.1	5	33.9	1.22	165,310	25
2388	D092B205	345	0.1	12	33.7	1.02	892,557	25
2389	D092B209	345	0.1	12	32.4	1.06	1,112,027	25
2390	D092B211	414	0.1	10	33.2	1.25	171,967	25
2639	D092B301	-684	*	13	----	----	1	25
2640	D092B302	-710	*	13	----	----	1	25
2641	D092B303	-708	*	13	----	----	1	25
2642	D092B305	-630	*	3	----	----	1	25
2643	D092B306	-610	*	3	----	----	1	25
2644	D092B308	-705	*	3	----	----	1	25

MATERIAL D092D

Lay-up = $[0]_7$, $V_F = 0.30$, Ave. thickness = 2.64 mm, S.D. = 0.11 mm, CoRezyn 63-AX-051 Polyester

2391	D092D105	736	*	13	25.4	2.89	1	25
2392	D092D107	722	*	13	25.6	2.81	1	25
2393	D092D111	734	*	13	25.8	2.84	1	25
2394	D092D108	482	0.1	2	24.4	1.98	3,342	25
2395	D092D110	482	0.1	4	23.6	2.04	2,650	25
2396	D092D103	414	0.1	8	25.4	1.63	113,301	25
2397	D092D109	345	0.1	10	25.6	1.35	813,359	25
2398	D092D104	414	0.1	8	27.4	1.51	75,856	25
2399	D092D102	345	0.1	12	24.3	1.42	291,147	25
2400	D092D106	345	0.1	15	26.1	1.30	948,810	25
2645	D092D301	-574	*	3	----	----	1	25
2646	D092D302	-515	*	3	----	----	1	25
2647	D092D303	-532	*	3	----	----	1	25
2648	D092D304	-538	*	3	----	----	1	25

MATERIAL D092F

Lay-up = $[0]_{12}$, $V_F = 0.50$, Ave. thickness = 3.00 mm, S.D. = 0.04 mm, CoRezyn 63-AX-051 Polyester

2178	D092F110	1090	*	13	35.9	3.04	1	25
2179	D092F112	1105	*	13	40.5	2.85	1	25 tab
2180	D092F103	1141	*	13	41.8	2.85	1	25
2181	D092F111	1203	*	13	42.2	2.86	1	25 tab
2182	D092F107	414	0.1	15	44.1	0.97	221,920	25
2183	D092F109	414	0.1	15	39.9	1.03	92,864	25
2184	D092F105	414	0.1	15	37.2	1.12	138,489	25

TEST & SAMPLE ID #		MAX. STRESS MPa	R	Q Hz	E GPa	e %	CYCLES TO FAIL	WIDTH (mm) and Notes
2185	D092F106	345	0.1	15	42.6	0.81	864,540	25
2186	D092F101	345	0.1	15	38.3	0.90	387,503	25
2187	D092F102	552	0.1	4	41.8	1.32	15,665	25 tab
2188	D092F124	552	0.1	4	44.6	1.24	31,284	25 tab
2653	D092F123	-615	*	3	----	----	1	25
2654	D092F126	-692	*	3	----	----	1	25
2655	D092F122	-697	*	3	----	----	1	25
2656	D092F121	-712	*	3	----	----	1	25

MATERIAL D092G

Lay-up = $[0]_{15}$, $V_F = 0.58$, Ave. thickness = 3.25 mm, S.D. = 0.05 mm, CoRezyn 63-AX-051 Polyester

2155	D092G113	1,130	*	13	42.2	2.70	1	25 tab
2156	D092G105	1,206	*	13	43.3	2.80	1	25 tab
2157	D092G103	1,182	*	13	41.8	2.80	1	25 tab
2158	D092G109	690	0.1	2	43.2	1.62	484	25 tab
2159	D092G112	414	0.1	4	44.1	0.94	12,691	25 tab
2160	D092G106	414	0.1	4	45.0	0.90	15,436	25 tab
2161	D092G101	552	0.1	1	46.0	1.31	2,113	25 tab
2162	D092G104	552	0.1	2	45.4	1.22	2,942	25 tab
2163	D092G102	414	0.1	2	43.4	0.97	11,735	25 tab
2164	D092G110	552	0.1	2	47.2	1.20	2,700	25 tab
2165	D092G108	276	0.1	10	6.79	0.62	261,247	25 tab
2166	D092G111	207	0.1	10	44.0	0.47	3,000,000	25 R tab
2167	D092G114	276	0.1	10	47.7	0.58	159,725	25 tab
2168	D092G107	276	0.1	10	50.0	0.55	95,939	25 tab
2169	D092G205	276	0.1	15	50.7	0.55	472,372	25 tab
2170	D092G207	276	0.1	10	51.1	0.56	494,104	25 tab
2171	D092G206	276	0.1	10	50.7	0.53	368,039	25 tab
2173	D092G201	414	0.1	10	46.8	0.90	36,932	25 tab
2174	D092G202	414	0.1	4	49.2	0.90	29,096	25 tab
2175	D092G-204	276	0.1	10	49.1	0.56	700,000	25 R tab
2177	D092G105	345	0.1	12	46.1	0.81	478,382	25 tab
2354	D092G205	1196	*	13	44.5	2.89	1	25 tab
2355	D092G209	1133	*	13	43.4	2.61	1	25 tab
2356	D092G201	1161	*	13	45.0	2.60	1	25 tab
2357	D092G212	276	0.1	12	47.8	0.58	874,379	25 tab
2358	D092G207	552	0.1	5	47.5	1.16	12,811	25 tab
2359	D092G202	552	0.1	5	41.5	1.33	9,807	25 tab
2360	D092G211	552	0.1	5	45.2	1.22	9,091	25 tab
2361	D092G216	690	0.1	2	42.1	1.64	1,360	25 tab
2362	D092G215	690	0.1	2	45.9	1.50	2,083	25 tab
2363	D092G214	414	0.1	10	41.9	0.99	113,852	25 tab
2364	D092G210	414	0.1	10	43.0	0.96	92,451	25 tab
2365	D092G213	276	0.1	15	45.6	0.60	6,654,291	25 tab
2366	D092G203	414	0.1	10	44.5	0.93	135,121	25 tab
2649	D092G301	-658	*	3	----	----	1	25
2650	D092G302	-645	*	3	----	----	1	25
2651	D092G303	-629	*	3	----	----	1	25

TEST & SAMPLE ID #		MAX. STRESS MPa	R	Q Hz	E GPa	e %	CYCLES TO FAIL	WIDTH (mm) and Notes
2652	D092G304	-837	*	3	----	----	1	25
2786	D092G130	-621	10	4	----	----	13,859	25
2787	D092G120	-621	10	5	----	----	7,978	25
2789	D092G126	-621	10	5	----	----	6,124	25
2790	D092G131	-552	10	12	----	----	19,386	25
2791	D092G123	-552	10	12	----	----	27,412	25
2792	D092G124	-552	10	12	----	----	11,391	25
2793	D092G132	-414	10	12	----	----	1,864,286	25
2794	D092G128	-483	10	10	----	----	481,468	25
2795	D092G121	-483	10	10	----	----	298,071	25
2796	D092G127	-483	10	10	----	----	331,041	25

MATERIAL D155

Lay-up = $[0]_6$, $V_F = 0.45$, Ave. thickness = 2.74 mm, S.D. = 0.10 mm, CoRezyn 63-AX-051 Polyester
Tests 2014 - 2035 in this section were done for Table 10.Compression tests involved a 13 mm gage length.

2014	D15501	984	*	0.25	39.0	2.90	1	ZERO
2015	D15502	898	*	0.25	36.3	2.69	1	ZERO
2016	D15503	976	*	0.25	38.9	2.87	1	ZERO
2017	D15504	93	*	0.25	12.8	----	1	±45
2018	D15505	25	*	0.25	9.12	0.43	1	90
2019	D15506	30	*	0.25	9.24	0.37	1	90
2022	D15509	-109	*	0.25	14.0	-3.2	1	±45
2023	D15510	-106	*	0.25	15.1	-3.72	1	±45
2024	D15511	-122	*	0.25	8.31	-1.62	1	90
2025	D15512	-118	*	0.25	7.65	-1.43	1	90
2026	D15513	-727	*	0.25	32.1	-2.48	1	ZERO
2027	D15514	-710	*	0.25	31.8	-1.77	1	ZERO
2028	D15515	-756	*	0.25	29.6	-1.34	1	ZERO
2029	D15516	104	*	0.25	12.3	----	1	±45
2030	D15517	103	*	0.25	10.8	----	1	±45
2031	D15550	-730	*	0.25	32.3	-2.18	1	ZERO
2032	D15551	-807	*	0.25	33.0	-2.14	1	ZERO
2033	D15552	-147	*	0.25	7.72	-1.96	1	90
2034	D15553	1088	*	0.25	39.0	2.85	1	ZERO
2035	D15554	86	*	0.25	13.2	----	1	±45

MATERIAL D155B

Lay-up = $[0]_5$, $V_F = 0.39$, Ave. thickness = 2.70 mm, S.D. = 0.11 mm, CoRezyn 63-AX-051 Polyester

2110	D155B65	935	*	13	34.8	2.80	1	25 tab
2111	D155B71	961	*	13	29.6	3.25	1	25 tab
2112	D155B61	911	*	13	33.8	2.80	1	25
2113	D155B60	552	0.1	2	31.9	1.86	1,831	25
2114	D155B72	552	0.1	2	29.8	1.92	3,911	25
2115	D155B63	414	0.1	5	31.9	1.44	85,156	25
2116	D155B70	414	0.1	10	28.6	1.49	108,103	25
2117	D155B69	276	0.1	20	28.5	1.08	8,000,000	25

TEST & SAMPLE ID #		MAX. STRESS MPa	R	Q Hz	E GPa	e %	CYCLES TO FAIL	WIDTH (mm) and Notes
2118	D155B68	552	0.1	4	30.9	1.83	6,582	25 tab
2119	D155B66	690	0.1	1	32.2	2.32	139	25
2120	D155B62	345	0.1	10	33.0	1.10	1,230,231	25 tab
2121	D155B64	414	0.1	10	33.0	1.28	75,774	25 tab
2122	D155B67	345	0.1	12	29.5	1.19	721,864	25 tab
2123	D155B81	345	0.1	10	32.5	1.15	572,173	25
2203	D155B200	755	*	13	31.1	2.43	1	25
2204	D155B209	779	*	13	28.2	2.76	1	25
2205	D155B215	785	*	13	28.5	2.75	1	25
2206	D155B201	483	0.1	4	32.6	1.48	6,979	25
2207	D155B207	483	0.1	4	33.1	1.46	16,497	25
2208	D155B205	414	0.1	7	32.2	1.28	82,605	25
2209	D155B203	414	0.1	8	36.8	1.13	68,483	25
2236	D155B212	345	0.1	15	33.6	1.02	967,901	25
2237	D155B210	345	0.1	15	30.1	1.15	1,104,634	25
2338	D155B202	483	0.1	5	30.4	1.59	19,814	25
2339	D155B213	552	0.1	3	32.2	1.71	2,141	25
2340	D155B208	552	0.1	4	30.3	1.82	2,305	25
2341	D155B211	552	0.1	4	31.8	1.73	1,733	25
2342	D155B214	414	0.1	10	30.8	1.34	48,181	25
2657	D155B301	-620	*	3	----	----	1	25
2658	D155B302	-666	*	3	----	----	1	25
2659	D155B303	-642	*	3	----	----	1	25
2660	D155B304	-656	*	3	----	----	1	25
2776	D155B174	-681	*	3	----	----	1	25
2777	D155B177	-517	10	1	----	----	178	25
2778	D155B175	-414	10	10	----	----	76,348	25
2779	D155B178	-414	10	10	----	----	61,956	25
2780	D155B180	-345	10	12	----	----	954,990	25
2781	D155B176	-345	10	12	----	----	893,962	25
2782	D155B173	-345	10	12	----	----	1,121,768	25
2783	D155B181	-414	10	10	----	----	172,874	25
2784	D155B179	-483	10	2	----	----	886	25
3735	D155B222	831	*	13	32.8	----	1	25
3736	D155B223	845	*	13	----	----	1	25
3737	D155B218	775	*	13	----	----	1	25
3738	D155B218	843	*	13	----	----	1	25

MATERIAL D155C

Lay-up = $[0]_7$, $V_F = 0.51$, Ave. thickness = 2.99 mm, S.D. = 0.09 mm, CoRezyn 63-AX-051 Polyester

2124	D155C111	1189	*	13	33.6	3.57	1	25
2125	D155C109	1184	*	13	32.3	3.66	1	25
2126	D155C107	1188	*	13	34.6	3.43	1	25
2127	D155C101	827	0.1	2	32.5	2.55	315	25
2128	D155C105	552	0.1	5	34.0	1.59	11,103	25
2129	D155C110	552	0.1	5	33.4	1.62	10,021	25
2130	D155C106	414	0.1	12	33.7	1.24	189,546	25
2131	D155C104	345	0.1	15	35.6	1.01	1,276,914	25

TEST & SAMPLE ID #		MAX. STRESS MPa	R	Q Hz	E GPa	e %	CYCLES TO FAIL	WIDTH (mm) and Notes
2132	D155C108	414	0.1	10	37.0	1.23	133,885	25
2133	D155C100	414	0.1	10	34.3	1.24	206,447	25
2134	D155C114	552	0.1	4	32.1	1.68	14,762	25
2135	D155C102	345	0.1	12	35.1	0.99	854,271	25
2136	D155C103	345	0.1	12	32.2	1.04	644,464	25
2220	D155C202	1129	*	13	43.0	2.62	1	25
2221	D155C205	1208	*	13	42.6	2.83	1	25
2222	D155C203	1152	*	13	43.8	2.63	1	25
2223	D155C206	552	0.1	5	46.7	1.18	19,546	25
2224	D155C207	552	0.1	5	43.0	1.28	19,611	25
2225	D155C209	552	0.1	5	46.7	1.09	25,014	25
2227	D155C210	345	0.1	10	41.4	0.83	1,369,554	25
2228	D155C213	345	0.1	12	43.4	0.75	1,251,972	25
2229	D155C211	690	0.1	2	42.5	1.65	3,370	25
2230	D155C208	690	0.1	2	42.8	1.61	2,480	25
2231	D155C201	414	0.1	5	45.0	0.92	196,825	25
2232	D155C212	414	0.1	10	43.4	0.95	278,697	25
2233	D155C204	414	0.1	10	41.8	0.99	188,541	25
2234	D155C216	690	0.1	2	40.5	1.70	3,610	25
2235	D155C217	345	0.1	15	42.4	0.81	1,182,710	25
2661	D155C301	-847	*	3	----	----	1	25
2662	D155C302	-734	*	3	----	----	1	25
2663	D155C303	-752	*	3	----	----	1	25
2664	D155C304	-841	*	3	----	----	1	25

MATERIAL D155G

Lay-up = $[0]_8$, $V_F = 0.59$, Ave. thickness = 2.81 mm, S.D. = 0.08 mm, CoRezyn 63-AX-051 Polyester

2189	D155G104	1318	*	13	48.4	2.72	1	25 tab
2190	D155G110	1320	*	13	48.2	2.74	1	25 tab
2191	D155G115	1303	*	13	46.7	2.80	1	25 tab
2192	D155G103	690	0.1	4	49.8	1.39	4,546	25 tab
2193	D155G107	690	0.1	2	46.3	1.49	1,839	25 tab
2194	D155G106	552	0.1	5	49.0	1.13	14,842	25 tab
2195	D155G109	552	0.1	5	51.3	1.08	10,796	25 tab
2196	D155G108	345	0.1	12	52.6	0.66	137,665	25 tab
2197	D155G105	345	0.1	12	46.2	0.75	164,363	25 tab
2198	D155G114	276	0.1	12	44.2	0.62	1,154,036	25 tab
2199	D155G102	276	0.1	12	41.4	0.66	817,204	25 tab
2200	D155G101	345	0.1	10	44.5	0.78	169,202	25 tab
2201	D155G112	690	0.1	2	45.2	1.53	2,546	25 tab
2202	D155G113	552	0.1	5	43.7	1.26	11,201	25 tab
2665	D155G301	-729	*	13	----	----	1	25
2666	D155G302	-647	*	13	----	----	1	25
2667	D155G303	-698	*	13	----	----	1	25
2668	D155G354	-783	*	13	----	----	1	25
2766	D155G305	-552	10	12	----	----	38,446	25
2767	D155G306	-552	10	12	----	----	130,068	25
2768	D155G309	-552	10	12	----	----	57,998	25

TEST & SAMPLE ID #		MAX. STRESS MPa	R	Q Hz	E GPa	e %	CYCLES TO FAIL	WIDTH (mm) and Notes
2770	D155G307	-483	10	12	----	----	161,615	25
2771	D155G305	-483	10	12	----	----	74,321	25
2772	D155G304	-730	*	13	----	----	1	25
2773	D155G316	-621	10	1	----	----	90	25
2774	D155G320	-621	10	1	----	----	136	25
2775	D155G310	-621	10	1	----	----	62	25
3117	D155G315	-821	*	13	----	----	1	25
3118	D155G302	-752	*	13	----	----	1	25
3119	D155G310	-722	*	13	----	----	1	25
Tests 3599 - 3613 involved a gage length of 13 mm (strain rate effect tests).								
3599	D155G314	-627	*	0.025	----	----	1	25 tab
3600	D155G321	-660	*	0.025	----	----	1	25 tab
3601	D155G323	-654	*	0.025	----	----	1	25 tab
3602	D155G311	-739	*	2.54	----	----	1	25 tab
3603	D155G322	-723	*	2.54	----	----	1	25 tab
3604	D155G324	-701	*	2.54	----	----	1	25 tab
3605	D155G317	-673	*	12.7	----	----	1	25 tab
3606	D155G313	-762	*	12.7	----	----	1	25 tab
3607	D155G319	-784	*	12.7	----	----	1	25 tab
3608	D155G335	-757	*	25.4	----	----	1	25 tab
3609	D155G330	-776	*	25.4	----	----	1	25 tab
3610	D155G333	-768	*	25.4	----	----	1	25 tab
3611	D155G332	-735	*	127	----	----	1	25 tab
3612	D155G331	-796	*	127	----	----	1	25 tab
3613	D155G336	-755	*	127	----	----	1	25 tab
Tests 3614 - 3625 involved a gage length of 100 mm (strain rate effect tests).								
3614	D155G217	964	*	0.025	----	----	1	25 tab
3615	D155G219	833	*	0.025	----	----	1	25 tab
3616	D155G214	897	*	0.025	----	----	1	25 tab
3617	D155G216	1086	*	2.54	----	----	1	25 tab
3618	D155G221	1143	*	2.54	----	----	1	25 tab
3619	D155G222	1061	*	2.54	----	----	1	25 tab
3620	D155G223	1140	*	12.7	----	----	1	25 tab
3621	D155G226	1222	*	12.7	----	----	1	25 tab
3622	D155G225	1024	*	12.7	----	----	1	25 tab
3623	D155G224	1086	*	63.5	----	----	1	25 tab
3624	D155G218	1100	*	63.5	----	----	1	25 tab
3625	D155G220	1136	*	63.5	----	----	1	25 tab

MATERIAL D155H

Lay-up = $[0]_7$, $V_F = 0.49$, Ave. thickness = 2.93 mm, S.D. = 0.10 mm, CoRezyn 63-AX-051 Polyester, No Stitching. Stitching in the D155 fabric was removed to study this effect.

2210	D155H106	961	*	13	34.3	2.80	1	25
2211	D155H111	886	*	13	33.1	2.68	1	25
2212	D155H103	903	*	13	34.7	2.61	1	25
2215	D155H108	552	0.1	5	34.4	1.60	39,227	25
2216	D155H109	552	0.1	5	35.4	1.56	22,154	25
2217	D155H122	1076	*	13	40.1	2.98	1	has stitch

TEST & SAMPLE ID #		MAX. STRESS MPa	R	Q Hz	E GPa	e %	CYCLES TO FAIL	WIDTH (mm) and Notes
2218	D155H121	1178	*	13	40.7	2.89	1	has stitch
2219	D155H120	1109	*	13	40.5	2.74	1	has stitch
2226	D155H102	552	0.1	5	33.9	1.62	41,215	25
2344	D155H210	483	0.1	10	37.0	1.30	156,200	25
2346	D155H204	1101	*	13	41.7	2.63	1	25
2347	D155H203	483	0.1	15	38.8	1.24	128,523	25
2348	D155H208	483	0.1	12	39.7	1.21	195,322	25
2349	D155H209	414	0.1	15	40.0	1.04	3,219,571	25
2350	D155H201	414	0.1	15	40.5	1.02	1,211,477	25
2351	D155H212	690	0.1	4	42.0	1.64	2,953	25
2352	D155H206	690	0.1	4	41.4	1.67	2,264	25
2353	D155H207	690	0.1	4	40.7	1.70	1,822	25
2669	D155H301	-718	*	3	----	----	1	25
2670	D155H302	-686	*	3	----	----	1	25
2671	D155H303	-623	*	3	----	----	1	has stitch
2672	D155H304	-864	*	3	----	----	1	has stitch
2673	D155H305	-795	*	3	----	----	1	has stitch
2674	D155H306	-846	*	3	----	----	1	has stitch

MATERIAL D155J

Lay-up = $[0]_6$, $V_F = 0.58$, Ave. thickness = 3.54 mm, S.D. = 0.11 mm, CoRezyn 63-AX-051 Polyester, No Stitching. Stitching in the D155 fabric was removed to study this effect.

2428	D155J111	1,098	*	13	49.8	2.65	1	25
2429	D155J114	1,190	*	13	47.5	2.51	1	25
2430	D155J101	1,140	*	13	48.6	2.43	1	25
2431	D155J103	690	0.1	5	44.9	1.54	6,213	25
2432	D155J115	690	0.1	5	50.0	1.38	7,977	25
2433	D155J106	690	0.1	5	46.8	1.47	4,784	25
2434	D155J108	552	0.1	5	50.0	----	20,345	25
2435	D155J105	552	0.1	5	50.0	1.10	73,109	25
2436	D155J109	414	0.1	12	47.0	0.88	684,350	25
2437	D155J113	552	0.1	5	47.8	1.15	35,652	25
2438	D155J116	414	0.1	12	47.8	0.79	912,579	25
2439	D155J107	552	0.1	5	45.2	1.22	89,980	25
2440	D155J104	414	0.1	12	47.3	0.86	485,216	25
2675	D155J301	-826	*	3	----	----	1	25
2676	D155J302	-704	*	3	----	----	1	25
2677	D155J303	-796	*	3	----	----	1	25
2678	D155J304	-777	*	3	----	----	1	25

MATERIAL D155K

Lay-up = $[0]_7$, $V_F = 0.33$, Ave. thickness = 4.45 mm, S.D. = 0.10 mm, CoRezyn 63-AX-051 Polyester

3673	D155K110	872	*	13	28.5	3.15	1	25
3674	D155K111	881	*	13	29.6	2.98	1	25
3675	D155K109	830	*	13	28.5	2.91	1	25
3676	D155K108	414	0.1	2	27.1	1.58	7,569	25

TEST & SAMPLE ID #		MAX. STRESS MPa	R	Q Hz	E GPa	e %	CYCLES TO FAIL	WIDTH (mm) and Notes
3677	D155K112	414	0.1	4	28.7	1.54	13,447	25
3678	D155K101	414	0.1	4	26.3	1.59	6,267	25
3679	D155K113	276	0.1	12	28.5	0.97	764,138	25
3680	D155K102	276	0.1	12	26.7	1.01	1,305,237	25
3681	D155K103	276	0.1	12	28.6	0.96	1,733,768	25
3682	D155K105	345	0.1	6	30.1	1.18	175,689	25
3683	D155K104	345	0.1	6	27.9	1.26	106,359	25
3684	D155K107	345	0.1	6	26.9	1.29	152,853	25
3685	D155K106	483	0.1	1	28.1	2.12	576	25
3686	D155K120	483	0.1	1	27.3	1.90	2,594	25
3687	D155K121T	23.8	*	13	8.00	0.30	1	25
3688	D155K122T	24.9	*	13	8.36	0.29	1	25
3689	D155K123T	18.9	*	13	8.52	0.22	1	25
3841	D155K125	-500	*	13	----	----	1	25
3842	D155K126	-624	*	13	----	----	1	25
3843	D155K127	-527	*	13	----	----	1	25

MATERIAL DB120

Lay-up = $[0]_{16}$, $V_F = 0.44$, Ave. thickness = 2.69 mm, S.D. = 0.10 mm, CoRezyn 63-AX-051 Polyester
Tests 2055 - 2074 in this section were done for Table 10.Compression tests involved a 13 mm gage length. ±45 degree fabric was separated into +45 and -45 degree plies and rotated to 0 degrees.

2055	DB12001	610	*	0.25	26.5	2.65	1	ZERO
2056	DB12002	596	*	0.25	26.8	2.41	1	ZERO
2057	DB12003	83	*	0.25	9.45	----	1	±45
2058	DB12004	85	*	0.25	9.10	----	1	±45
2059	DB12005	85	*	0.25	9.86	----	1	±45
2060	DB12006	87	*	0.25	8.89	----	1	±45
2061	DB12007	26	*	0.25	7.24	0.39	1	90
2062	DB12008	-554	*	0.25	18.9	----	1	ZERO
2063	DB12009	-555	*	0.25	19.7	----	1	ZERO
2064	DB12010	-545	*	0.25	19.4	----	1	ZERO
2065	DB12011	-116	*	0.25	8.83	----	1	±45
2066	DB12012	-120	*	0.25	9.86	----	1	±45
2067	DB12013	-123	*	0.25	9.31	----	1	±45
2068	DB12014	-120	*	0.25	6.96	-2.20	1	90
2069	DB12015	-117	*	0.25	6.41	-1.70	1	90
2070	DB12016	-104	*	0.25	6.55	-2.10	1	90
2071	DB12017	616	*	0.25	24.8	2.60	1	ZERO
2072	DB12018	24	*	0.25	7.72	0.32	1	90
2073	DB12050	619	*	0.25	28.2	2.30	1	ZERO
2074	DB12051	104	*	0.25	9.72	----	1	±45

TEST & SAMPLE ID #		MAX. STRESS MPa	R	Q Hz	E GPa	e %	CYCLES TO FAIL	WIDTH (mm) and Notes

MATERIAL DB240

Lay-up = $[0]_8$, V_F = 0.46, Ave. thickness = 2.77 mm, S.D. = 0.12 mm, CoRezyn 63-AX-051 Polyester
Tests 2075 - 2093 in this section were done for Table 10. Compression tests involved a 13 mm gage length. ±45 degree fabric was separated into +45 and -45 degree plies and rotated to 0 degrees.

2075	DB24001	701	*	0.25	30.8	2.60	1	ZERO
2076	DB24002	715	*	0.25	30.1	2.60	1	ZERO
2077	DB24003	669	*	0.25	31.1	2.50	1	ZERO
2078	DB24004	69	*	0.25	10.9	----	1	±45
2079	DB24005	69	*	0.25	10.1	----	1	±45
2080	DB24006	68	*	0.25	9.90	----	1	±45
2081	DB24007	-551	*	0.25	25.9	-1.60	1	ZERO
2082	DB24008	-507	*	0.25	24.8	-1.70	1	ZERO
2083	DB24009	-557	*	0.25	25.6	-1.60	1	ZERO
2084	DB24010	-122	*	0.25	11.0	----	1	±45
2085	DB24011	-101	*	0.25	10.3	----	1	±45
2086	DB24012	-128	*	0.25	10.3	----	1	±45
2087	DB24013	-125	*	0.25	6.32	-1.80	1	90
2088	DB24014	-118	*	0.25	6.69	-1.65	1	90
2089	DB24015	-122	*	0.25	7.08	-1.62	1	90
2090	DB24016	20	*	0.25	7.58	0.29	1	90
2091	DB24017	19	*	0.25	7.10	0.26	1	90
2092	DB24050	703	*	0.25	32.2	2.85	1	ZERO
2093	DB24051	70	*	0.25	10.1	----	1	±45

ANGLE PLY TESTING

The angled materials in this section were constructed using the D155 fabric.

MATERIAL D155B

Lay-up = $[0]_5$, $V_F = 0.39$, Ave. thickness = 2.70 mm, S.D. = 0.11 mm, CoRezyn 63-AX-051 Polyester

TEST & SAMPLE ID #		MAX. STRESS MPa	R	Q Hz	E GPa	e %	CYCLES TO FAIL	WIDTH (mm) and Notes
2203	D155B200	755	*	13	31.1	2.43	1	25
2204	D155B209	779	*	13	28.2	2.76	1	25
2205	D155B215	785	*	13	28.5	2.75	1	25
2206	D155B201	483	0.1	4	32.6	1.48	6,979	25
2207	D155B207	483	0.1	4	33.1	1.46	16,497	25
2208	D155B205	414	0.1	7	32.2	1.28	82,605	25
2209	D155B203	414	0.1	8	36.8	1.13	68,483	25
2236	D155B212	345	0.1	15	33.6	1.02	967,901	25
2237	D155B210	345	0.1	15	30.1	1.15	1,104,634	25
2338	D155B202	483	0.1	5	30.4	1.59	19,814	25
2339	D155B213	552	0.1	3	32.2	1.71	2,141	25
2340	D155B208	552	0.1	4	30.3	1.82	2,305	25
2341	D155B211	552	0.1	4	31.8	1.73	1,733	25
2342	D155B214	414	0.1	10	30.8	1.34	48,181	25

MATERIAL 10D155

Lay-up = $[\pm 10]_3$, $V_F = 0.38$, Ave. thickness = 3.47 mm, S.D. = 0.17 mm, CoRezyn 63-AX-051 Polyester

2513	10D155122	271	*	13	28.6	0.90	1	25
2514	10D155127	303	*	13	28.5	1.00	1	25
2515	10D155120	249	*	13	25.5	0.95	1	25
2566	10D155128	172	0.1	10	27.9	0.60	167,538	25
2569	10D155213	172	0.1	8	26.1	0.66	178,266	25
2570	10D155208	172	0.1	10	29.2	0.64	207,957	25
2571	10D155205	284	*	13	29.0	0.98	1	25
2572	10D155209	207	0.1	5	29.4	0.71	18,193	25
2573	10D155210	207	0.1	5	32.3	0.64	21,780	25
2574	10D155212	207	0.1	5	29.3	0.72	16,360	25
2575	10D155215	155	0.1	12	29.5	0.53	1,764,883	25
2583	10D155114	-405	*	13	----	----	1	25
2584	10D155106	-343	*	13	----	----	1	25
2585	10D155112	-406	*	13	----	----	1	25
2586	10D155113	-381	*	13	----	----	1	25

MATERIAL 20D155

Lay-up = $[\pm 20]_3$, $V_F = 0.39$, Ave. thickness = 3.21 mm, S.D. = 0.14 mm, CoRezyn 63-AX-051 Polyester

2510	20D155101	244	*	13	24.3	1.08	1	25
2511	20D155104	269	*	13	23.2	1.20	1	25
2512	20D155107	290	*	13	25.1	1.40	1	25
2558	20D155113	172	0.1	5	26.9	0.71	21,427	25

TEST & SAMPLE ID #		MAX. STRESS MPa	R	Q Hz	E GPa	e %	CYCLES TO FAIL	WIDTH (mm) and Notes
2559	20D155112	172	0.1	7	25.3	0.69	38,475	25
2560	20D155111	138	0.1	12	24.5	0.58	835,986	25
2561	20D155108	172	0.1	7	24.8	0.76	25,475	25
2562	20D155106	207	0.1	2	27.0	0.83	2,244	25
2563	20D155110	207	0.1	2	23.8	0.90	860	25
2564	20D155116	207	0.1	2	25.8	0.88	2,779	25
2565	20D155102	138	0.1	15	24.1	0.56	742,154	25
2587	20D155301	-284	*	13	----	----	1	25
2588	20D155302	-289	*	13	----	----	1	25
2589	20D155303	-271	*	13	----	----	1	25
2590	20D155304	-303	*	13	----	----	1	25

MATERIAL 30D155

Lay-up = $[\pm 30]_3$, $V_F = 0.40$, Ave. thickness = 3.11 mm, S.D. = 0.14 mm, CoRezyn 63-AX-051 Polyester

2507	30D155107	183	*	13	17.8	1.40	1	25
2508	30D155104	184	*	13	16.1	1.60	1	25
2509	30D155113	141	*	13	18.1	1.60	1	25
2537	30D155114	103	0.1	5	18.3	0.56	15,975	25
2538	30D155110	103	0.1	8	17.2	0.63	25,545	25
2539	30D155112	69	0.1	15	19.7	0.37	2,525,000	25 R
2540	30D155111	69	0.1	25	17.0	0.37	2,000,000	25 R
2541	30D155109	86	0.1	20	16.4	0.52	84,851	25
2542	30D155108	86	0.1	20	18.8	0.42	214,208	25
2543	30D155115	86	0.1	20	17.4	0.50	168,607	25
2544	30D155116	121	0.1	5	17.1	0.78	9,028	25
2545	30D155101	121	0.1	6	18.0	0.74	12,509	25
2546	30D155102	121	0.1	5	18.6	0.71	11,345	25
2547	30D155103	103	0.1	6	16.8	0.62	42,426	25
2591	30D155301	-195	*	13	----	----	1	25
2592	30D155302	-168	*	13	----	----	1	25
2593	30D155303	-169	*	13	----	----	1	25
2594	30D155304	-173	*	13	----	----	1	25
4445	30D155130	-103	10	4	----	----	28,562	25
4446	30D155130	-103	10	4	----	----	45,437	25
4447	30D155132	-103	10	4	----	----	44,837	25
4448	30D155133	-90	10	7	----	----	150,426	25
4449	30D155134	-90	10	8	----	----	142,051	25
4450	30D155135	-90	10	6	----	----	269,359	25
4451	30D155136	-83	10	10	----	----	530,475	25

MATERIAL 40D155

Lay-up = $[\pm 40]_3$, $V_F = 0.40$, Ave. thickness = 3.17 mm, S.D. = 0.09 mm, CoRezyn 63-AX-051 Polyester

2504	40D155110	147	*	13	11.5	14	1	25
2505	40D155105	142	*	13	11.2	16	1	25
2506	40D155102	142	*	13	11.4	11	1	25
2516	40D155103	86	0.1	4	10.8	0.89	7,598	25

TEST & SAMPLE ID #		MAX. STRESS MPa	R	Q Hz	E GPa	e %	CYCLES TO FAIL	WIDTH (mm) and Notes
2517	40D155104	86	0.1	4	11.8	0.97	6,950	25
2518	40D155106	86	0.1	4	12.2	0.93	3,054	25
2519	40D155107	69	0.1	5	11.7	0.69	27,264	25
2520	40D155108	55	0.1	12	12.3	0.46	631,703	25
2521	40D155109	55	0.1	15	11.9	0.49	275,777	25
2522	40D155111	69	0.1	5	11.8	0.67	36,776	25
2523	40D155112	69	0.1	8	12.0	0.62	34,920	25
2524	40D155113	55	0.1	20	11.1	0.52	857,164	25
2595	40D155301	-131	*	13	----	----	1	25
2596	40D155302	-135	*	13	----	----	1	25
2597	40D155303	-127	*	13	----	----	1	25
2598	40D155304	-134	*	13	----	----	1	25
4452	40D155137	-103	10	2	----	----	635	25
4453	40D155136	-90	10	4	----	----	5,021	25
4454	40D155135	-90	10	4	----	----	4,073	25
4455	40D155134	-90	10	4	----	----	2,494	25
4456	40D155133	-69	10	6	----	----	60,384	25
4457	40D155132	-69	10	6	----	----	82,612	25
4458	40D155131	-69	10	6	----	----	129,706	25
4459	40D155140	-59	10	10	----	----	460,369	25
4467	40D155141	-59	10	10	----	----	611,713	25

MATERIAL 45D155

Lay-up = $[\pm 45]_3$, $V_F = 0.38$, Ave. thickness = 3.17 mm, S.D. = 0.06 mm, CoRezyn 63-AX-051 Polyester

2441	45D155112	106	*	13	9.66	22.0	1	25
2442	45D155105	107	*	13	10.3	24.9	1	25
2443	45D155108	108	*	13	9.97	24.0	1	25
2444	45D155104	55	0.1	12	10.2	0.65	12,908	25
2445	45D155106	55	0.1	10	9.55	0.68	15,899	25
2446	45D155113	41	0.1	15	10.4	0.41	394,632	25
2447	45D155111	55	0.1	10	9.91	0.64	10,671	25
2448	45D155110	41	0.1	20	9.33	0.43	748,125	25
2449	45D155102	34	0.1	20	9.10	0.38	2,167,690	25 R
2450	45D155107	41	0.1	12	10.6	0.42	507,811	25
2451	45D155114	69	0.1	2	9.06	0.92	1,885	25
2452	45D155109	69	0.1	2	9.65	0.97	1,639	25
2453	45D155103	69	0.1	2	9.40	0.99	3,669	25
2599	45D155301	-139	*	13	----	----	1	25
2600	45D155302	-135	*	13	----	----	1	25
2601	45D155303	-135	*	13	----	----	1	25
2602	45D155304	-142	*	13	----	----	1	25
4399	45D155140	-97	10	2	----	----	1,236	25
4400	45D155143	-69	10	5	----	----	523,409	25
4401	45D155141	-69	10	10	----	----	597,040	25
4402	45D155142	-69	10	10	----	----	362,225	25
4403	45D155149	-69	10	10	----	----	367,979	25
4404	45D155145	34	-1	5	----	----	153,354	25
4405	45D155148	34	-1	5	----	----	64,588	25

4406	45D155144	34	-1	5	----	----	114,603	25
4407	45D155146	-83	10	8	----	----	19,588	25
4408	45D155147	-83	10	5	----	----	34,052	25
4409	45D155120	-83	10	5	----	----	28,684	25
4410	45D155119	-97	10	2	----	----	3,655	25
4411	45D155115	-97	10	2	----	----	4,822	25
4412	45D155121	28	-1	10	----	----	705,984	25
4413	45D155116	28	-1	10	----	----	791,693	25
4414	45D155164	41	-1	2	----	----	12,406	25
4415	45D155160	41	-1	2	----	----	10,061	25
4416	45D155161	41	-1	2	----	----	19,692	25

MATERIAL 45D155V2

Lay-up = $[\pm 45]_3$, $V_F = 0.38$, Ave. thickness = 3.10 mm, S.D. = 0.10 mm, Derakane 8084 Epoxy Vinyl ester

4417	45D155V349	-69	10	12	----	----	2,569,227	25
4418	45D155V322	-83	10	5	----	----	148,697	25
4419	45D155V326	-83	10	5	----	----	82,143	25
4420	45D155V344	-83	10	5	----	----	267,226	25
4421	45D155V320	-69	10	10	----	----	1,700,116	25
4422	45D155V325	-69	10	12	----	----	1,154,414	25
4423	45D155V330	-151	*	13	----	----	1	25
4424	45D155V329	-148	*	13	----	----	1	25
4425	45D155V331	-149	*	13	----	----	1	25
4426	45D155V314	136	*	13	9.9	----	1	25
4427	45D155V313	129	*	13	10.6	----	1	25
4428	45D155V316	141	*	13	11.0	----	1	25
4429	45D155V315	48	0.1	5	10.1	0.53	137,932	25
4430	45D155V311	48	0.1	5	----	----	262,388	25
4431	45D155V301	48	0.1	5	10.9	0.49	321,891	25
4432	45D155V304	55	0.1	5	----	----	27,606	25
4433	45D155V303	41	0.1	10	9.5	0.51	770,759	25
4434	45D155V302	41	0.1	10	9.5	0.50	1,233,580	25
4435	45D155V310	41	0.1	10	10.6	0.44	1,289,647	25
4436	45D155V161	-69	10	10	----	----	4,975,500	25 R

MATERIAL 45D155P2

Lay-up = $[\pm 45]_3$, $V_F = 0.40$, Ave. thickness = 3.05 mm, S.D. = 0.02 mm, CoRezyn 75-AQ-010 Isopolyester

4622	ISO45114	55	0.1	3	11.9	0.57	4,934	25
4623	ISO45101	55	0.1	2	10.9	0.63	5,740	25
4624	ISO45102	41	0.1	5	11.7	0.39	202,047	25
4625	ISO45103	41	0.1	5	11.3	0.42	192,822	25
4626	ISO45111	41	0.1	5	11.5	0.40	179,293	25
4627	ISO45110	38	0.1	7	11.3	0.37	811,700	25
4628	ISO45112	55	0.1	2	11.8	0.58	6,965	25
4629	ISO45109	48	0.1	3	----	----	21,334	25
4630	ISO45108	48	0.1	2	10.8	0.54	17,395	25
4631	ISO45107	48	0.1	2	----	----	9,479	25
4632	ISO45106	38	0.1	4	10.8	0.41	422,361	25
4633	ISO45105	95	*	13	12.0	1.30	1	25
4634	ISO45104	97	*	13	12.0	1.35	1	25

TEST & SAMPLE ID #		MAX. STRESS MPa	R	Q Hz	E GPa	e %	CYCLES TO FAIL	WIDTH (mm) and Notes
4635	ISO45113	96	*	13	11.3	1.4	1	25
4636	ISO45119	-156	*	13	----	----	1	25
4637	ISO45116	-165	*	13	----	----	1	25
4638	ISO45115	-158	*	13	----	----	1	25
4639	ISO45117	-161	*	13	----	----	1	25

MATERIAL 45D155V

Lay-up = $[45]_3$, $V_F = 0.40$, Ave. thickness = 3.00 mm, S.D. = 0.07 mm, Derakane 411C-50 vinyl ester

4869	41145113	41.4	0.1	10	10.2	0.40	4,000,000	25 R
4870	41145101	69	0.1		10.5	0.84	4,581	25
4871	41145109	130	*	13	10.8	21	1	25
4872	41145106	118	*	13	10.1	15	1	25
4873	41145107	116	*	13	10.5	23	1	25
4874	41145105	55.2	0.1	3	10.5	0.64	38,539	25
4875	41145104	55.2	0.1	4	10.8	0.61	51,501	25
4876	41145102	55.2	0.1	3	11.4	0.60	62,968	25
4877	41145110	69	0.1	2	11.2	0.86	7,247	25
4879	41145112	69	0.1	2	----	----	6,339	25
5908	41145116	-155	*	13	----	----	1	25
5909	41145115	-153	*	13	----	----	1	25
5910	41145119	-154	*	13	----	----	1	25
5911	41145118	-154	*	13	----	----	1	25

MATERIAL 50D155

Lay-up = $[\pm 50]_3$, $V_F = 0.39$, Ave. thickness = 3.23 mm, S.D. = 0.11 mm, CoRezyn 63-AX-051 Polyester

2454	50D155114	67	*	13	8.33	20	1	25
2455	50D155113	67	*	13	8.39	19	1	25
2456	50D155107	63	*	13	8.43	17	1	25
2457	50D155104	35	0.1	20	8.62	0.41	136,803	25
2458	50D155116	35	0.1	15	9.00	0.41	72,943	25
2459	50D155115	35	0.1	15	8.32	0.42	96,273	25
2460	50D155111	28	0.1	15	8.11	0.36	1,855,523	25
2461	50D155106	41	0.1	5	8.81	0.48	11,555	25
2462	50D155108	41	0.1	7	8.74	0.52	11,608	25
2463	50D155112	41	0.1	4	8.90	0.53	11,509	25
2464	50D155105	28	0.1	15	8.42	0.37	1,159,160	25
2465	50D155101	58	*	13	8.43	30.0	1	25
2466	50D155102	67	*	13	9.52	22.2	1	25
2603	50D155301	-132	*	13	----	----	1	25
2604	50D155302	-142	*	13	----	----	1	25
2605	50D155303	-139	*	13	----	----	1	25
2606	50D155304	-138	*	13	----	----	1	25
4468	50D155134	-90	10	3	----	----	10,617	25
4469	50D155133	-90	10	3	----	----	9,472	25
4470	50D155132	-90	10	3	----	----	11,783	25
4471	50D155131	-69	10	8	----	----	2,313,976	25

TEST & SAMPLE ID #		MAX. STRESS MPa	R	Q Hz	E GPa	e %	CYCLES TO FAIL	WIDTH (mm) and Notes
4472	50D155135	-79	10	4	----	----	38,964	25
4473	50D155136	-76	10	4	----	----	128,196	25
4613	50D155137	-79	10	4	----	----	83,779	25
4619	50D155145	-100	10	2	----	----	2,213	25

MATERIAL 60D155

Lay-up = $[\pm 60]_3$, $V_F = 0.40$, Ave. thickness = 3.11 mm, S.D. = 0.14 mm, CoRezyn 63-AX-051 Polyester

2482	60D155103	37	*	13	7.02	0.65	1	25
2483	60D155106	34	*	13	7.04	0.65	1	25
2484	60D155101	36	*	13	7.44	0.62	1	25
2576	60D155146	40	*	13	7.99	0.60	1	25
2548	60D155108	24	0.1	10	8.00	0.31	23,872	25
2549	60D155115	24	0.1	15	8.33	0.32	35,211	25
2550	60D155113	24	0.1	10	8.26	0.32	17,122	25
2551	60D155104	21	0.1	20	7.81	0.27	160,347	25
2552	60D155105	21	0.1	15	8.30	0.25	369,336	25
2553	60D155109	28	0.1	4	8.20	0.38	4,716	25
2554	60D155107	28	0.1	5	7.75	0.37	3,715	25
2555	60D155110	28	0.1	5	7.23	0.36	2,270	25
2556	60D155116	19	0.1	15	7.24	0.25	1,915,213	25
2557	60D155102	21	0.1	10	7.33	0.27	217,771	25
2607	60D155301	-144	*	13	----	----	1	25
2608	60D155302	-133	*	13	----	----	1	25
2609	60D155303	-143	*	13	----	----	1	25
2610	60D155304	-144	*	13	----	----	1	25
4437	60D155162	-103	10	4	----	----	2,461	25
4438	60D155141	-103	10	4	----	----	1,786	25
4439	60D155166	-103	10	4	----	----	4,011	25
4440	60D155160	-86	10	6	----	----	19,416	25
4441	60D155165	-86	10	6	----	----	21,746	25
4442	60D155142	-86	10	6	----	----	33,065	25
4443	60D155114	-79	10	10	----	----	573,969	25
4444	60D155164	-79	10	10	----	----	434,136	25

MATERIAL 70D155

Lay-up = $[\pm 70]_3$, $V_F = 0.40\%$, Ave. thickness = 3.17 mm, S.D. = 0.04 mm, CoRezyn 63-AX-051 Polyester

2485	70D155101	28	*	13	6.67	0.49	1	25
2486	70D155104	27	*	13	6.86	0.46	1	25
2487	70D155107	26	*	13	6.51	0.44	1	25
2577	70D155141	30	*	13	7.51	0.49	1	25
2525	70D155111	17	0.1	10	7.84	0.21	30,672	25
2526	70D155109	17	0.1	12	8.16	0.19	51,196	25
2527	70D155106	17	0.1	12	7.90	0.23	43,825	25
2528	70D155110	14	0.1	20	7.31	0.19	1,045,443	25
2529	70D155108	17	0.1	15	7.14	0.28	27,455	25
2530	70D155103	16	0.1	20	7.47	0.20	296,781	25

TEST & SAMPLE ID #		MAX. STRESS MPa	R	Q Hz	E GPa	e %	CYCLES TO FAIL	WIDTH (mm) and Notes
2531	70D155102	19	0.1	5	7.09	0.27	8,217	25
2532	70D155134	19	0.1	5	7.21	0.26	10,888	25
2533	70D155123	19	0.1	5	7.19	0.27	27,256	25
2534	70D155121	16	0.1	15	6.66	0.24	246,630	25
2535	70D155122	16	0.1	15	7.17	0.22	421,514	25
2611	70D155301	-133	*	13	----	----	1	25
2612	70D155302	-136	*	13	----	----	1	25
2613	70D155303	-138	*	13	----	----	1	25
2614	70D155304	-138	*	13	----	----	1	25

MATERIAL 80D155

Lay-up = $[\pm 80]_3$, $V_F = 0.38$, Ave. thickness = 3.32 mm, S.D. = 0.10 mm, CoRezyn 63-AX-051 Polyester

2488	80D155105	27	*	13	7.79	0.38	1	25
2489	80D155103	25	*	13	7.00	0.34	1	25
2490	80D155101	24	*	13	7.05	0.37	1	25
2578	80D155141	27	*	13	7.75	0.38	1	25
2580	80D155201	26	*	13	9.30	0.30	1	25
2581	80D155202	26	*	13	8.15	0.34	1	25
2582	80D155203	27	*	13	8.65	0.34	1	25
2494	80D155120	26	*	13	6.95	0.35	1	25
2495	80D155122	24	*	13	6.43	0.35	1	25
2491	80D155102	17	0.1	2	7.59	0.24	2,096	25
2492	80D155112	17	0.1	2	6.79	0.25	865	25
2493	80D155104	17	0.1	2	7.35	0.24	3,673	25
2496	80D155121	12	0.1	25	7.49	0.15	8,000,000	25 R
2497	80D155106	16	0.1	5	8.42	0.19	34,973	25
2498	80D155109	16	0.1	15	7.02	0.20	16,756	25
2499	80D155111	16	0.1	10	7.81	0.20	24,111	25
2500	80D155123	14	0.1	10	7.42	0.18	135,541	25
2501	80D155145	14	0.1	10	7.06	0.18	261,230	25
2502	80D155146	14	0.1	10	7.20	0.18	186,407	25
2619	80D155205	-148	*	13	----	----	1	25
2620	80D155206	-146	*	13	----	----	1	25
2621	80D155207	-156	*	13	----	----	1	25
2622	80D155208	-162	*	13	----	----	1	25

MATERIAL 90D155

Lay-up = $[\pm 90]_3$, $V_F = 0.38$, Ave. thickness = 3.32 mm, S.D. = 0.12 mm, CoRezyn 63-AX-051 Polyester

2467	90D155105	27	*	13	7.21	0.38	1	25
2468	90D155110	26	*	13	7.30	0.34	1	25
2469	90D155104	24	*	13	6.44	0.34	1	25
2579	90D155141	29	*	13	9.04	0.34	1	25
2470	90D155101	17	0.1	5	7.23	0.24	17,903	25
2471	90D155102	17	0.1	5	7.60	0.24	22,344	25
2472	90D155103	17	0.1	5	7.00	0.25	27,113	25
2473	90D155107	14	0.1	15	7.31	0.17	612,541	25

TEST & SAMPLE ID #		MAX. STRESS MPa	R	Q Hz	E GPa	e %	CYCLES TO FAIL	WIDTH (mm) and Notes
2474	90D155108	19	0.1	2	7.62	0.25	783	25
2475	90D155113	19	0.1	2	7.58	0.24	1,800	25
2476	90D155109	19	0.1	2	7.05	0.25	1,179	25
2477	90D155125	14	0.1	20	6.97	0.20	1,190,051	25
2578	90D155130	14	0.1	20	7.45	0.19	1,712,400	25
2479	90D155120	28	*	13	7.50	0.41	1	25
2480	90D155122	28	*	13	7.24	0.40	1	25
2481	90D155121	27	*	13	6.89	0.40	1	25
2623	90D155112	-108	*	13	----	----	1	25
2624	90D155111	-129	*	13	----	----	1	25
2625	90D155301	-126	*	13	----	----	1	25
2626	90D155302	-128	*	13	----	----	1	25
4614	90D155139	-66	10	15	----	----	20,000,000	25 R
4615	90D155130	-90	10	5	----	----	39,215	25
4616	90D155131	-79	10	8	----	----	400,785	25
4617	90D155132	-79	10	10	----	----	515,123	25
4618	90D155133	-79	10	10	----	----	780,009	25 R
4620	90D155134	-90	10	5	----	----	27,023	25
4621	90D155139	-90	10	5	----	----	26,104	25

MATERIAL 90D155V2

Lay-up = $[90]_6$, $V_F = 0.38$, Ave. thickness = 3.31 mm, S.D. = 0.09 mm, Derakane 8084 vinyl ester

4760	808490207	17.2	0.1	15	8.72	0.20	2,000,000	25 R
4761	808490213	51.1	*	13	9.32	0.56	1	25
4762	808490211	34.5	0.1	2	8.61	0.41	1,486	25
4763	808490215	27.6	0.1	2	9.32	0.32	85,350	25
4764	808490214	20.7	0.1	5	9.12	0.23	248,600	25
4765	808490212	20.7	0.1	7	8.76	0.24	153,624	25
4766	808490209	20.7	0.1	10	8.74	0.24	2,163,003	25
4767	808490208	27.6	0.1	5	9.38	0.30	10,162	25
4768	808490206	27.6	0.1	5	8.70	0.33	19,542	25
4769	808490216	34.5	0.1	1	8.42	0.41	422	25
4770	808490202	34.5	0.1	1	8.25	0.43	548	25
4771	808490217	55.8	*	13	9.66	0.58	1	25
4772	808490201	52.0	*	13	8.09	0.64	1	25
5912	808490218	-175	*	13	----	----	1	25
5913	808490219	-172	*	13	----	----	1	25
5914	808490221	-172	*	13	----	----	1	25
5915	808490200	-166	*	13	----	----	1	25

MATERIAL 90D155V

Lay-up = $[90]_6$, $V_F = 0.40$, Ave. thickness = 2.98 mm, S.D. = 0.10 mm, Derakane 411C-50 vinyl ester

4776	41190130	43.8	*	13	7.63	0.40	1	25
4777	41190140	51.2	*	13	9.81	0.52	1	25
4778	41190136	52.8	*	13	10.3	0.51	1	25
4779	41190141	20.7	0.1	10	11.8	0.19	223,965	25

TEST & SAMPLE ID #		MAX. STRESS MPa	R	Q Hz	E GPa	e %	CYCLES TO FAIL	WIDTH (mm) and Notes
4780	41190131	20.7	0.1	8	13.0	0.19	184,528	25
4781	41190149	20.7	0.1	10	11.1	0.19	138,110	25
4782	41190148	27.6	0.1	5	9.42	0.31	2,730	25
4783	41190135	27.6	0.1	5	10.8	0.26	15,581	25
4784	41190134	27.6	0.1	4	10.1	0.28	12,939	25
4785	41190147	24.1	0.1	5	8.21	0.31	77,719	25
4786	41190146	24.1	0.1	8	11.8	0.25	52,833	25
4787	41190138	24.1	0.1	4	10.1	0.24	30,181	25
4788	41190137	17.2	0.1	15	10.3	0.17	2,000,000	25 R
5916	41190145	-173	*	13	----	----	1	25
5917	41190144	-164	*	13	----	----	1	25
5918	41190132	-173	*	13	----	----	1	25
5919	41190139	-158	*	13	----	----	1	25

MATERIAL 90D155E2

Lay-up = $[90]_6$, $V_F = 0.38$, Ave. thickness = 3.41 mm, S.D. = 0.20 mm, SC14 epoxy

4789	SC1490216	27.6	0.1	0.1	9.29	0.35	254	25
4790	SC1490215	20.7	0.1	0.1	5.48	0.40	1,161	25
4791	SC1490207	38.2	*	13	6.72	0.57	1	25
4792	SC1490204	39.8	*	13	7.20	0.55	1	25
4793	SC1490208	43	*	13	8.34	0.52	1	25
4794	SC1490206	13.8	0.1	15	9.10	0.15	3,000,000	25 R
4795	SC1490209	20.7	0.1	3	5.30	0.40	8,141	25
4796	SC1490213	17.2	0.1	5	7.30	0.26	292,196	25
4797	SC1490210	20.7	0.1	3	8.06	0.27	27,984	25
4798	SC1490212	26.1	0.1	3	5.93	0.44	402	25
5904	SC1490211	-151	*	13	----	----	1	25
5905	SC1490201	-153	*	13	----	----	1	25
5906	SC1490203	-151	*	13	----	----	1	25
5907	SC1490205	-151	*	13	----	----	1	25

MATERIAL ROV1 (0/90 ROVING)

Lay-up = $[0/90]_7$, $V_F = 0.46$, Ave. thickness = 2.96 mm, S.D. = 0.16 mm, CoRezyn 63-AX-051 Polyester.
Tests 2095 - 2108 in this section were done for Table 10. Compression tests involved a 13 mm gage length.

2094	ROV01	380	*	0.25	22.8	2.40	1	ZERO
2095	ROV02	364	*	0.25	22.5	2.20	1	ZERO
2096	ROV03	374	*	0.25	24.8	2.20	1	ZERO
2097	ROV04	97	*	0.25	11.0	----	1	±45
2098	ROV05	102	*	0.25	11.4	----	1	±45
2099	ROV06	99	*	0.25	11.4	----	1	±45
2100	ROV07	-213	*	0.25	20.3	----	1	ZERO
2101	ROV08	-230	*	0.25	21.6	----	1	ZERO
2102	ROV09	-240	*	0.25	23.9	----	1	ZERO
2103	ROV10	98	*	0.25	10.6	----	1	±45
2104	ROV11	-100	*	0.25	11.2	----	1	±45
2105	ROV12	-97	*	0.25	11.3	----	1	±45

TEST & SAMPLE ID #		MAX. STRESS MPa	R	Q Hz	E GPa	e %	CYCLES TO FAIL	WIDTH (mm) and Notes
2106	ROV50	-207	*	0.25	13.7	----	1	ZERO
2107	ROV51	410	*	0.25	25.4	---	1	ZERO
2108	ROV52	102	*	0.25	13.9	----	1	±45

MATERIAL ROV2 (0/90 ROVING)

Lay-up = $[0/90]_4$, V_F = 0.30, Ave. thickness = 4.08 mm, S.D. = 0.10 mm, CoRezyn 63-AX-051 Polyester

4193	ROV217	326	*	13	----	----	1	25
4194	ROV215	103	0.1	10	----	----	3,200,000	25 R
4195	ROV218	380	*	13	21.0	1.9	1	25
4196	ROV206	381	*	13	21.6	1.8	1	25
4197	ROV205	241	0.1	1	21.3	1.45	1,642	25
4198	ROV201	172	0.1	3	21.7	0.96	13,794	25
4199	ROV200	138	0.1	5	21.2	0.74	608,189	25
4200	ROV204	172	0.1	2	22.4	0.87	40,071	25
4201	ROV203	172	0.1	3	23.1	0.89	63,917	25
4202	ROV214	138	0.1	10	21.2	0.78	723,201	25
4203	ROV212	138	0.1	10	21.0	0.81	483,611	25
4204	ROV207	241	0.1	1	20.9	1.50	1,043	25
4205	ROV219	241	0.1	1	20.7	1.58	494	25
4226	ROV231	-266	*	13	----	----	1	25
4227	ROV230	-245	*	13	----	----	1	25
4228	ROV232	-217	*	13	----	----	1	25
4229	ROV238	-247	*	13	----	----	1	25

MATERIAL ROV 3 (0/90 ROVING)

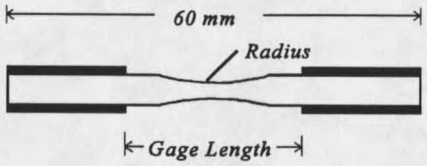
Lay-up = $[0/90]_5$, V_F = 0.40, Ave. thickness = 3.15 mm, S.D. = 0.05 mm, CoRezyn 63-AX-051 Polyester

4284	ROV3106	406	*	13	21.1	2.3	1	25
4285	ROV3109	443	*	13	21.4	2.4	1	25
4286	ROV3103	416	*	13	21.0	2.3	1	25
4287	ROV3107	207	0.1	2	20.1	1.35	3,055	25
4288	ROV3112	207	0.1	2	21.5	1.26	8,236	25
4289	ROV3108	207	0.1	3	20.9	1.34	3,720	25
4290	ROV3114	172	0.1	4	20.0	1.10	23,506	25
4291	ROV3110	172	0.1	4	20.2	1.06	14,233	25
4292	ROV3111	172	0.1	4	20.7	1.03	28,712	25
4293	ROV3102	103	0.1	10	21.2	0.58	4,320,474	25
4294	ROV3113	138	0.1	6	19.9	0.85	351,549	25
4295	ROV3115	138	0.1	6	22.0	0.79	690,805	25
4296	ROV3104	138	0.1	6	21.1	0.80	216,248	25
4297	ROV3101	138	0.1	6	20.7	0.84	264,008	25
4314	ROV3130	-201	*	13	----	----	1	25
4315	ROV3131	-204	*	13	----	----	1	25
4316	ROV3132	-204	*	13	----	----	1	25
4320	ROV3105	103	0.1	10	21.7	0.61	4,855,537	25
4327	ROV3130	103	0.1	8	21.0	0.63	5,981,053	25

TEST & SAMPLE ID #		MAX. STRESS MPa	R	Q Hz	E GPa	e %	CYCLES TO FAIL	WIDTH (mm) and Notes
MATERIAL ROV4 (0/90 ROVING)								
Lay-up = $[0/90]_6$, V_F = 0.53, Ave. thickness = 3.71 mm, S.D. = 0.09 mm, CoRezyn 63-AX-051 Polyester								
4298	ROV4109	207	0.1	2	27.5	1.04	1,501	25
4299	ROV4110	207	0.1	2	28.1	1.05	1,558	25
4300	ROV4111	207	0.1	2	26.4	1.11	2,319	25
4301	ROV4106	172	0.1	3	28.1	0.83	4,371	25
4302	ROV4105	172	0.1	3	24.4	0.98	3,514	25
4303	ROV4114	172	0.1	3	26.8	0.90	4,498	25
4304	ROV4115	138	0.1	5	27.0	0.67	14,689	25
4305	ROV4107	138	0.1	5	28.1	0.65	8,459	25
4306	ROV4113	138	0.1	5	27.2	0.67	11,994	25
4307	ROV4112	103	0.1	6	25.1	0.51	68,112	25
4308	ROV4104	502	*	13	25.3	2.2	1	25
4309	ROV4108	524	*	13	24.3	2.4	1	25
4310	ROV4102	488	*	13	25.4	2.1	1	25
4311	ROV4117	103	0.1	5	28.0	0.47	76,081	25
4312	ROV4116	103	0.1	5	27.7	0.46	147,753	25
4313	ROV4103	86	0.1	15	26.7	0.36	1,965,313	25
4317	ROV4130	-351	*	13	----	----	1	25
4318	ROV4131	-302	*	13	----	----	1	25
4319	ROV4132	-289	*	13	----	----	1	25
4321	ROV4101	86	0.1	15	26.9	0.35	924,136	25
4324	ROV4120	86	0.1	10	27.2	0.36	273,658	25
4326	ROV4121	86	0.1	5	27.1	0.35	1,135,918	25

HIGH CYCLE FATIGUE DATABASE

The High Cycle Fatigue Database studied two basic composite materials, a $(0)_2$ and a $(90)_4$ laminate, at R values of 2, 10, -1, 0.1 and 0.5. The Fatigue tests were carried out to 100 million cycles and involved testing frequencies up to 100 Hz. Smaller and thinner composites were necessary to avoid thermal failures.



Gage Length, Radius and Width of $[0]_2$ and $[90]_4$ Test Coupons in the High Cycle Database			
Direction and R value	Gage Length	Radius	Width
[0] R = 2, 10	5 mm	No radius	6 mm
[90] R = 2, 10, -1	5 mm		19 mm
[90] R = 0.1, 0.5	25 mm		19 mm
[0] R = 0.1, 0.5	10 mm	17 mm	6 mm
[0] R = -1	5 mm		

TEST & SAMPLE ID #		MAX. STRESS MPa	R	Q Hz	E GPa	e %	CYCLES TO FAIL	WIDTH (mm) and Notes
MATERIAL $(0)_2$								
Lay-up = $(0)_2$, V_F = 0.48 - 0.52, Average Thickness (Non-Tapered Coupons) = 0.82 mm, S.D. = 0.05 mm (min = 0.71 mm, max = 0.89 mm), Knytex D155 Fabric (527 g/m^2), CoRezyn 63-AX-051 Polyester								
5001	CT4	1627	*	6	46.2	3.53	1	6 tab
5002	AT2	1517	*	6	46.2	3.28	1	6 tab
5003	AT26	1393	*	3	46.2	3.01	1	6 tab
5004	CT3	1344	*	0.01	46.2	2.91	1	6 tab
5146	TF514	1332	*	5	39	2.88	1	6 tab
5147	TF510	1249	*	0.1	39	2.70	1	6 tab
5148	TF504	1398	*	5	39	3.03	1	6 tab
5149	TF505	1329	*	5	39	2.88	1	6 tab
5150	TF501A	1274	*	5	39	2.76	1	6 tab
5151	TF502A	1589	*	5	39	3.43	1	6 tab
5152	TF503A	1496	*	5	39	3.23	1	6 tab
5153	TF510	1249	*	5	39	2.70	1	6 tab
5154	AT5	1270	*	0.5	46.2	2.75	1	6 tab
5155	AT4	1343	*	0.5	46.2	2.91	1	6 tab
5156	T1	1684	*	5	46.2	3.64	1	6 tab
5157	TFT5	1692	*	5	39	3.66	1	6 tab
5158	TF501	1713	*	5	39	3.70	1	6 tab
5159	TF502	1391	*	5	39	3.01	1	6 tab

TEST & SAMPLE ID #		MAX. STRESS MPa	R	Q Hz	E GPa	e %	CYCLES TO FAIL	WIDTH (mm) and Notes
5005	AT27	690	0.1	20	46.2	1.49	2,982	6 tab
5006	CT1	690	0.1	20	46.2	1.49	45,845	6 tab
5007	AT19	469	0.1	60	46.2	1.01	157,502	6 tab
5008	AT18	469	0.1	60	46.2	1.01	702,844	6 tab
5009	AT23	414	0.1	80	46.2	0.90	602,984	6 tab
5010	AT20	414	0.1	80	46.2	0.90	2,269,945	6 tab
5011	CT5	310	0.1	100	46.2	0.67	5,902,329	6 tab
5012	CT7	310	0.1	100	46.2	0.67	78,810,903	6 R tab
5013	CT2	310	0.1	100	46.2	0.67	110,539,817	6 R tab
5160	T1	345	0.1	60	46.2	0.60	5,151,390	6 tab
5161	T2	345	0.1	40	46.2	0.60	772,447	6 tab
5162	FT6	538	0.1	60	46.2	1.16	144,728	6 tab
5163	TF503	345	0.1	60	46.2	0.75	6,889,310	6 R tab
5164	TF506	538	0.1	60	46.2	1.16	891,716	6 tab
5165	AT3	207	0.1	100	46.2	0.45	14,715,704	6 R tab
5166	AT21	414	0.1	80	46.2	0.90	80,439	6 tab
5167	AT22	414	0.1	80	46.2	0.90	98,566	6 tab
5014	TF513	1310	*	5	39.2	3.31	1	6 tab
5015	TF512	1426	*	5	39.2	3.64	1	6 tab
5016	TF515	1396	*	5	39.2	3.56	1	6 tab
5017	TF516	1295	*	20	39.2	3.34	1	6 tab
5018	TF525	602	0.5	60	39.2	1.54	235,881	6 tab
5019	TF526	602	0.5	60	39.2	1.54	284,150	6 tab
5168	TF524	602	0.5	40	39.2	1.54	2,513,501	6 tab
5020	TF527	606	0.5	60	39.2	1.54	850,428	6 tab
5021	TF521	535	0.5	80	39.2	1.36	417,082	6 tab
5022	TF528	535	0.5	80	39.2	1.36	1,095,381	6 tab
5023	TF522	535	0.5	80	39.2	1.36	4,112,276	6 tab
5169	TF517	535	0.5	60	39.2	1.36	486,856	6 tab
5170	TF518	535	0.5	60	39.2	1.36	368,725	6 tab
5024	TF529	468	0.5	100	39.2	1.19	11,927,857	6 tab
5025	TF520	468	0.5	100	39.2	1.19	16,711,593	6 tab
5026	TF519	401	0.5	100	39.2	1.02	100,686,430	6 R tab
5171	TF507	717	0.5	40	39.2	1.82	474,816	6 tab
5172	TF508	627	0.5	60	39.2	1.60	11,276,771	6 tab
5173	TF504A	807	0.5	40	39.2	2.06	245,223	6 tab
5174	TF505A	627	0.5	60	39.2	1.60	3,527,508	6 tab
Brackets after the sample ID indicate the coupon fiber volume in the radius								
5027	AC14 (57)	-742	*	0.8	35.6	-2.09	1	6 tab
5028	AC17 (46)	-741	*	0.8	35.6	-2.09	1	6 tab
5029	AC13 (45)	-683	*	0.8	35.6	-1.93	1	6 tab
5030	AC11 (48)	-414	10	40	35.6	-1.17	8,226	6 tab
5031	AC12 (49)	-414	10	40	35.6	-1.17	10,886	6 tab
5032	AC8 (61)	-414	10	40	35.6	-1.17	19,210	6 tab
5033	AC15 (61)	-345	10	60	35.6	-0.97	337,992	6 tab
5034	AC16 (46)	-345	10	60	35.6	-0.97	375,478	6 tab
5035	AC7 (50)	-345	10	60	35.6	-0.97	587,407	6 tab
5036	AC30 (48)	-276	10	100	35.6	-0.78	103,112,335	6 R tab
5037	AC10 (51)	-276	10	100	35.6	-0.78	103,573,682	6 R tab
5175	AC2	-414	10	40	35.6	-1.17	2,688	6 tab

TEST & SAMPLE ID #		MAX. STRESS MPa	R	Q Hz	E GPa	e %	CYCLES TO FAIL	WIDTH (mm) and Notes
5176	AC1	-345	10	60	35.6	-0.97	76,726	6 tab
5177	C2A	-264	10	80	35.6	-0.74	13,990,000	6 tab
5178	C6	-207	10	100	35.6	-0.58	51,028,261	6 R tab
5179	7A	-207	10	20	35.6	-0.58	10,188,704	6 R tab
5180	WA1	-276	10	30	35.6	-0.78	12,635,375	6 R tab
5181	WA4	-276	10	30	35.6	-0.78	9,707,898	6 R tab
5182	WA5	-345	10	30	35.6	-0.97	52,740	6 tab
5183	WA10	-276	10	30	35.6	-0.78	10,106,247	6 tab
5184	CC3	-345	10	60	35.6	-0.97	69,631	6 tab
5185	CC4	-345	10	10	35.6	-0.97	781,804	6 tab
5186	CC5	-379	10	10	35.6	-1.06	4,021	6 tab
5187	CC6	-379	10	10	35.6	-1.06	496,674	6 tab
5188	CC7	-379	10	50	35.6	-1.06	12,660	6 tab
5189	CC8	-379	10	10	35.6	-1.06	3,638,153	6 tab
5190	CC9	-379	10	50	35.6	-1.06	4,765	6 tab
5191	CC10	-379	10	50	35.6	-1.06	8,349	6 tab
5192	CC11	-379	10	10	35.6	-1.06	1,336,317	6 tab
5193	CC12	-379	10	30	35.6	-1.06	10,192	6 tab
5194	CC12A	-379	10	30	35.6	-1.06	6,550	6 tab
5195	C2	-345	10	30	35.6	-0.97	37,274	6 tab
5196	FC1	-234	10	60	35.6	-0.66	23,110,567	6 tab
5038	AC19 (49)	-552	2	60	35.4	-1.56	9,255	6 tab
5039	AC26 (49)	-552	2	60	35.4	-1.56	12,319	6 tab
5040	AC29 (49)	-552	2	60	35.4	-1.56	22,071	6 tab
5041	AC20 (51)	-552	2	60	35.4	-1.56	46,085	6 tab
5042	AC21 (47)	-483	2	80	35.4	-1.36	11,347	6 tab
5043	AC24 (52)	-483	2	80	35.4	-1.36	38,158	6 tab
5044	AC31 (44)	-483	2	80	35.4	-1.36	45,312	6 tab
5045	AC22 (46)	-483	2	80	35.4	-1.36	103,970	6 tab
5046	AC32 (46)	-448	2	100	35.4	-1.26	17,937	6 tab
5047	AC35 (48)	-448	2	100	35.4	-1.26	3,891,657	6 tab
5048	AC25 (49)	-448	2	100	35.4	-1.26	100,081,219	6 R tab
5049	AC23 (50)	-414	2	100	35.4	-1.17	107,413,026	6 R tab
5197	AC34	-448	2	100	35.4	-1.26	403,736	6 tab
5198	AC33	-448	2	100	35.4	-1.26	34,426	6 tab
5199	AC32	-448	2	100	35.4	-1.26	17,937	6 tab
5050	TCT1	1367	*	20	39.2	3.49	1	6 tab
5051	TCT2	1387	*	20	39.2	3.54	1	6 tab
5052	TCT3	1279	*	20	39.2	3.26	1	6 tab
5053	TCT4	1527	*	20	39.2	3.89	1	6 tab
5054	TCC1	-646	*	20	41.2	-1.57	1	6 tab
5055	TCC2	-463	*	20	41.2	-1.13	1	6 tab
5056	TCC3	-689	*	20	41.2	-1.68	1	6 tab
5057	TCC4	-537	*	20	41.2	-1.30	1	6 tab
5200	0STC1	-481	*	0.2	--	-----	1	6 tab
5201	0STC3	-478	*	0.2	--	-----	1	6 tab
5202	0FTC1	-513	*	5	--	-----	1	6 tab
5203	0FTC2	-534	*	5	--	-----	1	6 tab
5204	AC36	-592	*	5	--	-----	1	6 tab

TEST & SAMPLE ID #		MAX. STRESS MPa	R	Q Hz	E GPa	e %	CYCLES TO FAIL	WIDTH (mm) and Notes
5205	AC37	-639	*	5	--	-----	1	6 tab
5206	9A	-501	*	5	--	-----	1	6 tab
5207	10A	-500	*	5	--	-----	1	6 tab
5208	13A	-502	*	5	--	-----	1	6 tab
5209	WA7	-613	*	5	--	-----	1	6 tab
5210	WA8	-588	*	5	--	-----	1	6 tab
5211	WA9	-596	*	5	--	-----	1	6 tab
5212	TC1	293	-1	20	--	----	3,596	6 tab
5213	0FTS4	267	-1	10	--	----	146,258	6 tab
5058	TC15 (45)	264	-1	30	40.2	0.66	124,950	6 tab
5059	TC16 (45)	264	-1	30	40.2	0.66	337,226	6 tab
5060	TC13 (45)	264	-1	30	40.2	0.66	437,113	6 tab
5214	TC14	264	-1	30	40.2	0.66	1,260,397	6 tab
5215	TC12	234	-1	30	40.2	0.58	754,410	6 tab
5061	TC11 (40)	234	-1	30	40.2	0.58	591,914	6 tab
5062	TC7 (40)	234	-1	30	40.2	0.58	781,045	6 tab
5063	TC9 (40)	234	-1	30	40.2	0.58	1,981,821	6 tab
5064	TC22	205	-1	40	40.2	0.51	2,037,672	6 tab
5065	TC18 (35)	205	-1	40	40.2	0.51	6,141,627	6 tab
5066	TC6 (35)	205	-1	40	40.2	0.51	7,080,727	6 tab
5067	TC10 (35)	205	-1	40	40.2	0.51	7,605,707	6 tab
5068	TC21	176	-1	50	40.2	0.44	10,382,631	6 tab
5069	TC19	176	-1	50	40.2	0.44	17,272,745	6 tab
5070	TC20	176	-1	50	40.2	0.44	100,000,000	6 R tab
5216	0FTC11	160	-1	60	40.2	0.40	25,924,921	6 R tab
5217	0FTC12	187	-1	40	40.2	0.47	4,850,470	6 tab
5218	0FTS19	187	-1	30	40.2	0.47	3,267,903	6 tab
5219	0FTC20	187	-1	30	40.2	0.47	6,909,213	6 tab
5071	TC601	1618	*	20	40.2	4.02	1	6 tab
5072	TC602	1382	*	20	40.2	3.44	1	6 tab
5073	TC603	1410	*	20	40.2	3.51	1	6 tab
5074	TC604	-746	*	20	40.2	-1.86	1	6 tab
5075	TC605	-716	*	20	40.2	-1.78	1	6 tab
5076	TC606	-687	*	20	40.2	-1.71	1	6 tab
5077	TC608	294	-0.5	20	40.2	0.73	54,401	6 tab
5078	TC609	294	-0.5	20	40.2	0.73	151,631	6 tab
5079	TC613	294	-0.5	20	40.2	0.73	2,215,625	6 tab
5080	TC610	257	-0.5	20	40.2	0.64	338,635	6 tab
5081	TC611	257	-0.5	20	40.2	0.64	677,151	6 tab
5082	TC616	257	-0.5	20	40.2	0.64	4,237,939	6 tab
5083	TC614	257	-0.5	20	40.2	0.64	4,554,382	6 tab
5084	TC612	220	-0.5	20	40.2	0.55	3,089,148	6 tab
5085	TC615	220	-0.5	20	40.2	0.55	11,113,718	6 R tab

TEST & SAMPLE ID #		MAX. STRESS MPa	R	Q Hz	E GPa	e %	CYCLES TO FAIL	WIDTH (mm) and Notes
MATERIAL $(90)_4$								
Lay-up = $(90)_4$, V_F = 0.38, Average Thickness = 1.38 mm, S.D. = 0.15 mm (min = 1.07 mm, max = 1.75 mm)								
Hexcel D100 Fabric (340 g/m^2), CoRezyn 63-AX-051 Polyester								
5220	90CF7	-111	*	4	9.0	-1.23	1	13 tab
5221	90CF6	-127	*	4	9.0	-1.41	1	13 tab
5222	90CF5	-112	*	4	9.0	-1.24	1	13 tab
5223	90CF4	-128	*	4	9.0	-1.42	1	13 tab
5224	90CF4A	-157	*	4	9.0	-1.74	1	13 tab
5225	90CF4B	-136	*	4	9.0	-1.51	1	13 tab
5226	90CF8	-110	*	4	9.0	-1.22	1	13 tab
5227	90CF6A	-136	*	4	9.0	-1.51	1	13 tab
5086	90CF6T	-145	*	4	9.0	-1.61	1	13 tab
5087	90CF5T	-160	*	4	9.0	-1.78	1	13 tab
5088	90CF7T	-124	*	4	9.0	-1.38	1	13 tab
5228	90CF4A	-76	10	40	9.0	-0.84	76,674	13 tab
5089	90CF10T	-70	10	50	9.0	-0.79	13,122	13 tab
5090	90CF17T	-70	10	50	9.0	-0.79	33,632	13 tab
5091	90CF15T	-70	10	50	9.0	-0.79	268,262	13 tab
5092	90CF12T	-64	10	70	9.0	-0.72	290,252	13 tab
5093	90CF11T	-64	10	70	9.0	-0.72	697,512	13 tab
5094	90CF18T	-64	10	70	9.0	-0.72	1,330,488	13 tab
5229	90CF19	-59	10	70	9.0	-0.65	1,407,676	13 tab
5230	90CF16	-59	10	70	9.0	-0.65	2,218,971	13 tab
5231	90CF13	-59	10	100	9.0	-0.65	45,789,443	13 tab
5095	90CF21T	-59	10	100	9.0	-0.65	12,000,998	13 tab
5096	90CF9T	-59	10	100	9.0	-0.65	34,986,168	13 tab
5097	90CF20T	-55	10	100	9.0	-0.65	107,839,549	13 R tab
5232	90CF22	-55	10	100	9.0	-0.65	15,368,000	13 R tab
5098	CF501T	-113	*	20	9.0	-1.26	1	13 tab
5099	CF502T	-113	*	20	9.0	-1.26	1	13 tab
5100	CF503T	-121	*	20	9.0	-1.34	1	13 tab
5101	CF504T	-115	*	20	9.0	-1.27	1	13 tab
5102	CF518T	-88	2	40	9.0	-0.98	121,730	13 tab
5103	CF514T	-88	2	40	9.0	-0.98	511,744	13 tab
5104	CF517T	-88	2	40	9.0	-0.98	621,878	13 tab
5105	CF513T	-82	2	60	9.0	-0.92	853,552	13 tab
5106	CF512T	-82	2	60	9.0	-0.92	2,675,404	13 tab
5107	CF507T	-82	2	60	9.0	-0.92	3,705,190	13 tab
5108	CF511T	-76	2	80	9.0	-0.85	31,971,669	13 tab
5109	CF519T	-76	2	80	9.0	-0.85	100,682,804	13 R tab
5233	90CF505	-76	2	70	9.0	-0.79	11,667,961	13 tab
5110	90FT5T	22	*	20	8.6	0.25	1	13 tab
5111	90FT6T	18	*	20	8.6	0.21	1	13 tab
5112	90FT7T	23	*	20	8.6	0.27	1	13 tab
5113	90FT1T	22	*	20	8.6	0.36	1	13 tab
5234	90FT12	18	*	1	8.6	0.21	1	13 tab
5114	90FT18TA	14	0.1	60	8.6	0.16	9,383	13 tab
5234	90FT9	14	0.1	30	8.6	0.16	3,257	13 tab

TEST & SAMPLE ID #		MAX. STRESS MPa	R	Q Hz	E GPa	e %	CYCLES TO FAIL	WIDTH (mm) and Notes
5235	90FT11	13	0.1	40	8.6	0.14	2,720,600	13 R tab
5115	90FT15A	13	0.1	60	8.6	0.15	34,592	13 tab
5116	90FT3T	13	0.1	60	8.6	0.15	31,952	13 tab
5117	90FT26T	12	0.1	80	8.6	0.14	3,895,837	13 tab
5118	90FT14T	12	0.1	80	8.6	0.14	2,372,150	13 tab
5119	90FT15T	12	0.1	80	8.6	0.14	13,531,172	13 tab
5120	90FT8T	12	0.1	100	8.6	0.14	2,987,855	13 tab
5236	90FT13	12	0.1	80	8.6	0.14	3,810,385	13 tab
5121	90FT4T	11	0.1	100	8.6	0.13	21,111,725	13 tab
5122	90FT11T	11	0.1	100	8.6	0.12	102,350,298	13 R tab
5237	90FT19A	14	0.1	30	8.6	0.16	9,383	13 tab
5238	90FT13	11	0.1	40	8.6	0.12	1,813,684	13 tab
5239	90FT14A	12	0.1	40	8.6	0.14	2,372,150	13 tab
5240	90FT8	12	0.1	80	8.6	0.14	987,855	13 tab
5241	90FT10	10	0.1	100	8.6	0.11	208,516	13 tab
5242	90FT13A	13	0.1	70	8.6	0.15	2,759	13 tab
5243	90FT14	13	0.1	40	8.6	0.15	385	13 tab
5244	90FT15	12	0.1	70	8.6	0.14	1,471	13 tab
5245	90FT20	12	0.1	60	8.6	0.14	647	13 tab
5246	90TCA1	19	0.1	40	8.6	0.21	1,707,026	13 tab
5247	90TCB1	21	0.1	40	8.6	0.23	49,498	13 tab
5248	90FTC2	24	0.1	80	8.6	0.27	112,928	13 tab
5249	90FTC3	24	0.1	80	8.6	0.27	46,842	13 tab
5250	90FT18	20	*	1	8.6	0.22	1	13 tab
5251	90FT19B	19	*	1	8.6	0.21	1	13 tab
5252	90FT14	23	*	1	8.6	0.26	1	13 tab
5123	TI501T	21	*	20	8.7	0.24	1	13 tab
5124	TI502T	21	*	20	8.7	0.25	1	13 tab
5125	TI503T	23	*	20	8.7	0.27	1	13 tab
5126	TI509T	15	0.5	60	8.7	0.18	53,275	13 tab
5127	TI507T	15	0.5	60	8.7	0.18	114,090	13 tab
5128	TI505T	15	0.5	60	8.7	0.18	523,634	13 tab
5129	TI508T	14	0.5	80	8.7	0.16	1,308,671	13 tab
5130	TI504T	14	0.5	80	8.7	0.16	1,665,220	13 tab
5131	TI506T	14	0.5	80	8.7	0.16	9,806,694	13 tab
5132	TI514T	10	0.5	80	8.7	0.15	31,443,023	13 tab
5253	TI515T	10	0.5	80	8.7	0.15	34,693,646	13 tab
5133	TI513T	11	0.5	80	8.7	0.15	50,666,199	13 tab
5134	TCH1T	18	*	20	8.8	0.21	1	13 tab
5135	TCH2T	19	*	20	8.8	0.19	1	13 tab
5136	TCH3T	17	*	20	8.8	0.19	1	13 tab
5254	90FT16	21	*	5	8.8	0.24	1	13 tab
5255	90FT17	19	*	5	8.8	0.22	1	13 tab
5256	90FTC1	23	*	5	9.27	0.25	1	13 tab
5137	TCH12T	8	-1	20	8.8	0.09	45,172	13 tab
5138	TCH12T	8	-1	30	8.8	0.09	151,465	13 tab
5139	TCH10T	8	-1	30	8.8	0.09	794,513	13 tab
5140	TCH14T	7	-1	60	8.8	0.08	47,385	13 tab
5141	TCH13T	7	-1	60	8.8	0.08	1,043,369	13 tab

TEST & SAMPLE ID #		MAX. STRESS MPa	R	Q Hz	E GPa	e %	CYCLES TO FAIL	WIDTH (mm) and Notes
5142	TCH16T	7	-1	60	8.8	0.08	3,009,395	13 tab
5143	TCH7T	7	-1	60	8.8	0.08	3,973,407	13 tab
5144	TCH15T	6	-1	80	8.8	0.07	11,733,016	13 tab
5145	TCH19T	6	-1	100	8.8	0.07	100,151,319	13 R tab

FIBERGLASS PREPREG (3M - 250E) MATERIALS

MATERIAL PP

Lay-up = $[0]_{15}$, V_F = 0.56, Ave. thickness = 1.65 mm, S.D. = 0.03 mm, 3M-SP250E prepreg, Epoxy

TEST & SAMPLE ID #		MAX. STRESS MPa	R	Q Hz	E GPa	e %	CYCLES TO FAIL	WIDTH (mm) and Notes
3480	PP112	1,251	*	13	44.0	2.60	1	25
3481	PP114	1,279	*	13	49.0	2.70	1	25
3482	PP115	1,332	*	13	51.6	2.70	1	25
3483	PP116	758	0.1	4	52.0	1.52	4,545	25
3484	PP101	758	0.1	2	46.5	1.68	7,252	25
3485	PP117	758	0.1	2	46.0	1.65	4,825	25
3486	PP104	414	0.1	12	47.4	0.84	839,263	25
3487	PP118	414	0.1	12	48.7	0.83	491,518	25
3488	PP105	414	0.1	12	42.5	0.92	631,118	25
3489	PP111	620	0.1	4	43.0	1.40	11,696	25
3490	PP113	621	0.1	4	50.5	1.27	13,690	25
3491	PP110	620	0.1	4	44.3	1.36	26,209	25
3492	PP107	517	0.1	8	45.6	1.09	88,979	25
3493	PP104	517	0.1	8	----	----	125,521	25
3494	PP103	517	0.1	8	----	----	56,119	25
3495	PP102	517	0.1	10	45.9	1.14	124,781	25 tab
3496	PP106	621	0.1	4	47.6	----	17,314	25
3497	PP108	414	0.1	12	----	----	269,211	25
3844	PP131	-829	*	13	----	----	1	25 Z
3845	PP126	-842	*	13	----	----	1	25 Z
3846	PP136	-694	*	13	----	----	1	25 Z

MATERIAL PP45

Lay-up = $[(\pm 45)_2]_S$, V_F = 0.54, Ave. thickness = 1.65 mm, S.D. = 0.04 mm, 3M-SP250E prepreg, Epoxy

3503	PP45201	153	*	13	16.0	----	1	25
3504	PP45210	153	*	13	18.0	1.55	1	25
3505	PP45209	158	*	13	17.7	----	1	25
3506	PP45208	83	0.1	10	18.6	0.55	27,509	25
3507	PP45207	83	0.1	10	20.0	0.52	45,091	25
3508	PP45203	83	0.1	10	18.2	0.56	19,125	25
3509	PP45206	69	0.1	15	18.9	0.40	473,337	25
3510	PP45205	69	0.1	20	15.7	0.51	209,295	25
3511	PP45204	69	0.1	20	18.6	0.43	402,619	25
3512	PP45202	103	0.1	2	17.4	0.86	737	25
3847	PP45212	-160	*	13	----	----	1	25

MATERIAL PPDD5

Lay-up = $[(0)_3/\pm 45/(0)_3]_S$, V_F = 0.56, Ave. thickness = 3.31 mm, S.D. = 0.09 mm, 3M-SP250E prepreg, Epoxy

3658	PPDD5118	634	*	13	39.2	----	1	15
3659	PPDD5119	839	*	13	41.6	----	1	15

TEST & SAMPLE ID #		MAX. STRESS MPa	R	Q Hz	E GPa	e %	CYCLES TO FAIL	WIDTH (mm) and Notes
3660	PPDD5120	616	*	13	38.0	----	1	15
Problems with the previous static tests caused the following gage lengths widths to be heavily reduced.								
3662	PPDD5104	1,115	*	13	----	----	1	6
3663	PPDD5106	1,070	*	13	----	----	1	6
3664	PPDD5110	1,080	*	13	----	----	1	6
3665	PPDD5112	483	0.1	12	----	----	33,888	6
3666	PPDD5109	345	0.1	12	----	----	633,893	6
3667	PPDD5114	345	0.1	12	----	----	408,106	6
3668	PPDD5111	345	0.1	12	----	----	320,402	6
3669	PPDD5117	414	0.1	10	----	----	66,207	6
3670	PPDD5116	621	0.1	2	----	----	3,119	6
3671	PPDD5115	621	0.1	2	----	----	4,786	6
3672	PPDD5101	621	0.1	2	----	----	2,517	6
3708	PPDD5108	483	0.1	10	----	----	62,141	6
3709	PPDD5105	483	0.1	5	----	----	32,975	6
3969	PPDD5200	-716	*	13	----	----	1	25
3970	PPDD5202	-893	*	13	----	----	1	25
3971	PPDD5201	-779	*	13	----	----	1	25

GLASS CARBON HYBRIDS

MATERIAL DD23

Lay-up = $[0_2/\pm45/0/0^*]_S$, 0* - AS4-6K Carbon (TPI STYLE 4416), 220 g/m^2 , V_F = 0.45, Ave. thickness = 3.65 mm, S.D. = 0.11 mm, CoRezyn 63-AX-051 Polyester.

4077	DD23105	649	*	13	27.8	----	1	25 tab
4078	DD23106	276	0.1	10	28.9	0.96	1,681,606	25 tab
4079	DD23111	622	*	13	28.1	----	1	25 tab
4080	DD23107	685	*	13	27.1	----	1	25 tab
4081	DD23104	414	0.1	2	26.3	1.65	2,803	25 tab
4082	DD23110	634	*	13	27.9	----	1	25 tab
4083	DD23102	414	0.1	2	25.1	1.68	451	25 tab
4084	DD23103	345	0.1	4	28.6	1.17	295,281	25 tab
4085	DD23109	345	0.1	5	25.8	1.14	197,270	25 tab
4086	DD23108	647	*	0.1	26.1	----	1	25 tab
4087	DD23112	310	0.1	5	28.1	1.12	526,418	25 tab
4088	DD23101	310	0.1	10	26.6	1.08	493,197	25 tab
4101	DD23122	379	0.1	4	27.1	1.47	14,350	25 tab
4102	DD23121	379	0.1	4	28.0	1.37	22,335	25 tab
4103	DD23120	345	0.1	4	28.9	1.17	119,009	25 tab
4104	DD23119	379	0.1	2	27.6	1.42	4,324	25 tab
4214	DD23143	-467	*	13	----	----	1	25
4215	DD23142	-498	*	13	----	----	1	25
4216	DD23141	-505	*	13	----	----	1	25
4217	DD23140	-504	*	13	----	----	1	25

TEST & SAMPLE ID #		MAX. STRESS MPa	R	Q Hz	E GPa	e %	CYCLES TO FAIL	WIDTH (mm) and Notes
MATERIAL CG								
Lay-up = $[0_2/0_{2C}/0/0_{2C}/0_2]$,Glass = D155, C = AS4-6K Carbon (TPI STYLE 4416), 220g/m^2, V_F = 0.56, Ave. thickness = 2.66 mm, S.D. = 0.06 mm, CoRezyn 63-AX-051 Polyester								
4089	CG110	934	*	13	72.5	----	1	25 tab
4090	CG106	861	*	13	65.5	----	1	25 tab
4091	CG104	414	0.1	12	65.8	0.59	1,368,362	25 tab
4092	CG109	552	0.1	8	63.7	0.79	141,368	25 tab
4093	CG101	552	0.1	9	68.3	0.89	55,233	25 tab
4094	CG112	483	0.1	10	61.4	0.73	253,069	25 tab
4095	CG108	552	0.1	5	64.4	0.81	109,701	25 tab
4096	CG105	414	0.1	12	71.4	0.56	1,900,285	25 tab
4097	CG107	690	0.1	2	62.4	1.02	1,969	25 tab
4098	CG111	690	0.1	2	64.8	0.94	13,577	25 tab
4099	CG113	690	0.1	2	62.0	1.04	10,770	25 tab
4100	CG103	965	*	13	63.5	63.5	1	25 tab
MATERIAL CA								
Lay-up = $(0)_{12}$, AS4-6K Carbon (TPI STYLE 4416), 220g/m^2, V_F = 0.48, Ave. thickness = 2.82 mm, S.D. = 0.24 mm, CoRezyn 63-AX-051 Polyester								
4105	CA113	1504	*	13	112	1.34	1	18 tab
4106	CA109	1666	*	13	112	1.49	1	18 tab
4107	CA111	1364	*	13	118	1.15	1	18 tab
4108	CA110	1207	0.1	1	154	0.90	9	18 tab
4109	CA112	1034	0.1	5	112	0.82	28,497	18 tab
4110	CA108	862	0.1	12	112	0.70	1,030,350	18 tab
4111	CA106	862	0.1	12	118	0.68	77,101	18 R tab
4112	CA107	862	0.1	10	113	0.70	2,364,140	18 tab

GLASS ROVING TESTS

D155 STRAND TESTS

Owens Corning Fabrics roving number E-450-PVE, Catalog Number OC107B-AC-450, OC111A-AB-450, 2000 fibers (average fiber diameter = 15.98 µm, standard deviation = 1.53 µm, maximum = 19.4 µm, minimum = 12.5 µm, sample size = 14,000) The following six D155 fabric rolls were obtained over the time period of 1993 to 1999.

TEST & SAMPLE ID #		MAX. Load N	R	Q Hz	E GPa	e %	CYCLES TO FAIL	WIDTH (mm) and Notes
D155 Roll 1								
3739	D155TA1	1054	*	13	---	--	1	tow
3740	D155TA2	1061	*	13	---	--	1	tow
3741	D155TA3	993	*	13	---	--	1	tow
3742	D155TA4	940	*	13	---	--	1	tow
3743	D155TA5	1015	*	13	---	--	1	tow
3744	D155TA6	967	*	13	---	--	1	tow
3745	D155TA7	973	*	13	---	--	1	tow
3746	D155TA8	1014	*	13	---	--	1	tow
3747	D155TA9	987	*	13	---	--	1	tow
3748	D155TA10	1054	*	13	---	--	1	tow
3749	D155TA11	1019	*	13	---	--	1	tow
3750	D155TA12	1084	*	13	---	--	1	tow
3751	D155TA13	970	*	13	---	--	1	tow
3752	D155TA14	1084	*	13	---	--	1	tow
3753	D155TA15	975	*	13	---	--	1	tow
3754	D155TA16	1064	*	13	---	--	1	tow
3755	D155TA17	982	*	13	---	--	1	tow
3756	D155TA18	999	*	13	---	--	1	tow
3757	D155TA19	1015	*	13	---	--	1	tow
3758	D155TA20	981	*	13	---	--	1	tow
3759	D155TA21	1012	*	13	---	--	1	tow
3760	D155TA22	1040	*	13	---	--	1	tow
3761	D155TA23	1081	*	13	---	--	1	tow
3762	D155TA24	1036	*	13	---	--	1	tow
3763	D155TA25	1010	*	13	---	--	1	tow
3764	D155TA26	912	*	13	---	--	1	tow
3765	D155TA27	922	*	13	---	--	1	tow
3766	D155TA28	1051	*	13	---	--	1	tow
3767	D155TA29	991	*	13	---	--	1	tow
3768	D155TA30	995	*	13	---	--	1	tow
D155 Roll 2								
3769	D155TB1	1401	*	13	---	--	1	tow
3770	D155TB2	1310	*	13	---	--	1	tow

TEST & SAMPLE ID #		MAX. Load N	R	Q Hz	E GPa	e %	CYCLES TO FAIL	WIDTH (mm) and Notes
3771	D155TB3	1431	*	13	---	--	1	tow
3772	D155TB4	1403	*	13	---	--	1	tow
3773	D155TB5	1380	*	13	---	--	1	tow
3774	D155TB6	1347	*	13	---	--	1	tow
3775	D155TB7	1398	*	13	---	--	1	tow
3776	D155TB8	1361	*	13	---	--	1	tow
3777	D155TB9	1386	*	13	---	--	1	tow
3778	D155TB10	1362	*	13	---	--	1	tow
3779	D155TB11	1339	*	13	---	--	1	tow
3780	D155TB12	1413	*	13	---	--	1	tow
3781	D155TB13	1352	*	13	---	--	1	tow
3782	D155TB14	1366	*	13	---	--	1	tow
3783	D155TB15	1459	*	13	---	--	1	tow
3784	D155TB16	1412	*	13	---	--	1	tow
3785	D155TB17	1279	*	13	---	--	1	tow
3786	D155TB18	1381	*	13	---	--	1	tow
3787	D155TB19	1416	*	13	---	--	1	tow
3788	D155TB20	1420	*	13	---	--	1	tow
3789	D155TB21	1322	*	13	---	--	1	tow
3790	D155TB22	1263	*	13	---	--	1	tow
3791	D155TB23	1353	*	13	---	--	1	tow
3792	D155TB24	1446	*	13	---	--	1	tow
3793	D155TB25	1411	*	13	---	--	1	tow
3794	D155TB26	1310	*	13	---	--	1	tow
3795	D155TB27	1378	*	13	---	--	1	tow
3796	D155TB28	1372	*	13	---	--	1	tow
3797	D155TB29	1349	*	13	---	--	1	tow
3798	D155TB30	1319	*	13	---	--	1	tow
D155 Roll 3								
3799	D155TC1	1419	*	13	---	--	1	tow
3800	D155TC2	1256	*	13	---	--	1	tow
3801	D155TC3	1356	*	13	---	--	1	tow
3802	D155TC4	1375	*	13	---	--	1	tow
3803	D155TC5	1322	*	13	---	--	1	tow
3804	D155TC6	1410	*	13	---	--	1	tow
3805	D155TC7	1407	*	13	---	--	1	tow
3806	D155TC8	1392	*	13	---	--	1	tow
3807	D155TC9	1467	*	13	---	--	1	tow
3808	D155TC10	1456	*	13	---	--	1	tow
3809	D155TC11	1444	*	13	---	--	1	tow
3810	D155TC12	1367	*	13	---	--	1	tow
3811	D155TC13	1399	*	13	---	--	1	tow
3812	D155TC14	1336	*	13	---	--	1	tow
3813	D155TC15	1429	*	13	---	--	1	tow
3814	D155TC16	1326	*	13	---	--	1	tow
3815	D155TC17	1404	*	13	---	--	1	tow

TEST & SAMPLE ID #		MAX. Load N	R	Q Hz	E GPa	e %	CYCLES TO FAIL	WIDTH (mm) and Notes
3816	D155TC18	1353	*	13	---	--	1	tow
3817	D155TC19	1456	*	13	---	--	1	tow
3818	D155TC20	1336	*	13	---	--	1	tow
3819	D155TC21	1366	*	13	---	--	1	tow
3820	D155TC22	1379	*	13	---	--	1	tow
3821	D155TC23	1325	*	13	---	--	1	tow
3822	D155TC24	1250	*	13	---	--	1	tow
3823	D155TC25	1358	*	13	---	--	1	tow
3824	D155TC26	1401	*	13	---	--	1	tow
3825	D155TC27	1345	*	13	---	--	1	tow
3826	D155TC28	1387	*	13	---	--	1	tow
3827	D155TC29	1428	*	13	---	--	1	tow
3828	D155TC30	1350	*	13	---	--	1	tow

D155 Roll 4

4474	D155TD1	1117	*	13	---	--	1	tow
4475	D155TD2	1096	*	13	---	--	1	tow
4476	D155TD3	1123	*	13	---	--	1	tow
4477	D155TD4	1089	*	13	---	--	1	tow
4478	D155TD5	1078	*	13	---	--	1	tow
4479	D155TD6	1077	*	13	---	--	1	tow
4480	D155TD7	1075	*	13	---	--	1	tow
4481	D155TD8	1119	*	13	---	--	1	tow
4482	D155TD9	1108	*	13	---	--	1	tow
4483	D155TD10	1170	*	13	---	--	1	tow
4484	D155TD11	534	0.1	10	---	--	603,854	tow
4485	D155TD12	534	0.1	10	---	--	900,234	tow
4486	D155TD13	534	0.1	10	---	--	470,103	tow
4487	D155TD14	534	0.1	10	---	--	1,503,261	tow
4488	D155TD15	534	0.1	10	---	--	852,853	tow
4489	D155TD16	667	0.1	5	---	--	101,867	tow
4490	D155TD17	667	0.1	5	---	--	15,456	tow
4491	D155TD18	667	0.1	5	---	--	10,218	tow
4492	D155TD19	667	0.1	5	---	--	10,426	tow
4493	D155TD20	667	0.1	5	---	--	20,883	tow
4494	D155TD21	667	0.1	5	---	--	59,688	tow
4495	D155TD22	445	0.1	20	---	--	4,002,694	tow
4496	D155TD23	445	0.1	20	---	--	6,168,942	tow
4497	D155TD24	445	0.1	20	---	--	2,727,395	tow
4498	D155TD25	445	0.1	20	---	--	5,748,860	tow
4499	D155TD26	445	0.1	20	---	--	3,634,752	tow
4500	D155TD27	356	0.1	50	---	--	41,981,341	tow
4501	D155TD28	356	0.1	50	---	--	23,548,030	tow
4502	D155TD29	356	0.1	50	---	--	67,748,394	tow
4503	D155TD30	356	0.1	50	---	--	71,247,839	tow
4504	D155TD31	356	0.1	50	---	--	12,245,917	tow
4505	D155TD32	311	0.1	80	---	--	169,484,151	tow

TEST & SAMPLE ID #		MAX. Load N	R	Q Hz	E GPa	e %	CYCLES TO FAIL	WIDTH (mm) and Notes
4506	D155TD33	311	0.1	80	---	--	254,226,085	tow
4507	D155TD34	311	0.1	80	---	--	382,095,430	tow
4508	D155TD35	311	0.1	80	---	--	180,760,560	tow
4509	D155TD36	311	0.1	80	---	--	671,734,540	tow
4563	D155TD37	778	0.1	2	---	--	526	tow
4564	D155TD38	778	0.1	2	---	--	375	tow
4565	D155TD39	778	0.1	2	---	--	160	tow
4567	D155TD40	778	0.1	2	---	--	433	tow
4568	D155TD41	778	0.1	2	---	--	544	tow
D155 Roll 4B								
4640	D155TD42	1212	*	13	---	--	1	tow
4641	D155TD43	1287	*	13	---	--	1	tow
4642	D155TD44	1278	*	13	---	--	1	tow
4643	D155TD45	1187	*	13	---	--	1	tow
4644	D155TD46	1187	*	13	---	--	1	tow
4645	D155TD47	1195	*	13	---	--	1	tow
4646	D155TD48	1212	*	13	---	--	1	tow
4647	D155TD49	1212	*	13	---	--	1	tow
4648	D155TD50	1187	*	13	---	--	1	tow
4649	D155TD51	1295	*	13	---	--	1	tow
4650	D155TD52	1183	*	13	---	--	1	tow
4651	D155TD53	1195	*	13	---	--	1	tow
4652	D155TD54	1241	*	13	---	--	1	tow
4653	D155TD55	1095	*	13	---	--	1	tow
4654	D155TD56	1183	*	13	---	--	1	tow
4655	D155TD57	1145	*	13	---	--	1	tow
4656	D155TD58	1187	*	13	---	--	1	tow
4657	D155TD59	1053	*	13	---	--	1	tow
4658	D155TD60	1087	*	13	---	--	1	tow
4659	D155TD61	1303	*	13	---	--	1	tow
4660	D155TD62	1204	*	13	---	--	1	tow
4661	D155TD63	1212	*	13	---	--	1	tow
4662	D155TD64	1145	*	13	---	--	1	tow
4663	D155TD65	1062	*	13	---	--	1	tow
4664	D155TD66	1157	*	13	---	--	1	tow
4665	D155TD67	1287	*	13	---	--	1	tow
4666	D155TD68	1250	*	13	---	--	1	tow
4667	D155TD69	1129	*	13	---	--	1	tow
4668	D155TD70	1274	*	13	---	--	1	tow
4669	D155TD71	1254	*	13	---	--	1	tow
D155 Roll 5								
4510	D155TE551	1220	*	13	---	--	1	tow
4511	D155TE546	1208	*	13	---	--	1	tow
4512	D155TE515	1205	*	13	---	--	1	tow

TEST & SAMPLE ID #		MAX. Load N	R	Q Hz	E GPa	e %	CYCLES TO FAIL	WIDTH (mm) and Notes
4513	D155TE527	1182	*	13	---	--	1	tow
4514	D155TE547	1193	*	13	---	--	1	tow
4515	D155TE516	1161	*	13	---	--	1	tow
4516	D155TE564	1181	*	13	---	--	1	tow
4517	D155TE555	1143	*	13	---	--	1	tow
4518	D155TE572	1157	*	13	---	--	1	tow
4519	D155TE548	1122	*	13	---	--	1	tow
4520	D155TE549	1246	*	13	---	--	1	tow
4521	D155TE566	1203	*	13	---	--	1	tow
4522	D155TE556	1276	*	13	---	--	1	tow
4523	D155TE559	1205	*	13	---	--	1	tow
4524	D155TE517	1164	*	13	---	--	1	tow
4525	D155TE534	1233	*	13	---	--	1	tow
4526	D155TE538	1124	*	13	---	--	1	tow
4527	D155TE532	1162	*	13	---	--	1	tow
4528	D155TE520	1142	*	13	---	--	1	tow
4529	D155TE550	1171	*	13	---	--	1	tow
4530	D155TE557	1193	*	13	---	--	1	tow
4531	D155TE563	1264	*	13	---	--	1	tow
4532	D155TE539	1090	*	13	---	--	1	tow
4533	D155TE567	1128	*	13	---	--	1	tow
4534	D155TE554	1139	*	13	---	--	1	tow
4535	D155TE569	1146	*	13	---	--	1	tow
4536	D155TE558	1195	*	13	---	--	1	tow
4537	D155TE576	1249	*	13	---	--	1	tow
4538	D155TE570	1151	*	13	---	--	1	tow
4539	D155TE571	1201	*	13	---	--	1	tow
4540	D155TE553	778	0.1	5	---	--	11,640	tow
4541	D155TE552	778	0.1	5	---	--	2,983	tow
4542	D155TE518	778	0.1	5	---	--	4,596	tow
4543	D155TE561	778	0.1	5	---	--	3,678	tow
4544	D155TE562	778	0.1	5	---	--	4,817	tow
4546	D155TE509	667	0.1	5	---	--	30,953	tow
4547	D155TE505	667	0.1	5	---	--	10,943	tow
4548	D155TE512	667	0.1	5	---	--	19,520	tow
4549	D155TE511	667	0.1	5	---	--	10,173	tow
4550	D155TE510	667	0.1	5	---	--	14,350	tow
4551	D155TE531	534	0.1	10	---	--	858,810	tow
4552	D155TE542	534	0.1	10	---	--	159,944	tow
4553	D155TE541	534	0.1	10	---	--	254,240	tow
4554	D155TE525	534	0.1	10	---	--	386,380	tow
4555	D155TE533	534	0.1	10	---	--	235,364	tow
4556	D155TE514	534	0.1	10	---	--	525,623	tow
4557	D155TE591	445	0.1	20	---	--	3,218,504	tow
4558	D155TE592	445	0.1	20	---	--	3,924,363	tow
4559	D155TE596	445	0.1	20	---	--	2,319,792	tow
4560	D155TE593	445	0.1	20	---	--	6,759,244	tow
4561	D155TE597	445	0.1	20	---	--	2,535,198	tow
4562	D155TE598	445	0.1	20	---	--	4,468,170	tow

TEST & SAMPLE ID #		MAX. Load N	R	Q Hz	E GPa	e %	CYCLES TO FAIL	WIDTH (mm) and Notes
D155 Roll 5B								
4670	D155TE99	1412	*	13	---	--	1	tow
4671	D155TE100	1408	*	13	---	--	1	tow
4672	D155TE101	1462	*	13	---	--	1	tow
4673	D155TE102	1362	*	13	---	--	1	tow
4674	D155TE103	1391	*	13	---	--	1	tow
4675	D155TE104	1454	*	13	---	--	1	tow
4676	D155TE105	1462	*	13	---	--	1	tow
4677	D155TE106	1420	*	13	---	--	1	tow
4678	D155TE107	1437	*	13	---	--	1	tow
4679	D155TE108	1375	*	13	---	--	1	tow
4680	D155TE109	1475	*	13	---	--	1	tow
4681	D155TE110	1350	*	13	---	--	1	tow
4682	D155TE111	1337	*	13	---	--	1	tow
4683	D155TE112	1370	*	13	---	--	1	tow
4684	D155TE113	1375	*	13	---	--	1	tow
4685	D155TE114	1445	*	13	---	--	1	tow
4686	D155TE115	1342	*	13	---	--	1	tow
4687	D155TE116	1356	*	13	---	--	1	tow
4688	D155TE117	1387	*	13	---	--	1	tow
4689	D155TE118	1475	*	13	---	--	1	tow
4690	D155TE119	1429	*	13	---	--	1	tow
4691	D155TE120	1417	*	13	---	--	1	tow
4692	D155TE121	1387	*	13	---	--	1	tow
4693	D155TE122	1371	*	13	---	--	1	tow
4694	D155TE123	1446	*	13	---	--	1	tow
4695	D155TE124	1404	*	13	---	--	1	tow
4696	D155TE125	1362	*	13	---	--	1	tow
4697	D155TE126	1342	*	13	---	--	1	tow
4698	D155TE127	1471	*	13	---	--	1	tow
4699	D155TE128	1396	*	13	---	--	1	tow
D155 Roll 6								
4700	D155TF1	1195	*	13	---	--	1	tow
4701	D155TF2	1262	*	13	---	--	1	tow
4702	D155TF3	1171	*	13	---	--	1	tow
4702	D155TF4	1171	*	13	---	--	1	tow
4703	D155TF5	1321	*	13	---	--	1	tow
4704	D155TF6	1237	*	13	---	--	1	tow
4705	D155TF7	1171	*	13	---	--	1	tow
4706	D155TF8	1204	*	13	---	--	1	tow
4707	D155TF9	1208	*	13	---	--	1	tow
4708	D155TF10	1154	*	13	---	--	1	tow
4709	D155TF11	1287	*	13	---	--	1	tow
4710	D155TF12	1188	*	13	---	--	1	tow
4711	D155TF13	1197	*	13	---	--	1	tow

TEST & SAMPLE ID #		MAX. Load N	R	Q Hz	E GPa	e %	CYCLES TO FAIL	WIDTH (mm) and Notes
4712	D155TF14	1171	*	13	---	--	1	tow
4713	D155TF15	1229	*	13	---	--	1	tow
4714	D155TF16	1208	*	13	---	--	1	tow
4715	D155TF17	1213	*	13	---	--	1	tow
4716	D155TF18	1229	*	13	---	--	1	tow
4717	D155TF19	1146	*	13	---	--	1	tow
4718	D155TF20	1204	*	13	---	--	1	tow
4719	D155TF21	1262	*	13	---	--	1	tow
4720	D155TF22	1183	*	13	---	--	1	tow
4721	D155TF23	1487	*	13	---	--	1	tow
4722	D155TF24	1296	*	13	---	--	1	tow
4723	D155TF25	1137	*	13	---	--	1	tow
4724	D155TF26	1204	*	13	---	--	1	tow
4725	D155TF27	1271	*	13	---	--	1	tow
4726	D155TF28	1314	*	13	---	--	1	tow
4727	D155TF29	1246	*	13	---	--	1	tow
4728	D155TF30	1246	*	13	---	--	1	tow

D155 Roll 6B

4729	D155TF31	1404	*	13	---	--	1	tow
4730	D155TF32	1262	*	13	---	--	1	tow
4731	D155TF33	1221	*	13	---	--	1	tow
4732	D155TF34	1350	*	13	---	--	1	tow
4733	D155TF35	1179	*	13	---	--	1	tow
4734	D155TF36	1146	*	13	---	--	1	tow
4735	D155TF37	1338	*	13	---	--	1	tow
4736	D155TF38	1221	*	13	---	--	1	tow
4737	D155TF39	1262	*	13	---	--	1	tow
4738	D155TF40	1362	*	13	---	--	1	tow
4739	D155TF41	1254	*	13	---	--	1	tow
4740	D155TF42	1396	*	13	---	--	1	tow
4741	D155TF43	1313	*	13	---	--	1	tow
4742	D155TF44	1346	*	13	---	--	1	tow
4743	D155TF45	1387	*	13	---	--	1	tow
4744	D155TF46	1279	*	13	---	--	1	tow
4745	D155TF47	1287	*	13	---	--	1	tow
4746	D155TF48	1362	*	13	---	--	1	tow
4747	D155TF49	1096	*	13	---	--	1	tow
4748	D155TF50	1296	*	13	---	--	1	tow
4749	D155TF51	1246	*	13	---	--	1	tow
4750	D155TF52	1304	*	13	---	--	1	tow
4751	D155TF53	1287	*	13	---	--	1	tow
4752	D155TF54	1304	*	13	---	--	1	tow
4753	D155TF55	1237	*	13	---	--	1	tow
4754	D155TF56	1267	*	13	---	--	1	tow
4755	D155TF57	1304	*	13	---	--	1	tow
4756	D155TF58	1338	*	13	---	--	1	tow

TEST & SAMPLE ID #		MAX. Load N	R	Q Hz	E GPa	e %	CYCLES TO FAIL	WIDTH (mm) and Notes
4757	D155TF59	1304	*	13	---	--	1	tow
4758	D155TF60	1262	*	13	---	--	1	tow

D155 Roll 6C

4800	D155TF61	1393	*	13	---	--	1	tow
4801	D155TF62	1260	*	13	---	--	1	tow
4802	D155TF63	1268	*	13	---	--	1	tow
4803	D155TF64	1410	*	13	---	--	1	tow
4804	D155TF65	1385	*	13	---	--	1	tow
4805	D155TF66	1443	*	13	---	--	1	tow
4806	D155TF67	1402	*	13	---	--	1	tow
4807	D155TF68	1260	*	13	---	--	1	tow
4808	D155TF69	1318	*	13	---	--	1	tow
4809	D155TF70	1310	*	13	---	--	1	tow
4810	D155TF71	1314	*	13	---	--	1	tow
4811	D155TF72	1331	*	13	---	--	1	tow
4812	D155TF73	1277	*	13	---	--	1	tow
4813	D155TF74	1302	*	13	---	--	1	tow
4814	D155TF75	1393	*	13	---	--	1	tow
4815	D155TF76	1064	*	13	---	--	1	tow
4816	D155TF77	1210	*	13	---	--	1	tow
4817	D155TF78	1293	*	13	---	--	1	tow
4818	D155TF79	1314	*	13	---	--	1	tow
4819	D155TF80	1310	*	13	---	--	1	tow
4820	D155TF81	1427	*	13	---	--	1	tow
4821	D155TF82	1306	*	13	---	--	1	tow
4822	D155TF83	1277	*	13	---	--	1	tow
4823	D155TF84	1343	*	13	---	--	1	tow
4824	D155TF85	1368	*	13	---	--	1	tow
4825	D155TF86	1268	*	13	---	--	1	tow
4826	D155TF87	1335	*	13	---	--	1	tow
4827	D155TF88	1331	*	13	---	--	1	tow
4828	D155TF89	1352	*	13	---	--	1	tow
4829	D155TF90	1310	*	13	---	--	1	tow

D155 Roll 6D

4830	D155TF91	1168	*	13	---	--	1	tow
4831	D155TF92	1368	*	13	---	--	1	tow
4832	D155TF93	1389	*	13	---	--	1	tow
4833	D155TF94	1298	*	13	---	--	1	tow
4834	D155TF95	1285	*	13	---	--	1	tow
4835	D155TF96	1364	*	13	---	--	1	tow
4836	D155TF97	1318	*	13	---	--	1	tow
4837	D155TF98	1310	*	13	---	--	1	tow
4838	D155TF99	1326	*	13	---	--	1	tow
4839	D155TF100	1343	*	13	---	--	1	tow

TEST & SAMPLE ID #		MAX. Load N	R	Q Hz	E GPa	e %	CYCLES TO FAIL	WIDTH (mm) and Notes
4840	D155TF101	1310	*	13	---	--	1	tow
4841	D155TF102	1410	*	13	---	--	1	tow
4842	D155TF103	1343	*	13	---	--	1	tow
4842	D155TF104	1335	*	13	---	--	1	tow
4843	D155TF105	1210	*	13	---	--	1	tow
4844	D155TF106	1160	*	13	---	--	1	tow
4845	D155TF107	1385	*	13	---	--	1	tow
4846	D155TF108	1110	*	13	---	--	1	tow
4847	D155TF109	1352	*	13	---	--	1	tow
4848	D155TF110	1298	*	13	---	--	1	tow
4849	D155TF111	1343	*	13	---	--	1	tow
4850	D155TF112	1352	*	13	---	--	1	tow
4851	D155TF113	1318	*	13	---	--	1	tow
4852	D155TF114	1352	*	13	---	--	1	tow
4853	D155TF115	1335	*	13	---	--	1	tow
4854	D155TF116	1356	*	13	---	--	1	tow
4855	D155TF117	1285	*	13	---	--	1	tow
4856	D155TF118	1293	*	13	---	--	1	tow
4857	D155TF119	1243	*	13	---	--	1	tow
4858	D155TF120	1335	*	13	---	--	1	tow

DB120

Owens Corning Fabrics Roving number E-1200-PVE, catalog number OC-380-JC-451 (1200). (750 fibers)

DB120 Roll 5

4569	DB120TA1	370	*	13	---	--	1	tow
4570	DB120TA2	317	*	13	---	--	1	tow
4571	DB120TA3	374	*	13	---	--	1	tow
4572	DB120TA4	389	*	13	---	--	1	tow
4573	DB120TA5	396	*	13	---	--	1	tow
4574	DB120TA6	377	*	13	---	--	1	tow
4575	DB120TA7	284	*	13	---	--	1	tow
4576	DB120TA8	329	*	13	---	--	1	tow
4577	DB120TA9	310	*	13	---	--	1	tow
4578	DB120TA10	370	*	13	---	--	1	tow
4579	DB120TA11	378	*	13	---	--	1	tow
4580	DB120TA12	314	*	13	---	--	1	tow
4581	DB120TA13	304	*	13	---	--	1	tow
4582	DB120TA14	373	*	13	---	--	1	tow
4583	DB120TA15	348	*	13	---	--	1	tow
4584	DB120TA16	375	*	13	---	--	1	tow
4585	DB120TA17	344	*	13	---	--	1	tow
4586	DB120TA18	305	*	13	---	--	1	tow
4587	DB120TA19	371	*	13	---	--	1	tow
4588	DB120TA20	393	*	13	---	--	1	tow

TEST & SAMPLE ID #		MAX. Load N	R	Q Hz	E GPa	e %	CYCLES TO FAIL	WIDTH (mm) and Notes
4589	DB120TA21	351	*	13	---	--	1	tow
4590	DB120TA22	350	*	13	---	--	1	tow
4591	DB120TA23	332	*	13	---	--	1	tow
4592	DB120TA24	293	*	13	---	--	1	tow
4593	DB120TA25	387	*	13	---	--	1	tow
4594	DB120TA26	347	*	13	---	--	1	tow
4595	DB120TA27	358	*	13	---	--	1	tow
4596	DB120TA28	364	*	13	---	--	1	tow
4597	DB120TA29	307	*	13	---	--	1	tow
4598	DB120TA30	320	*	13	---	--	1	tow
4599	DB120TA31	403	*	13	---	--	1	tow
4600	DB120TA32	377	*	13	---	--	1	tow
4601	DB120TA33	346	*	13	---	--	1	tow
4602	DB120TA34	352	*	13	---	--	1	tow
4603	DB120TA35	377	*	13	---	--	1	tow
4604	DB120TA36	317	*	13	---	--	1	tow
4605	DB120TA37	376	*	13	---	--	1	tow
4606	DB120TA38	366	*	13	---	--	1	tow
4607	DB120TA39	319	*	13	---	--	1	tow
4608	DB120TA40	330	*	13	---	--	1	tow
4609	DB120TA41	351	*	13	---	--	1	tow
4610	DB120TA42	358	*	13	---	--	1	tow
4611	DB120TA43	376	*	13	---	--	1	tow
4612	DB120TA44	339	*	13	---	--	1	tow

Owens Corning 990-BC-2385-4093, 208 fiber strand

(Average fiber diameter = 10.71 µm, standard deviation = 0.94 µm, maximum = 13.96 µm, minimum = 8.33 µm, sample size = 1,820). The average area used for stress calculations was 0.004054 mm^2. A 45 fiber strand, impregnated with CoRezyn 63-AX-051, was manufactured from this strand. The gage length of these coupons were 25 ±5 mm. A special speaker cone based testing apparatus was used for these tests, see Reference 10.

TEST & SAMPLE ID #		MAX. Load grams	R	Q Hz	E GPa	e %	CYCLES TO FAIL	WIDTH (mm) and Notes
4900	STR63	1266	*	120	----	----	1	tow
4901	STR60	1506	*	120	----	----	1	tow
4902	STR54	1383	*	120	----	----	1	tow
4903	STR52	1181	*	120	----	----	1	tow
4904	STR40	1376	*	120	----	----	1	tow
4905	STR44	1687	*	120	----	----	1	tow
4906	STR33	1281	*	120	----	----	1	tow
4907	STR17	1367	*	120	----	----	1	tow
4908	STR14	1189	*	120	----	----	1	tow
4909	STR12	1126	*	120	----	----	1	tow
4910	STR10	1214	*	120	----	----	1	tow
4911	STR152	1349	*	120	----	----	1	tow
4912	STR141	1344	*	120	----	----	1	tow
4913	STR133	1300	*	120	----	----	1	tow
4914	STR122	1285	*	120	----	----	1	tow
4915	STR71	1192	*	120	----	----	1	tow
4916	STR102	1261	*	120	----	----	1	tow
4917	STR11	300	0.1	200	----	----	1,100,000,000	tow R
4918	STR16	500	0.1	80	----	----	3,151,637	tow
4919	STR13	500	0.1	80	----	----	521,416	tow
4920	STR19	500	0.1	80	----	----	1,887,512	tow
4921	STR61	500	0.1	80	----	----	10,590,546	tow
4922	STR34	500	0.1	80	----	----	660,762	tow
4923	STR43	500	0.1	80	----	----	2,970,613	tow
4924	STR51	500	0.1	80	----	----	6,271,853	tow
4925	STR32	500	0.1	80	----	----	1,163,044	tow
4926	STR64	500	0.1	80	----	----	2,371,532	tow
4927	STR42	500	0.1	80	----	----	23,198,205	tow
4928	STR50	500	0.1	80	----	----	877,701	tow
4929	STR31	500	0.1	80	----	----	1,867,185	tow
4930	STR53	400	0.1	100	----	----	21,256,335	tow
4931	STR41	400	0.1	100	----	----	541,168,069	tow
4932	STR154	700	0.1	50	----	----	28,026	tow
4933	STR150	700	0.1	50	----	----	117,135	tow
4934	STR153	700	0.1	50	----	----	87,956	tow
4935	STR143	700	0.1	50	----	----	820,108	tow
4936	STR121	700	0.1	50	----	----	37,208	tow
4937	STR130	700	0.1	50	----	----	119,137	tow
4938	STR151	700	0.1	50	----	----	834,738	tow
4939	STR72	700	0.1	50	----	----	446,679	tow
4940	STR120	700	0.1	50	----	----	174,072	tow

4941	STR132	700	0.1	50	----	----	204,871	tow
4942	STR144	700	0.1	50	----	----	154,706	tow
4943	STR123	700	0.1	50	----	----	14,218	tow
4944	STR140	600	0.1	100	----	----	2,313,678	tow
4945	STR84	600	0.1	100	----	----	4,138,791	tow
4946	STR83	600	0.1	100	----	----	3,185,311	tow
4947	STR131	600	0.1	100	----	----	2,564,971	tow
4948	STR94	600	0.1	100	----	----	19,248,908	tow
4949	STR30	400	0.1	120	----	----	1,000,000,000	tow R
4950	STR134	450	0.1	150	----	----	1,000,000,000	tow R
4951	STR142	1396	*	120	----	----	1	tow
4952	STR90	1284	*	120	----	----	1	tow
4953	STR70	1335	*	120	----	----	1	tow

RESIDUAL STRENGTH

(Covering Tests 5150 - 5234)

MATERIAL DD16A

Lay-up = $[90/0/\pm45/0]_S$, $V_F = 0.42$, Ave. thickness = 3.95 mm, S.D. = 0.08 mm, CoRezyn 63-AX-051 Polyester

TEST & SAMPLE ID #		MAX. STRESS MPa	R	Q Hz	E GPa	e %	CYCLES TO FAIL	WIDTH (mm) and Notes
Tests 5150 - 5188 were baseline static strength and fatigue tests								
5150	R59	661	*	13	----	----	1	8
5151	R27	658	*	13	----	----	1	8
5152	R26	657	*	13	----	----	1	8
5153	R16	701	*	13	----	----	1	8
5154	R102	685	*	13	----	----	1	8
5155	R61	686	*	13	----	----	1	8
5156	R120	658	*	13	----	----	1	8
5157	R121	678	*	13	----	----	1	8
5158	R122	683	*	13	----	----	1	8
5159	R123	691	*	13	----	----	1	8
5160	R124	625	*	13	----	----	1	8
5161	R125	675	*	13	----	----	1	8
5162	R42	684	*	13	----	----	1	8
5163	R74	673	*	13	----	----	1	8
5164	R56	705	*	13	----	----	1	8
5165	R71	674	*	13	----	----	1	8
5166	R110	664	*	13	----	----	1	8
5167	R111	665	*	13	----	----	1	8
5168	R21	665	*	13	----	----	1	8
5169	R11	680	*	13	----	----	1	8
5170	R35	207	0.1	10	----	----	192,780	8
5171	R58	207	0.1	10	----	----	636,742	8 R
5172	R22	207	0.1	10	----	----	1,694,879	8
5173	R57	207	0.1	10	----	----	961,214	8
5174	R44	276	0.1	6	----	----	38,152	8
5175	R23	241	0.1	8	----	----	104,645	8
5176	R13	241	0.1	8	----	----	256,923	8
5177	R46	241	0.1	8	----	----	169,108	8
5178	R7	241	0.1	8	----	----	236,617	8
5179	R48	241	0.1	8	----	----	176,479	8
5180	R50	241	0.1	8	----	----	149,778	8
5181	R43	241	0.1	8	----	----	325,439	8
5182	R41	241	0.1	8	----	----	78,445	8
5183	R64	241	0.1	8	----	----	52,320	8
5184	R68	241	0.1	8	----	----	67857	8
5185	R77	241	0.1	8	----	----	116,518	8
5186	R52	241	0.1	8	----	----	157,118	8
5187	R78	241	0.1	8	----	----	382,653	8
5188	R62	241	0.1	8	----	----	105,738	8

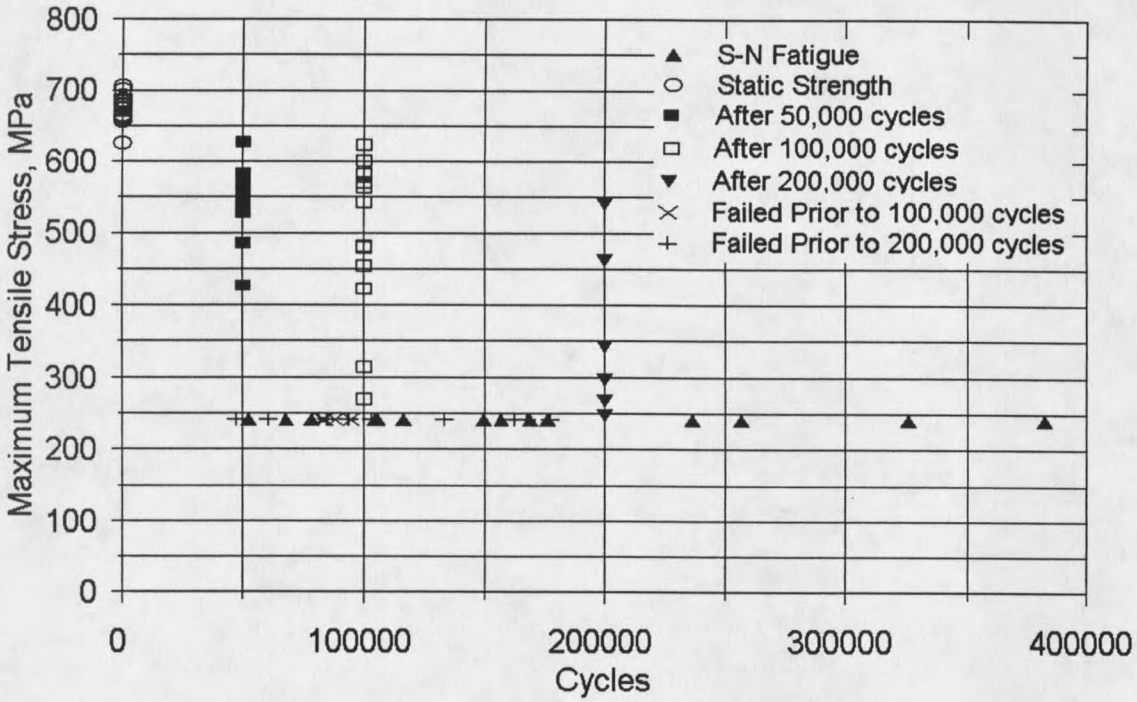
TEST & SAMPLE ID #		MAX. STRESS MPa	R	Q Hz	E GPa	e %	CYCLES TO FAIL	WIDTH (mm) and Notes

Test coupons were selected for three testing sequences: 50,000, 100,000 and 200,000 cycles at a maximum stress of 241 MPa (R = 0.1), after which the test coupon was statically tested for residual strength. Test coupons which failed prior to the completion of the designated number of cycles are listed, but should not be used in the baseline fatigue behavior due to sample biasing.

Tests 5189 - 5205, 100,000 cycles								
Tests 5189 - 5193 failed prior to completion of the 100,000 cycle sequence								
5189	R3	241	0.1	8	----	----	94,718	8 X
5190	R65	241	0.1	8	----	----	88,082	8 X
5191	R60	241	0.1	8	----	----	83,962	8 X
5192	R8	241	0.1	8	----	----	82,768	8 X
5193	R38	241	0.1	8	----	----	66,757	8 X
Tests 5194 - 5205 were cycled for 100,000 cycles at 241/24 MPa and then tested for residual strength								
5194	R5	241	0.1	8	----	----	100,000	8
	R5	602	*	13	----	----	1	8 RS
5195	R34	241	0.1	8	----	----	100,000	8
	R34	543	*	13	----	----	1	8 RS
5196	R101	241	0.1	8	----	----	100,000	8
	R101	583	*	13	----	----	1	8 RS
5197	R63	241	0.1	8	----	----	100,000	8
	R63	423	*	13	----	----	1	8 RS
5198	R29	241	0.1	8	----	----	100,000	8
	R29	482	*	13	----	----	1	8 RS
5199	R19	241	0.1	8	----	----	100,000	8
	R19	623	*	13	----	----	1	8 RS
5200	R6	241	0.1	8	----	----	100,000	8
	R6	563	*	13	----	----	1	8 RS
5201	R24	241	0.1	8	----	----	100,000	8
	R24	314	*	13	----	----	1	8 RS
5202	R39	241	0.1	8	----	----	100,000	8
	R39	571	*	13	----	----	1	8 RS
5203	R72	241	0.1	8	----	----	100,000	8
	R72	454	*	13	----	----	1	8 RS
5204	R45	241	0.1	8	----	----	100,000	8
	R45	480	*	13	----	----	1	8 RS
5205	R54	241	0.1	8	----	----	100,000	8
	R54	270	*	13	----	----	1	8 RS
Tests 5206 - 5217, 50,000 cycles								
5206	R12	241	0.1	8	----	----	50,000	8
	R12	485	*	13	----	----	1	8 RS
5207	R10	241	0.1	8	----	----	50,000	8
	R10	554	*	13	----	----	1	8 RS
5208	R20	241	0.1	8	----	----	50,000	8
	R20	628	*	13	----	----	1	8 RS
5209	R31	241	0.1	8	----	----	50,000	8
	R31	583	*	13	----	----	1	8 RS
5210	R67	241	0.1	8	----	----	50,000	8
	R67	427	*	13	----	----	1	8 RS

TEST & SAMPLE ID #		MAX. STRESS MPa	R	Q Hz	E GPa	e %	CYCLES TO FAIL	WIDTH (mm) and Notes
5211	R53	241	0.1	8	----	----	50,000	8
	R53	540	*	13	----	----	1	8 RS
5212	R28	241	0.1	8	----	----	50,000	8
	R28	568	*	13	----	----	1	8 RS
5213	R32	241	0.1	8	----	----	50,000	8
	R32	583	*	13	----	----	1	8 RS
5214	R37	241	0.1	8	----	----	50,000	8
	R37	582	*	13	----	----	1	8 RS
5215	R66	241	0.1	8	----	----	50,000	8
	R66	566	*	13	----	----	1	8 RS
5216	R117	241	0.1	8	----	----	50,000	8
	R117	529	*	13	----	----	1	8 RS
5217	R79	241	0.1	8	----	----	50,000	8
	R79	568	*	13	----	----	1	8 RS
Tests 5218 - 5234, 200,000 cycles								
Tests 5218 - 5228 failed prior to completion of the 200,000 cycle sequence								
5218	R17	241	0.1	8	----	----	162,465	8 X
5219	R47	241	0.1	8	----	----	47,182	8 X
5220	R25	241	0.1	8	----	----	177,640	8 X
5221	R55	241	0.1	8	----	----	93,300	8 X
5222	R9	241	0.1	8	----	----	84,703	8 X
5223	R36	241	0.1	8	----	----	168,069	8 X
5224	R15	241	0.1	8	----	----	93,877	8 X
5225	R75	241	0.1	8	----	----	113,114	8 X
5226	R40	241	0.1	8	----	----	60,592	8 X
5227	R70	241	0.1	8	----	----	103,240	8 X
5228	R18	241	0.1	8	----	----	133,677	8 X
Tests 5229 - 5234 were cycled for 200,000 cycles at 241/24 MPa and then tested for residual strength								
5229	R51	241	0.1	8	----	----	200,000	8
	R51	249	*	13	----	----	1	8 RS
5230	R4	241	0.1	8	----	----	200,000	8
	R4	464	*	13	----	----	1	8 RS
5231	R73	241	0.1	8	----	----	200,000	8
	R73	269	*	13	----	----	1	8 RS
5232	R14	241	0.1	8	----	----	200,000	8
	R14	541	*	13	----	----	1	8 RS
5233	R33	241	0.1	8	----	----	200,000	8
	R33	298	*	13	----	----	1	8 RS
5234	R69	241	0.1	8	----	----	200,000	8
	R69	337	*	13	----	----	1	8 RS

Static Strength, Residual Strength after 50,000, 100,000 and 200,000 Cycles at 241 MPa, and Fatigue Failure at a Maximum Stress of 241 MPa, R = 0.1 (Tension Fatigue), $[90/0/\pm45/0]_S$ Laminate



Environmental testing of different matrix materials in $[0/\pm45/0]_S$, $[90/\pm45/90]_S$, and $[\pm45]_3$ laminates.

Tests 5235 through 5714 involved static tests of five different matrix materials at different temperatures (25, 40, 55 and 70 °C) and different moisture contents. For composite moisture gain, the test coupons were placed in a distilled water bath at a temperature of 50 °C for 1,200 hours (433 hours for the Iso-Polyester). The temperature that the coupons were tested at is listed in the last data column.

TEST & SAMPLE ID #		MAX. STRESS MPa	R	Q Hz	E GPa	e %	CYCLES TO FAIL	WIDTH (mm) and Notes
Lay-up = $[0/\pm45/0]_S$, V_F = 0.36, Ave. thickness = 3.16 mm, S.D. = 0.11 mm, CoRezyn 63-AX-051 Polyester								
5235	p-t-1	478	*	0.1	23.7	----	1	25 °C
5236	p-t-2	489	*	0.1	23.4	----	1	25 °C
5237	p-t-3	495	*	0.1	22.9	----	1	25 °C
5238	p-t-15	477	*	0.1	21.9	----	1	40 °C
5239	p-t-5	517	*	0.1	22.7	----	1	40 °C
5240	p-t-6	496	*	0.1	23.5	----	1	40 °C
5241	p-t-7	460	*	0.1	22.0	----	1	55 °C
5242	p-t-8	482	*	0.1	23.5	----	1	55 °C
5243	p-t-9	497	*	0.1	23.9	----	1	55 °C
5244	p-t-10	422	*	0.1	19.9	----	1	70 °C
5245	p-t-11	432	*	0.1	22.2	----	1	70 °C
5246	p-t-12	403	*	0.1	20.5	----	1	70 °C
Tests 5247 - 5258 had an average moisture gain of 0.92% (conditioned 1,200 hours in 50°C water (DI))								
5247	w-p-t-1	434	*	0.1	20.3	----	1	25 °C
5248	w-p-t-2	441	*	0.1	21.2	----	1	25 °C
5249	w-p-t-3	455	*	0.1	23.0	----	1	25 °C
5250	w-p-t-4	444	*	0.1	20.6	----	1	40 °C
5251	w-p-t-5	442	*	0.1	22.7	----	1	40 °C
5252	w-p-t-6	411	*	0.1	20.2	----	1	40 °C
5253	w-p-t-7	409	*	0.1	22.2	----	1	55 °C
5254	w-p-t-8	387	*	0.1	22.5	----	1	55 °C
5255	w-p-t-9	401	*	0.1	20.8	----	1	55 °C
5256	w-p-t-10	390	*	0.1	21.4	----	1	70 °C
5257	w-p-t-11	392	*	0.1	21.3	----	1	70 °C
5258	w-p-t-12	383	*	0.1	21.1	----	1	70 °C
5259	p-c-1	-604	*	13	----	----	1	25 °C
5260	p-c-2	-634	*	13	----	----	1	25 °C
5261	p-c-3	-641	*	13	----	----	1	25 °C
5262	p-c-4	-522	*	13	----	----	1	40 °C
5263	p-c-5	-591	*	13	----	----	1	40 °C
5264	p-c-6	-580	*	13	----	----	1	40 °C
5265	p-c-7	-455	*	13	----	----	1	55 °C
5266	p-c-8	-480	*	13	----	----	1	55 °C
5267	p-c-9	-437	*	13	----	----	1	55 °C
5268	p-c-10	-348	*	13	----	----	1	70 °C
5269	p-c-11	-388	*	13	----	----	1	70 °C
5270	p-c-12	-405	*	13	----	----	1	70 °C
Tests 5271 - 5282 had an average moisture gain of 0.87% (conditioned 1,200 hours in 50 °C water (DI))								
5271	w-p-c-1	-327	*	13	----	----	1	25 °C
5272	w-p-c-2	-341	*	13	----	----	1	25 °C

TEST & SAMPLE ID #		MAX. STRESS MPa	R	Q Hz	E GPa	e %	CYCLES TO FAIL	WIDTH (mm) and Notes
5273	w-p-c-3	-334	*	13	----	----	1	25 °C
5274	w-p-c-4	-306	*	13	----	----	1	40 °C
5275	w-p-c-5	-307	*	13	----	----	1	40 °C
5276	w-p-c-6	-317	*	13	----	----	1	40 °C
5277	w-p-c-10	-266	*	13	----	----	1	55 °C
5278	w-p-c-11	-277	*	13	----	----	1	55 °C
5279	w-p-c-12	-268	*	13	----	----	1	55 °C
5280	w-p-c-7	-240	*	13	----	----	1	70 °C
5281	w-p-c-8	-243	*	13	----	----	1	70 °C
5282	w-p-c-9	-243	*	13	----	----	1	70 °C
Lay-up = $[90/\pm45/90]_S$, V_F = 0.36, Ave. thickness = 3.15 mm, S.D. = 0.10 mm, CoRezyn 63-AX-051 Polyester								
5283	p-tt-1	78.7	*	0.1	8.9	----	1	25 °C
5284	p-tt-2	75.0	*	0.1	9.6	----	1	25 °C
5285	p-tt-3	68.5	*	0.1	9.3	----	1	25 °C
5715	1T01	68.2	*	0.1	10.7	2.26	1	25 °C
5716	1T02	75.2	*	0.1	10.5	3.14	1	25 °C
5717	1T03	77.8	*	0.1	10.1	3.51	1	25 °C
5286	p-tt-4	86.0	*	0.1	8.3	----	1	40 °C
5287	p-tt-5	84.7	*	0.1	8.8	----	1	40 °C
5288	p-tt-6	85.1	*	0.1	8.3	----	1	40 °C
5289	p-tt-7	84.1	*	0.1	6.1	----	1	55 °C
5290	p-tt-8	84.0	*	0.1	6.0	----	1	55 °C
5291	p-tt-9	81.1	*	0.1	6.3	----	1	55 °C
5292	p-tt-10	70.8	*	0.1	4.7	----	1	70 °C
5293	p-tt-11	72.3	*	0.1	5.3	----	1	70 °C
5294	p-tt-12	70.6	*	0.1	3.8	----	1	70 °C
Tests 5295 - 5306 had an average moisture gain of 0.92% (conditioned 1,200 hours in 50 °C water (DI))								
5295	w-p-tt-1	56.4	*	0.1	7.3	----	1	25 °C
5296	w-p-tt-2	55.8	*	0.1	7.1	----	1	25 °C
5297	w-p-tt-3	56.3	*	0.1	7.0	----	1	25 °C
5839	1t04	77.2	*	0.1	8.94	2.95	1	25 °C
5840	1t05	71.9	*	0.1	8.68	2.78	1	25 °C
5841	1t06	75.8	*	0.1	9.02	2.79	1	25 °C
5298	w-p-tt-4	59.2	*	0.1	6.1	----	1	40 °C
5299	w-p-tt-5	58.5	*	0.1	6.2	----	1	40 °C
5300	w-p-tt-6	59.2	*	0.1	5.8	----	1	40 °C
5301	w-p-tt-7	53.1	*	0.1	5.4	----	1	55 °C
5302	w-p-tt-8	54.2	*	0.1	5.4	----	1	55 °C
5303	w-p-tt-9	53.8	*	0.1	5.4	----	1	55 °C
5304	w-p-tt-10	47.2	*	0.1	3.8	----	1	70 °C
5305	w-p-tt-11	48.5	*	0.1	3.7	----	1	70 °C
5306	w-p-tt-12	50.9	*	0.1	3.4	----	1	70 °C
Lay-up = $[\pm45]_3$, V_F = 0.36, Ave. thickness = 3.12 mm, S.D. = 0.08 mm, CoRezyn 63-AX-051 Polyester								
5307	p-45t-1	111	*	0.1	10.2	----	1	25 °C
5308	p-45t-2	115	*	0.1	11.3	----	1	25 °C
5309	p-45t-3	111	*	0.1	11.3	----	1	25 °C
5310	p-45t-4	108	*	0.1	8.9	----	1	40 °C
5311	p-45t-5	105	*	0.1	10.1	----	1	40 °C
5312	p-45t-6	108	*	0.1	9.2	----	1	40 °C

TEST & SAMPLE ID #		MAX. STRESS MPa	R	Q Hz	E GPa	e %	CYCLES TO FAIL	WIDTH (mm) and Notes
5313	p-45t-7	91.5	*	0.1	7.6	----	1	55 °C
5314	p-45t-8	90.3	*	0.1	7.7	----	1	55 °C
5315	p-45t-9	88.9	*	0.1	7.3	----	1	55 °C
5316	p-45t-10	72.8	*	0.1	5.1	----	1	70 °C
5317	p-45t-11	72.4	*	0.1	4.9	----	1	70 °C
5318	p-45t-12	72.9	*	0.1	5.4	----	1	70 °C
Tests 5319 - 5330 had an average moisture gain of 0.86% (conditioned 1,200 hours in 50 °C water (DI))								
5319	w-p-45t-1	65.8	*	0.1	7.6	----	1	25 °C
5320	w-p-45t-2	69.4	*	0.1	7.7	----	1	25 °C
5321	w-p-45t-3	66.6	*	0.1	7.5	----	1	25 °C
5322	w-p-45t-4	68.5	*	0.1	6.1	----	1	40 °C
5323	w-p-45t-5	69.2	*	0.1	7.1	----	1	40 °C
5324	w-p-45t-6	64.6	*	0.1	6.2	----	1	40 °C
5325	w-p-45t-7	58.7	*	0.1	5.4	----	1	55 °C
5326	w-p-45t-8	59.6	*	0.1	5.1	----	1	55 °C
5327	w-p-45t-9	61.2	*	0.1	5.5	----	1	55 °C
5328	w-p-45t-10	43.5	*	0.1	3.0	----	1	70 °C
5329	w-p-45t-11	45.1	*	0.1	3.3	----	1	70 °C
5330	w-p-45t-12	46.2	*	0.1	3.0	----	1	70 °C
Lay-up = $[0/\pm45/0]_S$, V_F = 0.36, Ave. thickness = 3.16 mm, S.D. = 0.11 mm, Derakane 411C-50, vinyl ester								
5331	411-t-1	599	*	0.1	27.0	----	1	25 °C
5332	411-t-2	525	*	0.1	25.6	----	1	25 °C
5333	411-t-3	621	*	0.1	25.9	----	1	25 °C
5334	411-t-4	546	*	0.1	24.6	----	1	40 °C
5335	411-t-5	518	*	0.1	25.4	----	1	40 °C
5336	411-t-6	595	*	0.1	25.2	----	1	40 °C
5337	411-t-7	546	*	0.1	25.6	----	1	55 °C
5338	411-t-8	558	*	0.1	25.4	----	1	55 °C
5339	411-t-9	562	*	0.1	24.5	----	1	55 °C
5340	411-t-10	463	*	0.1	30.0	----	1	70 °C
5341	411-t-11	538	*	0.1	27.9	----	1	70 °C
5342	411-t-12	502	*	0.1	23.2	----	1	70 °C
Tests 5343 - 5354 had an average moisture gain of 0.34% (conditioned 1,200 hours in 50 °C water (DI))								
5343	w-411-t-1	445	*	0.1	24.3	----	1	25 °C
5344	w-411-t-2	441	*	0.1	25.9	----	1	25 °C
5345	w-411-t-3	417	*	0.1	23.3	----	1	25 °C
5346	w-411-t-4	413	*	0.1	25.9	----	1	40 °C
5347	w-411-t-5	434	*	0.1	25.0	----	1	40 °C
5348	w-411-t-6	409	*	0.1	26.3	----	1	40 °C
5349	w-411-t-7	405	*	0.1	25.9	----	1	55 °C
5350	w-411-t-8	384	*	0.1	25.1	----	1	55 °C
5351	w-411-t-9	383	*	0.1	23.9	----	1	55 °C
5352	w-411-t-10	378	*	0.1	25.5	----	1	70 °C
5353	w-411-t-11	381	*	0.1	26.4	----	1	70 °C
5354	w-411-t-12	380	*	0.1	24.1	----	1	70 °C
5355	411-c-1	-555	*	13	----	----	1	25 °C
5356	411-c-2	-509	*	13	----	----	1	25 °C
5357	411-c-3	-594	*	13	----	----	1	25 °C
5358	411-c-4	-505	*	13	----	----	1	40 °C

TEST & SAMPLE ID #		MAX. STRESS MPa	R	Q Hz	E GPa	e %	CYCLES TO FAIL	WIDTH (mm) and Notes
5359	411-c-5	-513	*	13	----	----	1	40 °C
5360	411-c-6	-504	*	13	----	----	1	40 °C
5361	411-c-7	-438	*	13	----	----	1	55 °C
5362	411-c-8	-447	*	13	----	----	1	55 °C
5363	411-c-9	-492	*	13	----	----	1	55 °C
5364	411-c-10	-445	*	13	----	----	1	70 °C
5365	411-c-11	-453	*	13	----	----	1	70 °C
5366	411-c-12	-447	*	13	----	----	1	70 °C
Tests 5367 - 5378 had an average moisture gain of 0.32% (conditioned 1,200 hours in 50 °C water (DI))								
5367	w-411-c-1	-519	*	13	----	----	1	25 °C
5368	w-411-c-2	-536	*	13	----	----	1	25 °C
5369	w-411-c-3	-508	*	13	----	----	1	25 °C
5370	w-411-c-4	-522	*	13	----	----	1	40 °C
5371	w-411-c-5	-514	*	13	----	----	1	40 °C
5372	w-411-c-6	-505	*	13	----	----	1	40 °C
5373	w-411-c-10	-516	*	13	----	----	1	55 °C
5374	w-411-c-11	-477	*	13	----	----	1	55 °C
5375	w-411-c-12	-486	*	13	----	----	1	55 °C
5376	w-411-c-7	-455	*	13	----	----	1	70 °C
5377	w-411-c-8	-475	*	13	----	----	1	70 °C
5378	w-411-c-9	-494	*	13	----	----	1	70 °C
Lay-up = $[90/\pm45/90]_S$, $V_F = 0.36$, Ave. thickness = 3.15 mm, S.D. = 0.10 mm, Derakane 411C-50								
5379	411-tt-1	56.9	*	0.1	11.1	----	1	25 °C
5380	411-tt-2	56.2	*	0.1	11.7	----	1	25 °C
5381	411-tt-3	54.8	*	0.1	12.4	----	1	25 °C
5382	411-tt-4	61.5	*	0.1	10.9	----	1	40 °C
5383	411-tt-5	62.3	*	0.1	10.3	----	1	40 °C
5384	411-tt-6	63.3	*	0.1	10.8	----	1	40 °C
5385	411-tt-7	63.2	*	0.1	6.9	----	1	55 °C
5386	411-tt-8	61.5	*	0.1	7.1	----	1	55 °C
5387	411-tt-9	61.5	*	0.1	7.3	----	1	55 °C
5388	411-tt-10	60.4	*	0.1	6.6	----	1	70 °C
5389	411-tt-11	52.6	*	0.1	6.0	----	1	70 °C
5390	411-tt-12	56.4	*	0.1	6.4	----	1	70 °C
5718	ts4111	57.6	*	0.1	9.3	4.39	1	25 °C
5719	ts4112	54.8	*	0.1	9.2	4.92	1	25 °C
5720	ts4113	56.6	*	0.1	9.5	4.01	1	25 °C
Tests 5391 - 5402 had an average moisture gain of 0.34% (conditioned 1,200 hours in 50°C water (DI))								
5391	w-411-tt-1	51.1	*	0.1	8.6	----	1	25 °C
5392	w-411-tt-2	51.4	*	0.1	8.2	----	1	25 °C
5393	w-411-tt-3	50.9	*	0.1	8.5	----	1	25 °C
5394	w-411-tt-4	56	*	0.1	8.5	----	1	40 °C
5395	w-411-tt-5	55.5	*	0.1	8.2	----	1	40 °C
5396	w-411-tt-6	50.9	*	0.1	8.4	----	1	40 °C
5397	w-411-tt-7	48.4	*	0.1	8.1	----	1	55 °C
5398	w-411-tt-8	52.1	*	0.1	7.9	----	1	55 °C
5399	w-411-tt-9	52.1	*	0.1	8.2	----	1	55 °C
5400	w-411-tt-10	52.6	*	0.1	7.3	----	1	70 °C
5401	w-411-tt-11	52	*	0.1	7.5	----	1	70 °C

TEST & SAMPLE ID #		MAX. STRESS MPa	R	Q Hz	E GPa	e %	CYCLES TO FAIL	WIDTH (mm) and Notes
5402	w-411-tt-12	50.1	*	0.1	7.2	----	1	70 °C
Lay-up = $[\pm 45]_3$, V_F = 0.36, Ave. thickness = 3.12 mm, S.D. = 0.08 mm, Derakane 411C-50 vinyl ester								
5403	411-45t-1	140	*	0.1	11.0	----	1	25 °C
5404	411-45t-2	133	*	0.1	10.8	----	1	25 °C
5405	411-45t-3	130	*	0.1	10.9	----	1	25 °C
5406	411-45t-4	121	*	0.1	10.5	----	1	40 °C
5407	411-45t-5	121	*	0.1	10.6	----	1	40 °C
5408	411-45t-6	123	*	0.1	9.8	----	1	40 °C
5409	411-45t-7	112	*	0.1	9.8	----	1	55 °C
5410	411-45t-8	116	*	0.1	9.6	----	1	55 °C
5411	411-45t-9	117	*	0.1	10	----	1	55 °C
5412	411-45t-10	103	*	0.1	9.7	----	1	70 °C
5413	411-45t-11	100	*	0.1	8.5	----	1	70 °C
5414	411-45t-12	100	*	0.1	8.9	----	1	70 °C
Tests 5415 - 5426 had an average moisture gain of 0.24% (conditioned 1,200 hours in 50°C water (DI))								
5415	w-411-45t-1	135	*	0.1	11.4	----	1	25 °C
5416	w-411-45t-2	135	*	0.1	11.4	----	1	25 °C
5417	w-411-45t-3	133	*	0.1	10.2	----	1	25 °C
5418	w-411-45t-4	129	*	0.1	----	----	1	40 °C
5419	w-411-45t-5	125	*	0.1	9.7	----	1	40 °C
5420	w-411-45t-6	127	*	0.1	9.5	----	1	40 °C
5421	w-411-45t-7	110	*	0.1	9.0	----	1	55 °C
5422	w-411-45t-8	119	*	0.1	9.2	----	1	55 °C
5423	w-411-45t-9	121	*	0.1	10.3	----	1	55 °C
5424	w-411-45t-10	110	*	0.1	9.2	----	1	70 °C
5425	w-411-45t-11	112	*	0.1	9.2	----	1	70 °C
5426	w-411-45t-12	112	*	0.1	9.3	----	1	70 °C
Lay-up = $[0/\pm 45/0]_S$, V_F = 0.36, Ave. thickness = 3.16 mm, S.D. = 0.11 mm, SC-14 Epoxy								
5427	sc14-t-1	696	*	0.1	26.6	----	1	25 °C
5428	sc14-t-2	727	*	0.1	28.0	----	1	25 °C
5429	sc14-t-3	648	*	0.1	24.6	----	1	25 °C
5430	sc14-t-4	561	*	0.1	25.1	----	1	40 °C
5431	sc14-t-5	603	*	0.1	25.3	----	1	40 °C
5432	sc14-t-6	572	*	0.1	25.8	----	1	40 °C
5433	sc14-t-7	584	*	0.1	24.2	----	1	55 °C
5434	sc14-t-8	548	*	0.1	27.0	----	1	55 °C
5435	sc14-t-9	578	*	0.1	23.5	----	1	55 °C
5436	sc14-t-10	570	*	0.1	23.5	----	1	70 °C
5437	sc14-t-11	569	*	0.1	23.4	----	1	70 °C
5438	sc14-t-12	595	*	0.1	24.8	----	1	70 °C
Tests 5439 - 5450 had an average moisture gain of 1.34% (conditioned 1,200 hours in 50°C water (DI))								
5439	w-sc14-t-1	569	*	0.1	25.0	----	1	25 °C
5440	w-sc14-t-2	437	*	0.1	23.9	----	1	25 °C
5441	w-sc14-t-3	454	*	0.1	24.3	----	1	25 °C
5442	w-sc14-t-4	426	*	0.1	23.6	----	1	40 °C
5443	w-sc14-t-5	428	*	0.1	25.4	----	1	40 °C
5444	w-sc14-t-6	434	*	0.1	23.3	----	1	40 °C
5445	w-sc14-t-7	396	*	0.1	23.5	----	1	55 °C
5446	w-sc14-t-8	404	*	0.1	25.5	----	1	55 °C

TEST & SAMPLE ID #		MAX. STRESS MPa	R	Q Hz	E GPa	e %	CYCLES TO FAIL	WIDTH (mm) and Notes
5447	w-sc14-t-9	408	*	0.1	23.8	----	1	55 °C
5448	w-sc14-t-10	362	*	0.1	22.1	----	1	70 °C
5449	w-sc14-t-11	351	*	0.1	21.8	----	1	70 °C
5450	w-sc14-t-12	357	*	0.1	23.1	----	1	70 °C
5451	sc14-c-1	-563	*	13	----	----	1	25 °C
5452	sc14-c-2	-508	*	13	----	----	1	25 °C
5453	sc14-c-3	-532	*	13	----	----	1	25 °C
5454	sc14-c-4	-511	*	13	----	----	1	40 °C
5455	sc14-c-5	-555	*	13	----	----	1	40 °C
5456	sc14-c-6	-537	*	13	----	----	1	40 °C
5457	sc14-c-7	-492	*	13	----	----	1	55 °C
5458	sc14-c-8	-464	*	13	----	----	1	55 °C
5459	sc14-c-9	-480	*	13	----	----	1	55 °C
5460	sc14-c-10	-414	*	13	----	----	1	70 °C
5461	sc14-c-11	-406	*	13	----	----	1	70 °C
5462	sc14-c-12	-424	*	13	----	----	1	70 °C
Tests 5463 - 5474 had an average moisture gain of 1.41% (conditioned 1,200 hours in 50 °C water (DI))								
5463	w-sc14-c-1	-454	*	13	----	----	1	25 °C
5464	w-sc14-c-2	-456	*	13	----	----	1	25 °C
5465	w-sc14-c-3	-462	*	13	----	----	1	25 °C
5466	w-sc14-c-4	-428	*	13	----	----	1	40 °C
5467	w-sc14-c-5	-334	*	13	----	----	1	40 °C
5468	w-sc14-c-6	-412	*	13	----	----	1	40 °C
5469	w-sc14-c-10	-318	*	13	----	----	1	55 °C
5470	w-sc14-c-11	-371	*	13	----	----	1	55 °C
5471	w-sc14-c-12	-368	*	13	----	----	1	55 °C
5472	w-sc14-c-7	-375	*	13	----	----	1	70 °C
5473	w-sc14-c-8	-293	*	13	----	----	1	70 °C
5474	w-sc14-c-9	-349	*	13	----	----	1	70 °C
Lay-up = $[90/\pm45/90]_S$, $V_F = 0.36$, Ave. thickness = 3.15 mm, S.D. = 0.10 mm, SC-14 Epoxy								
5475	sc14-tt-14	86.6	*	0.1	9.1	----	1	25 °C
5476	sc14-tt-2	92.4	*	0.1	9.5	----	1	25 °C
5477	sc14-tt-3	91.8	*	0.1	8.8	----	1	25 °C
5478	sc14-tt-4	97	*	0.1	8.7	----	1	40 °C
5479	sc14-tt-5	89.7	*	0.1	8.4	----	1	40 °C
5480	sc14-tt-6	92.1	*	0.1	8.2	----	1	40 °C
5481	sc14-tt-7	93.4	*	0.1	7.9	----	1	55 °C
5482	sc14-t-8	93.1	*	0.1	7.6	----	1	55 °C
5483	sc14-t-9	88.3	*	0.1	7.7	----	1	55 °C
5484	sc14-tt-10	100	*	0.1	7.6	----	1	70 °C
5485	sc14-tt-11	93.4	*	0.1	7.4	----	1	70 °C
5486	sc14-tt-12	90.1	*	0.1	7.6	----	1	70 °C
5721	tsc141	109	*	0.1	9.4	3.21	1	25 °C
5722	tsc142	121	*	0.1	9.5	4.73	1	25 °C
5723	tsc143	104	*	0.1	9.4	3.45	1	25 °C
Tests 5487 - 5498 had an average moisture gain of 1.34% (conditioned 1,200 hours in 50 °C water (DI))								
5487	w-sc14-tt-1	76.2	*	0.1	8.6	----	1	25 °C
5488	w-sc14-tt-2	70.1	*	0.1	8.2	----	1	25 °C
5489	w-sc14-tt-3	69.9	*	0.1	7.8	----	1	25 °C

TEST & SAMPLE ID #		MAX. STRESS MPa	R	Q Hz	E GPa	e %	CYCLES TO FAIL	WIDTH (mm) and Notes
5490	w-sc14-tt-4	73.9	*	0.1	7.5	----	1	40 °C
5491	w-sc14-tt-5	68.3	*	0.1	7.1	----	1	40 °C
5492	w-sc14-tt-6	76.9	*	0.1	7.1	----	1	40 °C
5493	w-sc14-tt-7	68.1	*	0.1	6.3	----	1	55 °C
5494	w-sc14-tt-8	66.1	*	0.1	6.8	----	1	55 °C
5495	w-sc14-tt-9	71.1	*	0.1	6.3	----	1	55 °C
5496	w-sc14-tt-10	66.8	*	0.1	5.2	----	1	70 °C
5497	w-sc14-tt-11	67.3	*	0.1	5.1	----	1	70 °C
5498	w-sc14-tt-12	70.4	*	0.1	5.5	----	1	70 °C
Lay-up = $[\pm 45]_3$, V_F = 0.36, Ave. thickness = 3.12 mm, S.D. = 0.08 mm, SC-14 Epoxy								
5499	sc14-45t-1	92	*	0.1	9.6	----	1	25 °C
5500	sc14-45t-2	87.6	*	0.1	9.2	----	1	25 °C
5501	sc14-45t-3	92.7	*	0.1	8.8	----	1	25 °C
5502	sc14-45t-4	85.9	*	0.1	8.6	----	1	40 °C
5503	sc14-45t-5	84	*	0.1	7.4	----	1	40 °C
5504	sc14-45t-6	85.1	*	0.1	7.7	----	1	40 °C
5505	sc14-45t-7	75.7	*	0.1	6.4	----	1	55 °C
5506	sc14-45t-8	79.9	*	0.1	7.1	----	1	55 °C
5507	sc14-45t-9	74.7	*	0.1	6.9	----	1	55 °C
5508	sc14-45t-10	64.2	*	0.1	6.4	----	1	70 °C
5509	sc14-45t-11	73.6	*	0.1	6.7	----	1	70 °C
5510	sc14-45t-12	64.9	*	0.1	5.7	----	1	70 °C
Tests 5511 - 5522 had an average moisture gain of 1.24% (conditioned 1,200 hours in 50 °C water (DI))								
5511	w-sc1445t1	93.1	*	0.1	8.1	----	1	25 °C
5512	w-sc1445t2	81.4	*	0.1	7.8	----	1	25 °C
5513	w-sc1445t3	89	*	0.1	8.2	----	1	25 °C
5514	w-sc1445t4	84	*	0.1	7.2	----	1	40 °C
5515	w-sc1445t5	73.7	*	0.1	6.8	----	1	40 °C
5516	w-sc1445t6	75.4	*	0.1	6.5	----	1	40 °C
5517	w-sc1445t7	66.4	*	0.1	6.1	----	1	55 °C
5518	w-sc1445t8	67.6	*	0.1	6.0	----	1	55 °C
5519	w-sc1445t9	65	*	0.1	5.7	----	1	55 °C
5520	w-sc1445t10	55	*	0.1	4.0	----	1	70 °C
5521	w-sc1445t11	51.9	*	0.1	3.8	----	1	70 °C
5522	w-sc1445t12	49.5	*	0.1	3.5	----	1	70 °C
Lay-up = $[0/\pm 45/0]_S$, V_F = 0.36, Ave. thickness = 3.16 mm, S.D. = 0.11 mm, Derakane 8084 vinyl ester								
5523	8084-t-1	698	*	0.1	24.9	----	1	25 °C
5524	8084-t-2	684	*	0.1	25.1	----	1	25 °C
5525	8084-t-3	539	*	0.1	23.9	----	1	25 °C
5526	8084-t-4	480	*	0.1	22.9	----	1	40 °C
5527	8084-t-5	471	*	0.1	24.0	----	1	40 °C
5528	8084-t-6	550	*	0.1	24.4	----	1	40 °C
5529	8084-t-7	532	*	0.1	24.4	----	1	55 °C
5530	8084-t-8	656	*	0.1	23.6	----	1	55 °C
5531	8084-t-9	588	*	0.1	24.1	----	1	55 °C
5532	8084-t-10	556	*	0.1	23.5	----	1	70 °C
5533	8084-t-11	536	*	0.1	22.5	----	1	70 °C
5534	8084-t-12	550	*	0.1	22.3	----	1	70 °C

TEST & SAMPLE ID #		MAX. STRESS MPa	R	Q Hz	E GPa	e %	CYCLES TO FAIL	WIDTH (mm) and Notes
Tests 5535 - 5546 had an average moisture gain of 0.44% (conditioned 1,200 hours in 50 °C water (DI))								
5535	w-8084-t-1	461	*	0.1	25.6	----	1	25 °C
5536	w-8084-t-2	463	*	0.1	25.1	----	1	25 °C
5537	w-8084-t-3	472	*	0.1	24.3	----	1	25 °C
5538	w-8084-t-4	443	*	0.1	24.6	----	1	40 °C
5539	w-8084-t-5	435	*	0.1	23.6	----	1	40 °C
5540	w-8084-t-6	436	*	0.1	24.8	----	1	40 °C
5541	w-8084-t-7	423	*	0.1	23.9	----	1	55 °C
5542	w-8084-t-8	419	*	0.1	24.9	----	1	55 °C
5543	w-8084-t-9	413	*	0.1	26.2	----	1	55 °C
5544	w-8084-t-10	379	*	0.1	23.8	----	1	70 °C
5545	w-8084-t-11	397	*	0.1	24.2	----	1	70 °C
5546	w-8084-t-12	393	*	0.1	24.4	----	1	70 °C
5547	8084-c-1	-600	*	13	----	----	1	25 °C
5548	8084-c-2	-569	*	13	----	----	1	25 °C
5549	8084-c-3	-611	*	13	----	----	1	25 °C
5550	8084-c-4	-494	*	13	----	----	1	40 °C
5551	8084-c-5	-478	*	13	----	----	1	40 °C
5552	8084-c-6	-470	*	13	----	----	1	40 °C
5553	8084-c-7	-464	*	13	----	----	1	55 °C
5554	8084-c-8	-444	*	13	----	----	1	55 °C
5555	8084-c-9	-455	*	13	----	----	1	55 °C
5556	8084-c-10	-445	*	13	----	----	1	70 °C
5557	8084-c-11	-444	*	13	----	----	1	70 °C
5558	8084-c-12	-449	*	13	----	----	1	70 °C
Tests 5559 - 5570 had an average moisture gain of 0.42% (conditioned 1,200 hours in 50 °C water (DI))								
5559	w-8084-c-1	-521	*	13	----	----	1	25 °C
5560	w-8084-c-2	-492	*	13	----	----	1	25 °C
5561	w-8084-c-3	-513	*	13	----	----	1	25 °C
5562	w-8084-c-4	-487	*	13	----	----	1	40 °C
5563	w-8084-c-5	-502	*	13	----	----	1	40 °C
5564	w-8084-c-6	-450	*	13	----	----	1	40 °C
5565	w-8084-c-10	-431	*	13	----	----	1	55 °C
5566	w-8084-c-11	-466	*	13	----	----	1	55 °C
5567	w-8084-c-12	-465	*	13	----	----	1	55 °C
5568	w-8084-c-7	-414	*	13	----	----	1	70 °C
5569	w-8084-c-8	-435	*	13	----	----	1	70 °C
5570	w-8084-c-9	-388	*	13	----	----	1	70 °C
Lay-up = $[90/\pm45/90]_S$, $V_F = 0.36$, Ave. thickness = 3.15 mm, S.D. = 0.10 mm, Derakane 8084 vinyl ester								
5571	8084-tt-1	79.5	*	0.1	12.8	----	1	25 °C
5572	8084-tt-2	82.8	*	0.1	12.3	----	1	25 °C
5573	8084-tt-3	82	*	0.1	13.0	----	1	25 °C
5574	8084-tt-4	87.2	*	0.1	11.0	----	1	40 °C
5575	8084-tt-5	82.6	*	0.1	10.7	----	1	40 °C
5576	8084-tt-13	62.6	*	0.1	10.4	----	1	40 °C
5577	8084-tt-7	80.5	*	0.1	8.3	----	1	55 °C
5578	8084-tt-8	89.4	*	0.1	8.2	----	1	55 °C
5579	8084-tt-9	83.1	*	0.1	7.9	----	1	55 °C
5580	8084-tt-10	58.3	*	0.1	6.2	----	1	70 °C

TEST & SAMPLE ID #		MAX. STRESS MPa	R	Q Hz	E GPa	e %	CYCLES TO FAIL	WIDTH (mm) and Notes
5581	8084-tt-11	59.3	*	0.1	6.2	----	1	70 °C
5582	8084-tt-12	57.6	*	0.1	6.2	----	1	70 °C
5724	t80841	62.7	*	0.1	8.6	3.7	1	25 °C
5725	t80842	62.9	*	0.1	8.3	4.4	1	25 °C
5726	t80843	63.3	*	0.1	8.1	4.2	1	25 °C
Tests 5583 - 5594 had an average moisture gain of 0.44% (conditioned 1,200 hours in 50 °C water (DI))								
5583	w-8084-tt-1	47.5	*	0.1	8.4	----	1	25 °C
5584	w-8084-tt-2	48.4	*	0.1	8.5	----	1	25 °C
5585	w-8084-tt-3	49.5	*	0.1	8.3	----	1	25 °C
5586	w-8084-tt-4	51.3	*	0.1	8.3	----	1	40 °C
5587	w-8084-tt-5	49.5	*	0.1	7.4	----	1	40 °C
5588	w-8084-tt-6	49.7	*	0.1	8.0	----	1	40 °C
5589	w-8084-tt-7	49.2	*	0.1	7.3	----	1	55 °C
5590	w-8084-tt-8	53.1	*	0.1	7.3	----	1	55 °C
5591	w-8084-tt-9	45.7	*	0.1	7.4	----	1	55 °C
5592	w-8084-tt-10	53.4	*	0.1	6.6	----	1	70 °C
5593	w-8084-tt-11	51.2	*	0.1	7.0	----	1	70 °C
5594	w-8084-tt-12	52	*	0.1	6.8	----	1	70 °C
Lay-up = $[\pm 45]_3$, $V_F = 0.36$, Ave. thickness = 3.12 mm, S.D. = 0.08 mm, Derakane 8084 vinyl ester								
5595	8084-45t-1	122	*	0.1	9.7	----	1	25 °C
5596	8084-45t-2	134	*	0.1	10.4	----	1	25 °C
5597	8084-45t-3	125	*	0.1	10.8	----	1	25 °C
5598	8084-45t-4	118	*	0.1	9.0	----	1	40 °C
5599	8084-45t-5	117	*	0.1	9.6	----	1	40 °C
5600	8084-45t-6	116	*	0.1	9.3	----	1	40 °C
5601	8084-45t-7	113	*	0.1	8.7	----	1	55 °C
5602	8084-45t-8	114	*	0.1	8.6	----	1	55 °C
5603	8084-45t-9	113	*	0.1	8.5	----	1	55 °C
5604	8084-45t-10	100	*	0.1	7.4	----	1	70 °C
5605	8084-45t-11	104	*	0.1	7.8	----	1	70 °C
5606	8084-45t-12	103	*	0.1	7.3	----	1	70 °C
Tests 5607 - 5618 had an average moisture gain of 0.38% (conditioned 1,200 hours in 50°C water (DI))								
5607	w-8084-45t-1	115	*	0.1	10.3	----	1	25 °C
5608	w-8084-45t-2	115	*	0.1	10.1	----	1	25 °C
5609	w-8084-45t-3	116	*	0.1	10.3	----	1	25 °C
5610	w-8084-45t-4	108	*	0.1	9.6	----	1	40 °C
5611	w-8084-45t-5	112	*	0.1	10.1	----	1	40 °C
5612	w-8084-45t-6	110	*	0.1	9.7	----	1	40 °C
5613	w-8084-45t-7	102	*	0.1	9.1	----	1	55 °C
5614	w-8084-45t-8	102	*	0.1	9.4	----	1	55 °C
5615	w-8084-45t-9	101	*	0.1	9.4	----	1	55 °C
5616	w-8084-45t-10	95	*	0.1	8.0	----	1	70 °C
5617	w-8084-45t-11	88	*	0.1	7.3	----	1	70 °C
5618	w-8084-45t-12	94	*	0.1	7.8	----	1	70 °C
Lay-up = $[0/\pm 45/0]_S$, $V_F = 0.36$, Ave. thickness = 3.16 mm, S.D. = 0.11 mm, CoRezyn -AQ-051 Iso-Polyester								
5619	tp-t-1	694	*	0.1	24.9	----	1	25 °C
5620	tp-t-2	652	*	0.1	23.8	----	1	25 °C
5621	tp-t-3	557	*	0.1	23.9	----	1	25 °C
5622	tp-t-4	656	*	0.1	23.9	----	1	40 °C

TEST & SAMPLE ID #		MAX. STRESS MPa	R	Q Hz	E GPa	e %	CYCLES TO FAIL	WIDTH (mm) and Notes
5623	tp-t-5	578	*	0.1	25.3	----	1	40 °C
5624	tp-t-6	646	*	0.1	25.0	----	1	40 °C
5625	tp-t-7	629	*	0.1	23.8	----	1	55 °C
5626	tp-t-8	607	*	0.1	24.0	----	1	55 °C
5627	tp-t-9	660	*	0.1	24.2	----	1	55 °C
5628	tp-t-10	601	*	0.1	24.2	----	1	70 °C
5629	tp-t-11	529	*	0.1	23.5	----	1	70 °C
5630	tp-t-12	601	*	0.1	23.0	----	1	70 °C
Tests 5631 - 5642 had an average moisture gain of 0.5% (conditioned 430 hours in 50 °C water (DI))								
5631	w-tp-t-1	582	*	0.1	26.6	----	1	25 °C
5632	w-tp-t-2	635	*	0.1	24.1	----	1	25 °C
5633	w-tp-t-3	531	*	0.1	25.5	----	1	25 °C
5634	w-tp-t-4	618	*	0.1	25.0	----	1	40 °C
5636	w-tp-t-6	628	*	0.1	25.0	----	1	40 °C
5637	w-tp-t-7	609	*	0.1	24.9	----	1	55 °C
5638	w-tp-t-8	599	*	0.1	25.2	----	1	55 °C
5639	w-tp-t-9	618	*	0.1	25.0	----	1	55 °C
5640	w-tp-t-10	557	*	0.1	22.8	----	1	70 °C
5641	w-tp-t-11	553	*	0.1	24.4	----	1	70 °C
5642	w-tp-t-12	541	*	0.1	23.0	----	1	70 °C
5643	tp-c-1	-531	*	13	----	----	1	25 °C
5644	tp-c-2	-574	*	13	----	----	1	25 °C
5645	tp-c-3	-626	*	13	----	----	1	25 °C
5646	tp-c-4	-559	*	13	----	----	1	40 °C
5647	tp-c-5	-525	*	13	----	----	1	40 °C
5648	tp-c-6	-569	*	13	----	----	1	40 °C
5649	tp-c-7	-545	*	13	----	----	1	55 °C
5650	tp-c-8	-536	*	13	----	----	1	55 °C
5651	tp-c-9	-540	*	13	----	----	1	55 °C
5652	tp-c-10	-494	*	13	----	----	1	70 °C
5653	tp-c-11	-500	*	13	----	----	1	70 °C
5654	tp-c-12	-494	*	13	----	----	1	70 °C
Tests 5655 - 5666 had an average moisture gain of 0.5% (conditioned 430 hours in 50 °C water (DI))								
5655	w-tp-c-1	-595	*	13	----	----	1	25 °C
5656	w-tp-c-2	-583	*	13	----	----	1	25 °C
5657	w-tp-c-3	-547	*	13	----	----	1	25 °C
5658	w-tp-c-4	-534	*	13	----	----	1	40 °C
5659	w-tp-c-5	-495	*	13	----	----	1	40 °C
5660	w-tp-c-6	-580	*	13	----	----	1	40 °C
5661	w-tp-c-10	-476	*	13	----	----	1	55 °C
5662	w-tp-c-11	-514	*	13	----	----	1	55 °C
5663	w-tp-c-12	-539	*	13	----	----	1	55 °C
5664	w-tp-c-7	-480	*	13	----	----	1	70 °C
5665	w-tp-c-8	-499	*	13	----	----	1	70 °C
5666	w-tp-c-9	-509	*	13	----	----	1	70 °C
Lay-up = $[90/\pm45/90]_S$, $V_F = 0.36$, Ave. thickness = 3.15 mm, S.D. = 0.10 mm, CoRezyn Iso-Polyester								
5667	tp-tt-1	67.8	*	0.1	9.2	----	1	25 °C
5668	tp-tt-2	68.4	*	0.1	9.0	----	1	25 °C
5669	tp-tt-3	64.8	*	0.1	9.3	----	1	25 °C

TEST & SAMPLE ID #		MAX. STRESS MPa	R	Q Hz	E GPa	e %	CYCLES TO FAIL	WIDTH (mm) and Notes
5670	tp-tt-4	71.7	*	0.1	8.3	----	1	40 °C
5671	tp-tt-5	68.5	*	0.1	8.8	----	1	40 °C
5672	tp-tt-6	68.1	*	0.1	8.3	----	1	40 °C
5673	tp-tt-7	64.4	*	0.1	7.7	----	1	55 °C
5674	tp-tt-8	69.9	*	0.1	7.9	----	1	55 °C
5675	tp-tt-9	68.8	*	0.1	7.9	----	1	55 °C
5676	tp-tt-10	69.1	*	0.1	7.4	----	1	70 °C
5677	tp-tt-11	71.7	*	0.1	7.2	----	1	70 °C
5678	tp-tt-12	70.3	*	0.1	7.4	----	1	70 °C
Tests 5679 - 5690 had an average moisture gain of 0.5% (conditioned 430 hours in 50 °C water (DI))								
5679	w-tp-tt-1	64.8	*	0.1	9.4	----	1	25 °C
5680	w-tp-tt-2	68.8	*	0.1	9.7	----	1	25 °C
5681	w-tp-tt-3	66.6	*	0.1	9.1	----	1	25 °C
5682	w-tp-tt-4	66.6	*	0.1	9.0	----	1	40 °C
5683	w-tp-tt-5	69	*	0.1	9.1	----	1	40 °C
5684	w-tp-tt-6	70.8	*	0.1	9.0	----	1	40 °C
5685	w-tp-tt-7	67.9	*	0.1	8.5	----	1	55 °C
5686	w-tp-tt-8	66.3	*	0.1	8.9	----	1	55 °C
5687	w-tp-tt-9	61.6	*	0.1	8.4	----	1	55 °C
5688	w-tp-tt-10	64.6	*	0.1	7.6	----	1	70 °C
5689	w-tp-tt-11	66.2	*	0.1	7.6	----	1	70 °C
5690	w-tp-tt-12	67.7	*	0.1	7.1	----	1	70 °C
Lay-up = $[\pm 45]_3$, V_F = 0.36, Ave. thickness = 3.12 mm, S.D. = 0.08 mm, CoRezyn Iso-Polyester								
5691	tp-45t-1	133	*	0.1	11.5	----	1	25 °C
5692	tp-45t-2	135	*	0.1	12.3	----	1	25 °C
5693	tp-45t-3	132	*	0.1	11.2	----	1	25 °C
5694	tp-45t-4	124	*	0.1	11.5	----	1	40 °C
5695	tp-45t-5	127	*	0.1	10.7	----	1	40 °C
5696	tp-45t-6	128	*	0.1	10.0	----	1	40 °C
5697	tp-45t-7	116	*	0.1	10.1	----	1	55 °C
5698	tp-45t-8	116	*	0.1	10.2	----	1	55 °C
5699	tp-45t-9	114	*	0.1	10.0	----	1	55 °C
5700	tp-45t-10	93.2	*	0.1	8.9	----	1	70 °C
5701	tp-45t-11	93.2	*	0.1	9.6	----	1	70 °C
5702	tp-45t-12	100	*	0.1	8.8	----	1	70 °C
Tests 5703 - 5714 had an average moisture gain of 0.28% (conditioned 430 hours in 50 °C water (DI))								
5703	w-tp-45t-1	131	*	0.1	11.9	----	1	25 °C
5704	w-tp-45t-2	125	*	0.1	12.0	----	1	25 °C
5705	w-tp-45t-3	132	*	0.1	12.1	----	1	25 °C
5706	w-tp-45t-4	124	*	0.1	11.3	----	1	40 °C
5707	w-tp-45t-5	126	*	0.1	10.8	----	1	40 °C
5708	w-tp-45t-6	122	*	0.1	10.5	----	1	40 °C
5709	w-tp-45t-7	114	*	0.1	10.0	----	1	55 °C
5710	w-tp-45t-8	107	*	0.1	9.9	----	1	55 °C
5711	w-tp-45t-9	110	*	0.1	9.2	----	1	55 °C
5712	w-tp-45t-10	94.8	*	0.1	7.7	----	1	70 °C
5713	w-tp-45t-11	96.8	*	0.1	7.5	----	1	70 °C
5714	w-tp-45t-12	102	*	0.1	8.9	----	1	70 °C

Tests 5739 through 5838 involved (0/±45/0) laminates with D155/DB120 and A130/DB120 fabrics. These laminates were placed in distilled water and monitored for moisture absorption and ultimate compressive strength changes with moisture content. Two of these laminates were taken out of the water, bonded back-to-back, and compression tested. The back-to-back configuration gave the coupon added buckling resistance and simulated Material DD5P (denoted with a "D") and Material DD11 (denoted with an "A"). See Ref. 18.

TEST & SAMPLE ID #		MAX. STRESS MPa	R	Q Hz	E GPa	e %	CYCLES TO FAIL	Test Temperature
Tests 5739 - 5746 control group, no moisture conditioning, after 24 hours at 40 °C								
5739	D6456	-497	*	13	----	----	1	25 °C
5740	D6327	-565	*	13	----	----	1	25 °C
5741	D6533	-532	*	13	----	----	1	25 °C
5742	D6212	-476	*	13	----	----	1	25 °C
5743	A6034	-274	*	13	----	----	1	25 °C
5744	A6140	-302	*	13	----	----	1	25 °C
5745	A5962	-211	*	13	----	----	1	25 °C
5746	A5974	-272	*	13	----	----	1	25 °C
Tests 5747-5754 were tested after 24 hours in 40 °C water, (D-0.20% moisture gain, A-0.29% moisture gain)								
5747	D6229	-492	*	13	----	----	1	25 °C
5748	D6517	-529	*	13	----	----	1	25 °C
5749	D6559	-533	*	13	----	----	1	25 °C
5750	D5866	-509	*	13	----	----	1	25 °C
5751	A6046	-239	*	13	----	----	1	25 °C
5752	A6236	-334	*	13	----	----	1	25 °C
5753	A6141	-272	*	13	----	----	1	25 °C
5754	A6147	-205	*	13	----	----	1	25 °C
Tests 5755-5765 were tested after 144 hours in 40 °C water, (D-0.47% moisture gain, A-0.54% moisture gain)								
5755	D6229	-665	*	13	----	----	1	25 °C
5756	D6194	-464	*	13	----	----	1	25 °C
5757	D6112	-517	*	13	----	----	1	25 °C
5758	D6205	-464	*	13	----	----	1	25 °C
5759	A6070	-250	*	13	----	----	1	25 °C
5760	A6090	-314	*	13	----	----	1	25 °C
5761	A6236	-288	*	13	----	----	1	25 °C
5762	A5950	-295	*	13	----	----	1	25 °C
5763	D6441	-519	*	13	----	----	1	0 °C
5764	D6365	-486	*	13	----	----	1	0 °C
5765	D6369	-452	*	13	----	----	1	0 °C
Tests 5766-5765 were tested after 1315 hours in 40 °C water,(D-0.61% moisture gain, A-0.73% moisture gain)								
5766	D6443	-471	*	13	----	----	1	25 °C
5767	D6489	-519	*	13	----	----	1	25 °C
5768	D6846	-474	*	13	----	----	1	25 °C
5769	D6590	-420	*	13	----	----	1	25 °C
5770	A6570	-213	*	13	----	----	1	25 °C
5771	A5976	-211	*	13	----	----	1	25 °C
5772	A6021	-260	*	13	----	----	1	25 °C
5773	A6228	-191	*	13	----	----	1	25 °C
Tests 5774-5779 control group, no moisture conditioning, after 1315 hours at 40 °C								
5774	D6490	-509	*	13	----	----	1	25 °C
5775	D6370	-404	*	13	----	----	1	25 °C
5776	D5924	-621	*	13	----	----	1	25 °C

TEST & SAMPLE ID #		MAX. STRESS MPa	R	Q Hz	E GPa	e %	CYCLES TO FAIL	Test Temperature
5777	A6119	-283	*	13	----	----	1	25 °C
5778	A5980	-261	*	13	----	----	1	25 °C
5779	A6007	-279	*	13	----	----	1	25 °C
Tests 5780-5786 control group, no moisture conditioning, after 2000 hours at 40 °C, 2650 hours at 20 °C								
5780	D6210	-560	*	13	----	----	1	25 °C
5781	D6401	-568	*	13	----	----	1	25 °C
5782	D6219	-539	*	13	----	----	1	25 °C
5783	A5970	-218	*	13	----	----	1	25 °C
5784	A6070	-307	*	13	----	----	1	25 °C
5785	A5983	-300	*	13	----	----	1	25 °C
Tests 5786-5801 were tested after 2000 hours in 40 °C water and 2650 hours in 20 °C water, (D-0.62% moisture gain, A-0.64% moisture gain)								
5786	D6212	-405	*	13	----	----	1	25 °C
5787	D6220	-393	*	13	----	----	1	25 °C
5788	D6171	-473	*	13	----	----	1	25 °C
5789	D6794	-413	*	13	----	----	1	25 °C
5790	D5978	-352	*	13	----	----	1	50 °C
5791	D6349	-414	*	13	----	----	1	50 °C
5792	D6491	-423	*	13	----	----	1	50 °C
5793	D6270	-423	*	13	----	----	1	50 °C
5794	A6008	-228	*	13	----	----	1	25 °C
5795	A6506	-267	*	13	----	----	1	25 °C
5796	A6119	-240	*	13	----	----	1	25 °C
5797	A6034	-224	*	13	----	----	1	25 °C
5798	A6149	-176	*	13	----	----	1	50 °C
5799	A6396	-125	*	13	----	----	1	50 °C
5800	A6223	-216	*	13	----	----	1	50 °C
5801	A6149	-179	*	13	----	----	1	50 °C
Tests 5802-5817 were tested after 2000 hours in 40 °C water and 13355 hours in 20 °C water, (D-0.97% moisture gain, A-1.01% moisture gain)								
5802	D6223	-442	*	13	----	----	1	25 °C
5803	D6883	-406	*	13	----	----	1	25 °C
5804	D6037	-404	*	13	----	----	1	25 °C
5805	D5992	-366	*	13	----	----	1	25 °C
5806	A6026	-163	*	13	----	----	1	25 °C
5807	A5972	-215	*	13	----	----	1	25 °C
5808	A6188	-229	*	13	----	----	1	25 °C
5809	A6061	-203	*	13	----	----	1	25 °C
5810	D5864	-377	*	13	----	----	1	50 °C
5811	D5960	-332	*	13	----	----	1	50 °C
5812	D5842	-309	*	13	----	----	1	50 °C
5813	D6316	-375	*	13	----	----	1	50 °C
5814	A5975	-132	*	13	----	----	1	50 °C
5815	A6218	-154	*	13	----	----	1	50 °C
5816	A5894	-188	*	13	----	----	1	50 °C
5817	A6165	-225	*	13	----	----	1	50 °C
Tests 5818-5786 control group, no moisture conditioning, after 2000 hours at 40 °C, 13355 hours at 20 °C								
5818	D6394	-448	*	13	----	----	1	25 °C
5819	D6248	-361	*	13	----	----	1	25 °C

TEST & SAMPLE ID #		MAX. STRESS MPa	R	Q Hz	E GPa	e %	CYCLES TO FAIL	Test Temperature
5820	D6265	-434	*	13	----	----	1	25 °C
5821	D6472	-583	*	13	----	----	1	25 °C
5822	D6485	-532	*	13	----	----	1	25 °C
5823	D6428	-559	*	13	----	----	1	25 °C
5824	D6183	-516	*	13	----	----	1	50 °C
5825	D6351	-468	*	13	----	----	1	50 °C
5826	D6217	-542	*	13	----	----	1	50 °C
5827	D6411	-430	*	13	----	----	1	50 °C
5828	D6530	-405	*	13	----	----	1	50 °C
5829	A6040	-250	*	13	----	----	1	25 °C
5830	A6161	-283	*	13	----	----	1	25 °C
5831	A6008	-298	*	13	----	----	1	25 °C
5832	A6036	-222	*	13	----	----	1	25 °C
5833	A5911	-249	*	13	----	----	1	25 °C
5834	A5951	-251	*	13	----	----	1	50 °C
5835	A6259	-270	*	13	----	----	1	50 °C
5836	A6079	-232	*	13	----	----	1	50 °C
5837	A6420	-264	*	13	----	----	1	50 °C
5838	A6056	-233	*	13	----	----	1	50 °C

These tests are summarized in the two tables below [18].

Compression Testing Summary of Coupons (0/±45/0) Exposed to 20 - 40 °C Distilled Water (D155 and A130 0° fabric with DB120 ±45° fabric, V_F = 0.34)							
Exposure Time, hours	Test Temperature, °C	Average Moisture Gain (S.D.), %		D155 Ave. strength (S.D.), psi	% Change	A130 Ave. strength (S.D.), psi	% Change
		D155	A130				
0	20	0	0	517 (39)	--	265 (39)	--
24	20	0.20 (0.01)	0.29 (0.03)	516 (19)	-0.3	262 (55)	-0.8
144	20	0.47 (0.01)	0.54 (0.02)	481 (30)	-6.9	286 (27)	8.4
1,315	20	0.61 (0.06)	0.73 (0.04)	471(35)	-9.0	219 (26)	-17
4,650	20	0.62 (0.11)	0.64 (0.08)	420 (31)	-19	240 (17)	-9.3
4,650	50	0.62	0.64	403 (30)	-15	174 (32)	-30
15,355	20	0.94 (0.25)	1.02 (0.05)	404 (31)	-22	202 (28)	-23
15,355	50	0.99 (0.22)	0.99 (0.04)	348 (34)	-26	175 (40)	-30
Baseline D155 modulus = 24.8 GPa, Baseline A130 modulus = 23.7 GPa at 1% moisture - D155 = 24.8 GPa, at 1% moisture - A130 = 19.9 GPa Coupons were tested in a double thickness configuration at 13 mm/s with a 13 mm gage length.							

Compression Testing Summary of Dry Control Coupons (0/±45/0) (D155 and A130 0° fabric with DB120 ±45° fabric, $V_F = 0.34$)					
Exposure Time, hours	Testing Temperature, °C	D155 Ave. strength (S.D.), MPa	% Change	A130 Ave. strength (S.D.), MPa	% Change
0	20	517 (39)	--	265 (39)	--
1,315 dry control	20	511 (89)	-1.2	274 (10)	+3.8
4,650 dry control	20	556 (13)	+7.4	275 (40)	+3.9
15,355 dry control	20	486 (86)	-6.4	260 (30)	+1.6
15,355 dry control	50	472 (57)	-9.6	250 (17)	-5.8

DD5P Environmental Tests

Tests 4880 - 4899, 5860 - 5899 involved full thickness DD5P coupons which were immersed in distilled water for a total of 300 days The first 91 days were at a temperature of 40 °C with the remaining time at room temperature (18-22 °C). **These "WET" coupons averaged 1.0 percent moisture absorption at the time of testing.** All the tensile coupons in this series were dog boned shaped with a minimum width of 22 mm. The compression coupons were 25 mm wide and involved a gage length of 13 mm. The last column of data lists the temperature that the test was run under, and whether or not the coupon was "DRY" (not soaked in water, ~0 % moisture content) or WET (coupons that were soaked in distilled water, as described above). See Reference 18.

MATERIAL DD5P - Environmental

Lay-up = $[0/\pm45/0]_S$, $V_F = 0.36$, Ave. thickness (dry) = 3.13 mm, S.D. (dry) = 0.004 mm, Ave. thickness (wet) = 2.95 mm, S.D. (dry) = 0.004 mm, CoRezyn 63-AX-051 Polyester

TEST & SAMPLE ID #		MAX. STRESS MPa	R	Q Hz	E GPa	e %	CYCLES TO FAIL	Temperature and condition
4880	DD5P820	310	0.1	3	21.6	1.62	178,431	50 °C Dry
4881	DD5P816	310	0.1	3	20.8	1.64	233,742	50 °C Dry
4882	DD5P816	310	0.1	3	21.1	1.52	246,075	50 °C Dry
4883	DD5P819	710	*	13	19.5	3.6	1	50 °C Dry
4884	DD5P814	730	*	13	22.3	3.3	1	50 °C Dry
4885	DD5P817	742	*	13	22.3	3.4	1	50 °C Dry
4886	DD5P812	414	0.1	2	22.1	2.21	4,207	50 °C Dry
4887	DD5P821	414	0.1	2	22	2.03	3,614	50 °C Dry
4888	DD5P818	414	0.1	2	21.5	1.86	1,132	50 °C Dry
4891	DD5P908W	241	0.1	5	----	----	2,145,373	50 °C Wet
4892	DD5P900W	310	0.1	3	20	1.42	17,971	50 °C Wet
4893	DD5P901W	241	0.1	5	20.6	1.19	1,733,316	50 °C Wet
4894	DD5P902W	241	0.1	5	20.8	1.22	2,033,339	50 °C Wet
4895	DD5P903W	310	0.1	3	21.3	1.51	45,534	50 °C Wet
4896	DD5P904W	310	0.1	3	20	1.54	35,346	50 °C Wet
4897	DD5P905W	693	*	13	21.6	----	1	50 °C Wet
4898	DD5P907W	688	*	13	22	----	1	50 °C Wet
4899	DD5P906W	734	*	13	21	----	1	50 °C Wet

TEST & SAMPLE ID #		MAX. STRESS MPa	R	Q Hz	E GPa	e %	CYCLES TO FAIL	Temperature and condition
5860	DD5P909W	-345	10	1	----	----	16	50 °C Wet
5861	DD5P910W	-426	*	13	----	----	1	50 °C Wet
5862	DD5P911W	-384	*	13	----	----	1	50 °C Wet
5863	DD5P912W	-401	*	13	----	----	1	50 °C Wet
5864	DD5P913W	-381	*	13	----	----	1	50 °C Wet
5865	DD5P914W	-276	10	2	----	----	1,410	50 °C Wet
5866	DD5P915W	-207	10	2	----	----	37,673	50 °C Wet
5867	DD5P916W	-207	10	5	----	----	44,469	50 °C Wet
5868	DD5P917W	-207	10	5	----	----	54,737	50 °C Wet
5869	DD5P918W	-165	10	8	----	----	190,729	50 °C Wet
5870	DD5P919W	-165	10	10	----	----	342,905	50 °C Wet
5871	DD5P920W	-165	10	10	----	----	141,564	50 °C Wet
5872	DD5P921	-345	10	1	----	----	130	50 °C Dry
5873	DD5P930	-207	10	5	----	----	124,290	50 °C Dry
5874	DD5P926	-207	10	5	----	----	173,669	50 °C Dry
5875	DD5P929	-207	10	5	----	----	482,504	50 °C Dry
5876	DD5P924	-276	10	4	----	----	98,038	50 °C Dry
5877	DD5P931	-276	10	5	----	----	74,728	50 °C Dry
5878	DD5P925	-276	10	5	----	----	49,636	50 °C Dry
5879	DD5P923	-508	*	13	----	----	1	50 °C Dry
5880	DD5P922	-488	*	13	----	----	1	50 °C Dry
5881	DD5P927	-500	*	13	----	----	1	50 °C Dry
5900	DD5P963	-165	10	8	----	----	1,109,352	50 °C Dry
5882	DD5P928	-379	10	5	----	----	48,127	20 °C Dry
5883	DD5P932	-345	10	5	----	----	164,214	20 °C Dry
5884	DD5P933	-345	10	5	----	----	288,708	20 °C Dry
5885	DD5P945	-345	10	10	----	----	198,403	20 °C Dry
5898	DD5P940	-651	*	13	----	----	1	20 °C Dry
5886	DD5P944	-578	*	13	----	----	1	20 °C Dry
5887	DD5P937	-661	*	13	----	----	1	20 °C Dry
5892	DD5P936	-632	*	13	----	----	1	20 °C Dry
5888	DD5P957W	-523	*	13	----	----	1	20 °C Wet
5889	DD5P956W	-542	*	13	----	----	1	20 °C Wet
5890	DD5P955W	-539	*	13	----	----	1	20 °C Wet
5891	DD5P964W	-527	*	13	----	----	1	20 °C Wet
5893	DD5P963W	-276	10	5	----	----	333,063	20 °C Wet
5894	DD5P958W	-310	10	3	----	----	16,432	20 °C Wet
5895	DD5P959W	-276	10	5	----	----	836,080	20 °C Wet
5896	DD5P960W	-310	10	3	----	----	27,564	20 °C Wet
5897	DD5P961W	-310	10	3	----	----	22,185	20 °C Wet
5899	DD5P962W	-276	10	5	----	----	637,232	20 °C Wet

Neat Resin Tests

TEST & SAMPLE ID #		MAX. STRESS MPa	R	Q Hz	E GPa	e %	CYCLES TO FAIL	WIDTH (mm) and Notes

Maximum stress column lists the maximum stress/yield stress. The listed yield stress was determined using the 0.2% strain offset method.

CoRezyn 63-AX-051 (Interplastics Corporation)
Heat deflection temperature (3 tests) - 53.6 °C, 55.3 °C, 55.1 °C

5842	poly1	59.6/47.4	*	0.1	3.01	2.4	1	11
5843	poly2	48.3/41.7	*	0.1	3.25	1.66	1	11
5844	poly3	54.3/46.5	*	0.1	3.29	1.93	1	11

Derakane 411C-50 (Dow Chemical)
Heat deflection temperature (3 tests) - 73.5 °C, 80.2 °C, 79.6 °C

5845	411C1	57.2/47.1	*	0.1	3.26	2.02	1	11
5846	411C2	58.8/53.2	*	0.1	3.16	2.14	1	11
5847	411C3	57.1/50.9	*	0.1	3.21	2.02	1	11

Derakane 8084 (Dow Chemical)
Heat deflection temperature (3 tests) - 72.6 °C, 74.7 °C, 75.2 °C

5848	80841	75.1/58.4	*	0.1	3.04	3.36	1	11
5849	80842	73.8/54.5	*	0.1	3.33	2.95	1	11
5850	80843	68.8/52.6	*	0.1	3.38	2.6	1	11

System 41 (System Three)
Heat deflection temperature (3 tests) - 59.4 °C, 52.9 °C, 53.3 °C

5851	sys31	51.1/51.1	*	0.1	3.59	1.54	1	11
5852	sys32	53.1/53.1	*	0.1	3.63	1.58	1	11
5853	sys33	53.6/53.6	*	0.1	3.49	1.67	1	11

SC-12 (Applied Poleramic Inc.)
Heat deflection temperature (3 tests) - 92.7 °C, 94.8 °C, 95.0 °C

5854	sc121	41.1	*	0.1	3.48	1.26	1	11
5855	sc122	48.5	*	0.1	3.43	1.55	1	11
5856	sc123	43.4	*	0.1	3.52	1.32	1	11

SC-14 (Applied Poleramic Inc.)
Heat deflection temperature (3 tests) - 80.5 °C, 82.7 °C, 84.3 °C

5857	sc141	72.1/50.1	*	0.1	2.83	3.68	1	11
5858	sc142	66.3/46.8	*	0.1	2.76	3.15	1	11
5859	sc143	66.3/48.6	*	0.1	2.82	3.09	1	11

List of tests omitted from the database list due to testing irregularities, premature buckling, fiber orientation or gripping problems causing an invalid test.

TEST & SAMPLE ID #		MAX. STRESS MPa	R	Q Hz	E GPa	e %	CYCLES TO FAIL	WIDTH (mm) and Notes
A1	102A	454	*	0.02	----	----	1	50 tab
A3	101A	423	*	0.02	----	----	1	50 tab
A4	103A	347	*	----	----	----	1	50 tab
1	104A	185	0.5	----	----	----	1,400	50 tab
2	105A	130	0.1	10	----	----	155,201	50 tab
3	106A	333	0.1	0.5	----	----	210	50 tab
4	107A	288	0.1	1	----	----	873	50 tab
5	106B	338	*	----	----	----	----	50 tab
8	101B	361	0.1	0.5	----	----	1,860	50 tab
10	104B	408	0.1	0.1	----	----	40	50 tab
11	105B	420	0.1	0.1	----	----	160	50 tab
14	110B	356	0.1	0.1	----	----	480	50 tab
19	115B	399	0.1	0.1	18.3	----	180	50 tab
94	109J	188	*	--	22.6	0.82	1	25 tab
275	113R	155	0.1	15	----	----	1	50 tab
307	115X	345	0.1	5	25.1	1.42	1,441	25 tab
308	111X	345	0.1	5	23.6	1.46	2,114	25 tab
324	148X	-332	*	13	26.8	2.3	1	25 tab
325	146X	-378	*	13	25.9	1.73	1	25 tab
326	149X	-326	*	13	24.0	1.39	1	25 tab
327A	190X	-365	*	13	----	----	1	25
327B	191X	-317	*	13	----	----	1	25
338	155X	-241	10	10	30.9	0.74	2,000	25 tab
448	243AA	241	-1	2	18.9	----	17	25 tab
481	273AA	----	10	25	----	----	91,520	25 tab
698	165Y	-246	10	5	----	----	31	25 tab
700	174Y	-246	10	10	25.7	1.07	235	25 tab
703	171X	-345	10	2	----	----	137	25 tab
704	165X	-345	10	1	----	----	178	25 tab
705	177X	-310	10	2	----	----	14,129	25 tab
	Material DD3 had random mat in between the 0° and ±45°, $(0/M/\pm45/M/0)_S$, $V_F = 0.48$, thickness = 2.92 mm, D155 and DB120 fabrics with an unknown mat specification.							
1054	DD3104	792	*	13	29.3	2.70	1	22
1055	DD3106	483	0.1	2	29.0	1.66	687	22
1056	DD3105	483	0.1	2	27.4	1.76	869	22
1057	DD3103	414	0.1	5	27.4	1.50	1,932	22
1058	DD3102	345	0.1	10	----	----	6,629	22
1059	DD3101	345	0.1	10	----	----	4,909	22
1130	DD7130	-448	*	25	----	----	1	25
1131	DD7126	-460	*	25	----	----	1	25
1132	DD7121	-463	*	25	----	----	1	25
1133	DD7120	-451	*	25	----	----	1	25
1134	DD6127	-310	10	5	----	----	84,387	25
1135	DD6119	-345	10	5	----	----	13,297	25
1136	DD6120	-345	10	5	----	----	10,844	25
1137	DD7123	-345	10	10	----	----	89,517	25

TEST & SAMPLE ID #		MAX. STRESS MPa	R	Q Hz	E GPa	e %	CYCLES TO FAIL	WIDTH (mm) and Notes
1138	DD7122	-345	10	10	----	----	73,744	25
1139	DD7125	-345	10	15	----	----	100,821	25
1141	DD6122	-310	10	25	----	----	110,395	25
1150	DD6134	-480	*	13	----	----	1	25
1151	DD6117	-461	*	13	----	----	1	25
1152	DD6126	-379	10	10	----	----	6,797	25
1162	DD7127	-379	10	10	----	----	1,735	25
1176	DD6142	-425	*	13	----	----	1	25
1177	DD7149	-577	*	13	----	----	1	25
1205	DD8107	483	0.1	5	15.0	----	--	22
1208	DD8110	414	0.1	5	----	----	30	22
1222	DD9115	483	0.1	5	33.4	----	17	22
1225	DD9105	276	0.1	5	33.2	----	8,873	22
Tests 1690-1692 exhibited buckling during the fatigue tests.								
1690	CH12147	-241	10	12	----	----	18,512	25
1691	CH12134	-241	10	5	----	----	16,872	25
1692	CH12142	-241	10	5	----	----	12,942	25
1845	CC201	-166	*	13	----	----	1	25
1846	CC202	-186	*	13	----	----	1	25
1847	CC203	-176	*	13	----	----	1	25
2020	D15507	-598	*	13	31.2	-1.94	1	ZERO tab
2021	D15508	-619	*	13	32.0	-1.72	1	ZERO tab
3938	DD19A107	-172	10	5	----	----	13,650	25 Z
3939	DD19A105	-172	10	4	----	----	652	25 Z
Material D155D, $V_F = 0.29$, has fiber wash and fiber misalignment								
2137	D155D201	680	*	13	25.2	2.8	1	25
2138	D155D205	746	*	13	29.0	2.7	1	25
2139	D155D211	763	*	13	29.3	----	1	25
2140	D155D210	414	0.1	1	26.1	1.65	--	25
2213	D155H105	552	0.1	4	35.9	1.54	8,460	25
2214	D155H104	552	0.1	2	28.4	----	277	25
2345	D155H115	834	*	13	36.7	----	1	25
2769	D155G308	-500	10	5	----	----	46,980	25
Material 10D155 with a gage length of 100 mm (too short)								
2567	10D155125	172	0.1	5	27.6	0.66	1,747	25
2568	10D155126	172	0.1	5	21.2	0.87	9,287	25
2769	D155G308	-500	10	5	----	----	46,980	25
2785	D092G129	-690	10	1	----	----	4	25
4181	DD25B101	310	0.1	2	16.7	2.12	1,620	22 tab
END OF DATABASE								

APPENDIX B

SUMMARY OF I-BEAM TESTS

INDIVIDUAL BEAM TEST DETAILS FOR BEAMS NUMBERS 6 AND HIGHER

TABLE OF CONTENTS PAGE

Beams With AA Material (Triax) Flanges and CH10 Material Web 451
Beam 6 451
Beam 7 455
Beam 8 460
Beam 9 461
Beam 10 461
Beam 11 464
Beam 12 467
Beam 13 468
Beam 14 470
Beam 22 471
Beam 23 472
Beams With Improved Flange and Web Materials 473
Beams With DD5P Material Flanges and CH10 Material Webs 473
Beam 18 474
Beam 19 475
Beam 20 475
Beam 21 478
Beam 24 479
Beam 25 481
Beam 26 482
Beam 27 483
Beam 28 484
Beam 29 485
Beams With DD5P Material Flanges and CH3 Material Webs 486
Beam 30 487
Beam 31 488
Beam 32 489
Beam 33 490
Beams With DD5P Material Flanges and CH5 Material Webs 491
Beam 34 491
Beam 35 493
Beams With DD5P Material Flanges and DD5P Material Webs 494
Beam 51 494
Beam 52 494
Beam 53 497
Beam 54 498

Beams With Structural Details 499
Beams With Holes in Material AA (Triax) Flanges 499
Beam 15 500
Beam 16 501
Beam 17 502
DD27 Material Flanges (with balsa wood) and CH12 Web Material 504
Beam 58 504
Beam 59 504

AA Material (Triax) Flanges and CH10 Web Material

Beams 6 through 17, 22 and 23 all had Material AA (CDB200 Triax fabric) flanges, V_F = 0.42, consisting of a lay up of $((\pm 45°/0°)_2)_S$, except for Beams 9 and 10, which had the lay up reversed $((0°/\pm 45°)_2)_S$. The description of the I-beam flange lay up and ply numbering scheme for these beams is outlined in Tables B1 and B2. The web was CH10 material, $((\pm 45°)_3)_S$ with DB240 fabric.

BEAM 6

Beam 6 was tested statically to failure. The beam was loaded under actuator displacement control at a rate of 0.25 mm/s until failure, which involved a total ramp time of 74 seconds. An initial beam stiffness of 3,711 kN/m was measured. As the beam was loaded, the compression flange started to twist along the X-axis, prior to final compressive failure of the compression flange. The total amplitude of this twist was approximated at 6 to 8 mm prior to failure and the onset of this twisting occurred at approximately 90 to 95 percent of the ultimate load. This twisting was also evident in the failed beam as one side of the beam flange had fragmented ±45° strands pointing up, while the other side of the flange had the fragmented strands pointing down. Figures B1 and B2 show the failed beam. Further examination of the buckled compression flange indicated that the outside 0° ply (ply 3, Table B1) delaminated first from the adjacent +45° layer (ply 4, Table B1). This delamination arrested at x = 267 mm, which was evident by the white damage band in the outside plies at this point. It was not evident where the delamination started. From this initial arrest at x = 267 mm, the delamination continued to grow towards both inside compressive load pads at x = 152 mm and x = 464 mm.

The web had multiple delaminations under the initial flange failure site generated after the flange failure. Some delamination spots are visible at x = 191, 267, 343 and 394 mm, at the compression flange-web intersection that could be buckling nodal points. No shear stiffener, torsional stiffener or tension flange damage or delaminations were visible. The load-flange absolute maximum strain graph is shown in Figure B3 and indicates a maximum tension flange strain of 1.80 percent and a minimum compression flange strain of -1.6 percent which occurred at an ultimate applied load of 67.08 kN at a maximum mid-span deflection of 22 mm.

Table B1. Ply reference notation for Beams 6 through 9, 12 through 17, 22 and 23.

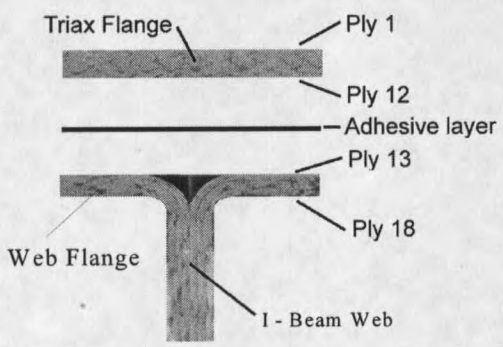
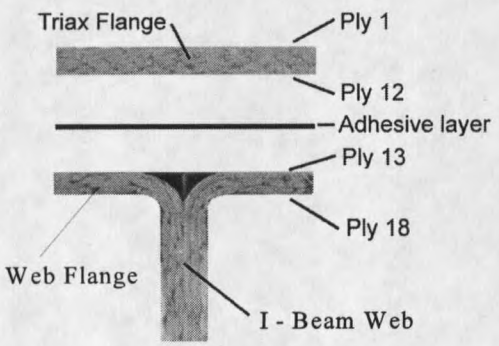
<table>
<tr><th>Ply number</th><th>Ply angle</th><th>Fabric</th><th>Description</th></tr>
<tr><td>1</td><td>+45°</td><td rowspan="3">CDB200</td><td rowspan="12">Material AA
triax flange, 2.9 mm thick
$V_F = 0.42$</td></tr>
<tr><td>2</td><td>-45°</td></tr>
<tr><td>3</td><td>0°</td></tr>
<tr><td>4</td><td>+45°</td><td rowspan="3">CDB200</td></tr>
<tr><td>5</td><td>-45°</td></tr>
<tr><td>6</td><td>0°</td></tr>
<tr><td>7</td><td>0°</td><td rowspan="3">CDB200</td></tr>
<tr><td>8</td><td>-45°</td></tr>
<tr><td>9</td><td>+45°</td></tr>
<tr><td>10</td><td>0°</td><td rowspan="3">CDB200</td></tr>
<tr><td>11</td><td>-45°</td></tr>
<tr><td>12</td><td>+45°</td></tr>
<tr><td colspan="4">Adhesive Layer Hysol EA 9309.2NA, 0.1 - 0.4 mm thick</td></tr>
<tr><td>13</td><td>+45°</td><td rowspan="2">DB240</td><td rowspan="6">Web material CH10
C-channel web flange,
5 mm thick
$V_F = 0.35$</td></tr>
<tr><td>14</td><td>-45°</td></tr>
<tr><td>15</td><td>+45°</td><td rowspan="2">DB240</td></tr>
<tr><td>16</td><td>-45°</td></tr>
<tr><td>17</td><td>+45°</td><td rowspan="2">DB240</td></tr>
<tr><td>18</td><td>-45°</td></tr>
<tr><td colspan="4">
</td></tr>
</table>

Table B2. Ply reference notation for Beams 10 and 11.

Ply number	Ply angle	Fabric	Description
1	0°	CDB200	Material AA2 triax flange, 2.9 mm thick $V_F = 0.42$
2	-45°		
3	+45°		
4	0°	CDB200	
5	-45°		
6	+45°		
7	+45°	CDB200	
8	-45°		
9	0°		
10	+45°	CDB200	
11	-45°		
12	0°		
Adhesive Layer Hysol EA 9309.2NA, 0.1 - 0.4 mm thick			
13	+45°	DB240	Web material CH10 C-channel web flange 5 mm thick $V_F = 0.35$
14	-45°		
15	+45°	DB240	
16	-45°		
17	+45°	DB240	
18	-45°		



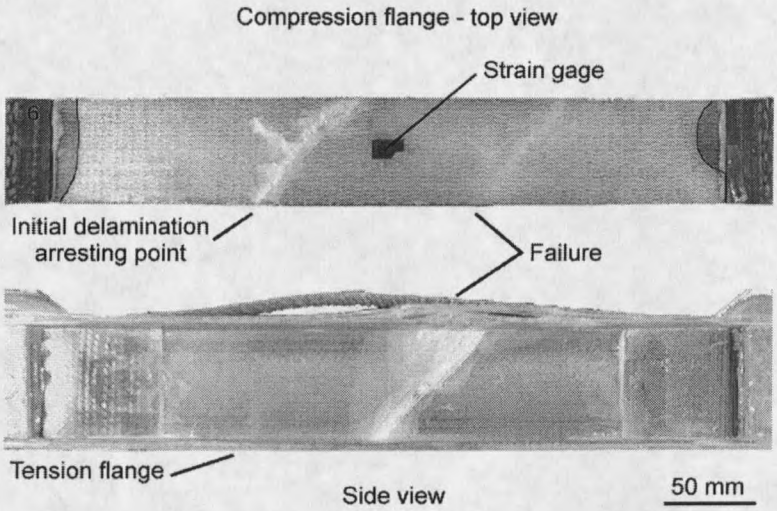


Figure B1. Beam 6.

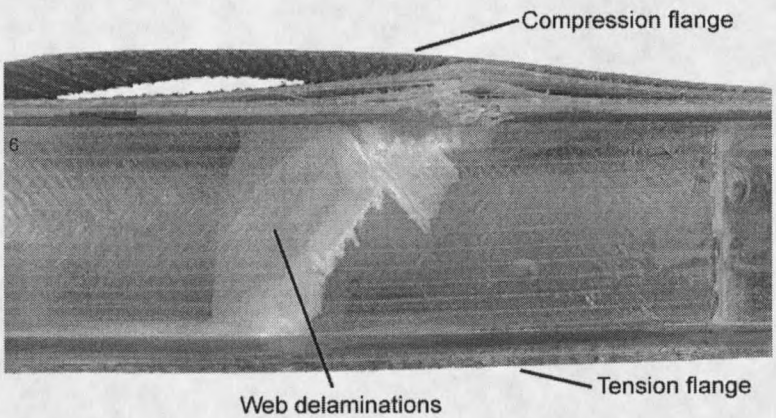


Figure B2. Beam 6.

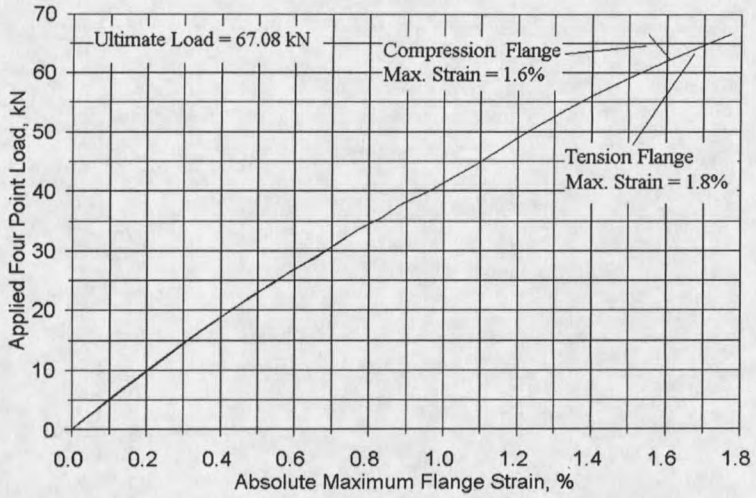


Figure B3. Load versus maximum flange strain, beam 6, static test.

BEAM 7

Beam number 7 was fatigued at a rate of 5 Hz under sinusoidal load control with a maximum load of 24.5 kN and a minimum load of 2.5 kN. The maximum load produced an initial maximum tension flange strain of 0.58 percent and a minimum compression flange strain of -0.56 percent. The initial beam stiffness was measured as 3,398 kN/m. The tensile flange had two additional strain gages on the flange edges to determine the strain distribution across the flange. At a static load of 27 kN, the center strain gage indicated 0.680percent strain, while the edge gages indicated 0.64 percent and 0.63 percent for a combined average strain of 0.65 percent. With the center strain gage directly over the web and the two other gages on the relatively flexible edges, this strain distribution is fairly uniform with only a ±4 percent change across the flange width. Initially, the beam was loaded to 32 kN with readings taken from all the strain gages, including a delta strain gage rosette (0°/120°/240°) centered 9 mm ahead of one of the shear stiffeners on the neutral axis of the beam. The strain rosette (Omega Engineering Inc. SG-3/350/RY11) was utilized to determine the nature of the strains ahead of the stiffener, which was a point of damage on the initial beams (1 to 5) and to also aid in finite element modeling of the beam.

The initial loading versus flange strain graph is shown in Figure B4 and is typical of all the other triax beams. Both the tension and compression flange indicate the same load-strain slope. The maximum absolute flange strain versus fatigue cycles is shown in Figure B5. The stiffness of the beam decreases during the fatigue test due to matrix cracking and delamination, and under load control, the maximum strain in the beam must increase during the fatigue test. The apparent increase in actuator amplitude, (maximum stroke minus minimum stroke), is shown in Figure B6 and is typical of all the beams tested. The initial strain rosette data is graphically shown in Figure B7. The shear stress 9 mm ahead

of the shear stiffener was calculated from this data and is shown in Figure B8. The shear stress is small, but present on the neutral axis of the beam at this point. During the fatigue test, white spots started to form at random locations on the tension flange. These damage nucleation locations involved fiber delamination and fiber breakage involving the stitching cross over points in the fabrics.

As the fatigue test continued, the damage sites increased in size and some damage spots coalesced to form failure lines. These sites continued to grow until the worst damage site extended across the tensile flange that caused final failure of the tension flange at 492,147 cycles. The failure site occurred at x = 356 ±5 mm and is shown in Figures B9 and B10.

The flange damage was very localized, while the delamination of the entire flange from the I-beam preform extended from x = 260 to x = 406 mm and was due to the flange failure. The delamination in the beam occurred between the +45° (ply 12, Table B1) and the adhesive, and between the ±45° plies (plies 15,16, Table B1). The failure also caused delaminations to extend 16 mm down into the shear web. No shear stiffener, torsional stiffener or compression flange damage or delaminations were visible. The Instron 8501 displacement interlocks were set so that any actuator travel ±3 mm above the nominal fatigue running displacement would stop the fatigue test and limit any post failure damage from being generated. This procedure was observed for all the beams.

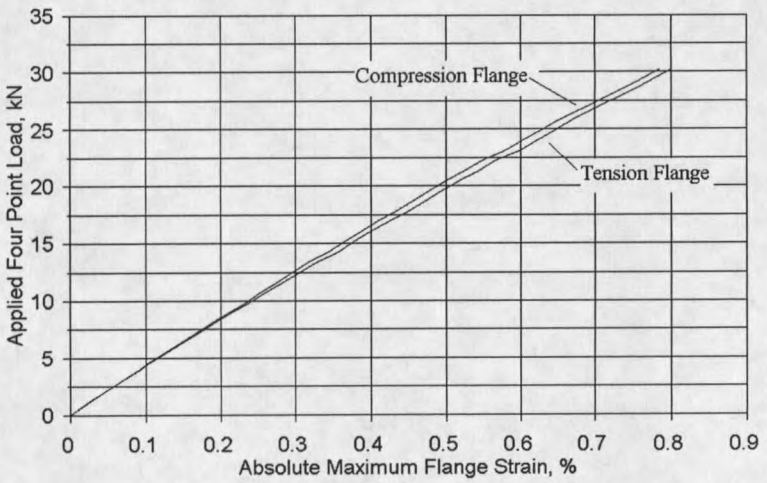


Figure B4. Load versus maximum flange strain, beam 7, initial loading.

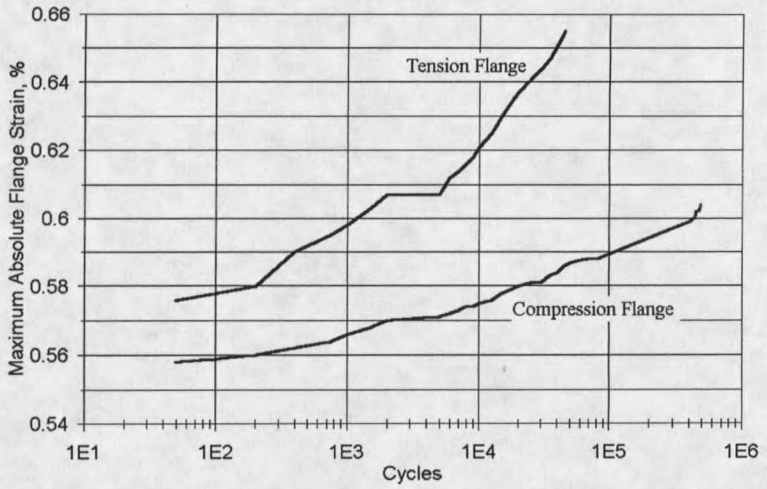


Figure B5. Maximum flange strain, beam 7. initial loading.

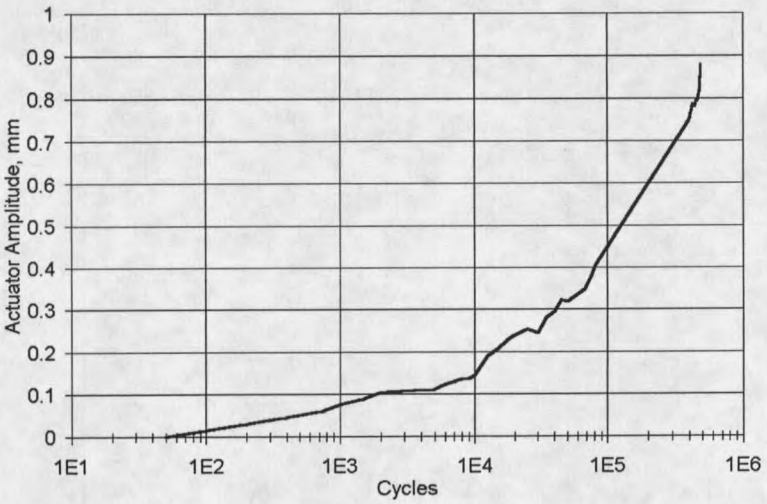


Figure B6. Actuator amplitude versus cycles, beam 7.

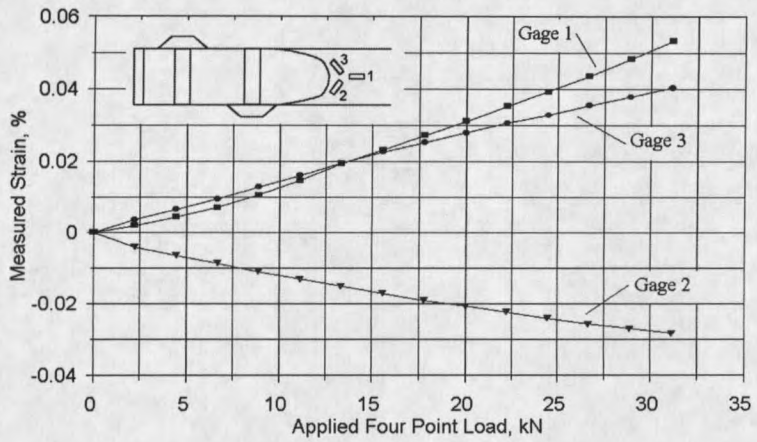


Figure B7. Load versus strain for beam 7, delta strain gage rosette on web.

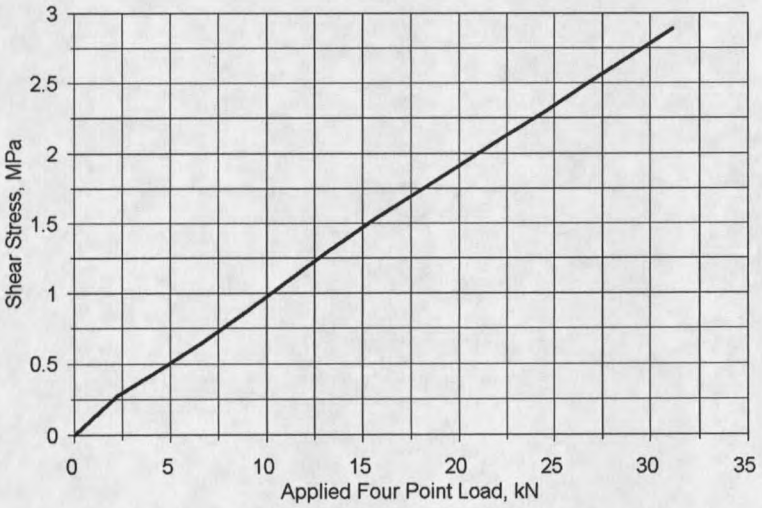


Figure B8. Load versus web shear stress for beam 7, 9 mm ahead of shear stiffener.

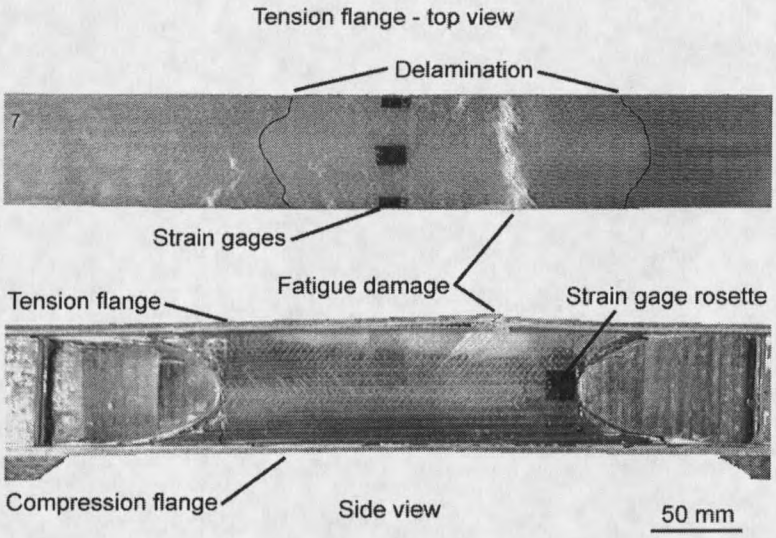


Figure B9. Beam 7.

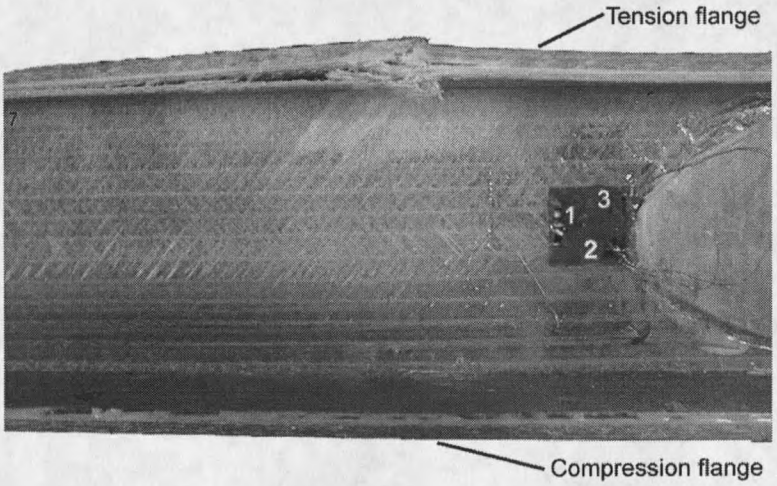


Figure B10. Beam 7.

BEAM 8

Beam number 8 was fatigued at a rate of 2 Hz with a maximum load of 31.1 kN and a minimum load of 3.1 kN. The maximum load produced an initial maximum tension flange strain of 0.79 percent and a minimum compression flange strain of -0.70 percent. The initial beam stiffness was measured as 3,499 kN/m. As with Beam 7, white damage spots were generated on the tension flange during the fatigue test.

At 29,051 cycles, the tensile flange failed and separated at x = 324 ± 9 mm, which caused the flange to delaminate from the preform between x = 255 to x = 368 mm and is shown in Figures B11 and B12. The delamination involved extensive fiber bridging between the inside flange +45° (ply 12, Table B1) and the adhesive on the preform. This beam was fatigued at a higher strain than Beam 7 and thus had more internal strain energy stored in it prior to failure, which is apparent by the amount of damage generated in the web as compared to Beam 7. The web delamination extended 45 mm from the tension flange and was located at x = 324 ± 44 mm. No shear stiffener, torsional stiffener or compression flange damage or delaminations were visible.

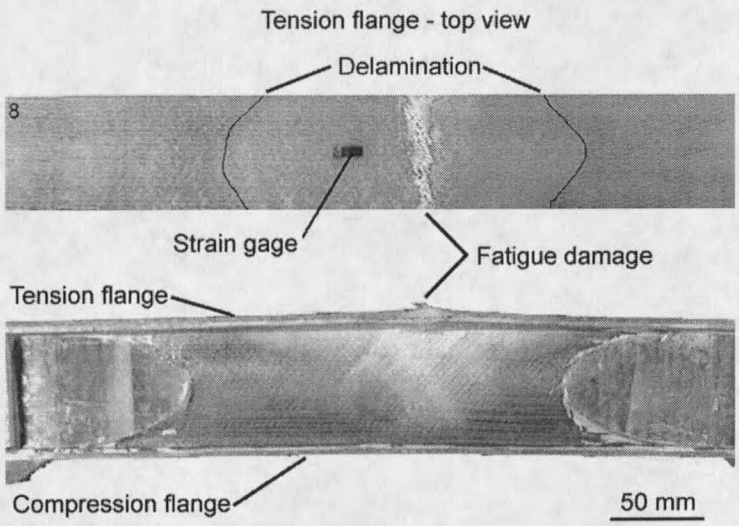


Figure B11. Beam 8.

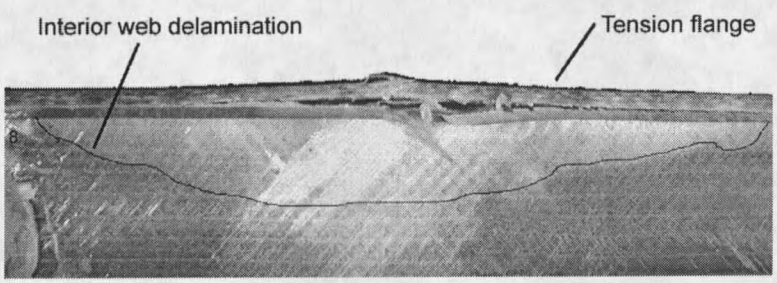


Figure B12. Beam 8.

BEAM 9

Beam 9 involved a static test. The beam was loaded under actuator displacement control at a rate of 0.25 mm/s until failure, which involved a total ramp time of 43 seconds. An initial beam stiffness of 3,556 kN/m was measured. Beams 9 and 10 were constructed with the 0° plies on the outside (Material AA2) of the flange rather than the +45° (Material AA). This layup reversal did not significantly affect the stiffness of the beam when compared to the other beams. It was apparent, after the static test, that there was substantial fiber waviness in the fabric that caused the beam to fail prematurely. Curved fiber tows, with a radius of 4 to 5 mm, turned white as they delaminated from the material around them on both the tension and compression flanges. Figures B13 and B14 show the failed beam. The ultimate load that the beam held was 59.2 kN and corresponded to a maximum tension flange strain of 1.78 percent and a minimum compression flange strain of -1.80 percent. The load versus maximum strain graph is shown in Figure B15. The buckling failure of the compression flange occurred at two sites: $x = 260 \pm 6$ mm on the flange and $x = 298 \pm 10$ mm on the preform. Delamination of the flange from the web flange occurred from $x = 203$ to $x = 419$ mm and was between the adhesive layer and 0° (ply 12, Table B2) ply and also between the 0° (ply 12, Table B2) and -45° (ply 11, 23) plies. The delamination also heavily affected the web, $x = 260$ mm to $x = 356$ mm, as the web delaminated fully between the interior -45° plies and also placed a spot delamination in the adhesive region on the tension flange. No shear stiffener, torsional stiffener or other tension flange damage or delaminations were visible.

BEAM 10

Beam number 10 was fatigued at a rate of 1 Hz with a maximum load of 40.0 kN and a minimum load of 4.0 kN. The maximum load produced an initial maximum tension flange strain of 1.07 percent and a minimum compression flange strain of -0.97 percent. The initial beam stiffness was measured as 3,694 kN/m. The initial hysteresis of the beam is shown in Figure B16. As with Beam 9, the fiber waviness caused premature damage to be generated on the tension flange. The test was stopped after 1,870 cycles due to the amount of damage present on the tension flange and the white delaminated regions had reached both sides of the flange at $x = 349 \pm 13$ mm. The beam stiffness was checked after the 1,870 cycles and equaled 3,384 kN/m, which was 92 percent of the initial stiffness. The failure site will probably occur at $x = 254 \pm 12$ mm due to the amount of accumulated damage in the 0° plies across the tension flange. No shear stiffener, torsional stiffener or compression flange damage or delaminations were visible at the end of the test. The failed beam is shown in Figure B17.

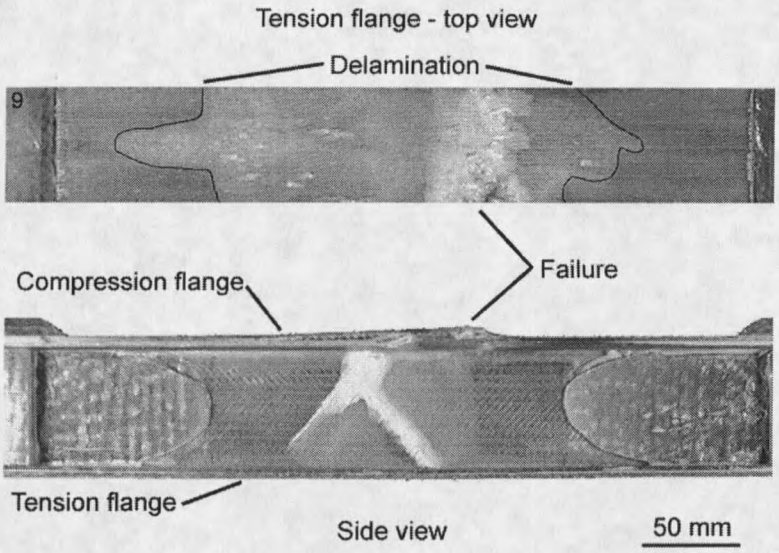


Figure B13. Beam 9.

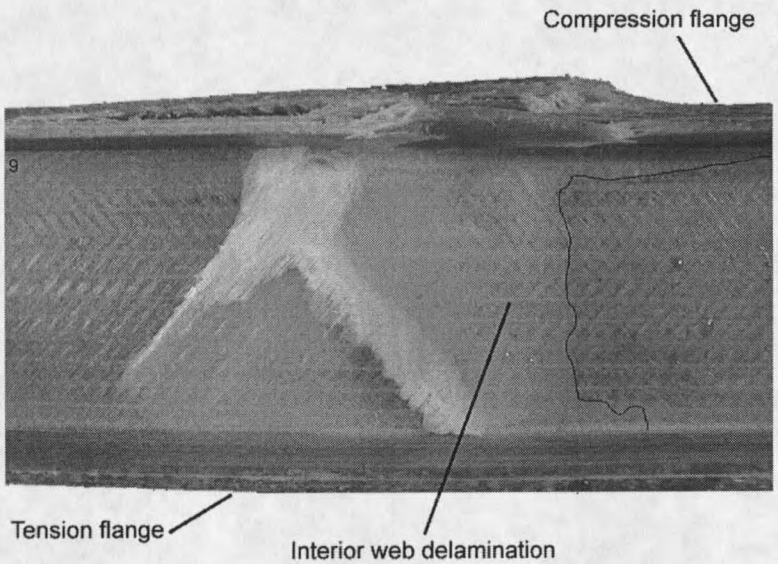


Figure B14. Beam 9.

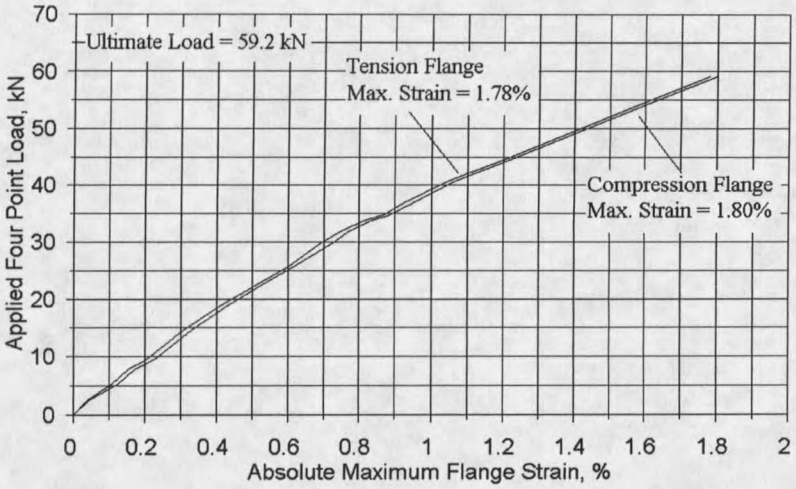


Figure B15. Load versus maximum flange strain beam 9, static test.

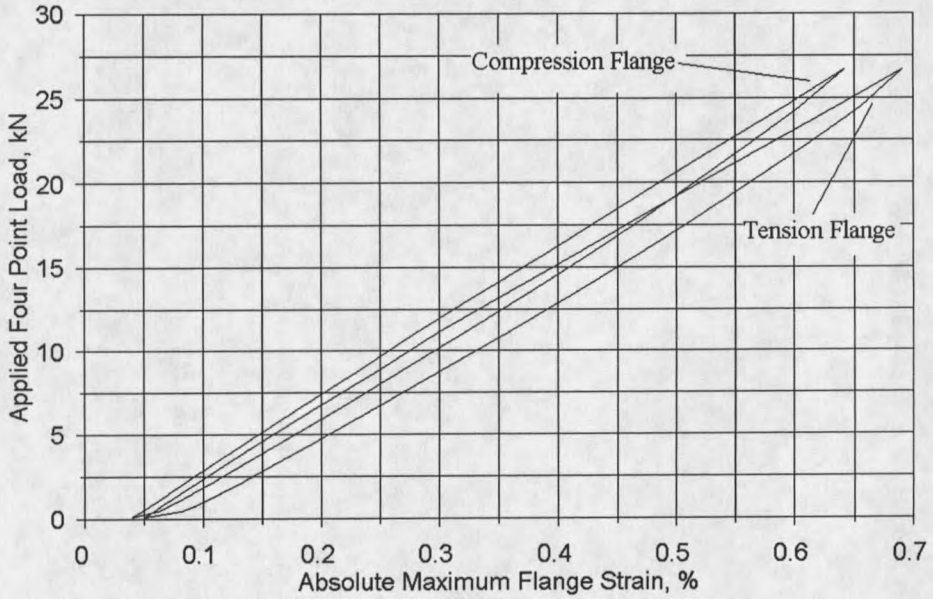


Figure B16. Initial hysteresis of beam 10.

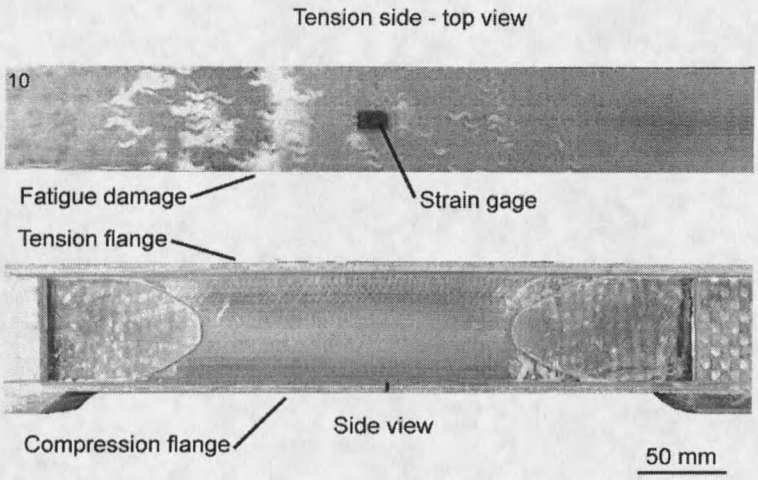


Figure B17. Beam 10.

BEAM 11

Beam number 11 was fatigued at a rate of 1 Hz with a maximum load of 40.0 kN and a minimum load of 4.0 kN. The maximum load produced an initial maximum tensile flange strain of 1.08 percent and a minimum compressive flange strain of -0.96 percent. The initial beam stiffness was measured as 3,436 kN/m. The fatigue test was stopped after 3,100 cycles to check the stiffness of the beam. The stiffness had decreased to 3,061 kN/m which was 89 percent of the initial stiffness. Figure B18 shows the initial beam stiffness and the stiffness after 3,100 cycles. The fatigue test was resumed and the beam failed after 4,620 cycles with a tension flange failure. The maximum flange strain versus fatigue cycles is shown in Figure B19. The offset in the graph at 3,100 cycles is due to the unloading of the beam for the stiffness check. Prior to failure, numerous white damage nucleation sites were evident on the tension flange.

Final failure of the flange occurred at x = 381 ± 17 mm and was very localized with some tearing of the top ±45° plies (ply 1 and 2, Table B1), which was noticed just prior to final failure. Delamination of the tensile flange occurred between the polyester matrix and the +45° ply (ply 13, Table B1) on the web flange with multiple amounts of fiber bridging and was located at x = 229 to x = 400 mm. Some delamination in the web was present and was caused by the flange failure. Figures B20 and B21 show the failed beam. No shear stiffener, torsional stiffener or compression flange damage or delaminations were visible. The load pads were manufactured as three separate plates that were then adhesively bonded together to get the required 12 mm load pad height. The upper most plate of this load pad assembly had partially delaminated in the adhesive interface from the rest of the pad. It is hypothesized that the adhesive layer was not thick enough to resist the applied compression loading on these pads. All four pads show the same partial delamination problem, but this did not influence the beam performance during the test.

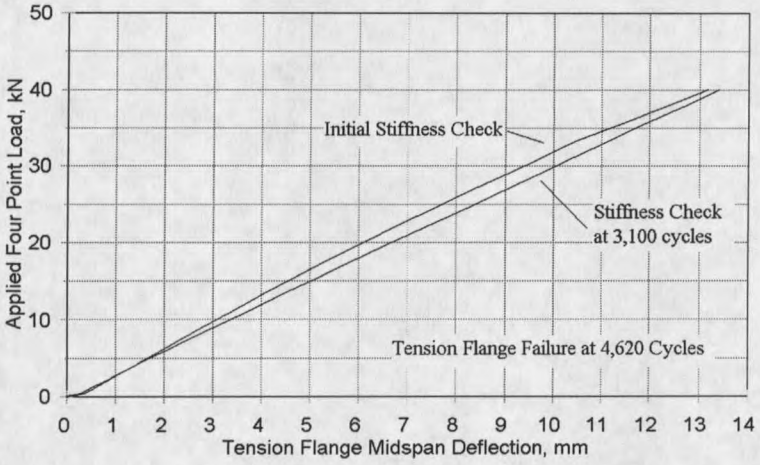


Figure B18. Load versus flange midspan deflection, beam 11.

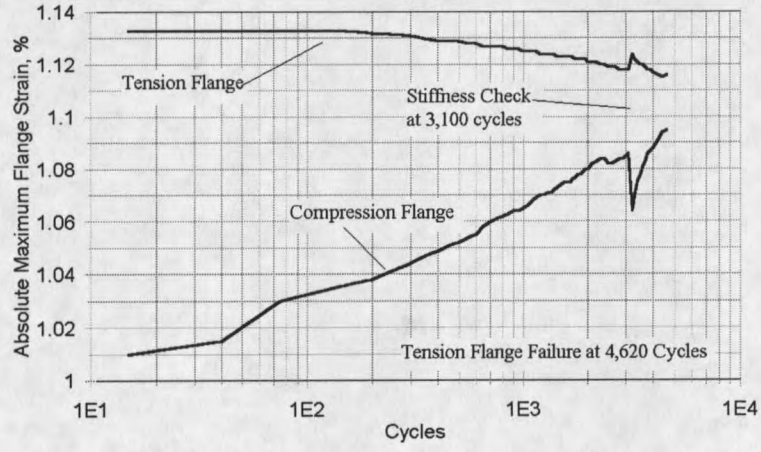


Figure B19. Absolute maximum flange fatigue strain versus cycles, beam 11.

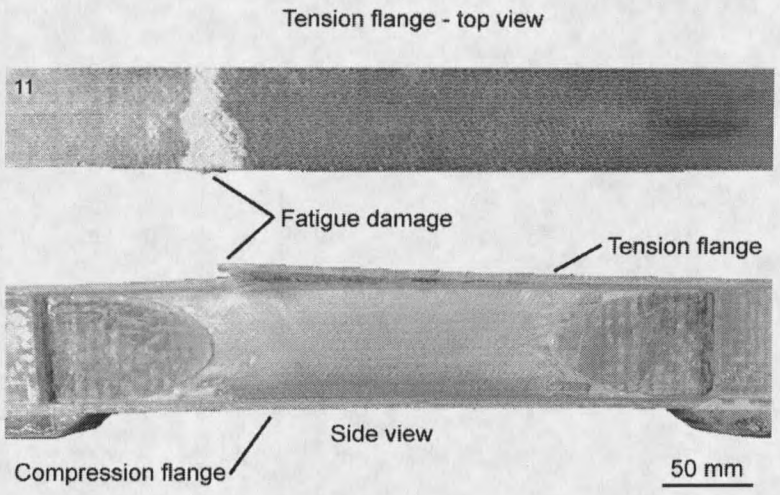


Figure B20. Beam 11.

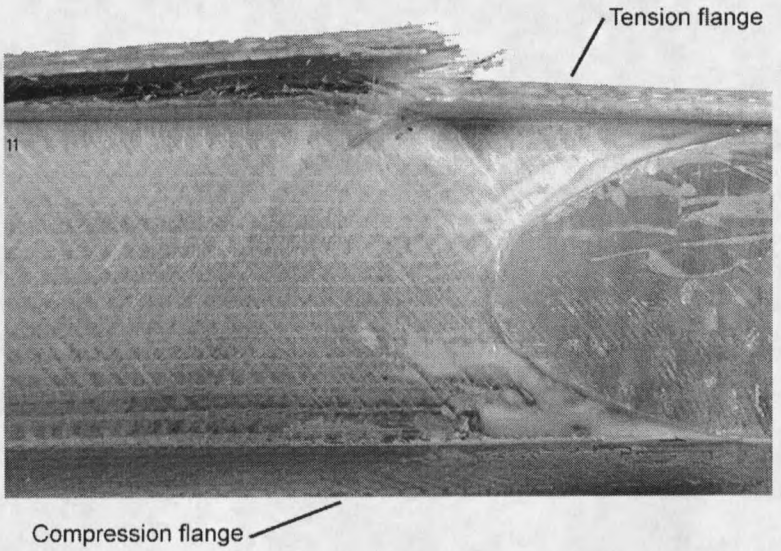


Figure B21. Beam 11.

BEAM 12

Beam number 12 was fatigued at a rate of 2 Hz with a maximum load of 28.9 kN and a minimum load of 2.9 kN. The maximum load produced an initial maximum tension flange strain of 0.73 percent and a minimum compression flange strain of -0.68 percent. The initial beam stiffness was measured as 3,498 kN/m. As with the other beams, numerous white damage nucleation spots appeared on the tension flange during the fatigue test. These damaged areas grew and coalesced until the damage spanned across the flange.

The final failure site started at one edge of the flange and grew to the other edge. After 30,290 cycles, the beam failed on the tension flange at x = 336 mm and is shown in Figure B22. The flange delaminated between the adhesive and the +45° ply (ply 12, Table B1) from x = 279 to x = 394 mm and contained multiple fiber bridging sites. The tension flange delamination traveled 45 mm into the web directly under the failure site. Some other minor cracks were evident on the flanges of the preform as the ±45° fabrics did not completely fill the C-channel mold, and thus created a matrix rich region on the flange edge, which cracked and segmented. These cracks were on the order of 10 mm in length, 5 mm wide and were located over the shear stiffener area of the beam. The load pads showed the same minor delamination problem as in Beam 11. Both these manufacturing flaws did not seem to cause any problems with the performance of the beam during the test. Otherwise, no shear stiffener, torsional stiffener or compression flange damage or delaminations were visible.

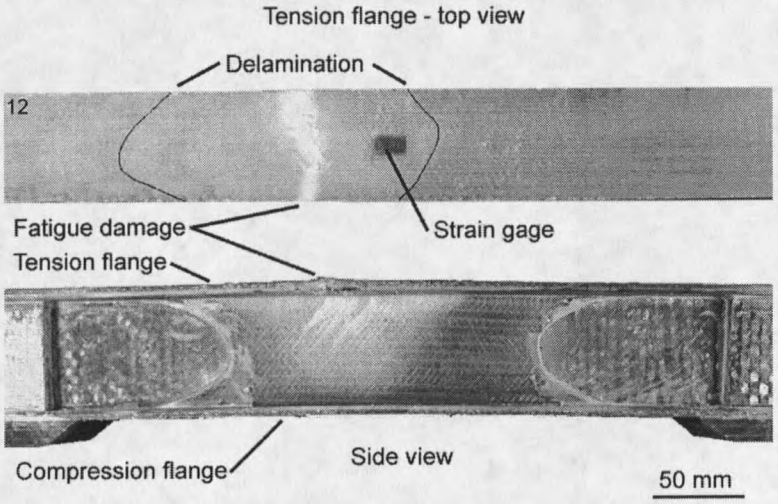


Figure B22. Beam 12.

BEAM 13

Beam 13 involved a static test. The beam was loaded under actuator displacement control at a rate of 0.51 mm/s until failure, which involved a total ramp time of 21 seconds. An initial beam stiffness of 3,516 kN/m was measured. The ultimate load was 60.72 kN and corresponded to a maximum tension flange strain of 2.10 percent, a minimum compression strain of -1.85 percent and a maximum mid-span deflection of 17 mm. The load versus maximum strain graph is shown in Figure B23. The beam failed in the compression flange at x = 330 ± 25 mm with delaminations between the 0° (ply 10, Table B1) and +45 plies (ply 11, 22) over the distance of x = 165 mm to x = 457 mm. The failed beam is shown in Figures B24 and B25. The failure at x = 330 mm caused the web to delaminate towards the tension flange under this failure point, causing an additional delamination spot under the tension flange. No shear stiffener, torsional stiffener or other tension flange damage or delaminations were visible.

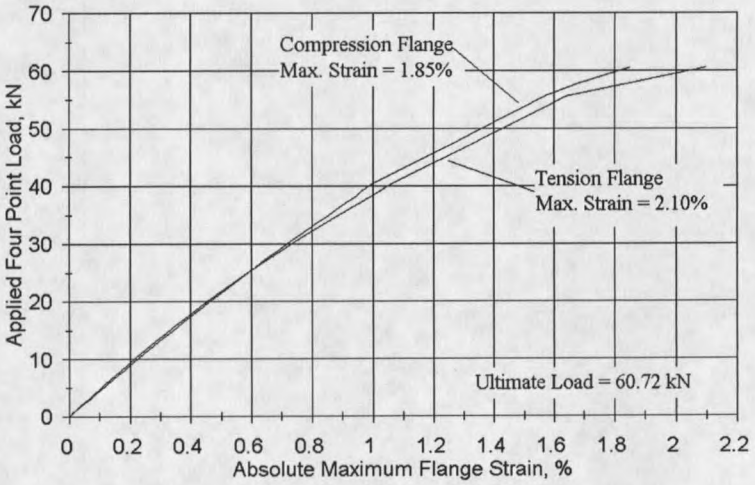


Figure B23. Load versus maximum flange strain, beam 13, static test.

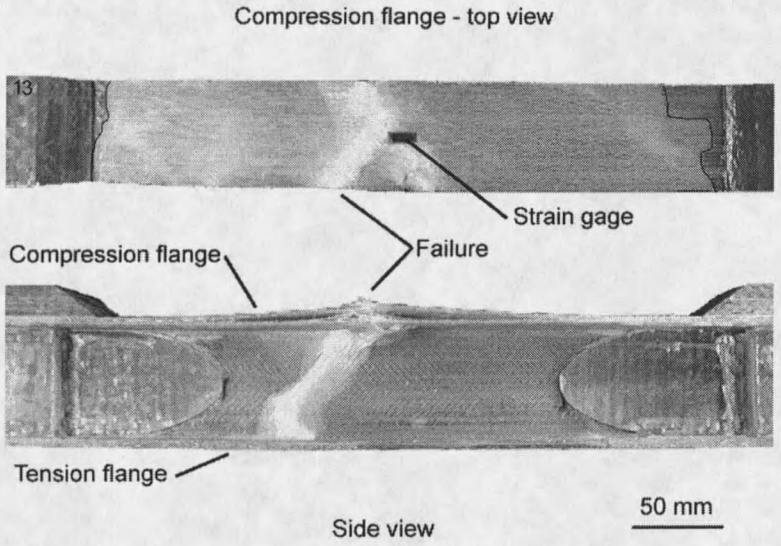


Figure B24. Beam 13.

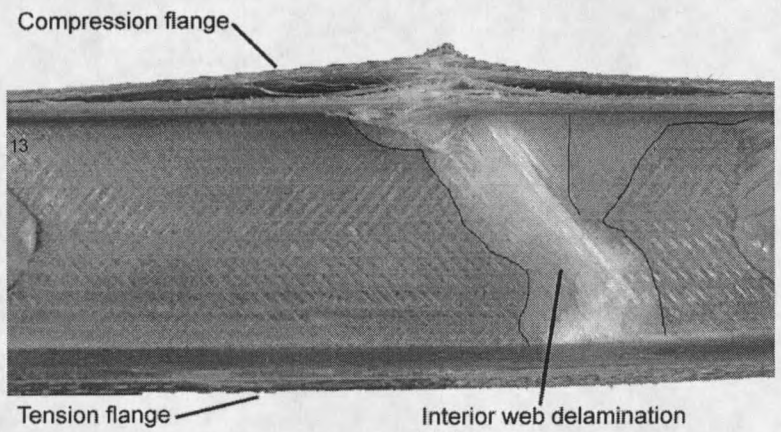


Figure B25. Beam 13.

BEAM 14

Beam number 14 was fatigued at a rate of 5 to 10 Hz with a maximum load of 24.5 kN and a minimum load of 2.5 kN. The maximum load produced an initial maximum tension flange strain of 0.59 percent and a minimum compression flange strain of -0.58 percent. The initial beam stiffness was measured as 3,407 kN/m. The fatigue test was stopped after 160,000 cycles to check the stiffness, which had reduced to 3,271 kN/m or 96 percent of the initial stiffness. After 389,175 cycles the tension flange failed at x = 248 ± 6 mm. The damage started at the edge of the tension flange and grew across the flange until final failure. The failure caused a delamination from x = 229 mm to x = 394 mm and was between the +45° ply (ply 16, 22) and the -45° ply (ply 17, Table B1) in the web flange. Figure B26 shows the failed beam. This delamination extended 10 mm down into the web. No shear stiffener, torsional stiffener or compressive flange damage or delaminations were visible.

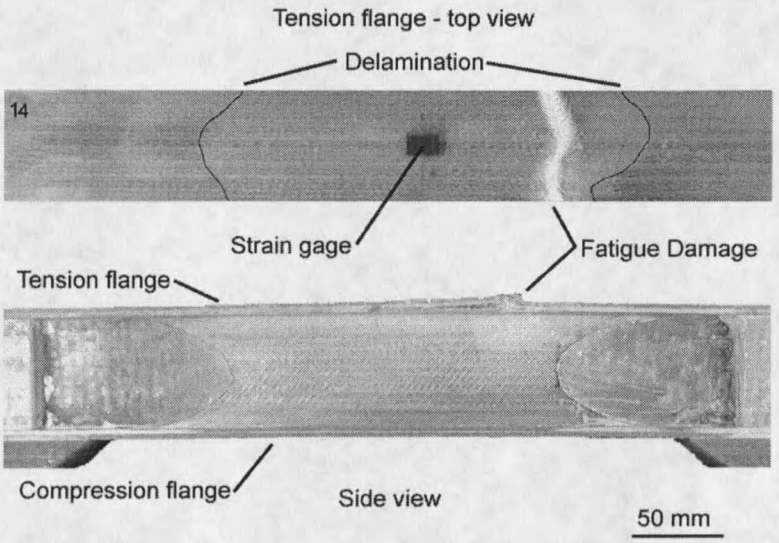


Figure B26. Beam 14.

BEAM 22

Beam number 22 was fatigued at a rate of 5 Hz with a maximum load of 31.1 kN and a minimum load of 3.1 kN. The maximum load produced an initial maximum tension flange strain of 0.84 percent and a minimum compression flange strain of -0.76 percent. The initial beam stiffness was measured as 3,637 kN/m. This beam had two acoustic emission sensors on the tension flange centered at x = 70 and 543 mm and two on the compression flange centered at x = 178 and 432 mm. The acoustic emission testing was performed with Dr. Al Beattie from Sandia National Laboratory and will not be discussed here. This beam showed less white damage sites on the tension flange than the previous beams during the fatigue test. Final failure occurred on the tension flange at x = 368 ± 10 mm with a delamination between the +45° ply (ply 11, Table B1) and the -45° ply (ply 12, Table B1). The delamination was between x = 330 and 406 mm and grew 25 mm into the web. The failed beam is shown in Figure B27. No shear stiffener, torsional stiffener or compression flange damage or delaminations were visible.

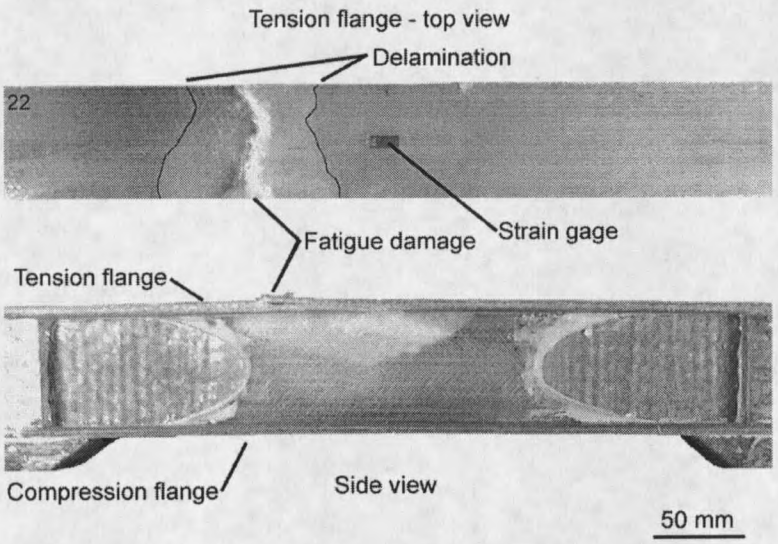


Figure B27. Beam 22.

BEAM 23

Beam number 23 was fatigued at a rate of 5 Hz with a maximum load of 28.9 kN and a minimum load of 2.9 kN. The maximum load produced an initial maximum tension flange strain of 0.71 percent and a minimum compression flange strain of -0.64 percent. The initial beam stiffness was measured as 3,542 kN/m. This beam also had two acoustic emission sensors on the tension flange centered at x = 64 and 543 mm and two on the compression flange centered at x = 178 and 438 mm. The beam failed in the tensile flange after 119,995 cycles. The failure site was at x = 318 ± 10 mm and created a delamination between the adhesive and the +45° ply (ply 13, 22) of the preform from x = 292 to x = 356 mm. This delamination extended 18 mm down into the web. The web flange had a matrix rich region on the edge of the flange between x = 279 and x = 470 mm and had a maximum depth towards the web of 8 mm. The failed beam is shown in Figure B28. The failure site of the tensile flange was within this matrix rich region and it is believed that the initial delamination did nucleate at this edge, between the adhesive and the preform. Although this beam went 89,705 cycles longer than Beam 12, it was assumed that this had some minor effect on the performance of the test, but not a large enough effect to be considered a structurally flawed beam. No shear stiffener, torsional stiffener or compression flange damage or delaminations were visible.

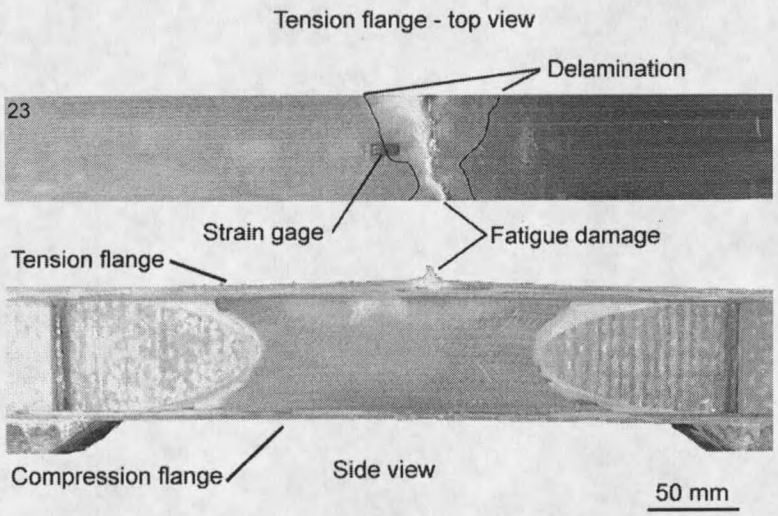


Figure B28. Beam 23.

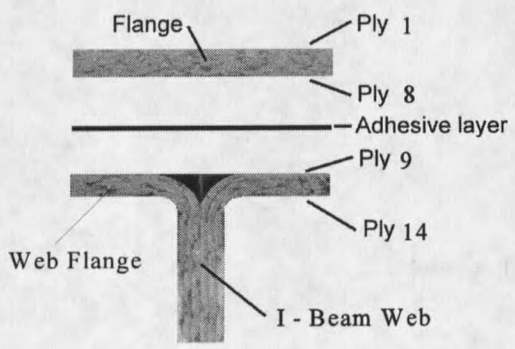
Beams With Improved Flange and Web Materials

Beams with DD5P Material Flanges and CH10 Web Material

Beams 18 through 21 and 24 through 29 all had DD5P flange material, $V_F = 0.36$, consisting of a lay up of $(0°/\pm45°/0°)_S$. The description of the I-beam flange layup and ply numbering scheme for these beams is outlined in Table B3.

Table B3. Ply reference notation for Beams 18 - 21 and 24 - 29.

Ply number	Ply angle	Fabric	Description
1	0°	D155	DD5P flange material, 2.9 mm thick $V_F = 0.36$
2	+45°	DB120	
3	-45°		
4	0°	D155	
5	0°		
6	-45°	DB120	
7	+45°		
8	0°	D155	
Adhesive Layer Hysol EA 9309.2NA, 0.1 - 0.4 mm thick			
9	+45°	DB240	Web material CH10 C-channel web flange 5 mm thick $V_F = 0.35$
10	-45°		
11	+45°	DB240	
12	-45°		
13	+45°	DB240	
14	-45°		



BEAM 18

Beam number 18 was fatigued at a rate of 1 Hz under sinusoidal load control with a maximum load of 62.3 kN and a minimum load of 6.3 kN. The maximum load produced an initial maximum tension flange strain of 1.42 percent and a minimum compression flange strain of -1.34 percent. The initial beam stiffness was measured as 4,134 kN/m. During the fatigue test, it was evident from the 0° fiber bundles delaminating from the flange surface that the DD5P flange material had been manufactured with a 2° to 3° angle. This angle caused the 0° edge terminated fibers to delaminate, starting from the flange edge and growing inward along the fiber bundle axis. This damage was confined to 4 to 6 mm from the flange edges and involved both the tension and compression flanges. The beam stiffness was checked throughout the test and is summarized in Table B4. As the fatigue test progressed, the tension flange started to delaminate from the C-channel between the 0° ply (ply 8, Table B3) and the +45° ply (ply 7, Table B3). This initial delamination started in the center of the beam and was located directly above the tapered shear stiffeners, x = 165 mm and x = 457 mm. This delamination grew until the test was stopped after 9,367 cycles. At this point, the delamination extended from x = 127 mm to x = 571 mm, but had not completely traveled across the width of the flange. The compression flange had some transverse tensile cracks under the edges of the web and extended from x = 152 to 457 mm. There was also major flange damage at x = 381 to 432 mm, directly below the tapered shear stiffener, that was 18 mm wide. This damage involved broken 0° on the surface and delaminations throughout the thickness of the flange. The web had delaminations extending into the shear stiffeners, but otherwise the center web, x = 215 to x = 394 mm, had no other noticeable damage. One shear stiffener showed cracking at x = 444 ±12 mm on the tension flange side and was involved with the web delamination underneath. The failed beam is shown in Figure B29.

Table B4. Beam 18 Stiffness versus Cycles.

Cycles	Stiffness (K), kN/m	Ratio (K/ 4,134)	n / N N = 9,367
0	4,134	1	--
1,000	3,714	0.90	0.11
2,000	3,619	0.88	0.21
3,000	3,632	0.88	0.32
4,000	3,659	0.88	0.43
5,000	3,486	0.84	0.53
6,000	3,509	0.85	0.64
8,000	3,428	0.83	0.85
9,367	3,150	0.76	1

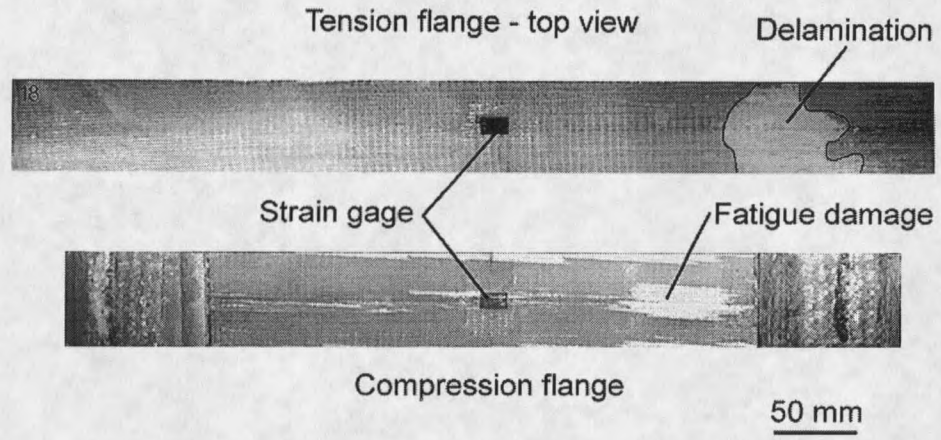


Figure B29. Beam 18.

BEAM 19

Beam 19 involved a static test. The beam was loaded under actuator displacement control at a rate of 0.05 mm/s until failure, which involved a total ramp time of 208 seconds and a total mid-span deflection of 13 mm. An initial beam stiffness of 4,245 kN/m was measured. As with the other static tests, the compression flange twisted prior to final failure. This twisting was also evident in the failed beam as one side of the beam flange had fragmented glass 0° and ±45° tows pointing up, while the other side of the flange had the fragmented glass tows pointing down. The compression flange failed at x = 305 ±15 mm with multiple delaminations throughout the flange thickness. The compression flange delaminated between the 0° ply (ply 5, 24) and -45° ply (ply 6, Table B3) from x = 305 to 457 mm. The flange also delaminated between the 0° ply (ply 8, Table B3) and the adhesive from x = 158 to 305 mm. The failure caused a delamination to travel into the web and created two spot delaminations on the tension flange in the adhesive layer. One shear stiffener showed some delamination at its tapered tip. No other shear stiffener, torsional stiffener or other tension flange damage or delaminations were visible. A maximum tension flange strain of 1.96 percent and a minimum compression flange strain of -1.82 percent, which occurred at a ultimate applied load of 89.2 kN, is shown in Figure B30. The failed beam is shown in Figure B31.

BEAM 20

Beam number 20 was fatigued at a rate of 4 Hz under sinusoidal load control with a maximum load of 53.4 kN and a minimum load of 5.3 kN. The maximum load produced an initial maximum tension flange strain of 1.09 percent and a minimum compression

flange strain of -1.09 percent. The initial beam stiffness was measured as 4,218 kN/m. The beam stiffness was checked throughout the test and is summarized in Table B5. The flanges of the beam showed the same 0° fiber misalignment, 2° to 3°, as in Beam number 18 and affected the edges of the flanges. The beam failed after 94,391 cycles due to the tension flange delaminating from the C-channel involving the 0° ply (ply 8, Table B3), the adhesive layer and the ±45° ply (ply 9, Table B3). This delamination was located between x = -75 to 521 mm. Along with the edge 0° fiber delamination, the compression flange also had transverse tension cracks from x = 178 to 445 mm on the flange located beneath the outside edge of the web. The web had delaminations extending 25 mm into the web towards the compression flange. The failed beam is shown in Figures B32 and B33.

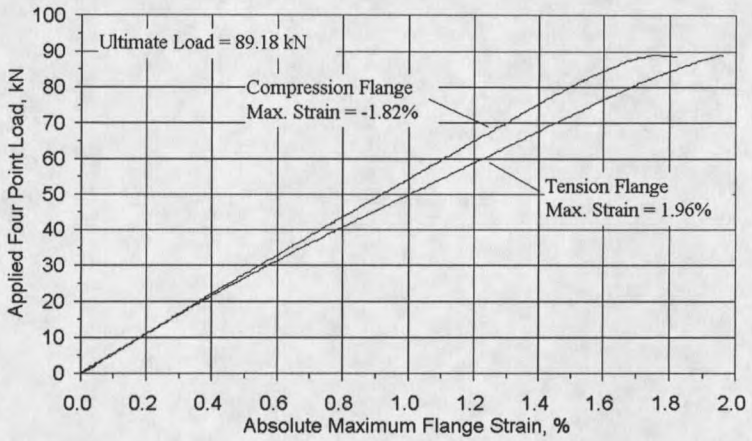


Figure B30. Load versus maximum flange strain, beam 19, static test.

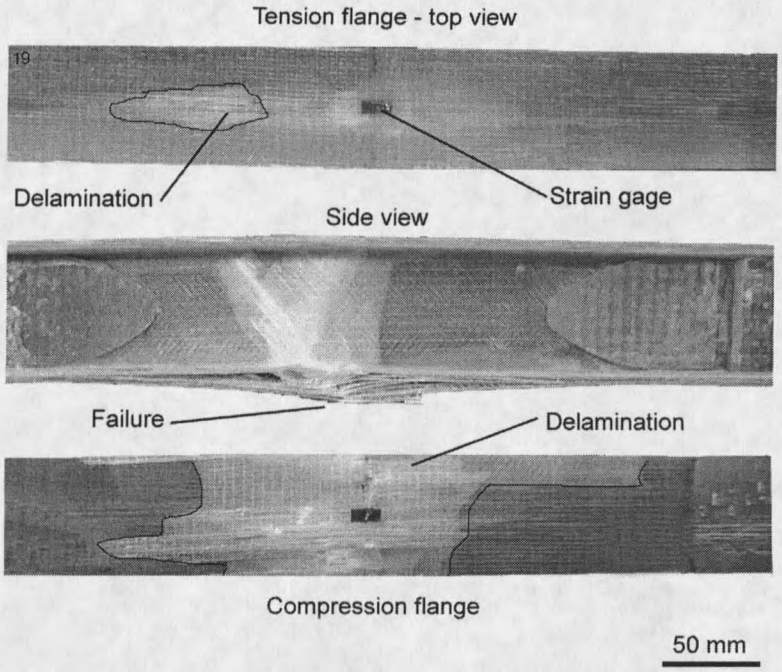


Figure B31. Beam 19.

Table B5. Beam 20 Stiffness versus Cycles.

Cycles	Stiffness (K), kN/m	Ratio (K/ 4,218)	n / N N = 94,391
0	4,218	1	---
2,000	4,133	0.98	0.02
10,000	4,009	0.95	0.11
30,000	3,726	0.88	0.32
50,000	3,522	0.83	0.53
73,000	3,022	0.72	0.77
90,000	2,978	0.71	0.95

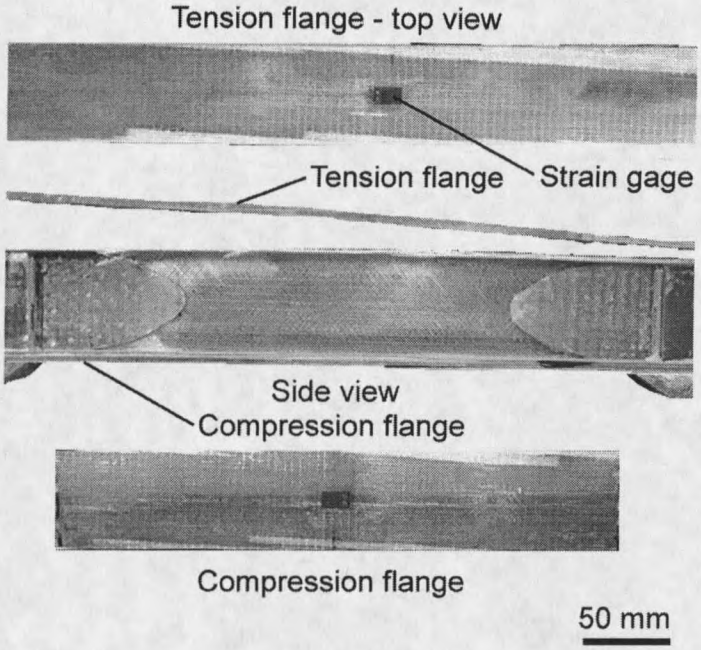


Figure B32. Beam 20.

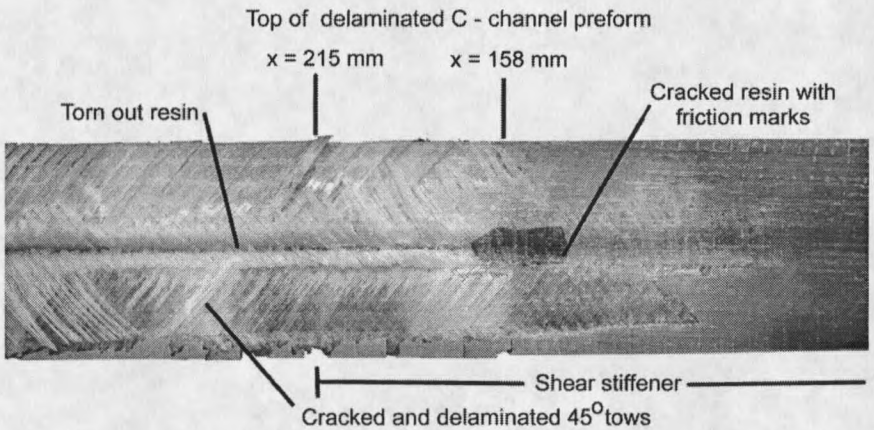


Figure B33. Beam 20.

BEAM 21

Beam number 21 was fatigued at a rate of 2 Hz under sinusoidal load control with a maximum load of 53.4 kN and a minimum load of 5.3 kN. The maximum load produced an initial maximum tension flange strain of 1.14 percent and a minimum compression

flange strain of -0.99 percent. The initial beam stiffness was measured as 4,110 kN/m. The beam stiffness was checked throughout the test and is summarized in Table B6. This beam had a edge flaw on the tension flange edge at x = 400 ±5 mm and was 1 mm deep. This flaw was large enough to start flange delamination from the C-channel between the 0° ply (ply 8, Table B3) and the adhesive. After 23,000 cycles, the flange damage was 13 mm wide and extended from x = 342 mm to 440 mm. The delamination extended towards the web and 5 mm down into it. The compression flange had some transverse tension cracks centered about the web. No shear stiffener, torsional stiffener or other compression flange damage or delaminations were visible. The beam is shown in Figure B34.

BEAM 24

Beam 24 involved a static test. The beam was loaded under actuator displacement control at a rate of 0.075 mm/s until failure, which involved a total ramp time of 190 seconds and a total mid-span deflection of 20 mm. An initial beam stiffness of 4,221 kN/m was measured. The beam had four acoustic emission sensors on the flanges: two on the tension flange centered at x = 76 and 549 mm, and two on the compression flange centered at x = 165 and 432 mm. A maximum tension flange strain of 1.93 percent and a minimum compression flange strain of -1.77 percent that occurred at a ultimate applied load of 88.29 kN. As with the other static tests, the compression flange twisted prior to final failure. This twisting was also evident in the failed beam as both sides of the beam flange had fragmented glass 0° and ±45° tows pointing up. This was a different mode of buckling than the other beams had shown. The compression flange failed at x = 320 ±10 mm with multiple delaminations throughout the flange thickness. The compression flange delaminated between the 0° ply (ply 5, Table B3) and -45° ply (ply 6, Table B3) from x = 146 to 437 mm. The failure caused delaminations to travel through the web and into the tension flange adhesive layer. Transverse tension cracks were present on the tension flange from x = 250 to 458 mm. The failed beam is shown in Figure B35. No shear stiffener, torsional stiffener or other tension flange damage or delaminations were visible.

Table B6. Beam 21 Stiffness versus Cycles.

Cycles	Stiffness (K), kN/m	Ratio (K/ 4,110)	n / N N = 23,000
0	4,110	1	---
1,000	3,984	0.97	0.04
1,500	3,943	0.96	0.07
2,000	3,893	0.95	0.09
8,000	3,830	0.93	0.35
15,000	3,811	0.93	0.65
21,000	3,689	0.90	0.91
22,500	3,523	0.86	0.98

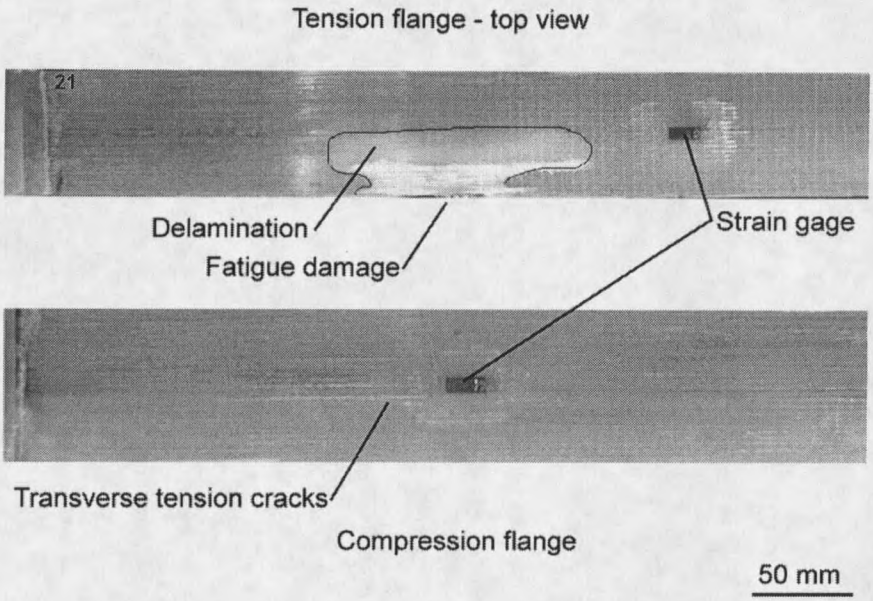


Figure B34. Beam 21.

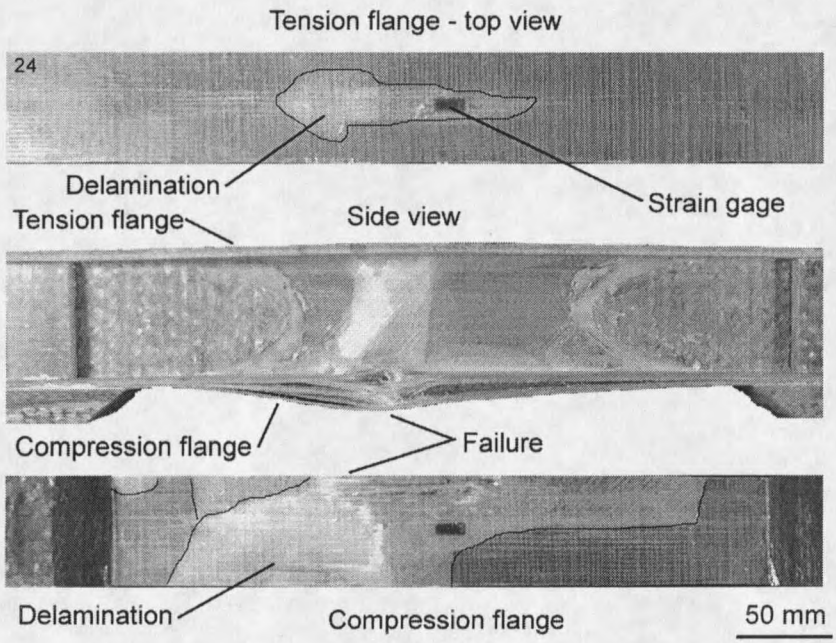


Figure B35. Beam 24.

BEAM 25

Beam number 25 was fatigued at a rate of 2 Hz under sinusoidal load control with a maximum load of 62.3 kN and a minimum load of 6.2 kN. The maximum load produced an initial maximum tension flange strain of 1.43 percent and a minimum compression flange strain of -1.13 percent. The initial beam stiffness was measured as 4,305 kN/m. The beam had four acoustic emission sensors on the flanges: two on the tension flange centered at x = 63 and 533 mm, and two on the compression flange centered at x = 170 and 430 mm. After 7,636 cycles, the compression flange failed at x = 229 ± 13 mm. A loud pop was heard one cycle prior to failure and it is suspected that a partial delamination grew to a point where it compromised the stability of the compression flange, lowering the strength of the beam to below the maximum fatigue stress. The final failure of the beam indicates a twisting of the compression flange at failure. The flange delamination extended from x = 170 to 432 mm and involved all the 0° to 45° interfaces and the adhesive layer. The delamination traveled into the web towards the tension flange and created two spot delaminations. Transverse tension cracks were also present on the tension flange over the web. It is not known if these transverse cracks were present prior to flange failure. No shear stiffener, torsional stiffener or other tension flange damage or delaminations were visible. The failed beam is shown in Figure B36.

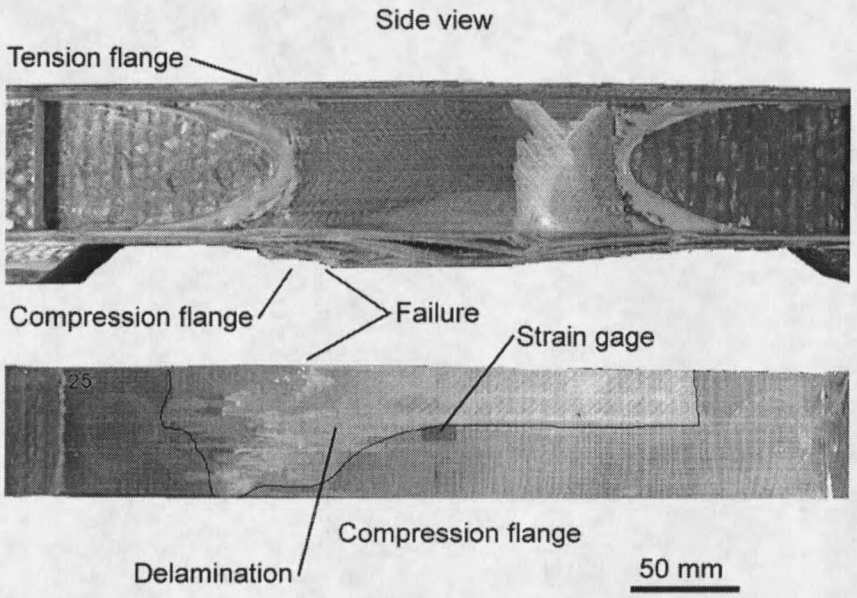


Figure B36. Beam 25.

BEAM 26

Beam number 26 was fatigued at a rate of 2 Hz under sinusoidal load control with a maximum load of 57.8 kN and a minimum load of 5.8 kN. The maximum load produced an initial maximum tension flange strain of 1.22 percent and a minimum compression flange strain of -1.05 percent. The initial beam stiffness was measured as 4,355 kN/m. The beam stiffness was checked throughout the test and is summarized in Table B7. After 104,407 cycles, the beam failed by compression flange delamination and shear stiffener failure. Shear failure of the compression flange occurred at x = 133 mm. This was under the compression flange load pad. The compression flange delaminated between the 0° ply (ply 8, 24) and the adhesive layer. Delamination of the tension flange above the shear stiffeners, x = 178 and 428 mm, was noticed at 10,000 cycles and continued to grow until failure. The beam is shown in Figure B37. All shear stiffeners showed some signs of delamination from the web.

Table B7. Beam 26 Stiffness versus Cycles.

Cycles	Stiffness (K), kN/m	Ratio (K/ 4,355)	n / N N = 104,407
0	4,355	1	---
20,000	4,078	0.94	0.19
50,000	3,939	0.91	0.48
60,000	3,919	0.90	0.57
75,000	3,878	0.89	0.72
100,000	3,853	0.89	0.96

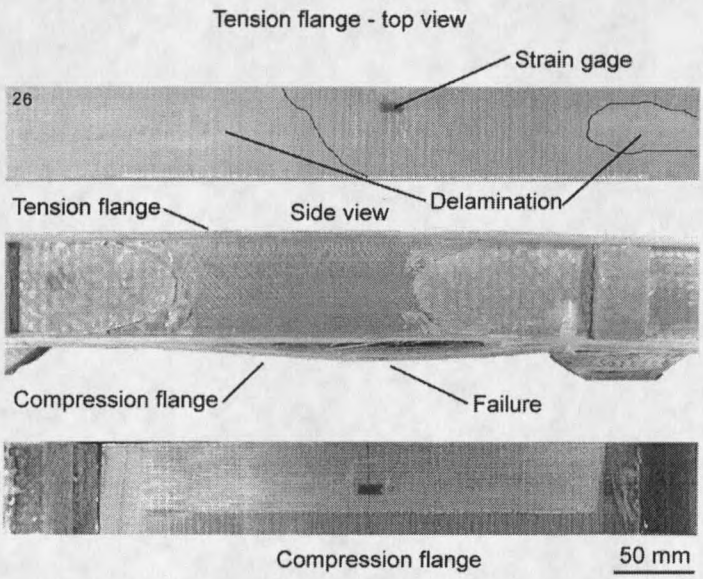


Figure B37. Beam 26.

BEAM 27

Beam number 27 was fatigued at a rate of 3 Hz under sinusoidal load control with a maximum load of 53.4 kN and a minimum load of 5.3 kN. The maximum load produced an initial maximum tension flange strain of 1.07 percent and a minimum compression flange strain of -1.00 percent. The initial beam stiffness was measured as 4,069 kN/m. As with the other DD5P beams, two tension flange delamination spots started over the tapered shear stiffener area, x = 178 and 445 mm. These spots grew during the fatigue test until the delamination was under a tension flange load pad. After 243,876 cycles, the tension flange delaminated. The delamination involved the adhesive layer and the adjacent 0° and 45° plies and was from x = -75 to 483 mm. Some transverse cracks were present on both the tensile and compression flanges prior to failure. The shear stiffeners under the delamination show some damage, but it is not known if this was present prior to failure. The web also has delaminations extending 15 mm down towards the compression flange. The failed beam is shown in Figure B38.

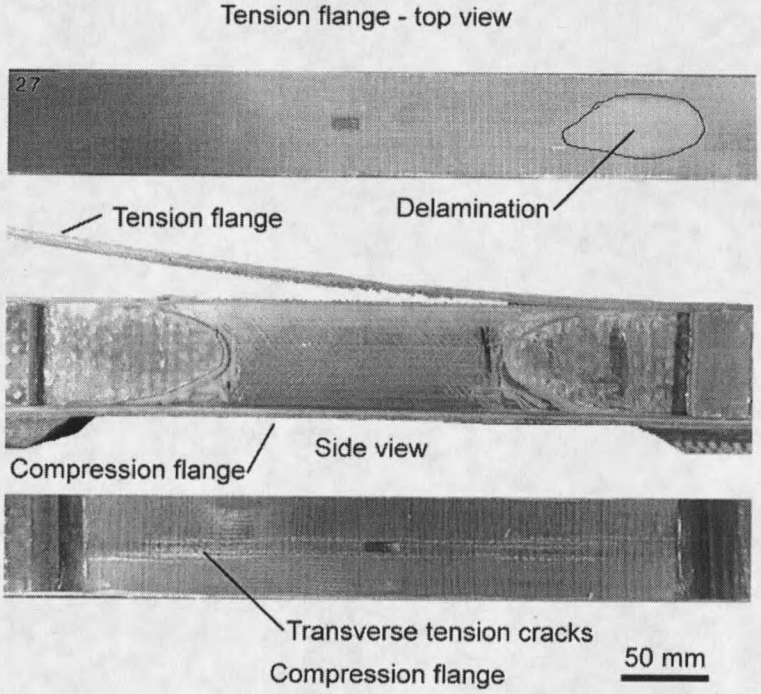


Figure B38. Beam 27.

BEAM 28

Beam number 28 was fatigued at a rate of 5 to 12 Hz under sinusoidal load control with a maximum load of 44.5 kN and a minimum load of 4.4 kN. The maximum load produced an initial maximum tension flange strain of 0.86 percent and a minimum compression flange strain of -0.85 percent. The initial beam stiffness was measured as 4,142 kN/m. Tension flange delamination spots started to develop over the tapered shear stiffener area, x = 178 and 445 mm, after approximately 600,000 cycles. After 2,000,000 cycles, the beam was stopped and the only damage present was the delamination between the tension flange and the adhesive layer. This is shown in Figure B39. The compression flange has two transverse tension cracks, x = 406 to 445 mm extending under the load pad. No shear stiffener, torsional stiffener or other flange damage or delaminations were visible.

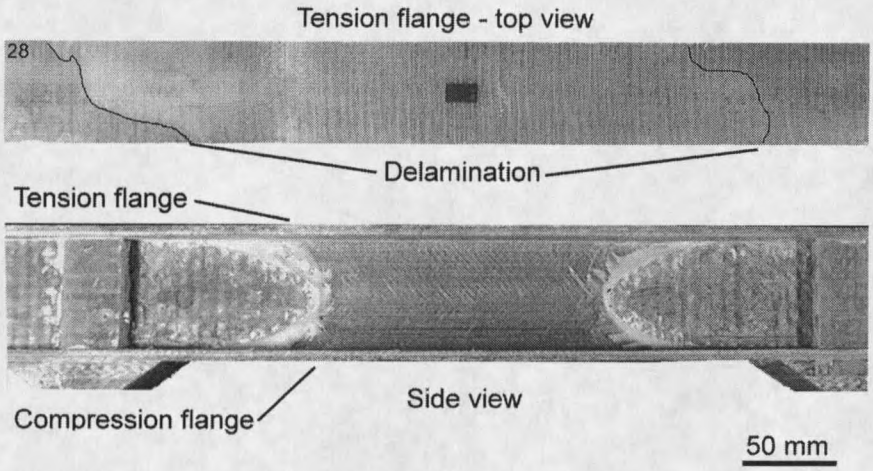


Figure B39. Beam 28.

BEAM 29

Beam number 29 was fatigued at a rate of 4 Hz under sinusoidal load control with a maximum load of 48.9 kN and a minimum load of 4.9 kN. The maximum load produced an initial maximum tension flange strain of 0.92 percent and a minimum compression flange strain of -0.96 percent. The initial beam stiffness was measured as 4,100 kN/m. Kapton film was placed between the strain gages and the flanges in hopes of preventing the matrix cracks from traveling into the strain gages. The traveling was not stopped and the gages failed after 4,000 cycles. No significant improvement in strain gage lifetime, with the Kapton film, was observed. The beam was stopped after 815,684 cycles prior to beam failure. At this point the tension flange delamination extended between the 0° ply (ply 5, Table B3) and the -45° ply (ply 6, Table 4), x = 0 to 115 mm, and between the adhesive and the 0°ply (ply 8, Table B3), x = 115 to 260 mm. The compression flange showed three small transverse tensile cracks but otherwise no other damage. The beam is shown is Figure B40.

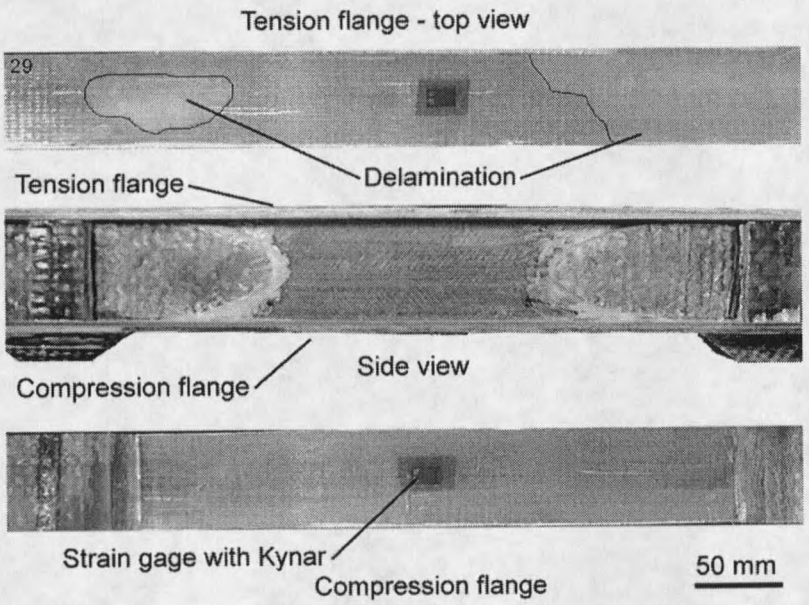


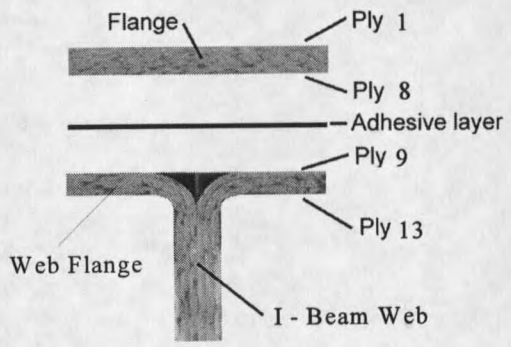
Figure B40. Beam 29.

Beams with DD5P Material Flanges and CH3 Web Material

Beams 30, 31, 32 and 33 had a stiffer web, CH3 versus CH10, to try to eliminate the tension flange from delaminating from the I-beam preform. The description of the I-beam flange lay up and ply numbering scheme for these beams is outlined in Table B8 below.

Table B8. Ply reference notation for Beams 30, 31, 32 and 33.

Ply number	Ply angle	Fabric	Description
1	0°	D155	DD5P flange material, 2.9 mm thick $V_F = 0.36$
2	+45°	DB120	
3	-45°		
4	0°	D155	
5	0°		
6	-45°	DB120	
7	+45°		
8	0°	D155	
Adhesive Layer Hysol EA 9309.2NA, 0.1 - 0.4 mm thick			
9	+45°	DB240	Web material CH3 I-shape 3 mm thick $V_F = 0.35$
10	-45°		
11	0°	D155	
12	+45°	DB240	
13	-45°		



BEAM 30

Beam number 30 was fatigued at a rate of 2 Hz under sinusoidal load control with a maximum load of 62.3 kN and a minimum load of 6.2 kN. The maximum load produced an initial maximum tension flange strain of 1.20 percent and a minimum compression flange strain of -1.05 percent. The initial beam stiffness was measured as 4,345 kN/m. The beam had four acoustic emission sensors on the flanges: two on the tension flange centered at x = 64 and 533 mm, and two on the compression flange centered at x = 178 and 432 mm. After 5,741 cycles, the test was stopped as the failure mode was identical to Beam number 26. The shear stiffeners had delaminated and the compression flange had a shear failure through its thickness at x = 120 mm, under a compression flange load pad. The shear stiffener had a crack at x = 120 mm, which was the start of the stiffener taper, 30 mm up towards the tension flange. The compression flange had a few transverse tension cracks. The tension flange had started to delaminate over the shear stiffeners. No torsional stiffener or other tension flange damage or delaminations were visible. The failed beam is shown in Figures B41 and B42.

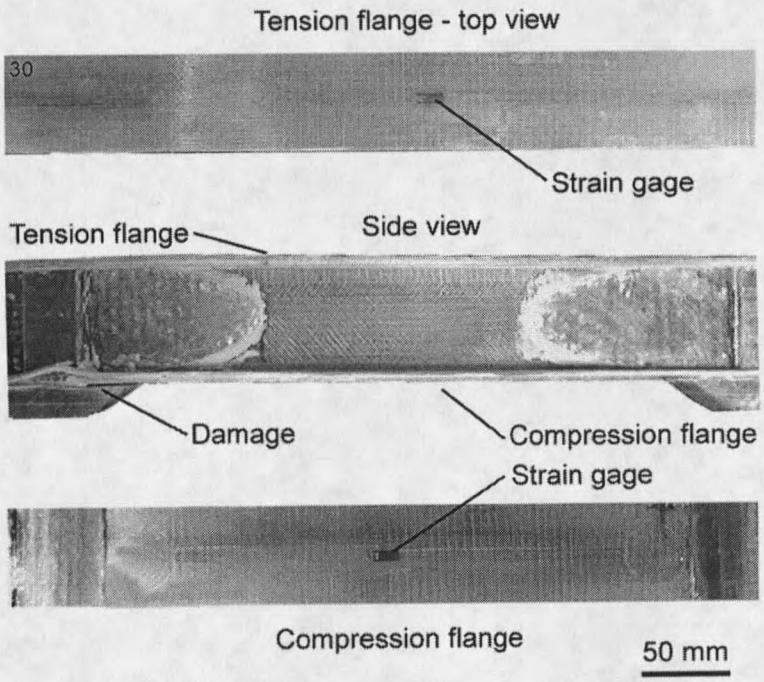


Figure B41. Beam 30.

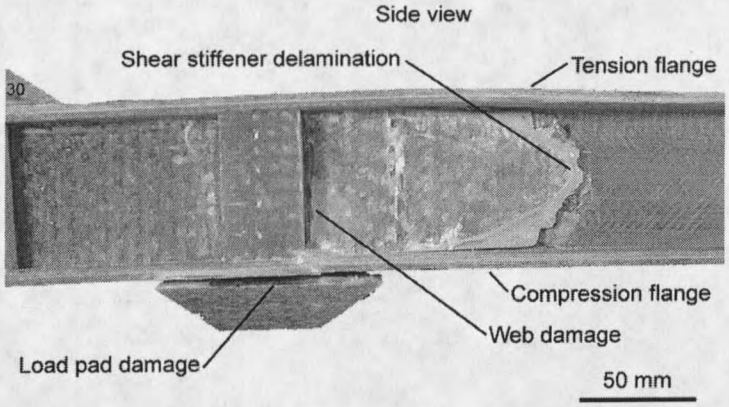


Figure B42. Beam 30.

BEAM 31

Beam number 31 was fatigued at a rate of 4 Hz under sinusoidal load control with a maximum load of 53.4 kN and a minimum load of 5.3 kN. The maximum load produced an initial maximum tension flange strain of 1.92 percent and a minimum compression flange strain of -0.89 percent. The initial beam stiffness was measured as 4,764 kN/m. The stiffness was also checked after a power outage at 796,633 cycles, 4,170 kN/m and after 2,030,240 cycles 3,248 kN/m. The test was stopped after 2,030,240 cycles. After these cycles 3 of the shear stiffeners had started to delaminate from the web and the tension flange had delaminated from the C-channel between x = 25 and 280 mm. There was also web delamination damage at x = 195 mm that extended down from the tension flange into the tapered shear stiffener area. The compression flange also had multiple transverse tension cracks under this shear stiffener area. The beam is shown in Figure B43.

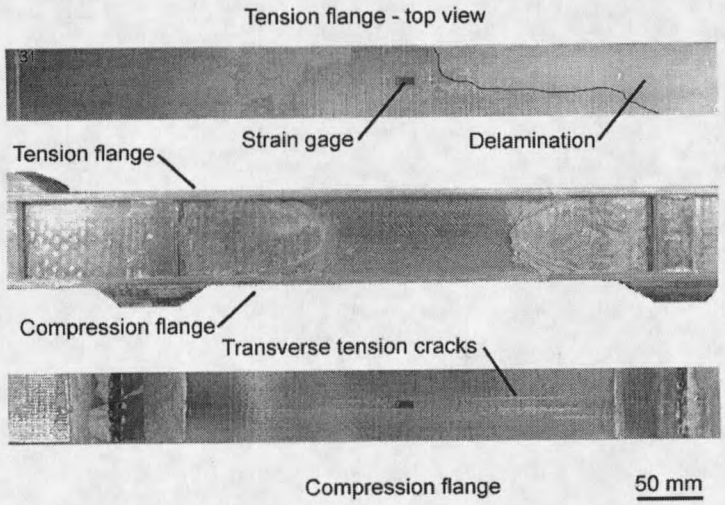


Figure B43. Beam 31.

BEAM 32

Beam number 32 was fatigued at a rate of 5 Hz under sinusoidal load control with a maximum load of 53.4 kN and a minimum load of 5.3 kN. The maximum load produced an initial maximum tension flange strain of 0.86 percent and a minimum compression flange strain of -0.73 percent. The initial beam stiffness was measured as 4,639 kN/m. The beam stiffness was checked throughout the test and is summarized in Table B9. The fatigue test was stopped after 783,153 cycles. Like Beams 26 and 30, this beam started to have the same failure mode. The compression flange has sheared through the thickness at x = 127 mm under a compression flange load pad at the edge of the torsional stiffener. The compression flange did not have any visible transverse tension cracks. The only other damage on the beam was the spot delaminations on the tension flange over the shear stiffeners. The beam is shown in Figure B44.

Table B9 Beam 32 Stiffness versus Cycles.

Cycles	Stiffness (K), kN/m	Ratio (K/ 4,639)	n / N N = 783,153
0	4,639	1	---
5,000	4,231	0.91	0.01
10,000	4,149	0.89	0.01
15,000	4,161	0.90	0.02
20,000	4,180	0.90	0.03
65,000	3,863	0.83	0.08
75,000	3,844	0.83	0.10
85,000	3,869	0.83	0.11
250,000	3,823	0.82	0.32

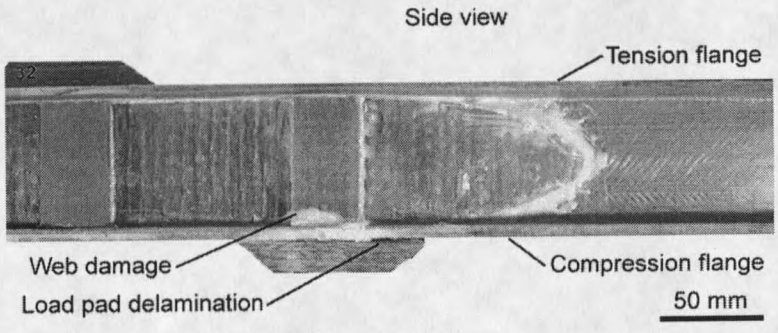


Figure B44. Beam 32.

BEAM 33

Beam number 33 was fatigued at a rate of 4 Hz under sinusoidal load control with a maximum load of 53.4 kN and a minimum load of 5.3 kN. The maximum load produced an initial maximum tension flange strain of 0.94 percent and a minimum compression flange strain of -0.93 percent. The initial beam stiffness was measured as 4,606 kN/m. The beam stiffness was checked throughout the test and is summarized in Table B10. The beam was stopped after 3,200,000 cycles. Although the beam had not failed, there was some tension flange delamination, three spots, which were growing and extended down into the C-channel at x = 318 mm. The compression flange had some minor transverse tension cracks. The beam is shown in Figure B45.

Table B10. Beam 33 Stiffness versus Cycles.

Cycles	Stiffness (K), kN/m	Ratio (K/ 4,606)	n / N N = 3,200,000
0	4,606	1	---
200,000	4,184	0.91	0.06
300,000	4,215	0.92	0.09
500,000	4,150	0.90	0.16
3,200,000	3,873	0.84	1

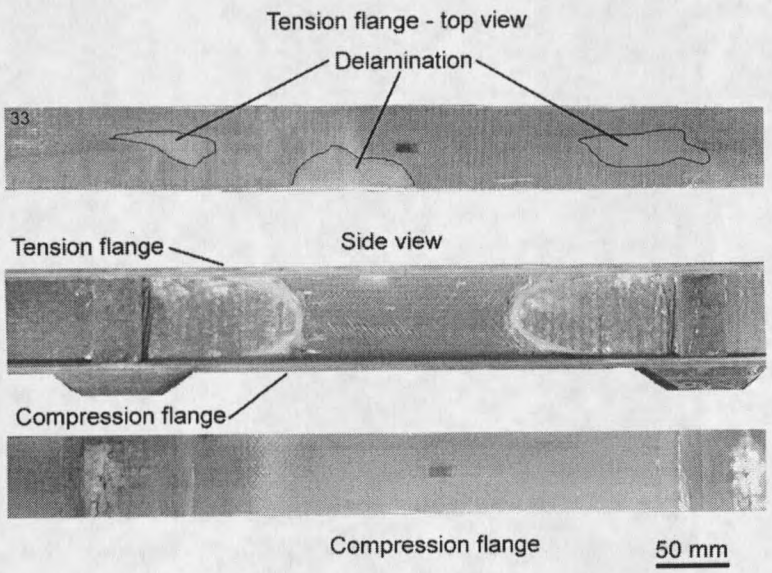


Figure B45. Beam 33.

Beams With DD5P Material Flanges With CH12 Material Webs

Although the tension flanges were still delaminating from the web flange, Beams 34 and 35 had their fiber volume reduced to 0.34, CH12 material, with the same $(\pm 45°/0°/\pm 45°)_2$ layup as the previous beams. This fiber volume showed promising fatigue response in standard coupon tests.

Beam 34

Beam 34 involved a static test. The beam was loaded under actuator displacement control at a rate of 0.075 mm/s until failure, which involved a total ramp time of 65 seconds and a total mid-span deflection of approximately 8 mm. An initial beam stiffness of 4,990 kN/m was measured. The beam had two additional strain gages on the compression flange edges, both top and bottom of the flange. This was done to determine when the flange starts to buckle. The beam was loaded statically to 60 kN three times before the actual static test. The initial load - flange absolute maximum strain graph is shown in Figure B46 and shows the two standard strain gages on the center of the tension and compression flanges. Figure B47 shows the two compression flange edge gages, back-to-back, which indicates that the onset of buckling in this beam occurs at approximately 75 kN or 1.4 percent strain. The third load-up involved the static test and indicated a maximum tension flange strain of 1.92 percent and a minimum compression flange strain of -1.69 percent that occurred at a ultimate applied load of 83.22 kN. The failure occurred on the compression flange at x = 292 ± 20 mm. The compression flange had transverse tension cracks and multiple delaminations between x = 150 and 457 mm. The delaminations extended through the web and into the adhesive layer on the tension flange, producing a delamination from x = 178 to 381 mm. The failed beam is shown in Figures B48 and B49.

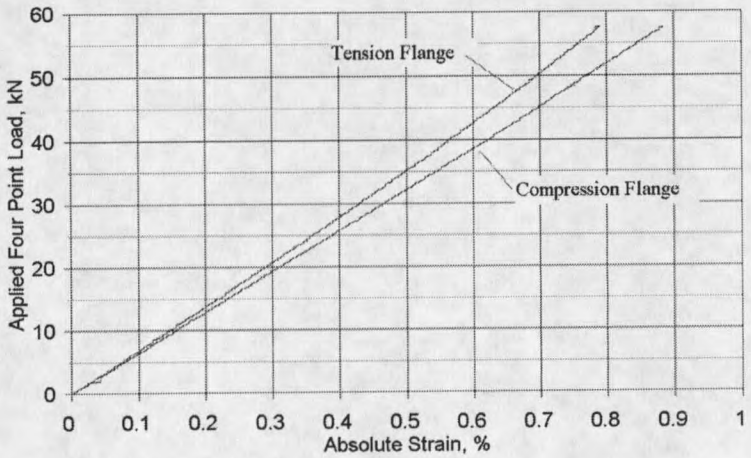


Figure B46. Absolute flange strain versus load, initial four point loading, beam 34.

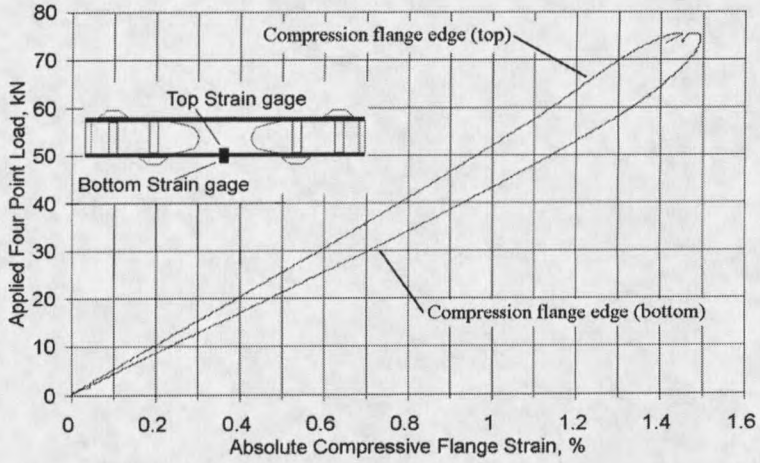


Figure B47. Load versus compressive flange strain, beam 34.

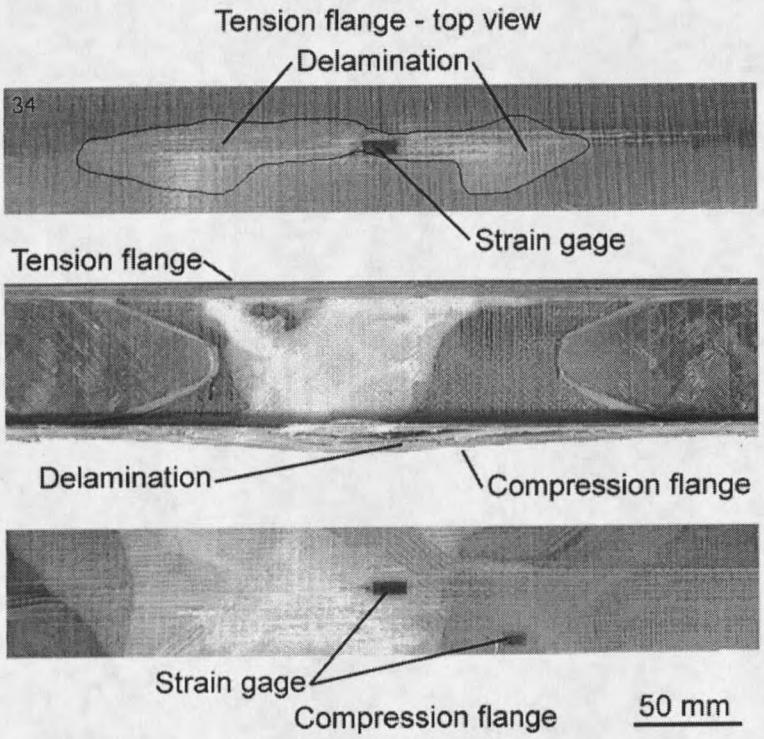


Figure B48. Beam 34.

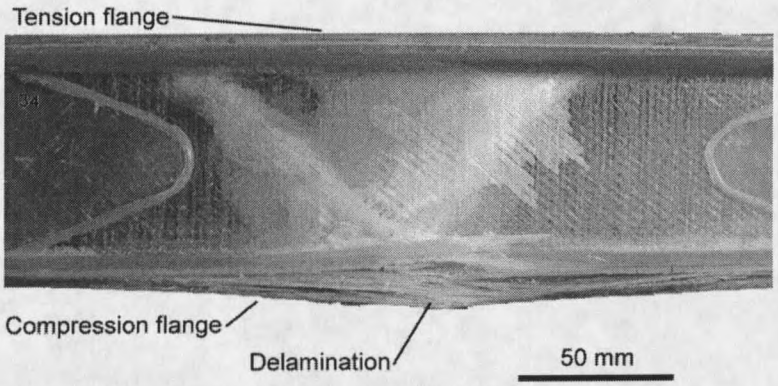


Figure B49. Beam 34.

BEAM 35

Beam number 35 was fatigued at a rate of 2 Hz under sinusoidal load control with a maximum load of 62.3 kN and a minimum load of 6.3 kN. The maximum load produced an initial maximum tension flange strain of 1.04 percent and a minimum compression flange strain of -1.02 percent. The initial beam stiffness was measured as 4,347 kN/m. The compression flange delaminated from x = -75 to 458 mm, after 9,771 cycles. The delamination of the flange caused the web to fail at x = 190 mm with delamination in the web from x = 178 to 267 mm. There were two spot delaminations on the tension flange, caused by the failure, at x = 190 to 356 mm. The failed beam is shown in Figures B50 and B51.

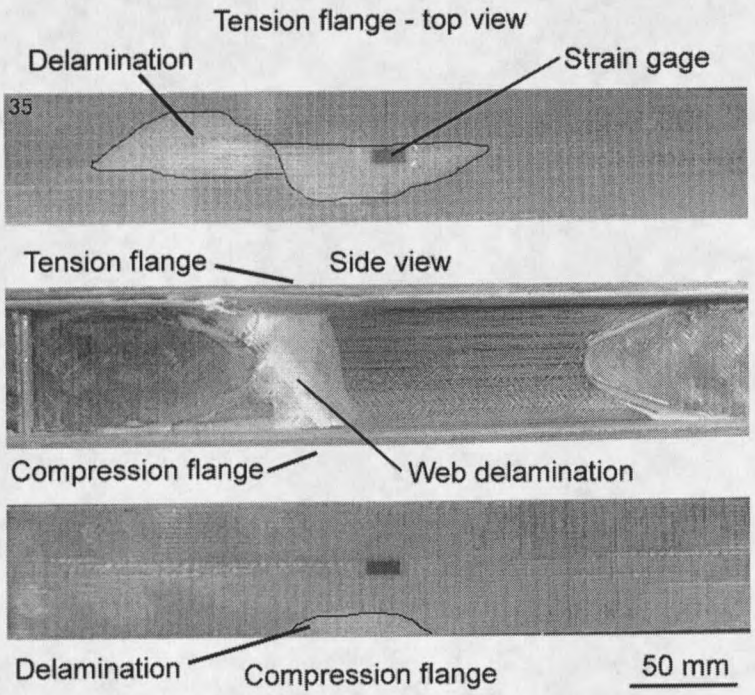


Figure B50. Beam 35.

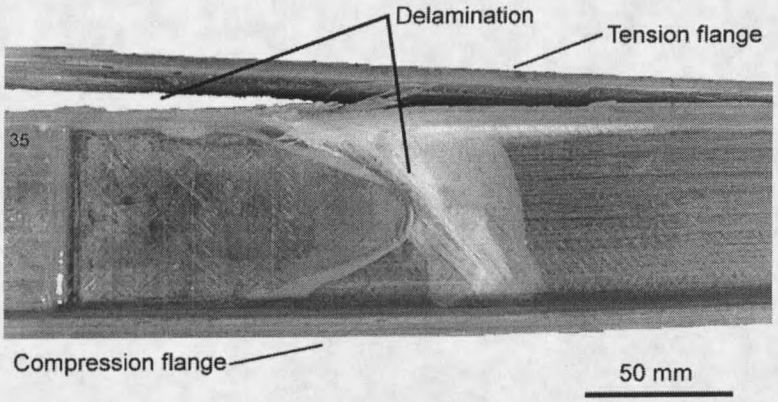


Figure B51. Beam 35.

DD5P Material Flanges with DD5P Web Material

Beams 51 through 55 were manufactured with both the flange and web consisting of DD5P material. This was done to increase the stiffness and fatigue response of the web. Beam 53 was tested first, which resulted in a shear stiffener failure. It was therefore necessary to increase the stiffener reinforcement under the load pads to handle the increased loads. The ply lay-up and numbering scheme is shown in Table B11.

BEAM 51

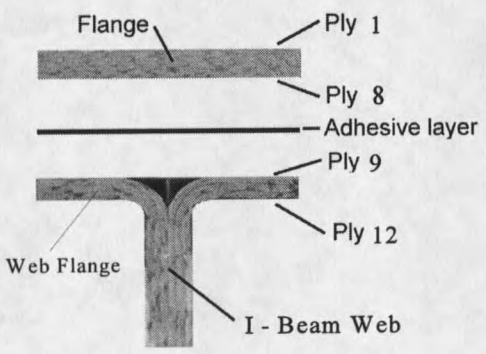
Beam number 51 was fatigued at a rate of 6 Hz under sinusoidal load control with a maximum load of 53.4 kN and a minimum load of 5.3 kN. The maximum load produced an initial maximum tension flange strain of 0.76 percent and a minimum compression flange strain of -0.75 percent. The initial beam stiffness was measured as 4,867 kN/m. The beam was stopped after 3,000,000 cycles with no significant change in stiffness and no major damage. Figure B52 shows the only noticeable damage on the beam, transverse tension cracks on the compression flange. Figure B53 shows the additional shear stiffener material that was added to the beam.

BEAM 52

Beam number 52 was fatigued at a rate of 3 Hz under sinusoidal load control with a maximum load of 62.3 kN and a minimum load of 6.2 kN. The maximum load produced an initial maximum tension flange strain of 0.93 percent and a minimum compression flange strain of -0.89 percent. The initial beam stiffness was measured as 5,145 kN/m. Initially the compression flange showed no evidence of buckling, but after 16,000 cycles, it was noticed that the compression flange had a small localized buckling node at x = 395 mm that was present on only one flange edge. This node, or area of increased localized displacement, did not change until the failure of the beam after 62,843 cycles. The

compression flange failed at x = 395 mm, the node, with multiple delaminations in the preform and flange. The compression flange delaminations extended from x = 200 to 460 mm and were between the 0°ply and adjacent 45° plies throughout the flange and preform thickness. This delamination also traveled into the web. The failed beam is shown in Figure B54.

Table B11. Ply reference notation for Beams 51 through 55.

<table>
<tr><th>Ply Number</th><th>Ply Angle</th><th>Fabric</th><th>Description</th></tr>
<tr><td>1</td><td>0°</td><td>D155</td><td rowspan="8">DD5P flange material,
2.9 mm thick
$V_F = 0.36$</td></tr>
<tr><td>2</td><td>+45°</td><td rowspan="2">DB120</td></tr>
<tr><td>3</td><td>-45°</td></tr>
<tr><td>4</td><td>0°</td><td rowspan="2">D155</td></tr>
<tr><td>5</td><td>0°</td></tr>
<tr><td>6</td><td>-45°</td><td rowspan="2">DB120</td></tr>
<tr><td>7</td><td>+45°</td></tr>
<tr><td>8</td><td>0°</td><td>D155</td></tr>
<tr><td colspan="4">Adhesive Layer Hysol EA 9309.2NA, 0.1 - 0.4 mm thick</td></tr>
<tr><td>9</td><td>0°</td><td>D155</td><td rowspan="4">DD5P web material
I-shape
3 mm thick
$V_F = 0.36$</td></tr>
<tr><td>10</td><td>+45°</td><td rowspan="2">DB240</td></tr>
<tr><td>11</td><td>-45°</td></tr>
<tr><td>12</td><td>0°</td><td>D155</td></tr>
<tr><td colspan="4">
</td></tr>
</table>

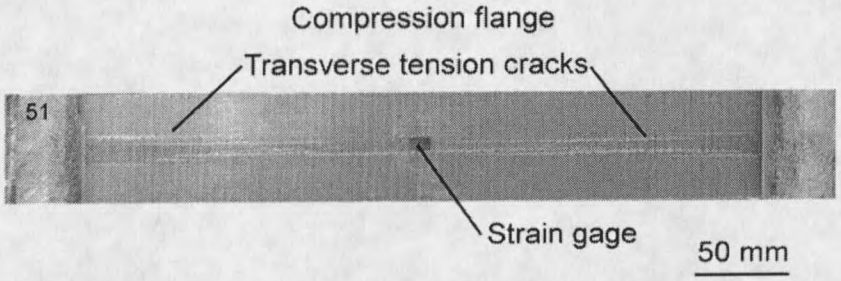


Figure B52. Beam 51.

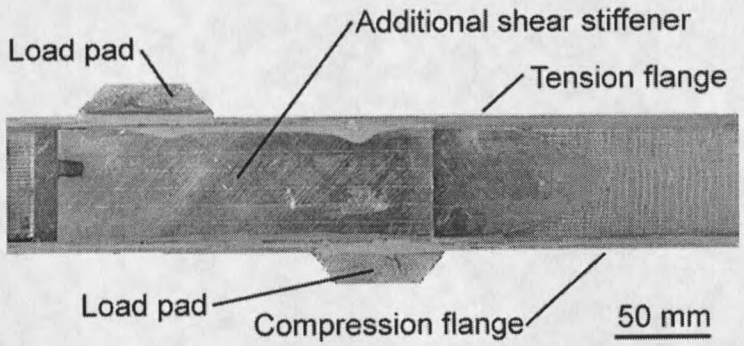


Figure B53. Additional shear stiffener material.

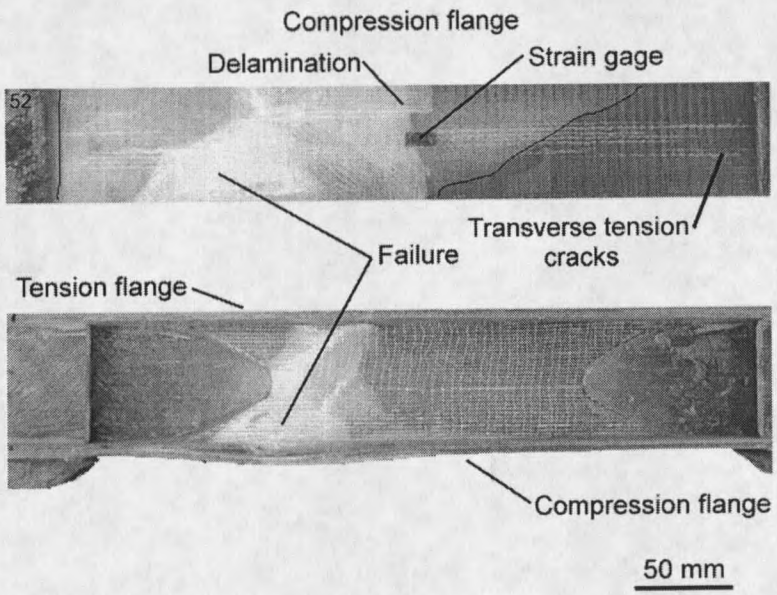


Figure B54. Beam 52.

BEAM 53

Beam number 53 was fatigued at a rate of 3 Hz under sinusoidal load control with a maximum load of 62.3 kN and a minimum load of 6.2 kN. The maximum load produced an initial maximum tension flange strain of 0.94 percent and a minimum compression flange strain of -0.89 percent. The initial beam stiffness was measured as 4,901 kN/m. The beam was stopped after 8,700 cycles due to a shear stiffener and web failure inside the shear loading area of the load pads. This damage is shown in Figure B55. Due to this failure, additional stiffener material was added to the other beams (51, 52 and 54) tested at this or higher loads.

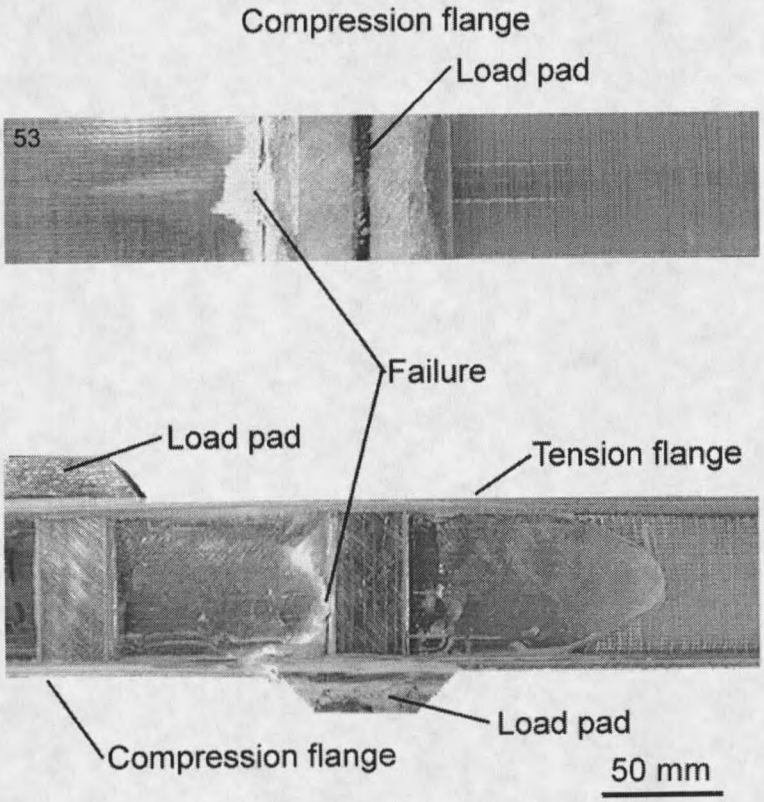


Figure B55. Beam 53.

BEAM 54

Beam number 54 was fatigued at a rate of 4 Hz under sinusoidal load control with a maximum load of 62.3 kN and a minimum load of 6.2 kN. The maximum load produced an initial maximum tension flange strain of 0.88 percent and a minimum compression flange strain of -0.88 percent. The initial beam stiffness was measured as 4,951 kN/m. The compression flange showed no evidence of buckling throughout the test. The beam failed after 2,744,704 cycles with a web and shear stiffener failure shown in Figure B56.

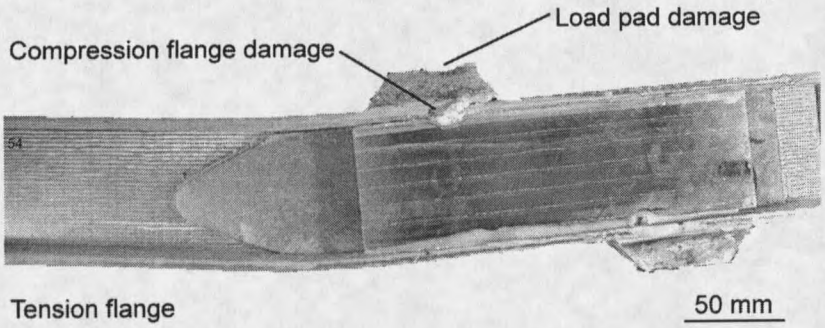


Figure B56. Beam 54.

BEAMS WITH STRUCTURAL DETAILS

Beams With Holes In AA Material (Triax) Flanges

To study the effects of severe flaws in flanges, 13 mm diameter holes were drilled on 102 mm centers along the length of each flange, through the flange thickness. This geometry, shown in Figure B57, included two holes on the compression flange and four holes on the tension flange. The holes were drilled into the flanges prior to the adhesive bonding to the preform. This was done to ensure that no damage was initiated in the web. Therefore, the flange hole penetrated the flange thickness, but stopped at the adhesive layer above the web flange. The tension flange had four-13 mm diameter holes located at x = 152, 254, 365 and 457 mm on the center line of the flange (y = 0). The compression flange had two -13 mm diameter holes at x = 254 and 356 mm. The web was CH10 Material, as in the foregoing series.

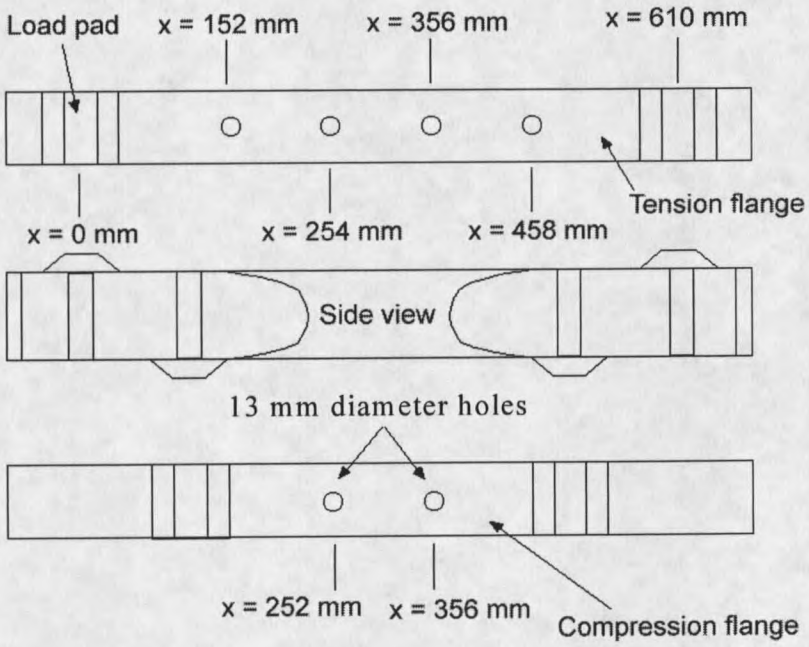


Figure B57. Beams 15, 16 and 17 flange geometry.

BEAM 15

Beam number 15 was fatigued at a rate of 1 Hz under sinusoidal load control with a maximum load of 31.1 kN and a minimum load of 3.1 kN. The maximum load produced an initial maximum tension flange strain of 0.83 percent and a minimum compression flange strain of -0.78 percent, both measured between hole locations. The initial beam stiffness was measured as 3,260 kN/m. The stiffness was checked after 2,163 cycles and was 3,064 kN/m or 94 percent of the original stiffness. The tension flange had two strain gages: one in the center of the flange and another at the edge. During the initial load up, at 18 kN, the center gage indicated 0.419 percent strain, while the edge gage was 0.429 percent, which is no significant difference. During the fatigue test, damage started to develop at all the holes and grew until it reached the edge of the flange. The beam failed after 2,772 cycles, in compression with the compression damage at x = 254 mm. Multiple delaminations between the 0° and +45° plies from x = 229 to x = 286 mm were also present. The compression flange failure and delamination caused an additional delamination to travel into the web at x = 244 to x = 279 mm. The failed beam is shown in Figure B58. No shear stiffener, torsional stiffener damage or delaminations were visible.

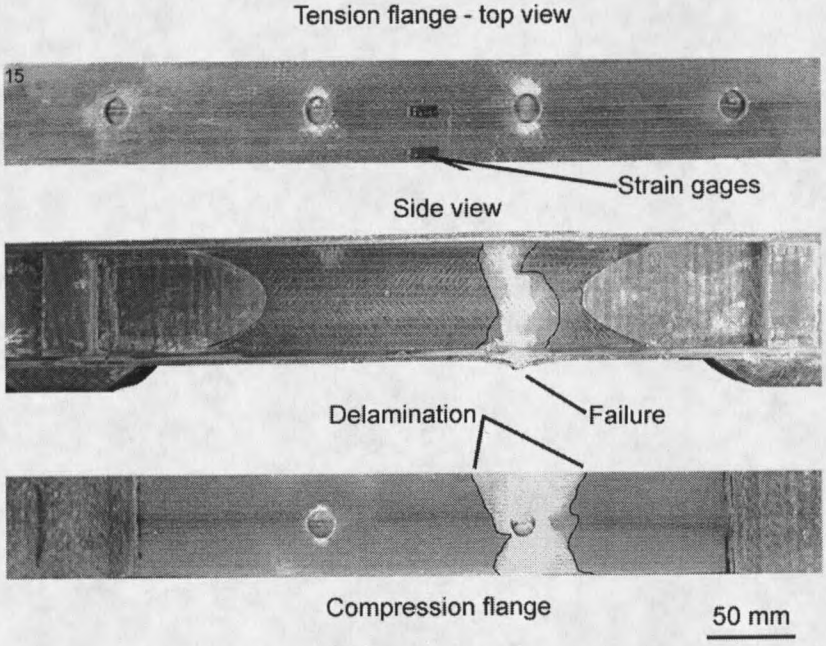


Figure B58. Beam 15.

BEAM 16

Beam number 16 was fatigued at a rate of 5 Hz under sinusoidal load control with a maximum load of 24.5 kN and a minimum load of 2.5 kN. The maximum load produced an initial maximum tension flange strain of 0.58 percent and a minimum compression flange strain of -0.53 percent. The initial beam stiffness was measured as 3,340 kN/m. During the fatigue test, damage started at the outside edges of the holes and continued to grow until failure after 40,448 cycles. The beam failed on the tension flange at x = 356 ± 13 mm with the underlying delamination between x = 325 to x = 394 mm. This delamination also traveled 25 mm down into the web. Prior to failure, the web had a large number of 1.0 to 1.5 mm long tensile cracks, all located at stitching cross over points. Although these small cracks probably did not have any influence on the failure, it is still disconcerting that every stitch cross-over point on the tension side of the neutral axis had a crack. Some minor delamination damage was present on the tension flange around the holes. No shear stiffener, torsional stiffener damage or delaminations were visible. The failed beam is shown in Figures B59 and B60.

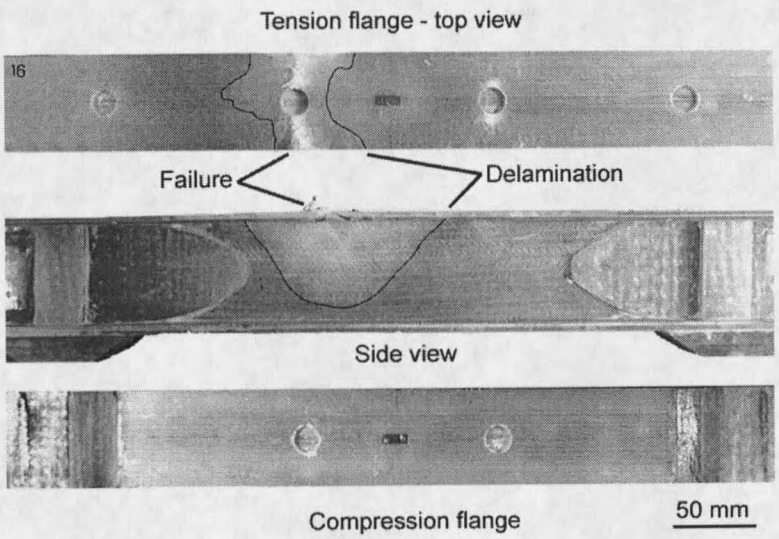


Figure B59. Beam 16.

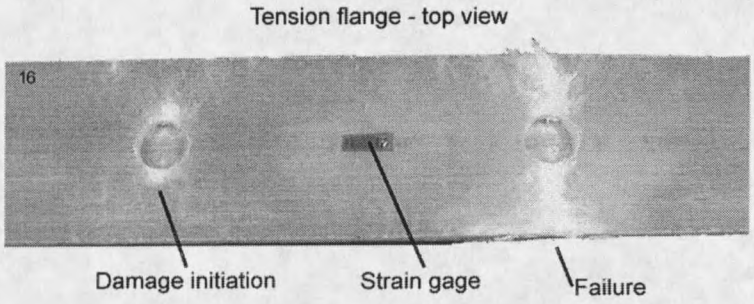


Figure B60. Beam 16.

BEAM 17

Beam 17 was tested statically to failure. The beam was loaded under actuator displacement control at a rate of 0.05 mm/s until failure, which had a total ramp time of 196 seconds. An initial beam stiffness of 3,350 kN/m was measured. The beam had a total of six strain gages, with three on the tension flange and three on the compression flange. At 18 kN, the tension flange indicated a center strain of 0.33 percent while the two edge gages indicated 0.42 percent and 0.42 percent. The compression flange center gage indicated -0.37 percent and the two edge gages indicated -0.39 percent and -0.37 percent. The difference in strain from the center, where the flange is discontinuous, and the edge is more pronounced than the strains recorded from Beam 15. As the beam was loaded, the compression flange did not appear to twist as in the other beam static tests. The load-flange absolute maximum strain graph is shown in Figure B61, indicating a maximum tension flange center strain of 1.30 percent and a minimum compression flange center strain of -1.08 percent. These strains occurred at a ultimate applied load of 47.0 kN at a maximum mid-span deflection of 15 mm. The failed beam is shown in Figure B62. The compression flange failed at $x = 260 \pm 15$ mm and created a flange delamination from $x = 178$ to $x = 419$ mm. The delamination was between the 0° ply (ply 10, Table B1) and +45° ply (ply 11, Table B1). This delamination traveled up towards the tension flange and produced a spot delamination at the tension flange hole. The second hole on the compression flange had a 12 mm delamination going towards the edge, but the damage at the other hole produced the flange failure first.

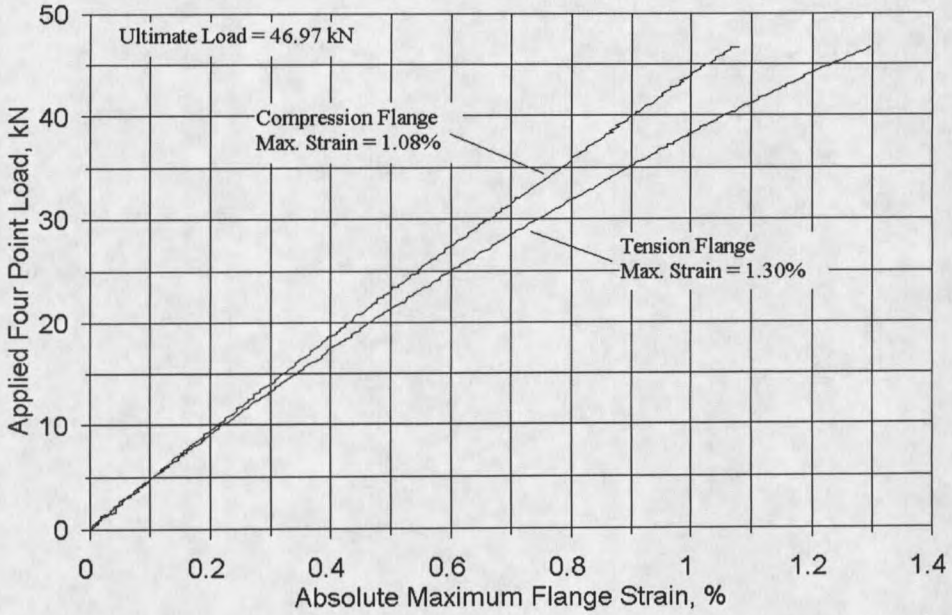


Figure B61. Load versus maximum flange strain, beam 17, static test.

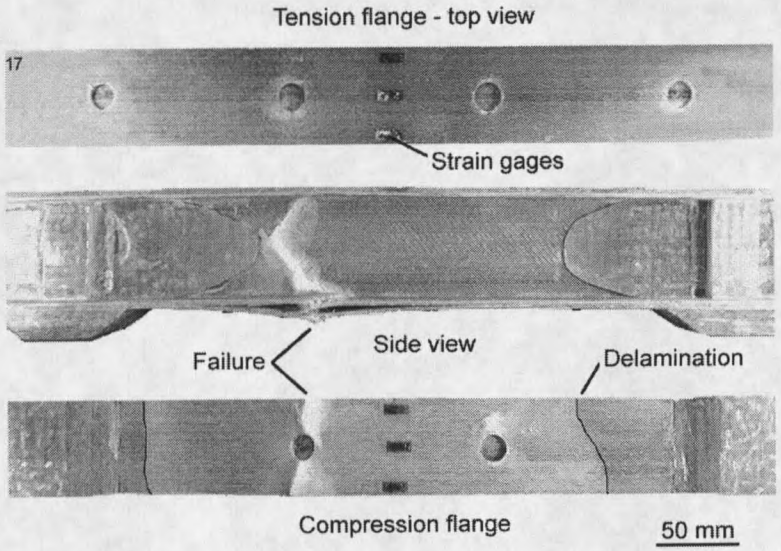


Figure B62. Beam 17.

DD27 Material Flanges (with balsa wood) and CH12 Web Material

Beams 58 and 59 involved 6 mm thick balsa wood, Baltek AL600, in the DD5P flange material to simulate actual wind turbine lay-up configurations. The ply lay-up and numbering scheme is listed in Table B12. The balsa wood core was replaced with ±45° ply DB400 under the load pads to prevent crushing damage.

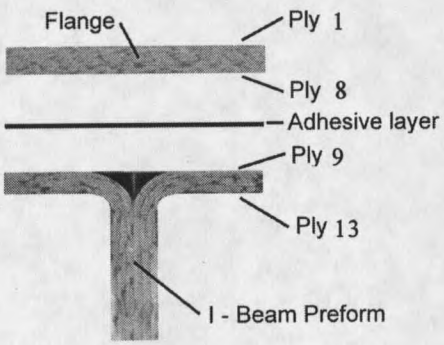
BEAM 58

Beam number 58 was fatigued at a rate of 1 Hz under sinusoidal load control with a maximum load of 62.3 kN and a minimum load of 6.2 kN. The maximum load produced an initial maximum tension flange strain of 0.97% and a minimum compression flange strain of -1.00%. The initial beam stiffness was measured as 5,341 kN/m. The compression flange failed after 230 cycles. The fiberglass plies delaminated from the balsa wood from x = 160 to 410 mm. This was a buckling induced compression flange failure. It is a possibility that the load pad / balsa wood core drop area influenced the failure. The failed beam is shown in Figure B63.

BEAM 59

Beam number 59 was initially fatigued at a rate of 4 Hz under sinusoidal load control with a maximum load of 35.6 kN and a minimum load of 3.6 kN. The maximum load produced an initial maximum tension flange strain of 0.58% and a minimum compression flange strain of -0.59%. The initial beam stiffness was measured as 5,512 kN/m. The beam was stopped after 1,000,000 cycles with no major noticeable damage. At this point the fatigue load was increased to a maximum load of 44.5 kN/m and a minimum load of 4.4 kN/m. This resulted in a maximum strain of 0.75% and a minimum strain of -0.75%. The compression flange failed after 88,993 cycles. The compression flange appeared to be sheared off at the edge of the load pad, which then delaminated from the balsa wood core from x = 160 to 350 mm. The delamination traveled into the web and produced two spot delaminations on the tension flange. The failed beam is shown in Figure B64.

Table B12. Ply reference notation for Beams 58 and 59.

<table>
<tr><th>Ply number</th><th>Ply angle</th><th>Fabric</th><th>Description</th></tr>
<tr><td>1</td><td>0°</td><td>D155</td><td rowspan="4"></td></tr>
<tr><td>2</td><td>+45°</td><td rowspan="2">DB120</td></tr>
<tr><td>3</td><td>-45°</td></tr>
<tr><td>4</td><td>0°</td><td>D155</td></tr>
<tr><td colspan="4">6 mm balsa wood core</td></tr>
<tr><td>5</td><td>0°</td><td>D155</td><td rowspan="4"></td></tr>
<tr><td>6</td><td>-45°</td><td rowspan="2">DB120</td></tr>
<tr><td>7</td><td>+45°</td></tr>
<tr><td>8</td><td>0°</td><td>D155</td></tr>
<tr><td colspan="4">Adhesive layer Hysol EA 9309.2NA, 0.1 - 0.4 mm thick</td></tr>
<tr><td>9</td><td>+45°</td><td rowspan="2">DB240</td><td rowspan="5">Material CH12
I-shape
5 mm thick
$V_F = 0.37$</td></tr>
<tr><td>10</td><td>-45°</td></tr>
<tr><td>11</td><td>0°</td><td>D155</td></tr>
<tr><td>12</td><td>-45°</td><td rowspan="2">DB240</td></tr>
<tr><td>13</td><td>+45°</td></tr>
<tr><td colspan="4">
</td></tr>
</table>

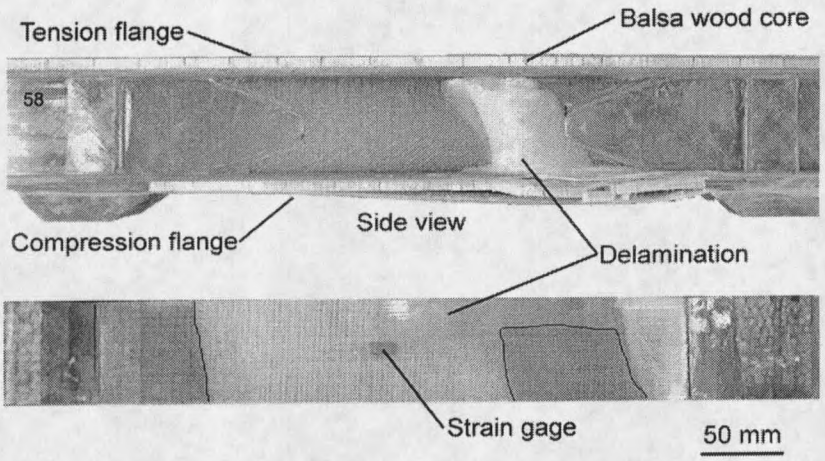


Figure B67. Beam 58

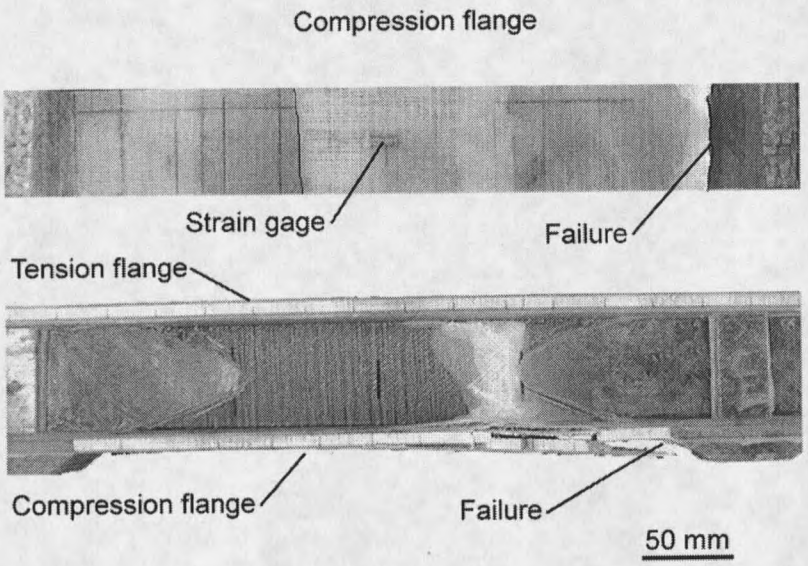


Figure B68. Beam 59

MONTANA STATE UNIVERSITY - BOZEMAN
3 1762 10428332 8